

# STRENGTH OF MATERIALS

---

## PART II

### *Advanced Theory and Problems*

---

By

S. TIMOSHENKO

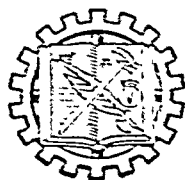
*Professor Emeritus of Engineering Mechanics  
Stanford University*

---

THIRD EDITION

---

CHECKED



D. VAN NOSTRAND COMPANY, Inc.

PRINCETON, NEW JERSEY

TORONTO

NEW YORK

LONDON

D. VAN NOSTRAND COMPANY, INC.

120 Alexander St., Princeton, New Jersey  
257 Fourth Avenue, New York 10, New York

25 Hollinger Rd., Toronto 16, Canada

Macmillan & Co., Ltd., St. Martin's St., London, W.C. 2, England

*All correspondence should be addressed to the  
principal office of the company at Princeton, N. J.*

MBM LIBRARY



4489

Copyright, ©, 1930, 1941, 1956 by  
D VAN NOSTRAND COMPANY, INC.

Published simultaneously in Canada by  
D VAN NOSTRAND COMPANY (Canada), LTD

*All Rights Reserved*

*This book, or any parts thereof, may not be  
reproduced in any form without written per  
mission from the author and the publishers.*

Library of Congress Catalogue Card No 55-6497

*First Published, June 1930*

*Two Reprintings*

*Second Edition, August 1941*

*Fourteen Reprintings*

*Third Edition, March 1956*

PRINTED IN THE UNITED STATES OF AMERICA

## PREFACE TO THE THIRD EDITION

In preparing the latest edition of this book, a considerable amount of new material has been added. Throughout the text, the latest references have been inserted, as well as new problems for solution and additional figures. The major changes in text material occur in the chapters on torsion, plastic deformation and mechanical properties of materials.

With regard to torsion, the problem of the twist of tubular members with intermediate cells is considered, as well as the torsional buckling of thin-walled members of open cross section. Each of these topics is important in the design of thin-walled structures such as the structural components of airplanes. In the chapter on plastic deformation the fundamental principles of limit design are discussed. Several examples of the application of the method to structural analysis are presented.

Major additions were made to the chapter on mechanical properties of materials, so that this single chapter now contains over 160 pages. The purpose of this expanded chapter is to focus attention on the recent developments in the field of experimental studies of the properties of structural materials. Some of the topics discussed are (1) the influence of imperfections on the ultimate strength of brittle materials and the "size effect"; (2) comparison of test results for single-crystal and polycrystal specimens; (3) the testing of materials under two- and three-dimensional stress conditions and various strength theories; (4) the strength of materials under impact; (5) fatigue of metals under various stress conditions and methods for improving the fatigue resistance of machine parts; and (6) strength of materials at high temperature, creep phenomenon and the use of creep test data in design. For the reader who desires to expand his knowledge of these topics further, the numerous references to the recent literature will be helpful. Finally, in the concluding article of the book, information for the proper

selection of working stresses is presented in considerable detail.

It is the author's hope that with these additions, the book will be more complete for the teaching of graduate courses in mechanics of materials and also more useful for designers and research engineers in mechanical and structural engineering.

In conclusion the author wishes to thank Professor James M. Gere of Stanford University for his assistance and numerous suggestions in revising the book and in reading the proofs

S. TIMOSHENKO

STANFORD UNIVERSITY

February 10, 1956



## PREFACE TO THE SECOND EDITION

In the preparation of the new edition of this volume, the general character of the book has remained unchanged; the only effort being to make it more complete and up-to-date by including new theoretical and experimental material representing recent developments in the fields of stress analysis and experimental investigation of mechanical properties of structural materials.

The most important additions to the first edition include:

1. A more complete discussion of problems dealing with bending, compression, and torsion of slender and thin-walled structures. This kind of structure finds at present a wide application in airplane constructions, and it was considered desirable to include in the new edition more problems from that field.

2. A chapter on plastic deformations dealing with bending and torsion of beams and shafts beyond the elastic limit and also with plastic flow of material in thick-walled cylinders subjected to high internal pressures.

3. A considerable amount of new material of an experimental character pertaining to the behavior of structural materials at high temperatures and to the fatigue of metals under reversal of stresses, especially in those cases where fatigue is combined with high stress concentration.

4. Important additions to be found in the portion of the book dealing with beams on elastic foundations; in the chapters on the theory of curved bars and theory of plates and shells; and in the chapter on stress concentration, in which some recent results of photoelastic tests have been included.

Since the appearance of the first edition of this book, the author's three volumes of a more advanced character, "Theory of Elasticity," "Theory of Elastic Stability," and "Theory of Plates and Shells" have been published. Reference to these

books are made in various places in this volume, especially in those cases where only final results are given without a complete mathematical derivation.

It is hoped that with the additions mentioned above the book will give an up-to-date presentation of the subject of strength of materials which may be useful both to graduate students interested in engineering mechanics and to design engineers dealing with complicated problems of stress analysis.

STEPHEN P. TIMOSHENKO

PALO ALTO, CALIFORNIA

June 12, 1941

## PREFACE TO THE FIRST EDITION

The second volume of *THE STRENGTH OF MATERIALS* is written principally for advanced students, research engineers, and designers. The writer has endeavored to prepare a book which contains the new developments that are of practical importance in the fields of strength of materials and theory of elasticity. Complete derivations of problems of practical interest are given in most cases. In only a comparatively few cases of the more complicated problems, for which solutions cannot be derived without going beyond the limit of the usual standard in engineering mathematics, the final results only are given. In such cases, the practical applications of the results are discussed, and, at the same time, references are given to the literature in which the complete derivation of the solution can be found.

In the first chapter, more complicated problems of bending of prismatical bars are considered. The important problems of bending of bars on an elastic foundation are discussed in detail and applications of the theory in investigating stresses in rails and stresses in tubes are given. The application of trigonometric series in investigating problems of bending is also discussed, and important approximate formulas for combined direct and transverse loading are derived.

In the second chapter, the theory of curved bars is developed in detail. The application of this theory to machine design is illustrated by an analysis of the stresses, for instance, in hooks, fly wheels, links of chains, piston rings, and curved pipes.

The third chapter contains the theory of bending of plates. The cases of deflection of plates to a cylindrical shape and the symmetrical bending of circular plates are discussed in detail and practical applications are given. Some data regarding the bending of rectangular plates under uniform load are also given.

In the fourth chapter are discussed problems of stress distribution in parts having the form of a generated body and symmetrically loaded. These problems are especially important for designers of vessels submitted to internal pressure and of rotating machinery. Tensile and bending stresses in thin-walled vessels, stresses in thick-walled cylinders, shrink-fit stresses, and also dynamic stresses produced in rotors and rotating discs by inertia forces and the stresses due to non-uniform heating are given attention.

The fifth chapter contains the theory of sidewise buckling of compressed members and thin plates due to elastic instability. These problems are of utmost importance in many modern structures where the cross sectional dimensions are being reduced to a minimum due to the use of stronger materials and the desire to decrease weight. In many cases, failure of an engineering structure is to be attributed to elastic instability and not to lack of strength on the part of the material.

In the sixth chapter, the irregularities in stress distribution produced by sharp variations in cross sections of bars caused by holes and grooves are considered, and the practical significance of stress concentration is discussed. The photo-elastic method, which has proved very useful in investigating stress concentration, is also described. The membrane analogy in torsional problems and its application in investigating stress concentration at reentrant corners, as in rolled sections and in tubular sections, is explained. Circular shafts of variable diameter are also discussed, and an electrical analogy is used in explaining local stresses at the fillets in such shafts.

In the last chapter, the mechanical properties of materials are discussed. Attention is directed to the general principles rather than to a description of established, standardized methods of testing materials and manipulating apparatus. The results of modern investigations of the mechanical properties of single crystals and the practical significance of this information are described. Such subjects as the fatigue of metals and the strength of metals at high temperature are

of decided practical interest in modern machine design. These problems are treated more particularly with reference to new developments in these fields.

In concluding, various strength theories are considered. The important subject of the relation of the theories to the method of establishing working stresses under various stress conditions is developed.

It was mentioned that the book was written partially for teaching purposes, and that it is intended also to be used for advanced courses. The writer has, in his experience, usually divided the content of the book into three courses as follows: (1) A course embodying chapters 1, 3, and 5 principally for advanced students interested in structural engineering. (2) A course covering chapters 2, 3, 4, and 6 for students whose chief interest is in machine design. (3) A course using chapter 7 as a basis and accompanied by demonstrations in the material testing laboratory. The author feels that such a course, which treats the fundamentals of mechanical properties of materials and which establishes the relation between these properties and the working stresses used under various conditions in design, is of practical importance, and more attention should be given this sort of study in our engineering curricula.

The author takes this opportunity of thanking his friends who have assisted him by suggestions, reading of manuscript and proofs, particularly Messrs. W. M. Coates and L. H. Donnell, teachers of mathematics and mechanics in the Engineering College of the University of Michigan, and Mr. F. L. Everett of the Department of Engineering Research of the University of Michigan. He is indebted also to Mr. F. C. Wilharm for the preparation of drawings, to Mrs. E. D. Webster for the typing of the manuscript, and to the D. Van Nostrand Company for their care in the publication of the book.

S. TIMOSHENKO

ANN ARBOR, MICHIGAN  
May 1, 1930

## NOTATIONS

$\alpha$ .....	Angle, coefficient of thermal expansion, numerical coefficient
$\beta$ ..	Angle, numerical coefficient
$\gamma$	Shearing strain, weight per unit volume
$\Delta$ .	Unit volume expansion, distance
$\delta$ ..	Total elongation, total deflection, distance
$\epsilon$ .	Unit strain
$\epsilon_x, \epsilon_y, \epsilon_z$	Unit strains in $x, y$ , and $z$ directions
$\theta$ .	Angle, angle of twist per unit length of a shaft
$\mu$ .	Poisson's ratio
$\rho$ .	Distance, radius
$\sigma$	Unit normal stress
$\sigma_1, \sigma_2, \sigma_3$	Principal stresses
$\sigma_x, \sigma_y, \sigma_z$	Unit normal stresses on planes perpendicular to the $x, y$ , and $z$ axes
$\sigma_E$ ...	Unit stress at endurance limit
$\sigma_{ult}$ .	Ultimate stress
$\sigma_{uc}, \sigma_{ut}$	Ultimate stresses in compression and tension
$\sigma_W$ .	Working stress
$\sigma_{YP}$	Yield point stress
$\tau$ .	Unit shear stress
$\tau_{xy}, \tau_{yz}, \tau_{zx}$	Unit shear stresses on planes perpendicular to the $x, y$ , and $z$ axes, and parallel to the $y, z$ , and $x$ axes
$\tau_E$ .. . .	Endurance limit in shear
$\tau_{oct}$	Unit shear stress on octahedral plane
$\tau_{ult}$	Ultimate shear stress
$\tau_W$ ..	Working stress in shear
$\tau_{YP}$	Yield point stress in shear
$\varphi$ . . .	Angle, angle of twist of shaft
$\omega$ ...	Angular velocity

$A$ .....	Cross-sectional area
$a, b, c, d, e$ ..	Distances
$C$ .....	Torsional rigidity
$C_1$ .....	Warping rigidity
$D$ .....	Flexural rigidity
$d$ .....	Diameter
$E, E_t, E_r$ ....	Modulus of elasticity, tangent modulus, reduced modulus
$f$ .....	Shear flow
$G$ .....	Modulus of elasticity in shear
$h$ .....	Height, thickness
$I_p, I_o$ .....	Polar moments of inertia of a plane area with respect to centroid and shear center
$I_x, I_y, I_z$ ....	Moments of inertia of a plane area with respect to $x, y$ , and $z$ axes
$k$ .....	Modulus of foundation, radius of gyration, stress concentration factor, numerical constant
$l$ .....	Length, span
$M$ .....	Bending moment
$M_{ult}$ .....	Ultimate bending moment
$M_{Y.P.}$ .....	Bending moment at which yielding begins
$M_t$ .....	Torque
$(M_t)_{ult}$ .....	Ultimate torque
$(M_t)_{Y.P.}$ .....	Torque at which yielding begins
$n$ .....	Factor of safety
$P, Q$ .....	Concentrated forces
$p$ .....	Pressure, frequency of vibration
$q$ .....	Load per unit length, reduction in area, sensitivity factor
$R$ .....	Reaction, force, radius, range of stress
$r$ .....	Radius, radius of curvature
$S$ .....	Axial force, surface tension
$s$ .....	Length
$T$ .....	Axial force, absolute temperature
$t$ .....	Temperature, thickness
$U$ .....	Strain energy
$u$ .....	Rate of strain, displacement in $x$ direction
$V$ .....	Volume, shearing force

$v$	Velocity, creep rate, displacement in $y$ direction
$W$	Weight
$w$	Strain energy per unit volume, displacement in $z$ direction
$x, y, z$	Rectangular coordinates
$Z$	Section modulus



# CONTENTS

CHAPTER	PAGE
I. BEAMS ON ELASTIC FOUNDATIONS . . . . .	1
1. Beams of Unlimited Length . . . . .	1
2. Semi-infinite Beams . . . . .	11
3. Beams of Finite Length on Elastic Foundations . . .	15
II. BEAMS WITH COMBINED AXIAL AND LATERAL LOADS . .	26
4. Direct Compression and Lateral Load . . . . .	26
5. Continuous Struts . . . . .	37
6. Tie Rod with Lateral Loading . . . . .	41
7. Representation of the Deflection Curve by a Trigonometric Series . . . . .	46
8. Deflection of Bars with Small Initial Curvature . .	54
III. SPECIAL PROBLEMS IN THE BENDING OF BEAMS . . .	57
9. Local Stresses in the Bending of Beams . . . . .	57
10. Shearing Stresses in Beams of Variable Cross Section	62
11. Effective Width of Thin Flanges . . . . .	64
12. Limitations of the Method of Superposition . . . .	69
IV. THIN PLATES AND SHELLS . . . . .	76
13. Bending of a Plate to a Cylindrical Surface . . . .	76
14. Bending of a Long, Uniformly Loaded Rectangular Plate . . . . .	78
15. Deflection of Long Rectangular Plates Having a Small Initial Cylindrical Curvature . . . . .	84
16. Pure Bending in Two Perpendicular Directions . .	86
17. Thermal Stresses in Plates . . . . .	90
18. Bending of Circular Plates Loaded Symmetrically with Respect to the Center . . . . .	92
19. Bending of a Uniformly Loaded Circular Plate . . .	96
20. Bending of Circular Plates of Variable Thickness .	102
21. Bending of a Circular Plate Loaded at the Center .	103
22. Bending of a Circular Plate Concentrically Loaded	107
23. Deflection of a Symmetrically Loaded Circular Plate with a Circular Hole at the Center . . . . .	109
24. Bending of Rectangular Plates . . . . .	114

CHAPTER	PAGE
25 Thin walled Vessels Subjected to Internal Pressure	117
26 Local Bending Stresses in Thin Vessels	124
27 Thermal Stresses in Cylindrical Shells	134
28 Twisting of a Circular Ring by Couples Uniformly Distributed along Its Center Line	138
V BUCKLING OF BARS, PLATES AND SHELLS	145
29 Lateral Buckling of Prismatic Bars Simpler Cases	145
30 Lateral Buckling of Prismatic Bars More Complicated Cases	153
31 Energy Method of Calculating Critical Compressive Loads	161
32 Buckling of Prismatic Bars under the Action of Uniformly Distributed Axial Forces	167
33 Buckling of Bars of Variable Cross Section	169
34 Effect of Shearing Force on the Critical Load	171
35 Buckling of Latticed Struts	173
36 Inelastic Buckling of Straight Columns	178
37 Buckling of Circular Rings and Tubes under External Pressure	186
38 Buckling of Rectangular Plates	193
39 Buckling of Beams without Lateral Supports	199
VI DEFORMATIONS SYMMETRICAL ABOUT AN AXIS	205
40 Thick walled Cylinder	205
41 Stresses Produced by Shrink Fit	210
42 Rotating Disc of Uniform Thickness	214
43 Rotating Disc of Variable Thickness	223
44 Thermal Stresses in a Long, Hollow Cylinder	228
VII TORSION	235
45 Shafts of Noncircular Cross Section	235
46 Membrane Analogy	237
47 Torsion of Rolled Profile Sections	244
48 Torsion of Thin Tubular Members	247
49 Torsion of Thin walled Members of Open Cross Section in Which Some Cross Sections Are Prevented from Warping	255
50 Combined Bending and Torsion of Thin walled Members of Open Cross Section	267
51 Torsional Buckling of Thin walled Members of Open Cross Section	273

# CONTENTS

CHAPTER	XV PAGE
52. Buckling of Thin-walled Members of Open Cross Section by Simultaneous Bending and Torsion . . .	279
53. Longitudinal Normal Stresses in Twisted Bars . . .	286
54. Open-coiled Helical Spring . . . . .	292
VIII. STRESS CONCENTRATION . . . . .	300
55. Stress Concentration in Tension or Compression Members . . . . .	300
56. Stresses in a Plate with a Circular Hole . . . . .	301
57. Other Cases of Stress Concentration in Tension Members . . . . .	306
58. Stress Concentration in Torsion . . . . .	312
59. Circular Shafts of Variable Diameter . . . . .	318
60. Stress Concentration in Bending . . . . .	324
61. The Investigation of Stress Concentration with Models . . . . .	329
62. Photoelastic Method of Stress Measurements . . .	333
63. Contact Stresses in Balls and Rollers . . . . .	339
IX. DEFORMATIONS BEYOND THE ELASTIC LIMIT . . . . .	346
64. Structures of Perfectly Plastic Materials . . . . .	346
65. Ultimate Strength of Structures . . . . .	354
66. Pure Bending of Beams of Material Which Does Not Follow Hooke's Law . . . . .	366
67. Bending of Beams by Transverse Loads beyond the Elastic Limit . . . . .	374
68. Residual Stresses Produced by Inelastic Bending .	377
69. Torsion beyond the Elastic Limit . . . . .	381
70. Plastic Deformation of Thick Cylinders under the Action of Internal Pressure . . . . .	386
X. MECHANICAL PROPERTIES OF MATERIALS . . . . .	393
71. General . . . . .	393
72. Tensile Tests of Brittle Materials . . . . .	395
73. Tensile Tests of Ductile Materials . . . . .	400
74. Tests of Single-Crystal Specimens in the Elastic Range . . . . .	403
75. Plastic Stretching of Single-Crystal Specimens . .	407
76. Tensile Tests of Mild Steel in the Elastic Range . .	411
77. Yield Point . . . . .	417
78. Stretching of Steel beyond the Yield Point . . . .	420
79. Types of Fractures in Tension . . . . .	430

CHAPTER	PAGE
80 Compression Tests	435
81 Tests of Materials under Combined Stresses	438
82 Strength Theories	444
83 Impact Tests	462
84 Fatigue of Metals	470
85 Fatigue under Combined Stresses	479
86 Factors Affecting the Endurance Limit	483
87. Fatigue and Stress Concentrations	489
88 Reduction of the Effect of Stress Concentrations in Fatigue	498
89 Surface Fatigue Failure	505
90 Causes of Fatigue	509
91 Mechanical Properties of Metals at High Temperatures	516
92 Bending of Beams at High Temperatures	527
93 Stress Relaxation	530
94 Creep under Combined Stresses	533
95 Particular Cases of Two-dimensional Creep	537
96 Working Stresses	544
AUTHOR INDEX	559
SUBJECT INDEX . . . . .	565

## PART II

### CHAPTER I

#### BEAMS ON ELASTIC FOUNDATIONS

1. **Beams of Unlimited Length.**—Let us consider a prismatic beam supported along its entire length by a continuous elastic foundation, such that when the beam is deflected, the intensity of the continuously distributed reaction at every point is proportional to the deflection at that point.<sup>1</sup> Under such conditions the reaction per unit length of the beam can be represented by the expression  $ky$ , in which  $y$  is the deflection and  $k$  is a constant usually called the *modulus of the foundation*. This constant denotes the reaction per unit length when the deflection is equal to unity. The simple assumption that the continuous reaction of the foundation is proportional to the deflection is a satisfactory approximation in many practical cases. For instance, in the case of railway tracks the solution obtained on this assumption is in good agreement with actual measurements.<sup>2</sup> In studying the deflection curve of the beam we use the differential equation<sup>3</sup>

$$EI_z \frac{d^4 y}{dx^4} = q, \quad (a)$$

---

<sup>1</sup> The beam is imbedded in a material capable of exerting downward as well as upward forces on it.

<sup>2</sup> See S. Timoshenko and B. F. Langer, *Trans. A.S.M.E.*, Vol. 54, p. 277, 1932. The theory of the bending of beams on an elastic foundation has been developed by E. Winkler, *Die Lehre von der Elastizität und Festigkeit*, Prague, p. 182, 1867. See also H. Zimmermann, *Die Berechnung des Eisenbahn-Oberbaues*, Berlin, 1888. Further development of the theory will be found in: Hayashi, *Theorie des Trägers auf elastischer Unterlage*, Berlin, 1921; Wieghardt, *Z. angew. Math. u. Mech.*, Vol. 2, 1922; K. v. Sanden and Schleicher, *Beton u. Eisen*, Heft 5, 1926; Pasternak, *Beton u. Eisen*, Hefte 9 and 10, 1926; W. Prager, *Z. angew. Math. u. Mech.*, Vol. 7, p. 354, 1927; M. A. Biot, *J. Appl. Mech.*, Vol. 4, p. A-1, 1937; M. Hetényi, *Beams on Elastic Foundation*, Ann Arbor, 1946.

<sup>3</sup> See S. Timoshenko, *Strength of Materials*, Part I, eq. (80), p. 140.

in which  $q$  denotes the intensity of the load acting on the beam. For an unloaded portion the only force on the beam is the continuously distributed reaction force from the foundation of intensity  $ky$ . Hence  $q = -ky$ , and eq. (a) becomes

$$EI_z \frac{d^4 y}{dx^4} = -ky. \quad (1)$$

Using the notation

$$\sqrt[4]{\frac{k}{4EI_z}} = \beta, \quad (2)$$

the general solution of eq. (1) can be represented as follows:

$$y = e^{\beta x}(A \cos \beta x + B \sin \beta x) + e^{-\beta x}(C \cos \beta x + D \sin \beta x). \quad (b)$$

This can easily be verified by substituting the value from eq. (b) into eq. (1). In particular cases the constants  $A$ ,  $B$ ,  $C$  and  $D$  of the solution must be determined from the known conditions at certain points.

Let us consider as an example the case of a single concentrated load acting on an infinitely long beam (Fig. 1a), taking the origin of coordinates at the point of application of the

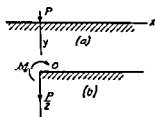


FIG. 1.

force. Because of the condition of symmetry, only that part of the beam to the right of the load need be considered (Fig. 1b). In applying the general solution, eq. (b), to this case, the arbitrary constants must first be found. It is reasonable to assume that at points infinitely distant from the force  $P$  the deflection

and the curvature vanish. This condition can be fulfilled only if the constants  $A$  and  $B$  in eq. (b) are taken equal to zero. Hence the deflection curve for the right portion of the beam becomes

$$y = e^{-\beta x}(C \cos \beta x + D \sin \beta x). \quad (c)$$

The two remaining constants of integration  $C$  and  $D$  are found from the conditions at the origin,  $x = 0$ . At this point

the deflection curve must have a horizontal tangent; therefore

$$\left(\frac{dy}{dx}\right)_{x=0} = 0,$$

or, substituting the value of  $y$  from eq. (c),

$$e^{-\beta x}(C \cos \beta x + D \sin \beta x + C \sin \beta x - D \cos \beta x)_{x=0} = 0,$$

from which

$$C = D.$$

Eq. (c) therefore becomes

$$y = Ce^{-\beta x}(\cos \beta x + \sin \beta x). \quad (d)$$

The consecutive derivatives of this equation are

$$\frac{dy}{dx} = -2\beta Ce^{-\beta x} \sin \beta x,$$

$$\frac{d^2y}{dx^2} = 2\beta^2 Ce^{-\beta x}(\sin \beta x - \cos \beta x), \quad (e)$$

$$\frac{d^3y}{dx^3} = 4\beta^3 Ce^{-\beta x} \cos \beta x. \quad (f)$$

The constant  $C$  can now be determined from the fact that at  $x = 0$  the shearing force for the right part of the beam (Fig. 1b) is equal to  $-(P/2)$ . The minus sign follows from our convention for signs of shearing forces (see Part I, pp. 75-6). Then

$$(V)_{x=0} = \left(\frac{dM}{dx}\right)_{x=0} = -EI_z \left(\frac{d^3y}{dx^3}\right)_{x=0} = -\frac{P}{2},$$

or, using eq. (f),

$$EI_z \cdot 4\beta^3 C = \frac{P}{2},$$

from which

$$C = \frac{P}{8\beta^3 EI_z}.$$

Substituting this value into eqs. (d) and (e), we obtain the following equations for the deflection and bending moment curves:

$$y = \frac{P}{8\beta^3 EI_z} e^{-\beta x} (\cos \beta x + \sin \beta x)$$

$$= \frac{P\beta}{2k} e^{-\beta x} (\cos \beta x + \sin \beta x), \quad (3)$$

$$M = -EI_z \frac{d^2 y}{dx^2} = -\frac{P}{4\beta} e^{-\beta x} (\sin \beta x - \cos \beta x). \quad (4)$$

Eqs. (3) and (4) each have, when plotted, a wave form with gradually diminishing amplitudes. The length  $a$  of these

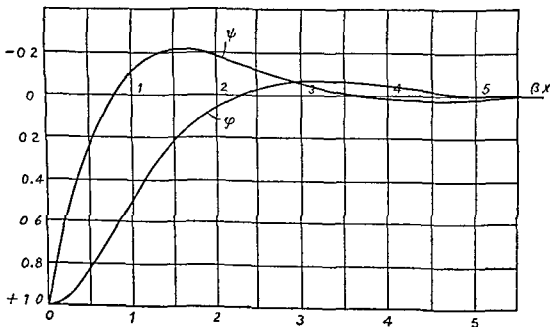


FIG. 2

waves is given by the period of the functions  $\cos \beta x$  and  $\sin \beta x$ , i.e.,

$$a = \frac{2\pi}{\beta} = 2\pi \sqrt[4]{\frac{4EI_z}{k}}. \quad (5)$$



To simplify the calculation of deflections, bending moments and shearing forces a numerical table is given (Table 1), in

TABLE 1: FUNCTIONS  $\varphi$ ,  $\psi$ ,  $\theta$  AND  $\zeta$ 

$\beta x$	$\varphi$	$\psi$	$\theta$	$\zeta$	$\beta x$	$\varphi$	$\psi$	$\theta$	$\zeta$
0	1.0000	1.0000	1.0000	0	3.6	-0.0366	-0.0124	-0.0245	-0.0121
0.1	0.9907	0.8100	0.9003	0.0903	3.7	-0.0341	-0.0079	-0.0210	-0.0131
0.2	0.9651	0.6398	0.8024	0.1627	3.8	-0.0314	-0.0040	-0.0177	-0.0137
0.3	0.9267	0.4888	0.7077	0.2189	3.9	-0.0286	-0.0008	-0.0147	-0.0140
0.4	0.8784	0.3564	0.6174	0.2610	4.0	-0.0258	0.0019	-0.0120	-0.0139
0.5	0.8231	0.2415	0.5323	0.2908	4.1	-0.0231	0.0040	-0.0095	-0.0136
0.6	0.7628	0.1431	0.4530	0.3099	4.2	-0.0204	0.0057	-0.0074	-0.0131
0.7	0.6997	0.0599	0.3798	0.3199	4.3	-0.0179	0.0070	-0.0054	-0.0125
0.8	0.6354	-0.0093	0.3131	0.3223	4.4	-0.0155	0.0079	-0.0038	-0.0117
0.9	0.5712	-0.0657	0.2527	0.3185	4.5	-0.0132	0.0085	-0.0023	-0.0108
1.0	0.5053	-0.1108	0.1988	0.3096	4.6	-0.0111	0.0089	-0.0011	-0.0100
1.1	0.4476	-0.1457	0.1510	0.2967	4.7	-0.0092	0.0090	0.0001	-0.0091
1.2	0.3899	-0.1716	0.1091	0.2807	4.8	-0.0075	0.0089	0.0007	-0.0082
1.3	0.3355	-0.1897	0.0729	0.2626	4.9	-0.0059	0.0087	0.0014	-0.0073
1.4	0.2849	-0.2011	0.0419	0.2430	5.0	-0.0046	0.0084	0.0019	-0.0065
1.5	0.2384	-0.2068	0.0158	0.2226	5.1	-0.0033	0.0080	0.0023	-0.0057
1.6	0.1959	-0.2077	-0.0059	0.2018	5.2	-0.0023	0.0075	0.0026	-0.0049
1.7	0.1576	-0.2047	-0.0235	0.1812	5.3	-0.0014	0.0069	0.0028	-0.0042
1.8	0.1234	-0.1985	-0.0376	0.1610	5.4	-0.0006	0.0064	0.0029	-0.0035
1.9	0.0932	-0.1899	-0.0484	0.1415	5.5	0.0000	0.0058	0.0029	-0.0029
2.0	0.0667	-0.1794	-0.0563	0.1230	5.6	0.0005	0.0052	0.0029	-0.0023
2.1	0.0439	-0.1675	-0.0618	0.1057	5.7	0.0010	0.0046	0.0028	-0.0018
2.2	0.0244	-0.1548	-0.0652	0.0895	5.8	0.0013	0.0041	0.0027	-0.0014
2.3	0.0080	-0.1416	-0.0668	0.0748	5.9	0.0015	0.0036	0.0026	-0.0010
2.4	-0.0056	-0.1282	-0.0669	0.0613	6.0	0.0017	0.0031	0.0024	-0.0007
2.5	-0.0166	-0.1149	-0.0658	0.0492	6.1	0.0018	0.0026	0.0022	-0.0004
2.6	-0.0254	-0.1019	-0.0636	0.0383	6.2	0.0019	0.0022	0.0020	-0.0002
2.7	-0.0320	-0.0895	-0.0608	0.0287	6.3	0.0019	0.0018	0.0018	+0.0001
2.8	-0.0369	-0.0777	-0.0573	0.0204	6.4	0.0018	0.0015	0.0017	0.0003
2.9	-0.0403	-0.0666	-0.0534	0.0132	6.5	0.0018	0.0012	0.0015	0.0004
3.0	-0.0423	-0.0563	-0.0493	0.0070	6.6	0.0017	0.0009	0.0013	0.0005
3.1	-0.0431	-0.0469	-0.0450	0.0019	6.7	0.0016	0.0006	0.0011	0.0006
3.2	-0.0431	-0.0383	-0.0407	-0.0024	6.8	0.0015	0.0004	0.0010	0.0006
3.3	-0.0422	-0.0306	-0.0364	-0.0058	6.9	0.0014	0.0002	0.0008	0.0006
3.4	-0.0408	-0.0237	-0.0323	-0.0085	7.0	0.0013	0.0001	0.0007	0.0006
3.5	-0.0389	-0.0177	-0.0283	-0.0106					

which the following notations are used:

$$\left. \begin{aligned} \varphi &= e^{-\beta x}(\cos \beta x + \sin \beta x); \\ \psi &= -e^{-\beta x}(\sin \beta x - \cos \beta x); \\ \theta &= e^{-\beta x} \cos \beta x; \quad \zeta = e^{-\beta x} \sin \beta x. \end{aligned} \right\} \quad (6)$$

In Fig. 2 the functions  $\varphi$  and  $\psi$  are shown graphically.

Using notations (6) and eqs. (d)-(f), we obtain

$$\left. \begin{aligned} y &= \frac{P\beta}{2k} \varphi(\beta x), & \frac{dy}{dx} &= -\frac{P\beta^2}{k} \zeta(\beta x), \\ M &= -EI_z \frac{d^2 y}{dx^2} = \frac{P}{4\beta} \psi(\beta x), \\ V &= -EI_z \frac{d^3 y}{dx^3} = -\frac{P}{2} \theta(\beta x). \end{aligned} \right\} \quad (7)$$

From these equations and Table 1, the deflection, slope, bending moment and shearing force for any cross section of the beam can be readily calculated. The maximum deflection and maximum bending moment occur at the origin and are, respectively,

$$\delta = (y)_{x=0} = \frac{P\beta}{2k}, \quad (8)$$

$$M_0 = (M)_{x=0} = \frac{P}{4\beta}. \quad (9)$$

By using the solution (eq. 3) for a single load and the principle of superposition, the deflection produced in an infinitely long beam on an elastic foundation by any other type of loading can be readily obtained.

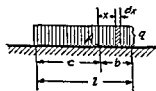


FIG. 3.

As an example let us consider the case of a uniform load distributed over a length  $l$  of an infinitely long beam (Fig. 3). Consider any point  $A$ , and let  $c$  and  $b$  represent the distances from this point to the ends of the loaded part of the beam. The deflection at  $A$ , produced by an element  $q dx$  of the load, is obtained by substituting  $q dx$  for  $P$  in eq. (3), which gives

$$\frac{q dx}{8\beta^3 EI_z} e^{-\beta x} (\cos \beta x + \sin \beta x).$$

The deflection produced at  $A$  by the loading distributed over the length  $l$  then becomes

$$\begin{aligned}
 y &= \int_0^b \frac{q dx}{8\beta^3 EI_z} e^{-\beta z} (\cos \beta x + \sin \beta x) \\
 &\quad + \int_0^c \frac{q dx}{8\beta^3 EI_z} e^{-\beta z} (\cos \beta x + \sin \beta x) \\
 &= \frac{q}{2k} (2 - e^{-\beta b} \cos \beta b - e^{-\beta c} \cos \beta c). \quad (g)
 \end{aligned}$$

If  $c$  and  $b$  are large, the values  $e^{-\beta b}$  and  $e^{-\beta c}$  will be small and the deflection (eq.  $g$ ) will be equal approximately to  $q/k$ ; i.e., at points remote from the ends of the loaded part of the bar the bending of the bar can be neglected and it can be assumed that the uniform loading  $q$  is transmitted directly to the elastic foundation. Taking the point  $A$  at the end of the loaded part of the bar, we have  $c = 0$ ,  $b = l$ ,  $e^{-\beta c} \cos \beta c = 1$ . Assuming that  $l$  is large, we have also  $e^{-\beta b} \cos \beta b \approx 0$ . Then  $y = q/2k$ ; i.e., the deflection now has only one-half of the value obtained above.

In a similar manner, by using eq. (4), the expression for the bending moment at  $A$  can be derived. If the point  $A$  is taken outside the loaded portion of the beam and if the quantities  $b$  and  $c$  represent, respectively, the larger and the smaller distance from this point to the ends of the loaded part of the beam, the deflection at  $A$  is

$$\begin{aligned}
 y &= \int_0^b \frac{q dx}{8\beta^3 EI_z} e^{-\beta z} (\cos \beta x + \sin \beta x) \\
 &\quad - \int_0^c \frac{q dx}{8\beta^3 EI_z} e^{-\beta z} (\cos \beta x + \sin \beta x) \\
 &= \frac{q}{2k} (e^{-\beta c} \cos \beta c - e^{-\beta b} \cos \beta b). \quad (h)
 \end{aligned}$$

When  $c = 0$  and if  $b = l$  is a large quantity, we obtain for the deflection the value  $q/2k$ , which coincides with our previous conclusion. As the distances  $b$  and  $c$  increase, the deflection, eq. (h), decreases, approaching zero as  $b$  and  $c$  grow larger.

The case of a couple acting on an infinitely long beam, Fig.

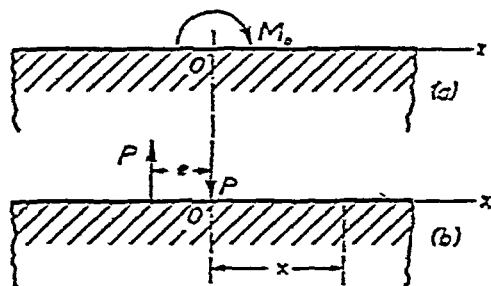


FIG. 4.

4a, can also be analyzed by using the solution, eq. (3), for a single load. The action of the couple is equivalent to that of the two forces  $P$

shown in Fig. 4*b*, if  $Pe$  approaches  $M_0$  while  $e$  approaches zero. Using the first of eqs. (7), we find the deflection at a distance  $x$  from the origin:

$$y = \frac{P\beta}{2k} \{ \varphi(\beta x) - \varphi[\beta(x+e)] \}$$

$$= \frac{M_0\beta}{2k} \cdot \frac{\varphi(\beta x) - \varphi[\beta(x+e)]}{e} = -\frac{M_0\beta}{2k} \frac{d\varphi}{dx}.$$

From eqs. (7),

$$\frac{d\varphi}{dx} = -2\beta\zeta,$$

and the deflection curve produced by the couple  $M_0$  becomes

$$y = \frac{M_0\beta^2}{k} \zeta(\beta x). \quad (10)$$

By differentiating this equation, we obtain

$$\frac{dy}{dx} = \frac{M_0\beta^3}{k} \psi(\beta x),$$

$$M = -EI_z \frac{d^2y}{dx^2} = \frac{M_0}{2} \theta(\beta x), \quad (10')$$

$$V = -EI_z \frac{d^3y}{dx^3} = -\frac{M_0\beta}{2} \varphi(\beta x).$$

Using these equations together with Table 1, we can readily calculate the deflection, slope, bending moment and shearing force for any cross section of the beam.

We shall now consider the case of several loads acting on an infinite beam. As an example, bending of a rail produced by the wheel pressures of a locomotive will be discussed. The following method of analyzing stresses in rails is based upon the assumption that there is a continuous elastic support under the rail. This assumption is a good approximation,<sup>4</sup> since the distance between the ties is small in comparison to the wavelength  $a$  of the deflection curve, given by eq. (5). In order to obtain the magnitude  $k$  of the modulus of the foundation, the load required to produce unit deflection of a tie must be divided by the tie spacing. It is assumed that the tie is

<sup>4</sup> See the author's paper, "Strength of Rails," *Memoirs Inst. Engrs. Ways of Communication (St. Petersburg)*, 1915; and the author's paper in *Proc. 2d Internat. Congr. Appl. Mech.*, Zürich, 1926. See also footnote 2.

symmetrically loaded by two loads corresponding to the rail pressures. Suppose, for example, that the tie is depressed 0.3 in. under each of two loads of 10,000 lb and that the tie spacing is 22 in.; then

$$k = \frac{10,000}{0.3 \times 22} = 1,500 \text{ lb per sq in.}$$

For the case of a single wheel load  $P$ , eqs. (8) and (9) are used for the maximum deflection and maximum bending moment. The maximum stress due to the bending of the rail will be

$$\sigma_{\max} = \frac{M_{\max}}{Z} = \frac{P}{4\beta Z} = \frac{P}{4Z} \sqrt[4]{\frac{4EI_z}{k}}, \quad (i)$$

where  $Z$  denotes the section modulus of the rail.<sup>5</sup>

In order to compare the stresses in rails which have geometrically similar cross sections, eq. (i) may be put in the following form:

$$\sigma_{\max} = \frac{P}{A} \cdot \frac{A\sqrt[4]{I_z}}{4Z} \sqrt[4]{\frac{4E}{k}}, \quad (j)$$

in which  $A$  is the area of the cross section of the rail. Since the second factor on the right-hand side of eq. (j) remains constant for geometrically similar cross sections and since the third factor does not depend on the dimensions of the rail, the maximum stress is inversely proportional to the area of the cross section, i.e., inversely proportional to the weight of the rail per unit length.

An approximate value of the maximum pressure  $R_{\max}$  on a tie is obtained by multiplying the maximum depression by the tie spacing  $l$  and by the modulus of the foundation. Thus, using eq. (8), we have

$$R_{\max} = \frac{P\beta}{2k} lk = \frac{P\beta l}{2} = \frac{P}{2} \sqrt[4]{\frac{k l^4}{4EI_z}}. \quad (k)$$

It may be seen from this that the pressure on the tie depends principally on the tie spacing  $l$ . It should also be noted that  $k$  occurs in both eqs. (j) and (k) as a fourth root. Hence an error in the determination of  $k$  will introduce only a much smaller error in the magnitude of  $\sigma_{\max}$  and  $R_{\max}$ .

<sup>5</sup> In writing eq. (i) it was assumed that the elementary beam formula can be used at the cross section where the load  $P$  is applied. More detailed investigations show that because of local stresses, considerable deviation from the elementary eq. (i) may be expected.

When several loads are acting on the rail, the method of superposition must be used. To illustrate the method of calculation we shall discuss a numerical example. Consider a 100-lb rail section with  $I_z = 44 \text{ in.}^4$  and with a tie spacing such that  $k = 1,500 \text{ lb per sq in.}$ ; then from eq. (2)

$$\beta = \sqrt[4]{\frac{k}{4EI_z}} = \sqrt[4]{\frac{1,500}{4 \times 30 \times 10^6 \times 44}} = \frac{1}{43.3} \text{ in.}^{-1},$$

and from eq. (5)

$$a = \frac{2\pi}{\beta} = 272 \text{ in.}$$

We take as an example a system of four equal wheel loads, 66 in. apart. If we fix the origin of coordinates at the point of contact of the first wheel, the values of  $\beta x$  for the other wheels will be those given in Table 2. Also given are the corresponding values of the functions  $\varphi$  and  $\psi$ , taken from Table 1.

TABLE 2

Loads	1	2	3	4
$\beta x$	0	1 52	3 05	4 57
$\psi$	1	-0 207	-0 051	0 008
$\varphi$	1	0 230	-0 042	-0 012

After superposing the effects of all four loads acting on the rail, the bending moment under the first wheel is, from eq. (4),

$$M_1 = \frac{P}{4\beta} (1 - 0.207 - 0.051 + 0.008) = 0.75 \frac{P}{4\beta},$$

i.e., the bending moment is 25 per cent less than that produced by a single load  $P$ . Proceeding in the same manner for the point of contact of the second wheel we obtain

$$M_2 = \frac{P}{4\beta} (1 - 2 \times 0.207 - 0.051) = 0.535 \frac{P}{4\beta}.$$

It may be seen that owing to the action of adjacent wheels the bending moment under the second wheel is much smaller than that under

the first. This fact was proved by numerous experimental measurements of track stresses.

Using eq. (3) and the values in the last line of Table 2, we find the following deflection under the first wheel:

$$\delta_1 = \frac{P\beta}{2k} (1 + 0.230 - 0.042 - 0.012) = 1.18 \frac{P\beta}{2k}.$$

The deflections at other points can be obtained in a similar manner.

It is seen that the method of superposition may be easily applied to determine the bending of a rail produced by a combination of loads having any arrangement and any spacing.

The above analysis is based on the assumption that the rail support is capable of developing negative reactions. Since there is usually play between the rail and the spikes, there is little resistance to the upward movement of the rail, and this tends to increase the bending moment in the rail under the first and the last wheels. Nevertheless, in general the above theory for the bending of a rail by static loading is in satisfactory agreement with the experiments which have been made.

### Problems

1. Using the information given in Table 2, construct the bending moment diagram for a rail, assuming that the wheel pressures are equal to 40,000 lb. Such a diagram should show that the moments are negative in sections midway between the wheels, indicating that during locomotive motion the rail is subjected to the action of reversal of bending stresses, which may finally result in fatigue cracks.

2. Find the bending moment at the middle of the loaded portion of the beam shown in Fig. 3 and the slope of the deflection curve at the left end of the same portion.

3. Find the deflection at any point *A* under the triangular load acting on an infinitely long beam on an elastic foundation, Fig. 5.

*Answer.* Proceeding as in the derivation of eq. (g), p. 7, we obtain

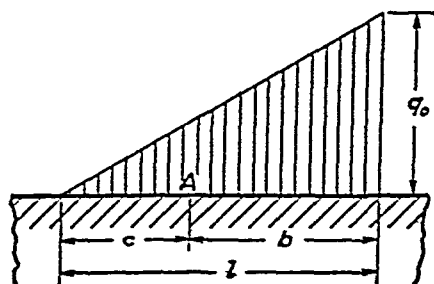


FIG. 5.

$$v = \frac{q_0}{4\beta k l} \frac{1}{l} [\psi(\beta c) - \psi(\beta b) - 2\beta l \theta(\beta b) + 4\beta c].$$

**2. Semi-infinite Beams.**—If a long beam on an elastic foundation is bent by a force *P* and a moment *M*<sub>0</sub> applied at the end as shown

in Fig 6, we can again use the general solution, eq (b), of the preceding article. Since the deflection and the bending moment approach zero as the distance  $x$  from the loaded end increases, we must take  $A = B = 0$  in that solution. We obtain

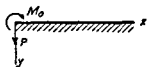


FIG 6

$$y = e^{-\beta x}(C \cos \beta x + D \sin \beta x) \quad (a)$$

For determining the constants of integration  $C$  and  $D$  we have the conditions at the origin, i.e., under the load  $P$

$$EI_z \left( \frac{d^2 y}{dx^2} \right)_{x=0} = -M_0,$$

$$EI_z \left( \frac{d^3 y}{dx^3} \right)_{x=0} = -V = P$$

Substituting from eq (a) into these equations, we obtain two linear equations in  $C$  and  $D$ , from which

$$C = \frac{1}{2\beta^3 EI_z} (P - \beta M_0), \quad D = \frac{M_0}{2\beta^2 EI_z}$$

Substituting into eq (a), we obtain

$$y = \frac{e^{-\beta x}}{2\beta^3 EI_z} [P \cos \beta x - \beta M_0 (\cos \beta x - \sin \beta x)] \quad (11)$$

or, using notations (6),

$$y = \frac{2\beta}{k} \{ P\theta(\beta x) - \beta M_0 [\theta(\beta x) - \zeta(\beta x)] \}$$

To get the deflection under the load we must substitute  $x = 0$  into eq (11). Then

$$\delta = (y)_{x=0} = \frac{1}{2\beta^3 EI_z} (P - \beta M_0) \quad (11')$$

The expression for the slope is obtained by differentiating eq (11). At the end ( $x = 0$ ) this becomes

$$\left( \frac{dy}{dx} \right)_{x=0} = -\frac{1}{2\beta^2 EI_z} (P - 2\beta M_0) \quad (12)$$

By using eqs (11') and (12) in conjunction with the principle of superposition, more complicated problems can be solved. Take as an example a uniformly loaded long beam on an elastic foundation,



having a simply supported end, Fig. 7a. The reaction  $R$  at the end is found from the condition that the deflection at the support is zero. Observing that at a large distance from the support, the bending of the beam is negligible, and that its depression into the foundation can be taken equal to  $q/k$ , we calculate the value of  $R$  by substituting  $M_0 = 0$  and  $\delta = q/k$  into eq. (11'). This yields the result

$$R = 2\beta^3 EI_z \cdot \frac{q}{k} = \frac{q}{2\beta}. \quad (13)$$

The deflection curve is now obtained by subtracting the deflections given by eq. (11) for  $P = R$ ,  $M_0 = 0$  from the uniform depression  $q/k$  of the beam, which gives

$$v = \frac{q}{k} - \frac{e^{-\beta x}}{2\beta^3 EI_z} R \cos \beta x = \frac{q}{k} (1 - e^{-\beta x} \cos \beta x). \quad (14)$$

In the case of a built-in end, Fig. 7b, the magnitudes of the reaction  $R$  and of the moment  $M_0$  are obtained from the conditions that at the support the deflection and the slope are zero. Observing that at a large distance from the support the deflection is equal to  $q/k$  and using eqs. (11') and (12), we obtain the following equations<sup>6</sup> for calculating  $R$  and  $M_0$ :

$$-\frac{q}{k} = -\frac{1}{2\beta^3 EI_z} (R + \beta M_0)$$

and

$$0 = \frac{1}{2\beta^2 EI_z} (R + 2\beta M_0)$$

from which

$$M_0 = -2\beta^2 EI_z \frac{q}{k}, \quad R = 4\beta^3 EI_z \frac{q}{k} = \frac{q}{\beta}. \quad (15)$$

The minus sign of  $M_0$  indicates that the moment has the direction shown by the arrow at the left in Fig. 7b.

<sup>6</sup> In eqs. (11') and (12),  $P = -R$  is substituted, since the positive direction for the reaction is taken upwards.

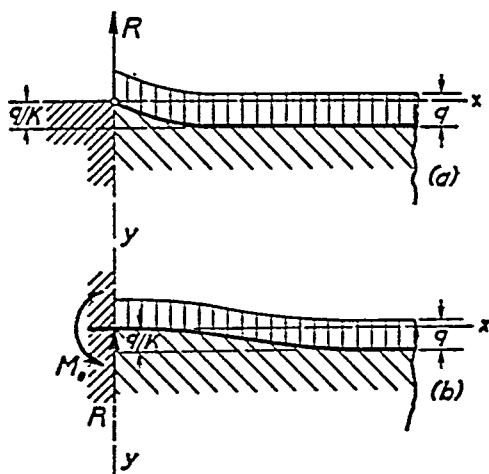


FIG. 7.

## Problems

1 Find the deflection curve for a semi-infinite beam on an elastic foundation hinged at the end and acted upon by a couple  $M_0$ ,

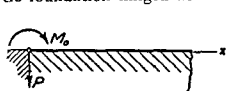


FIG 8

Fig 8

*Solution* The reaction at the hinge is obtained from eq (11') by substituting  $\delta = 0$ , which gives

$$P = \beta M_0$$

Substituting this value of  $P$  in eq (11) we obtain

$$y = \frac{M_0}{2\beta^2 EI_z} e^{-\beta x} \sin \beta x = \frac{M_0}{2\beta^2 EI_z} \zeta(\beta x). \quad (16)$$

By subsequent differentiation, we find

$$\left. \begin{aligned} \frac{dy}{dx} &= \frac{2\beta^3 M_0}{k} \psi(\beta x), \\ M &= -EI_z \frac{d^2 y}{dx^2} = M_0 \cdot \theta(\beta x), \\ V &= -EI_z \frac{d^3 y}{dx^3} = -\beta M_0 \varphi(\beta x). \end{aligned} \right\} \quad (b)$$

2 Find the bending moment  $M_0$  and the force  $P$  acting on the end of a semi-infinite beam on an elastic foundation, Fig 9, if the deflection  $\delta$  and the slope  $\alpha$  at the end are given

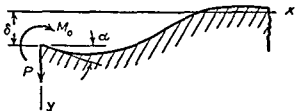


FIG 9

*Solution* The values  $M_0$  and  $P$  are obtained from eqs (11') and (12) by substituting the given quantities for  $\delta$  and  $(dy/dx)_{x=0} = \alpha$

3 Find the deflection curve for a semi-infinite beam on an elastic foundation produced by a load  $P$  applied at a distance  $c$  from the free end  $A$  of the beam, Fig 10.

*Solution.* Assume that the beam extends to the left of the end  $A$  as shown by the dotted line. In such a case eq. (3) gives the deflection curve for  $x > 0$ , and at the cross section  $A$  of the fictitious infinite beam we have, from eqs. (7), and using the condition of symmetry,

$$M = \frac{P}{4\beta} \psi(\beta c), \quad V = \frac{P}{2} \theta(\beta c). \quad (c)$$

To obtain the required deflection curve for the semi-infinite beam free at the end  $A$ , we evidently must superpose the deflection of the semi-infinite beam produced by the forces shown in Fig 10*b* on the deflection of the fictitious infinite beam. By using equations (3), (11) and (c) in this way we obtain for  $x > 0$ :

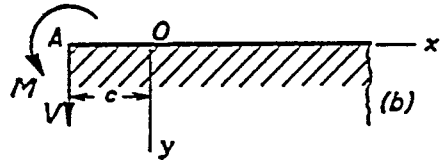
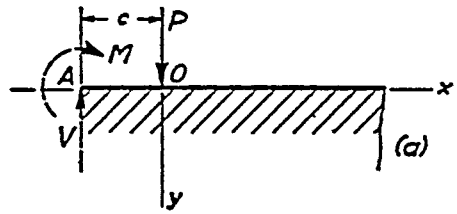


FIG. 10.

$$\begin{aligned} y &= \frac{P\beta}{2k} \varphi(\beta x) + \frac{2\beta}{k} \{V\theta[\beta(x+c)] \\ &\quad + \beta M\theta[\beta(x+c)] - \beta M\zeta[\beta(x+c)]\} \\ &= \frac{P\beta}{2k} \varphi(\beta x) + \frac{\beta P}{k} \{\theta(\beta c)\theta[\beta(x+c)] \\ &\quad + \frac{1}{2}\psi(\beta c)\theta[\beta(x+c)] - \frac{1}{2}\psi(\beta c)\zeta[\beta(x+c)]\}. \end{aligned} \quad (d)$$

This expression can also be used for  $-c < x < 0$ ; in this case we have only to substitute the absolute value of  $x$ , instead of  $x$ , in  $\varphi(\beta x)$ .

**3. Beams of Finite Length on Elastic Foundations.**—The bending of a beam of finite length on an elastic foundation can also be investigated by using the solution, eq. (3), for an infinitely long beam together with the method of superposition.<sup>7</sup> To illustrate the method let us consider the case of a beam of finite length with free ends which is loaded by two symmetrically applied forces  $P$ , Fig. 11*a*. A similar condition exists in the case of a tie under the action of rail pressures. To each of the three portions of the beam the general solution, eq. (b) of Art. 1, can be applied, and the constants of integration can be calculated from the conditions at the ends and at the points of application of the loads. The required solution can, however, be

<sup>7</sup> This method of analysis was developed by M. Hetényi, *Final Report, 2d Congr. Internat. Assoc. Bridge and Structural Engng.*, Berlin, 1938. See also his *Beams on Elastic Foundation*, p. 38.

obtained much more easily by superposing the solutions for the two kinds of loading of an infinitely long beam shown in Fig. 11*b* and *c*. In Fig. 11*b* the two forces  $P$  are acting on an infinitely long beam. In Fig. 11*c* the infinitely long beam is loaded by forces  $Q_0$  and moments  $M_0$ , both applied outside the portion  $AB$  of the beam, but infinitely close to points  $A$  and  $B$  which correspond to the free ends of the given beam, Fig. 11*a*. It is easy to see that by a proper selection of the forces  $Q_0$  and the moments  $M_0$ , the bending moment and

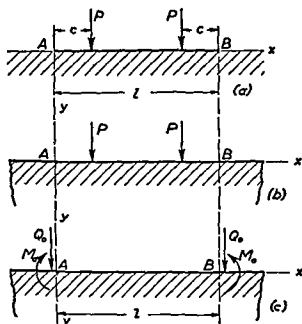


FIG 11

the shearing force produced by the forces  $P$  at the cross sections  $A$  and  $B$  of the infinite beam (shown in Fig. 11*b*) can be made equal to zero. Then the middle portion of the infinite beam will evidently be in the same condition as the finite beam represented in Fig. 11*a*, and all necessary information regarding bending of the latter beam will be obtained by superposing the cases shown in Figs. 11*b* and 11*c*.

To establish the equations for determining the proper values of  $M_0$  and  $Q_0$ , let us consider the cross section  $A$  of the infinitely long beam. Taking the origin of the coordinates at this point and using eqs. (7), the bending moment  $M'$  and the shearing force  $V'$  produced at this point by the two forces  $P$ , Fig. 11*b*, are

$$\begin{aligned} M' &= \frac{P}{4\beta} \{ \psi[\beta(l-c)] + \psi(\beta c) \} \\ V' &= \frac{P}{2} \{ \theta'[\beta(l-c)] + \theta(\beta c) \} \end{aligned} \quad (a)$$

The moment  $M''$  and the shearing force  $V''$  produced at the same point by the forces shown in Fig. 11c are obtained by using eqs. (7) together with eqs. (10'), which give

$$\left. \begin{aligned} M'' &= \frac{Q_0}{\pm\beta} [1 + \psi(\beta l)] + \frac{M_0}{2} [1 + \theta(\beta l)], \\ V'' &= -\frac{Q_0}{2} [1 - \theta(\beta l)] - \frac{M_0\beta}{2} [1 - \varphi(\beta l)]. \end{aligned} \right\} \quad (b)$$

The proper values of  $M_0$  and  $Q_0$  are now obtained from the equations

$$\left. \begin{aligned} M' + M'' &= 0, \\ V' + V'' &= 0, \end{aligned} \right\} \quad (c)$$

which can be readily solved in each particular case by using Table 1. Once  $M_0$  and  $Q_0$  are known, the deflection and the bending moment at any cross section of the actual beam, Fig. 11a, can be obtained by using eqs. (7), (10) and (10') together with the method of superposition.

The particular case shown in Fig. 12 is obtained from our previous discussion by taking  $c = 0$ .

Proceeding as previously explained, we obtain for the deflections at the ends and at the middle the following expressions:

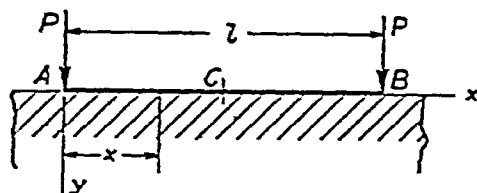


FIG. 12.

$$y_a = y_b = \frac{2P\beta}{k} \frac{\cosh \beta l + \cos \beta l}{\sinh \beta l + \sin \beta l}, \quad (d)$$

$$y_c = \frac{4P\beta}{k} \frac{\cosh \frac{\beta l}{2} \cos \frac{\beta l}{2}}{\sinh \beta l + \sin \beta l}. \quad (e)$$

The bending moment at the middle is

$$M_c = -\frac{2P}{\beta} \frac{\sinh \frac{\beta l}{2} \sin \frac{\beta l}{2}}{\sinh \beta l + \sin \beta l}. \quad (f)$$

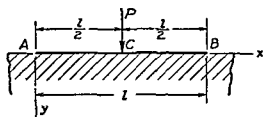


FIG 13

The case of a single load at the middle, Fig 13, can also be obtained from the previous case, shown in Fig 11a. It is only necessary to take  $c = l/2$  and to substitute  $P$  for  $2P$ . In this way we obtain for the deflections at the middle and at the ends the following expressions:

$$y_a = y_b = \frac{2P\beta}{k} \frac{\cosh \frac{\beta l}{2} \cos \frac{\beta l}{2}}{\sinh \beta l + \sin \beta l}, \quad (g)$$

$$y_c = \frac{P\beta}{2k} \frac{\cosh \beta l + \cos \beta l + 2}{\sinh \beta l + \sin \beta l}. \quad (h)$$

For the bending moment under the load we find

$$M_c = \frac{P}{4\beta} \frac{\cosh \beta l - \cos \beta l}{\sinh \beta l + \sin \beta l}. \quad (i)$$

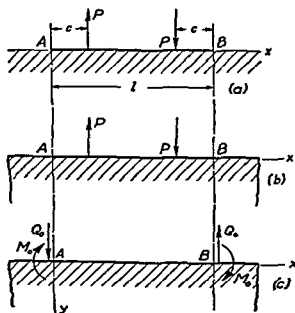


FIG 14

The method used for the symmetrical case shown in Fig 11a can also be applied in the antisymmetrical case shown in Fig 14a.  $Q_0$  and  $M_0$  in this case will also represent an antisymmetrical system as shown in Fig 14c. For the determination of the proper values of

$Q_0$  and  $M_0$ , a system of equations similar to eqs. (a), (b) and (c) can be readily written. As soon as  $Q_0$  and  $M_0$  are calculated, all necessary information regarding the bending of the beam shown in Fig. 14a can be obtained by superposing the cases shown in Figures 14b and 14c.

Having the solutions for the symmetrical and for the antisymmetrical loading of a beam, we can readily obtain the solution for any kind of loading by using the principle of superposition. For example, the solution of the unsymmetrical case shown in Fig. 15a is obtained by superposing the solutions of the symmetrical and the antisymmetrical cases shown in Fig. 15b and c. The problem shown

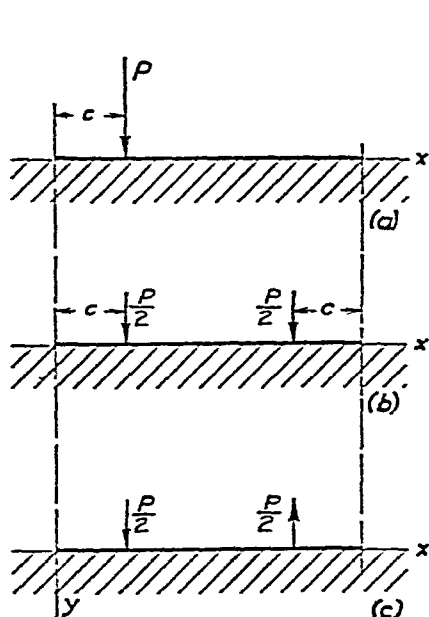


FIG. 15.

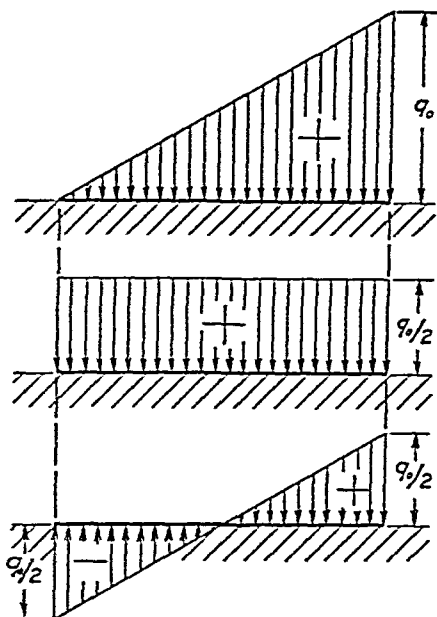


FIG. 16.

in Fig. 16 can be treated in the same manner. In each case the problem is reduced to the determination of the proper values of the forces  $Q_0$  and moments  $M_0$  from the two eqs. (c).

In discussing the bending of beams of finite length we note that the action of forces applied at one end of the beam on the deflection at the other end depends on the magnitude of the quantity  $\beta l$ . This quantity increases with the increase of the length of the beam. At the same time, as may be seen from Table 1, the functions  $\varphi$ ,  $\psi$  and  $\theta$  are rapidly decreasing, and beyond a certain value of  $\beta l$  we can assume that the force acting at one end of the beam has only a negligible effect at the other end. This justifies our considering the beam as an infinitely long one. In such a case the quantities  $\varphi^{(m)}$ ,  $\psi(\beta l)$  and  $\theta(\beta l)$  can be neglected in comparison with unity in eqs. (c) by so doing eqs. (c) are considerably simplified.

ormly

In general, a discussion of the bending of beams of finite length falls naturally into the three groups

- I Short beams,  $\beta l < 0.60$
- II Beams of medium length,  $0.60 < \beta l < 5$
- III Long beams,  $\beta l > 5$

In discussing beams of group I we can entirely neglect bending and consider these beams as absolutely rigid, since the deflection due to bending is usually negligibly small in comparison with the deflection of the foundation. Taking, for example, the case of a load at the middle, Fig. 13, and assuming  $\beta l = 0.60$ , we find from the formulas given above for  $y_a$  and  $y_c$  that the difference between the deflection at the middle and the deflection at the end is only about one half of one per cent of the total deflection. This indicates that the deflection of the foundation is obtained with very good accuracy by treating the beam as infinitely rigid and by using for the deflection the formula

$$y = \frac{P}{kl}$$

The characteristic of beams of group II is that a force acting on one end of the beam produces a considerable effect at the other end. Thus such beams must be treated as beams of finite length.

In beams of group III we can assume in investigating one end of the beam that the other end is infinitely far away. Hence the beam can be considered as infinitely long.

In the preceding discussion it has been assumed that the beam is supported by a continuous elastic foundation, but the results obtained can also be applied when the beam is supported by a large number of equidistant elastic supports. As an example of this kind, let us consider a horizontal beam  $AB$ , Fig. 17, supporting a system of equidistant vertical beams which are carrying a uniformly distributed load  $q$ .<sup>8</sup> All beams are simply supported at the ends. Denoting by  $EI_1$  and  $l_1$  the flexural rigidity and the length of the vertical beams, we find the deflection at their middle to be

$$y = \frac{5}{384} \frac{ql_1^4}{EI_1} - \frac{Rl_1^3}{48EI_1} \quad (j)$$

where  $R$  is the pressure on the horizontal beam  $AB$  of the vertical

<sup>8</sup> Various problems of this kind are encountered in ship structures. A also be a complete discussion of such problems is given by I. G. Boobnov in his *Monograph of Structure of Ships*, St. Petersburg, Vol. 2, 1914. See also P. F. Papinov in his *Structural Mechanics of Ships*, Moscow, Vol. 2, Part I, pp. 318-314,



beam under consideration. Solving eq. (j) for  $R$ , we find that the horizontal beam  $AB$  is under the action of a concentrated force, Fig. 17c, the magnitude of which is

$$R = \frac{5}{8} q l_1 - \frac{48EI_1}{l_1^3} y. \quad (k)$$

Assuming that the distance  $a$  between the vertical beams is small in comparison with the length  $l$  of the horizontal beam and replacing

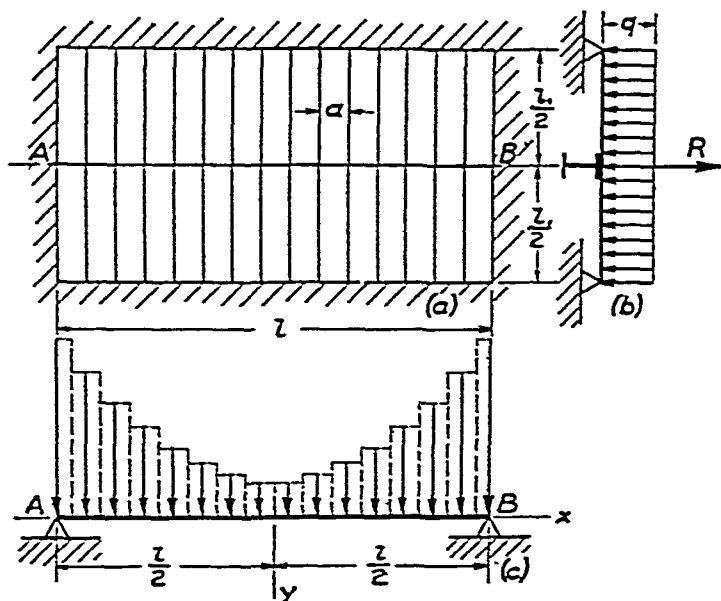


FIG. 17.

the concentrated forces by the equivalent uniform load, as shown in Fig. 17c, we also replace the stepwise load distribution (indicated in the figure by the broken lines) by a continuous load distribution of the intensity

$$q_1 - ky,$$

where

$$q_1 = \frac{5}{8} \frac{ql_1}{a}; \quad k = \frac{48EI_1}{al_1^3}. \quad (l)$$

The differential equation of the deflection curve for the beam  $AB$  then is

$$EI \frac{d^4 y}{dx^4} = q_1 - ky. \quad (m)$$

It is seen that the horizontal beam is in the condition of a uniformly

loaded beam on an elastic foundation. The intensity of the load and the modulus of the foundation are given by eqs (l)

In discussing the deflection of the beam we can use the method of superposition previously explained or we can directly integrate eq (m). Using the latter method, we may write the general integral of eq (m) in the following form

$$y = \frac{q_1}{k} + C_1 \sin \beta x \sinh \beta x + C_2 \sin \beta x \cosh \beta x + C_3 \cos \beta x \sinh \beta x + C_4 \cos \beta x \cosh \beta x \quad (n)$$

Taking the origin of the coordinates at the middle, Fig 17c, we conclude from the condition of symmetry that

$$C_2 = C_3 = 0$$

Substituting this into eq (n) and using the conditions at the simply supported ends,

$$(y)_{x=l/2} = 0, \quad \left( \frac{d^2 y}{dx^2} \right)_{x=l/2} = 0,$$

we find

$$C_1 = -\frac{q_1}{k} \frac{2 \sin \frac{\beta l}{2} \sinh \frac{\beta l}{2}}{\cos \beta l + \cosh \beta l},$$

$$C_4 = -\frac{q_1}{k} \frac{2 \cos \frac{\beta l}{2} \cosh \frac{\beta l}{2}}{\cos \beta l + \cosh \beta l}$$

The deflection curve then is

$$y = \frac{q_1}{k} \left( 1 - \frac{2 \sin \frac{\beta l}{2} \sinh \frac{\beta l}{2}}{\cos \beta l + \cosh \beta l} \sin \beta x \sinh \beta x - \frac{2 \cos \frac{\beta l}{2} \cosh \frac{\beta l}{2}}{\cos \beta l + \cosh \beta l} \cos \beta x \cosh \beta x \right) \quad (o)$$

The deflection at the middle is obtained by substituting  $x = 0$ , which gives

$$(y)_{x=0} = \frac{q_1}{k} \left( 1 - \frac{2 \cos \frac{\beta l}{2} \cosh \frac{\beta l}{2}}{\cos \beta l + \cosh \beta l} \right) \quad (p)$$

loaded beam on an elastic foundation. The intensity of the load and the modulus of the foundation are given by eqs (l)

In discussing the deflection of the beam we can use the method of superposition previously explained or we can directly integrate eq (m). Using the latter method, we may write the general integral of eq (m) in the following form

$$y = \frac{q_1}{k} + C_1 \sin \beta x \sinh \beta x + C_2 \sin \beta x \cosh \beta x + C_3 \cos \beta x \sinh \beta x + C_4 \cos \beta x \cosh \beta x \quad (n)$$

Taking the origin of the coordinates at the middle, Fig 17c, we conclude from the condition of symmetry that

$$C_2 = C_3 = 0$$

Substituting this into eq (n) and using the conditions at the simply supported ends,

$$(y)_{x=l/2} = 0, \quad \left( \frac{d^2 y}{dx^2} \right)_{x=l/2} = 0,$$

we find

$$C_1 = -\frac{q_1}{k} \frac{2 \sin \frac{\beta l}{2} \sinh \frac{\beta l}{2}}{\cos \beta l + \cosh \beta l},$$

$$C_4 = -\frac{q_1}{k} \frac{2 \cos \frac{\beta l}{2} \cosh \frac{\beta l}{2}}{\cos \beta l + \cosh \beta l}$$

The deflection curve then is

$$y = \frac{q_1}{k} \left( 1 - \frac{2 \sin \frac{\beta l}{2} \sinh \frac{\beta l}{2}}{\cos \beta l + \cosh \beta l} \sin \beta x \sinh \beta x - \frac{2 \cos \frac{\beta l}{2} \cosh \frac{\beta l}{2}}{\cos \beta l + \cosh \beta l} \cos \beta x \cosh \beta x \right) \quad (o)$$

The deflection at the middle is obtained by substituting  $x = 0$ , which gives

$$(y)_{x=0} = \frac{q_1}{k} \left( 1 - \frac{2 \cos \frac{\beta l}{2} \cosh \frac{\beta l}{2}}{\cos \beta l + \cosh \beta l} \right) \quad (p)$$

4 Find the deflection and the bending moment at the middle of the uniformly loaded beam with hinged ends, Fig 20

*Answer*

$$y_c = \frac{q}{k} \left( 1 - \frac{2 \cosh \frac{\beta l}{2} \cos \frac{\beta l}{2}}{\cosh \beta l + \cos \beta l} \right),$$

$$M_c = \frac{q}{\beta^2} \frac{\sinh \frac{\beta l}{2} \sin \frac{\beta l}{2}}{\cosh \beta l + \cos \beta l}$$

5 Find the bending moments at the ends of the beam with built-in ends, carrying a uniform load and a load at the middle, Fig 21

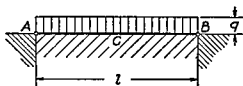


FIG 20

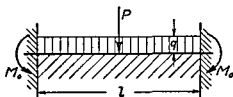


FIG 21

*Answer*

$$M_0 = -\frac{P}{\beta} \frac{\sinh \frac{\beta l}{2} \sin \frac{\beta l}{2}}{\sinh \beta l + \sin \beta l} - \frac{q}{2\beta^2} \frac{\sinh \beta l - \sin \beta l}{\sinh \beta l + \sin \beta l}$$

6 Find the deflection curve for the beam on an elastic foundation with a load applied at one end, Fig 22

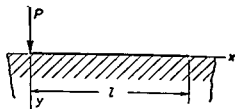


FIG 22

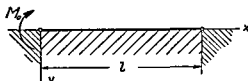


FIG 23

*Answer*

$$y = \frac{2P\beta}{k(\sinh^2 \beta l - \sin^2 \beta l)} [\sinh \beta l \cos \beta x \cosh \beta(l-x) - \sin \beta l \cosh \beta x \cos \beta(l-x)]$$

7. A beam on an elastic foundation and with hinged ends is bent by a couple  $M_0$  applied at the end, Fig. 23. Find the deflection curve of the beam.

*Answer.*

$$y = \frac{2M_0\beta^2}{k(\cosh^2 \beta l - \cos^2 \beta l)} [\cosh \beta l \sin \beta x \sinh \beta(l - x) - \cos \beta l \sinh \beta x \sin \beta(l - x)].$$

## CHAPTER II

### BEAMS WITH COMBINED AXIAL AND LATERAL LOADS

4. **Direct Compression and Lateral Load.**—Let us begin with the simple problem of a strut with hinged ends, loaded by a single lateral force  $P$  and centrally compressed by two equal and opposite forces  $S$ , Fig 24. Assuming that the strut

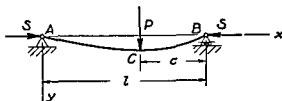


FIG 24

has a plane of symmetry and that the force  $P$  acts in that plane, we see that bending proceeds in the same plane. The differential equations of the deflection curve for the two portions of the strut are

$$EI \frac{d^2 y}{dx^2} = -Sy - \frac{Pc}{l} x, \quad (a)$$

$$EI \frac{d^2 y}{dx^2} = -Sy - \frac{P(l-c)}{l} (l-x). \quad (b)$$

Using the notation

$$\frac{S}{EI} = p^2, \quad (17)$$

we represent the solutions of eqs. (a) and (b) in the following form:

$$y = C_1 \cos px + C_2 \sin px - \frac{Pc}{Sl} x, \quad (c)$$

$$y = C_3 \cos px + C_4 \sin px - \frac{P(l-c)}{Sl} (l-x). \quad (d)$$

Since the deflections vanish at the ends of the strut, we conclude that

$$C_1 = 0,$$

$$C_3 = -C_4 \tan pl.$$

The remaining two constants of integration are found from the conditions of continuity at the point of application of the load  $P$ , which require that eqs. (c) and (d) give the same deflection and the same slope for  $x = l - c$ . In this way we obtain

$$C_2 \sin p(l - c) = C_4 [\sin p(l - c) - \tan pl \cos p(l - c)],$$

$$C_2 p \cos p(l - c) = C_4 p [\cos p(l - c) + \tan pl \sin p(l - c)] + \frac{P}{S},$$

from which

$$C_2 = \frac{P \sin pc}{Sp \sin pl}, \quad C_4 = -\frac{P \sin p(l - c)}{Sp \tan pl}.$$

Substituting in eq. (c), we obtain for the left portion of the strut

$$y = \frac{P \sin pc}{Sp \sin pl} \sin px - \frac{Pc}{Sl} x, \quad (18)$$

and by differentiation we find

$$\left. \begin{aligned} \frac{dy}{dx} &= \frac{P \sin pc}{S \sin pl} \cos px - \frac{Pc}{Sl}, \\ \frac{d^2y}{dx^2} &= -\frac{Pp \sin pc}{S \sin pl} \sin px. \end{aligned} \right\} \quad (19)$$

The corresponding expressions for the right portion of the strut are obtained by substituting  $(l - x)$  instead of  $x$ , and  $(l - c)$  instead of  $c$ , and by changing the sign of  $dy/dx$  in eqs.

(18) and (19). These substitutions give

$$y = \frac{P \sin p(l-c)}{Sp \sin pl} \sin p(l-x) - \frac{P(l-c)}{Sl} (l-x), \quad (20)$$

$$\frac{dy}{dx} = -\frac{P \sin p(l-c)}{S \sin pl} \cos p(l-x) + \frac{P(l-c)}{Sl}, \quad (21)$$

$$\frac{d^2y}{dx^2} = -\frac{Pp \sin p(l-c)}{S \sin pl} \sin p(l-x). \quad (22)$$

In the particular case when the load  $P$  is applied at the middle, we have  $c = l/2$ , and by introducing the notation

$$\frac{Sl^2}{4EI} = \frac{p^2 l^2}{4} = u^2, \quad (23)$$

we obtain from eq. (18)

$$\begin{aligned} (y)_{\max} &= (y)_{x=l/2} = \frac{P}{2Sp} \left( \tan \frac{pl}{2} - \frac{pl}{2} \right) \\ &= \frac{Pl^3}{48EI} \cdot \frac{\tan u - u}{\frac{1}{3}u^3}. \end{aligned} \quad (24)$$

The first factor in eq. (24) represents the deflection produced by the lateral load  $P$  acting alone. The second factor indicates in what proportion the deflection produced by  $P$  is magnified by the axial compressive force  $S$ . When  $S$  is small in comparison with the Euler load ( $S_e = EI\pi^2/l^2$ ), the quantity  $u$  is small and the second factor in eq. (24) approaches unity, which indicates that under this condition the effect on the deflection of the axial compressive force is negligible. When  $S$  approaches the Euler value, the quantity  $u$  approaches the value  $\pi/2$  (see eq. 23) and the second factor in eq. (24) increases indefinitely, as should be expected from our previous discussion of critical loads (see Part I, p. 263).

The maximum value of the bending moment is under the load, and its value is obtained from the second of eqs. (19), which gives

$$M_{\max} = -EI \left( \frac{d^2y}{dx^2} \right)_{x=l/2} = EI \frac{Pp}{2S} \tan \frac{pl}{2} = \frac{Pl}{4} \cdot \frac{\tan u}{u}. \quad (25)$$



Again we see that the first factor in eq. (25) represents the bending moment produced by the load  $P$  acting alone, while the second factor is the *magnification factor*, representing the effect of the axial force  $S$  on the maximum bending moment.

Having solved the problem for one lateral load  $P$ , Fig. 24, we can readily obtain the solution for the case of a strut bent by a couple applied at the end, Fig. 25. It is only necessary



FIG. 25.

to assume that in our previous discussion the distance  $c$  is indefinitely diminishing and approaching zero, while  $Pc$  remains a constant equal to  $M_0$ . Substituting  $Pc = M_0$  and  $\sin pc = pc$  in eq. (18), we obtain the deflection curve

$$y = \frac{M_0}{S} \left( \frac{\sin px}{\sin pl} - \frac{x}{l} \right), \quad (26)$$

from which

$$\frac{dy}{dx} = \frac{M_0}{S} \left( \frac{p \cos px}{\sin pl} - \frac{1}{l} \right).$$

The slopes of the beam at the ends are

$$\begin{aligned} \left( \frac{dy}{dx} \right)_{x=0} &= \frac{M_0}{S} \left( \frac{p}{\sin pl} - \frac{1}{l} \right) \\ &= \frac{M_0 l}{6EI} \cdot 6 \left( \frac{1}{2u \sin 2u} - \frac{1}{(2u)^2} \right), \end{aligned} \quad (27)$$

$$\begin{aligned} \left( \frac{dy}{dx} \right)_{x=l} &= \frac{M_0}{S} \left( \frac{p}{\tan pl} - \frac{1}{l} \right) \\ &= \frac{M_0 l}{3EI} \cdot 3 \left( \frac{1}{2u \tan 2u} - \frac{1}{(2u)^2} \right). \end{aligned} \quad (28)$$

Again the first factors in eqs. (27) and (28) taken with proper signs represent the slopes produced by the couple  $M_0$  acting alone (see Part I, p. 158), and the second factors represent the effect of the axial force  $S$ .

Considering eqs. (18) and (26), we see that the lateral force  $P$  and the couple  $M_0$  occur in these expressions linearly, while the axial force  $S$  occurs in the same expressions in a more complicated manner, since  $p$  also contains  $S$  (see eq. 17). From this we conclude that if at point  $C$ , Fig. 24, two forces  $P$  and  $Q$  are applied, the deflection at any point may be obtained by superposing the deflections produced by the load  $Q$  and the axial forces  $S$  on the deflection produced by the load  $P$  and the same axial forces. A similar conclusion can be reached regarding couples applied to one end of the beam.

This conclusion regarding superposition can be readily generalized and extended to cover the case of several loads, Fig. 26. For each portion of the strut an equation similar to

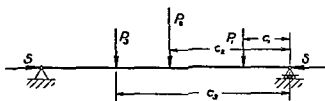


FIG. 26.

eqs. (a) and (b) can be written, and a solution similar to those in (c) and (d) can be obtained. The constants of integration can be found from the conditions of continuity at the points of load application and from the conditions at the ends of the strut. In this way it can be shown that the deflection at any point of the strut is a linear function of the loads  $P_1, P_2, \dots$  and that the deflection at any point can be obtained by superposing the deflections produced at that point by each of the lateral loads acting together with the axial force  $S$ .

Let us consider a general case when  $n$  forces are acting and  $m$  of these forces are applied to the right of the cross section for which we are calculating the deflection. The expression for this deflection is obtained by using eq. (18) for the forces  $P_1, P_2, \dots, P_m$  and eq. (20) for the forces  $P_{m+1}, P_{m+2}, \dots, P_n$ .

In this way we obtain the required deflection:

$$y = \frac{\sin px}{Sp \sin pl} \sum_{i=1}^{i=m} P_i \sin pc_i - \frac{x}{Sl} \sum_{i=1}^{i=m} P_i c_i \\ + \frac{\sin p(l-x)}{Sp \sin pl} \sum_{i=m+1}^{i=n} P_i \sin p(l-c_i) \\ - \frac{l-x}{Sl} \sum_{i=m+1}^{i=n} P_i (l-c_i). \quad (29)$$

If, instead of concentrated forces, there is a uniform load of intensity  $q$  acting on the strut, each element  $qdc$  of this load, taken at a distance  $c$  from the right end, can be considered as a concentrated force. Substituting it, instead of  $P_i$ , in eq. (29) and replacing summation signs by integration, we obtain the following expression for the deflection curve:

$$y = \frac{\sin px}{Sp \sin pl} \int_0^{l-x} q \sin pc dc - \frac{x}{Sl} \int_0^{l-x} q dc \\ + \frac{\sin p(l-x)}{Sp \sin pl} \int_{l-x}^l q \sin p(l-c) dc - \frac{l-x}{Sl} \int_{l-x}^l q(l-c) dc.$$

Performing the integrations, we obtain

$$y = \frac{q}{Sp^2} \left[ \frac{\cos\left(\frac{pl}{2} - px\right)}{\cos \frac{pl}{2}} - 1 \right] - \frac{q}{2S} x(l-x) \quad (30)$$

and

$$y_{\max} = (y)_{x=l/2} = \frac{q}{Sp^2} \left( \frac{1}{\cos u} - 1 - \frac{u^2}{2} \right) \\ = \frac{5}{384} \frac{ql^4}{EI} \cdot \frac{1}{\frac{5}{24}u^4} \left( \frac{1}{\cos u} - 1 - \frac{u^2}{2} \right). \quad (31)$$

By differentiating eq. (30) we readily obtain the expressions for the slope and for the bending moment. The slope at the

left end of the strut is

$$\left(\frac{dy}{dx}\right)_{x=0} = \frac{ql}{2S} \left( \frac{\tan \frac{pl}{2}}{\frac{pl}{2}} - 1 \right) = \frac{ql^3}{24EI} \frac{\tan u - u}{\frac{1}{3}u^3}. \quad (32)$$

The maximum bending moment is at the middle where

$$\begin{aligned} M_{\max} &= -EI \left( \frac{d^2y}{dx^2} \right)_{x=l/2} \\ &= EI \frac{q \left( 1 - \cos \frac{pl}{2} \right)}{S \cos \frac{pl}{2}} = \frac{ql^2}{8} \cdot \frac{2(1 - \cos u)}{u^2 \cos u}. \end{aligned} \quad (33)$$

By using the solution for the case of a couple together with the solutions for lateral loads and applying the method of superposition, various statically indeterminate cases of bending of struts can be readily solved. Taking as an example the case of a uniformly loaded strut built in at one end, Fig. 27,

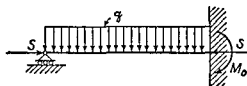


FIG. 27.

we find the bending moment  $M_0$  at the built-in end from the condition that this end does not rotate during bending. By using eqs. (28) and (32) this condition is found to be

$$-\frac{ql^3}{24EI} \frac{\tan u - u}{\frac{1}{3}u^3} + \frac{M_0 l}{3EI} \cdot \left( \frac{3}{2u \tan 2u} - \frac{3}{(2u)^2} \right) = 0$$

from which

$$M_0 = -\frac{ql^2}{8} \cdot \frac{4 \tan 2u (\tan u - u)}{u(\tan 2u - 2u)}. \quad (34)$$

In the case of a uniformly loaded strut with both ends built in, the moments  $M_0$  at the ends are obtained from the equation

$$-\frac{ql^3}{24EI} \frac{\tan u - u}{\frac{1}{3}u^3} + \frac{M_0 l}{3EI} \left[ \frac{3}{2u \tan 2u} - \frac{3}{(2u)^2} \right] - \frac{M_0 l}{6EI} \left( \frac{6}{2u \sin 2u} - \frac{6}{(2u)^2} \right) = 0,$$

from which

$$M_0 = -\frac{ql^2}{12} \cdot \frac{\tan u - u}{\frac{1}{3}u^2 \tan u}. \quad (35)$$

It is seen from eqs. (34) and (35) that the values of the statically indeterminate moments are obtained by multiplying the corresponding moments produced by the lateral loads acting alone by certain magnification factors.

The necessary calculations can be greatly simplified by using prepared numerical tables for determining the magnification factors.<sup>1</sup> In Table 3 are given the magnification factors for a uniformly loaded strut, using the notation:

$$\varphi_0(u) = \frac{\frac{1}{\cos u} - 1 - \frac{u^2}{2}}{\frac{5}{24}u^4}$$

$$\psi_0(u) = \frac{2(1 - \cos u)}{u^2 \cos u}.$$

When the maximum bending moment for a strut is found, the numerically maximum stress is obtained by combining the direct stress with the maximum bending stress, which gives

$$[\sigma]_{\max} = \frac{S}{A} + \frac{M_{\max}}{Z} \quad (e)$$

where  $A$  and  $Z$  are, respectively, the cross-sectional area and

<sup>1</sup> Various particular cases of laterally loaded struts have been discussed by A. P. Van der Fleet, *Bull. Soc. Engrs. Ways of Communication*, St. Petersburg, 1900-03. Numerous tables of magnification factors are given in that work.

TABLE 3. MAGNIFICATION FACTORS FOR UNIFORMLY LOADED STRUTS

$u =$	0	0.10	0.20	0.30	0.40	0.50
$\varphi_0(u) =$	1.000	1.004	1.016	1.037	1.070	1.114
$\psi_0(u) =$	1.000	1.004	1.016	1.038	1.073	1.117
$u =$	0.60	0.70	0.80	0.90	1.00	1.10
$\varphi_0(u) =$	1.173	1.250	1.354	1.494	1.690	1.962
$\psi_0(u) =$	1.176	1.255	1.361	1.504	1.704	1.989
$u =$	1.20	1.30	1.40	1.45	1.50	$\frac{\pi}{2}$
$\varphi_0(u) =$	2.400	3.181	4.822	6.790	11.490	$\infty$
$\psi_0(u) =$	2.441	3.240	4.938	6.940	11.670	$\infty$

the section modulus for the strut. Taking as an example the case of a uniformly loaded strut with hinged ends, we obtain from eq. (33)

$$|\sigma|_{\max} = \frac{S}{A} + \frac{ql^2}{8Z} \cdot \frac{2(1 - \cos u)}{u^2 \cos u}. \quad (f)$$

In selecting the proper cross-sectional dimensions of the strut it is necessary to first establish the relation between the longitudinal and lateral loads. If the conditions are such that the axial force  $S$  remains constant and only the lateral load  $q$  can vary, then the maximum stress in eq. (f) is proportional to the load  $q$ . Then the required cross-sectional dimensions are obtained by substituting  $\sigma_{YP}/n$  for  $\sigma_{\max}$  in this equation,  $n$  being the factor of safety with respect to the yield point of the material.<sup>2</sup>

If the conditions are as shown for the strut  $AB$  in Fig. 28, so that the axial force  $S$  varies in the same proportion as the

<sup>2</sup> It is assumed that the material of the strut has a pronounced yield point.

lateral load  $q$ , the problem of selecting safe dimensions becomes more complicated. The right-hand side of eq. (f) is no longer linear in  $q$  since the quantity  $u$ , defined by eq. (23), also depends on the magnitude of  $q$ . Owing to this fact, the maximum stress in eq. (f) increases at a greater rate than the load  $q$ , and if we proceed as in the preceding case and use  $\sigma_{Y.P.}/n$  for  $\sigma_{\max}$  in this equation, the actual factor of safety of the structure will be smaller than  $n$ , and the load at which yielding begins will be smaller than  $nq$ . To satisfy conditions of safety we use eq. (f) to define conditions at the beginning of yielding and write

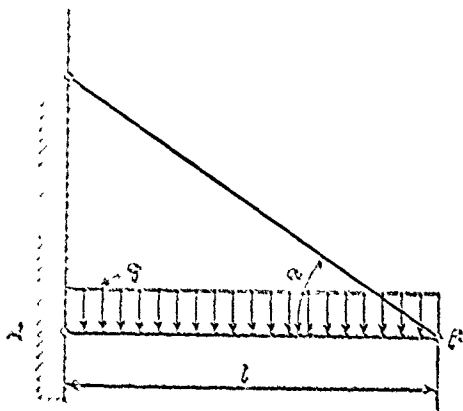


FIG. 28.

$$\sigma_{Y.P.} = \frac{S_{Y.P.}}{A} + \frac{q_{Y.P.} l^2}{8Z} \cdot \frac{2(1 - \cos u_{Y.P.})}{u_{Y.P.}^2 \cos u_{Y.P.}} \quad (g)$$

Since  $S_{Y.P.}$  in each particular case (such as Fig. 28) is a certain function of  $q_{Y.P.}$  and  $u$  is defined by eq. (23), the right-hand side of eq. (g) for any assumed values of  $A$  and  $Z$  is a function of the limiting value  $q_{Y.P.}$  of the load, and this value can be found from the equation by trial and error. Knowing  $q_{Y.P.}$ , we determine the safe load  $q_{Y.P.}/n$  for the assumed cross-sectional dimensions of the strut. Repeating this calculation several times, we can finally find the cross-sectional dimensions<sup>3</sup> which will provide the required factor of safety,  $n$ . A similar method was used previously in the article, *Design of Columns on the Basis of Assumed Inaccuracies* (see Part I, p. 274).

<sup>3</sup> This method of design of struts was developed by K. S. Zavriev; see *Memoirs Inst. of Engrs. Ways of Communication* (St. Petersburg), 1913.

## Problems

1 The dimensions of the strut  $AB$  in Fig 28 are such that its Euler load is equal to 2,000 lb Using Table 3, find the magnification factors  $\varphi_0(u)$  and  $\psi_0(u)$  if  $\alpha = 45^\circ$  and  $ql = 2,000$  lb

*Answer*  $\varphi_0(u) = 2.01$ ,  $\psi_0(u) = 2.03$

2 Find the slope at the left end of a strut with hinged ends which is loaded at the middle by a load  $P$  and with the axial load  $S$

*Answer*

$$\left(\frac{dy}{dx}\right)_{x=0} = \frac{P}{2S} \frac{1 - \cos u}{\cos u} = \frac{Pl^2}{16EI} \frac{1 - \cos u}{\frac{1}{2}u^2 \cos u}$$

3 Find the slopes at the ends of a strut carrying a triangular load, Fig 29

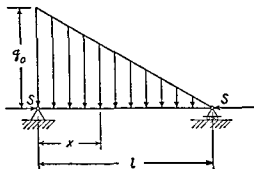


FIG 29

*Solution* Substituting  $q_0 c dc/l$  into eq (29) instead of  $P$ , and replacing summation by integration, we find

$$\begin{aligned} y = & \frac{\sin px}{Sp \sin pl} \int_0^{l-x} \frac{q_0 c}{l} \sin pc dc - \frac{x}{Sl} \int_0^{l-x} \frac{q_0 c^2}{l} dc \\ & + \frac{\sin p(l-x)}{Sp \sin pl} \int_{l-x}^l \frac{q_0 c}{l} \sin p(l-c) dc - \frac{l-x}{Sl} \int_{l-x}^l \frac{q_0 c}{l} (l-c) dc \end{aligned}$$

Differentiating this with respect to  $x$ , we find that

$$\left(\frac{dy}{dx}\right)_{x=0} = \frac{2q_0 l}{6p^2 EI} (\beta - 1)$$



and

$$\left(\frac{dy}{dx}\right)_{x=l} = -\frac{q_0 l}{6p^2 EI}(\alpha - 1),$$

where  $\alpha$  and  $\beta$  are the functions given by eqs. (36) (see p. 38).

4. Find the slopes at the ends of a strut symmetrically loaded by two loads  $P$ , as shown in Fig. 30.

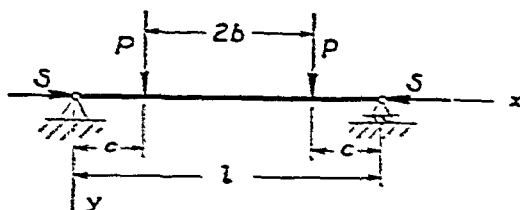


FIG. 30.

*Answer.*

$$\left(\frac{dy}{dx}\right)_{x=0} = -\left(\frac{dy}{dx}\right)_{x=l} = \frac{P}{S} \left( \frac{\cos pb}{\cos \frac{p l}{2}} - 1 \right).$$

5. A strut with built-in ends is loaded as shown in Fig. 30. Find the bending moments  $M_0$  at the ends.

*Solution.* The moments  $M_0$  are found from the conditions that the ends of the strut do not rotate. By using the answer to the preceding problem and also eqs. (27) and (28), the following equation for calculating  $M_0$  is obtained:

$$\frac{M_0 l}{6EI} \alpha + \frac{M_0 l}{3EI} \beta + \frac{P}{S} \left( \frac{\cos pb}{\cos \frac{p l}{2}} - 1 \right) = 0,$$

from which

$$M_0 = -\frac{2PEI}{Sl} \frac{u}{\tan u} \left( \frac{\cos pb}{\cos u} - 1 \right).$$

If  $b = 0$ , we obtain the case of a load  $2P$  concentrated at the middle.

5. Continuous Struts.—In the case of a continuous strut we proceed as in the case of continuous beams (see Part I, p. 203) and consider two adjacent spans, Fig. 31.<sup>4</sup> Using eqs. (23), (27) and (28)

<sup>4</sup> The theory is due to H. Zimmermann, *Sitzungsber. Akad. Wissensch.*, Berlin, 1907 and 1909.

and introducing the following notation for the  $n$ th span

$$u_n^2 = \frac{S_n l_n^2}{4EI_n},$$

$$\alpha_n = 6 \left[ \frac{1}{2u_n \sin 2u_n} - \frac{1}{(2u_n)^2} \right],$$

(36)

$$\beta_n = 3 \left[ \frac{1}{(2u_n)^2} - \frac{1}{2u_n \tan 2u_n} \right],$$

$$\gamma_n = \frac{\tan u_n - u_n}{\frac{1}{3}u_n^3},$$

(37)

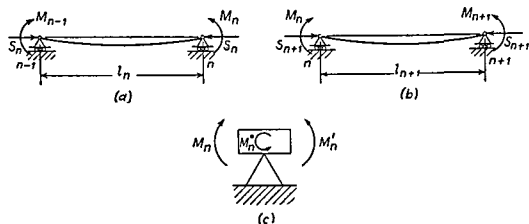


FIG 31

we conclude that the slope at the right end of the  $n$ th span, Fig 31a, produced by the end moments  $M_{n-1}$  and  $M_n$ , is

$$-\beta_n \frac{M_n l_n}{3EI_n} - \alpha_n \frac{M_{n-1} l_n}{6EI_n}$$

(a)

The slope produced at the left end of the  $n+1$  span by the moments  $M_n$  and  $M_{n+1}$  is

$$\alpha_{n+1} \frac{M_{n+1} l_{n+1}}{6EI_{n+1}} + \beta_{n+1} \frac{M_n l_{n+1}}{3EI_{n+1}}$$

(b)

If there is no lateral load acting on the two spans under consideration, expressions (a) and (b) must be equal, and we obtain

$$\frac{\alpha_n l_n}{I_n} M_{n-1} + 2 \left( \beta_n \frac{l_n}{I_n} + \beta_{n+1} \frac{l_{n+1}}{I_{n+1}} \right) M_n + \alpha_{n+1} \frac{l_{n+1}}{I_{n+1}} M_{n+1} = 0. \quad (38)$$

This is the three-moment equation for a continuous strut if there is no lateral load on the two spans under consideration.

If there is a lateral load acting, the corresponding slopes produced by this load must be added to expressions (a) and (b). Taking, for example, the case of uniform load  $q_n$  and  $q_{n+1}$  acting on the spans  $n$  and  $n+1$  in a downward direction, we obtain the corresponding slopes from eq. (32) and, instead of expressions (a) and (b), we obtain

$$-\beta_n \frac{M_n l_n}{3EI_n} - \alpha_n \frac{M_{n-1} l_n}{6EI_n} - \gamma_n \frac{q_n l_n^3}{24EI_n}, \quad (c)$$

$$\alpha_{n+1} \frac{M_{n+1} l_{n+1}}{6EI_{n+1}} + \beta_{n+1} \frac{M_n l_{n+1}}{3EI_{n+1}} + \gamma_{n+1} \frac{q_{n+1} l_{n+1}^3}{24EI_{n+1}}. \quad (d)$$

Equating these two expressions we obtain

$$\begin{aligned} \frac{\alpha_n l_n}{I_n} M_{n-1} + 2 \left( \beta_n \frac{l_n}{I_n} + \beta_{n+1} \frac{l_{n+1}}{I_{n+1}} \right) M_n + \alpha_{n+1} \frac{l_{n+1}}{I_{n+1}} M_{n+1} \\ = -\gamma_n \frac{q_n l_n^3}{4I_n} - \gamma_{n+1} \frac{q_{n+1} l_{n+1}^3}{4I_{n+1}}. \end{aligned} \quad (39)$$

This is the three-moment equation for a strut with a uniform load in each span. It is similar to the three-moment equation for a continuous beam and coincides with it when  $S = 0$  and the functions  $\alpha, \beta, \gamma$  become equal to unity.

For any other kind of lateral load we have to change only the right-hand side of eq. (39), which depends on the rotation of the adjacent ends of the two spans produced by the lateral loading. Taking for example the case of a trapezoidal load shown in Fig. 32 and dividing the load into two parts, uniform loads and triangular loads, we use for the uniform loads the terms already written on the right-hand side of eq. (39). To these terms we must add the terms corresponding to the triangular loads.

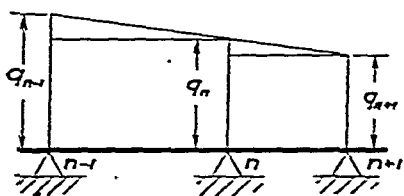


FIG. 32.

Using the expressions for the slopes in Prob. 3 of the preceding article, we find that the two terms which we have to add to the right-

hand side of eq (39) in the case of the load shown in Fig 32 are

$$-\frac{(q_{n-1} - q_n)l_n}{p^2 I_n} (\alpha_n - 1) - \frac{2(q_n - q_{n+1})l_{n+1}}{p^2 I_{n+1}} (\beta_{n+1} - 1), \quad (e)$$

in which  $\alpha_n$  and  $\beta_{n+1}$  are defined by eqs (36). If concentrated forces are acting on the spans under consideration, the required expressions for the rotations are readily obtainable from the general expression for the deflection curve, eq (29).

The calculation of moments from the three moment eqs (39) can be considerably simplified by using numerical tables of functions  $\alpha$ ,  $\beta$  and  $\gamma$ .<sup>5</sup>

In the derivation of eq (39) it was assumed that the moment  $M_n$  at the  $n$ th support had the same value for both adjacent spans. There are cases, however, in which an external moment  $M_n^0$  is applied at the support as shown in Fig 31c, in such cases we must distinguish between the values of the bending moment to the left and of that to the right of the support. The relation between these two moments is given by the equation of statics.<sup>6</sup>

$$M_n - M_n^0 - M_n = 0,$$

from which

$$M_n' = M_n - M_n^0 \quad (f)$$

Eq (39) in such a case is replaced by the following equation

$$\begin{aligned} \frac{\alpha_n l_n}{I_n} M_{n-1} + 2\beta_n \frac{l_n}{I_n} M_n + 2\beta_{n+1} \frac{l_{n+1}}{I_{n+1}} M_n + \alpha_{n+1} \frac{l_{n+1}}{I_{n+1}} M_{n+1} \\ = -\gamma_n \frac{q_n l_n^3}{4I_n} - \gamma_{n+1} \frac{q_{n+1} l_{n+1}^3}{4I_{n+1}} \end{aligned} \quad (40)$$

If the supports of a continuous strut are not in a straight line, then additional terms, depending on the differences in the levels of the three consecutive supports, must be put on the right hand side of eq (39) or (40). These terms are not affected by the presence of the axial forces, and are the same as in the case of a beam without axial load (see Part I, p. 205).

<sup>5</sup> Such tables can be found in the book by A. S. Niles and J. S. Newell, *Airplane Structures*, New York, Vol. 2, 1943, see also the writer's book *Theory of Elastic Stability*, New York, 1936.

<sup>6</sup> The direction of  $M_n^0$  indicated in Fig 31c is taken as the positive direction for an external moment.

## Problems

1. Write the right-hand side of the three-moment equation if there is a concentrated force  $P$  in the span  $n + 1$  at a distance  $c_{n+1}$  from the support  $n + 1$ .

*Answer.*

$$-\frac{6P}{p_{n+1}^2 I_{n+1}} \left( \frac{\sin p_{n+1} c_{n+1}}{\sin p_{n+1} l_{n+1}} - \frac{c_{n+1}}{l_{n+1}} \right).$$

2. Write the right-hand side of the three-moment equation if the  $n$ th span is loaded as shown in Fig. 30, p. 37, and if there is no load on span  $n + 1$ .

*Answer.* Using the solution of Prob. 4, p. 37, we obtain the following expression:

$$-\frac{6P}{p_n^2 I_n} \left( \frac{\cos p_n b_n}{\cos \frac{p_n l_n}{2}} - 1 \right).$$

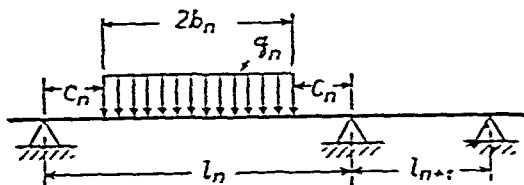


FIG. 33.

3. Find the right-hand side of the three-moment equation if the load is as shown in Fig. 33.

*Answer.*

$$-\frac{6q_n}{p_n^2 I_n} \left( \frac{\cos p_n b_n}{p_n \cos \frac{p_n l_n}{2}} - b_n \right).$$

6. Tie Rod with Lateral Loading.—If a tie rod is subjected to the action of tensile forces  $S$  and a lateral load  $P$  (Fig. 34) we can write the differential equation of the deflection curve for each portion of the rod in exactly the same manner as we did for a strut, Art. 4. It is only necessary to change the sign of  $S$ . In such a case instead of quantities  $p^2$  and  $u^2$  defined by eqs. (17) and (23), respectively, we shall have  $-p^2$  and  $-u^2$ ; and instead of  $p$  and  $u$  we shall have  $p\sqrt{-1} = pi$  and

$u\sqrt{-1} = ui$ . Substituting  $-S$ ,  $pi$  and  $ui$  in place of  $S$ ,  $p$  and  $u$  in the formulas obtained for the strut in Fig. 24, we

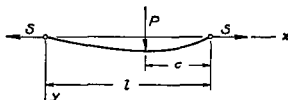


FIG. 34.

obtain the necessary formulas for the tie rod in Fig. 34. In making this substitution we use the known relations:

$$\sin ui = i \sinh u, \quad \cos ui = \cosh u, \quad \tan ui = i \tanh u.$$

In this way we obtain for the left-hand portion of the tie rod in Fig. 34, from eqs. (18) and (19),

$$y = -\frac{P \sinh pc}{Sp \sinh pl} \sinh px + \frac{Pc}{Sl} x, \quad (41)$$

$$\frac{dy}{dx} = -\frac{P \sinh pc}{S \sinh pl} \cosh px + \frac{Pc}{Sl},$$

$$\frac{d^2y}{dx^2} = -\frac{Pp \sinh pc}{S \sinh pl} \sinh px. \quad (42)$$

Similar formulas can also be obtained for the right-hand portion of the tie rod by using eqs. (20)–(22). Having the deflection curve for the case of one load  $P$  acting on the tie rod, we can readily obtain the deflection curve for any other kind of loading by using the method of superposition.

Considering for example a uniformly loaded tie rod and using eqs. (30) and (31) we obtain

$$y = \frac{q}{Sp^2} \left[ \frac{\cosh\left(\frac{pl}{2} - px\right)}{\cosh \frac{pl}{2}} - 1 \right] + \frac{q}{2S} x(l-x),$$

and the maximum deflection is

$$y_{\max} = (y)_{x=l/2} = \frac{5}{384} \frac{ql^4}{EI} \cdot \frac{\frac{1}{\cosh u} - 1 + \frac{u^2}{2}}{\frac{5}{24}u^4}$$

$$= \frac{5}{384} \frac{ql^4}{EI} \cdot \varphi_1(u), \quad (43)$$

where

$$\varphi_1(u) = \frac{\frac{1}{\cosh u} - 1 + \frac{u^2}{2}}{\frac{5}{24}u^4}.$$

The slope of the deflection curve at the left-hand end, from eq. (32), is

$$\left(\frac{dy}{dx}\right)_{x=0} = \frac{ql^3}{24EI} \frac{u - \tanh u}{\frac{1}{3}u^3}. \quad (44)$$

The maximum bending moment, which in this case is at the middle of the span, is obtained from eq. (33):

$$M_{\max} = \frac{ql^2}{8} \cdot \frac{2(\cosh u - 1)}{u^2 \cosh u} = \frac{ql^2}{8} \psi_1(u), \quad (45)$$

where

$$\psi_1(u) = \frac{2(\cosh u - 1)}{u^2 \cosh u}.$$

It is seen that the deflection and the maximum bending moment are obtained by multiplying the corresponding expressions for a simple beam without axial load by the factors  $\varphi_1(u)$  and  $\psi_1(u)$ , which depend on the magnitude of the axial tensile force  $S$ . The numerical values of these factors are given in Table 4.<sup>7</sup>

<sup>7</sup> Various cases of bending of tie rods are investigated in the papers by A. P. Van der Fleet, *loc. cit.*, p. 33, and also in the book by I. G. Boobnov, *loc. cit.*, p. 20. Table 4 is taken from the latter book.

TABLE 4: DEFLECTION AND MAXIMUM BENDING MOMENT CONSTANTS IN  
LATERALLY LOADED TIE RODS

$u$	$\varphi_1$	$\varphi_2$	$\psi_1$	$\psi_2$	$\psi_3$	$u$	$\varphi_1$	$\varphi_2$	$\psi_1$	$\psi_2$	$\psi_3$
0	1.000	1.000	1.000	1.000	1.000	6.5	0.054	0.197	0.047	0.391	0.139
0.5	0.908	0.976	0.905	0.984	0.972	7.0	0.047	0.175	0.041	0.367	0.121
1.0	0.711	0.909	0.704	0.939	0.894	7.5	0.041	0.156	0.036	0.347	0.106
1.5	0.523	0.817	0.511	0.876	0.788	8.0	0.036	0.141	0.031	0.328	0.093
2.0	0.380	0.715	0.367	0.806	0.673	8.5	0.032	0.127	0.028	0.311	0.083
2.5	0.281	0.617	0.268	0.736	0.563	9.0	0.029	0.115	0.025	0.296	0.074
3.0	0.213	0.529	0.200	0.672	0.467	9.5	0.026	0.105	0.022	0.283	0.066
3.5	0.166	0.453	0.153	0.614	0.386	10.0	0.024	0.096	0.020	0.270	0.060
4.0	0.132	0.388	0.120	0.563	0.320	10.5	0.021	0.088	0.018	0.259	0.054
4.5	0.107	0.335	0.097	0.519	0.267	11.0	0.020	0.081	0.017	0.248	0.050
5.0	0.088	0.291	0.079	0.480	0.224	11.5	0.018	0.075	0.015	0.238	0.045
5.5	0.074	0.254	0.066	0.446	0.189	12.0	0.016	0.069	0.014	0.229	0.042
6.0	0.063	0.223	0.055	0.417	0.162						

In the case of bending of a tie rod by a couple applied at the right-hand end, the deflection curve is obtained from eq. (26), which gives

$$y = \frac{M_0}{S} \left( \frac{x}{l} - \frac{\sinh px}{\sinh pl} \right). \quad (46)$$

If there are two equal and opposite couples applied at the ends of a tie rod, the deflection curve is obtained by the method of superposition:

$$\begin{aligned} y &= \frac{M_0}{S} \left( \frac{x}{l} - \frac{\sinh px}{\sinh pl} \right) + \frac{M_0}{S} \left[ \frac{l-x}{l} - \frac{\sinh p(l-x)}{\sinh pl} \right] \\ &= \frac{M_0}{S} \left[ 1 - \frac{\cosh p \left( \frac{l}{2} - x \right)}{\cosh \frac{pl}{2}} \right]. \end{aligned} \quad (47)$$

From this equation we find the deflection at the middle and the slope at the left-hand end of the tie rod:

$$\left. \begin{aligned} (y)_{x=l/2} &= \frac{M_0}{S} \cdot \frac{\cosh u - 1}{\cosh u} = \frac{M_0 l^2}{8EI} \cdot \frac{\cosh u - 1}{\frac{1}{2} u^2 \cosh u}, \\ \left( \frac{dy}{dx} \right)_{x=0} &= \frac{M_0}{S} p \tanh u = \frac{M_0 l}{2EI} \cdot \frac{\tanh u}{u}. \end{aligned} \right\} \quad (48)$$



The bending moment at the middle is

$$(M)_{z=l/2} = -EI \left( \frac{d^2 y}{dz^2} \right)_{z=l/2} = M_0 \cdot \frac{1}{\cosh u}. \quad (49)$$

Having the deflection curves for a tie rod with hinged ends bent by transverse loading and by couples at the ends, we can readily obtain various statically indeterminate cases of bending of tie rods by the method of superposition. Taking for example the case of a uniformly loaded tie rod with built-in ends and using eqs. (44) and (48), we obtain the bending moments  $M_0$  at the ends from the equation

$$\frac{ql^3}{24EI} \cdot \frac{u - \tanh u}{\frac{1}{3}u^3} + \frac{M_0 l}{2EI} \cdot \frac{\tanh u}{u} = 0$$

from which

$$M_0 = -\frac{ql^2}{12} \cdot \frac{u - \tanh u}{\frac{1}{3}u^2 \tanh u} = -\frac{ql^2}{12} \psi_2(u), \quad (50)$$

where

$$\psi_2(u) = \frac{u - \tanh u}{\frac{1}{3}u^2 \tanh u}.$$

The numerical values of the function  $\psi_2(u)$  are given in Table 4. By using eqs. (45) and (49) the bending moment  $M_1$  at the middle is obtained:

$$\begin{aligned} M_1 &= \frac{ql^2}{8} \cdot \frac{2(\cosh u - 1)}{u^2 \cosh u} - \frac{ql^2}{12} \cdot \frac{u - \tanh u}{\frac{1}{3}u^2 \sinh u} \\ &= \frac{ql^2}{24} \cdot \frac{6(\sinh u - u)}{u^2 \sinh u} = \frac{ql^2}{24} \psi_3(u). \end{aligned} \quad (51)$$

The deflection at the middle is obtained by using eqs. (43) and (48), which give

$$\begin{aligned} y_{\max} = (y)_{z=l/2} &= \frac{5}{384} \frac{ql^4}{EI} \cdot \frac{\frac{1}{\cosh u} - 1 + \frac{u^2}{2}}{\frac{5}{32}u^4} \\ &\quad - \frac{ql^4}{16EI} \frac{(u - \tanh u)(\cosh u - 1)}{u^4 \sinh u} \\ &= \frac{ql^4}{384EI} \cdot \varphi_2(u), \end{aligned} \quad (52)$$

where

$$\varphi_2(u) = \frac{24}{u^4} \left( \frac{u^2}{2} - \frac{u \cosh u - u}{\sinh u} \right)$$

The functions  $\varphi_1$ ,  $\psi_3$ , are equal to unity at  $u = 0$ , i.e., when only a transverse load is acting. As the longitudinal tensile force increases, each function decreases, i.e., the longitudinal tensile forces diminish the deflections and the bending moments in laterally loaded tie rods. Some applications of the above table will be given later in discussing the bending of thin plates (see p. 80).

### Problems

1 Find the maximum deflection and the maximum bending moment for a tie rod loaded at the middle.

*Answer*

$$(y)_{\max} = \frac{Pl^3}{48EI} \frac{u - \tanh u}{\frac{1}{3}u^3},$$

$$M_{\max} = \frac{Pl}{4} \frac{\tanh u}{u}$$

2 Find the bending moments  $M_0$  at the ends of a tie rod with built-in ends symmetrically loaded by two forces  $P$  as shown in Fig. 30.

*Solution* The bending moments at the ends are obtained from the equation

$$\frac{P}{S} \left( 1 - \frac{\cosh pb}{\cosh \frac{pl}{2}} \right) + \frac{M_0 l}{2EI} \frac{\tanh u}{u} = 0$$

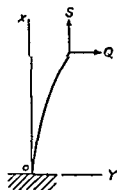


FIG. 35

3 Find the bending moments at the ends of a tie rod with built-in ends loaded by a triangular load as shown in Fig. 29.

*Hint* Use the solution of Prob. 3 on p. 36 together with eq. (46).

4 Find the maximum deflection and the maximum bending moment for the bar shown in Fig. 35.

*Hint* Consider the bar as one half of a tie rod loaded at the middle.

7. Representation of the Deflection Curve by a Trigonometric Series.—In discussing the deflection of beams, it is sometimes very useful to represent the deflection curve in the form of a trigonometric

series.<sup>8</sup> This representation has the advantage that a single mathematical expression for the curve holds for the entire length of the span. Taking the case of the beam with supported ends<sup>9</sup> shown in Fig. 36, the deflection at any point may be represented by the following series:

$$y = a_1 \sin \frac{\pi x}{l} + a_2 \sin \frac{2\pi x}{l} + a_3 \sin \frac{3\pi x}{l} + \dots \quad (a)$$

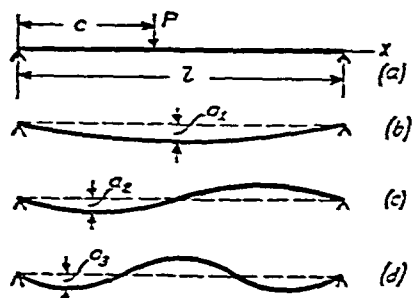


FIG. 36.

Geometrically, this means that the deflection curve may be obtained by superposing simple sinusoidal curves such as are shown in Fig. 36*b*, *c* and *d*, etc. The first term in the series of eq. (a) represents the first curve, the second term represents the second curve, etc. The coefficients  $a_1$ ,  $a_2$ ,  $a_3$  of the series give the maximum ordinates of these sine curves, and the numbers 1, 2, 3, ... give the number of half-waves. By properly determining the coefficients  $a_1$ ,  $a_2$ , ..., the series (eq. a) can be made to represent any deflection curve<sup>10</sup> with a degree of accuracy which depends upon the number of terms taken. These coefficients may be calculated by a consideration of the strain energy of the beam (Part I, eq. 191, p. 317) as given by the equation

$$U = \frac{EI}{2} \int_0^l \left( \frac{d^2 y}{dx^2} \right)^2 dx. \quad (b)$$

The second derivative of  $y$ , from eq. (a), is

$$\frac{d^2 y}{dx^2} = -a_1 \frac{\pi^2}{l^2} \sin \frac{\pi x}{l} - a_2 \frac{2^2 \pi^2}{l^2} \sin \frac{2\pi x}{l} - a_3 \frac{3^2 \pi^2}{l^2} \sin \frac{3\pi x}{l} \dots$$

Eq. (b) involves the square of this derivative, which contains terms of two kinds:

$$a_n^2 \frac{n^4 \pi^4}{l^4} \sin^2 \frac{n\pi x}{l} \quad \text{and} \quad 2a_n a_m \frac{n^2 m^2 \pi^4}{l^4} \sin \frac{n\pi x}{l} \sin \frac{m\pi x}{l}.$$

<sup>8</sup> See the author's paper, "Application of General Coordinates in the Solution of Problems in Bending of Bars and Plates," *Bull. Polytech. Inst. (Kiev)*, 1909 (in Russian); see also H. M. Westergaard, *Proc. Am. Soc. Civ. Engrs.*, Vol. 47, pp. 455-533.

<sup>9</sup> For other cases the analysis becomes too complicated for most practical purposes.

<sup>10</sup> See Byerly, *Fourier Series and Spherical Harmonics*, §§ 19-24. See also Osgood, *Advanced Calculus*, p. 391, 1928.

By direct integration it may be shown that

$$\int_0^l \sin^2 \frac{n\pi x}{l} dx = \frac{l}{2}$$

and

$$\int_0^l \sin \frac{n\pi x}{l} \sin \frac{m\pi x}{l} dx = 0, \quad \text{for } n \neq m$$

Hence, in the integral of eq (b), all terms containing products of coefficients such as  $a_n a_m$  disappear and only the terms with squares of those coefficients remain. Then

$$\begin{aligned} U &= \frac{EI\pi^4}{4l^3} (1 a_1^2 + 2^4 a_2^2 + 3^4 a_3^2 + \dots) \\ &= \frac{EI\pi^4}{4l^3} \sum_{n=1}^{\infty} n^4 a_n^2 \end{aligned} \quad (53)$$

In a previous discussion (see Part I, eq a, p 360)<sup>11</sup> it was shown that if an elastic system undergoes a small displacement from its position of equilibrium, the corresponding increase in the potential energy of the system is equal to the work done by the external forces during such a displacement. When the deflection curve is given by the series of eq (a), small displacements can be obtained by small variations of the coefficients  $a_1, a_2, a_3, \dots$ . If any coefficient  $a_n$  is given an increment  $da_n$ , we have the term  $(a_n + da_n) \sin(n\pi x/l)$  in eq (a) instead of the term  $a_n \sin(n\pi x/l)$ , the other members remaining unchanged. This increment  $da_n$  in the coefficient  $a_n$  represents an additional small deflection given by the sine curve  $da_n \sin(n\pi x/l)$ , superposed upon the original deflection curve. During this additional deflection the external loads do work. In the case of a single load  $P$ , applied at a distance  $c$  from the left support, the point of application of the load undergoes a vertical displacement  $da_n \sin(n\pi c/l)$  and the load does work equal to

$$da_n \left( \sin \frac{n\pi c}{l} \right) P. \quad (c)$$

The increase in the strain energy, given by eq (53), due to the increase  $da_n$  in  $a_n$ , is

$$dU = \frac{\partial U}{\partial a_n} da_n = \frac{EI\pi^4}{2l^3} n^4 a_n da_n \quad (d)$$

<sup>11</sup> See also S. Timoshenko and D. H. Young, *Theory of Structures*, New York, p. 229, 1945.

Equating this to the work given by eq. (c), we obtain

$$\frac{EI\pi^4}{2l^3} n^4 a_n = P \sin \frac{n\pi c}{l},$$

from which

$$a_n = \frac{2Pl^3}{EI\pi^4} \cdot \frac{1}{n^4} \sin \frac{n\pi c}{l}.$$

From this we can determine each of the coefficients in the series of eq. (a), and the deflection curve becomes

$$\begin{aligned} y &= \frac{2Pl^3}{EI\pi^4} \left( \sin \frac{\pi c}{l} \sin \frac{\pi x}{l} + \frac{1}{2^4} \cdot \sin \frac{2\pi c}{l} \sin \frac{2\pi x}{l} + \dots \right) \\ &= \frac{2Pl^3}{EI\pi^4} \sum_{n=1}^{\infty} \frac{1}{n^4} \sin \frac{n\pi c}{l} \sin \frac{n\pi x}{l}. \end{aligned} \quad (54)$$

By using this equation the deflection may be calculated for any value of  $x$ . For example, the deflection at the middle when the load is at the middle ( $c = x = l/2$ ) will be

$$\delta = (y)_{x=l/2} = \frac{2Pl^3}{EI\pi^4} \left( 1 + \frac{1}{3^4} + \frac{1}{5^4} + \dots \right).$$

By taking only the first term of this series we obtain

$$\delta = \frac{2Pl^3}{EI\pi^4} = \frac{Pl^3}{48.7EI}.$$

Comparison with eq. (90) of Part I (p. 146) shows that we obtained 48.7 where the exact value was 48, so that the error made in using only the first term instead of the whole series is about  $1\frac{1}{2}$  per cent. Such accuracy is sufficient in many practical cases, and we shall have other examples where a satisfactory accuracy is obtained by using only one term in the series of eq. (a).

From the solution (eq. 54) for a single load, more complicated problems can be studied by using the method of superposition. For example, consider a beam carrying a uniformly distributed load of intensity  $q$ . Each elemental load  $qdc$  at distance  $c$  from the left support produces a deflection obtained from eq. (54), with  $P = qdc$ , equal to

$$dy = \frac{2qdc l^3}{EI\pi^4} \sum_{n=1}^{\infty} \frac{\sin \frac{n\pi c}{l} \sin \frac{n\pi x}{l}}{n^4}.$$

Integrating this with respect to  $x$  between the limits  $x = 0$  and  $x = l$ , we obtain the deflection produced by the entire load

$$y = \frac{4ql^4}{EI\pi^5} \sum_{n=1}^{\infty} \frac{1}{n^5} \sin \frac{n\pi x}{l} \quad (55)$$

If we use the first term only, the deflection at the middle of a uniformly loaded beam is

$$\delta = \frac{4ql^4}{EI\pi^5} = \frac{ql^4}{76.5EI}$$

Comparing this with the exact solution

$$\delta = \frac{5}{384} \frac{ql^4}{EI} = \frac{ql^4}{76.8EI},$$

we find that the error in taking only the first term was less than  $\frac{1}{2}$  per cent in this case

The trigonometric series of eq (a) is especially useful when the beam is subjected to the action of a longitudinal compressive or tensile force in addition to lateral loading. In the problem shown in Fig 37 the hinge  $B$  approaches the fixed hinge  $A$ , during bending,

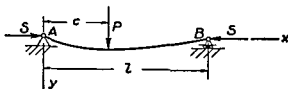


FIG 37

by an amount equal to the difference between the length of the deflection curve and the length of the chord  $AB$ <sup>12</sup>. For a flat curve this difference is (see Part I, p 178)

$$\lambda = \frac{1}{2} \int_0^l \left( \frac{dy}{dx} \right)^2 dx \quad (56)$$

With  $y$  as given by eq (a), the square of its derivative contains terms of the two forms

$$a_n^2 \frac{n^2 \pi^2}{l^2} \cos^2 \frac{n\pi x}{l} \quad \text{and} \quad 2a_n a_m \frac{nm\pi^2}{l^2} \cos \frac{n\pi x}{l} \cos \frac{m\pi x}{l}$$

<sup>12</sup> Longitudinal contraction due to the axial force can be considered as constant for small deflections

By integration it can be shown that

$$\int_0^l \cos^2 \frac{n\pi x}{l} dx = \frac{l}{2}; \quad \int_0^l \cos \frac{n\pi x}{l} \cos \frac{m\pi x}{l} dx = 0, \quad \text{for } n \neq m.$$

The equation for  $\lambda$  then becomes

$$\lambda = \frac{\pi^2}{2I} \sum_{n=1}^{\infty} n^2 a_n^2. \quad (57)$$

To calculate the coefficients  $a_1, a_2, a_3, \dots$  in the series of eq. (a) we again consider the work done by the external forces during a small displacement  $da_n \sin (n\pi x/l)$  from the position of equilibrium. In the case represented in Fig. 37 both the force  $P$  and the longitudinal force  $S$  do work during such a displacement. The displacement  $\lambda$ , due to the increment  $da_n$  in the coefficient  $a_n$ , increases by an amount

$$d\lambda = \frac{\partial \lambda}{\partial a_n} da_n = \frac{\pi^2}{2I} n^2 a_n da_n.$$

Then the work done by the force  $S$  is

$$S \frac{\pi^2}{2I} n^2 a_n da_n.$$

This is added to the work (eq. c) done by the lateral force and the sum is equated to the increase in the potential energy (eq. d). This gives us the following equation for determining any coefficient  $a_n$  in eq. (a):

$$P \sin \frac{n\pi c}{l} da_n + S \frac{\pi^2}{2I} n^2 a_n da_n = \frac{EI\pi^4}{2I^3} n^4 a_n da_n,$$

from which

$$a_n = \frac{2P I^3}{EI\pi^4} \frac{1}{n^2 \left( n^2 - \frac{SI^2}{EI\pi^2} \right)} \sin \frac{n\pi c}{l}.$$

If the ratio of the longitudinal force to the critical value of the axial load (see p. 28) be denoted by  $\alpha = SI^2/EI\pi^2$ , we obtain

$$a_n = \frac{2P I^3}{EI\pi^4} \frac{1}{n^2 (n^2 - \alpha)} \sin \frac{n\pi c}{l}.$$

When this value is substituted into eq (a), the deflection curve is

$$y = \frac{2Pl^3}{EI\pi^4} \left( \frac{1}{1-\alpha} \sin \frac{\pi c}{l} \sin \frac{\pi x}{l} + \frac{1}{2^2(2^2-\alpha)} \sin \frac{2\pi c}{l} \sin \frac{2\pi x}{l} + \dots \right) \\ = \frac{2Pl^3}{EI\pi^4} \sum_{n=1}^{\infty} \frac{1}{n^2(n^2-\alpha)} \sin \frac{n\pi c}{l} \sin \frac{n\pi x}{l} \quad (58)$$

Comparing this with eq (54) for the case of a lateral force  $P$  only, we see that the deflection of the bar increases due to the action of the longitudinal compressive force  $S$ . We have seen that the first term in the series of eq (a) represents a good approximation for the deflection, hence the increase of the deflection produced by the longitudinal force will be approximately in the ratio  $1/(1-\alpha)$ .

This conclusion also holds if there are several transverse loads in the same direction or if there is a continuous load acting on the beam. Denoting by  $\delta_0$  the maximum deflection produced by a lateral load acting alone, we can assume with satisfactory accuracy that under the combined action of compressive forces  $S$  and the lateral load the maximum deflection is

$$\delta = \frac{\delta_0}{1-\alpha} \quad (59)$$

This expression for the maximum deflection can be used also for an approximate calculation of bending moments in a strut. For example, in the case of a uniformly loaded strut with hinged ends the maximum bending moment can be calculated from the following approximate formula.

$$M_{\max} = \frac{ql^2}{8} + \frac{S\delta_0}{1-\alpha} \quad (60)$$

If the longitudinal force is tensile instead of compressive, the method discussed above still holds, with  $-\alpha$  instead of  $\alpha$  in the expressions for the deflection curve (58). If we use only the first term in this expression, the approximate formula for the deflection at the middle becomes

$$\delta = \frac{\delta_0}{1+\alpha}, \quad (61)$$

where  $\delta_0$  denotes the deflection produced by lateral loads only. It must be noted that in the case of longitudinal tensile forces  $\alpha$  can be larger than unity, and the accuracy of the approximate equation



(eq. 61) decreases with increase of  $\alpha$ . For example, for a uniformly distributed lateral load the error in eq. (61) at  $\alpha = 1$  is about 0.3 per cent. At  $\alpha = 2$  the error is 0.7 per cent, and at  $\alpha = 10$  the error is 1.7 per cent.

In the case of a bar with built-in ends an approximate equation, analogous to eq. (61), may be derived for calculating the deflection at the middle, which gives

$$\delta = \frac{\delta_0}{1 + \frac{\alpha}{4}}, \quad (62)$$

in which  $\delta_0$  is the deflection at the middle produced by lateral loads acting alone and  $\alpha$  has the same meaning as before.

The applications of these approximate equations will be shown later in considering the deflection of thin rectangular plates. The method of trigonometric series can also be extended to analyzing beams of variable cross sections.<sup>13</sup>

### Problems

1. Find the deflection curve of the beam shown in Fig. 36a produced by a couple  $M$  applied at the left end, using an infinite series.

*Solution.* Considering  $c$  as very small and substituting  $Pc = M$ ,  $\sin(n\pi c/l) \sim (n\pi c/l)$  into the series of eq. (54), we obtain

$$y = \frac{2Ml^2}{EI\pi^3} \sum_{n=1}^{\infty} \frac{1}{n^3} \sin \frac{n\pi x}{l}.$$

2. Find the deflection curve of a simply supported strut loaded as shown in Fig. 38.

*Answer.*

$$y = \frac{2ql^2}{EI\pi^5} \sum_{n=1}^{\infty} \frac{1}{n^3(n^2 - \alpha)} \left( \cos \frac{n\pi a}{l} - \cos \frac{n\pi b}{l} \right) \sin \frac{n\pi x}{l}.$$

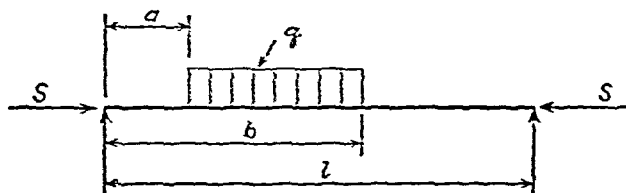


FIG. 38.

<sup>13</sup> See the paper by M. Hetényi, *J. Appl. Mech.*, Vol. 4, p. A-49, 1937.

3 Find the deflection  $\delta$  of the end  $B$  of the vertical column  $AB$ . The column is built in at  $A$  and loaded at  $B$ , as shown in Fig 39

$$\text{Answer } \delta = \frac{Ql^3}{3EI} \frac{1}{1 - \alpha} \quad \text{where} \quad \alpha = \frac{P(2l)^2}{EI\pi^2}$$

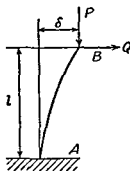


FIG 39

8 Deflection of Bars with Small Initial Curvature —If a bar with a small initial curvature is bent by transverse forces only, the deflections may be calculated by the method used for a straight bar. The conditions are quite different, however, if there are longitudinal forces in addition to the transverse forces. A small initial curvature makes a great change in the effect of these longitudinal forces on the deflection. The solution of this involved problem may be greatly simplified by using trigonometric series for repre-

senting the initial shape of the curve and the deflection due to bending.<sup>14</sup> It is assumed as before that the curved bar has a plane of symmetry in which the external forces act, and the bar is taken as simply supported at the ends. Let  $y_0$  denote the initial ordinates of the center line of the bar, measured from the chord joining the centroids of the ends, and  $y_1$  the deflections produced by the external forces, so that the total ordinates after bending are

$$y = y_0 + y_1 \quad (a)$$

Let the initial deflection curve be represented by the series

$$y_0 = b_1 \sin \frac{\pi x}{l} + b_2 \sin \frac{2\pi x}{l} + \dots \quad (b)$$

and let the deflection produced by the load be

$$y_1 = a_1 \sin \frac{\pi x}{l} + a_2 \sin \frac{2\pi x}{l} + \dots \quad (c)$$

In this case the same expression (eq 53) for strain energy can be used as for straight bars. For the loading shown in Fig 37 it is necessary, in calculating the work done by the longitudinal forces  $S$ , to replace the quantity  $\lambda$  (see eq 56) by

$$\begin{aligned} \lambda_1 - \lambda_0 &= \frac{1}{2} \int_0^l \left[ \frac{d(y_1 + y_0)}{dx} \right]^2 dx - \frac{1}{2} \int_0^l \left( \frac{dy_0}{dx} \right)^2 dx \\ &= \frac{\pi^2}{4l} \left( 2 \sum_{n=1}^{\infty} n^2 a_n b_n + \sum_{n=1}^{\infty} n^2 a_n^2 \right) \end{aligned} \quad (63)$$

<sup>14</sup> See the author's paper, *Festschrift zum 70. Geburtstage August Föppl*, Berlin, p 74, 1924

This represents the longitudinal displacement of one end of the curved bar with respect to the other end during deflection.

We proceed as in the case of straight bars (p. 48) and give to the bar an infinitely small additional deflection  $da_n \sin (n\pi x/l)$ . The work done by the longitudinal forces  $S$  during this deflection is

$$S \frac{\partial(\lambda_1 - \lambda_0)}{\partial a_n} da_n = S \frac{n^2 \pi^2}{2l} (a_n + b_n) da_n.$$

The work done by the load  $P$  is

$$P \sin \frac{n\pi c}{l} da_n,$$

and the increase in strain energy, from eq. (53), is

$$\frac{EI\pi^4}{2l^3} n^4 a_n da_n.$$

The equation for calculating  $a_n$  is

$$\frac{EI\pi^4}{2l^3} n^4 a_n da_n = P \sin \frac{n\pi c}{l} da_n + S \frac{n^2 \pi^2}{2l} (a_n + b_n) da_n,$$

from which

$$a_n = \frac{2Pl^3 \sin \frac{n\pi c}{l} + Sn^2 \pi^2 l^2 b_n}{EI\pi^4 n^4 - Sn^2 \pi^2 l^2}.$$

Substituting into eq. (c) and using the notation

$$\alpha = \frac{Sl^2}{EI\pi^2},$$

we obtain

$$\begin{aligned} y_1 = \frac{2Pl^3}{EI\pi^4} & \left( \frac{\sin \frac{\pi c}{l} \sin \frac{\pi x}{l}}{1 - \alpha} + \frac{\sin \frac{2\pi c}{l} \sin \frac{2\pi x}{l}}{2^4 - 2^2 \alpha} + \dots \right) \\ & + \alpha \left( \frac{b_1 \sin \frac{\pi x}{l}}{1 - \alpha} + \frac{b_2 \sin \frac{2\pi x}{l}}{2^2 - \alpha} + \dots \right). \quad (64) \end{aligned}$$

The first expression on the right-hand side of eq. (64) represents the

deflection of a straight bar (see eq 58), while the second gives the additional deflection due to the initial curvature

Take, for example, a bar which has an initial deflection  $y_0 = b \sin (\pi x/l)$ . The maximum deflection is at the middle of the span and is equal to  $b$ . If only the longitudinal forces  $S$  act on the bar ( $P = 0$ ), the deflection at the middle produced by these forces is obtained from eq (64) by substituting  $P = 0$ ,  $b_1 = b$ ,  $b_2 = b_3 = \dots = 0$ . Then

$$y_1 = \frac{\alpha b \sin \frac{\pi x}{l}}{1 - \alpha} \quad (d)$$

The total ordinates of the center line after bending are

$$y = y_1 + y_0 = \frac{\alpha b \sin \frac{\pi x}{l}}{1 - \alpha} + b \sin \frac{\pi x}{l} = \frac{b}{1 - \alpha} \sin \frac{\pi x}{l} \quad (65)$$

Because of the longitudinal compressive forces  $S$ , the ordinates of the center line increase in the ratio  $1/(1 - \alpha)$ , i e, the increase of the ordinates depends upon the quantity  $\alpha$ , which is the ratio of the longitudinal force to the critical force

If longitudinal tensile forces, instead of compressive forces, act on the bar, it is only necessary to substitute  $-\alpha$  instead of  $\alpha$  in the previous equations. In the particular case in which  $y_0 = b \sin (\pi x/l)$  the ordinates of the center line after deformation become

$$y = \frac{b}{1 + \alpha} \sin \frac{\pi x}{l} \quad (66)$$

It is seen that the longitudinal tensile force diminishes the initial ordinates. Taking, for example, the longitudinal force equal to its critical value ( $\alpha = 1$ ), we find

$$y = \frac{1}{2} b \sin \frac{\pi x}{l},$$

and this longitudinal force reduces the initial ordinates of the bar by half.

## CHAPTER III

### SPECIAL PROBLEMS IN THE BENDING OF BEAMS

9. Local Stresses in the Bending of Beams.—The elementary formula for bending stresses in prismatic bars gives satisfactory results only at some distance from the point of application of the load. Near this point there will be irregularities in stress distribution. In the case of a narrow rectangular cross section, these irregularities can be studied by using the rigorous solution for stress distribution in an infinitely large plate subjected to the action of a concentrated force  $P$ , Fig. 40. The force  $P$  acts in the middle plane of the plate and

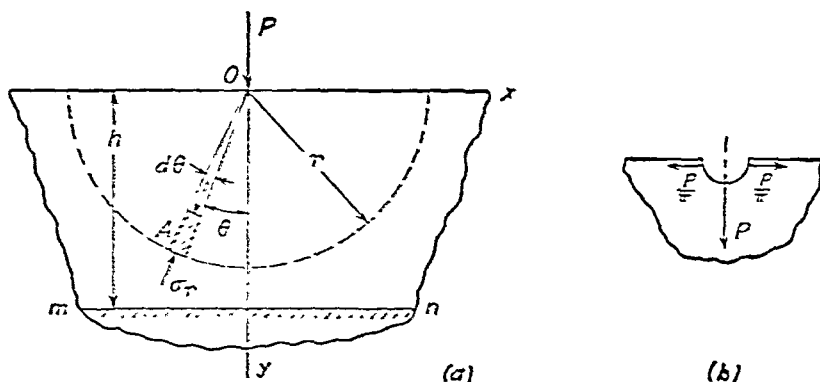


FIG. 40.

perpendicular to the edge of the plate. The stress distribution in this case is a simple radial stress distribution.<sup>1</sup> An element such as is shown at point  $A$  undergoes a simple compression in the radial direction, and the stress is

$$\sigma_r = -k \frac{P \cos \theta}{br}, \quad (a)$$

<sup>1</sup> See S. Timoshenko and J. N. Goodier, *Theory of Elasticity*, New York, p. 85, 1951. Local stresses in built-up girders subjected to a concentrated load were studied by E. W. Parkes, *Proc. Roy. Soc., A*, Vol. 231, No. 1186, 1955, pp. 379-387.

where  $r$  is the radial distance from the point of application of the load and  $b$  is the thickness of the plate. The factor  $k$  is determined from the fact that the stresses  $\sigma_r$  distributed along the length of the semicircle shown in the figure by the broken line maintain equilibrium with the load  $P$ . Hence

$$-2b \int_0^{\pi/2} \sigma_r \cos \theta r d\theta = P.$$

Substituting for  $\sigma_r$  its expression (eq.  $a$ ) we obtain

$$k = \frac{2}{\pi}$$

and eq. (a) becomes

$$\sigma_r = \frac{-2P}{\pi} \cdot \frac{\cos \theta}{br}. \quad (67)$$

If we consider a horizontal plane  $mn$  at a distance  $h$  from the edge of the plate, Fig. 40, the normal stress acting on that plane is

$$\sigma_v = \sigma_r \cos^2 \theta = \frac{-2P}{\pi} \frac{\cos^3 \theta}{br} = \frac{-2P}{\pi} \frac{\cos^4 \theta}{bh}. \quad (68)$$

It is seen that the pressure rapidly diminishes as the angle  $\theta$  increases. It is also seen that the stresses increase with a decrease of the distance  $h$ . Knowing the stresses produced by the action of the concentrated load  $P$  and using the method of superposition, we can readily discuss cases in which several loads are acting.

If a concentrated force is acting at the middle of a rectangular beam of narrow cross section of depth  $h$ , the highly concentrated stresses given by eq. (67) are superposed on bending stresses in the beam, and a complicated stress distribution results near the point of the load application. This perturbation in stress distribution produced by the concentrated load is of a localized character and is of importance only in the close vicinity of the point of application of the load. If we consider a cross section of the beam at a distance from the load larger, say, than one-half the depth of the beam, the stress

distribution in that cross section is approximately that given by the simple beam formula.

By determining the resultant of the horizontal components of the radial pressures  $b\sigma_r r d\theta$  for each half of the broken-line semicircle in Fig. 40*a*, it can be shown that the concentrated force  $P$  produces a wedging action, represented in Fig. 40*b* by the two equal and opposite forces of magnitude  $P/\pi$ . In the case of the beam of depth  $h$  and thickness  $b$ , these forces, acting at a distance  $h/2$  from the axis of the beam, produce in the middle cross section not only tensile stresses given by

$$\sigma_z' = \frac{P}{\pi h b} \quad (b)$$

but also bending stresses given by the expression

$$\sigma_z'' = -\frac{Ph}{2\pi} \frac{y}{I_z}, \quad (c)$$

in which  $Ph/2\pi$  is the bending moment produced by the horizontal forces  $P/\pi$ ,  $y$  is the distance from the axis of the beam, taken positive downwards, and  $I_z = bh^3/12$  is the moment of inertia of the cross section. Superposing the stresses of eqs. (b) and (c) upon the bending stresses given by the ordinary beam formula, we find that the tensile stress in the most remote fiber of the beam in the loaded cross section is

$$\begin{aligned} (\sigma_z)_{y=h/2} &= \frac{Pl}{4} \cdot \frac{6}{bh^2} + \frac{P}{\pi bh} - \frac{3P}{\pi bh} \\ &= \frac{Pl}{4} \cdot \frac{6}{bh^2} \left(1 - \frac{4}{3\pi} \frac{h}{l}\right). \end{aligned} \quad (d)$$

The second term in the parentheses represents the stress produced by the wedging action of the load  $P$ . It is seen that in the case of short beams this stress is of considerable magnitude.

Eq. (d) was developed for a beam of narrow rectangular cross section, but it can also be used for I beams. Assuming that the local action of the load  $P$  will be taken entirely by

the web of the beam, we will again obtain wedging forces  $P/\pi$ , and the corresponding stresses will be

$$\sigma_x' = \frac{P}{\pi A}, \quad \sigma_x'' = -\frac{Ph}{2\pi} \frac{y}{I_z},$$

where  $A$  and  $I_z$  are the area and moment of inertia of the cross section of the beam. Superposing these stresses on the stresses given by the simple beam formula, we obtain for the maximum tensile stress

$$(\sigma_x)_{y=h/2} = \left(\frac{Pl}{4} - \frac{Ph}{2\pi}\right) \frac{h}{2I_z} + \frac{P}{\pi A}. \quad (e)$$

This stress is in satisfactory agreement with experimental results.<sup>2</sup>

To investigate the local stresses at the supports of a beam of narrow rectangular cross section we can utilize the known solutions<sup>3</sup> for the two cases of a wedge loaded as shown in Fig. 41. In these cases we again have simple radial stress dis-

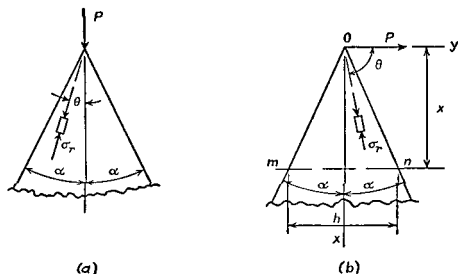


FIG. 41.

tribution and can use formula (a) for the radial compressive stress. The constant  $k$ , for the case of compression of a wedge, Fig. 41a, will be found from the equation

<sup>2</sup> See the paper by Arnold W. Hendry, *Proc. Soc. Exp. Stress Anal.*, Vol. 72, p. 91, 1949.

<sup>3</sup> See Timoshenko and Goodier, *Theory of Elasticity*, p. 96, 1951.



$$\begin{aligned}
 2b \int_0^\alpha \sigma_r \cos \theta r d\theta &= 2 \int_0^\alpha kP \cos^2 \theta d\theta \\
 &= kP \left( \alpha + \frac{\sin 2\alpha}{2} \right) = P,
 \end{aligned}$$

from which

$$k = \frac{1}{\left( \alpha + \frac{\sin 2\alpha}{2} \right)}.$$

Then we obtain from eq. (a) the stress

$$\sigma_r = - \frac{P \cos \theta}{br \left( \alpha + \frac{\sin 2\alpha}{2} \right)}. \quad (69)$$

In the case of the bending of a wedge, Fig. 41*b*, the angle  $\theta$  is again measured from the direction of the force  $P$ , and the equation of statics becomes

$$b \int_{(\pi/2)-\alpha}^{(\pi/2)+\alpha} \sigma_r \cos \theta r d\theta = -P,$$

from which

$$k = \frac{1}{\alpha - \frac{\sin 2\alpha}{2}}.$$

We then obtain for the radial compressive stress the formula

$$\sigma_r = - \frac{P \cos \theta}{br \left( \alpha - \frac{\sin 2\alpha}{2} \right)}. \quad (70)$$

It is seen that if  $\theta$  is larger than  $\pi/2$  the radial stress becomes positive, or tension.

Combining the two solutions, eqs. (69) and (70), the radial stress distribution at the support of a rectangular beam, Fig. 42, can be obtained.

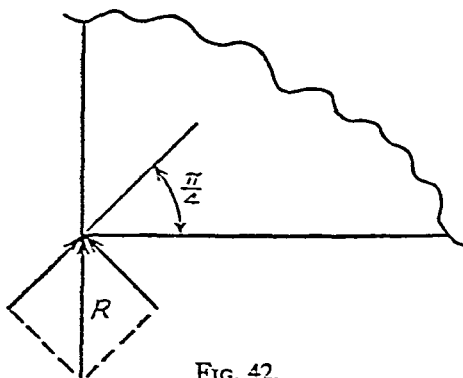


FIG. 42.

### 10. Shearing Stresses in Beams of Variable Cross Section.

—Using eq. (70) of the preceding article, let us now consider the bending stresses in a cantilever having the form of a wedge, Fig. 41*b*. Taking a cross section  $mn$  perpendicular to the  $x$  axis, we obtain (see Part I, eqs. (17) and (18), p. 38)

$$\begin{aligned}\sigma_x &= \sigma_r \sin^2 \theta = \frac{My}{I_z} \frac{4 \tan^3 \alpha \sin^4 \theta}{3(2\alpha - \sin 2\alpha)}; \\ \tau_{xy} &= \frac{\sigma_r}{2} \sin 2\theta = \frac{P}{bh} \frac{16y^2}{h^2} \frac{\tan^3 \alpha \sin^4 \theta}{2\alpha - \sin 2\alpha},\end{aligned}\tag{a}$$

in which

$$h = 2x \tan \alpha; \quad I_z = \frac{bh^3}{12}; \quad M = -Px.$$

For the neutral plane of the wedge,  $\theta = \pi/2$  and the normal and shearing stresses become zero. The maximum normal and shearing stresses occur at  $\theta = (\pi/2) + \alpha$ . They can be calculated from eqs. (a) which give

$$(\sigma_x)_{\max} = -\beta \frac{Mh}{2I_z}, \quad (\tau_{xy})_{\max} = 3\beta \frac{P}{bh},\tag{b}$$

where

$$\beta = \frac{4}{3} \cdot \frac{\tan^3 \alpha \cos^4 \alpha}{2\alpha - \sin 2\alpha}.$$

For  $\alpha = 5^\circ, 10^\circ, 15^\circ$  and  $20^\circ$ , the factor  $\beta$  has the magnitudes 1.00, 0.970, 0.947 and 0.906, respectively.

It is seen that the maximum normal stress  $\sigma_x$ , from the first of formulas (b), is approximately the same as that obtained from the usual beam formula provided the angle  $\alpha$  is sufficiently small. For  $\alpha = 20^\circ$  the error of the simple beam formula, as it is seen from the value of the factor  $\beta$ , is about 10 per cent. The maximum shearing stress, given by the second of formulas (b), is about three times the average shearing stress  $P/bh$  and occurs at points most remote from the neutral axis. This latter fact is in direct opposition to the results obtained for prismatic bars (Part I, p. 116). In many cases the practical shear stresses are of no great importance

and only the normal bending stresses are considered. Then the formula for maximum bending stress, derived for prismatic beams, can also be used with sufficient accuracy for bars of variable cross section, provided the variation of the cross section is not too rapid.

On the assumption that the simple beam formula can be used with sufficient accuracy in calculating the normal bending stresses in beams of variable cross section, the magnitude of the shearing stresses in these beams can be calculated by applying the method already used for prismatic beams (see Part I, p. 116). Assume that a rectangular beam of variable depth  $h$  and constant width  $b$  is bent by a load  $P$  applied at the end, Fig. 43. Taking two adjacent cross sections  $mn$  and  $m_1n_1$

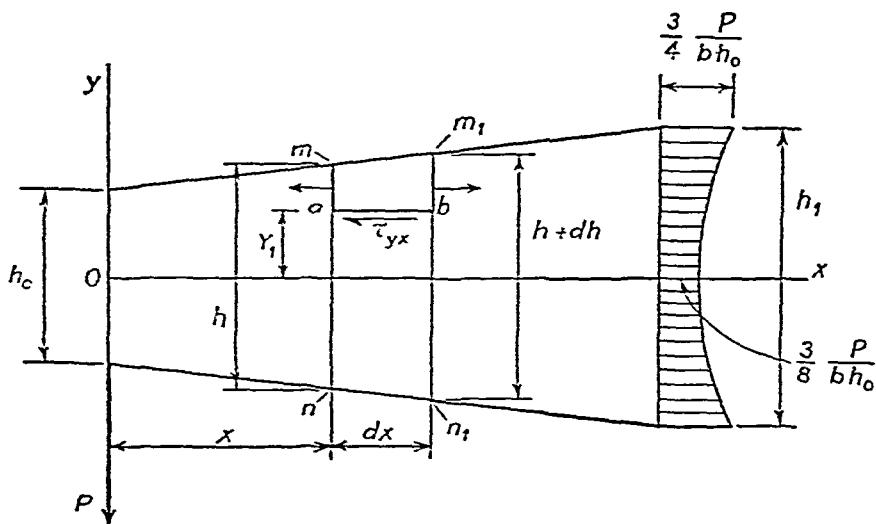


FIG. 43.

and cutting out an element  $mm_1ba$  by a horizontal plane  $ab$ , we find the magnitude of the shearing stress  $\tau_{yx}$  from the equation of equilibrium of this element

$$b \int_{y_1}^{(h+dh)/2} (\sigma_x + d\sigma_x) dy - b \int_{y_1}^{h/2} \sigma_x dy = b \tau_{yx} dx, \quad (c)$$

where

$$\sigma_x = \frac{12Pxy}{bh^3}, \quad \sigma_x + \frac{d\sigma_x}{dx} dx = \frac{12Py}{b} \left[ \frac{x}{h^3} + \frac{d}{dx} \left( \frac{x}{h^3} \right) dx \right].$$

Substituting into eq. (c), we obtain

$$\frac{3Px}{h^2} dh + 6P \frac{d}{dx} \left( \frac{x}{h^3} \right) dx \left( \frac{h}{4} - y_1^2 \right) = b\tau_{yz}dx,$$

from which

$$\tau_{yz} = \frac{3Px}{bh^2} \frac{dh}{dx} + \frac{6P}{b} \left( \frac{h^2}{4} - y_1^2 \right) \frac{d}{dx} \left( \frac{x}{h^3} \right). \quad (d)$$

If  $h$  is given as a certain function of  $x$ ,  $\tau_{yz}$  can be readily calculated from this equation. Assume, for example, that  $h$  is a linear function of  $x$  and that  $h_1 = 2h_0$ , Fig. 43. Then we have  $h = h_0(1 + x/l)$  and we obtain, from eq. (d),

$$\tau_{yz} = \frac{6Ph_0}{bh^2} \left[ \frac{1}{4} + \left( \frac{y_1}{h} \right)^2 \left( \frac{2x - l}{l} \right) \right].$$

It is seen that the distribution of shearing stresses depends not only on  $y_1$  but also on the distance  $x$  from the loaded end. For  $x = 0$  we obtain a parabolic stress distribution as for a prismatic rectangular beam. For the built-in end at  $x = l$  we obtain

$$\tau_{yz} = \frac{3P}{8bh_0} \left( 1 + \frac{y_1^2}{h_0^2} \right).$$

This stress distribution is shown in Fig. 43 by the shaded area.

Eq. (d) was derived by assuming the particular case of loading shown in Fig. 43. Observing that the bending moment is equal to  $Px$  in this case, and substituting  $M$  for  $Px$  in eq. (d), we obtain the equation

$$\tau_{yz} = \frac{3M}{bh^2} \frac{dh}{dx} + \frac{6}{b} \left( \frac{h^2}{4} - y_1^2 \right) \frac{d}{dx} \left( \frac{M}{h^3} \right), \quad (e)$$

which can be used for any loading of the beam.

**11. Effective Width of Thin Flanges.**—The simple bending formula (see Part I, eq. 55, p. 94) shows that bending stresses in a beam are proportional to the distance from the neutral axis. This conclusion is correct as long as we are dealing with beams for which the cross-sectional dimensions are small in comparison with their length, and as long as we are considering points at a considerable distance from the ends. In

practical applications we sometimes use beams with wide flanges, to which the elementary beam formula cannot be applied with sufficient accuracy. Take as an example the case of a beam consisting of a rib and a wide flange shown in Fig. 44. Assuming that the beam is simply supported at the

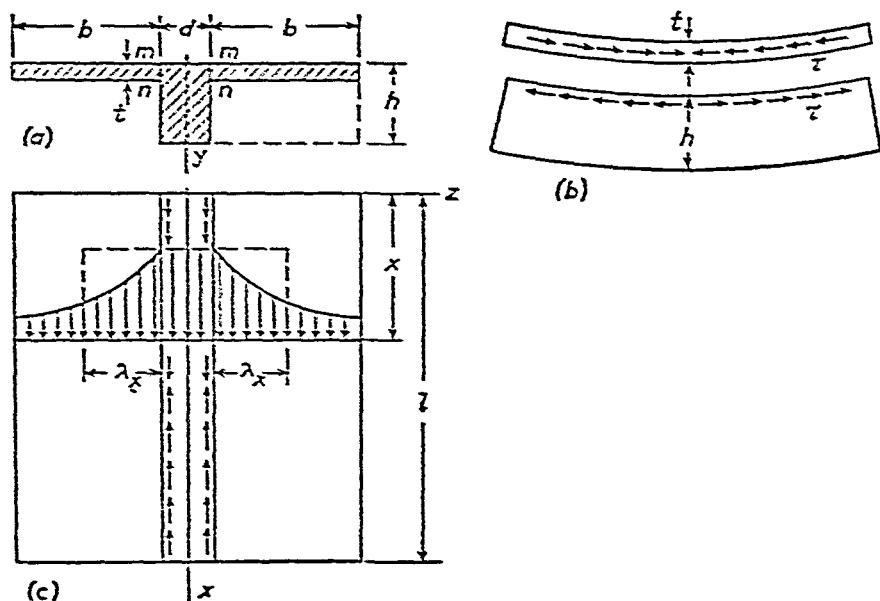


FIG. 44.

ends and loaded in the middle plane  $xy$ , we observe that there are shearing stresses acting between the flanges and the rib along the surfaces  $mn$ , Fig. 44a, and directed as shown in Fig. 44b. It is seen that these stresses tend to reduce the deflection of the rib, i.e., to make it stiffer. At the same time they produce compression of the flanges. Considering a flange at one side of the rib as a rectangular plate subjected to the action of shearing forces along one edge, Fig. 44c, we see that the compressive stresses will not be uniformly distributed along the width of the flange, and a rigorous analysis shows<sup>4</sup> that

<sup>4</sup>A discussion of the rigorous solution, obtained by Th. v. Kármán, is given in Timoshenko and Goodier, *Theory of Elasticity*, p. 171, 1951. See also W. Metzger, *Luftfahrtforsch.*, Vol. 4, p. 1, 1929; K. Girkmann, *Stahlbau*, Vol. 6, p. 98, 1933; H. Reissner, *Z. angew. Math. u. Mech.*, Vol. 14, p. 312, 1934; E. Reissner, *Stahlbau*, Vol. 7, p. 206, 1934; E. Chwalla, *Stahlbau*, Vol. 9, p. 73, 1936; L. Beschkin, *Publ. Internat. Assoc. Bridge and Structural Engrs.*, Vol. 5, p. 65, 1937-8.

the distribution will be as indicated by the shaded area, the maximum stress in the flange being the same as in the upper fibers of the rib. From this nonuniformity of stress distribution it can be concluded that in applying to the beam in Fig. 44a the simple beam formula for maximum bending stress we must use a *reduced width*  $2\lambda_x$ , instead of the actual width  $2b$  of the two flanges, in order to obtain the correct value of the maximum stress. This reduced width, usually called the *effective width*, can be calculated if the compressive stress distribution, shown by the shaded area in Fig. 44c, is known. It is only necessary to make the area of the rectangle, indicated in the figure by the broken lines, equal to the shaded area. The magnitude of  $2\lambda_x$  usually varies along the span of the beam, for it depends on the proportions of the beam and also on the shape of the bending moment diagram.

In the particular case when the width of the flange is very large, say  $2b \geq l$ , and the bending moment diagram is given by the sine curve

$$M = M_1 \sin \frac{\pi x}{l}, \quad (a)$$

the reduced width becomes constant and equal to

$$2\lambda_x = \frac{4l}{\pi(1 + \mu)(3 - \mu)},$$

where  $\mu$  is Poisson's ratio. For  $\mu = 0.3$  we obtain

$$2\lambda_x = 0.363l. \quad (71)$$

Hence, in this particular case the actual beam can be replaced by an *equivalent T beam* of a constant cross section and with the width of the two flanges equal to  $0.363l$ . Applying to this beam the simple beam formulas, we obtain the same maximum stress as for the actual beam.

In a general case of transverse loading, the bending moment diagram can be represented by a sine series:

$$M_x = \Sigma M_n \sin \frac{n\pi x}{l}, \quad (b)$$

in which the coefficients  $M_n$  can be calculated, in each particular case, from the known formula:<sup>5</sup>

$$M_n = \frac{2}{l} \int_0^l M_x \sin \frac{n\pi x}{l} dx. \quad (c)$$

In the case of a uniform load, for example, we have

$$M_x = \frac{qx(l-x)}{2}$$

and formula (c) gives

$$M_n = \frac{4ql^2}{n^3\pi^3}, \quad (d)$$

where  $n = 1, 3, 5, \dots$ .

Having the coefficients  $M_n$  in the series of eq. (b), we obtain the effective width from the rigorous solution, which, in the case of a large width of the flanges, gives

$$\frac{l}{2\lambda_x} = \beta \left[ \frac{M_x}{\sum_{n=1,3,5,\dots} \frac{M_n \sin(n\pi x/l)}{\frac{1}{k} + (k/\beta)n\pi}} - \frac{1}{k} \right], \quad (72)$$

in which  $\beta = A/dh$  is the ratio of the area  $A$  to the cross-sectional area of the rib, and

$$k = \frac{(1 + \mu)(3 - \mu)}{\frac{1}{2}} = 0.878 \quad \text{for } \mu = 0.3.$$

Taking, for example, the case of a beam with uniformly distributed load and substituting eq. (d) for  $M_n$  into formula (72), we find that for various values of the ratio  $\beta$  the variation of the effective width along the length of the beam is as shown in Fig. 45. It is seen that in the middle portion of the span the effective width varies very little and is approximately the same as for a sinusoidal bending moment diagram (see eq. 71). When the effective width is found from formula (72), the maximum stress and maximum deflection are found by applying simple beam formulas to the equivalent beam.

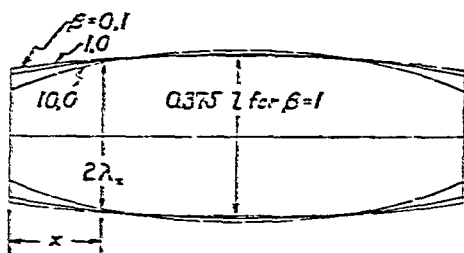


FIG. 45.

We discussed the case in which the flanges of the beam have a very large width. There are also rigorous solutions for the case in

<sup>5</sup> See Art. 7.

which the flanges are not very wide and also for the case of a long rectangular slab reinforced by a system of identical and equidistant ribs. In all these cases the problem is reduced to that of calculating stresses and deflections in an equivalent beam<sup>6</sup>

A problem of the same general nature as that discussed above occurs in aircraft structures. Consider a box beam, Fig 46, formed from

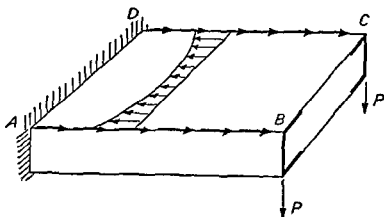


FIG 46

two channels to which are attached two thin sheets by riveting or welding along the edges. If the whole beam is built in at the left hand end and loaded as a cantilever by two forces  $P$  applied to the channels at the other end, the elementary bending theory will give a tensile bending stress in the sheet  $ABCD$  uniformly distributed across any section parallel to  $BC$ . Actually, however, the sheet acquires its tensile stress from shear stresses on its edges communicated to it by the channels, as indicated in Fig 46. The distribution of tensile stress across the width of the sheet will not be uniform, but, as in Fig 46, will be higher at the edges than at the middle. This departure from the uniformity assumed by the elementary theory is known as *shear lag*, since it involves a shear deformation in the sheets. The problem has been analyzed by strain-energy considerations with the help of some simplifying assumptions.<sup>7</sup>

<sup>6</sup> These rigorous solutions have found application in specifications for concrete slabs reinforced by ribs. In airplane design the presence of non uniform stress distribution in wide flanges is taken care of by using an approximate theory which is discussed in papers by P. Kuhn, *Nat. Advisory Comm. Aeronaut. Repts.*, No 608, 1937, and No 636, 1938. See also H. Ebner, *Luftfahrtforsch.*, Vol 14, p 93, 1937, and Vol 15, p 527, 1938.

<sup>7</sup> See the papers by E. Reissner, *Quart. Appl. Math.*, Vol 4, p 268, 1946, J. Hadji Argyris, *Aeronaut. Research Council (Brit.) Repts. and Mem.*, No 2038, 1944, J. Hadji Argyris and H. L. Cox, *ibid.*, No 1969, 1944. References to earlier publications are given in these papers.



**12. Limitations of the Method of Superposition.**—In discussing the bending of beams it was shown that the calculation of deflections can be greatly simplified by using the method of superposition (see Part I, p. 162). This method can always be used provided the bending of the beam does not introduce any changes in the action of the external forces. For example, small deflections of beams by lateral loads do not change the bending moment diagrams for these loads, and superposition can be successfully used. But if we have bending combined with axial tension or compression, the deflection produced by the lateral loads changes the action of the axial forces, and the latter produce not only axial tension or compression but also some additional bending. In such cases, as we have seen (Art. 4), there are some limitations of the method of superposition; we can use this method only with regard to the lateral loads, assuming that the axial force always remains constant. There are other cases in which small deflections of beams may introduce considerable changes in the action of forces. In such cases the method of superposition fails. Some examples of this kind will now be discussed.

As a first example let us consider the bending of the cantilever  $AB$ , Fig. 47, if during bending it comes gradually into contact with a rigid cylindrical supporting surface  $AC$  having a

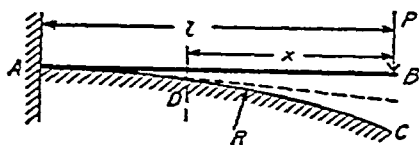


FIG. 47.

a constant curvature  $1/R$  and a horizontal tangent at  $A$ . It is seen that as long as the curvature of the beam at the end  $A$ , as given by the formula

$$\frac{1}{r} = \frac{M}{EI_z} = \frac{Pl}{EI_z}, \quad (a)$$

is less than the curvature of the support  $1/R$ , the cantilever will touch the surface  $AC$  only at the point  $A$ , and the deflection  $\delta$  at the end  $B$  will be given by the known formula

$$\delta = \frac{Pl^3}{3EI_z}. \quad (b)$$

From the equation

$$\frac{1}{r} = \frac{Pl}{EI_z} = \frac{1}{R} \quad (c)$$

we can obtain the limiting value of the load  $P$ , for which the beam begins to come into contact with the cylindrical supporting surface beyond the point  $A$ . Let  $P_1 = EI_z/lR$  be this limiting value of the load; then for  $P > P_1$  a part  $AD$  of the beam will be supported as indicated in Fig. 47 by the broken line. The length  $x$  of the unsupported portion of the cantilever is obtained from the condition that at  $D$  the curvature  $1/r$  of the beam is equal to the curvature of the supporting surface; hence

$$\frac{Px}{EI_z} = \frac{1}{R},$$

and we obtain

$$x = \frac{EI_z}{PR}. \quad (d)$$

The total deflection at the end  $B$  of the cantilever consists of three parts: (1) deflection of the portion  $DB$  of the beam as a simple cantilever, which is

$$\delta_1 = \frac{Px^3}{3EI_z} = \frac{(EI_z)^2}{3P^2R^3}, \quad (e)$$

(2) deflection owing to the slope at  $D$ , which is

$$\delta_2 = \frac{x(l-x)}{R} = \frac{EI_z}{PR^2} \left( l - \frac{EI_z}{PR} \right), \quad (f)$$

and (3) deflection representing the distance of the point  $D$  from the horizontal tangent at  $A$ , which is

$$\delta_3 \approx \frac{(l-x)^2}{2R} = \left( l - \frac{EI_z}{PR} \right)^2 \frac{1}{2R}. \quad (g)$$

Summing up these three parts, we obtain the total deflection:

$$\delta = \delta_1 + \delta_2 + \delta_3 = \frac{l^2}{2R} - \frac{1}{6} \frac{(EI_z)^2}{P^2R^3}. \quad (h)$$

This expression for the deflection must be used instead of eq. (b) if  $P$  is larger than the limiting value  $P_1 = EI_z/lR$ . Note that the deflection is no longer proportional to  $P$ . If, in addition to  $P$ , there is a load  $Q$  applied at the end  $B$  of the cantilever, the total deflection will not be equal to the sum of the deflections produced by  $P$  and produced by  $Q$  if both are considered to be acting alone. Hence the method of superposition does not hold in this case.

As a second example let us consider the case of a uniformly loaded beam with built-in ends, as shown in Fig. 48. It is

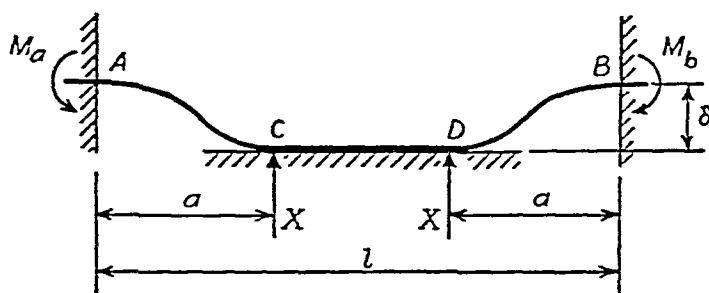


FIG. 48.

assumed that during bending the middle portion of the beam is supported by a rigid horizontal foundation so that along this portion the deflection is constant and equal to  $\delta$ . It is seen that if the deflection at the middle is less than  $\delta$ , we have an ordinary case of the bending of a beam with built-in ends. The limiting value  $q_1$  of the load is obtained from the known equation

$$\frac{1}{384} \frac{q_1 l^4}{EI_z} = \delta. \quad (i)$$

For a load of intensity  $q_1$  the beam just touches the horizontal foundation at the middle point. With a further increase of the load  $q$  a reaction  $2X$  appears at the point of contact. The magnitude of the reaction can be determined from the equation

$$\frac{q l^4}{384 EI_z} - \frac{2X l^3}{192 EI_z} = \delta. \quad (j)$$

This condition holds up to the value  $q_2$  of the load, when the

bending moment and curvature at the middle of the beam vanish. The value of  $q_2$  may be found from the equation

$$\frac{q_2 l^2}{24} - \frac{2Xl}{8} = 0, \quad (k)$$

which gives

$$2X = \frac{q_2 l}{3}.$$

Substituting into eq. (j) we obtain

$$\frac{1}{3} \frac{q_2 l^4}{384EI_z} = \delta. \quad (l)$$

Comparing this with eq. (i), we find that  $q_2 = 3q_1$ . For an intensity of load equal to  $q_2$  the element of the beam at the middle becomes straight and touches the horizontal foundation.

For an intensity of load larger than  $q_2$ , a portion of the beam will be supported by the foundation as shown in Fig. 48. This part remains straight so that there is no bending moment acting in the portion  $CD$  of the beam, and the load is balanced by the uniformly distributed reaction. At the ends  $C$  and  $D$ , however, concentrated reactions  $X$  will act on the unsupported portions of the beam. The length  $a$  of the unsupported portions of the beam and the magnitude  $X$  of the concentrated reactions can be obtained by considering the portion  $AC$  of the beam as a cantilever with a uniform load  $q$  and with a concentrated load  $X$  at the end. Observing that the cross section at  $C$  does not rotate during bending and using eqs. (94) and (100) from Part I, pp. 150 and 151, we obtain

$$\frac{qa^3}{6EI_z} = \frac{Xa^2}{2EI_z},$$

from which

$$X = \frac{qa}{3}. \quad (m)$$

Another equation is obtained from the condition that the deflection at  $C$  is equal to  $\delta$ . Using the known formulas for

the deflection of the cantilever, we obtain

$$\frac{qa^4}{8EI_z} - \frac{Xa^3}{3EI_z} = \delta. \quad (n)$$

Solving eqs. (m) and (n) we find

$$a = \sqrt[4]{\frac{72\delta EI_z}{q}}, \quad X = \sqrt[4]{\frac{8\delta EI_z q^3}{9}}. \quad (o)$$

It is immediately apparent that the reaction  $X$  is not proportional to the load. The numerical maximum of the bending moment, which is at the built-in ends, is obtained from the equation

$$|M_a| = |M_b| = \frac{qa^2}{2} - Xa,$$

which gives

$$M_a = \frac{qa^2}{6} = \sqrt{2\delta EI_z q}. \quad (p)$$

Again we see that the bending moment does not increase in the same proportion as the load. Hence the method of superposition cannot be used.

### Problems

1. Find the deflection of the cantilever shown in Fig. 47 if there is a uniformly distributed load  $q$  instead of a force  $P$ .

2. Find an expression for the deflection at the center of a beam loaded at the middle by a force  $P$ , Fig. 49, and supported by two identical cylindrical surfaces of radius  $R$ .

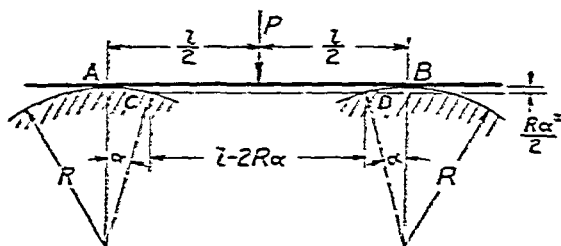


FIG. 49.

*Solution.* As the load  $P$  increases, the points of contact of the beam with the supporting surfaces move inwards and the span dimin-

ishes; hence the deflection increases in a smaller proportion than does the load  $P$ . The angle  $\alpha$ , defining the positions of the points of contact, is found from the condition that at these points the deflection curve is tangent to the supporting surfaces; hence, for small values of  $\alpha$ ,

$$\alpha = \frac{P(l - 2R\alpha)^2}{16EI_z}.$$

Having  $\alpha$ , we obtain the deflection at the middle from the equation:

$$\delta = \frac{P(l - 2R\alpha)^3}{48EI_z} + \frac{R\alpha^2}{2}.$$

3. Solve the preceding problem assuming that the beam is built in at the points  $A$  and  $B$ .

4. Solve Prob. 2 if the load is not at the middle of the span  $AB$ .

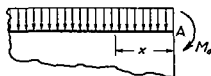


FIG 50

5. A long, uniformly loaded beam is supported by a horizontal rigid foundation, Fig. 50. Find the angle  $\alpha$  of rotation of the end  $A$  and the length  $x$  which will be bent by the moment  $M_0$  applied at the end.

*Solution.* The length  $x$  is found from the equation

$$\frac{qx^3}{24EI} = \frac{M_0x}{6EI}.$$

The angle of rotation at the end  $A$  is

$$\alpha = \frac{M_0x}{3EI} - \frac{qx^3}{24EI}.$$

6. A vertical force  $P$  is applied to the end  $A$  of a prismatic bar  $AB$  supported along the entire length by a horizontal rigid plane,

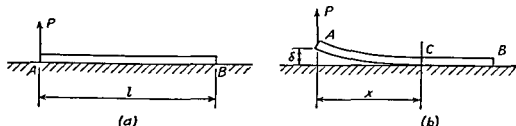


FIG 51.

Fig. 51. Investigate bending of the bar assuming that  $P$  is less than half of the weight  $ql$  of the bar.

*Solution.* The portion  $BC$  of the bar (Fig. 51*b*) remains straight and the bending moment at  $C$  is zero. Hence the length  $x$  of the portion  $AC$  of the bar subjected to bending will be found from the equation

$$\frac{qx^2}{2} = Px,$$

from which

$$x = \frac{2P}{q}.$$

At point  $C$  there will act a concentrated vertical reaction equal to  $P$ , and the portion  $AC$  of the bar is in the same condition as a uniformly loaded beam of span  $x$ . The deflection of the end  $A$  of the bar is

$$\delta = \frac{qx^4}{24EI_z}.$$

## CHAPTER IV

### THIN PLATES AND SHELLS

13. **Bending of a Plate to a Cylindrical Surface.**—Assume that a rectangular plate of uniform thickness  $h$  is bent to a cylindrical surface (Fig 52)<sup>1</sup> In such a case it is sufficient to consider only one strip of unit width, such as  $AB$ , as a beam of rectangular cross section and of length  $l$  From the condition of continuity it may be concluded that there will be no distortion in the cross section of the strip during bending, such as shown in Fig 82*b*, Part I, p 93 Hence a fiber lengthwise of the strip such as  $ss$  (Fig 53) suffers not only the longi-

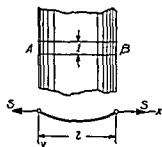


FIG 52

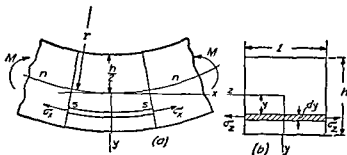


FIG 53

tudinal tensile stress  $\sigma_x$  but also tensile stress  $\sigma_z$  in the lateral direction, which must be such as to prevent lateral contraction of the fiber We assume, as before (see Part I, p 92), that cross sections of the strip remain plane during bending Hence the unit elongations in the  $x$  and  $z$  directions

<sup>1</sup> Such bending occurs in the case of long rectangular plates if the acting forces do not vary along the length of the plate and if only the portion of the plate at a sufficient distance from the ends is considered



are

$$\epsilon_z = \frac{y}{r}; \quad \epsilon_x = 0.$$

The corresponding stresses in the  $x$  and  $z$  directions are then obtained as in the case of tension in two perpendicular directions. By the use of eqs. (38), Part I, p. 55, we find

$$\sigma_z = \frac{\epsilon_z E}{1 - \mu^2} = \frac{Ey}{(1 - \mu^2)r}; \quad \sigma_x = \frac{\mu \epsilon_z E}{1 - \mu^2} = \frac{\mu Ey}{(1 - \mu^2)r}.$$

We now proceed as in the case of the bending of a bar and calculate the bending moment at any cross section of the strip. Then

$$M = \int_{-h/2}^{+h/2} \sigma_z y dy = \frac{E}{(1 - \mu^2)r} \int_{-h/2}^{+h/2} y^2 dy = \frac{Eh^3}{12(1 - \mu^2)r},$$

from which

$$\frac{1}{r} = \frac{M}{D}, \quad (73)$$

where

$$D = \frac{Eh^3}{12(1 - \mu^2)}. \quad (74)$$

This quantity is called the *flexural rigidity* of a plate and takes the place of  $EI_z$  which was used in discussing bending of beams. Comparison of eq. (73) for the strip with eq. (56), Part I, p. 95, for a bar shows that the rigidity of the strip within the plate is larger than that of an isolated bar of the same cross section in the ratio  $1:(1 - \mu^2)$ .

The experiments show that in the case of the bending of an isolated thin strip of large width  $b$ , distortion of the cross section takes place only near the edges (Fig. 54*b*) and the middle portion  $aa$  of the strip is bent into a cylindrical form;<sup>2</sup> hence

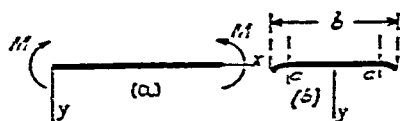


FIG. 54.

<sup>2</sup> Explanation of this phenomenon is given by G. F. C. Searle, *Experimental Elasticity*, Cambridge, 1908. See also H. Lamb, *Proc. London Math. Soc.*, Vol. 21, p. 70, 1891, and the author's paper in *Mech. Engrg.*, p. 259, 1923.

eq. (73) is applicable in calculating deflections and the strip will prove more rigid than would be expected from the simple beam formula.

For small deflections of the strip  $AB$  (Fig. 52) the curvature  $1/r$  can be replaced by its approximate value  $d^2y/dx^2$  and the differential equation for the deflection curve of the strip is

$$D \frac{d^2y}{dx^2} = -M. \quad (75)$$

The discussion of the bending of a plate to a cylindrical surface involves the integration of this equation. The particular case in which bending to a cylindrical surface is brought about by a uniformly distributed load is discussed in the next article.

#### 14. Bending of a Long, Uniformly Loaded Rectangular Plate.—

If a rectangular plate whose length is large in comparison with its width is uniformly loaded, then it may be assumed that near the center, where the maximum deflection and stresses occur, the deflection surface is nearly cylindrical and eq (75) may be used to calculate the deflections<sup>3</sup> Let us consider this important problem<sup>4</sup> for two extreme conditions. (1) the edges of the plate are simply supported and can rotate freely during bending, and (2) the edges are built-in. In both cases it is assumed that there are no displacements at the edges in the plane of the plate. Then an elemental strip such as  $AB$  in Fig 52 is in the same condition as a tie rod with uniform lateral loading (see Art. 6) and the tensile forces  $S$ . The magnitude of the forces  $S$  is found from the condition that the extension of the strip is equal to the difference between the length of the deflection curve and the length  $l$  of the chord  $AB$  (Fig. 52).

*Simply Supported Edges.* In the case of simply supported edges, a good approximation for  $S$  is obtained by assuming that the deflection curve is a sine curve

$$y = \delta \sin \frac{\pi x}{l}, \quad (a)$$

<sup>3</sup> If the length is three times the width for a simply supported plate and twice the width for a clamped plate, the solution derived on this assumption is sufficiently accurate

<sup>4</sup> A solution of the problem was given by I G Boobnov. See his book, *Theory of Structure of Ships*, St Petersburg, Vol 2, p 545, 1914 A discussion of this problem, together with calculation of stresses in the hull of a ship, is given in S. Timoshenko, *Theory of Plates and Shells*, New York, 1940

where  $\delta$  denotes the deflection at the middle. Then, from eq. (56), p. 50, the extension of the center line of the strip is

$$\lambda = \frac{1}{2} \int_0^l \left( \frac{dy}{dx} \right)^2 dx = \frac{\pi^2 \delta^2}{4l}. \quad (b)$$

Taking for the deflection at the middle the approximate eq. (61), we have

$$\delta = \frac{\delta_0}{1 + \alpha}, \quad (c)$$

in which

$$\delta_0 = \frac{5}{384} \frac{ql^4}{D} \quad \text{and} \quad \alpha = \frac{S}{S_{cr}} = \frac{Sl^2}{\pi^2 D}. \quad (76)$$

Substituting in eq. (b), we obtain

$$\lambda = \frac{\pi^2}{4l} \cdot \frac{\delta_0^2}{(1 + \alpha)^2}. \quad (d)$$

The lateral contraction of the strip in the plane of the plate during bending is assumed to be zero; hence from eqs. (74) and (76) the elongation of the center line of the strip produced by forces  $S$  is

$$\lambda = \frac{Sl(1 - \mu^2)}{Ek} = \frac{\pi^2 \alpha k^2}{12l}. \quad (e)$$

Equating (d) and (e), the equation for determining  $\alpha$  and hence the longitudinal force  $S$ , is obtained in the form

$$\alpha(1 + \alpha)^2 = \frac{3\delta_0^2}{k^2}. \quad (77)$$

If the load  $q$  and the dimensions of the plate are given, the right side of eq. (77) can easily be calculated. The solution of eq. (77) can be simplified by letting

$$1 + \alpha = x. \quad (f)$$

Then this equation becomes

$$x^3 - x^2 = \frac{3\delta_0^2}{k^2},$$

i.e., the quantity  $x$  is such that the difference between its cube and its square has a known value. Thus  $x$  can be determined from a slide rule or a suitable table and  $\alpha$  found from eq. (f). The deflection and stresses in the strip  $AB$  are then calculated by using Table 4

for tie rods (see p 44) In using this table it is necessary to remember that, from eqs (23) and (76),

$$u = \frac{pl}{2} = \frac{\pi}{2} \sqrt{\alpha} \quad (78)$$

Take, for example, a steel plate of dimensions  $l = 45$  in and  $h = \frac{3}{8}$  in loaded by a uniformly distributed load  $q = 10$  lb per sq in Then eq (77) becomes

$$\alpha(1 + \alpha)^2 = 290, \quad (g)$$

from which

$$\alpha = 5.97 \quad \text{and} \quad u = \frac{\pi}{2} \sqrt{\alpha} = 3.83$$

The tensile stress produced by the longitudinal force  $S$  is

$$\sigma_x' = \frac{S}{h} = \frac{\alpha S_{cr}}{h} = \frac{\alpha \pi^2 D}{hl^2} = 11,300 \text{ lb per sq in}$$

and the maximum bending moment at the middle of the strip, from eq (45), is

$$M_{\max} = \frac{ql^2}{8} \psi_1(u) \quad (h)$$

Again using Table 4, we find by interpolation that for  $u = 3.83$ ,  $\psi_1(u) = 0.131$  This shows that owing to the action of the longitudinal force  $S$ , the bending moment is greatly diminished and is only about 13 per cent of the moment produced by the action of transverse loading alone Using eq (h),

$$M_{\max} = \frac{10 \times 45^2}{8} \times 0.131 = 332 \text{ in lb}$$

The corresponding maximum bending stress is

$$\sigma_x'' = \frac{6M_{\max}}{h^2} = \frac{6 \times 332 \times 8^2}{3^2} = 14,200 \text{ lb per sq in}$$

and, superposing the tensile and bending stresses, the maximum stress is

$$\sigma_{\max} = \sigma_x' + \sigma_x'' = 11,300 + 14,200 = 25,500 \text{ lb per sq in}$$

It may be seen that owing to the action of the longitudinal force the maximum stress does not increase in the same proportion as the intensity of the load For example, in the above numerical illustra

tion if we take  $q = 20$  lb per sq in., then from eq. (g)

$$\alpha(1 + \alpha)^2 = 290 \times 4 = 1,160,$$

from which

$$\alpha = 9.85; \quad u = 4.93.$$

The tensile stress produced by the longitudinal force  $S$  is

$$\sigma_z' = \frac{S}{h} = 18,600 \text{ lb per sq in.}$$

and  $\psi_1(u) = 0.082$  for  $u = 4.93$ . The maximum bending stress is

$$\sigma_z'' = \frac{6M_{\max}}{h^2} = \frac{6 \times 20 \times 45^2 \times 8^2}{8 \times 3^2} \times 0.082 = 17,900 \text{ lb per sq in.}$$

and the maximum total stress is

$$\sigma_{\max} = \sigma_z' + \sigma_z'' = 18,600 + 17,900 = 36,500 \text{ lb per sq in.}$$

In other words, because of the action of the longitudinal forces  $S$  the stresses increase less rapidly than the load. In this case, when the load was doubled the maximum stress increased only 43 per cent.

*Clamped Edges.* In the case of clamped edges eq. (a) is replaced by <sup>5</sup> the equation

$$y = \frac{\delta}{2} \left( 1 - \cos \frac{2\pi x}{l} \right), \quad (i)$$

which satisfies conditions at the clamped edges because the deflection  $y$  and the slope  $dy/dx$  both become zero at  $x = 0$  and at  $x = l$ . Substituting eq. (i) into eq. (b), the extension of the center line of the strip is

$$\lambda = \frac{1}{2} \int_0^l \left( \frac{dy}{dx} \right)^2 dx = \frac{\pi^2 \delta^2}{4l}. \quad (j)$$

For the deflection at the middle we use the approximate eq. (62)

$$\delta = \frac{\delta_0}{1 + \frac{\alpha}{4}}$$

and find, from eqs. (j) and (e), the following equation for  $\alpha$ :

$$\alpha \left( 1 + \frac{\alpha}{4} \right)^2 = \frac{3\delta_0^2}{h^2} \quad (79)$$

<sup>5</sup> See the author's paper, *loc. cit.*, p. 47.

or, by letting  $1 + (\alpha/4) = x$ ,

$$x^3 - x^2 = \frac{3}{4} \frac{\delta_0^2}{h^2} \quad (k)$$

In the previous numerical example with  $q = 10$  lb per sq in, eq (k) becomes

$$x^3 - x^2 = 2.90,$$

from which  $x = 1.849$  and  $\alpha = 3.40$ . Hence the tensile force is less than in the case of simply supported edges by the ratio  $3.40/5.97$ , and we obtain

$$\sigma_x' = \frac{3.40}{5.97} \times 11,300 = 6,430 \text{ lb per sq in}$$

In calculating the bending stresses Table 4, p 44, is used. Noting that in our case  $u = (\pi/2)\sqrt{\alpha} = 2.89$ , we find from the table by interpolating that  $\psi_2 = 0.686$ ,  $\psi_3 = 0.488$ . The bending moment at each clamped edge is

$$M = -0.686 \frac{ql^2}{12} = -1,150 \text{ in lb}$$

The corresponding maximum bending stress is

$$\sigma_x'' = 49,300 \text{ lb per sq in}$$

The maximum total stress is <sup>6</sup>

$$\sigma_{\max} = \sigma_x' + \sigma_x'' = 6,430 + 49,300 = 55,700 \text{ lb per sq in}$$

Comparison of this stress with that obtained above for the same plate with simply supported edges shows that clamping the edges increases the maximum stress. This result can be explained as follows. As a result of clamping the edges, the deflection of the plate is diminished, and the longitudinal force  $S$  and its effect on the bending moment are also diminished. In the case of simply supported edges, the maximum bending moment was only 0.131 of that produced by the transverse load alone. But in the case of clamped edges, the bending moment at these edges is 0.686 of that produced by the transverse load alone, i.e., the effect of the longitudinal force is more pronounced in the case of simply supported edges.

This approximate method can be used in the calculation of stresses in the plates of a ship's hull submitted to hydrostatic pressure.

The maximum stress evidently depends on the intensity of the load  $q$  and on the ratio  $l/h$ . The magnitude of this stress for the case

<sup>6</sup> It is assumed that the steel has a proportional limit above the stress calculated.

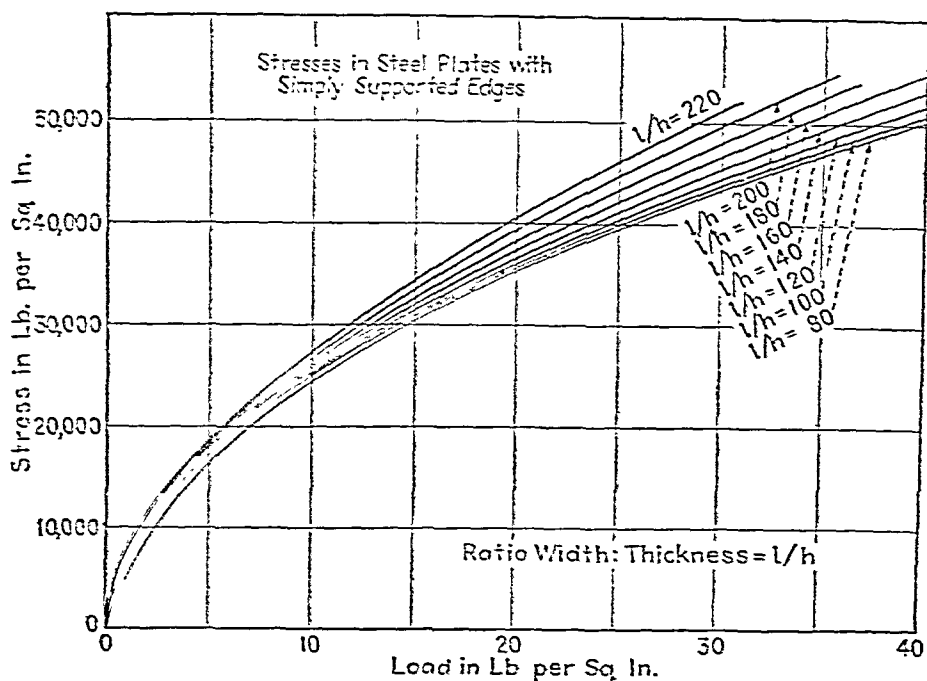


FIG. 55.

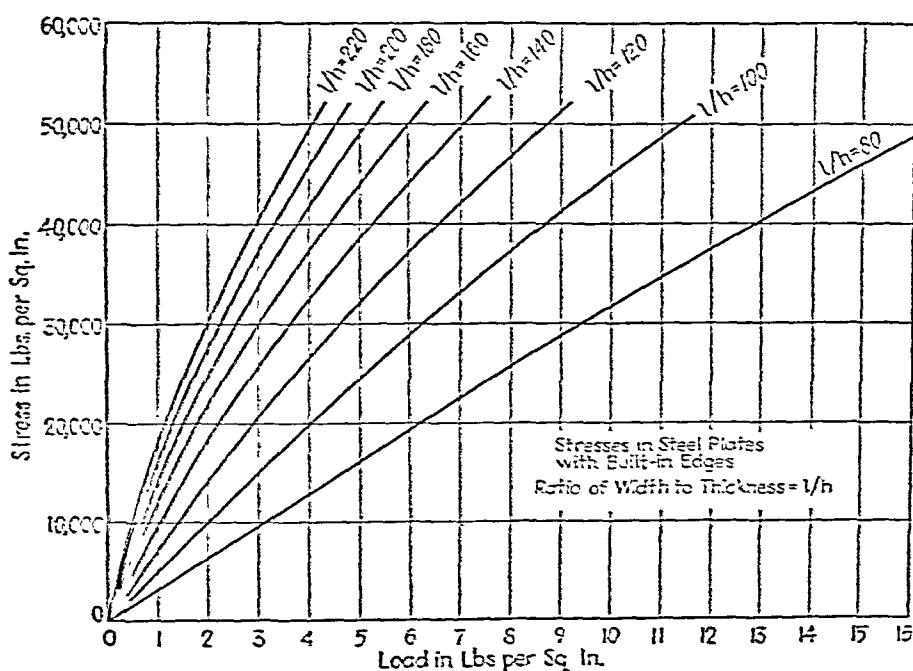


FIG. 56.

of simply supported edges and for various values of the ratio  $l/h$  is represented by curves <sup>7</sup> in Fig 55. It is seen that because of the presence of tensile forces  $S$ , which increase with the load, the maximum stress is not proportional to the load  $q$ .

In Fig 56 the curves for maximum stress in the case of plates with built in edges are given. It is seen that for small values of the intensity of the load  $q$ , when the effect of the axial force on the deflections of the strip is small, the maximum stress increases approximately in the same ratio as  $q$  increases. But for larger values of  $q$  the relation between the load and the maximum stress becomes non linear.

**15 Deflection of Long Rectangular Plates Having a Small Initial Cylindrical Curvature** <sup>8</sup>—In this problem, we may use the results already obtained for the bending of bars with small initial curvature (p 54). The edges of the plate are assumed to be simply supported, and the coordinate axes and an elemental strip are taken as in Fig 52. Let

$$y_0 = b \sin \frac{\pi x}{l} \quad (a)$$

represent the small initial deflection of the plate, with the maximum deflection at the middle equal to  $b$ . If a uniform load  $q$  is applied, an additional deflection is produced, accompanied by an extension of the *middle surface* <sup>9</sup> of the plate. As before, let  $S$  denote the tensile force on the strip  $AB$  of unit width and  $\alpha$  the ratio of this force to the critical force  $S_{cr} = \pi^2 D/l^2$ . Then the additional deflection produced by the load  $q$  is

$$y_1 = \frac{\delta_0}{1 + \alpha} \sin \frac{\pi x}{l} - \frac{\alpha b}{1 + \alpha} \sin \frac{\pi x}{l} \quad (b)$$

The first term on the right hand side represents the approximate expression for the deflection of a straight line strip, which was used before for flat plates, the second term represents the effect of the initial curvature (see eq (d), p 56). By adding together eqs (a) and (b) we obtain the total ordinates of the center line

$$\begin{aligned} y = y_0 + y_1 &= b \sin \frac{\pi x}{l} + \frac{\delta_0}{1 + \alpha} \sin \frac{\pi x}{l} - \frac{\alpha b}{1 + \alpha} \sin \frac{\pi x}{l} \\ &= \frac{b + \delta_0}{1 + \alpha} \sin \frac{\pi x}{l} \end{aligned} \quad (c)$$

<sup>7</sup> These curves are taken from the paper by S. Way presented at the meeting of the Applied Mechanics Division, A S M E, New Haven, June 1932.

<sup>8</sup> See the author's article, *loc cit*, p 54.

<sup>9</sup> The middle surface is the surface midway between the faces of the plate.



The magnitude of  $\alpha$  is determined by considering the extension of the strip  $AB$ . Using the same reasoning as in Art. 14, we obtain the following expression for this extension:

$$\lambda = \frac{1}{2} \int_0^l \left( \frac{dy}{dx} \right)^2 dx - \frac{1}{2} \int_0^l \left( \frac{dy_0}{dx} \right)^2 dx.$$

Substituting from eqs. (a) and (c) for  $y_0$  and  $y$  and integrating, we obtain

$$\lambda = \frac{\pi^2}{4l} \left[ \left( \frac{b + \delta_0}{1 + \alpha} \right)^2 - b^2 \right].$$

Setting this quantity equal to the extension produced by the longitudinal force  $S$  (eq. e, Art. 14, p. 79), we obtain

$$\frac{\pi^2}{4l} \left[ \left( \frac{b + \delta_0}{1 + \alpha} \right)^2 - b^2 \right] = \frac{\pi^2 \alpha h^2}{12l}$$

or

$$\alpha(1 + \alpha)^2 = 3 \left( \frac{b + \delta_0}{h} \right)^2 - 3 \frac{b^2}{h^2} (1 + \alpha)^2. \quad (80)$$

If  $b = 0$ , this reduces to eq. (77) for a flat plate.

Take as an example a steel plate of the same dimensions as in Art. 14:

$$l = 45 \text{ in.}, \quad h = \frac{3}{8} \text{ in.}, \quad q = 10 \text{ lb per sq in.},$$

and assume  $b = \frac{3}{8} \text{ in.}$  Then

$$\delta_0 = \frac{5}{384} \frac{ql^4}{D} = 3.686 \text{ in.},$$

and eq. (80) becomes

$$\alpha(1 + \alpha)^2 = 351.6 - 3(1 + \alpha)^2. \quad (d)$$

As before, let

$$1 + \alpha = x;$$

then

$$x^3 + 2x^2 = 351.6,$$

from which

$$x = 6.45, \quad \alpha = 5.45.$$

The tensile stress produced by the longitudinal force  $S$  is

$$\sigma_z' = \frac{S}{h} = \frac{\alpha \pi^2 D}{hl^2} = 10,200 \text{ lb per sq in.}$$

These stresses are proportional to the distance  $z$  from the neutral surface. The moments of the internal forces acting on the sides of the element are equated to the moments of the external couples, giving the following equations.

$$\int_{-h/2}^{+h/2} \sigma_x z dy dz = M_1 dy, \quad (d)$$

$$\int_{-h/2}^{+h/2} \sigma_y z dx dz = M_2 dx \quad (e)$$

Substituting from eqs (b) and (c) for  $\sigma_x$  and  $\sigma_y$  and noting that

$$\frac{E}{1 - \mu^2} \int_{-h/2}^{+h/2} z^2 dz = \frac{Eh^3}{12(1 - \mu^2)} = D,$$

where  $D$  denotes the *flexural rigidity of the plate* (eq 74), we find

$$D \left( \frac{1}{r_1} + \mu \frac{1}{r_2} \right) = M_1, \quad (81)$$

$$D \left( \frac{1}{r_2} + \mu \frac{1}{r_1} \right) = M_2, \quad (82)$$

which correspond to eq (56), Part I, p 95, for the pure bending of a straight bar. Denoting by  $w$  the small deflections of the plate in the  $z$  direction, the approximate formulas for the curvatures are

$$\frac{1}{r_1} = - \frac{\partial^2 w}{\partial x^2} \quad \text{and} \quad \frac{1}{r_2} = - \frac{\partial^2 w}{\partial y^2}$$

In terms of  $w$ , eqs (81) and (82) then become

$$-D \left( \frac{\partial^2 w}{\partial x^2} + \mu \frac{\partial^2 w}{\partial y^2} \right) = M_1 \quad (83)$$

$$-D \left( \frac{\partial^2 w}{\partial y^2} + \mu \frac{\partial^2 w}{\partial x^2} \right) = M_2 \quad (84)$$

These equations correspond to eq (79), Part I, p 139, for the deflection curve of a straight bar

In the particular case in which  $M_1 = M_2 = M$ , the curvatures of the deflection surface in two perpendicular directions are equal and the surface is spherical. The curvature of the sphere, from eq. (81), is

$$\frac{1}{r} = \frac{M}{D(1 + \mu)}. \quad (85)$$

Such a spherical deflection surface is obtained for a plate of any shape if bending moments  $M$  are uniformly distributed along its edge.

In the preceding discussion it has been assumed that there is no change in the length of the fibers of the middle surface, i.e., that this surface is the neutral surface in the bent plate. This condition can be rigorously satisfied only if the surface of the bent plate is a *developable* surface, such as the cylindrical surface discussed in Art. 15. For nondevelopable surfaces the above assumption is sufficiently accurate only if the deflection  $w$  of the plate is small in comparison with its thickness  $h$ . To show this, let us consider the bending of a circular plate produced by couples  $M$  uniformly distributed along the edge. It follows from the preceding theory that the deflection surface is a sphere with radius given by eq. (85).

Let  $AOB$  (Fig. 59) represent a diametral section of the bent circular plate, with  $a$  the outer radius of the plate and  $\delta$  the deflection at the middle. (We assume first that there is no stretching of the middle plane of the plate along a meridian such as  $AOB$ .) Then arc  $OB = a$ ,  $\varphi = a/r$ , and  $CB = a_1 = r \sin \varphi$ . In such a case the deflection of the plate is obviously accompanied by a compressive strain in the circumferential direction. The magnitude of this strain at the edge of the plate is

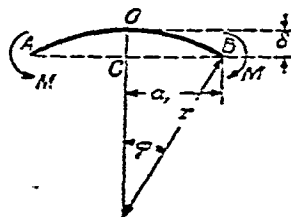


FIG. 59.

$$\epsilon = \frac{a - a_1}{a} = \frac{r\varphi - r \sin \varphi}{r\varphi}.$$

For a small deflection  $\delta$ , the angle  $\varphi$  is small, and therefore

$\sin \varphi \approx \varphi - (\varphi^3/6)$ , so that

$$\epsilon = \frac{\varphi^2}{6}, \quad (f)$$

or, noting that

$$\delta = r(1 - \cos \varphi) \approx \frac{r\varphi^2}{2},$$

we obtain

$$\epsilon = \frac{\delta}{3r} \quad (g)$$

This represents the upper limit of circumferential strain at the edge. It was obtained by assuming that the meridional strain is zero. Under actual conditions there will be a certain amount of strain in the meridional direction and the true circumferential compression will be smaller than that given by eq (g).<sup>10</sup>

The approximate theory of the bending of plates neglects entirely the strain in the middle plane and considers only strains such as are given by eqs (a), for which the maximum value in the above example is  $h/2r$ . Hence a strain such as that given by eq (g) can be neglected and the middle surface considered as unstrained if  $\delta/3r$  is small in comparison with  $h/2r$ , that is, if the deflection  $\delta$  is small in comparison with the thickness of the plate  $h$ . Only within this assumption can the results given later for various special cases of the bending of plates be used with sufficient accuracy.

**17. Thermal Stresses in Plates.**—Eq (85) in Art 16, for bending to a spherical shape, is very useful in calculating thermal stresses produced in a plate by nonuniform heating. Let  $t$  denote the difference in temperature between the upper and the lower face of the plate, and let  $\alpha$  denote the coefficient of

<sup>10</sup> If the deflections are not small and the strain in the middle surface is taken into consideration, it has been shown that in the case of the pure bending of a circular plate of radius  $a \approx 23h$ , the circumferential compressive stress in the middle surface at the edge is about 18 per cent of the maximum bending stress when the deflection at the middle is equal to 0.6 of the thickness of the plate. See the author's paper in *Memoirs Inst Engrs Ways of Communication*, St Petersburg, 1915. See also his *Theory of Plates and Shells*, p 332, 1940.

linear expansion of the material. Assuming that the variation of the temperature through the thickness of the plate follows a linear law, then the corresponding expansions follow the same law; and if the edge of the plate is free, the deflection produced by these expansions will be spherical.<sup>11</sup> The difference between the maximum expansion and the expansion at the middle surface is  $\alpha t/2$ , and the curvature resulting from this nonuniform expansion is given by the equation

$$\frac{\alpha t}{2} = \frac{h}{2r},$$

from which

$$\frac{1}{r} = \frac{\alpha t}{h}. \quad (86)$$

This bending of the plate does not produce any stresses provided the edges are free and the deflection is small as compared with the thickness.

However, if the edge of the plate be clamped, heating will produce bending moments along the edge. The magnitude of these moments is such as to eliminate the curvature produced by the nonuniform heating and given by eq. (86), since only in this manner can the conditions at the clamped edge be satisfied. From eqs. (85) and (86) we obtain the following equation for the bending moment per unit length of the clamped edge:

$$M = \frac{\alpha t(1 + \mu)D}{h}.$$

Since  $M$  acts on a rectangular area of unit width and of depth  $h$ , the corresponding maximum bending stress is

$$\sigma_{\max} = \frac{6M}{h^2} = \frac{6\alpha t(1 + \mu)D}{h^3} = \frac{\alpha t}{2} \frac{E}{1 - \mu}. \quad (87)$$

This stress is proportional to the coefficient of thermal expansion

<sup>11</sup> It is assumed that the deflections are small in comparison with the thickness  $h$  of the plate.

sion  $\alpha$ , to the difference in temperature  $t$  at the two faces<sup>12</sup> of the plate and to the modulus of elasticity. The difference in temperature  $t$  is likely to increase with the thickness of the plate, therefore greater thermal stress can be expected in thick plates than in thin ones. Note that eq (87), developed for flat plates, can also be used with sufficient accuracy in cases of spherical and cylindrical shells (see p 135).

**18. Bending of Circular Plates Loaded Symmetrically with Respect to the Center.**<sup>13</sup>—The deflection surface in this case is

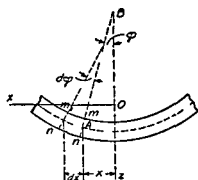


FIG 60

symmetrical about the axis perpendicular to the plate through its center, and a consideration of a diametral section through this axis is sufficient for calculating deflections and stresses. Fig 60 represents such a diametral section, with the axis of symmetry  $Oz$ . Let  $w$  denote the deflection of the plate in the  $z$  direction at any point  $A$  at distance

$x$  from the axis. For small values of  $w$  we may let  $\varphi = -(dw/dx)$  represent the slope of the deflection surface at the same point. Then the curvature of the plate in the diametral section  $xz$  is

$$\frac{1}{r_1} = -\frac{d^2w}{dx^2} = \frac{d\varphi}{dx} \quad (a)$$

In determining the radius of curvature  $r_2$  in the direction perpendicular to the  $xz$  plane it is necessary to note that after deflection of the plate, sections such as  $nm$  form a conical surface whose apex  $B$  is the point of intersection of  $nm$  with the axis  $Oz$ . Then  $AB$  represents the radius  $r_2$ , and from Fig 60 we obtain

$$\frac{1}{r_2} = \frac{\varphi}{x} \quad (b)$$

<sup>12</sup> It must be noted that  $t$  denotes the difference in temperature between the two faces of the plate and not that between liquids or gases in contact with the plate. The latter, owing to abrupt change in temperature at the plate surface, may be much greater than  $t$ .

<sup>13</sup> This case of bending was developed by Poisson, *Mém de l'Acad (Paris)*, Vol 8, 1829.

We now neglect the effect of shear on bending and assume the same relations between the bending moments and the curvatures as in the case of the pure bending of a plate (Art. 16). Eqs. (81) and (82) can therefore be used; and substituting from eqs. (a) and (b) into them, we find

$$M_1 = D \left( \frac{d\varphi}{dx} + \mu \frac{\varphi}{x} \right), \quad (88)$$

$$M_2 = D \left( \frac{\varphi}{x} + \mu \frac{d\varphi}{dx} \right). \quad (89)$$

In these equations  $M_1$  and  $M_2$  denote bending moments per unit length,  $M_1$  acting along cylindrical sections such as  $mn$ , and  $M_2$  acting along diametral sections  $xz$ .

Eqs. (88) and (89) contain only one variable,  $\varphi$ , which can be determined from the equation of equilibrium of an element  $abcd$  (Fig. 61) cut out from the plate by two cylindrical sections  $ab$  and  $cd$  and by two diametral sections  $aO$  and  $bO$ . The couple acting on the side  $cd$  of the element is

$$M_1 x d\theta. \quad (c)$$

The corresponding couple on the side  $ab$  is

$$\left( M_1 + \frac{dM_1}{dx} dx \right) (x + dx) d\theta. \quad (d)$$

The couples on the sides  $ad$  and  $bc$  are each equal to  $M_2 dx$ , and they have a resultant in the plane  $xz$  equal to

$$M_2 dx d\theta \quad (e)$$

In addition to these couples there are shearing forces  $V$  on the sides  $ab$  and  $cd$ .<sup>14</sup> If  $V$  represents the shearing force per unit length, the total shearing force acting on the side  $cd$  of

<sup>14</sup> It follows from symmetry that there are no shearing forces on the sides  $bc$  and  $ad$  of the element.

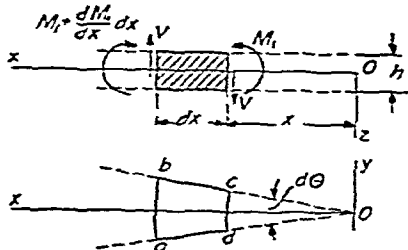


FIG. 61.

the element is  $Vxd\theta$ . Neglecting small quantities of higher order, a shearing force of the same magnitude acts on the side  $ab$ . These two forces give a couple in the plane  $xz$  equal to

$$Vxd\theta dx. \quad (f)$$

Summing up moments (c), (d), (e) and (f) with proper signs, the equation of equilibrium of the element  $abcd$  is

$$\left(M_1 + \frac{dM_1}{dx} dx\right)(x + dx)d\theta - M_1xd\theta - M_2dxd\theta + Vxdxd\theta = 0,$$

from which we find, by neglecting small quantities of higher order,

$$M_1 + \frac{dM_1}{dx} x - M_2 + Vx = 0. \quad (g)$$

On substituting the values of eqs. (88) and (89) for  $M_1$  and  $M_2$ , eq. (g) becomes

$$\frac{d^2\varphi}{dx^2} + \frac{1}{x} \frac{d\varphi}{dx} - \frac{\varphi}{x^2} = -\frac{V}{D}. \quad (90)$$

In any particular case of a symmetrically loaded circular plate the shearing force  $V$  may be determined from statics, and then eq. (90) can be used for determining the slope  $\varphi$  and the deflection  $w$  of the plate.

Consider, for example, a circular plate loaded with a uniformly distributed load of intensity  $q$  and a concentrated load  $P$  applied at the center. Taking a section of the plate cut out by a cylindrical surface with axis  $Oz$  and radius  $x$ , we can find the shearing force  $V$  per unit length of this section from an equation of equilibrium of the inner part of the plate cut out by the cylindrical surface. The load acting on this part of the plate is  $P + \pi x^2 q$ . This load must be equal to the resultant of the shearing forces distributed over the cylindrical section; hence

$$2\pi xV = P + \pi x^2 q$$

and

$$V = \frac{qx}{2} + \frac{P}{2\pi x}. \quad (91)$$



Substituting into eq. (90), we obtain

$$\frac{d^2\varphi}{dx^2} + \frac{1}{x} \frac{d\varphi}{dx} - \frac{\varphi}{x^2} = -\frac{1}{D} \left( \frac{qx}{2} + \frac{P}{2\pi x} \right),$$

or

$$\frac{d}{dx} \left[ \frac{1}{x} \frac{d}{dx} (x\varphi) \right] = -\frac{1}{D} \left( \frac{qx}{2} + \frac{P}{2\pi x} \right),$$

from which by integration we obtain

$$\frac{1}{x} \frac{d}{dx} (x\varphi) = -\frac{1}{D} \left( \frac{qx^2}{4} + \frac{P}{2\pi} \log_e x \right) + C_1, \quad (h)$$

where  $C_1$  is a constant of integration. The integration of eq. (h) gives

$$x\varphi = -\frac{qx^4}{16D} - \frac{P}{2\pi D} \left( \frac{x^2 \log_e x}{2} - \frac{x^2}{4} \right) + C_1 \frac{x^2}{2} + C_2,$$

or

$$\varphi = -\frac{qx^3}{16D} - \frac{Px}{8\pi D} (2 \log_e x - 1) + \frac{C_1 x}{2} + \frac{C_2}{x}, \quad (92)$$

where  $C_2$  is the second constant of integration. For small deflections (Fig. 60) we have

$$\varphi = -\frac{dw}{dx},$$

which gives the following equation for the deflection:

$$\frac{dw}{dx} = \frac{qx^3}{16D} + \frac{Px}{8\pi D} (2 \log_e x - 1) - \frac{C_1 x}{2} - \frac{C_2}{x},$$

from which, by integration,

$$w = \frac{qx^4}{64D} + \frac{Px^2}{8\pi D} (\log_e x - 1) - \frac{C_1 x^2}{4} - C_2 \log_e x + C_3. \quad (93)$$

The constants of integration  $C_1$ ,  $C_2$  and  $C_3$  must be determined in each particular case from the conditions at the edge of the plate.

In the discussion above, eqs. (81) and (82) were used on the assumption that the middle surface of the plate is a neutral surface, i.e., that there is no strain in this plane. This assumption, as we have seen (p. 90), is justified only if the edges of the plate are free from stresses in the middle plane of the plate and if the deflections are small in comparison with the thickness of the plate.

**19. Bending of a Uniformly Loaded Circular Plate.**—*Plate Clamped at the Edge.*—The slope and the deflection in this case are given by eqs. (92) and (93) by putting  $P = 0$  in those equations. Denoting by  $a$  the outer radius of the plate, we have, for clamped edges,  $\varphi = 0$  for  $x = a$  and for  $x = 0$ . These conditions give the following equations for calculating the arbitrary constants  $C_1$  and  $C_2$  from eq. (92):

$$\left( \frac{qx^3}{16D} - \frac{C_1x}{2} - \frac{C_2}{x} \right)_{x=a} = 0,$$

$$\left( \frac{qx^3}{16D} - \frac{C_1x}{2} - \frac{C_2}{x} \right)_{x=0} = 0,$$

from which

$$C_2 = 0 \quad \text{and} \quad C_1 = \frac{qa^2}{8D}. \quad (a)$$

Substituting these values into eq. (92), we obtain

$$\varphi = \frac{qx}{16D} (a^2 - x^2). \quad (94)$$

The deflections are now calculated from eq. (93). In this equation we first set  $P = 0$  and then substitute the values of the arbitrary constants  $C_1$  and  $C_2$  from eqs. (a), obtaining

$$w = \frac{qx^4}{64D} - \frac{qa^2x^2}{32D} + C_3. \quad (b)$$

The constant  $C_3$  is found from the condition that at the edge of the plate the deflection is zero. Hence

$$\frac{qa^4}{64D} - \frac{qa^4}{32D} + C_3 = 0,$$

from which

$$C_3 = \frac{qa^4}{64D}.$$

Substituting this value in eq. (b), we obtain

$$w = \frac{q}{64D} (a^2 - x^2)^2. \quad (95)$$

The maximum deflection is at the center of the plate and is

$$\delta = \frac{qa^4}{64D}. \quad (96)$$

This deflection is equal to  $\frac{3}{8}$  of the deflection of a strip (Fig. 52) clamped at the ends and of length equal to the diameter of the plate.

The bending moments in the plate are obtained from eqs. (88) and (89) by substituting the value from eq. (94) for  $\varphi$  into those equations. In this way we obtain

$$M_1 = \frac{q}{16} [a^2(1 + \mu) - x^2(3 + \mu)], \quad (c)$$

$$M_2 = \frac{q}{16} [a^2(1 + \mu) - x^2(1 + 3\mu)]. \quad (d)$$

At the edge of the plate ( $x = a$ ) the moments are

$$M_1 = -\frac{qa^2}{8}; \quad M_2 = -\frac{\mu qa^2}{8}; \quad (e)$$

and at the center ( $x = 0$ ) the moments are

$$M_1 = M_2 = \frac{1 + \mu}{16} qa^2. \quad (f)$$

The maximum stress is at the edge of the plate and is equal to

$$(\sigma_x)_{\max} = \frac{6}{h^2} \frac{qa^2}{8} = \frac{3}{4} \frac{qa^2}{h^2}. \quad (97)$$

*Plate Simply Supported at the Edge.*—The method of superposition will be used in calculating the deflections of a plate

simply supported at the edge. It was shown above that in the

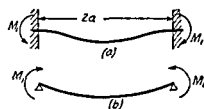


FIG 62

case of a clamped edge there are negative bending moments  $M_1 = -(qa^2/8)$  acting along the edge (Fig. 62a). If this case is combined with that of pure bending, shown in Fig. 62b, so as to eliminate the bending moment at the edge, we obtain

the bending of a plate simply supported at the edge. The deflections due to pure bending (Fig. 62b) are obtained from eq. (85). Substituting in this equation  $M = qa^2/8$ , we find

$$\frac{1}{r} = \frac{qa^2}{8D(1 + \mu)}.$$

The corresponding deflection at the middle for a spherical surface is (Part I, p. 97)

$$\delta_1 = \frac{a^2}{2r} = \frac{qa^4}{16D(1 + \mu)}.$$

This must be added to the deflection (eq. 96) of a plate clamped at the edge in order to obtain the deflection of a plate simply supported at the edge. Thus for the deflection at the center we obtain

$$\delta = \frac{qa^4}{64D} + \frac{qa^4}{16D(1 + \mu)} = \frac{5 + \mu}{64(1 + \mu)D} qa^4. \quad (98)$$

For  $\mu = 0.3$ , this deflection is about four times as large as when the edges are clamped.

In calculating bending moments the constant bending moment  $qa^2/8$  must be superposed on the moments of eqs. (c) and (d) found above for the case of a clamped edge. Hence

$$M_1 = \frac{q}{16} (3 + \mu)(a^2 - x^2),$$

$$M_2 = \frac{q}{16} [a^2(3 + \mu) - x^2(1 + 3\mu)].$$

The maximum bending moment is at the center, where

$$M_1 = M_2 = \frac{3 + \mu}{16} qa^2.$$

The corresponding maximum stress is

$$(\sigma_x)_{\max} = (\sigma_y)_{\max} = \frac{6M_1}{h^2} = \frac{3(3 + \mu)}{8} \cdot \frac{qa^2}{h^2}. \quad (99)$$

For comparison of the bending stresses  $\sigma_x$  and  $\sigma_y$  at the lower sides of the plates with clamped and simply supported edges, the variation in these stresses along the radius of the plates is graphically represented in Fig. 63. Measuring the ordi-

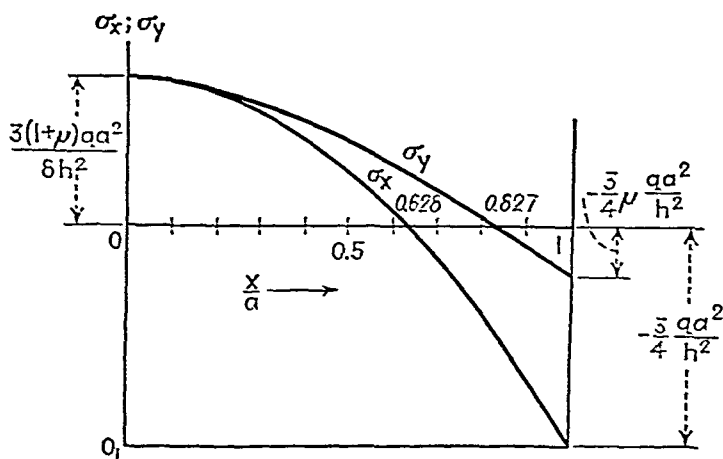


FIG. 63.

nates from the horizontal axis passing through the point  $O$ , we obtain the stresses for a plate with a clamped edge. Adding to these stresses the constant value  $3qa^2/4h^2$ , i.e., measuring the ordinates from the horizontal axis passing through the point  $O_1$  in Fig. 63, we obtain the stresses for a simply supported plate. It may be seen that a more favorable stress condition is obtained by clamping the edge.

In the preceding discussion the effect of shearing strain on the deflection has been neglected. When the thickness of the plate is not small in comparison with its radius, this effect may

be considerable and must be taken into account <sup>15</sup> The additional deflection due to shear is found by the same method as in the case of beams (see Part I, p 170) In the case of uniform loading the shearing force, from eq (91), is

$$V = \frac{qx}{2}$$

If we assume the same distribution of shearing stresses over the thickness of the plate as in the case of a bar of rectangular cross section, the maximum shearing stress is at the middle surface and its magnitude at a distance  $x$  from the center of the plate is

$$\tau = \frac{3}{2} \frac{V}{h} = \frac{3}{4} \frac{qx}{h}$$

The corresponding shearing strain at the middle surface of the plate is

$$\gamma = \frac{\tau}{G} = \frac{3}{4} \frac{qx}{Gh},$$

and the additional deflection due to distortion of an element such as  $abcd$  in Fig 61 is

$$\gamma dx = \frac{3}{4} \frac{qxdx}{Gh}$$

Summing up these deflections along the length of the radius of the plate and noting that at the edge the deflection is zero, we find

$$w_1 = \frac{3}{4} \frac{q}{Gh} \int_x^a x dx = \frac{3}{8} \frac{q}{Gh} (a^2 - x^2)$$

This is added to the deflection (eq 95) due to the bending moment in order to obtain the total deflection for a plate with a clamped edge,

$$w = \frac{q}{64D} (a^2 - x^2)^2 + \frac{3}{8} \frac{q}{Gh} (a^2 - x^2),$$

<sup>15</sup> The increase in deflection due to shear was demonstrated by experiments made by G M Russell, *Engineering*, Vol 123, p 343, 1927 See also the paper by H Carrington, *ibid*, Vol 125, p 31, 1928

or, using eq. (74),

$$w = \frac{q}{64D} \left[ (a^2 - x^2)^2 + \frac{4}{1 - \mu} h^2 (a^2 - x^2) \right]. \quad (100)$$

The deflection at the center is

$$\delta = \frac{qa^4}{64D} \left( 1 + \frac{4}{1 - \mu} \frac{h^2}{a^2} \right). \quad (101)$$

In the case of thick plates the second term in the parentheses, which represents the effect of shearing stresses, may be of practical importance.

The above theory of the bending of circular plates is based on the assumption that the deflections are small in comparison with the thickness. For larger deflections the stretching of the middle surface of the plate must be considered. If this is done it can be shown that at larger deflections the plate becomes stiffer than the theory above indicates,<sup>16</sup> and the deflections are no longer proportional to the load. In the case of a uniformly loaded circular plate clamped at the edge, this deflection can be calculated from the following equation:<sup>17</sup>

$$\delta + 0.58 \frac{\delta^3}{h^2} = \frac{qa^4}{64D}, \quad (102)$$

which is in good agreement with experiments.

In practical applications, very thin uniformly loaded plates are sometimes used. In such cases the bending stresses may be small in comparison with the stresses due to the stretching of the middle surface, and the plate can be considered as a thin membrane which has no flexural rigidity.<sup>18</sup> The deflection at the middle of a uniformly loaded circular membrane is given by the equation

$$\delta = 0.662a \sqrt[3]{\frac{qa}{Eh}}. \quad (103)$$

<sup>16</sup> See the author's paper, *loc. cit.*, p. 90. See also his *Theory of Plates and Shells*, 1940.

<sup>17</sup> *Ibid.*, p. 336.

<sup>18</sup> H. Hencky, *Z. Math. u. Phys.*, Vol. 63, p. 311, 1915.

We obtain an analogous equation by neglecting  $\delta$  in comparison with the term containing  $\delta^3$  in eq (102). Experiments made on thin membranes are in good agreement with eq (103)<sup>19</sup>

**20 Bending of Circular Plates of Variable Thickness**—In the case of a uniformly loaded circular plate of variable thickness the variation of the thickness with the radial distance can be expressed with sufficient accuracy by the equation

$$\frac{h}{h_0} = e^{-\beta x^2/6a^2},$$

in which  $h/h_0$  is the ratio of the thickness at the radial distance  $x$  to the thickness  $h_0$  at the center, and  $\beta$  is a constant. The shapes of the diametral sections of plates for various values of the constant  $\beta$  are shown in Fig. 64.

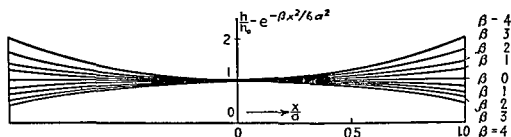


FIG. 64

The maximum bending stress  $\sigma_x$  in the radial direction at a radial distance  $x$  from the center can be expressed by the equation

$$\sigma_x = \gamma \frac{3qa^2}{h_0^2},$$

in which  $\gamma$  is a factor varying with the radial distance  $x$ . The values of this factor<sup>20</sup> for a plate with clamped edges are given

<sup>19</sup> Bruno Eck, *Z angew Math u Mech*, Vol 7, p 498, 1927. For information on corrugated diaphragms see *Nat Advisory Comm Aeronaut Tech Notes*, No 738, 1939.

<sup>20</sup> These values are given in the dissertation by O Pichler, *Die Biegung kreissymmetrischer Platten von veränderlicher Dicke*, Berlin, 1928. A more recent investigation of the bending of circular plates of variable thickness was made by Henri Favre and Eric Chabloz, *Z angew Math u Mech*, Vol 1, p 317, 1950, and *Bull tech Suisse romande*, No 1, 1952. See also H Favre's paper presented at the International Congress of Applied Mechanics, Istanbul, 1952.



by the curves in Fig. 65. For a simply supported plate these values are given in Fig. 66.

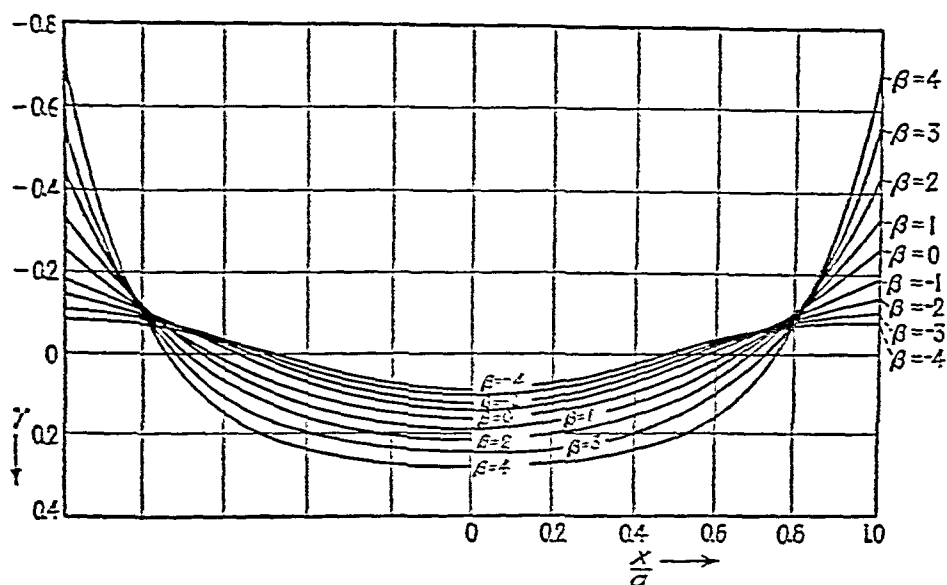


FIG. 65.

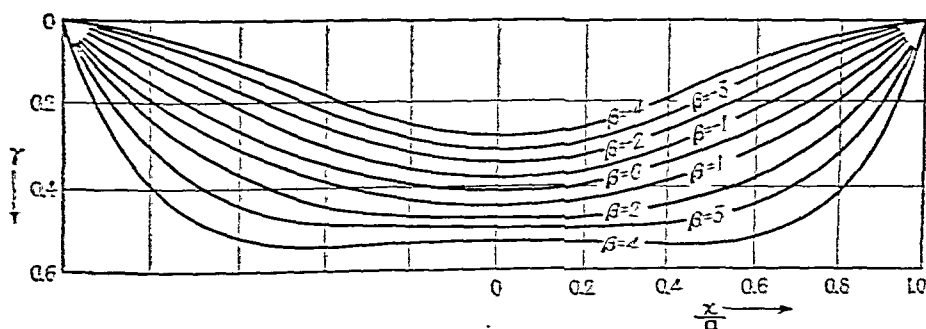


FIG. 66.

21. Bending of a Circular Plate Loaded at the Center.—*Plate Clamped at the Edge.*—For this case  $q = 0$  is substituted into eq. (92), which gives

$$\varphi = -\frac{Px}{8\pi D} (2 \log_e x - 1) + \frac{C_1 x}{2} + \frac{C_2}{x}. \quad (a)$$

The constants of integration  $C_1$  and  $C_2$  are found from the conditions that  $\varphi$  is equal to zero at the clamped edge and at

the center of the plate; hence

$$\left[ -\frac{Px}{8\pi D} (2 \log_e x - 1) + \frac{C_1 x}{2} + \frac{C_2}{x} \right]_{x=0} = 0, \quad (b)$$

$$\left[ -\frac{Px}{8\pi D} (2 \log_e x - 1) + \frac{C_1 x}{2} + \frac{C_2}{x} \right]_{x=a} = 0.$$

Since  $(x \log_e x)_{x=0} = 0$ , the following values of the arbitrary constants are obtained from eqs. (b):

$$C_1 = \frac{P}{4\pi D} (2 \log_e a - 1); \quad C_2 = 0, \quad (c)$$

and eq. (a) becomes

$$\varphi = \frac{Px}{4\pi D} \log_e \frac{a}{x}. \quad (d)$$

The equation for the deflection surface is obtained by substituting  $q = 0$  and the values from eq. (c) of the arbitrary constants into eq. (93), which gives

$$w = \frac{Px^2}{8\pi D} \left( \log_e \frac{x}{a} - \frac{1}{2} \right) + C_3. \quad (e)$$

The constant  $C_3$  is obtained from the condition that at the clamped edge the deflection is zero, giving  $C_3 = Pa^2/16\pi D$ . Substituting this into eq. (e), we obtain

$$w = \frac{Px^2}{8\pi D} \log_e \frac{x}{a} + \frac{P}{16\pi D} (a^2 - x^2). \quad (f)$$

The deflection at the middle is

$$\delta = \frac{Pa^2}{16\pi D}. \quad (104)$$

This deflection is four times as great as that produced by a uniformly distributed load of the same magnitude (eq. 96).

The bending moments are calculated from eqs. (88) and (89) by using eq. (d), which gives

$$M_1 = \frac{P}{4\pi} \left[ (1 + \mu) \log_e \frac{a}{x} - 1 \right], \quad (g)$$

$$M_2 = \frac{P}{4\pi} \left[ (1 + \mu) \log_e \frac{a}{x} - \mu \right]. \quad (h)$$

At the edge ( $x = a$ ) these moments become

$$M_1 = -\frac{P}{4\pi}; \quad M_2 = -\mu \frac{P}{4\pi}; \quad (105)$$

and the corresponding maximum stresses are

$$(\sigma_z)_{\max} = \frac{3}{2} \frac{P}{\pi h^2}, \quad (\sigma_y)_{\max} = \frac{3\mu}{2} \frac{P}{\pi h^2}. \quad (106)$$

Comparison with eq. (97) for a uniform load shows that a load concentrated at the center produces stresses at the clamped edge of the plate which are twice as great as the stresses produced by a load of the same magnitude uniformly distributed over the plate.

At the center of the plate eqs. (g) and (h) give infinitely large values for the bending moments and the stresses. This result is due to the assumption that the load is concentrated at a point.<sup>21</sup> If the distribution of the load is taken over a small circle, the stresses become finite (see p. 109).

In determining the safe dimensions of a circular plate loaded at the center we can limit our investigation to the calculation of the maximum tensile bending stresses at the bottom of the plate. It has already been mentioned that eqs. (g) and (h) are not suitable for this purpose, and a more detailed investigation<sup>22</sup> indicates that the proper formula for calculating

<sup>21</sup> Local stresses at the point of application of a concentrated load are discussed in the paper by H. Hencky, *Der Spannungszustand in rechteckigen Platten*, Darmstadt, p. 54, 1915. See also A. Nadai, *Elastische Platten*, p. 97, 1925.

<sup>22</sup> This question is discussed in S. Timoshenko, *Theory of Plates and Shells*, p. 75, 1940.

the above-mentioned tensile stress is

$$(\sigma_x)_{\max} = \frac{P}{h^2} (1 + \mu) \left( 0.485 \log_e \frac{a}{h} + 0.52 \right). \quad (107)$$

Although the compressive stresses at the top of the plate may be many times larger than the tensile stresses at the bottom in the case of a strong concentration of the load, they do not represent a direct danger, because of their highly localized character. The local yielding which occurs in the case of a ductile material will not affect the general deformation of the plate if the tensile stresses at the bottom of the plate remain within safe limits. Since the compressive strength of a brittle material is usually many times greater than its tensile strength, a plate of brittle material will also be safe if the tensile stress at the bottom is within the limit of safety.

*Plate Simply Supported at the Edge.*—The deflection of a plate simply supported at the edge is obtained by the method of superposition. On the deflections (eq. *f*) found above for the case of a clamped edge, we superpose the deflection produced in the plate by moments  $M_1 = P/4\pi$  uniformly distributed along the edge and thus obtain the case of a simply supported plate. The curvature produced by the moments  $M_1 = P/4\pi$  is found from eq. (85) to be

$$\frac{1}{r} = \frac{P}{4\pi(1 + \mu)D},$$

and the corresponding deflection at the middle is

$$\delta_1 = \frac{a^2}{2r} = \frac{Pa^2}{8\pi(1 + \mu)D}.$$

This is added to the deflection of eq. (104) to give the deflection at the middle of a simply supported plate:

$$\delta = \frac{Pa^2}{16\pi D} + \frac{Pa^2}{8\pi(1 + \mu)D} = \frac{Pa^2}{16\pi D} \cdot \frac{3 + \mu}{1 + \mu}. \quad (108)$$

This deflection is about 2.5 times as great as that for the case of a clamped plate.

For the outer portion ( $x > b$ ),

$$w = \frac{P}{8\pi D} \left[ -(x^2 + b^2) \log_e \frac{a}{x} + \frac{(3 + \mu)a^2 - (1 - \mu)b^2}{2(1 + \mu)a^2} (a^2 - x^2) \right] \quad (d)$$

Any other case of the bending of a circular plate loaded symmetrically with respect to the center can be solved by using these equations together with the method of superposition. Consider, for example, the case shown in Fig 68,

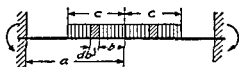


FIG 68

$c$  Substituting  $P = 2\pi b q db$  into eq (a), we obtain the deflection produced at the center of the plate by the elemental ring loading shown in the figure

$$dw = \frac{q}{4D} \left[ -b^2 \log_e \frac{a}{b} - b^2 + \frac{1}{2} (a^2 + b^2) \right] b db \quad (e)$$

The deflection produced at the center of the plate by the entire load is then

$$\begin{aligned} \delta &= \int_0^c dw = \frac{q}{4D} \int_0^c \left[ -b^2 \log_e \frac{a}{b} - b^2 + \frac{1}{2} (a^2 + b^2) \right] b db \\ &= \frac{q}{4D} \left[ -\frac{c^4}{4} \log_e \frac{a}{c} - \frac{3}{16} c^4 + \frac{a^2 c^2}{4} \right] \end{aligned} \quad (109)$$

If  $c = a$ , this equation coincides with eq (96) for a uniformly loaded plate. By substituting  $c = 0$  and  $\pi c^2 q = P$  into eq (109) we obtain eq (104) for the deflection due to a concentrated load.

To determine bending moments and stresses at the center of the plate we calculate the second derivative with respect to  $x$  of eq (a). Setting  $x = 0$  and  $P = 2\pi b q db$  in this derivative, the curvature at the center produced by the elemental ring loading (Fig 68) becomes

$$\frac{q}{4D} \left( -2 \log_e \frac{a}{b} + 1 - \frac{b^2}{a^2} \right) b db$$

The curvature at the center produced by the entire load is then

$$\begin{aligned} \left( \frac{d^2 w}{dx^2} \right)_{x=0} &= \frac{q}{4D} \int_0^c \left( -2 \log_e \frac{a}{b} + 1 - \frac{b^2}{a^2} \right) b db \\ &= -\frac{qc^2}{4D} \left( \log_e \frac{a}{c} + \frac{c^2}{4a^2} \right). \end{aligned} \quad (110)$$

The corresponding bending moment at the center from eqs. (83) and (84) is

$$M_1 = M_2 = -D(1 + \mu) \frac{d^2 w}{dx^2} = \frac{1 + \mu}{4} qc^2 \left( \log_e \frac{a}{c} + \frac{c^2}{4a^2} \right), \quad (111)$$

and the maximum bending stresses at the center are

$$(\sigma_x)_{\max} = (\sigma_y)_{\max} = \frac{3}{2} (1 + \mu) \frac{qc^2}{h^2} \left( \log_e \frac{a}{c} + \frac{c^2}{4a^2} \right). \quad (112)$$

Using the notation  $P$  for the entire load  $\pi c^2 q$ , this becomes

$$(\sigma_x)_{\max} = (\sigma_y)_{\max} = \frac{3}{2} (1 + \mu) \frac{P}{\pi h^2} \left( \log_e \frac{a}{c} + \frac{c^2}{4a^2} \right). \quad (113)$$

By diminishing the radius  $c$  of the circle over which the load is distributed, we approach the condition of a concentrated load. The stresses at the center increase as  $c$  decreases, but remain finite as long as  $c$  is finite.

**23. Deflection of a Symmetrically Loaded Circular Plate with a Circular Hole at the Center.**—*Bending by Couples.*—Let us denote by  $M_{1a}$  and  $M_{1b}$  the bending moments per unit length on the outer and the inner edge respectively (Fig. 69a). For this case we have  $P = q = 0$ , and from eqs. (92) and (93) we find

$$\varphi = \frac{C_1 x}{2} + \frac{C_2}{x}, \quad (a)$$

$$w = -\frac{C_1 x^2}{4} - C_2 \log_e \frac{x}{a} + C_3. \quad (b)$$

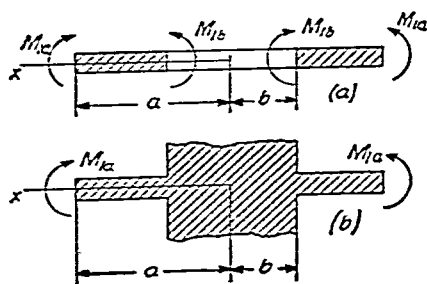


FIG. 69.

The arbitrary constants  $C_1$ ,  $C_2$  and  $C_3$  are now to be determined from the conditions at the edges. Substituting from eq (a) into eq (88) we obtain

$$M_1 = D \left[ \frac{C_1}{2} - \frac{C_2}{x^2} + \mu \left( \frac{C_1}{2} + \frac{C_2}{x^2} \right) \right] \quad (c)$$

By substituting  $x = a$  and also  $x = b$  we obtain the following equations for determining  $C_1$  and  $C_2$

$$D \left[ \frac{C_1}{2} (1 + \mu) - \frac{C_2}{a^2} (1 - \mu) \right] = M_{1a},$$

$$D \left[ \frac{C_1}{2} (1 + \mu) - \frac{C_2}{b^2} (1 - \mu) \right] = M_{1b},$$

from which

$$C_1 = \frac{2(a^2 M_{1a} - b^2 M_{1b})}{(1 + \mu)D(a^2 - b^2)}, \quad C_2 = \frac{a^2 b^2 (M_{1a} - M_{1b})}{(1 - \mu)D(a^2 - b^2)} \quad (d)$$

The constant  $C_3$  is determined by considering the deflection of the plate. Assume, for example, that the plate is simply supported at the outer edge, then the deflection at this edge is zero and  $C_3$  is calculated from eq (b), which becomes, for  $x = a$ ,

$$-\frac{C_1 a^2}{4} + C_3 = 0,$$

so that

$$C_3 = \frac{a^2}{4} C_1$$

The deflection surface of the plate can now be obtained by substituting  $C_1$ ,  $C_2$  and  $C_3$  into eq (b)

As a second example let us consider the case of the bending of the plate by the couples  $M_{1a}$  when the inner edge is built in (Fig 69b). The arbitrary constants  $C_1$  and  $C_2$  in eq (a) are determined in this case from the conditions  $\varphi = 0$  for  $x = b$  and  $M_1 = M_{1a}$  for  $x = a$ . Then from eqs (a) and (c) we find

$$\frac{C_1 b}{2} + \frac{C_2}{b} = 0,$$

$$\frac{C_1}{2} (1 + \mu) - \frac{C_2}{a^2} (1 - \mu) = \frac{M_{1a}}{D},$$

and we obtain

$$C_1 = \frac{2a^2 M_{1a}}{D[a^2(1 + \mu) + b^2(1 - \mu)]},$$

$$C_2 = -\frac{a^2 b^2 M_{1a}}{D[a^2(1 + \mu) + b^2(1 - \mu)]}.$$

Substituting these values into eqs. (a) and (c), we find

$$\varphi = \frac{a^2 M_{1a}}{D[a^2(1 + \mu) + b^2(1 - \mu)]} \left( x - \frac{b^2}{x} \right), \quad (e)$$

$$M_1 = \frac{a^2 M_{1a}}{a^2(1 + \mu) + b^2(1 - \mu)} \left[ 1 + \mu + (1 - \mu) \frac{b^2}{x^2} \right]. \quad (f)$$

*Bending by a Load Uniformly Distributed along Inner and Outer Edges.*—If bending is produced by a loading uniformly distributed along the edges (Fig. 70a), then  $q = 0$  and  $P$  is equal to the total load on the inner edge. These values are substituted into eqs. (92) and (93). Thus, from eq. (92) we obtain

$$\varphi = -\frac{Px}{8\pi D} (2 \log_e x - 1) + \frac{C_1 x}{2} + \frac{C_2}{x}. \quad (g)$$

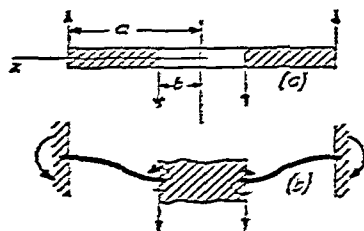


FIG. 70.

The constants of integration  $C_1$  and  $C_2$  are to be determined from the conditions at the edges. For example, if the plate is clamped at the edges (Fig. 70b), the arbitrary constants are determined from the conditions that  $\varphi = 0$  for  $x = a$  and  $x = b$ . Thus, from eq. (g),

$$-\frac{Pa}{8\pi D} (2 \log_e a - 1) + \frac{C_1 a}{2} + \frac{C_2}{a} = 0,$$

$$-\frac{Pb}{8\pi D} (2 \log_e b - 1) + \frac{C_1 b}{2} + \frac{C_2}{b} = 0.$$

The expression for  $\varphi$  is obtained after  $C_1$  and  $C_2$  are calculated from



these equations and substituted into eq (g). The bending moments may then be calculated from eqs (88) and (89)

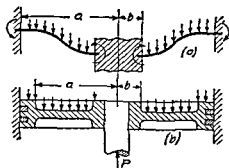


FIG 71

If, instead of a load distributed along the edges, there acts a load uniformly distributed over the plate as shown in Fig 71a, the shearing force  $V$  at any point a distance  $x$  from the center is

$$V = \frac{1}{2\pi x} \pi q (x^2 - b^2) = \frac{qx}{2} - \frac{qb^2}{2x}$$

This quantity must be substituted into eq (90), and then eqs (92) and (93) become

$$\varphi = -\frac{qx^3}{16D} + \frac{qb^2x}{8D} (2 \log_e x - 1) + \frac{C_1x}{2} + \frac{C_2}{x},$$

$$w = \frac{qx^4}{64D} - \frac{b^2qx^2}{8D} (\log_e x - 1) - \frac{C_1x^2}{4} - C_2 \log_e x + C_3$$

For determining the arbitrary constants the conditions at the edges must be used. For example, if the plate is clamped at the edges, the equations for determining  $C_1$  and  $C_2$  are

$$\begin{aligned} -\frac{qa^3}{16D} + \frac{qab^2}{8D} (2 \log_e a - 1) + \frac{C_1a}{2} + \frac{C_2}{a} &= 0, \\ -\frac{qb^3}{16D} + \frac{qb^3}{8D} (2 \log_e b - 1) + \frac{C_1b}{2} + \frac{C_2}{b} &= 0 \end{aligned}$$

Solutions of such problems as the bending of pistons of steam engines and the bending of flanges<sup>25</sup> of cylinders and tubes may be obtained by combining the solutions discussed in this article. For example, by combining the cases shown in Figs 70b and 71a an approximate solution of the problem of the bending of a piston (Fig 71b) by steam pressure may be obtained<sup>26</sup>

<sup>25</sup> See the paper by Everett O. Waters and J. Hall Taylor, *Trans A S M E*, 1927

<sup>26</sup> Several problems of this kind are considered in the paper by M. Ensslin, *Dinglers Polytech J*, 1903 and 1904. See also Pfeleiderer, *Forschungsarb*, No 97, 1911. Experiments with pistons are described in the paper by C. Codron, *Re ue de mecanique*, Vol 13, p 340, 1903. Circular plates reinforced by ribs are discussed by M. Schulhansl, *Z angew Math u Mech*, Vol 6, p 484, 1926, and *Z Ver deut Ing*, Vol 71, p 1154, 1927. A further discussion of circular plates is given in S. Timoshenko, *Theory of Plates and Shells*, 1940.

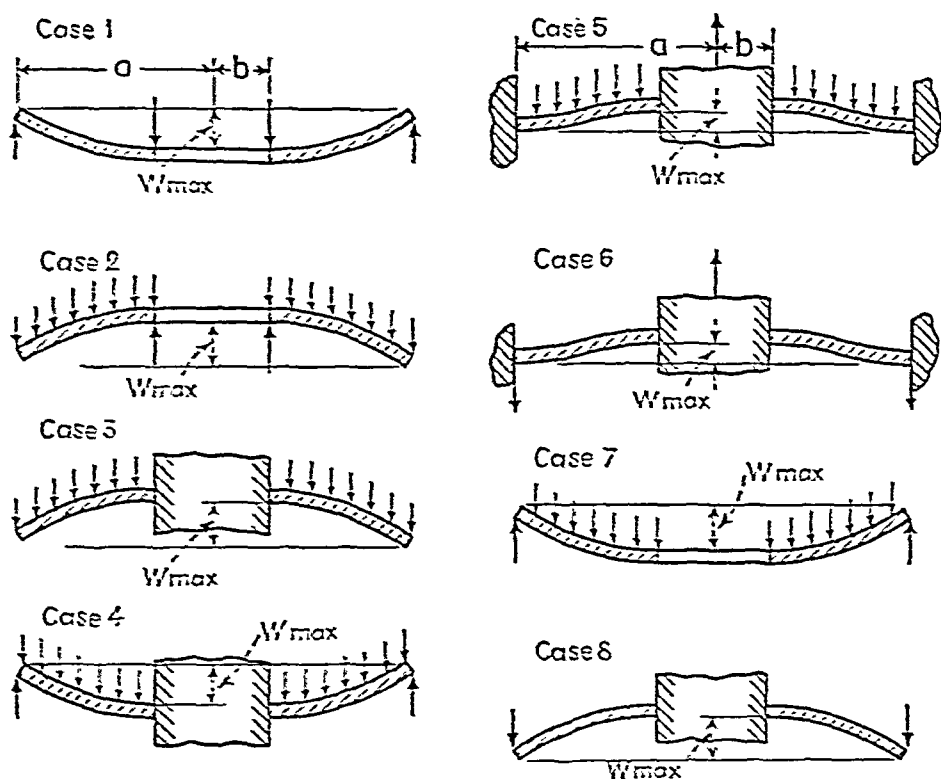


FIG. 72.

Several cases of practical importance are represented in Fig. 72.<sup>27</sup> In all these cases the maximum stress can be represented by a formula of the type

$$\sigma_{\max} = k \frac{qa^2}{k^2} \quad \text{or} \quad \sigma_{\max} = \frac{kP}{k^2} \quad (114)$$

depending on whether the applied load is uniformly distributed over the surface or concentrated along the edge. The numerical values of the factor  $k$ , calculated for several values of the ratio  $a/b$  and for Poisson's ratio  $\mu = 0.3$ , are given in Table 5. The maximum deflections in the same cases are given by formulas of the type

$$w_{\max} = k_1 \cdot \frac{qa^4}{Ek^3} \quad \text{or} \quad w_{\max} = k_1 \cdot \frac{Pa^2}{Ek^3} \quad (115)$$

The numerical factors  $k_1$  are also given in Table 5.<sup>28</sup>

<sup>27</sup> See the paper by A. M. Wahl and G. Lobo, *Trans. A.S.M.E.*, Vol. 52, 1929.

<sup>28</sup> For more complete information regarding symmetrically loaded circular plates see the paper by W. E. Trumpler, *J. Appl. Mech.*, Vol. 10, p. 173, 1943.

TABLE 5 COEFFICIENTS  $k$  AND  $k_1$  IN EQS (114) AND (115) FOR THE EIGHT CASES SHOWN IN FIG 72

$a/b =$	1.25		1.5		2		3		4		5	
Case	$k$	$k_1$	$k$	$k_1$	$k$	$k_1$	$k$	$k_1$	$k$	$k_1$	$k$	$k_1$
1	1.10	0.341	1.26	0.519	1.48	0.672	1.88	0.734	2.17	0.724	2.34	0.704
2	0.66	0.202	1.19	0.491	2.04	0.902	3.34	1.220	4.30	1.300	5.10	1.310
3	0.135	0.00231	0.410	0.0183	1.04	0.0938	2.15	0.293	2.99	0.448	3.69	0.564
4	0.122	0.00343	0.336	0.0313	0.74	0.1250	1.21	0.291	1.45	0.417	1.59	0.492
5	0.090	0.00077	0.273	0.0062	0.71	0.0329	1.54	0.110	2.23	0.179	2.80	0.234
6	0.115	0.00129	0.220	0.0064	0.405	0.0237	0.703	0.062	0.933	0.092	1.13	0.114
7	0.592	0.184	0.976	0.414	1.440	0.664	1.880	0.824	2.08	0.830	2.19	0.813
8	0.227	0.00510	0.428	0.0249	0.753	0.0877	1.205	0.209	1.514	0.293	1.745	0.350

**24 Bending of Rectangular Plates**—The theory of the bending of rectangular plates is more complicated than that for circular plates, and therefore only some final results for the bending moments and deflections are given below.<sup>29</sup> In deriving these results it is assumed that the deflections are small in comparison with the thickness of the plate, and that during bending the edges can be freely displaced in the plane of the plate, i.e., there are no stresses acting in the middle plane of the plate.

*Plate Simply Supported at the Edges*—In the case of a uniformly distributed load  $q$  the maximum deflection occurs at the center of the plate (Fig 73) and can be represented by the equation

$$\delta = \alpha \frac{qa^4}{Eh^3} \quad (116)$$

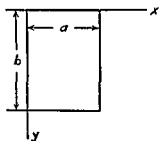


FIG 73

in which  $a$  is the shorter side of the plate,  $h$  the thickness of the plate and  $\alpha$  a numerical factor depending on the magnitude of the ratio  $b/a$ .

As before, we use the notations  $M_1$  and  $M_2$  for the bending moments per unit length on the sections parallel to the  $y$  and  $x$  axes respectively. The maximum bending moments occur at the center of the plate and are

$$(M_1)_{\max} = \beta_1 qa^2, \quad (M_2)_{\max} = \beta_2 qa^2, \quad (117)$$

in which  $\beta_1$  and  $\beta_2$  denote numerical factors depending upon the ratio

<sup>29</sup> A more complete discussion of bending of rectangular plates is given in the author's *Theory of Plates and Shells*, New York, 1940.

$b/a$ . Several values of the coefficients  $\alpha$ ,  $\beta_1$  and  $\beta_2$  are given in Table 6. These values are calculated on the assumption that Poisson's ratio is equal to 0.3.

TABLE 6: CONSTANTS FOR UNIFORMLY LOADED RECTANGULAR PLATES WITH SIMPLY SUPPORTED EDGES

$b/a =$	1.0	1.1	1.2	1.3	1.4	1.5	1.6	1.7
$\alpha =$	0.0443	0.0530	0.0516	0.0597	0.0770	0.0843	0.0906	0.0964
$\beta_1 =$	0.0479	0.0553	0.0526	0.0593	0.0753	0.0812	0.0862	0.0908
$\beta_2 =$	0.0479	0.0494	0.0501	0.0504	0.0506	0.0500	0.0493	0.0486
$b/a =$	1.8	1.9	2.0	3.0	4.0	5.0	$\infty$	
$\alpha =$	0.1017	0.1054	0.1106	0.1336	0.1400	0.1416	0.1422	
$\beta_1 =$	0.0948	0.0985	0.1017	0.1189	0.1235	0.1246	0.1250	
$\beta_2 =$	0.0479	0.0471	0.0464	0.0404	0.0384	0.0375	0.0375	

It may be seen from Table 6 that for  $b/a > 3$  the maximum deflection and the maximum bending moment do not differ substantially from those calculated for  $b/a = \infty$ . This means that for long rectangular plates ( $b/a > 3$ ) the effect of the short sides can be neglected and the formulas derived in Arts. 13-15 for bending to a cylindrical surface can be used with sufficient accuracy.

*Plate Built In at the Edges.*—The maximum deflection takes place at the center of the plate and can be expressed by the same equation (116) as was used for a plate with simply supported edges. The numerically maximum bending moment occurs at the middle of the longer sides and is given by the equation

$$|M_1|_{\max} = \beta q a^2 \quad (118)$$

Several values of the coefficients  $\alpha$  and  $\beta$  are given in Table 7.

The values in Table 7 indicate that clamping the edges of a plate considerably diminishes the maximum deflection. However, the effect of clamping the edges on the magnitude of the maximum bending stress is not very great. It is also seen that in the case of clamped edges the maximum deflection and the maximum bending moment for  $b/a = 2$  nearly coincide with those obtained for  $b/a = \infty$ . This justifies the use of the results obtained in Art. 14 for bending to a

TABLE 7: CONSTANTS FOR UNIFORMLY LOADED RECTANGULAR PLATES WITH CLAMPED EDGES

$b/a =$	1.00	1.25	1.50	1.75	2.00	$\infty$
$\alpha =$	0.0138	0.0199	0.0240	0.0264	0.0277	0.0284
$\beta =$	0.0513	0.0665	0.0757	0.0806	0.0829	0.0833

cylindrical surface in making calculations for comparatively long rectangular plates ( $b/a \geq 2$ ) with clamped edges.

*Plate with Two Opposite Sides Simply Supported, Third Side Built In and Fourth Side Free (Fig. 74).* In the case of a uniformly dis-

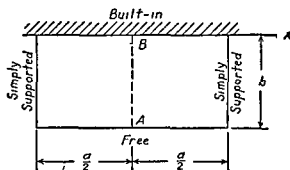


FIG. 74.

tributed load, the maximum deflection is at the middle of the free side at point  $A$ . This deflection can be represented by the equation

$$\delta = \alpha \frac{qb^4}{Eh^3} \quad (119)$$

The values of the numerical factor  $\alpha$  in this equation are given in Table 8. The maximum bending moment  $M_1$  also occurs at point  $A$ , and its magnitude is given by the equation

$$(M_1)_{\max} = \beta_1 qa^2. \quad (120)$$

The numerically maximum bending moment  $M_2$  occurs at point  $B$ , at the middle of the built-in side, and is given by the equation

$$(M_2)_{\max} = \beta_2 qb^2. \quad (121)$$

Several values of the factors  $\beta_1$  and  $\beta_2$  are given in Table 8.

TABLE 8: CONSTANTS FOR UNIFORMLY LOADED RECTANGULAR PLATE SHOWN IN FIG. 74

$b/a =$	0	$\frac{1}{3}$	$\frac{1}{2}$	$\frac{2}{3}$	1
$\alpha =$	1.37	1.03	0.635	0.366	0.123
$\beta_1 =$	0	0.0078	0.0293	0.0558	0.0972
$\beta_2 =$	0.500	0.428	0.319	0.227	0.119

It can be seen from the table that when  $a$  is large compared to  $b$ , the middle strip  $AB$  approaches the condition of a cantilever built in at  $B$  and uniformly loaded.

*Uniformly Loaded Plate Supported at Many Equidistant Points (Fig. 75).* In this case we can obtain a good approximation to the maximum stress and to the stress distribution near a support as follows: A part of the plate near the support, bounded by a circle of radius  $a = 0.22c$  (where  $c$  is the distance between supports), is considered as a circular plate simply supported at the outer edge, loaded at the inner edge by the load  $P = qc^2$  acting upward, and uniformly loaded by a load of intensity  $q$  acting downward. This loading is shown in Fig. 75b.<sup>30</sup> The problem may be solved by using the methods developed in Art. 23.

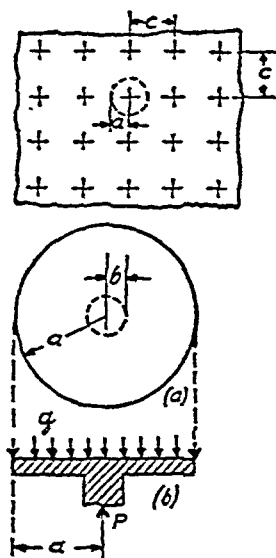


FIG. 75.

The bending of rectangular plates on an elastic foundation in connection with a stress analysis in concrete roads was discussed by H. M. Westergaard.<sup>31</sup>

## 25. Thin-walled Vessels Subjected to Internal Pressure.—

This consideration will be confined to vessels having the form of a surface of revolution and subjected to a continuous internal pressure of intensity  $p$ , not necessarily uniform but sym-

<sup>30</sup> See the paper by H. M. Westergaard and A. Slater, *Proc. Am. Concrete Inst.*, Vol. 17, 1921. See also V. Lewe, *Die strenge Lösung des Pflzdecken-problems*, Berlin, 1922.

<sup>31</sup> See his paper in *Ingeniøren*, Copenhagen, p. 513, 1923, and also in *Public Roads*, Vol. 7, p. 25, 1926. See also S. Timoshenko, *Theory of Plates and Shells*, 1940.

metrically distributed with reference to the axis of revolution  $O-O$  (Fig 76) If the thickness of the wall is small in comparison with the radii of curvature and there are no discontinuities such as sharp bends in the meridional curves, the stresses can be calculated with sufficient accuracy by neglecting the bending of the wall of the vessel, i.e., by assuming

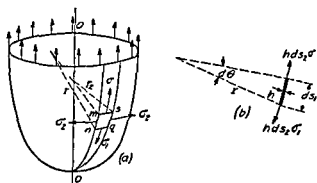


FIG 76

that the tensile stresses in the wall are uniformly distributed across the thickness.<sup>32</sup> The magnitudes of the stresses may then be easily calculated from the equations of statics

Let us consider an element  $mnsq$  cut from the wall of the vessel by two meridional sections  $mn$  and  $sq$  and two sections  $ms$  and  $nq$  normal to the meridians. From the condition of symmetry it is seen that only normal stresses act on the sides of this element. The following notation will now be used

$\sigma_1$  = tensile stress in the meridional direction, or the *meridional stress*,

$\sigma_2$  = tensile stress along a parallel circle, or the *hoop stress*,

$h$  = uniform thickness of the shell,

$ds_1$  = dimension of the element in the meridional direction,

$ds_2$  = dimension of the element in the direction of a parallel circle,

<sup>32</sup> Shells which do not resist bending are sometimes called *membranes* and the stresses calculated by neglecting bending are called *membrane stresses*. It is assumed that the external forces, uniformly distributed along the edge of the shell, are tangent to the meridians.

$r_1$  = meridional radius of curvature,

$r_2$  = radius of curvature of a section taken perpendicular to the meridian.

Then the total tensile forces acting on the sides of the element are  $h\sigma_1 ds_2$  and  $h\sigma_2 ds_1$ . The tensile forces  $h\sigma_1 ds_2$  acting on the sides  $ms$  and  $nq$  of the element have a component in the direction normal to the element equal to (see Fig. 76b)

$$h\sigma_1 ds_2 d\theta_1 = \frac{h\sigma_1 ds_1 ds_2}{r_1}. \quad (a)$$

In the same manner the tensile forces acting on the sides  $mn$  and  $sq$  have a normal component,

$$h\sigma_2 ds_1 d\theta_2 = \frac{h\sigma_2 ds_1 ds_2}{r_2}. \quad (b)$$

The sum of these normal components is in equilibrium with the normal pressure on the element; hence

$$\frac{h\sigma_1 ds_1 ds_2}{r_1} + \frac{h\sigma_2 ds_1 ds_2}{r_2} = p ds_1 ds_2 \quad (c)$$

or

$$\frac{\sigma_1}{r_1} + \frac{\sigma_2}{r_2} = \frac{p}{h}. \quad (122)$$

Some applications of this equation will now be discussed.

*Spherical Vessel under Uniform Internal Pressure.*—In this case  $r_1 = r_2 = r$  and  $\sigma_1 = \sigma_2 = \sigma$ . Eq. (122) becomes

$$\sigma = \frac{pr}{2h}.$$

*Conical Tank.*—Let us consider an open conical tank filled with liquid (Fig. 77). In this case the curvature of the meridian  $1/r_1 = 0$ , and the hoop stress  $\sigma_2$  due to the liquid pressure can be calculated from eq. (122). The internal pressure at points  $m-n$  at distance

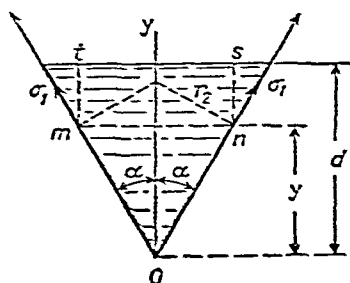


FIG. 77.



$d - y$  from the surface of the liquid is

$$p = \gamma(d - y),$$

where  $\gamma$  is the weight per unit volume of the liquid. The radius of curvature  $r_2$  at these points is

$$r_2 = \frac{y \tan \alpha}{\cos \alpha}.$$

Eq. (122) then becomes

$$\sigma_2 \frac{\cos \alpha}{y \tan \alpha} = \frac{\gamma(d - y)}{h},$$

from which

$$\sigma_2 = \frac{\gamma(d - y)}{h} \frac{y \tan \alpha}{\cos \alpha}. \quad (d)$$

The maximum value of this stress occurs at points where the product  $(d - y)y$  is a maximum. If we set the derivative of  $(d - y)y$  equal to zero, we find  $y = d/2$  and the stress at this point is

$$(\sigma_2)_{\max} = \frac{\gamma d^2 \tan \alpha}{4h \cos \alpha}. \quad (e)$$

The stress  $\sigma_1$  at the level  $m-n$  is found from the condition that the vertical components of the meridional tensile forces in the shell support the weight of the volume  $tmOns$  of the liquid (Fig. 77); hence

$$2\pi y(\tan \alpha)h\sigma_1 \cos \alpha = \pi y^2(\tan^2 \alpha)(d - y + \frac{1}{3}y)\gamma,$$

from which

$$\sigma_1 = \frac{y(\tan \alpha)(d - \frac{2}{3}y)\gamma}{2h \cos \alpha}. \quad (f)$$

This stress is maximum when  $y = \frac{3}{4}d$ . Substituting this value into eq. (f), we find

$$(\sigma_1)_{\max} = \frac{3}{16} \frac{d^2 \gamma \tan \alpha}{h \cos \alpha}. \quad (g)$$

Eqs. (d) and (f) represent the complete solution of the problem as long as the bending stresses in the wall of the tank may be neglected.

In the case of a *cylindrical shell* of diameter  $d$ , subjected to uniform pressure  $p$ , we found before (see Part I, p. 45)

$$\sigma_1 = \frac{pd}{4h}; \quad \sigma_2 = \frac{pd}{2h}.$$

### Problems

1. The tank of Fig. 78 contains liquid at the level shown.

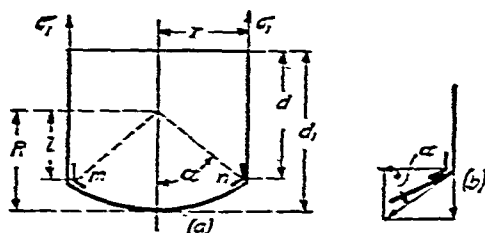


FIG. 78.

Determine the maximum stresses  $\sigma_1$  and  $\sigma_2$  in the cylindrical and the spherical portions of the tank and also the compressive force in the reinforcing ring  $mn$ .

*Solution.* The weight of the liquid in the container is

$$Q = \left[ \pi d r^2 + \pi \left( \frac{2}{3} R^3 - R^2 l + \frac{l^3}{3} \right) \right] \gamma.$$

For the cylindrical portion of the tank,

$$\sigma_1 = \frac{Q}{2\pi r h} = \text{const.} \quad \text{and} \quad (\sigma_2)_{\max} = \frac{d\gamma r}{h}.$$

For the spherical portion of the tank the maximum stress is at the bottom, where the liquid pressure is  $\gamma d_1$  and  $\sigma_1 = \sigma_2 = \gamma d_1 R / 2h$ . The tensile force in the spherical portion of the tank per unit length of the ring  $mn$  is  $Q / (2\pi r \sin \alpha)$ . The radial component of this force, producing compression of the ring (Fig. 78b), is  $(Q / 2\pi r) \cot \alpha$ , and

the compressive force in the ring is  $(Q/2\pi) \cot \alpha$ . This is only an approximation obtained on the assumption that the cylindrical and spherical portions are membranes, resisting only tension. In calculating the compressive stress in the ring, adjacent portions of the cylindrical and spherical shells must be added to the cross section of the ring  $mn$  itself.

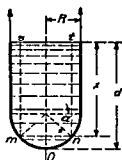


FIG. 79

2. Determine the stresses at the points  $mn$  of a cylindrical tank with a hemispherical bottom which contains liquid at the level indicated (Fig. 79).

*Solution* From eq (122) for any point of the spherical portion at a distance  $x$  from the surface of the liquid we have

$$\frac{\sigma_1 + \sigma_2}{R} = \frac{\gamma x}{h} \quad (h)$$

Since the meridional stresses along the section  $mn$  support the weight of the volume  $smOnt$  of the liquid, a second equation is

$$\sigma_1 = \frac{\gamma R}{h} \left( \frac{d - R}{2} + \frac{R}{3} \frac{1 - \sin^3 \alpha}{\cos^2 \alpha} \right), \quad (i)$$

and eq (h) becomes

$$\sigma_2 = \frac{\gamma R}{h} \left( \frac{d - R}{2} + \frac{R \sin^3 \alpha + 3 \sin \alpha \cos^2 \alpha - 1}{3 \cos^2 \alpha} \right).$$

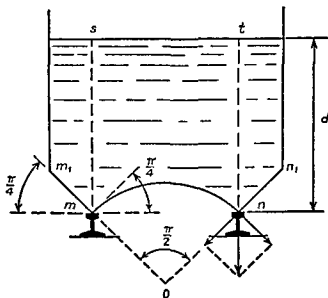


FIG. 80

3. In Fig. 80 determine the relation between the outer diameter of the tank, the diameter of the supporting ring  $mn$ , and the depth  $d$  of the liquid, in order that the ring  $mn$  may be subjected to vertical pressure only. The middle portion of the bottom of the tank is a spherical surface of central angle  $\pi/2$ . The conical portion  $mm_1nn_1$  also has the same angle.

*Hint.* The necessary relation may be obtained from the condition that the pressures on the ring from the side of the spherical bottom and from the conical lateral surface both inclined  $45^\circ$  give no horizontal component. From this it follows that the volume of the liquid inside the surface  $mstn$  must be equal to the volume outside that surface.

4. Determine the maximum stress in the tank represented in Fig. 78 if  $R = 10$  ft,  $r = 8$  ft,  $d = 20$  ft,  $\gamma = 62.5$  lb per cu ft and  $h = \frac{1}{4}$  in.

5. Determine the stresses  $\sigma_1$  and  $\sigma_2$  in the wall of a torus subjected to uniform internal pressure  $p$  (Fig. 81).

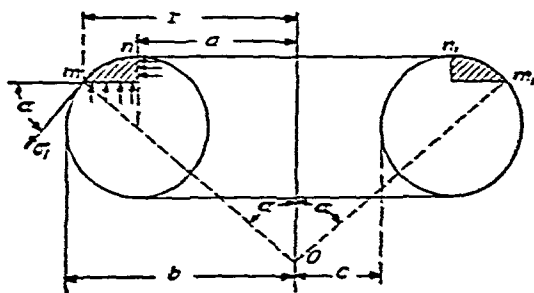


FIG. 81.

*Solution.* The condition of equilibrium with respect to vertical forces of the portion  $mm_1nn_1$  cut from the vessel by a vertical cylindrical surface of radius  $a$  and conical surface  $mOm_1$  gives

$$\pi(r^2 - a^2)p - \sigma_1 h 2\pi r \sin \alpha = 0,$$

from which

$$\sigma_1 = \frac{p(r^2 - a^2)}{2rh \sin \alpha}.$$

The stress  $\sigma_2$  can now be calculated from eq. (122).

6. Determine the maximum stress in the wall of the vessel represented in Fig. 81 if  $a = 10$  ft,  $b = 12$  ft,  $h = \frac{1}{4}$  in. and  $p = 50$  lb per sq in.

7. A spherical dome of constant thickness  $h$ , Fig. 82, is loaded by

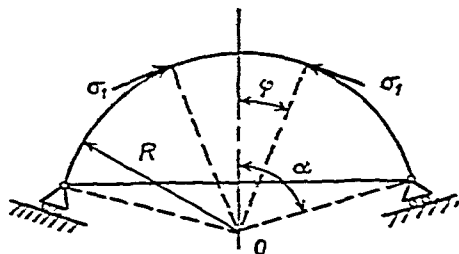


FIG. 82.

its own weight  $q$  per unit area

Find the stresses in the meridional direction and also perpendicular to the meridians

*Answer*

$$\sigma_1 = -\frac{qR}{h(1 + \cos \varphi)}$$

$$\sigma_2 = \frac{qR}{h} \left( \frac{1}{1 + \cos \varphi} - \cos \varphi \right)$$

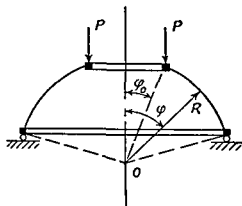


FIG 83

uniformly distributed load  $P$  per unit length is applied to the upper edge

*Answer*

$$\sigma_1 = -\frac{qR(\cos \varphi_0 - \cos \varphi)}{h \sin^2 \varphi} - \frac{P \sin \varphi_0}{h \sin^2 \varphi}$$

$$\sigma_2 = \frac{qR}{h} \left( \frac{\cos \varphi_0 - \cos \varphi}{\sin^2 \varphi} - \cos \varphi \right) + \frac{P \sin \varphi_0}{h \sin^2 \varphi}$$

9 A spherical tank, Fig 84, supported along a parallel circle  $AA$  is completely filled with a liquid of specific weight  $\gamma$ . Find  $\sigma_1$  and  $\sigma_2$

*Answer* If  $\varphi < \alpha$

$$\sigma_1 = \frac{\gamma R^2}{6h} \left( 1 - \frac{2 \cos^2 \varphi}{1 + \cos \varphi} \right),$$

$$\sigma_2 = \frac{\gamma R^2}{6h} \left( 5 - 6 \cos \varphi + \frac{2 \cos^2 \varphi}{1 + \cos \varphi} \right)$$

If  $\varphi > \alpha$

$$\sigma_1 = \frac{\gamma R^2}{6h} \left( 5 + \frac{2 \cos^2 \varphi}{1 - \cos \varphi} \right),$$

$$\sigma_2 = \frac{\gamma R^2}{6h} \left( 1 - 6 \cos \varphi - \frac{2 \cos^2 \varphi}{1 - \cos \varphi} \right)$$

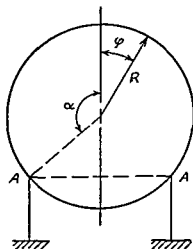


FIG 84

26 Local Bending Stresses in Thin Vessels—In the previous article, bending of the wall of the vessel was neglected and only tensile stresses, called *membrane stresses*, were considered. The dis

placements due to membrane stresses cause bending of the wall, and the resulting bending stresses may be of practical importance. This is especially so at points of discontinuity in the meridian. If the meridian consists of curves which are not tangent to one another at the points of juncture, a reinforcing ring such as is shown in Fig. 85 is required in order to prevent large bending of the wall of the vessel.

The stresses may also become very high at the points of juncture in a meridian consisting of several curves tangent to one another. The additional stresses set up at such points are called *discontinuity stresses*. The method of calculating them will now be shown for the simple case of a cylindrical vessel with hemispherical ends subjected to the action of uniform internal pressure (Fig. 85). We consider first the membrane stresses only, and find for the cylindrical portion

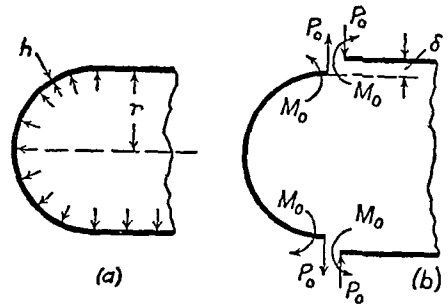


FIG. 85.

$$\sigma_1 = \frac{pr}{2h}; \quad \sigma_2 = \frac{pr}{h}, \quad (a)$$

where  $r$  is the radius of the cylinder and of the hemisphere and  $h$  is the thickness of the wall. For the spherical portion,

$$\sigma_1 = \sigma_2 = \sigma = \frac{pr}{2h}.$$

The corresponding radial displacements for the cylindrical and spherical portions are

$$\frac{r}{E} (\sigma_2 - \mu\sigma_1) = \frac{pr^2}{2hE} (2 - \mu) \quad \text{and} \quad \frac{pr^2}{2hE} (1 - \mu)$$

respectively.

If the spherical and cylindrical parts of the vessel were disjointed (Fig. 85*b*), the difference in radii due to deformation produced by the membrane stresses would be

$$\delta = \frac{pr^2}{2hE}. \quad (b)$$

In the actual vessel the head and the cylinder are kept together at the joint by shearing forces  $P_0$  and bending moments  $M_0$  (Fig. 85*b*) per unit length of the circumference of the middle surface of the

vessel These forces produce bending of the adjacent parts of the

vessel In discussing bending in the cylindrical part it is sufficient to consider the bending of an elemental strip (Fig 86), since the deformation is symmetrical with respect to the axis and the deflection of this strip will be in the meridional plane For simplicity it is assumed that the strip is of unit width If  $y$  denotes the radial displacement at any cross section of the strip, then the radius of the cylinder shortens at this section

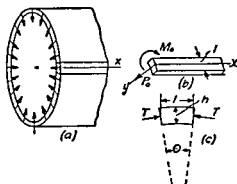


FIG 86

tion by  $y$  and as a result there appears a compressive strain in the circumferential direction of the magnitude  $y/r$  The corresponding compressive stress is  $Ey/r$  Hence when the strip deflects towards the axis of the cylinder, lateral compressive forces  $T$  (Fig 86c) are produced whose magnitude per unit length of the strip is

$$T = \frac{Ey}{r} h \quad (c)$$

Since the angle  $\theta$  is equal to  $1/r$ , these forces have a radial resultant

$$\frac{Eyh}{r} \theta = \frac{Eyh}{r^2}, \quad (d)$$

which opposes the deflection of the strip (It is assumed that  $\theta$  is a small angle) These reactive forces are distributed along the strip and are proportional to the deflection  $y$ , so that the strip is in the same condition with respect to bending as a beam on an elastic foundation<sup>33</sup> (Art 1) with  $k = Eh/r^2$  Since any change in the shape of the cross section of the strip is prevented by the adjacent strips in a manner similar to that in plates (see p 76),  $D = Eh^3/12(1 - \mu^2)$  is to be used for its flexural rigidity The differential equation of the deflection curve of the strip is then (see eq 1, p 2)

$$D \frac{d^4 y}{dx^4} = - \frac{Eh}{r^2} y$$

<sup>33</sup> It appears that this method of analysis of the local bending in cylindrical shells was introduced by H Scheffler, see *Organ f Eisenbahnwesen*, 1859

Introducing, as before, the notation

$$\beta = \sqrt[4]{\frac{Eh}{4Dr^2}} = \sqrt[4]{\frac{3(1-\mu^2)}{r^2h^2}}, \quad (123)$$

the deflection curve of the strip becomes (see eq. 11, p. 12)

$$y = \frac{e^{-\beta x}}{2\beta^3 D} [P_0 \cos \beta x - \beta M_0 (\cos \beta x - \sin \beta x)]. \quad (e)$$

This is a rapidly damped oscillatory curve of wavelength

$$l = \frac{2\pi}{\beta} = 2\pi \sqrt[4]{\frac{r^2h^2}{3(1-\mu^2)}}, \quad (f)$$

which is small in comparison with  $r$  if  $h$  is small. From this it can be shown that bending at the joint of the cylinder and head is of *local character* and has an appreciable effect on the stresses only in a narrow zone in the vicinity of the joint. This narrow zone at the edge of the head can be considered as nearly cylindrical in shape and hence eq. (e), which was developed for the cylindrical portion of the vessel, can also be used for an approximate calculation of the deflections and stresses in the head.<sup>34</sup>

In the simplest case, in which the cylindrical wall and spherical head are of the same thickness, the deflections and the slopes produced at the edges of the spherical and cylindrical parts by the forces  $P_0$  are equal. Then the conditions of continuity at the joint are satisfied if  $M_0 = 0$  and if  $P_0$  has such a magnitude as to produce a deflection at the edge of the cylinder equal to  $\delta/2$ . Substituting  $M_0 = 0$  and  $x = 0$  into eq. (e), the equation for calculating  $P_0$  becomes

$$\frac{P_0}{2\beta^3 D} = \frac{\delta}{2},$$

from which

$$P_0 = \delta\beta^3 D = \frac{pr^2}{2hE} \frac{Eh}{4\beta r^2} = \frac{p}{8\beta}. \quad (124)$$

With  $P_0$  known, the deflection and the bending moment at any cross section of the strip may be calculated from eq. (e). The corresponding discontinuity stresses must be added to the membrane stresses given by eqs. (a).

<sup>34</sup> A proof that this is a sufficiently accurate assumption was given by E. Meissner, *Schweiz. Bauzeitung*, Vol. 86, p. 1, 1925.



If the head and the cylindrical portion of the vessel have different thicknesses, there will be both a shearing force  $P_0$  and a moment  $M_0$  at the joint. These two quantities are calculated from the conditions (1) the sum of edge deflections in the spherical and in the cylindrical parts must be equal to  $\delta$  (Fig 85b), (2) the angles of rotation of the two edges must be equal.

The above method can also be used for cases in which the ends of the vessel are not of hemispherical shape<sup>35</sup>. If the thickness of the wall of a pressure vessel is not small, the bending stresses in the wall may become of primary importance and a more detailed investigation of the stress distribution becomes necessary<sup>36</sup>.

### Problems

1 Determine the discontinuity stresses in the vessel shown in Fig 85 if  $p = 150$  lb per sq in,  $r = 25$  in,  $h = \frac{1}{2}$  in,  $\mu = 0.3$ .

*Solution* From eq (123) we obtain  $\beta = 0.364$ , and from eq (124) we find

$$P_0 = \frac{150}{8 \times 0.364} = 51.5 \text{ lb per in}$$

The bending moment in the elemental strip is

$$M = -D \frac{d^2 y}{dx^2}$$

and, by using eq (e) and substituting

$$y = \frac{P_0}{2\beta^3 D} e^{-\beta x} \cos \beta x,$$

<sup>35</sup> This method was used in investigating the stress distribution in various shapes of steam boiler heads, see E. Hohn and A. Huggenberger, *Über die Festigkeit der Gewölbten Boden und der Zylinderschale*, Zürich, 1927, and W. M. Coates, 'The State of Stress in Full Heads of Pressure Vessels,' *Trans. A.S.M.E., Appl. Mech. Div.*, 1929. The method was also used in investigating local bending in tanks containing liquids, see T. Poschl and K. Terzaghi, *Berechnung von Behältern*, Berlin, 1926; H. Reissner, *Beton u. Eisen*, Vol. 7, 1908, and C. Runge, *Z. Math. u. Phys.*, Vol. 51, p. 254, 1904. Cylindrical shells with flat ends were discussed by E. O. Holmberg and K. Axelson, *Trans. A.S.M.E.*, Vol. 54, p. 13, 1932. The method was also applied to thick walled cylinders and gave satisfactory results, see the paper by C. W. MacGregor and L. F. Coffin, *J. Appl. Mech.*, Vol. 14, p. A 301, 1947. A further discussion of cylindrical shells is given in S. Timoshenko, *Theory of Plates and Shells*, 1940.

<sup>36</sup> See S. Timoshenko, *ibid*.

we obtain

$$M = -\frac{P_0}{\beta} e^{-\beta x} \sin \beta x.$$

The numerically largest value of this moment occurs at  $\beta x = \pi/4$ , where  $M_{\max} = 45.4$  in. lb. The corresponding maximum bending stress in the strip is  $6M_{\max}/h^2 = 1,090$  lb per sq in. This stress must be added to the membrane stress

$$\sigma_1 = \frac{pr}{2h} = 150 \times 25 = 3,750 \text{ lb per sq in.}$$

The bending of the strip also produces hoop stresses. These are made up of two parts: (1) stresses which prevent cross sections of the strip from distortion (see p. 76) and which have a maximum value at any cross section of the strip of  $\pm 6\mu M/h^2$ ; and (2) stresses of magnitude  $-yE/r$  due to shortening of the circumference. Substituting the above expressions for  $y$  and  $M$ , the discontinuity stress which must be added to the membrane stress  $\sigma_2$  is

$$\begin{aligned} -\frac{P_0 E}{2\beta^3 D r} e^{-\beta x} \cos \beta x + \frac{6\mu P_0}{\beta h^2} e^{-\beta x} \sin \beta x \\ = \frac{6\mu P_0}{\beta h^2} e^{-\beta x} (\sin \beta x - 1.83 \cos \beta x). \end{aligned}$$

The maximum value of this stress can easily be found by the usual method. It is small in comparison with the membrane hoop stress  $pr/h = 7,500$  lb per sq in., so that discontinuity stresses in this case do not materially affect the maximum stress.

2. A thin cylindrical drum attached to two solid discs rotates about the axis  $O-O$  (Fig. 87) with a peripheral velocity  $v$ . Determine the local bending stresses in the drum if it is built in along the edges  $mn$  and  $m_1 n_1$ .

*Solution.* If the drum were separated from the discs, the increase in the radius of the drum due to centrifugal force would be equal to  $\gamma v^2 r / gE$  (see Part I, eq. 15, p. 32). The increase in the radius of the solid discs is (see eq. 194, p. 218)

$$\frac{1 - \mu}{4} \frac{\gamma v^2 r}{gE}.$$

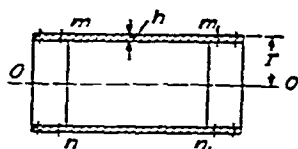


FIG. 87.

The difference of these two quantities is

$$\delta = \frac{3 + \mu}{4} \frac{\gamma v^2 r}{gE}$$

(It is assumed that  $\gamma$ ,  $\mu$  and  $E$  are the same for the drum and the discs.) Applying the same method as in the previous problem and considering a strip of unit width, the magnitudes of the shearing force  $P_0$  and the bending moment  $M_0$  at the edge  $mn$  are found by using eqs (11) and (12). These equations may be used if the strip is considered as very long. In addition, we may consider the discs as very rigid in comparison with the drum and neglect the deformations produced in them by the forces  $P_0$  and the couples  $M_0$ . The equations for calculating  $P_0$  and  $M_0$  then are

$$\frac{1}{2\beta^3 D} (P_0 - \beta M_0) = \delta,$$

$$\frac{1}{2\beta^2 D} (P_0 - 2\beta M_0) = 0.$$

from which

$$P_0 = 4\delta\beta^3 D, \quad M_0 = 2\delta\beta^2 D.$$

By use of these quantities the deflections and the bending stresses in the drum are found from an equation analogous to eq (11)

3 Determine the maximum bending stress in the drum of the preceding problem if  $r = 25$  in,  $h = \frac{1}{2}$  in,  $v = 500$  ft per sec and the material is steel

4 Determine the bending stresses produced in a pipe by a narrow ring shrunk onto it (Fig 88)

*Solution* Consider a longitudinal strip of unit width and denote by  $P$  the pressure between the ring and the pipe, per unit length of the circumference of the pipe. The bending of the strip is the same as that of a long bar on an elastic foundation which carries a single load  $P$  (Art 1). The decrease in the radius of the pipe due to  $P$ , from eq (8), is  $P/8\beta^3 D$ . The increase in the radius of the ring is  $Pr^2/AE$ , where  $A$  is the cross sectional area of the ring.

(The dimension of the ring in the radial direction is assumed to be small in comparison with the radius  $r$ .) If  $\delta$  is the initial difference in the inner radius of the ring and the outer radius of the pipe, the



FIG 88

equation for calculating  $P$  is

$$\frac{P}{8\beta^3 D} + \frac{Pr^2}{AE} = \delta$$

or, by using eq. (123) and taking  $\mu = 0.3$ , we obtain

$$0.643 \frac{P}{E} \left( \frac{r}{h} \right)^{3/2} + \frac{Pr^2}{AE} = \delta. \quad (g)$$

$P$  is determined from this equation, and the maximum bending moment in the strip is found from eq. (9).<sup>37</sup> The maximum bending stress in the strip is then

$$\sigma = \frac{3}{2} \frac{P}{h^2} \sqrt{\frac{r^2 h^2}{3(1 - \mu^2)}}.$$

The same method is also applicable to cases in which a cylindrical tube with reinforcing rings is subjected to either a uniform internal or a uniform external pressure. If the distance between the rings is large enough for the effect of any ring on the deflections produced by any other ring to be neglected,  $P$  can be obtained from eq. (g) by substituting  $\delta \approx pr^2/Eh$ . This represents the change in the radius of the pipe due to the uniform pressure.<sup>38</sup>

5. Solve the preceding problem assuming that the length  $l$  of the pipe is not large and that the ring is at the middle of the length. The material is steel and the dimensions are  $r = 25$  in.,  $h = \frac{1}{2}$  in.,  $l = 50$  in.,  $A = 4$  sq in., and  $\delta = 0.05$  in.

*Hint.* In calculating the pressure  $P$  per unit length of the ring, use the results obtained for the beam shown in Fig. 13, p. 18. Thus, the deflection produced in the pipe by the pressure  $P$  is

$$\frac{P}{8\beta^3 D} \cdot \frac{\cosh \beta l + \cos \beta l + 2}{\sinh \beta l + \sin \beta l}.$$

The equation for calculating  $P$  is then

$$\frac{P}{8\beta^3 D} \cdot \frac{\cosh \beta l + \cos \beta l + 2}{\sinh \beta l + \sin \beta l} + \frac{Pr^2}{AE} = \delta.$$

<sup>37</sup> An example of such calculations is given in the paper by G. Cook, *Engineering*, Vol. 116, p. 479, 1923. See also R. Lorenz, *Z. Ver. deut. Ing.*, Vol. 52, p. 1706, 1908; M. Westphal, *ibid.*, Vol. 41, p. 1036, 1897.

<sup>38</sup> The application of this method to the calculation of hull stresses in a submarine having a circular cross section is given in a paper by K. v. Sanden, *Werft u. Reederei*, p. 189, 1920.

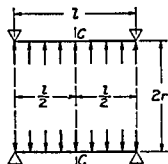


FIG 89

6 A circular cylindrical pipe with simply supported edges is subjected to a uniform internal pressure  $p$ . Find the longitudinal bending stress and the deflection at the middle of the pipe, Fig 89. The dimensions of the pipe are the same as in the preceding problem.

*Hint* From the results of the problem shown in Fig 20, p 24, the deflection and the bending moment per unit length of the

circumference at the middle cross section  $c-c$  are

$$y_c = \frac{pr^2}{Eh} \left( 1 - \frac{2 \cosh \frac{\beta l}{2} \cos \frac{\beta l}{2}}{\cosh \beta l + \cos \beta l} \right),$$

$$M = \frac{p}{\beta^2} \frac{\sinh \frac{\beta l}{2} \sin \frac{\beta l}{2}}{\cosh \beta l + \cos \beta l}$$

7 Solve the preceding problem assuming that the edges of the pipe are built in rigidly.

*Hint* Use the results of the problem shown in Fig 21, p 24.

8 A circular steel pipe is reinforced by rings which are at distance  $l$  apart, Fig 90a, and subjected to internal pressure  $p$ . Find the pressure  $P$  produced per unit length of the inner circumference of a ring. Find the maximum bending stresses in the pipe.

*Solution* Let us begin with a consideration of the portion of the pipe between two rings under the action of shearing forces  $V_0$  (Fig 90b) and bending moments  $M_0$  (Fig 90c) per unit length of the

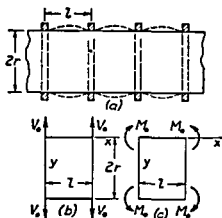


FIG 90

circumference of the pipe. (The width of the ring is assumed to be negligible in comparison with the distance  $l$  between the rings.) Considering a longitudinal strip of unit width as a beam on an elastic foundation and using the results of the problems in Fig. 12, p. 17, and in Fig. 18, p. 23, we find for the deflection and the slope at the left end of the strip in Fig. 90*b*

$$(w_1)_{z=0} = -\frac{2V_0\beta r^2}{Ek} \cdot \frac{\cosh \beta l + \cos \beta l}{\sinh \beta l + \sin \beta l}, \quad (h)$$

$$\left(\frac{dw_1}{dx}\right)_{z=0} = \frac{2V_0\beta^2 r^2}{Ek} \cdot \frac{\sinh \beta l - \sin \beta l}{\sinh \beta l + \sin \beta l}. \quad (i)$$

For the left end of the strip in Fig. 90*c* we obtain

$$(w_2)_{z=0} = -\frac{2M_0\beta^2 r^2}{Ek} \cdot \frac{\sinh \beta l - \sin \beta l}{\sinh \beta l + \sin \beta l}, \quad (j)$$

$$\left(\frac{dw_2}{dx}\right)_{z=0} = \frac{4M_0\beta^3 r^2}{Ek} \cdot \frac{\cosh \beta l - \cos \beta l}{\sinh \beta l + \sin \beta l}. \quad (k)$$

From our definition of  $P$  it follows that

$$V_0 = -\frac{P}{2}.$$

Substituting this in eq. (i) and observing that in the pipe (Fig. 90*a*) the tangent to the strip must be parallel to the axis of the pipe, we obtain

$$\left(\frac{dw_1}{dx}\right)_{z=0} + \left(\frac{dw_2}{dx}\right)_{z=0} = 0,$$

from which

$$M_0 = \frac{P}{4\beta} \cdot \frac{\sinh \beta l - \sin \beta l}{\cosh \beta l - \cos \beta l}. \quad (l)$$

In calculating  $P$  we assume first that the rings are absolutely rigid. In such a case the deflection in the pipe produced by the forces  $P$  under the rings must be equal to the radial expansion  $pr^2/Ek$  which

the pipe would have in the absence of the reinforcing rings. Hence the equation for calculating  $P$  is

$$(w_1)_{x=0} + (w_2)_{x=0} = \frac{pr^2}{Eh},$$

or

$$\frac{P\beta r^2}{Eh} \frac{\cosh \beta l + \cos \beta l}{\sinh \beta l + \sin \beta l}$$

$$- \frac{P\beta r^2}{2Eh} \cdot \frac{(\sinh \beta l - \sin \beta l)^2}{(\sinh \beta l + \sin \beta l)(\cosh \beta l - \cos \beta l)} = \frac{pr^2}{Eh} \quad (m)$$

In each particular case this equation can be readily solved for  $P$ . Substituting the value of  $P$  in eq (l), we obtain the required value of the bending moment  $M_0$ .

To take into account the expansion of the reinforcing rings, we observe that the forces  $P$  produce an extension of the inner radius of the ring equal to  $Pr^2/AE$ , where  $A$  is the cross sectional area of the ring. The deflection of the pipe is diminished by the same amount. Hence to obtain the force  $P$  in this case we have only to substitute

$$\frac{pr^2}{Eh} - \frac{Pr^2}{AE}$$

instead of  $pr^2/Eh$  on the right-hand side of eq (m).

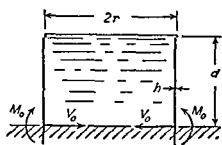


FIG 91

9 Find the bending moment  $M_0$  and the shearing force  $V_0$  per unit length of circumference at the bottom of the cylindrical steel tank filled with liquid, Fig 91, if  $r = 30$  ft,  $d = 26$  ft,  $h = 14$  in,  $\gamma = 0.03613$  lb per cu in, and  $\mu = 0.25$ .

Answer  $M_0 = 13,960$  in lb per in,  $V_0 = 563.6$  lb per in.

10 Solve Prob 5 assuming that the ring is fitted at the left end of the pipe. The resistance of the ring to torsion may be neglected.

*Hint* Use the result obtained for Prob 6, p. 24.

**27. Thermal Stresses in Cylindrical Shells**—If a cylindrical shell with free edges undergoes a uniform temperature

change, no thermal stresses will be produced. But if the edges are supported or clamped, free expansion of the shell is prevented, and local bending stresses are set up at the edges. Assume, for example, that the edges of a long cylindrical pipe are built in; then the shearing forces and the bending moments at the edges are obtained as in Prob. 2 of Art. 26. It is only necessary to substitute into the equation of that problem the quantity  $\delta = r\alpha t$ , representing the increase in the radius of the shell due to thermal expansion. If the length of the pipe is not large and both ends have to be considered simultaneously, the bending moments and the shearing forces can be readily obtained by using the results of Prob. 8 of Art. 26.

Let us now consider the case in which there is a temperature gradient in the radial direction. Assume that  $t_1$  and  $t_2$  are the uniform temperatures of the cylindrical wall at the inside and the outside surface, respectively, and that the variation of the temperature through the thickness is linear. In such a case, at points at a large distance from the ends of the shell there will be no bending, and the stresses can be calculated by using eq. (87), p. 91, derived for a plate with a clamped edge. This gives for the maximum bending stress

$$\sigma_{\max} = \frac{\alpha E(t_1 - t_2)}{2(1 - \mu)}. \quad (a)$$

(It is assumed that  $t_1 > t_2$ .) Then the tensile stress will act at the outer surface of the shell.

Near the ends of the shell there will be some bending of the shell and the total thermal stresses will be obtained by superposing upon the stresses of eq. (a) the stresses due to that bending. Let us consider as an example the stresses at a free end of a long cylindrical pipe. In calculating the stresses in this case we observe that at the edge the stresses represented by eq. (a) result in uniformly distributed moments  $M_0$ , Fig. 92a, of the magnitude

$$M_0 = \frac{\alpha E(t_1 - t_2)h^2}{12(1 - \mu)}. \quad (b)$$



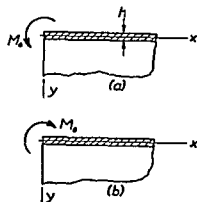


FIG. 92.

To obtain a free edge, moments of the same magnitude but opposite in direction must be superposed, Fig. 92*b*. Hence the thermal stresses at the free edge are obtained by superposing upon the stresses of eq. (a) the stresses produced by the moments shown in Fig. 92*b*. These latter stresses can be readily obtained by considering the bending of an

elemental strip and then using eq. (11), p. 12, which gives

$$y = -\frac{M_0}{2\beta^2 D} e^{-\beta x} (\cos \beta x - \sin \beta x), \quad (c)$$

where  $\beta$  is given by eq. (123). The largest deflection, obtained at the free edge ( $x = 0$ ), is

$$y_{\max} = -\frac{M_0}{2\beta^2 D} \quad (d)$$

and the corresponding hoop stresses are

$$\frac{M_0}{2\beta^2 D} \cdot \frac{E}{r} = \frac{E\alpha(t_1 - t_2)}{2\sqrt{3}(1 - \mu)} \sqrt{1 - \mu^2}. \quad (e)$$

The bending moment acting on the end of the elemental strip is given by eq. (b). The bending moments preventing the cross sections of the strip from distortion during bending are

$$\mu M_0 = \mu \frac{\alpha E(t_1 - t_2) h^2}{12(1 - \mu)}. \quad (f)$$

The maximum thermal stress acts at the outer surface of the pipe in the circumferential direction and consists of three parts: (1) stress given by eq. (a), (2) stress given by eq. (e), and (3) stress produced by the moments given by eq. (f). Hence

$$\sigma_{\max} = \frac{\alpha E(t_1 - t_2)}{2(1 - \mu)} \left( 1 + \frac{\sqrt{1 - \mu^2}}{\sqrt{3}} - \mu \right). \quad (125)$$

For  $\mu = 0.3$  this stress is about 25 per cent greater than the stress from eq. (a) calculated at points at a large distance from the ends. We can therefore conclude that if a crack occurs in a brittle material such as glass due to a temperature difference  $t_1 - t_2$ , it will start at the edge and will proceed in the axial direction. In a similar manner the stresses can also be calculated in cases in which the edges are clamped or supported.<sup>32</sup>

### Problems

1. Find the thermal stresses produced in a long steel pipe with built-in edges if  $r = 25$  in.,  $t = \frac{1}{8}$  in.,  $\mu = 0.3$ , coefficient of thermal expansion  $\alpha = 70 \times 10^{-7}$ , and the increase in the uniform temperature of the pipe is  $100^\circ \text{F}$ .

*Solution.* With the given dimensions we find

$$\beta = 0.364 \text{ in.}^{-1}, \quad D = 343 \times 10^3 \text{ lb in.}$$

The free elongation of the radius of the pipe due to the temperature rise is  $\delta = \alpha r(t - t_0) = 70 \times 25 \times 100 \times 10^{-7} = 175 \times 10^{-4}$  in. Substituting in the equations of Prob. 2 of the preceding article, we find the shearing force and the bending moment per unit length of the circumference at the built-in edge:

$$P_0 = 4\beta^3 D = 1,160 \text{ lb per in.}$$

$$M_0 = 2\beta^2 D = 1,590 \text{ in. lb per in.}$$

With these values of  $P_0$  and  $M_0$  the stresses in the axial and circumferential directions at the built-in edge can be readily calculated. (It is assumed that the tube is free to expand in the axial direction.)

2. Solve the preceding problem assuming that the edges are simply supported.

3. A steel tube of the same dimensions as in Prob. 1 has the temperatures  $t_1$  and  $t_2$  at the inside and the outside surfaces respectively. Find the maximum stress in the tube if  $t_1 - t_2 = 100^\circ \text{F}$  and the edges are free.

*Answer.*  $\sigma_{\max} = 18,750 \text{ lb per sq in.}$

4. Solve the preceding problem assuming that the edges of the tube were built in when the tube had a uniform temperature equal to  $(t_1 + t_2)/2$ .

<sup>32</sup> Several examples of this kind are discussed by C. H. Kent, *Trans. A.S.M.E.*, Vol. 53, p. 167, 1931. The case of a temperature gradient in the axial direction is discussed in S. Timoshenko, *Theory of Plates and Shells*, p. 423, 1940.

28. **Twisting of a Circular Ring by Couples Uniformly Distributed along Its Center Line.**—There are cases in which a circular ring of uniform cross section is subjected to the action of twisting couples uniformly distributed along its center line.<sup>40</sup> Considering half of the ring, Fig 93*a*, as a free body,

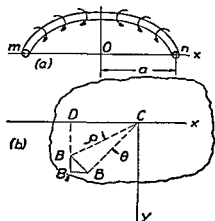


FIG 93

we conclude from the condition of equilibrium with respect to moments about the diameter  $Ox$  that there must be a bending moment acting on the cross sections  $m$  and  $n$  of the magnitude

$$M = M_t a, \quad (a)$$

where  $a$  is the radius of the center line and  $M_t$  is the twisting couple per unit length of the center line

Let us consider now the deformation of the ring. From the condition of symmetry it can be concluded that during twist each cross section rotates in its own plane through the same angle  $\theta$ , which is assumed to be small in the following discussion.<sup>41</sup> Let  $C$  be the center of rotation (Fig 93*b*) and  $B$  a point in the cross section at distance  $\rho$  from  $C$ . Owing to rotation of the cross section the point  $B$  describes a small

<sup>40</sup> Examples of such problems are the calculation of stresses in the retaining rings of commutators of electric motors and the stress analysis of pipe flanges

<sup>41</sup> A general discussion of the problem when  $\theta$  is not small is given by R. Grammel, *Z angew Math u Mech*, Vol 3, p 429, 1923, and Vol 7, p 198, 1927. See also the book by C. B. Biezeno and R. Grammel, *Technische Dynamik*, Vol 1, p 430, 1953.

arc  $\overline{BB_1} = \rho\theta$ . Due to this displacement the annular fiber of the ring, which is perpendicular to the section at the point  $B$ , increases its radius by  $\overline{B_2B_1}$ . If the coordinate axes are taken as indicated, we have from the similarity of the triangles  $BB_1B_2$  and  $BDC$ ,

$$\overline{B_1B_2} = \overline{BB_1}(\overline{DB}/\overline{BC}) = \rho\theta \frac{y}{\rho} = \theta y. \quad (b)$$

Let us consider first the case in which the cross-sectional dimensions of the ring are small in comparison with the radius  $a$  of the center line. Then the radius of any ring fiber may be taken equal to  $a$  without great error, and the unit elongation of the fiber  $B$ , due to the displacement given by eq. (b), is

$$\epsilon = \frac{\theta y}{a}. \quad (c)$$

If there is no lateral pressure between the ring fibers, the fiber stress due to elongation  $\epsilon$  is

$$\sigma = \frac{E\theta y}{a}. \quad (d)$$

Now, from the equilibrium of the half ring, the sum of all the normal forces acting on the cross section of the ring must be equal to zero, and the moment of these forces about the  $x$  axis must be equal to  $M$  (see eq. a). If  $dA$  denotes an elemental area of the cross section, these equations of equilibrium become

$$\int_A \frac{E\theta y}{a} dA = 0; \quad \int_A \frac{E\theta y^2}{a} dA = M, \quad (e)$$

where the integration is extended over the cross-sectional area  $A$ . The first of these equations shows that the centroid of the cross section must be on the  $x$  axis; from the second we find

$$\theta = \frac{Ma}{EI_x} = \frac{M_t a^2}{EI_x}, \quad (126)$$

where  $I_x$  is the moment of inertia of the cross section of the

ring with respect to the  $x$  axis. Substituting in eq. (d), we find

$$\sigma = \frac{M_t a y}{I_x}, \quad (127)$$

i.e., the distribution of the normal stresses over the cross section of the ring is the same as in the bending of straight bars; the stress is proportional to the distance from the neutral axis  $x$ , and the maximum stress occurs at the points most remote from this axis.

As a second example let us consider a ring of rectangular cross

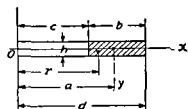


FIG 94

section (Fig 94) whose width  $b$  is not small in comparison with the radius  $a$  of the center line. Let  $c$  and  $d$  denote the inner and the outer radius of the ring respectively, and  $r$  the radius of any fiber of the ring, and assume as before that the deformation of the ring consists of a rotation of its cross section<sup>42</sup> through an

angle  $\theta$ . The elongation of the fiber at a radius  $r$  and the corresponding stress are

$$\epsilon = \frac{\theta y}{r}; \quad \sigma = \frac{E \theta y}{r}. \quad (f)$$

The equation of equilibrium analogous to the second of eqs. (e) becomes

$$\int_{-h/2}^{+h/2} \int_c^d \frac{E \theta y^2 dr dy}{r} = M$$

and, by performing the integration,

$$\frac{E \theta h^3}{12} \log_e \frac{d}{c} = M,$$

from which

$$\theta = \frac{12M}{E h^3 \log_e \frac{d}{c}} = \frac{12M_t a}{E h^3 \log_e \frac{d}{c}}. \quad (128)$$

<sup>42</sup> The possibility of distortion of the cross section is neglected in this consideration. The corresponding error is small, provided  $d/c < 1.5$ . See A. M. Wahl, *loc. cit.*, p. 113.

Substituting this value into the second of eqs. (f) we obtain

$$\sigma = \frac{12My}{h^3 r \log_e \frac{d}{c}}$$

The maximum stress is found at the inner corners of the ring where  $r = c$  and  $y = h/2$ :

$$\sigma_{\max} = \frac{6M}{h^2 c \log_e \frac{d}{c}} = \frac{6M_t a}{h^2 c \log_e \frac{d}{c}} \quad (129)$$

If  $b$  is small, eq. (128) can easily be changed to the form of eq. (126). Thus by using  $d = a + (b/2)$  and  $c = a - (b/2)$  we find

$$\log_e \frac{d}{c} = \log_e \frac{a + \frac{b}{2}}{a - \frac{b}{2}} \cong \log_e \left( 1 + \frac{b}{a} \right).$$

For small values of the ratio  $b/a$  the above logarithm is approximately equal to  $b/a$ . Substitution of this into eq. (128) gives eq. (126).

These results can be used in calculating the stresses produced at the joint of a pipe and a flange<sup>43</sup> by forces  $R$  (Fig. 95).  $R$  is the force per unit length of the inner circumference of the pipe. The force per unit length of the outer circumference of the flange is  $R(c/d)$ . Under the action of these forces the cross section of the flange rotates through the angle  $\theta$ , and the wall of the pipe bends as shown in Fig. 95b by the broken lines. Let  $M_0$  and  $P_0$  be the bending moment and the shearing force at the joint per unit length of the inner circumference of the pipe. The magnitude of these quantities can be found from the condition of continuity at the junction of pipe and flange. Since ordinarily the flange is very rigid in the plane perpendicular to the

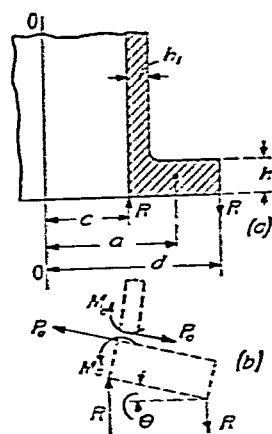


FIG. 95.

<sup>43</sup> Another method of calculating these stresses is given by E. O. Waters, *J. Appl. Mech.*, Vol. 59, p. 161, 1937. See also J. D. Mattimore, N. O. Smith-Petersen and H. C. Bell, *Trans. A.S.M.E.*, Vol. 60, p. 297, 1938. The method was extended to noncylindrical shells by G. Horvay and I. M. Clausen; see Paper No. 53-A-43 presented at the annual meeting of the American Society of Mechanical Engineers, Dec. 1953.

axis of the pipe, the radial displacement produced in the flange by forces  $P_0$  is negligible, and the deflection at the edge of the pipe can be considered zero. The angle of rotation of the edge of the pipe is equal to  $\theta$ , the angle of rotation of cross sections of the flange. Then eqs (11) and (12) (see p. 12) give the following equations for calculating  $M_0$  and  $P_0$

$$\begin{aligned}\frac{1}{2\beta^3 D}(P_0 - \beta M_0) &= 0, \\ -\frac{1}{2\beta^2 D}(P_0 - 2\beta M_0) &= \theta.\end{aligned}$$

From the first of these equations

$$P_0 = \beta M_0 \quad (g)$$

Then

$$M_0 = 2\beta D\theta \quad \text{and} \quad P_0 = 2\beta^2 D\theta \quad (h)$$

For a pipe of thickness  $h_1$  and inner radius  $c$ , we find  $\beta$  by eq. (123)

$$\beta = \sqrt[4]{\frac{3(1 - \mu^2)}{c^2 h_1^2}} \quad (i)$$

(If the thickness of the pipe is small, the difference between the inner radius and the radius of the middle surface can be neglected.) The torque per unit length of the center line of the flange, produced by the forces shown in the figure, is

$$\begin{aligned}M_t &= \frac{c}{a} \left[ R(d - c) - M_0 - P_0 \frac{h}{2} \right] \\ &= \frac{c}{a} \left[ R(d - c) - M_0 - M_0 \frac{h}{2} \beta \right] \quad (j)\end{aligned}$$

The substitution of eq. (j) into eq. (128) gives the angle  $\theta$ , and then from the first of eqs. (h)

$$M_0 = 2\beta D \frac{12c}{Eh^3 \log_e \frac{d}{c}} \left[ R(d - c) - M_0 - M_0 \frac{h}{2} \beta \right].$$

Replacing  $D$  by its magnitude  $Eh_1^3/12(1 - \mu^2)$ , we obtain

$$M_0 = \frac{R(d - c)}{1 + \frac{\beta h}{2} + \frac{1 - \mu^2}{2\beta c} \left( \frac{h}{h_1} \right)^3 \log_e \frac{d}{c}} \quad (130)$$

The quantities  $M_0$  and  $P_0$  can be calculated from eqs. (130) and (g), provided we are given the dimensions of the pipe, Poisson's ratio, and the forces  $R$ . Then the bending stresses in the pipe may be found as in Art. 26.

### Problems

1. Determine the bending moment  $M_0$  and the shearing force  $P_0$  in the pipe shown in Fig. 95 if  $d = 6\frac{1}{2}$  in.,  $c = 3\frac{5}{16}$  in.,  $h = 1\frac{7}{16}$  in.,  $h_1 = \frac{13}{16}$  in.,  $\mu = 0.3$ .

*Solution.* From eq. (i)

$$\beta = \frac{\sqrt[4]{2.73}}{\sqrt{ch_1}} = 0.784 \text{ in.}^{-1}$$

and in addition

$$\log_e \frac{d}{c} = 0.635; \quad \frac{\beta h}{2} = 0.564.$$

Substituting these values into eq. (130), we obtain

$$M_0 = 0.459R(d - c); \quad P_0 = \beta M_0 = 0.360R(d - c).$$

The maximum bending stress in the pipe is obtained from the equation

$$\sigma = \frac{6M_0}{h_1^2}.$$

2. Find an expression for the small deflection of the conical ring, shown in Fig. 96, which represents an element of a Belleville spring.  $R$  is the load per unit length of the inner edge of the ring.

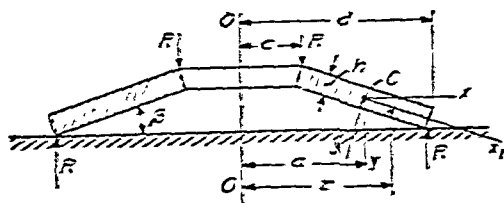


FIG. 95.

*Solution.* Take, as before, the coordinates  $x$  and  $y$  with the origin at the center of rotation  $C$ . The unit elongation and the unit stress for any fiber with the radius  $r$  are given by eqs. (f). From the equilibrium of the half ring, we obtain

$$\int_{\frac{\pi}{2}} \frac{E\beta y}{r} dA = 0; \quad \int_{\frac{\pi}{2}} \frac{E\beta y^2}{r} dA = M = Rc(d - c). \quad (k)$$



The position of the center of rotation  $C$  can be determined from the first of these two equations. Let  $a$  be the radius at the point  $C$  and assume the angle  $\beta$  of the cone to be small so that we can take  $\sin \beta = \beta$ ,  $\cos \beta = 1$ . Then by taking the axes  $x_1$  and  $y_1$  parallel to the sides of the rectangular cross section and noting that  $y = y_1 + \beta x_1 = y_1 + \beta(r - a)$ , the first of eqs (k) becomes

$$\begin{aligned} \int_{-h/2}^{+h/2} \int_c^d \frac{E\theta}{r} [y_1 + \beta(r - a)] dr dy_1 &= E\theta\beta h \left| r - a \log_e r \right|_c^d \\ &= E\theta\beta h \left( d - c - a \log_e \frac{d}{c} \right) = 0, \end{aligned}$$

from which

$$a = \frac{d - c}{\log_e \frac{d}{c}} \quad (l)$$

The second of eqs (k) becomes

$$\begin{aligned} \int_{-h/2}^{+h/2} \int_c^d \frac{E\theta}{r} [y_1 + \beta(r - a)]^2 dr dy_1 \\ = E\theta \left[ \frac{h^3}{12} \log_e \frac{d}{c} + \beta^2 h \left( \frac{d^2 - c^2}{2} - 2a(d - c) + a^2 \log_e \frac{d}{c} \right) \right] \\ = Rc(d - c), \end{aligned}$$

and by substituting the value from eq (l) for  $a$  we obtain for the vertical deflection of the upper edge of the cone

$$\delta = \theta(d - c) = \frac{Rc(d - c)}{E \left[ \frac{h^3}{12(d - c)} \log_e \frac{d}{c} + \beta^2 h \left( \frac{d + c}{2} - \frac{d - c}{\log_e \frac{d}{c}} \right) \right]} \quad (m)$$

This equation gives  $\delta$  if we know the dimensions of the ring, the modulus of elasticity of the material and the load  $R$ . The derivation neglects the effect of the change in the angle  $\beta$  due to the rotation  $\theta$ .<sup>44</sup>

<sup>44</sup> For larger deflections the change in the angle  $\beta$  must be considered. In such cases the deflection is no longer proportional to the load. See the paper by W. A. Brecht and A. M. Wahl, *Trans. A. S. M. E. Appl. Mech. Div.*, Vol. 52, p. 52, 1930. See also papers by J. O. Almen and A. Laszlo, *ibid.*, Vol. 58, p. 305, 1936, and Siegfried Gross, *Z. Ver. deut. Ing.*, Vol. 79, p. 865, 1935.

## CHAPTER V

### BUCKLING OF BARS, PLATES AND SHELLS<sup>1</sup>

#### 29. Lateral Buckling of Prismatic Bars: Simpler Cases.—

The previous discussion of simultaneous bending and compression of struts (Part I, p. 263) showed that there is a certain *critical value* of the compressive force at which large lateral deflections may be produced by the slightest lateral load. For a prismatic bar with hinged ends and having two planes of symmetry<sup>2</sup> this *critical compressive force* is

$$P_{cr} = \frac{\pi^2 EI}{l^2}, \quad (a)$$

where  $I$  is the smaller principal moment of inertia of the cross section. Experiments show that when the compressive force in a slender<sup>3</sup> strut approaches this value, lateral deflection begins and increases so rapidly with increase of the compressive force that a load equal to the critical value is usually sufficient to produce complete failure of the structure. Consequently this *critical load* must be considered the criterion of strength for slender columns and struts.

From eq. (a) it is seen that this critical load does not depend upon the strength of the *material* of the bar, but only upon the dimensions of the structure and the modulus of elasticity of the material. Two equal slender struts, one of high-strength steel and the other of common structural steel, will buckle at the same compressive force, although the strength of the material in the two cases is very different. Eq. (a) shows also that the load-carrying capacity of a strut may be raised by in-

<sup>1</sup> For more information on problems of buckling see S. Timoshenko, *Theory of Elastic Stability*, New York, 1936.

<sup>2</sup> The more general case in which lateral buckling is combined with torsion is discussed later (p. 279).

<sup>3</sup> When the strut is not slender enough, lateral buckling occurs at a compressive stress which is above the proportional limit. This case is discussed later (p. 178).

creasing  $I$ . This may be done without changing the cross sectional area by distributing the material as far as possible from the principal axes of the cross section. Hence tubular sections are more economical than solid sections for compression members. By diminishing the wall thickness of such sections and increasing the transverse dimensions their stability can be increased. There is a lower limit for the wall thickness, however, below which the wall itself becomes unstable, and instead of buckling of the strut as a whole, there occurs a local buckling which brings about a corrugation of the wall.

This discussion shows that the *elastic stability*, or the side-wise buckling of compression members, is of great practical importance. This is especially true in many modern structures where the cross-sectional dimensions are being made smaller and smaller owing to the use of stronger materials and the desire to save weight. In many cases failure of an engineering structure may be attributed to elastic instability and not to the lack of strength on the part of the material.

In the previous discussion (Part I, p. 263) the magnitude of the critical load of a strut was obtained by considering the simultaneous action of compressive and bending forces. The same result may be obtained by assuming that the bar is compressed by a centrally applied load only.<sup>4</sup> Let us consider the

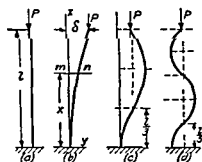


FIG 97

case of a bar in the form of a slender vertical prism built in at the bottom and loaded axially at the top (Fig. 97). If the load  $P$  is less than its critical value the bar remains straight and undergoes only axial compression. This straight form of elastic equilibrium is *stable*, i.e., if a lateral force be applied and

<sup>4</sup> The values of the critical loads, for various conditions at the ends of a compressed prismatic bar, were first obtained by L. Euler, see *Additamentum, De curvis elasticis*, in the *Methodus inveniendi lineas curvas maximi minive proprietate gaudentes*, Lausanne, 1744. See also *Histoire de l'Académie*, Berlin, Vol. 13, 1757. An English translation of this work is given in *Isis*, No. 58, Vol. 20, 1933.

a small deflection produced, the deflection disappears when the lateral force is removed and the bar becomes straight again. By increasing  $P$  gradually we arrive at a condition in which the straight form of equilibrium becomes unstable and a slight lateral force produces a lateral deflection which does not disappear when the force is removed. The critical load is then defined as the axial load which is sufficient to keep the bar in a slightly bent form (Fig. 97*b*).

This load can be calculated by means of the differential equation of the deflection curve. With axes taken as indicated in Fig. 97*b*, the bending moment at any cross section  $mn$  becomes  $P(\delta - y)$ , and the differential equation of the deflection curve is <sup>5</sup>

$$EI \frac{d^2 y}{dx^2} = P(\delta - y). \quad (b)$$

It is apparent that with the upper end free, buckling of the bar will occur in the plane of *smallest flexural rigidity*. Denoting by  $EI$  the smallest flexural rigidity and letting

$$p^2 = \frac{P}{EI}, \quad (c)$$

eq. (b) becomes

$$\frac{d^2 y}{dx^2} + p^2 y = p^2 \delta. \quad (d)$$

The general solution of this equation is

$$y = \delta + C_1 \cos px + C_2 \sin px, \quad (e)$$

in which  $C_1$  and  $C_2$  are constants which must be adjusted so as to satisfy the following conditions at the built-in end:

$$(y)_{x=0} = 0; \quad \left( \frac{dy}{dx} \right)_{x=0} = 0.$$

These conditions are fulfilled if we take

$$C_1 = -\delta; \quad C_2 = 0.$$

<sup>5</sup> For the deflection shown in Fig. 97*b*,  $d^2 y/dx^2$  is positive; hence we use a positive sign on the right-hand side of eq. (b).

Then

$$y = \delta(1 - \cos px). \quad (f)$$

The condition at the upper end is

$$(y)_{x=l} = \delta,$$

which is satisfied if  $\cos pl = 0$  or if

$$pl = (2n + 1) \frac{\pi}{2}, \quad (g)$$

where  $n$  is an integer. The smallest value of  $pl$ , and therefore of  $P$ , which satisfies eq. (g) is obtained by putting  $n = 0$ . Then, using eq. (c), we obtain

$$pl = l \sqrt{\frac{P}{EI}} = \frac{\pi}{2},$$

from which

$$P_{cr} = \frac{\pi^2 EI}{4l^2}. \quad (131)$$

This is the *critical load* for the bar represented in Fig. 97a, i.e., the smallest load which can keep the bar in a slightly bent shape.

With  $n = 1, n = 2, \dots$ , in eq. (g) we obtain

$$P = \frac{9\pi^2 EI}{4l^2}, \quad P = \frac{25\pi^2 EI}{4l^2}, \quad \dots$$

The corresponding deflection curves are shown in Fig. 97c and d. For the shape shown in Fig. 97c a force 9 times larger than the critical is necessary, and for the shape in Fig. 97d the force must be 25 times larger. These forms of buckling are unstable and have no practical meaning, because the structure fails when the load reaches the value in eq. (131).

The critical load for certain other cases can easily be obtained from the solution for the foregoing case. For example, in the case of a bar with hinged ends (Fig. 98) it is evident from symmetry that each half of the bar is in the same condition as the bar

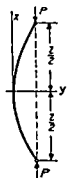


FIG. 98.

of Fig. 97*b*. Hence the critical load for this case is obtained by using  $l/2$ , instead of  $l$ , in eq. (131), which gives

$$P_{cr} = \frac{\pi^2 EI}{l^2}. \quad (132)$$

The case of a bar with hinged ends is very often encountered in practical applications and is called the *fundamental case* of buckling of a prismatic bar.

In the case of a bar with built-in ends (Fig. 99) there are reactive moments which keep the ends from rotating during buckling. The combination of the compressive force and the end moments is equivalent to the compressive force  $P$  applied eccentrically, Fig. 99. There are inflection points where the line of action of  $P$  intersects the deflection curve, because the bending moment at these points is zero. These points and the mid-point of the span divide the bar into four equal portions, each of which is in the same condition as the bar represented in Fig. 97*b*. Hence the critical load for a bar with built-in ends is found from eq. (131) by using  $l/4$  instead of  $l$ , which gives

$$P_{cr} = \frac{4\pi^2 EI}{l^2}. \quad (133)$$

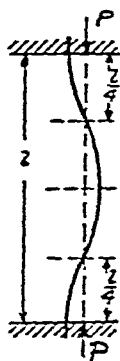


Fig. 99.

It has been assumed in the preceding discussion that the bar is very slender so that the stresses which occur during buckling remain within the proportional limit. Only under this condition can eq. (b) be applied. To establish the limit of applicability of the formulas derived above for the critical loads, let us consider the *fundamental case* (Fig. 98). Dividing eq. (132) by the cross-sectional area  $A$  of the bar and denoting by  $k$  the smaller radius of gyration, we obtain

$$\sigma_{cr} = \frac{P_{cr}}{A} = \pi^2 E \left( \frac{k}{l} \right)^2. \quad (134)$$

This equation is applicable as long as the stress  $\sigma_{cr}$  remains below the proportional limit of the material. With this limit

and also with the modulus  $E$  known for a given material, the limiting value of the ratio  $l/k$  (which is called the *slenderness ratio* of the bar) can easily be obtained from eq (134) for each particular case. In Fig 100 the relation (eq. 134) between

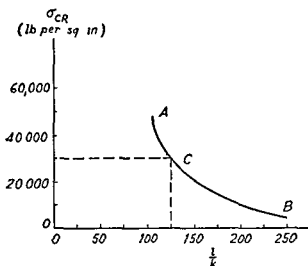


FIG 100

the slenderness ratio  $l/k$  and the value of  $\sigma_{cr}$  is given by the curve  $ACB$  for structural steel having  $E = 30 \times 10^6$  lb per sq in. Assuming that the proportional limit of the material is 30,000 lb per sq in, we conclude that only the portion  $CB$  of the curve can be used for determining  $\sigma_{cr}$ .

Proceeding in the same manner as above, we find the following equations for the cases represented in Figs. 97 and 99.

$$\sigma_{cr} = \pi^2 E \left( \frac{k}{2l} \right)^2, \quad (135)$$

$$\sigma_{cr} = \pi^2 E \left( \frac{k}{\frac{1}{2}l} \right)^2 \quad (136)$$

The equation for the fundamental case (eq 134) may be applied to these cases if we use a *reduced length*  $l_1$  instead of the actual length of the bar. In the case of a prismatic bar with one end built in and the other end free, the reduced length (eq 135) is twice as great as the actual length, so that  $l_1 = 2l$ . In the case of a prismatic bar with both ends built in, the reduced length (eq. 136) is half the actual length, or

$l_1 = l/2$ . The equation for the critical stress in the general case may consequently be represented in the form

$$\sigma_{cr} = \pi^2 E \left( \frac{k}{\alpha l} \right)^2 = \pi^2 E \left( \frac{k}{J_1} \right)^2, \quad (137)$$

in which  $\alpha$  depends upon the conditions at the ends of the bar and is sometimes called the *length coefficient*.

In discussing the design of columns (Part I, p. 268) the fundamental case of a column with hinged ends was considered. The information given there can now be applied to columns with other end conditions, provided the reduced length  $l_1$  instead of the actual length  $l$  is used. Thus in each particular case the design of a column reduces to the determination of the proper value of the *length coefficient*.

In the derivation of eq. (f) for the deflection curve after buckling, the maximum deflection  $\delta$  remained indeterminate, i.e., at the critical load the bar may have any small deflection. The above theory may be applied only to *small* deflections because only in such cases may we use the approximate expression  $d^2y/dx^2$  for the curvature, in place of the exact expression

$$\frac{\frac{d^2y}{dx^2}}{\left[ 1 + \left( \frac{dy}{dx} \right)^2 \right]^{3/2}}.$$

The solution of the exact differential equation for the deflection curve has been found for several cases<sup>6</sup> and shows that there is really no such indeterminateness in the deflection as is implied above. For example, for a bar with hinged ends the maximum deflection may be represented by the equation<sup>7</sup>

$$\delta = \frac{l\sqrt{8}}{\pi} \sqrt{\frac{P}{P_{cr}} - 1} \left[ 1 - \frac{1}{8} \left( \frac{P}{P_{cr}} - 1 \right) \right], \quad (138)$$

<sup>6</sup> See Saalschütz, *Der belastete Stab*, Leipzig, 1880. See also Halphen, *Traité des fonctions elliptiques*, Vol. 2, p. 192, 1888.

<sup>7</sup> See R. v. Mises, *Z. angew. Math. u. Mech.*, Vol. 4, p. 435, 1924; see also O. Domke, *Bautechnik*, Vol. 4, p. 747, 1926, and R. W. Burges, *Phys. Rev.*, 1917.



which shows that the deflection increases very rapidly when the load is above the critical value. Assuming, for example, that the load is 1 per cent larger than  $P_{cr}$ , we find from eq (138) that the deflection is about 9 per cent of the length  $l$  of the bar. (It is assumed that the strains remain within the proportional limit.)

The relation between the load and the deflection may be represented graphically (Fig

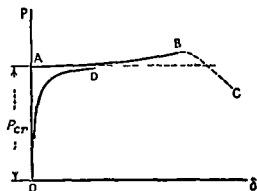


FIG 101

101) by the curve  $OAB$ , in which the load is represented by the ordinates and the deflections by the abscissas. As long as the load is smaller than  $P_{cr}$ , the deflection is zero. Beyond this limit the deflection increases rapidly with the load. (When yielding begins, the curve  $AB$  is no longer

applicable and further buckling proceeds as indicated by the broken line  $BC$ , Fig 101.)

In experimental investigations of the lateral buckling of compressed bars, the relation between the deflection and the load depends considerably upon the accuracy with which the load is centrally applied and upon the straightness and homogeneity of the bar. The load deflection curve is usually similar to curve  $OD$  in Fig 101. Because of inaccuracies of various kinds, deflection begins at small loads, but progresses very slowly as long as the load is far below the critical value. As the load approaches the critical value, the deflection proceeds very rapidly. The more accurately the bar is constructed and loaded, the more nearly the curve approaches the theoretical curve  $OAB$ .\*

\* A very close coincidence of experimental and calculated values of critical loads was obtained by Th v Karman, *Forschungsarb*, No 81, 1910. See also K Memmler, *Proc 2d Internat Congr Appl Mech*, Zurich, p 357, 1926.

# Problems

1. A steel bar of rectangular cross section  $1 \times 2$  in. with hinged ends is axially compressed. Determine the minimum length at which eq. (132) can be applied if  $E = 30 \times 10^6$  lb per sq in. and the limit of proportionality is 30,000 lb per sq in. Determine the magnitude of the critical stress if the length is 5 ft.

*Solution.* The smaller radius of gyration is  $k = 1/\sqrt{12}$  in.; hence the minimum length is found from eq. (134):

$$30,000 = \pi^2 \times 30 \times 10^6 \times \frac{1}{12} \times \frac{1}{l_{\min}^2},$$

and

$$l_{\min} = 28.7 \text{ in.}$$

The critical stress for  $l = 5$  ft is found from eq. (134) to be

$$\sigma_{cr} = 6,850 \text{ lb per sq in.}$$

2. Solve the preceding problem, assuming a bar of circular cross section with a diameter of 1 in. and with built-in ends.

*Answer.* Minimum length = 50 in. For  $l = 5$  ft,  $\sigma_{cr} = 20,800$  lb per sq in.

3. Determine the critical compressive load for a standard 6 I 12.5 section with a length of 6 ft and with hinged ends.

*Answer.*

$$P_{cr} = \frac{\pi^2 EI}{l^2} = \frac{9.87 \times 30 \times 10^6 \times 1.8}{72^2} = 103,000 \text{ lb}$$

**30. Lateral Buckling of Prismatic Bars: More Complicated Cases.**—As an example of a more complicated case of lateral buckling of bars, let us consider a centrally compressed strut with the lower end built in and the upper end hinged (Fig. 102). The critical value of the compressive force is that value  $P_{cr}$  which can keep the strut in a slightly buckled shape. It may be seen that in this case, during buckling a lateral reaction  $Q$  will be produced and the differential equation of the deflection curve becomes

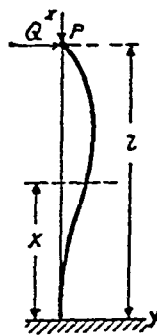


FIG. 102.

$$EI \frac{d^2 y}{dx^2} = -Py + Q(l - x). \quad (a)$$

The general solution of this equation, using the notation of eq. (c) in Art. 29, is

$$y = C_1 \cos px + C_2 \sin px + \frac{Q}{P}(l - x). \quad (b)$$

For determining the constants  $C_1$  and  $C_2$  and the unknown reaction  $Q$ , we have the following conditions at the ends:

$$(y)_{x=0} = 0, \quad (y)_{x=l} = 0, \quad \left(\frac{dy}{dx}\right)_{x=0} = 0.$$

Substituting the value of  $y$  from eq. (b), we obtain from these conditions

$$C_1 + \frac{Q}{P}l = 0, \quad C_1 \cos pl + C_2 \sin pl = 0, \quad pC_2 - \frac{Q}{P} = 0. \quad (c)$$

Determining the constants  $C_1$  and  $C_2$  from the first and the third of these equations and then substituting into the second equation, we obtain the following transcendental equation for calculating the critical load:

$$\tan pl = pl \quad (d)$$

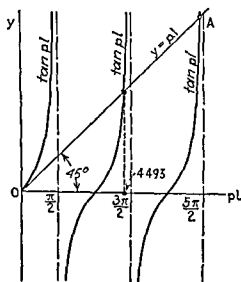


FIG. 103.

A graphical method is useful in solving this equation. In Fig. 103 curves are drawn representing  $\tan pl$  as a function of  $pl$ . These curves are asymptotic to the vertical lines  $pl = \pi/2, 3\pi/2, \dots$ , and for these values  $\tan pl$  becomes infinite. The roots of eq. (d) are now obtained as the abscissas of the intersection points of the above curves with the straight line  $y = pl$ . The smallest root obtained in this way is

$$pl = 4.493.$$

Then

$$P_{cr} = p^2 EI = \frac{20.19EI}{l^2} \approx \frac{\pi^2 EI}{(0.7l)^2}. \quad (139)$$

Thus the critical load is the same as for a strut with hinged ends having a reduced length:

$$l_1 = 0.7l.$$

As a second example let us consider a strut on three supports and centrally compressed by forces  $P$ , Fig. 104. In calculating the critical value of the compressive force we continue with our previous definition

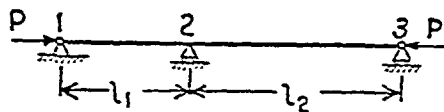


FIG. 104.

and assume that  $P_{cr}$  is the force which can keep the strut in a slightly buckled shape. As a result of buckling there will be a bending moment  $M_2$  at the middle support,<sup>9</sup> which can be calculated from eq. (38), p. 39, derived for continuous struts. By observing that in our case the ends of the strut are hinged, we obtain  $M_1 = M_3 = 0$  and eq. (38) becomes

$$\left( \beta_1 \frac{l_1}{I_1} + \beta_2 \frac{l_2}{I_2} \right) M_2 = 0. \quad (e)$$

This equation is satisfied and a buckled shape of the strut becomes possible if

$$\beta_1 \frac{l_1}{I_1} + \beta_2 \frac{l_2}{I_2} = 0. \quad (f)$$

In these equations the following notation is used (see eqs. 36 and 23):

$$\begin{aligned} \beta_1 &= 3 \left[ \frac{1}{(2u_1)^2} - \frac{1}{2u_1 \tan 2u_1} \right], \\ \beta_2 &= 3 \left[ \frac{1}{(2u_2)^2} - \frac{1}{2u_2 \tan 2u_2} \right] \end{aligned} \quad (g)$$

<sup>9</sup> An exception is the trivial case when the two spans are equal and the cross section is constant along the entire length. In this case  $M_2 = 0$  at the intermediate support, and each span is in the same condition as a strut with hinged ends.

and

$$u_1 = \frac{l_1}{2} \sqrt{\frac{P}{EI_1}}, \quad u_2 = \frac{l_2}{2} \sqrt{\frac{P}{EI_2}}. \quad (h)$$

If the dimensions of the strut are given, the ratio  $u_1:u_2$  is known from eqs. (h), and the ratio  $\beta_1:\beta_2$  from eq. (f) is

$$\frac{\beta_1}{\beta_2} = -\frac{l_2 I_1}{l_1 I_2}. \quad (i)$$

Having a numerical table of the functions  $\beta$ , we can readily solve this equation for the proper values of  $u_1$  and  $u_2$ . Then the critical value of  $P$  is obtained from eqs. (h).

Take, for example,  $I_1 = I_2 = I$  and  $l_2 = 2l_1$ . Then  $u_2 = 2u_1$  and

$$\frac{\beta_1}{\beta_2} = -2. \quad (j)$$

To solve this equation we have to find a value  $2u_1$  of the argument  $2u$  such that after doubling it the function  $\beta$  changes sign and reduces to half of its numerical value at the argument  $2u_1$ . Using a table<sup>10</sup> of numerical values of  $\beta$ , we readily find that this condition is satisfied if

$$2u_1 = 1.93.$$

Hence, from equations (h),

$$P_{cr} = \frac{1.93^2 EI}{l_1^2} = \frac{3.72 EI}{l_1^2} = \frac{14.9 EI}{l_2^2}.$$

It is seen that the value of the critical load lies between the two values  $\pi^2 EI/l_1^2$  and  $\pi^2 EI/l_2^2$ , calculated for the separate spans as if each were a strut with hinged ends. The stability of the shorter span is reduced, owing to the action of the longer span, while the stability of the longer span is increased.

<sup>10</sup> Such a table is given in S. Timoshenko, *Theory of Elastic Stability*, 1936.

## Problems

1. Solve Prob. 1 of Art. 29 assuming that one end of the bar is hinged and the other built in as shown in Fig. 102.

2. Determine the critical value of the forces  $P$  which compress the vertical members of the rectangular frame shown in Fig. 105.

*Solution.* Symmetrical buckling, shown in Fig. 105, produces reactive bending moments  $M_0$  which resist free rotation of the ends of the vertical members. The differential equation for the deflection curve of the vertical member is

$$EI \frac{d^2 y}{dx^2} = -Py + M_0.$$

The general solution of this equation is

$$y = C_1 \cos px + C_2 \sin px + \frac{M_0}{P}. \quad (k)$$

The constants of integration and the moments  $M_0$  are to be determined from the following conditions, based on the symmetrical form of the buckled frame (Fig. 105):

$$(y)_{x=0} = 0; \quad \left(\frac{dy}{dx}\right)_{x=l/2} = 0; \quad \left(\frac{dy}{dx}\right)_{x=0} = \theta = \frac{M_0 l_1}{2EI_1}.$$

Substituting the value from eq. (k) for  $y$  we obtain

$$C_1 + \frac{M_0}{P} = 0; \quad -C_1 p \sin \frac{pl}{2} + C_2 p \cos \frac{pl}{2} = 0; \quad C_2 p = \frac{M_0 l_1}{2EI_1}.$$

These equations give the following transcendental equation for determining  $p$  and the critical load:

$$\tan \frac{pl}{2} + \frac{Pl_1}{2pEI_1} = 0,$$

or, using the notation of eq. (c) in Art. 29,

$$\tan \frac{pl}{2} + \frac{I}{I_1} \frac{l_1}{l} \frac{pl}{2} = 0. \quad (l)$$

When  $(I/I_1)(l_1/l)$  is large, i.e., when the resistance of the horizontal members of the frame to buckling of the vertical members is small,

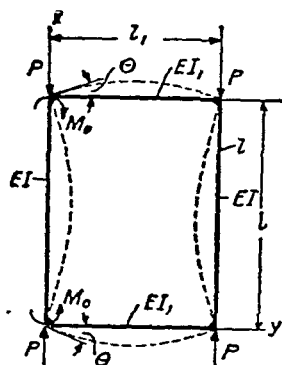


FIG. 105.

$\tan(pl/2)$  is a large negative number and  $pl/2$  approaches  $\pi/2$ . The critical load then approaches the value  $\pi^2 EI/l^2$  obtained before for a bar with hinged ends (eq 132)

When  $(I/I_1)(l_1/l)$  is small, i.e., when the resistance of the horizontal members of the frame to buckling of the vertical members is very great,  $\tan(pl/2)$  is a small negative number and  $pl/2$  approaches  $\pi$ . Then the critical load approaches the value  $4\pi^2 EI/l^2$  obtained before (eq 133) for a bar with built-in ends.

In the case of a square frame with all members of the same cross section ( $l = l_1$ ,  $I = I_1$ ) the equation for determining the critical load becomes

$$\tan \frac{pl}{2} + \frac{pl}{2} = 0,$$

from which

$$\frac{pl}{2} = 2.029,$$

$$P_{cr} = \frac{16.47EI}{l^2} = \frac{\pi^2 EI}{(0.774l)^2} \quad (m)$$

The reduced length in this case is therefore equal to  $0.774l$ . (Curves similar to those in Fig 103 can be used also in this case.)

3 Solve the preceding problem assuming that in addition to vertical forces  $P$  there are two pairs of horizontal forces  $Q$  which produce compression of the horizontal members of the frame.

*Hint* Since the horizontal bars are compressed, the angle of rotation  $\theta$  indicated in Fig 105 is <sup>11</sup>

$$\theta = \frac{M_0 l_2 \tan u}{2EI_1 u},$$

where

$$u^2 = \frac{Ql_1^2}{4EI_1}$$

The equation for calculating the critical value of  $P$  is obtained by substituting  $I_1 u / \tan u$  instead of  $I_1$  in eq (I) of Prob 2.

4 A strut  $AB$  with hinged ends, Fig 106, is compressed by the two forces  $P_1$  and  $P_2$ . Find the critical value of the force  $P_1 + P_2$  if  $(P_1 + P_2)/P_1 = m$ ,  $I_2/I_1 = n$ , and  $l_2/l_1 = r$ .

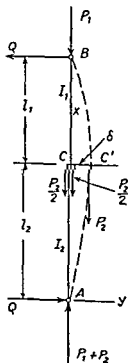


FIG 106

<sup>11</sup> It is obtained from eq (48), p 44, by substituting  $u$  for  $u$

*Solution.* Assuming that the buckled shape of the strut is as shown in Fig. 106 by the broken line, there will be horizontal reactions  $Q = \delta P_2/l$  produced during buckling. The differential equations of the upper and lower portions of the deflection curve are

$$\begin{aligned} EI_1 \frac{d^2 y_1}{dx^2} &= -P_1 y_1 - \frac{\delta P_2}{l} (l - x), \\ EI_2 \frac{d^2 y_2}{dx^2} &= -P_1 y_2 - \frac{\delta P_2}{l} (l - x) + P_2 (\delta - y_2). \end{aligned} \quad (n)$$

Using the notation

$$\frac{P_1}{EI_1} = p_1^2, \quad \frac{P_2}{EI_2} = p_2^2, \quad \frac{P_1 + P_2}{EI_2} = p_3^2, \quad \frac{P_2}{EI_1} = p_4^2, \quad (o)$$

we obtain the following solutions of eqs. (n):

$$\begin{aligned} y_1 &= C_1 \sin p_1 x + C_2 \cos p_1 x - \frac{\delta p_4^2}{l p_1^2} (l - x) \\ y_2 &= C_3 \sin p_3 x + C_4 \cos p_3 x + \frac{\delta p_2^2}{l p_3^2} x. \end{aligned}$$

The constants of integration are obtained from the end conditions of the two portions of the buckled bar:

$$(y_1)_{x=l} = 0, \quad (y_1)_{x=l_2} = \delta, \quad (y_2)_{x=l_2} = \delta, \quad (y_2)_{x=0} = 0.$$

From these conditions we obtain

$$\begin{aligned} C_1 &= \frac{\delta(p_1^2 l + p_4^2 l_1)}{p_1^2 l (\sin p_1 l_2 - \tan p_1 l \cos p_1 l_2)}, & C_2 &= -C_1 \tan p_1 l \\ C_3 &= \frac{\delta(p_3^2 l - p_2^2 l_2)}{p_3^2 l \sin p_3 l_2}, & C_4 &= 0. \end{aligned}$$

Substituting into the continuity condition

$$\left( \frac{dy_1}{dx} \right)_{x=l} = \left( \frac{dy_2}{dx} \right)_{x=l_2}$$

we obtain the following transcendental equation for calculating the critical loads:

$$\frac{p_4^2}{p_1^2} - \frac{p_1^2 l + p_4^2 l_1}{p_1 \tan p_1 l_1} = \frac{p_2^2}{p_3^2} + \frac{p_3^2 l - p_2^2 l_2}{p_3 \tan p_3 l_2}, \quad (p)$$



which can be solved in each particular case by trial and error or by plotting both sides of the equation and determining the intersection point of the two curves. Taking as an example  $l_1 = l_2$ ,  $I_1 = I_2 = I$  and  $P_1 = P_2$ , we obtain

$$(P_1 + P_2)_{cr} = \frac{\pi^2 EI}{(0.87l)^2}$$

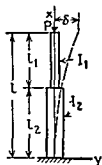


FIG 107

5 Find the critical load for a column built in at the bottom and free at the top and consisting of two prismatic portions with moments of inertia  $I_1$  and  $I_2$ ,  
FIG 107

*Solution* If  $\delta$  is the deflection at the top of the column the differential equations for the two portions of the deflection curve are

$$EI_1 \frac{d^2 y_1}{dx^2} = P(\delta - y_1),$$

$$EI_2 \frac{d^2 y_2}{dx^2} = P(\delta - y_2)$$

By making use of the notation from eqs (o) the solutions of these equations are

$$y_1 = \delta + C \cos p_1 x + D \sin p_1 x,$$

$$y_2 = \delta(1 - \cos p_2 x)$$

The constants of integration are obtained from the conditions

$$(y_1)_{x=l} = \delta, \quad (y_1)_{x=l_1} = (y_2)_{x=l_1},$$

which give

$$\delta + C \cos p_1 l + D \sin p_1 l = \delta,$$

$$\delta + C \cos p_1 l_2 + D \sin p_1 l_2 = \delta(1 - \cos p_2 l_2),$$

from which

$$C = -D \tan p_1 l, \quad D = \frac{\delta \cos p_2 l_2 \cos p_1 l}{\sin p_1 l_1}$$

Since the two portions of the deflection curve have the same tangent at  $x = l_2$  we have the equation

$$\delta p_2 \sin p_2 l_2 = -C p_1 \sin p_1 l_2 + D p_1 \cos p_1 l_2$$

Substituting for  $C$  and  $D$  the above values, we finally obtain the

following equation for calculating  $P_{cr}$ :

$$\tan p_1 l_1 \tan p_2 l_2 = \frac{p_1}{p_2}. \quad (q)$$

In the particular case when both portions of the column are the same, we have

$$p_1 l_1 = p_2 l_2 = \frac{l}{2} \sqrt{\frac{P}{EI}},$$

and eq. (q) becomes

$$\tan^2 \left( \frac{l}{2} \sqrt{\frac{P}{EI}} \right) = 1 \quad \text{or} \quad \frac{l}{2} \sqrt{\frac{P}{EI}} = \frac{\pi}{4}$$

and

$$P_{cr} = \frac{\pi^2 EI}{4l^2}.$$

This is the critical load for a column of constant cross section.

**31. Energy Method of Calculating Critical Compressive Loads.**<sup>12</sup>—Euler's formulas, derived in Art. 29, were derived by solving the differential equation of the deflection curve for a compression member with given end conditions. Other cases arise in which this equation is complicated and the exact solution becomes difficult. We may then use an approximate method, based on a consideration of the energy of the system.

As a simple example, consider a column built in at the bottom and carrying a load at the top (Fig. 97*a* and *b*). The straight form of equilibrium of the compressed bar is *stable* if the compressive force  $P$  is small, but *unstable* after  $P$  reaches its critical value at which lateral buckling begins. This critical value of  $P$  may be found by comparing the energy of the system in the two cases: (1) when the bar is simply *compressed* and (2) when it is *compressed and bent*. The strain energy in the bent bar is larger than that in the straight compressed form, because the energy of bending must be added to the energy of compression, which may be considered constant for

<sup>12</sup> See the writer's papers in *Bull. Polytech. Inst. (Kiev)*, 1910, and *Ann. ponts et chaussées*, 1913.

small lateral deflections The potential energy of the load  $P$  must also be considered The deflection of the bar is accompanied by a lowering of the point of application of the load  $P$  so that the potential energy of the load diminishes Let  $U$  be the strain energy of bending and  $U_1$  the decrease in the potential energy of the load Then if  $U_1$  is less than  $U$ , deflection of the bar is accompanied by an increase in the potential energy of the system This means that it would be necessary to apply some additional lateral force to produce bending In such a case the straight form of equilibrium is *stable* On the other hand, if  $U_1 > U$ , deflection of the bar is accompanied by a decrease in the potential energy of the system and the bending will proceed without the application of any lateral force, i.e., the straight form of equilibrium is *unstable* The critical value of the compressive force is therefore obtained from the condition

$$U = U_1. \quad (140)$$

To calculate the magnitude of the critical load from this equation we must have expressions for  $U$  and  $U_1$  From eq (f), p 148, the deflection curve of the bar when under the action of a compressive load equal to the critical load ( $pl = \pi/2$ ), is

$$y = \delta \left( 1 - \cos \frac{\pi x}{2l} \right) \quad (a)$$

With this value for  $y$ , the expression for the strain energy of bending becomes

$$U = \frac{1}{2} EI \int_0^l \left( \frac{d^2 y}{dx^2} \right)^2 dx = \frac{\delta^2 \pi^4}{64 l^3} EI \quad (b)$$

The lowering of the point of application of the load during bending is (see p 50)

$$\lambda = \frac{1}{2} \int_0^l \left( \frac{dy}{dx} \right)^2 dx = \frac{\delta^2 \pi^2}{16 l}, \quad (c)$$

and therefore

$$U_1 = P\lambda = \frac{\delta^2 \pi^2 P}{16 l} \quad (d)$$

Substituting from eqs. (b) and (d) into the fundamental equation (140), we obtain

$$P_{cr} = \frac{\pi^2 EI}{4l^2},$$

which coincides with eq. (131) obtained previously.

In this example the deflection curve (eq. a) was known in advance, and therefore the exact solution for the critical load was obtained from eq. (140). In cases where the deflection curve is unknown an approximation to the critical load may be obtained by assuming a *suitable curve* (i.e., one satisfying the conditions at the ends of the bar) for the deflection curve, and proceeding in exactly the same manner as described above.

In order to show the accuracy which can be achieved by using this method, the preceding problem will be considered again. Assume, for example, that in the case shown in Fig. 97b the deflection curve is the same as for a cantilever loaded at the end by a transverse force  $Q$ . Then from eq. (97), Part I, p. 150, we obtain  $y = (Qx^2/6EI)(3l - x)$ . This expression is substituted into eq. (b) for the strain energy  $U$  of bending and also into eq. (d) for  $U_1$ , and we obtain

$$U = \frac{EI}{2} \int_0^l \left( \frac{d^2y}{dx^2} \right)^2 dx = \frac{Q^2 l^3}{6EI},$$

$$U_1 = P\lambda = \frac{P}{2} \int_0^l \left( \frac{dy}{dx} \right)^2 dx = \frac{P}{15} \frac{Q^2 l^5}{(EI)^2}.$$

Substituting into eq. (140) we obtain  $P_{cr} = 2.5EI/l^2$ . Comparing this result with the exact formula (eq. 131), we see that the error arising from the approximation is only about 1 per cent.

The error can be considerably reduced and a better approximation obtained if we take for the strain energy of bending the expression

$$U = \frac{1}{2EI} \int_0^l M^2 dx. \quad (e)$$

Substituting in this expression

$$\begin{aligned} M &= P(\delta - y) = P \left[ \delta - \frac{Qx^2}{6EI} (3l - x) \right] \\ &= P\delta \left[ 1 - \frac{x^2}{2l^3} (3l - x) \right], \end{aligned} \quad (f)$$

we find

$$U = \frac{P^2 \delta^2}{2EI} \frac{17l}{35}.$$

The decrease in the potential energy of the load  $P$  is

$$U_1 = \frac{P}{15} \cdot \frac{Q^2 l^5}{(EI)^2} = \frac{3P}{5} \cdot \frac{\delta^2}{l}.$$

Substituting into eq. (140), we obtain

$$\frac{P^2 \delta^2}{2EI} \frac{17l}{35} = \frac{3P}{5} \frac{\delta^2}{l},$$

from which

$$P_{cr} = \frac{42}{17} \cdot \frac{EI}{l^2} = 2.4706 \frac{EI}{l^2}.$$

The correct value is

$$P_{cr} = \frac{\pi^2 EI}{4l^2} = 2.4674 \frac{EI}{l^2}.$$

Hence the error in the approximate solution is only 0.13 per cent. In using eq. (e) instead of eq. (b) for the strain energy we introduce into the calculations the deflection  $y$  of the assumed curve, instead of the derivative  $d^2y/dx^2$ . Since  $y$  is represented with better accuracy by the assumed curve than is  $d^2y/dx^2$ , the second method of calculation results in a better approximation for  $P_{cr}$ .

The energy method usually gives a very satisfactory approximation provided the assumed curve is properly chosen. Sometimes we can make a very rough assumption for the shape of the curve and still obtain a satisfactory result. For example, we might assume the deflection curve in the above example to be a parabola given by the equation

$$y = \frac{\delta x^2}{l^2}.$$

Then

$$U = \int_0^l \frac{M^2 dx}{2EI} = \frac{P^2 \delta^2}{2EI} \int_0^l \left(1 - \frac{x^2}{l^2}\right)^2 dx = \frac{P^2 \delta^2}{2EI} \frac{8}{15} l,$$

$$U_1 = \frac{P}{2} \int_0^l \left(\frac{dy}{dx}\right)^2 dx = \frac{2}{3} \frac{\delta^2}{l} P.$$

By substituting these values into eq. (140) we obtain

$$\frac{P^2 \delta^2}{2EI} \frac{8}{15} l = \frac{2}{3} \frac{\delta^2}{l} P$$

and

$$P_{cr} = 2.5 \frac{EI}{l^2}.$$

A satisfactory approximation to the critical load is thus obtained, although the assumed parabolic curve cannot be considered a very satisfactory one. It has an approximately constant curvature along the length, while in the actual curve the curvature is proportional to the bending moment. It is zero at the top of the bar and a maximum at the bottom.

Applying the energy method by using an assumed curve which satisfies the end conditions, we always obtain a value for the critical load which is higher than the true value. This follows from the fact that the actual deflection curve of a buckled bar is the one that corresponds to the least resistance of the bar. Only by merest chance will an assumed curve be the true curve of least resistance. In almost every case the assumed curve will be different from this curve of least resistance, thus giving high values for the critical loads.<sup>15</sup>

### Problems

1. Solve the problem shown in Fig. 102, assuming that the deflection curve is the same as for a uniformly loaded beam with one end built in and the other hinged.

2. Solve by the energy method Prob. 4 of Art. 30 (p. 158) assuming  $l_1 = l_2 = l/2$ .

<sup>15</sup> For a further discussion of the energy method see S. Timoshenko, *Theory of Elastic Stability*, p. 120, 1936.

*Solution.* Assuming that the deflection curve is a sine curve,

$$y = \delta \sin \frac{\pi x}{l},$$

the bending moments for the two portions of the curve are

$$M_1 = P_1 y + \frac{\delta P_2}{l} (l - x),$$

$$M_2 = (P_1 + P_2)y - \frac{\delta P_2 x}{l}.$$

The strain energy of bending is

$$\begin{aligned} U &= \int_{l/2}^l \frac{M_1^2 dx}{2EI_1} + \int_0^{l/2} \frac{M_2^2 dx}{2EI_2} \\ &= \frac{\delta^2}{2EI_1} \left( P_1^2 \frac{l}{4} + P_2^2 \frac{l}{24} + P_1 P_2 \frac{2l}{\pi^2} \right) \\ &\quad + \frac{\delta^2}{2EI_2} \left[ (P_1 + P_2)^2 \frac{l}{4} + P_2^2 \frac{l}{24} - P_2 (P_1 + P_2) \frac{2l}{\pi^2} \right] \end{aligned}$$

The decrease in the potential energy due to lowering of the points of application of the loads  $P_1$  and  $P_2$  is

$$U_1 = \frac{P_1}{2} \int_0^l \left( \frac{dy}{dx} \right)^2 dx + \frac{P_2}{2} \int_0^{l/2} \left( \frac{dy}{dx} \right)^2 dx = \frac{\delta^2 \pi^2}{4l} \left( P_1 + \frac{1}{2} P_2 \right).$$

Substituting in eq. (140) and using the previous notation (p. 158), we obtain

$$\begin{aligned} (P_1 + P_2)_{cr} &= \frac{(\pi^2 EI_2 / l^2)(m+1)}{m + \frac{m(m-1)^2}{6} - \frac{8}{\pi^2}(m-1) + n \left[ \frac{1}{m} + \frac{m(m-1)^2}{6} + \frac{8}{\pi^2} \frac{m-1}{m} \right]}. \quad (141) \end{aligned}$$

3. Solve Prob. 5 of Art. 30 by using the energy method.

*Answer.* Assuming the deflection curve

$$y = \delta \left( 1 - \cos \frac{\pi x}{2l} \right),$$

we obtain

$$P_{cr} = \pi^2 \frac{EI_2}{4l^2} \cdot \frac{1}{\frac{l_2}{l} + \frac{l_1}{l} \frac{I_2}{I_1} - \frac{1}{\pi} \left( \frac{I_2}{I_1} - 1 \right) \sin \frac{\pi l_2}{l}}. \quad (142)$$

**32. Buckling of Prismatic Bars under the Action of Uniformly Distributed Axial Forces.**—Assuming that under the action of a uniform axial load a slight lateral buckling occurs, Fig. 108, we can obtain the critical value of the load by integrating the differential equation of the deflection curve. The equation in this case is not as simple as that we had before, and its exact solution requires the use of Bessel functions.<sup>14</sup> However, an approximate solution can readily be obtained by using the energy method.

As an approximate expression for the deflection curve let us take

$$y = \delta \left( 1 - \cos \frac{\pi x}{2l} \right) \quad (a)$$

which is the true curve for the case where buckling occurs under the action of a compressive load applied at the end. The bending moment at cross section  $mn$ , resulting from the load above that cross section, is

$$M = \int_x^l q(\eta - y) d\xi.$$

Substituting from eq. (a) for  $y$  and setting

$$\eta = \delta \left( 1 - \cos \frac{\pi \xi}{2l} \right),$$

we obtain after integration with respect to  $\xi$

$$M = \delta q \left[ (l - x) \cos \frac{\pi x}{2l} - \frac{2l}{\pi} \left( 1 - \sin \frac{\pi x}{2l} \right) \right].$$

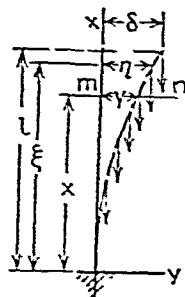


FIG. 108.

<sup>14</sup> See S. Timoshenko, *Theory of Elastic Stability*, p. 115, 1936.



Substituting this in the expression for the strain energy of bending, we obtain

$$U = \int_0^l \frac{M^2 dx}{2EI} = \frac{\delta^2 q^2 l^3}{2EI} \left( \frac{1}{6} + \frac{9}{\pi^2} - \frac{32}{\pi^3} \right) \quad (b)$$

In calculating the decrease of the potential energy of the distributed load during lateral buckling, we note that owing to the inclination of an element  $ds$  of the deflection curve at the cross section  $mn$ , the upper part of the load undergoes a downward displacement equal to

$$ds - dx \approx \frac{1}{2} \left( \frac{dy}{dx} \right)^2 dx,$$

and the corresponding reduction in the potential energy is

$$\frac{1}{2} \left( \frac{dy}{dx} \right)^2 q(l-x) dx$$

The total decrease of the potential energy of the load during buckling is then

$$U_1 = \frac{1}{2} q \int_0^l \left( \frac{dy}{dx} \right)^2 (l-x) dx = \frac{\pi^2 \delta^2 q}{8} \left( \frac{1}{4} - \frac{1}{\pi^2} \right) \quad (c)$$

Substituting from eqs (b) and (c) into eq (140), we obtain

$$\frac{\delta^2 q^2 l^3}{2EI} \left( \frac{1}{6} + \frac{9}{\pi^2} - \frac{32}{\pi^3} \right) = \frac{\pi^2 \delta^2 q}{8} \left( \frac{1}{4} - \frac{1}{\pi^2} \right),$$

from which

$$(ql)_{cr} = \frac{7.89EI}{l^2}$$

The exact solution for this case is

$$(ql)_{cr} = \frac{7.83EI}{l^2} = \frac{\pi^2 EI}{(1.122l)^2} \quad (143)$$

Thus the error in the approximate solution is less than 1 per cent.

### Problems

1. A prismatic bar with hinged ends, Fig. 109, is subjected to the action of a uniformly distributed axial load of intensity  $q$  and an axial compressive force  $P$ . Find the critical value of  $P$  by assuming for the deflection curve the equation

$$y = \delta \sin \frac{\pi x}{l}.$$

Answer.

$$P_{cr} = \frac{\pi^2 EI}{l^2} - \frac{ql}{2}.$$

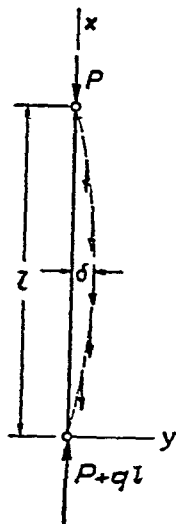


FIG. 109.

### 33. Buckling of Bars of Variable Cross Section.—

A bar of variable cross section, symmetrical with respect to the middle and having two axial planes of symmetry, is shown in Fig. 110. The middle portion is of uniform cross section with its smaller moment of inertia equal to  $I_0$ . At the ends the cross section varies, and the smaller moments of inertia follow the law

$$I = I_0 \left( \frac{x}{a} \right)^m, \quad (a)$$

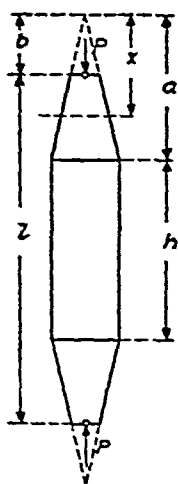


FIG. 110.

in which  $x$  and  $a$  are distances from a fixed point (Fig. 110) and  $m$  is a number depending upon the type of column. When the middle portion is a solid cylinder and the ends are solid cones,  $I$  varies as the fourth power of  $x$  and  $m = 4$  in eq. (a). When the column has a constant thickness in the direction perpendicular to the plane of Fig. 110, the moments of inertia  $I$  with respect to axes parallel to the plane of the figure are proportional to  $x$  and  $m = 1$  in eq. (a). (When the column consists of four angles connected by lat-

tices, as in Fig. 111, the cross-sectional area remains constant, and  $I$  can be taken proportional to  $x^2$ , so that  $m = 2$  in eq. (a).) Calculations made for  $m = 1, 2, 3, 4$ , show<sup>15</sup> that the critical load within the elastic limit can be represented by the equation

$$P_{cr} = \alpha \frac{EI_0}{l^2}, \quad (144)$$

<sup>15</sup> See A. N. Dinnik, *Bull. Engrs. (Vestnik Ingenerov)*, 1927 (in Russian). Table 9 is taken from this paper.

in which  $\alpha$  is a numerical factor depending upon the ratios  $h/l$  and  $I_1/I_0$ , where  $I_1 = I_0(b/a)^m$  is the moment of inertia of the end cross section. Assuming the ends of the column hinged, the magnitudes of  $\alpha$  for various ratios are given in Table 9. It can be seen that as

TABLE 9 COEFFICIENT  $\alpha$  IN EQ (144)

$I_1/I_0$	$h/l =$	0	0.2	0.4	0.6	0.8	1
0.1	$m = 1$	6.48	7.58	8.68	9.46	9.82	$\pi^2$
	$m = 2$	5.40	6.67	8.08	9.25	9.79	"
	$m = 3$	5.01	6.32	7.84	9.14	9.77	"
	$m = 4$	4.81	6.11	7.68	9.08	9.77	"
0.2	$m = 1$	7.01	7.99	8.91	9.63	9.82	"
	$m = 2$	6.37	7.49	8.61	9.44	9.81	"
	$m = 3$	6.14	7.31	8.49	9.39	9.81	"
	$m = 4$	6.02	7.20	8.42	9.38	9.80	"
0.4	$m = 1$	7.87	8.60	9.19	9.70	9.84	"
	$m = 2$	7.61	8.42	9.15	9.63	9.84	"
	$m = 3$	7.52	8.38	9.10	9.63	9.84	"
	$m = 4$	7.48	8.33	9.10	9.62	9.84	"
0.6	$m = 1$	8.60	9.12	9.55	9.74	9.85	"
	$m = 2$	8.51	9.03	9.48	9.74	9.85	"
	$m = 3$	8.50	9.02	9.47	9.74	9.85	"
	$m = 4$	8.47	9.01	9.45	9.74	9.85	"
0.8	$m = 1$	9.27	9.54	9.69	9.83	9.86	"
	$m = 2$	9.24	9.50	9.69	9.82	9.86	"
	$m = 3$	9.23	9.50	9.69	9.81	9.86	"
	$m = 4$	9.23	9.49	9.69	9.81	9.86	"
1		$\pi^2$	$\pi^2$	$\pi^2$	$\pi^2$	$\pi^2$	"

the ratio  $h/l$  or the ratio  $I_1/I_0$  approaches unity the factor  $\alpha$  approaches  $\pi^2$  and eq (144) approaches eq (132) for a prismatic bar.

As an example of the application of this table consider a wooden strut 6 ft 6 in. long of rectangular cross section. The thickness of the strut remains constant and equal to  $\frac{3}{4}$  in. The width varies according to a straight line law and is 4 in. at the middle and 2.4 in. at the ends. Determine  $P_{cr}$  if  $E = 1.2 \times 10^6$  lb per sq in. In this case  $h/l = 0$ ,  $m = 1$  and  $I_1/I_0 = (2.4)/4 = 0.6$ . From Table 9 we find  $\alpha = 8.60$ , and the critical load, from eq (144), is

$$P_{cr} = 8.60 \frac{1.2 \times 10^6 \times \frac{1}{4} \times 3^3}{\frac{1}{4}^3 \times 12 \times 78^2} = 239 \text{ lb}$$

As a second example let us consider a pyramidal column (Fig. 111) whose square cross section consists of four angles  $3\frac{1}{2} \times 3\frac{1}{2} \times \frac{3}{8}$  in. The outside width of the column at the ends is 12 in. and at the middle  $20\frac{1}{2}$  in. The length of the column is 65 ft. Determine the critical load for this column, taking for structural steel  $E = 30 \times 10^6$  lb per sq in. and assuming that the lattice bars are rigid enough to allow the application of eq. (144), derived for solid bars. The cross-sectional area is  $A = 2.48 \times \frac{1}{4} = 9.92$  sq in.; and in addition  $I_1 = 2.9 \times \frac{1}{4} + 2.48 \times \frac{1}{4} \times (6 - 1.01)^2 = 259 \text{ in.}^4$ ;  $I_0 = 2.9 \times \frac{1}{4} + 2.48 \times \frac{1}{4} \times (10.25 - 1.01)^2 = 860 \text{ in.}^4$ . Taking  $I_1/I_0 = 0.3$ ,  $m = 2$  approximately, and  $h/l = 0$ , we find from Table 9 by interpolation that  $\alpha = 7$ , approximately. Then from eq. (144)

$$P_{cr} = 7 \times \frac{30 \times 10^6 \times 860}{65^2 \times 12^2} = 297,000 \text{ lb}$$



FIG. 111.

34. Effect of Shearing Force on the Critical Load.—In the preceding derivations of the equations for the critical loads, we used the differential equation of the deflection curve (see p. 147) in which the effect of shearing force on the deflection was neglected. But when buckling occurs, the cross sections of the bar are no longer perpendicular to the compressive force and there will be shearing forces acting in these cross sections. The effect of these forces may be found by using the energy method developed in Art. 31. In using this method the energy of shear must be added to the energy of bending in calculating the strain energy  $U$  due to buckling. Let  $AB$  (Fig. 112) represent a solid strut with hinged ends, buckled under the action of compressive forces  $P$ . The magnitudes of the bending moment and the shearing force at any cross section  $mn$  are

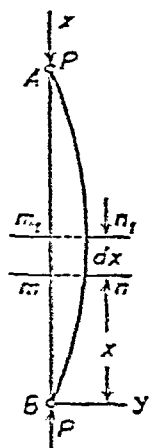


FIG. 112.

$$M = Py; \quad V = P \frac{dy}{dx}. \quad (a)$$

From previous considerations (see Part I, Art. 69) the potential energy stored in an element of the bar is

$$dU = \frac{M^2 dx}{2EI} + \frac{\alpha V^2 dx}{2GA}, \quad (b)$$

where

$A$  = cross-sectional area,

$\alpha$  = numerical factor depending on the shape of the cross section (see Part I, p. 171).

The displacement of the section  $mn$  with respect to  $m_1n_1$ , due to shear, can be taken equal to  $(\alpha V/GA)dx$ , and the second member on the right-hand side of eq. (b) represents the potential energy of shear stored in the element. By using eqs. (a) and (b), the strain energy stored in the strut during buckling is

$$U = \int_0^l \frac{P^2 y^2 dx}{2EI} + \int_0^l \frac{\alpha P^2}{2GA} \left( \frac{dy}{dx} \right)^2 dx. \quad (c)$$

The decrease in the potential energy of the load  $P$  is

$$U_1 = \frac{P}{2} \int_0^l \left( \frac{dy}{dx} \right)^2 dx. \quad (d)$$

Assuming that the deflection curve of the buckled strut is a sine curve,

$$y = \delta \sin \frac{\pi x}{l}, \quad (e)$$

and substituting this value into eqs. (c) and (d) we obtain

$$U = \delta^2 \frac{P^2 l}{4EI} + \delta^2 \frac{P^2 l}{4GA} \frac{\alpha \pi^2}{l^2}, \quad (f)$$

$$U_1 = \delta^2 \frac{P \pi^2}{4l}.$$

Eq. (140) then gives

$$P_{cr} = \frac{\pi^2 EI}{l^2} \frac{1}{1 + \frac{EI}{GA} \frac{\alpha \pi^2}{l^2}}. \quad (g)$$

Comparison with Euler's formula (eq. 132) shows that owing to the action of shear the critical load is diminished in the ratio

$$\frac{1}{1 + \frac{EI}{GA} \frac{\alpha \pi^2}{l^2}}. \quad (145)$$

If we let

$$\frac{\pi^2 EI}{l^2} = P_e; \quad \frac{GA}{\alpha} = P_d; \quad (h)$$

then eq. (g) becomes

$$P_{cr} = P_e \frac{1}{1 + \frac{P_e}{P_d}}. \quad (146)$$

For solid bars,  $P_d$  is very large in comparison with  $P_e$ , and the effect of the shearing force can be neglected. In the case of latticed bars, especially when spacing plates or battens are used (Fig. 114a),  $P_d$  may become of the same order as  $P_e$ , and in this case the effect of shearing force can no longer be neglected. This problem is considered in the following article.

**35. Buckling of Latticed Struts.**<sup>18</sup>—Latticed struts are sometimes used in steel structures. Their resisting capacities are always less than those of solid columns having the same cross-sectional area and the same slenderness ratio  $l/k$ , and depend

<sup>18</sup> See F. Engesser, *Zentr. Bauverwalt.*, p. 483, 1891, and p. 609, 1907; L. Prandtl, *Z. Ver. deut. Ing.*, 1907, and also the writer's paper in *Bull. Polytech. Inst. (Kiev)*, 1908. These papers discuss the problem of the buckling of latticed struts in connection with the collapse of a compression member of the Quebec bridge.

greatly on the details of spacing the lattice bars, spacing plates and battens. This lowering of the critical

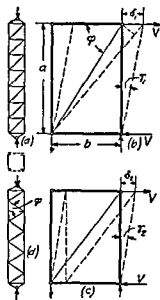


FIG. 113.

stresses is due principally to the fact that in the case of latticed columns shearing forces produce a much larger effect on the deflections than in the case of solid bars. To calculate the effect of shearing force on the critical load, eq. (146), which was derived for solid bars, can be adapted to latticed struts. As before, let  $P_c$  be the critical load obtained from eq. (132). In the case of solid struts,  $P_d$  in eq. (146) has a simple physical meaning, namely that  $V/P_d$  represents the additional slope  $\gamma$  in the deflection curve produced by the shearing forces.  $P_d$  also has the same meaning in the case of lat-

ticed struts, provided the number of panels is large. To determine  $P_d$  in any particular case we must therefore investigate the lateral displacements produced by the shearing forces.

Consider first one panel of the latticed bar shown in Fig. 113a. The shear displacement is due to the elongation and contraction of the diagonals and battens in each panel (Fig. 113b). Assuming hinges at the joints, the elongation of the diagonal produced by the shearing force  $V$  is  $Va/(\sin \varphi \cos \varphi EA_d)$ , in which

- $\varphi$  = angle between the batten and the diagonal,
- $V/\cos \varphi$  = tensile force in the diagonal,
- $a/\sin \varphi$  = length of the diagonal,
- $A_d$  = cross-sectional area of two diagonals.

The corresponding lateral displacement, Fig. 113b, is

$$\delta_1 = \frac{Va}{\sin \varphi \cos^2 \varphi EA_d}. \quad (a)$$

The shortening of a batten and the corresponding lateral dis-

placement (Fig. 113*c*) is

$$\delta_2 = \frac{Vb}{EA_b}, \quad (b)$$

where

$b$  = length of the batten

$A_b$  = cross-sectional area of two battens

From eqs. (a) and (b), the angular displacement produced by the shearing force  $V$  is

$$\gamma = \frac{\delta_1 + \delta_2}{a} = \frac{V}{\sin \varphi \cos^2 \varphi EA_c} + \frac{Vb}{aEA_b}.$$

Then using the definition introduced above,  $V/P_c = \gamma$ , we find

$$\frac{1}{P_c} = \frac{1}{\sin \varphi \cos^2 \varphi EA_c} + \frac{b}{aEA_b}.$$

Substituting into eq. (146) we obtain

$$P_c = \frac{\pi^2 EI}{l^2} \frac{1}{1 + \frac{\pi^2 EI}{l^2} \left( \frac{1}{\sin \varphi \cos^2 \varphi EA_c} + \frac{b}{aEA_b} \right)}. \quad (147)$$

If the cross-sectional areas  $A_c$  and  $A_b$  are very small in comparison with the cross-sectional area of the channels (Fig. 113*a*), the critical load (eq. 147) may be considerably lower than that obtained from Euler's formula (eq. 132).

Eq. (147) can also be used in the case represented in Fig. 113*d* if the angle  $\varphi$  is measured as shown in the figure and if the term in eq. (147) due to the deformation of the battens is omitted.



In the case of a strut made with battens only, as in Fig. 114a, to obtain the lateral displacement produced by the shearing force  $V$  we must consider the deformation of a

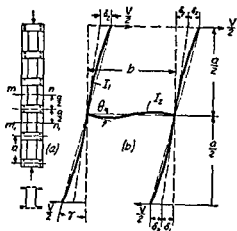


FIG 114

portion of the strut cut out by the cross sections  $mn$  and  $m_1n_1$ . Assuming that the deflection curves of the channels have points of inflection at these sections, the condition of bending will be as shown in Fig. 114b. (The tension and compression forces acting on the channels

are not shown in the figure.) The deflection consists of two parts: the displacement  $\delta_1$  due to bending of the batten, and the displacement  $\delta_2$  due to bending of the channels. There are couples  $Va/2$  at the ends of the batten and the angle of rotation  $\theta$  (see eqs. 103 and 104, Part I, p. 158) is

$$\theta = \frac{Va}{2} \frac{b}{3EI_2} - \frac{Va}{2} \frac{b}{6EI_2} = \frac{Vab}{12EI_2},$$

where  $b$  is the length of the battens and  $EI_2$  is their flexural rigidity. The lateral displacement  $\delta_1$  produced by the bending of the battens is

$$\delta_1 = \theta \frac{a}{2} = \frac{Va^2b}{24EI_2}. \quad (c)$$

The displacement  $\delta_2$  can be calculated from the cantilever formula

$$\delta_2 = \frac{V \left(\frac{a}{2}\right)^3}{2 \cdot 3EI_1} = \frac{Va^3}{48EI_1}. \quad (d)$$

The total angular displacement produced by the shearing force  $V$  is

$$\gamma = \frac{\delta_1 + \delta_2}{\frac{a}{2}} = \frac{Vab}{12EI_2} + \frac{Va^2}{24EI_1};$$

then, since  $V/P_d = \gamma$ , we obtain

$$\frac{1}{P_d} = \frac{ab}{12EI_2} + \frac{a^2}{24EI_1},$$

and eq. (146) for determining the critical load becomes

$$P_{cr} = \frac{\pi^2 EI}{l^2} \frac{1}{1 + \frac{\pi^2 EI}{l^2} \left( \frac{ab}{12EI_2} + \frac{a^2}{24EI_1} \right)}, \quad (148)$$

where, as before,  $\pi^2 EI/l^2$  represents the critical load calculated for the entire column by Euler's formula. It may be seen that when the flexural rigidity of the battens is small, the actual critical load is much lower than that given by Euler's formula.

From eqs. (147) and (148) we note that in calculating critical loads for built-up columns the actual length of a column is replaced by a *reduced length* which is to be determined in the case of a latticed column, Fig. 113, from the equation

$$l_1 = l \sqrt{1 + \frac{\pi^2 EI}{l^2} \left( \frac{1}{\sin \varphi \cos^2 \varphi EA_d} + \frac{b}{aEA_b} \right)},$$

and in the case of a batten-plate column as shown in Fig. 114, from the equation

$$l_1 = l \sqrt{1 + \frac{\pi^2 EI}{l^2} \left( \frac{ab}{12EI_2} + \frac{a^2}{24EI_1} \right)}.$$

When the reduced length of a built-up column is determined, the allowable stress is obtained as for a solid column with the slenderness ratio equal to  $l_1/k$ .

In the design of built-up columns the proper dimensioning of the lattice bars and batten plates is of great practical importance. As a basis for determining stresses in these details, an eccentricity in the application of compressive forces should

be assumed in the design of shorter columns<sup>17</sup> If the eccentricities at the two ends are equal to  $e$  and are in opposite directions, the compressive forces  $P$  form a couple of magnitude  $2Pe$  which produces at the ends of the strut the shearing forces

$$V = \frac{2Pe}{l}. \quad (149)$$

The maximum value of  $V$  is obtained by substituting for  $P$  in this equation the maximum load  $P_{cr}$  which the column can support The eccentricity  $e$  is usually taken as a certain fraction of the core radius  $r$ , say  $e/r = 0.3$  The details should then be designed in such a way that the maximum stresses produced in them by  $V_{\max}$  does not exceed the yield-point stress

In the case of a compressed latticed member of a truss with rigid joints, some bending moments at the ends of the member are produced during loading of the truss If the magnitudes  $M_1$  and  $M_2$  of these moments are calculated from the *secondary stress* analysis, the corresponding eccentricities  $e_1 = M_1/P$  and  $e_2 = M_2/P$  in the point of application of the compressive force  $P$  are known, and the magnitude of their algebraic sum must be substituted in eq (149) in place of  $2e$

**36. Inelastic Buckling of Straight Columns.**—In the preceding discussion of buckling problems it has always been assumed that the material of the column is perfectly elastic and follows Hooke's law Let us assume now that the material, although perfectly elastic, does not follow Hooke's law and that the compression test diagram is as shown in Fig 115a If a bar of such a material is under a compressive stress corresponding to point  $C$  on the diagram and then some small change in stress is produced (positive or negative), the relation between the change in stress and the change in strain

<sup>17</sup> This question is discussed in more detail in the paper by D H Young, *Proc Am Soc Civil Engrs*, Dec 1934, and another paper by the same author in *Publ Internat Assoc Bridge and Structural Engrg*, Zurich, Vol 2, p 480, 1934 See also S Timoshenko, *Theory of Elastic Stability*, p 197, 1936, and Friedrich Bleich, *Buckling Strength of Metal Structures*, New York, p 167, 1952.

depends on the magnitude of the initial stress. This relation is given by the slope of the compression test diagram at point  $C$ , as shown in the figure by the heavy-line element. The

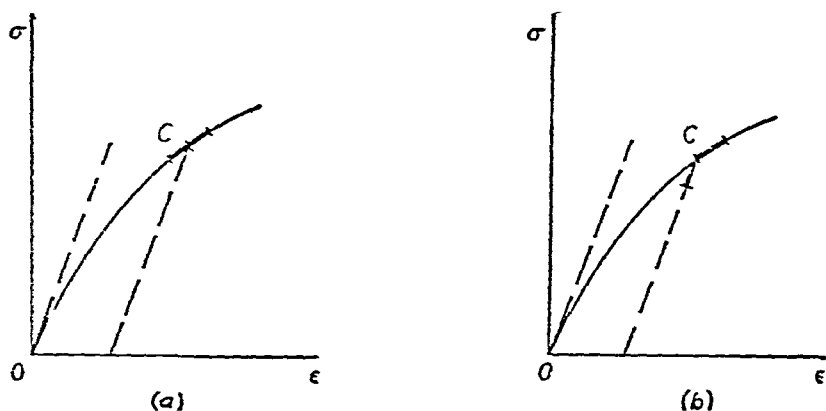


FIG. 115.

magnitude of the ratio  $d\sigma/d\epsilon$  can be considered as a variable modulus of elasticity of the material and will be called the *tangent modulus* and denoted by  $E_t$ .

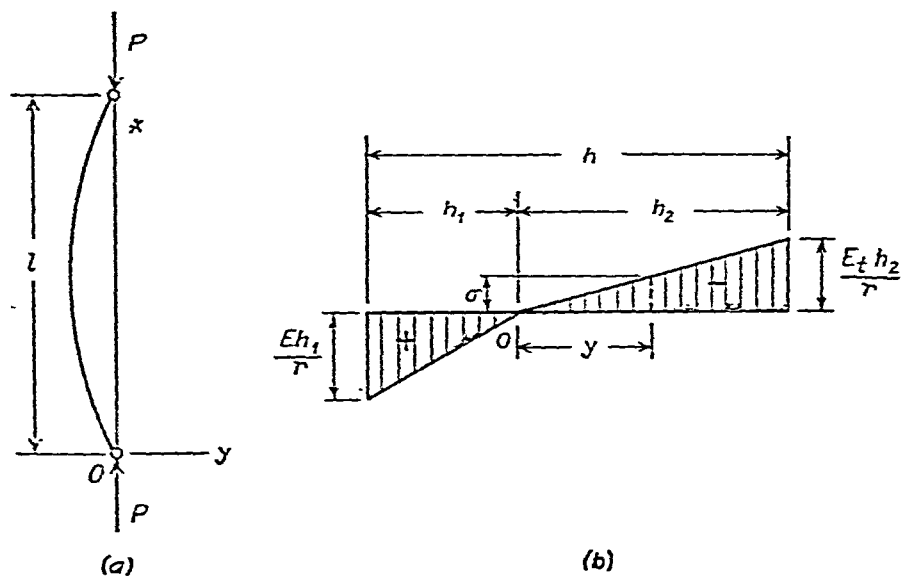


FIG. 116.

Let us consider now an axially compressed prismatic bar with hinged ends (Fig. 116a) and assume that the elastic properties of the material are represented by the diagram in Fig. 115a. In determining the value of the critical load for such a

bar we can proceed as before and assume that after applying the forces  $P$  an infinitesimal deflection of the bar is produced. Then the force  $P_{cr}$  is calculated as the force required to keep the bar in this slightly deflected shape. Since the assumed deflection is infinitely small, the corresponding bending stresses are small in comparison with the initial compressive stress, and the relation between bending stress and bending strain will be determined by the corresponding value of the tangent modulus  $E_t$ . In such a case the differential equation of the deflection curve will have the same form as for materials following Hooke's law, but the tangent modulus  $E_t$  will appear instead of  $E$ . The integration of that equation gives

$$P_{cr} = \frac{\pi^2 E_t I}{l^2}, \quad (150)$$

and

$$\sigma_{cr} = \pi^2 E_t \frac{k^2}{l^2} \quad (151)$$

The difference between these formulas and eqs (132) and (134), for materials following Hooke's law, consists only in the replacement of the constant modulus  $E$  by the tangent modulus  $E_t$ , which is a function of the direct stress  $\sigma$ .

If the compression test diagram such as that in Fig 115a is known, then the value of  $E_t$  can be readily determined for any value of  $\sigma$ . To establish the relation between  $\sigma_{cr}$  and the slenderness ratio  $l/k$  we take a series of values of  $\sigma_{cr}$  with the corresponding values of  $E_t$  and substitute them into eq (151). The equation then determines the corresponding values of  $l/k$ . Using these values the relation between  $l/k$  and  $\sigma_{cr}$  can be represented by a curve analogous to the curve in Fig 100 obtained for a material following Hooke's law.

This method of calculating  $\sigma_{cr}$  for the case when the material does not follow Hooke's law was proposed by F. Engesser,<sup>18</sup> who also suggested its use for metallic struts compressed beyond the proportional limit. In this case, however, the problem is more complicated. If a bar is compressed beyond the elastic

<sup>18</sup> F. Engesser, *Z. Architekt u. Ingenieurw.*, p. 455, 1889. See also Conside, *Congr. internat. procédés de construction*, Paris, Vol. 3, p. 371, 1889.

limit and then a small deflection is produced, Fig. 116*a*, the compressive strain on the concave side increases, and the relation between strain and stress is defined by the magnitude of the tangent modulus  $E_t$ . At the same time the compressive strain on the convex side diminishes, and in such a case the stress-strain relation is defined by the initial value  $E$  of the modulus. Thus the conditions are the same as for a material having two different moduli, one for tension and the other for compression. The corresponding slopes are indicated in Fig. 115*b* by the two short heavy-line elements. Assuming that cross sections of the bar remain plane during bending, the small bending stresses will be represented by the two triangles shown in Fig. 116*b*. These bending stresses are superposed on the uniformly distributed initial compressive stresses. If  $r$  denotes the radius of curvature of the deflection curve at the cross section under consideration, the maximum tensile and compressive bending stresses are  $Eh_1/r$  and  $E_th_2/r$  respectively, and the position of the neutral axis  $O$ , Fig. 116*b*, is found from the condition that the resultants of the tensile and compressive bending stresses must be equal and must provide a couple which balances the bending moment  $M$ . In the case of a rectangular cross section of depth  $h$  and width  $b$  these conditions require

$$Eh_1^2 = E_t h_2^2 \quad (a)$$

and

$$\frac{Eh_1}{r} \frac{bh_1}{2} \frac{2h}{3} = M. \quad (b)$$

Observing that  $h_1 + h_2 = h$ , we obtain from eq. (a)

$$h_1 = \frac{h\sqrt{E_t}}{\sqrt{E} + \sqrt{E_t}}, \quad h_2 = \frac{h\sqrt{E}}{\sqrt{E} + \sqrt{E_t}}. \quad (c)$$

Then eq. (b) gives

$$\frac{1}{r} \frac{bh^3}{12} \frac{4EE_t}{(\sqrt{E} + \sqrt{E_t})^2} = M. \quad (d)$$

Introducing the notation

$$E_r = \frac{4EE_t}{(\sqrt{E} + \sqrt{E_t})^2}, \quad (152)$$

we obtain from eq (d)

$$\frac{E_r I}{r} = M \quad (153)$$

Eq (153) has the same form as the equation for the elastic curve when the material follows Hooke's law. We have only to replace the modulus  $E$  by the quantity  $E_r$ , given by eq (152) and called the *reduced modulus of elasticity*. Using for  $1/r$  its approximate expression  $d^2y/dx^2$  and integrating eq (153), we obtain for a bar with hinged ends (Fig 116a)

$$P_{cr} = \frac{\pi^2 E_r I}{l^2}, \quad (154)$$

$$\sigma_{cr} = \pi^2 E_r \frac{k^2}{l^2} \quad (155)$$

Comparing these equations with eqs (150) and (151), we see that the difference is only in the replacement of the tangent modulus  $E_t$ , used in Engesser's original equations, by the reduced modulus  $E_r$ . Since  $E_t < E$ , it is seen from eq (152) that  $E_r > E_t$ <sup>19</sup> and hence the values of  $P_{cr}$  from eq (154) are larger than from eq (150). This increased value arises from considering that during the assumed bending (Fig 116a) the strain on the convex side of the bar represents a decrease in the initial compressive strain. Thus strain hardening has an influence on the bending. In Fig 117 are presented curves giving the relation between  $\sigma_{cr}$  and  $l/k$  as calculated from eqs (151) and (155) for rectangular bars of structural steel.<sup>20</sup>

For many years eq (155) based on the reduced modulus  $E_r$  was used by engineers in dealing with such ductile mate

<sup>19</sup> It can be shown that this is true not only for the case of a rectangular bar but also for a bar with any symmetrical cross section and which is bent in the plane of symmetry.

<sup>20</sup> Figs 117 and 118 are taken from F. Bleich, *Buckling Strength of Metal Structures*, New York, McGraw Hill Book Company, Inc., 1952.

rials as aluminum alloys and structural steel, but certain experiments have shown that test results are in better agreement with eq. (151). Fig. 118, for example, represents test results

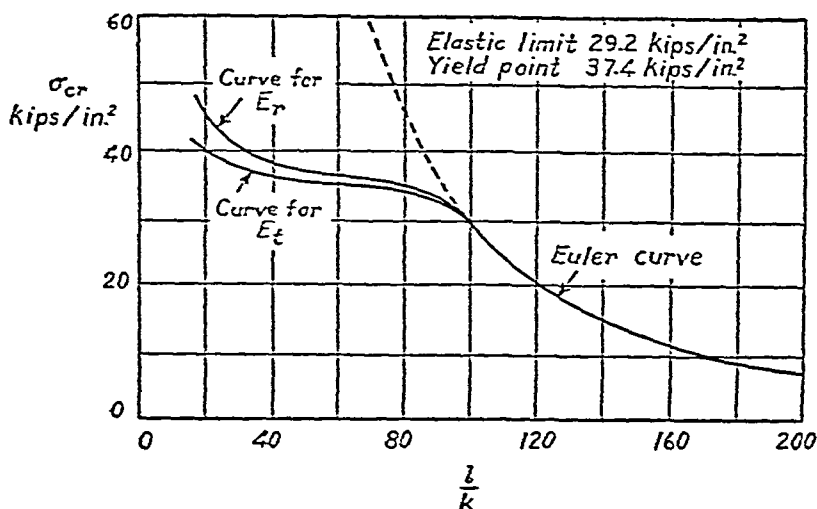


FIG. 117.

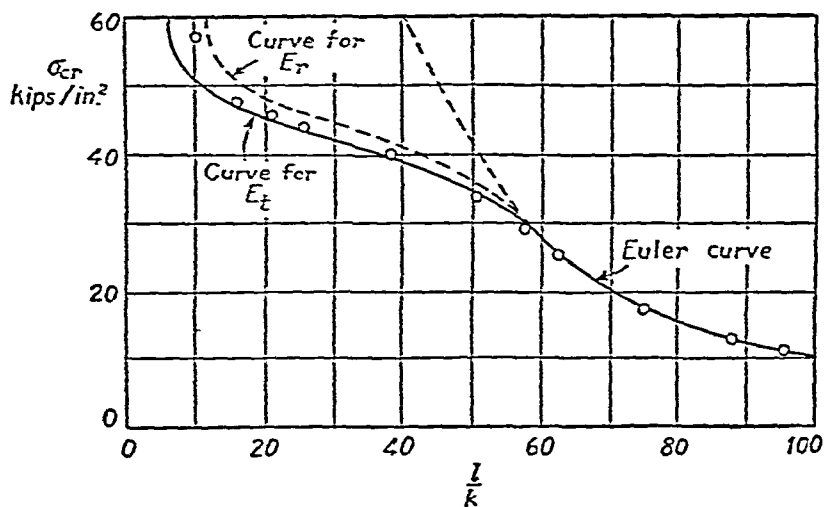


FIG. 118.

for solid circular rods of aluminum alloy.<sup>21</sup> It is seen that for larger values of the slenderness ratio the results coincide with Euler's curve, and for shorter bars the results agree satisfac-

<sup>21</sup> See the paper by R. L. Templin, R. G. Sturm, E. C. Hartmann and M. Holt, *Aluminum Research Laboratories*, Aluminum Company of America, Pittsburgh, 1938.



torily with the tangent modulus curve. Thus the method of reasoning used in calculating  $\sigma_{er}$  in the elastic range becomes unsatisfactory beyond the elastic limit, since the  $E_t$  curve, based on that method, does not agree with test results.

To explain<sup>22</sup> the failure of this generally used method, we have to keep in mind that in the case of plastic deformation of a bar the magnitude of the deflections may depend not only on the values of the acting forces, but also on the order in

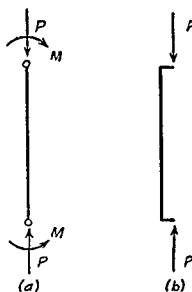


FIG. 119.

which these forces are applied. Take, for example, the case of combined compression and bending, Fig. 119a.

If the deformations are perfectly elastic, the deflections of the bar depend only on the magnitude of  $P$  and  $M$  and are independent of the order in which they are applied. Conditions are quite different if plastic deformations are produced during loading. Assume, for example, that the axial forces  $P$  are applied first and that their magnitude is such that plastic deformation is produced.

If now the couples  $M$  are applied, the bending of the bar due to the couples will be affected by the cold working produced in the material by  $P$ . This cold working must be taken into account and the reduced modulus  $E_r$  used in calculating deflections. As another way of loading consider next the case when gradually increasing loads  $P$  and  $M$  are applied simultaneously. Such a condition of loading is obtained, for example, in the compression of a bar by forces  $P$  applied with some eccentricity, as shown in Fig. 119b. In this case the strains in each longitudinal fiber are continuously increasing, and the relation between stress and strain is defined for each step of loading by the corresponding value of tangent modulus  $E_t$ .

In the experimental study of lateral buckling of columns,

<sup>22</sup> The explanation was given by F. R. Shanley, *J. Aeronaut. Sci.*, Vol. 14, p. 261, 1947.

conditions are usually similar to those in Fig. 119*b*. Owing to unavoidable eccentricities, bending of the column begins immediately with the initial loading. However, since the eccentricities are very small, the deflections are negligible up to the stage when the load begins to approach its critical value. At this last stage the deflections begin to increase rapidly, and their magnitude is defined by the magnitude of  $E_t$  corresponding to the critical value of the load. From this consideration it therefore follows that Engesser's original eq. (151) will give the critical stresses with better accuracy than eq. (155), as the test results indicate.

The preceding discussion, developed for the fundamental case of buckling (Fig. 98), can also be applied to other cases of buckling such as are shown in Figs. 99 and 102. The critical stress can be calculated from eq. (137) upon substituting  $E_t$  for  $E$ . In general, however, buckling problems in the plastic range are more complicated, since the end conditions and length coefficients usually cease to be constant and vary with the value of  $P_{cr}$ . Take, for example, the case shown in Fig. 105. In the elastic range the length coefficient for this case depends only on the ratio (see eq. *l*, p. 157)

$$\frac{II_1}{I_1 l}, \quad (e)$$

which is independent of the value of  $P_{cr}$ . But in the plastic range,  $E_t$  must be used instead of  $E$  and instead of ratio (e) we obtain

$$\frac{E_t II_1}{EI_1 l}, \quad (f)$$

where  $E_t$  is smaller than  $E$  and depends on the magnitude of  $P_{cr}$ . Hence the ratio of the flexural rigidity of the horizontal members of the frame to that of the vertical members becomes larger, and as a result of this, the length coefficient becomes smaller in the plastic range than for the case of perfect elasticity. From this we conclude that if in the design of the vertical members of the frame in the plastic region we use for the reduced length the same value as that calculated for per-

fectly elastic conditions, we will be on the safe side. Similar conclusions are also obtained for the cases discussed in Arts 32, 33 and 35.

**37. Buckling of Circular Rings and Tubes under External Pressure.**—*Buckling of a Circular Ring*—It is well known that a circular ring or tube may collapse owing to external pressure alone. If the flexural rigidity of the ring is insufficient, such a failure may occur at stresses far below the elastic limit of the material. This phenomenon must be taken into consideration in such problems as the design of boiler tubes subjected to external steam pressure and the design of reinforcing rings for submarines.

The pressure at which the circular form becomes unstable and buckling occurs is known as the *critical pressure*. Its value will be obtained by use of the general equation (eq 235, Part I, p 404) for the deflection curve.

Assume that under external pressure the ring (Fig 120) is

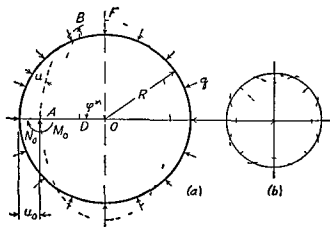


FIG 120

buckled into an elliptical shape as shown by the broken line. The following notation is then used

- $q$  = external pressure per unit length of center line,
- $R$  = radius of center line of ring,
- $u$  = radial displacement during buckling,
- $u_0$  = radial displacement for cross section  $A$ ,
- $M_0$  = bending moment at cross section  $A$ ,
- $N_0 = q(R - u_0)$  = longitudinal compressive force at cross section  $A$ .

The bending moment at any cross section  $B$  of the buckled ring then is

$$M = M_0 + q\overline{AO} \cdot \overline{AD} - \frac{q}{2} \overline{AB}^2. \quad (a)$$

Now, in the triangle  $AOB$

$$\overline{OB}^2 = \overline{AB}^2 + \overline{AO}^2 - 2\overline{AO} \cdot \overline{AD}$$

or

$$\begin{aligned} \frac{1}{2}\overline{AB}^2 - \overline{AO} \cdot \overline{AD} &= \frac{1}{2}(\overline{OB}^2 - \overline{AO}^2) \\ &= \frac{1}{2}[(R - u)^2 - (R - u_0)^2]. \end{aligned}$$

Since  $u$  is small in comparison to  $R$ , terms in  $u^2$  or  $u_0^2$  can be neglected, whence

$$\frac{1}{2}\overline{AB}^2 - \overline{AO} \cdot \overline{AD} = R(u_0 - u).$$

Substituting this value in eq. (a), we obtain

$$M = M_0 - qR(u_0 - u).$$

Eq. (235), Part I, p. 404, becomes

$$\frac{d^2u}{d\varphi^2} + u = -\frac{R^2}{EI} [M_0 - qR(u_0 - u)]$$

or

$$\frac{d^2u}{d\varphi^2} + u \left( 1 + \frac{qR^3}{EI} \right) = \frac{-M_0R^2 + qR^3u_0}{EI}. \quad (b)$$

The general solution of this equation is

$$u = C_1 \sin p\varphi + C_2 \cos p\varphi + \frac{-M_0R^2 + qR^3u_0}{EI + qR^3}, \quad (c)$$

in which  $C_1$  and  $C_2$  are constants to be determined from the conditions at the cross sections  $A$  and  $F$  of the buckled ring, and

$$p^2 = 1 + \frac{qR^3}{EI}. \quad (d)$$

From symmetry, it follows that

$$\left( \frac{du}{d\varphi} \right)_{\varphi=0} = 0; \quad \left( \frac{du}{d\varphi} \right)_{\varphi=\pi/2} = 0. \quad (e)$$

From the first of these conditions we obtain  $C_1 \approx 0$ , and from the second,

$$\sin \frac{p\pi}{2} = 0. \quad (f)$$

The smallest root of this equation is

$$\frac{p\pi}{2} = \pi$$

or

$$p = 2.$$

Substituting this in eq (d), we obtain the value for the critical pressure <sup>23</sup>

$$q_{cr} = \frac{3EI}{R^3}. \quad (156)$$

Other roots of eq (f) such as  $p\pi/2 = 2\pi$ ,  $p\pi/2 = 3\pi$ , etc, correspond to a larger number of waves in the buckled ring and give greater values for the pressure  $q$ . Figure 120b

shows, for example, the buckled form for  $p\pi/2 = 2\pi$ . These higher forms of buckling are of interest in studying the stability of short cylindrical tubes with fastened ends.

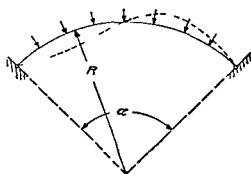


FIG 121

broken line in Fig 121. The critical value of the pressure depends upon the magnitude of the angle  $\alpha$  and may be calculated from the equation <sup>24</sup>

<sup>23</sup> This problem was solved by M. Bresse, *Cours de mécanique appliquée*, Paris, Part I, p. 334, 1866.

<sup>24</sup> See the author's paper on the stability of elastic systems, *Bull. Polytech. Inst. (Kiev)*, 1910, French translation, *Ann. ponts et chaussées*, 1913. See also E. Hurlbrink, *Schiffbau*, Vol. 9, p. 640, 1907-08; E. Chwalla and C. F. Kollbrunner, *Stahlbau*, 1937 and 1938, and A. N. Dinnik, *Buckling of Bars*, Moscow, 1939 (in Russian).

$$q_{cr} = \frac{EI}{R^3} \left( \frac{4\pi^2}{\alpha^2} - 1 \right). \quad (157)$$

The problem of the buckling of a ring in the direction perpendicular to its plane has also been solved.<sup>25</sup>

*Buckling of Circular Tubes.*—The theory of buckling developed above for a circular ring can also be used in the case of a long circular tube subjected to uniform external pressure. Consider an elementary ring cut out of the tube by two cross sections unit distance apart. The moment of inertia of the cross section of this ring is

$$I = \frac{1 \cdot h^3}{12},$$

where  $h$  denotes the thickness of the wall of the tube. Since the cross section of the ring will not be distorted during bending, the quantity

$$\frac{E}{1 - \mu^2}$$

must be used instead of  $E$ . Eq. (156), for calculating the critical pressure, becomes

$$p_{cr} = \frac{Eh^3}{4(1 - \mu^2)R^3}. \quad (158)$$

The preceding equation may be used as long as the corresponding compressive stress in the tube is less than the proportional limit of the material. Beyond the elastic limit the true critical pressure will be less than that obtained from eq. (158), and the following equation may be used for a material with a pronounced yield point:<sup>26</sup>

$$p_{cr} = \frac{h}{R} \frac{\sigma_{Y.P.}}{1 + 4 \frac{\sigma_{Y.P.} R^2}{E h^2}}, \quad (159)$$

<sup>25</sup> Nicolai, *Z. angew. Math. u. Mech.*, Vol. 3, p. 227, 1923. See also the author's paper, *ibid.*, p. 358.

<sup>26</sup> See R. V. Southwell, *Phil. Mag.*, Vol. 29, p. 67, 1915.

in which  $\sigma_{YP}$  denotes the yield point of the material in compression. As the thickness reduces, the critical pressure approaches the limiting value  $Eh^3/4R^3$ , which is slightly less than that given by eq (158), and in all cases its value is less than  $h\sigma_{YP}/R$ , i.e., less than the pressure corresponding to the yield point stress<sup>27</sup>

In the region beyond the elastic limit, we can proceed as in the case of struts and use  $E_t$  instead of  $E$  in eq (158). In this way a relation is established between  $p_{cr}$  and  $h/R$  in the plastic range.

*Tubes with an Initial Ellipticity*—The failure of tubes under uniform external pressure depends considerably upon the various kinds of imperfections in them. The most important imperfection is an initial ellipticity, the limiting value of which in each type of tube is usually well known from numerous inspection measurements. Hence it seems desirable to have a design formula in which this initial ellipticity appears explicitly. To derive such a formula<sup>28</sup> let us assume

that the initial deviation of the shape of the tube from a perfect circular form, indicated by the broken line in Fig 122, is given by the equation

$$u_1 = u_0 \cos 2\varphi, \quad (g)$$

in which  $u_0$  is the maximum initial radial deviation, considered small in comparison with  $R$ , and  $\varphi$  is the central angle measured as shown in the figure. The initial shape of the tube is then represented by the solid line.

If on such a noncircular tube an external pressure  $p$  is applied, a further flattening of the tube occurs. Denoting

<sup>27</sup> Experiments on the collapse of short tubes from external pressure are described by G. Cook, *Phil Mag*, p 51, 1914. For a bibliography on the subject by the same author see *Brit Assoc Adv Sci (Birmingham) Repts*, 1913.

<sup>28</sup> See the writer's paper, *J Appl Mech*, Vol 1, p 173, 1933.

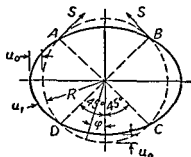


FIG 122

the radial displacements corresponding to the latter flattening by  $u_2$  and considering an elemental ring of unit width, we obtain from eq. (235), Part I, p. 404:

$$\frac{d^2 u_2}{d\varphi^2} + u_2 = -\frac{1}{D} MR^2, \quad (h)$$

where

$$D = \frac{Eh^3}{12(1 - \mu^2)},$$

i.e.,  $D$  is the flexural rigidity of the elemental ring. Regarding the bending moment  $M$  due to pressure  $p$ , we see that a decrease in curvature occurs in the portions  $AB$  and  $CD$  of the elemental ring; hence  $M$  is positive in these regions, while in the remaining portions of the ring the moment is negative. At points  $A$ ,  $B$ ,  $C$  and  $D$  the bending moment is zero, and the interaction between the parts of the elemental ring is given by forces  $S$  tangential to the broken-line circle representing the ideal shape of the tube. (The action of the forces  $S$  on the portion  $AB$  of the ring is shown in the figure.) This circle can be considered as a funicular curve for the external uniform pressure  $p$ . The compressive force along this curve remains constant and equal to  $S \approx pR$ . Thus the bending moment at any cross section is obtained by multiplying  $S$  by the total radial deviation  $u_1 + u_2$  at this cross section. Then

$$M = pR(u_2 + u_0 \cos 2\varphi), \quad (i)$$

and eq. (h) becomes

$$\frac{d^2 u_2}{d\varphi^2} + u_2 = -\frac{1}{D} pR^3(u_2 + u_0 \cos 2\varphi)$$

or

$$\frac{d^2 u_2}{d\varphi^2} + u_2 \left(1 + p \frac{R^3}{D}\right) = -\frac{1}{D} pR^3 u_0 \cos 2\varphi.$$

The solution of this equation satisfying the conditions of continuity at the points  $A$ ,  $B$ ,  $C$  and  $D$  is

$$u_2 = \frac{u_0 p}{p_{cr} - p} \cos 2\varphi, \quad (160)$$



in which  $p_{cr}$  is given by eq. (158). It is seen that at the points  $A$ ,  $B$ ,  $C$  and  $D$  the displacement  $u_2$  and its second derivative vanish. Hence the bending moments at these points are zero, as was previously assumed. The maximum bending moment occurs at  $\varphi = 0$  and  $\varphi = \pi$  where

$$M_{\max} = pR \left( u_0 + \frac{u_0 p}{p_{cr} - p} \right) = \frac{p u_0 R}{1 - \frac{p}{p_{cr}}}. \quad (161)$$

It is seen that for small values of the ratio  $p/p_{cr}$  the change in the ellipticity of the tube due to pressure  $p$  can be neglected, and that the maximum bending moment is obtained by multiplying the compressive force  $S = pR$  by the initial deviation  $u_0$ . If the ratio  $p/p_{cr}$  is not small, the change in the initial ellipticity of the tube must be considered, and eq. (161) must be used in calculating  $M_{\max}$ .

The maximum compressive stress is now obtained by adding the maximum compressive stress due to bending moment  $M_{\max}$  to the stress produced by the compressive force  $pR$ . Thus we find

$$|\sigma|_{\max} = \frac{pR}{h} + \frac{6pRu_0}{h^2} \cdot \frac{1}{1 - \frac{p}{p_{cr}}}. \quad (j)$$

With the aid of this equation a method of pipe design can be developed which is similar to the design of columns on the basis of assumed imperfections.

The limiting value of the pressure  $p$  is that value at which yielding of the material begins. Denoting this value by  $p_{YP}$ , and substituting  $\sigma_{YP}$  for  $\sigma_{\max}$  in eq. (j) we obtain

$$\sigma_{YP} = \frac{p_{YP} R}{h} + \frac{6p_{YP} Ru_0}{h^2} \cdot \frac{1}{1 - \frac{p_{YP}}{p_{cr}}} \quad (k)$$

from which the value of the limiting pressure  $p_{YP}$  can be calculated if  $\sigma_{YP}$  and the initial deviation  $u_0$  are known. By

using the notation

$$\frac{R}{h} = m \quad \text{and} \quad \frac{u_0}{R} = n, \quad (I)$$

eq. (k) for calculating  $p_{Y.P.}$  becomes

$$p_{Y.P.}^2 - \left[ \frac{\sigma_{Y.P.}}{m} + (1 + 6mn)p_{cr} \right] p_{Y.P.} + \frac{\sigma_{Y.P.} p_{cr}}{m} = 0. \quad (162)$$

From this equation curves can be plotted giving the average compressive stress  $p_{Y.P.}R/h$  as a function of  $R/h$  for various values of the ratio  $u_0/R$  and for various values of  $\sigma_{Y.P.}$ . By using such curves, together with a proper factor of safety, the suitable wall thickness of a pipe can be readily calculated. It should be noted that the pressure  $p_{Y.P.}$  determined in this manner is smaller than the pressure at which complete collapse of the tube occurs; hence by using  $p_{Y.P.}$  as the ultimate value of pressure we are always on the safe side.

In the preceding discussion it was assumed that the length of the tube  $l$  is large in comparison with its radius, say  $l/R > 20$ . For shorter tubes, if the edges are built in or supported, the value of  $p_{cr}$  is larger than that given by eq. (158) and depends on the ratio  $l/R$ . The theory of buckling of such tubes is more complicated,<sup>29</sup> since the tube subdivides during buckling in several waves along the circumference, and the number of these waves depends on the ratio  $l/R$ .<sup>30</sup>

The problem of the buckling of tubes closed at the ends and subjected to uniform pressure on both the ends and the sides<sup>31</sup> has also been solved.<sup>32</sup>

**38. Buckling of Rectangular Plates.**—The problem of the buckling of compressed rectangular plates is of practical im-

<sup>29</sup> For a discussion of this problem see S. Timoshenko, *Theory of Elastic Stability*, p. 445, 1936.

<sup>30</sup> Some curves for calculating critical pressures on short tubes were prepared by the Research Committee on the Strength of Vessels under External Pressure, A.S.M.E., Dec. 1933.

<sup>31</sup> This condition arises in the investigation of the stability of the hull of a submarine between two reinforcing rings.

<sup>32</sup> See the paper by R. v. Mises in *Festschrift f. Prof. A. Stodola*, Zürich, 1929.

portance in discussing the elastic stability of compression members built up of plates such as are often used in steel structures (Fig. 123). The failure of such members may be brought about by buckling of the web or of the side plates instead of by buckling of the member as a whole. For example, in the cases shown in Fig. 123, buckling of the plates as

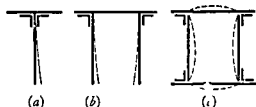


FIG. 123.

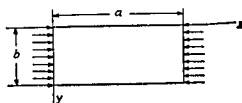


FIG. 124.

indicated by the broken lines may occur if the thickness of the plate is not satisfactorily chosen. Since the length of a compression member is usually large in comparison with the cross-sectional dimensions, the problem reduces to that of the buckling of a long, compressed plate, Fig. 124. The short sides of the plate can be considered as simply supported; the conditions along the other two sides depend on the shape of the cross section. For example, if a column section has a square form, Fig. 123c, and the side plates are all of the same thickness, they have the tendency to buckle simultaneously. Each side can be considered as a compressed rectangular plate with all four sides simply supported. In the cases shown in Figs. 123a and 123b, the lower edges of the vertical webs are free and the upper edges are elastically built in.<sup>33</sup>

Rigorous solutions of the buckling problem for various conditions along the longitudinal sides of a plate such as is shown in Fig. 124 have been worked out.<sup>34</sup> We give here only some final results and the values of the critical stresses obtained from these solutions.

<sup>33</sup> The first experiments in which the question of buckling of thin-walled structures was discussed were made by William Fairbairn and described in his book, *Britannia and Conway Tubular Bridges*, London, 1849. See also the work of E. Hodgkinson published as Appendix AA to the *Report of the Commissioners Appointed to Inquire into the Application of Iron to Railway Structures*, London, 1849.

<sup>34</sup> See S. Timoshenko, *Theory of Elastic Stability*, 1936.

*Rectangular Plate Simply Supported on Four Sides.*—A simply supported plate under uniform compression in the direction of the  $x$  axis (Fig. 124) buckles by subdividing into squares or rectangles which approximate squares. The critical value of the compressive stress is given by the equation<sup>32</sup>

$$\sigma_{cr} = \beta \sigma_e, \quad (163)$$

in which

$$\sigma_e = \frac{\pi^2 E k^2}{12 b^2 (1 - \mu^2)}, \quad (164)$$

where  $k$  is the thickness of the plate and  $b$  its width. The factor

$$\beta = \left( \frac{a}{mb} + \frac{mb}{a} \right)^2 \quad (a)$$

denotes a coefficient depending upon the magnitude of the ratio  $a/b$ , and the integer  $m$  represents the number of waves into which the

TABLE 10: CONSTANTS FOR CALCULATING CRITICAL COMPRESSIVE STRESS FOR SIMPLY SUPPORTED RECTANGULAR PLATES

$a/b =$	0.4	0.6	0.8	1.0	1.2	1.4	1.6
$\beta =$	8.41	5.14	4.23	4.00	4.13	4.47	4.20
$\sigma_{cr} =$	22,830	14,000	11,400	10,900	11,200	12,100	11,400

$a/b =$	1.8	2.0	2.2	2.4	2.7	3
$\beta =$	4.04	4.00	4.04	4.13	4.04	4.00
$\sigma_{cr} =$	11,000	10,900	11,000	11,200	11,000	10,900

plate divides in buckling. The integer  $m$  must be so chosen as to make  $\beta$  a minimum.<sup>33</sup> Several values of the coefficient  $\beta$  are given in Table 10. For longer plates ( $a/b > 3$ ) a good approximation is  $\beta = 4$ .

<sup>32</sup> The solution of this problem is due to G. H. Bryan; see *Proc. London Math. Soc.*, Vol. 22, p. 54, 1891. Other cases of buckling of rectangular plates were considered by the writer. See his papers: "On the Stability of Compressed Plates," *Bull. Polytech. Inst. (Kiev)*, 1907; *Z. Math. u. Phys.*, Vol. 58, 1910; *Eisenbau*, Vol. 12, 1911; *Proc. Am. Soc. Civil Engrs.*, Vol. 55, p. 855, 1929. See also H. Reissner, *Zentr. Bauverstat.*, p. 93, 1909.

<sup>33</sup> It may be seen that this minimum value of  $\beta$  is equal to 4 and occurs when  $a = mb$ , i.e., when the plate subdivides during buckling into squares.

The values of  $\sigma_{cr}$  given in Table 10 are calculated on the assumption that  $E = 30 \times 10^6$  lb per sq in,  $\mu = 0.3$  and  $h/b = 0.01$ . The critical stress for any other value of the ratio  $h/b$  can be obtained by multiplying the tabular values by  $10^4(h^2/b^2)$ . To illustrate, consider a long steel plate having a yield point stress of 40,000 lb per sq in. Suppose we wish to determine the value of the ratio  $b/h$  at which the critical stress is equal to the yield point stress. Assuming  $\beta = 4$  and using Table 10, we obtain

$$\sigma_{cr} = 10,900 \times 10^4 \times \frac{h^2}{b^2} = 40,000 \text{ lb per sq in,}$$

from which

$$\frac{b}{h} = 52.2 \quad (b)$$

For larger values of the ratio  $b/h$  failure occurs by buckling at a compressive stress smaller than the yield point of the material. Under such conditions the critical stress and not the yield point of the material must be taken as the basis for determining working stress.

*Three Sides of the Plate Simply Supported and the Fourth Side Free*—If one of the longitudinal edges such as  $y = b$  (see Fig. 124) is free, the previous equation (eq. 163) can be used for calculating the critical values of the compressive stress. The values of the coefficient  $\beta$  are given in Table 11.

TABLE 11 CONSTANT  $\beta$  FOR CALCULATING CRITICAL COMPRESSIVE STRESS FOR A RECTANGULAR PLATE WITH THREE EDGES SIMPLY SUPPORTED AND THE FOURTH ( $y = b$ ) FREE

$a/b =$	0.5	1.0	1.2	1.4	1.6	1.8	2.0	2.5	3.0	4.0	5.0
$\beta =$	4.40	1.440	1.135	0.952	0.835	0.755	0.698	0.610	0.564	0.516	0.506

*Two Opposite Sides Simply Supported, the Third Side Built In, and the Fourth Side Free*—The sides  $x = 0$ ,  $x = a$  in Fig. 124 are considered as simply supported and the side  $y = 0$  as built in. The same equation (eq. 163) can be used and the values of the coefficient  $\beta$  are given in Table 12. (For larger values of the ratio  $a/b$ , a good approximation is  $\beta = 1.33$ .)

*Two Opposite Sides Simply Supported and the Other Two Built In*<sup>37</sup> The sides  $x = 0$  and  $x = a$  are considered simply supported

<sup>37</sup> We have this condition when two opposite sides of the compressed member shown in Fig. 123c are very rigid and only the other two may buckle.

TABLE 12: CONSTANT  $\beta$  FOR CALCULATING CRITICAL COMPRESSIVE STRESS FOR A RECTANGULAR PLATE WITH TWO OPPOSITE SIDES SIMPLY SUPPORTED, THE THIRD BUILT IN, AND THE FOURTH ( $y = b$ ) FREE

$a/b =$	1.0	1.1	1.2	1.3	1.4	1.5	1.6	1.7	1.8	1.9	2.0	2.2	2.4	2.6	2.8	3
$\beta =$	1.70	1.56	1.47	1.41	1.36	1.34	1.33	1.33	1.34	1.36	1.38	1.45	1.47	1.41	1.36	1.34

The corresponding values of the coefficient  $\beta$  in eq. (163) are given in Table 13.

 TABLE 13: CONSTANT  $\beta$  FOR CALCULATING CRITICAL COMPRESSIVE STRESS FOR A RECTANGULAR PLATE WITH TWO OPPOSITE SIDES SIMPLY SUPPORTED AND THE OTHER TWO BUILT IN

$a/b =$	0.4	0.5	0.6	0.7	0.8	0.9	1.0	1.2	1.4	1.6	1.8	2.1
$\beta =$	9.44	7.69	7.05	7.00	7.29	7.83	7.69	7.05	7.00	7.29	7.05	7.00

*Rectangular Plate Simply Supported on Four Sides and Subjected to the Action of Shearing Stresses Uniformly Distributed along the Sides (Fig. 125). The critical value of the shearing stress which may produce buckling of the plate is*

$$\tau_{cr} = \beta \sigma_e. \quad (165)$$

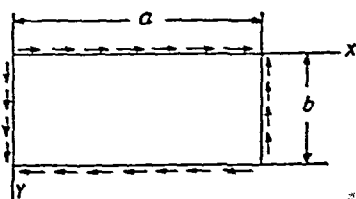


FIG. 125.

The values of the numerical coefficient  $\beta$  are given in Table 14.

 TABLE 14: CONSTANT  $\beta$  FOR CALCULATING CRITICAL STRESS FOR A RECTANGULAR PLATE SIMPLY SUPPORTED ON FOUR SIDES AND SUBJECTED TO THE ACTION OF A UNIFORM SHEAR

$a/b =$	1	1.2	1.4	1.5	1.6	1.8	2.0	2.5	3	$\infty$
$\beta =$	9.42	8.0	7.3	7.1	7.0	6.8	6.6	6.3	6.1	5.4

Table 14 can be used in choosing the thickness of the web of a plate girder. Near the supports the shearing force is the most important factor. Therefore the part of the web between two stiffeners may be considered as a rectangular plate with simply supported edges,

subjected only to the action of shearing stresses. For example, if the distance between the stiffeners is 5 ft,  $E = 30 \times 10^6$  lb per sq in and  $\mu = 0.3$ , the following values of the critical stress in lb per sq in are obtained for girders of thickness  $h$  and depth  $b$  by using Table 15<sup>38</sup>

TABLE 15

$b$	$h = \frac{3}{8}$ in	$h = \frac{7}{16}$ in	$h = \frac{1}{2}$ in	$h = \frac{9}{16}$ in
5 ft	9,980	13,600	17,700	22,400
7 ft	7,730	10,500	13,700	17,400
10 ft	6,990	9,510	12,400	15,700

The necessary thicknesses of the steel plates used in the built-up compression members whose sections are shown in Fig. 123 can be obtained from Tables 10–15. If the sides of the hollow section (Fig. 123c) are considered to be long rectangular plates simply supported, the critical compressive stress is

$$\sigma_{cr} = 4\sigma_e = \frac{\pi^2 h^2}{3b^2} \frac{E}{1 - \mu^2} \quad (c)$$

Taking, for example,  $h/b = 0.01$  we find

$$\sigma_{cr} = 10,900 \text{ lb per sq in}$$

This stress is far below the proportional limit of structural steel. If the longitudinal edges of the same plate are assumed to be built in, we find

$$\sigma_{cr} = 7\sigma_e = \frac{7}{4}(10,900) \approx 19,100 \text{ lb per sq in.}$$

In the cases of Fig. 123a and 123b, the compressed vertical steel plates may be considered as long plates built in<sup>39</sup> along the upper

<sup>38</sup> Additional data regarding the buckling of the web and the design of stiffeners are given in the writer's papers, *Proc Am Soc Civil Engrs*, Vol 55, p 855, 1929, and *Engineering*, Vol 138, p 207, 1934. See also E. Chwalla, *Repts 2d Congr Internat Assoc Bridge and Structural Engrg*, Berlin, 1936, *Stahlbau*, 1936.

<sup>39</sup> This assumption gives an upper limit for the critical stress. The true critical stress will be somewhat lower, since the fastening of the upper edge is not absolutely rigid.

edge and free along the lower edge. The critical stress is therefore

$$\sigma_{cr} = 1.33\sigma_e = \frac{1.33\pi^2}{12} \frac{h^2}{b^2} \frac{E}{1 - \mu^2}. \quad (d)$$

Again the stability of the plate depends on the magnitude of the ratio  $b/h$ . Assuming that the yield point of structural steel is 30,000 lb per sq in., the value of  $b/h$  which makes  $\sigma_{cr}$  equal to this stress is, from eq. (d),

$$\frac{b}{h} = \sqrt{\frac{1.33\pi^2}{12 \times 30\,000} \times \frac{30 \times 10^6}{0.91}} \approx 35.$$

Consequently, if  $b/h > 35$ , the critical stress becomes less than the yield point of the material. This fact must be considered in choosing the magnitude of the working stress. The stability of the plate can be increased by reinforcing the free edge of the plate.

In all the above cases it was assumed that the critical stress is below the proportional limit. For stresses beyond the proportional limit our equations give exaggerated values of the critical stresses.<sup>40</sup>

**39. Buckling of Beams without Lateral Supports.**—It is well known that in the absence of lateral supports, I beams loaded in the plane of the web may prove to be insufficiently stable in a lateral direction. If the load is increased beyond a certain *critical limit* such beams buckle sidewise, and further loading causes them to collapse.<sup>41</sup> The energy method may be used to determine this limit.

As an illustration consider a beam  $AB$  (Fig. 126) of narrow rectangular cross section with a central concentrated load  $P$  acting in the longitudinal vertical plane of symmetry. If this force is small, the deflection of the beam is in the vertical plane only and the bending is stable. This means that if the beam is deflected sideways by a lateral force, this deflection disappears with the removal of the

<sup>40</sup> This question is discussed in S. Timoshenko, *Theory of Elastic Stability*, p. 384, 1936.

<sup>41</sup> The collapse of girders as a consequence of sideways buckling is illustrated by the bridge disaster near Tarbes, France; see *Revue technique*, Nov. 15, 1897. The lateral buckling of beams of a narrow rectangular cross section was discussed by L. Prandtl, dissertation, Nürnberg, 1899, and A. G. M. Michell, *Phil. Mag.*, Vol. 48, 1899. Buckling of I beams was discussed by the writer; see *Bull. Polytech. Inst. (St. Petersburg)*, Vols. 4 and 5, 1905 and 1906. See also *Ann. ponts et chaussées*, 1913, and *Trans. Am. Soc. Civil Engrs.*, Vol. 87, p. 1247, 1924. The practical application of the theory is discussed by E. Chwalla, *Die Kipp-Stabilität gerader Träger mit doppelt-symmetrischem I-Querschnitt*, Berlin, 1939. See also the book by F. Bleich, *loc. cit.*, p. 182, Chap. 4.



force and the beam returns to its initial form. If  $P$  is increased, however, a limiting value is reached at which bending in the vertical plane becomes unstable. The beam then buckles sideways, and large lateral deflections may occur with a very small increase of the load. This limiting value of  $P$  is called the *critical load*.

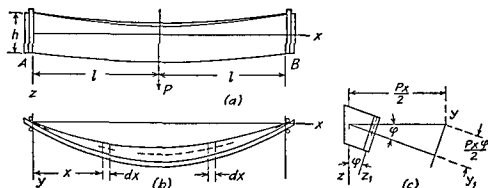


FIG 126

The critical load is determined by considering the potential energy of the system. Any lateral deflection of the beam is accompanied by an increase of the strain energy. After a small lateral buckling we have not only the strain energy of bending in the vertical plane, which may be considered unchanged, but also the strain energy of bending in the lateral direction and the strain energy of twist. At the same time the potential energy of the load diminishes, because sidewise buckling is accompanied by a lowering of its point of application. Let  $U_1$  denote this decrease in the potential energy of the load,  $U$  the strain energy due to bending in the lateral direction, and  $U_2$  the strain energy due to twist. Then the critical load is determined by eq (140), p 162, which becomes

$$U + U_2 = U_1 \quad (a)$$

We must now calculate the quantities entering into this equation. The bending moment in the vertical plane at any cross section a distance  $x$  from the left support (see Fig 126) is  $Px/2$ . In calculating sidewise buckling, the bending moment with respect to the  $z_1$  axis (Fig 126c) must be considered. This moment is equal to  $(Px/2)\varphi$ , in which  $\varphi$  denotes the small angle of twist, variable along the length of the beam. Then for small lateral deflections<sup>42</sup> we have the following differential equation

$$EI_z \frac{d^2 y}{dx^2} = -\frac{Px}{2} \varphi \quad (b)$$

<sup>42</sup> For small deflections we may take  $d^2 y/dx^2$  for the curvature instead of  $d^2 y_1/dx^2$ .

The corresponding strain energy of bending is

$$U = EI_z \int_0^l \left( \frac{d^2 y}{dx^2} \right)^2 dx = \frac{P^2}{4EI_z} \int_0^l x^2 \varphi^2 dx. \quad (c)$$

The strain energy of twist is (see Part I, eq. 186)

$$U_2 = C \int_0^l \left( \frac{d\varphi}{dx} \right)^2 dx, \quad (d)$$

in which the torsional rigidity  $C$  for a rectangular cross section is obtained from Part I, eq. 159.

Let us consider now the lowering of the point of application of the load  $P$  due to the lateral deflection. Take two symmetrically situated elements  $dx$  of the beam (Fig. 126*b* and *c*) and consider the effect of the bending in the plane  $xy_1$  of these two elements only. The angular deflection due to this bending is equal to  $-(d^2 y/dx^2)dx$ . As this bending occurs in the plane  $xy_1$  inclined at an angle  $\varphi$  to the horizontal (Fig. 126*c*), it causes a lowering of the load  $P$  equal to  $-x\varphi(d^2 y/dx^2)dx$ . The total lowering of  $P$  due to such bending of all the elements of the beam in buckling is therefore

$$\delta = - \int_0^l x\varphi \frac{d^2 y}{dx^2} dx,$$

or, using eq. (b),

$$\delta = \frac{P}{2EI_z} \int_0^l x^2 \varphi^2 dx.$$

Hence

$$U_1 = P\delta = \frac{P^2}{2EI_z} \int_0^l x^2 \varphi^2 dx. \quad (e)$$

Substituting from eqs. (c), (d) and (e) in eq. (a), we find

$$P_{cr}^2 = \frac{4EI_z C \int_0^l \left( \frac{d\varphi}{dx} \right)^2 dx}{\int_0^l x^2 \varphi^2 dx}. \quad (f)$$

By taking for the angle of twist  $\varphi$  a suitably chosen function of  $x$  to satisfy the end conditions we obtain an approximate value of the critical load from eq. (f). Assume, for instance, that

$$\varphi = a \sin \frac{\pi x}{2l}. \quad (g)$$

Consider as an example a structural steel I beam of the following dimensions

$$\text{Length } 2l = 20 \text{ ft}$$

$$\text{Depth } h = 24 \text{ in}$$

$$\text{Flange width } b = 7 \text{ in}$$

$$\text{Thickness of web } \delta_1 = 0.5 \text{ in}$$

$$\text{Mean thickness of flanges } \delta = \frac{1}{2}(0.60 + 1.14) = 0.87 \text{ in}$$

$$\text{Area of section } A = 23.3 \text{ in}^2$$

$$\text{Principal rigidity } EI_y = 2,087E \text{ lb in}^2$$

$$\text{Principal rigidity } EI_z = 42.7E \text{ lb in}^2$$

From eq (224), p 245,

$$C = G(\frac{2}{3}b\delta^3 + \frac{1}{3}h\delta_1^3) = 4.07G$$

Then, from eq (h), assuming  $E = 2.6G$ ,

$$\alpha = 3.67,$$

and from eq (i),

$$\gamma = \frac{42.7}{2,087 \times 100} = 205 \times 10^{-6}$$

Table 16 gives, by interpolation for  $\alpha = 3.67$ ,

$$\sigma_{cr} = 11,300 + \frac{1}{2}(13,600 - 11,300)1.67 = 13,200 \text{ lb per sq in}$$

This is the critical stress for  $\gamma = 0.0001$ . The critical stress in the example considered will be  $13,200 \times \gamma \times 10^4 = 26,900 \text{ lb per sq in}$ . The load corresponding to this stress must be considered the ultimate load for the beam.

This numerical result shows that sideways buckling may occur at stresses smaller than the ultimate stress of the material under direct compression, and even less than the elastic limit. This fact must be considered and the critical stress instead of the yield point must be taken as the basis for the determination of working stresses. In this example, using a factor of safety of 3, the working stress will be equal to  $26,900/3 = 8,970 \text{ lb per sq in}$ .

## CHAPTER VI

### DEFORMATIONS SYMMETRICAL ABOUT AN AXIS

40. **Thick-walled Cylinder.**—If a circular cylinder of constant wall thickness is subjected to the action of uniformly distributed internal and external pressures, the deformation produced is symmetrical about the axis of the cylinder and does not change along its length. In Fig. 127 we consider a

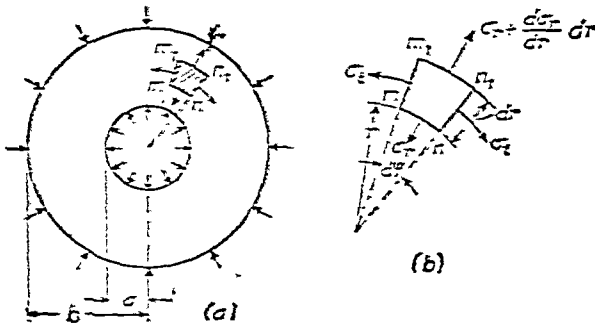


FIG. 127.

ring cut from the cylinder by two planes perpendicular to the axis and at unit distance apart. From the condition of symmetry it follows that there are no shearing stresses on the sides of an element  $mm_1n_1$  of this ring, Fig. 127. The element  $mm_1n_1$  is bounded by two axial planes and two concentric cylindrical surfaces. Let  $\sigma_t$  denote the hoop stress acting normal to the sides  $mm_1$  and  $n_1n_1$  of the element, and  $\sigma_r$  the radial stress normal to the side  $mn$ . This stress varies with the radius  $r$  and changes by an amount  $(d\sigma_r/dr)dr$  in the distance  $dr$ . The normal radial stress on the side  $m_1n_1$  is consequently

$$\sigma_r + \frac{d\sigma_r}{dr} dr.$$

Summing up the forces on the element in the direction of the

equations for determining the constants  $C_1$  and  $C_2$ , from which

$$C_1 = \frac{1 - \mu}{E} \frac{a^2 p_1 - b^2 p_0}{b^2 - a^2}; \quad C_2 = \frac{1 + \mu}{E} \frac{a^2 b^2 (p_1 - p_0)}{b^2 - a^2}. \quad (j)$$

With these values for the constants in eqs. (g) and (h) the general expressions for the normal stresses  $\sigma_r$  and  $\sigma_t$  become<sup>2</sup>

$$\begin{aligned} \sigma_r &= \frac{a^2 p_1 - b^2 p_0}{b^2 - a^2} - \frac{(p_1 - p_0) a^2 b^2}{r^2 (b^2 - a^2)}, \\ \sigma_t &= \frac{a^2 p_1 - b^2 p_0}{b^2 - a^2} + \frac{(p_1 - p_0) a^2 b^2}{r^2 (b^2 - a^2)}. \end{aligned} \quad (171)$$

It is important to note that the sum of these two stresses remains constant, so that the deformation of all elements in the direction of the axis of the cylinder is the same, and cross sections of the cylinder remain plane after deformation. This justifies our consideration of the problem as a two dimensional one.

Let us consider now the particular case when  $p_0 = 0$ , i.e., the cylinder is subjected to *internal pressure only*. Then eqs. (171) become

$$\sigma_r = \frac{a^2 p_1}{b^2 - a^2} \left( 1 - \frac{b^2}{r^2} \right), \quad (172)$$

$$\sigma_t = \frac{a^2 p_1}{b^2 - a^2} \left( 1 + \frac{b^2}{r^2} \right). \quad (173)$$

These equations show that  $\sigma_r$  is always a compressive stress and  $\sigma_t$  a tensile stress. The latter is maximum at the inner surface of the cylinder, where

$$(\sigma_t)_{\max} = \frac{p_1 (a^2 + b^2)}{b^2 - a^2}. \quad (174)$$

This equation shows that  $(\sigma_t)_{\max}$  is always numerically greater than the internal pressure, and approaches this quantity as  $b$  increases. The minimum value of  $\sigma_t$  is at the outer surface of

<sup>2</sup>This solution appeared first in the paper by Lamé and Clapeyron, "Mémoire sur l'équilibre intérieur des corps solides homogènes," *Mém. divers savans*, Vol. 4, 1833.

the cylinder. The ratio

$$\frac{(\sigma_t)_{\max}}{(\sigma_t)_{\min}} = \frac{a^2 + b^2}{2a^2}$$

increases with increase in the thickness of the wall of the cylinder. For a comparatively small thickness there is not a great difference between the maximum and minimum values of  $\sigma_t$ . Taking, for example,  $b = 1.1a$ ,  $(\sigma_t)_{\max}$  exceeds  $(\sigma_t)_{\min}$  by only  $10\frac{1}{2}$  per cent. The error is therefore small if we assume the tensile stresses  $\sigma_t$  to be uniformly distributed over the thickness of the wall and use the equation

$$\sigma_t = \frac{p_i a}{b - a},$$

which coincides with the equation given on p. 121 for thin cylinders. The shearing stress is maximum at the inner surface of the cylinder where

$$\tau_{\max} = \frac{\sigma_t - \sigma_r}{2} = \frac{1}{2} \left[ \frac{p_i(a^2 + b^2)}{b^2 - a^2} + \frac{p_i(b^2 - a^2)}{b^2 - a^2} \right] = \frac{p_i b^2}{b^2 - a^2}. \quad (k)$$

When only an *external pressure* acts on the cylinder we have  $p_i = 0$  and eqs. (171) give

$$\sigma_r = -\frac{p_0 b^2}{b^2 - a^2} \left( 1 - \frac{a^2}{r^2} \right), \quad (175)$$

$$\sigma_t = -\frac{p_0 b^2}{b^2 - a^2} \left( 1 + \frac{a^2}{r^2} \right). \quad (176)$$

In this case  $\sigma_r$  and  $\sigma_t$  are both compressive stresses, and  $\sigma_t$  is always numerically greater than  $\sigma_r$ . The maximum compressive stress is at the inner surface of the cylinder, where

$$(\sigma_t)_{r=a} = -\frac{2p_0 b^2}{b^2 - a^2}. \quad (177)$$

It is interesting to note that as the ratio  $b/a$  of the radii of the cylinder is increased, this maximum compressive stress

approaches twice the value of the external pressure acting on the cylinder, namely,  $-2p_0$ .

Let us consider now the *deformation of the cylinder*. Substituting from eqs. (j) for the arbitrary constants in eq. (f), we find

$$u = \frac{1 - \mu}{E} \frac{a^2 p_1 - b^2 p_0}{b^2 - a^2} r + \frac{1 + \mu}{E} \frac{a^2 b^2 (p_1 - p_0)}{(b^2 - a^2) r}. \quad (178)$$

This gives the radial displacement of any point in the wall of the cylinder. In the particular case of a cylinder subjected to internal pressure only ( $p_0 = 0$ ), the radial displacement at the inner surface, from eq. (178), is

$$(u)_{r=a} = \frac{a p_1}{E} \left( \frac{a^2 + b^2}{b^2 - a^2} + \mu \right). \quad (179)$$

When the cylinder is subjected to external pressure only ( $p_1 = 0$ ), the radial displacement at the outer surface is

$$(u)_{r=b} = -\frac{b p_0}{E} \left( \frac{a^2 + b^2}{b^2 - a^2} - \mu \right). \quad (180)$$

The minus sign indicates that the displacement is towards the axis of the cylinder.

41. **Stresses Produced by Shrink Fit.**—If it is necessary to produce contact pressure between a hub and a shaft or between two rings mounted one inside the other, it is the usual practice to make the inner radius of the outer part smaller than the outer radius of the inner part and to assemble the structure after a preliminary heating of the outer part. After cooling, a contact pressure between the two parts is produced, which is called the *shrink-fit pressure*. The magnitude of this pressure and the stresses produced by it can easily be calculated by using the equations of the preceding article.

Assume, for example, that the external radius of the inner cylinder in the unstressed condition is larger than the internal radius of the outer cylinder (Fig. 128) by the amount  $\delta$ . Then after assembly a pressure  $p$  is produced between the cylinders. The magnitude of  $p$  is found from the condition that the in-

crease in the inner radius of the outer cylinder plus the decrease in the outer radius of the inner cylinder must be equal

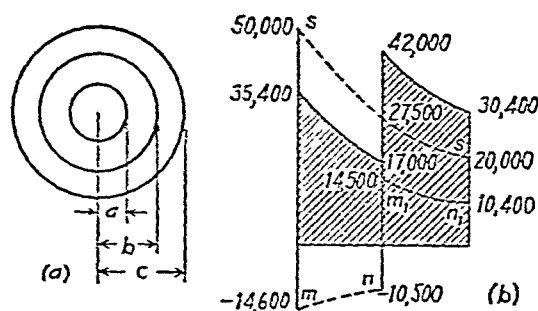


FIG. 128.

to  $\delta$ . Hence, from eqs. (179) and (180),

$$\frac{bp}{E} \left( \frac{b^2 + c^2}{c^2 - b^2} + \mu \right) + \frac{bp}{E} \left( \frac{a^2 + b^2}{b^2 - a^2} - \mu \right) = \delta,$$

from which

$$p = \frac{E\delta (b^2 - a^2)(c^2 - b^2)}{b \cdot 2b^2(c^2 - a^2)}. \quad (181)$$

Eqs. (172) and (173) then give the stresses in the outer cylinder, and eqs. (175) and (176) give the stresses in the inner cylinder. Usually the stresses to be considered in design are those at the inner surface of the outer cylinder. These stresses are

$$\sigma_t = \frac{p(b^2 + c^2)}{c^2 - b^2}, \quad \sigma_r = -p.$$

The maximum shearing stress at this surface is (see eq.  $k$ , p. 209)

$$\tau_{\max} = \frac{pc^2}{c^2 - b^2}$$

or, substituting from eq. (181) for  $p$ ,

$$\tau_{\max} = \frac{E\delta c^2(b^2 - a^2)}{2b^3(c^2 - a^2)}. \quad (182)$$

In the particular case of a solid shaft and a hub we have  $a = 0$ ,



which gives

$$p = \frac{E\delta}{2bc^2} (c^2 - b^2) \quad (183)$$

$$\tau_{\max} = \frac{E\delta}{2b}, \quad (184)$$

i.e., the maximum shearing stress is the same as in a simple tie rod which undergoes a unit elongation equal to  $\delta/b$

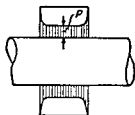


FIG 129

The above discussion assumed that both cylinders have the same length. In dealing with a hub and a shaft (Fig 129) the projecting portions of the shaft resist compression, which results in an increased pressure near the faces of the hub as indicated by the shaded areas.<sup>3</sup>

If a built-up cylinder such as is represented in Fig 128 is subjected to internal pressure, the stresses produced by this pressure are the same as in a cylinder with a solid wall of thickness  $c - a$ . These stresses are superposed on the shrink fit stresses. The shrink fit produces a tangential compressive stress at the inner surface of the cylinder which reduces the maximum tangential tensile stress produced by the internal pressure at this point, so that a more favorable stress distribution may be obtained than in the case of a solid tube (see Prob 2, p 213). Hence cylinders built up of several tubes are used in situations where the internal pressures are very high, as in gun barrels.

A distribution of initial stresses analogous to those described above in the case of built up cylinders can also be

<sup>3</sup> An experimental investigation of shrink fit stresses is given in a paper by A Huggenberger, *Technische Blätter*, Schweiz Lokomotiv und Maschinenfabrik, Winterthur, 1926. A further discussion of shrink fit stresses is given in the paper by W Janicki, *Schweiz Bauzeitung*, Vol 88, p 93, 1926, and Vol 90, p 127, 1927. See also J W Baugher, *Trans A S M E*, Vol 52, 1930, and O J Horger and C W Nelson, *J Appl Mech*, Vol 4, p 183, 1937, and Vol 5, p 32, 1938. For practical information on shrink fits see O J Horger, ed., *A S M E Handbook*, New York, p 178, 1953. For a rigorous solution of the problem see S Timoshenko and J N Goodier, *Theory of Elasticity*, p 388, 1951.

obtained in a solid tube by applying a high internal pressure sufficient to produce permanent set in the inner part of the tube. After removing this internal pressure some stresses remain in the tube due to the permanent set, so that the inner part is then in a state of compression, and the outer part in a state of tension.<sup>4</sup>

### Problems

1. Determine the tangential stresses at the inner and outer surfaces and at the middle thickness of the wall of a cylinder with inner radius  $\frac{1}{2}$  in. and outer radius 8 in., subjected to an internal pressure  $p_i = 30,000$  lb per sq in.

*Answer.* From eq. (173):  $(\sigma_t)_{r=\frac{1}{2}''} = 50,000$  lb per sq in.;  $(\sigma_t)_{r=6''} = 27,500$  lb per sq in.;  $(\sigma_t)_{r=8''} = 20,000$  lb per sq in.

2. Determine the stresses in a built-up steel cylinder (Fig. 128) subjected to an internal pressure  $p_i = 30,000$  lb per sq in. if  $a = 4$  in.,  $b = 6$  in.,  $c = 8$  in., and the shrinkage  $\delta = 0.005$  in.

*Solution.* Determine first the initial stresses in the cylinder due to shrinkage. From eq. (181)

$$p = \frac{30 \times 10^6 \times 0.005(6^2 - 4^2)(8^2 - 6^2)}{6 \times 2 \times 6^2(8^2 - 4^2)} = 4,050 \text{ lb per sq in.}$$

The tangential stresses produced by this pressure in the inner cylinder, from eq. (176), are

$$(\sigma_t)_{r=\frac{1}{2}''} = -\frac{2pb^2}{b^2 - a^2} = -\frac{2 \times 4,050 \times 6^2}{6^2 - 4^2} = -14,600 \text{ lb per sq in.,}$$

$$(\sigma_t)_{r=6''} = -\frac{p(b^2 + a^2)}{b^2 - a^2} = -10,500 \text{ lb per sq in.}$$

The stresses for the outer cylinder, from eq. (173), are

$$(\sigma_t)_{r=8''} = \frac{p(b^2 + c^2)}{c^2 - b^2} = \frac{4,050(6^2 + 8^2)}{8^2 - 6^2} = 14,500 \text{ lb per sq in.,}$$

$$(\sigma_t)_{r=6''} = \frac{2pb^2}{c^2 - b^2} = \frac{4,050 \times 2 \times 6^2}{8^2 - 6^2} = 10,400 \text{ lb per sq in.}$$

The distribution of initial stresses  $\sigma_t$  over the thickness of the wall is shown in Fig. 128*b* by the broken lines  $mn$  and  $m_1n_1$ . The stresses

<sup>4</sup> A further discussion of this question is given in Art. 70.

produced by the internal pressure are the same as in the previous problem and are represented in the figure by the dotted line  $ss$ . Superposition of the two stress distributions gives the distribution represented by the shaded area. It may be seen that owing to assembly stresses, the maximum stress when the cylinder is subjected to internal pressure is reduced from 50,000 to 42,000 lb per sq in.

3 Referring to Fig 128, find the shrink fit stresses  $\sigma_t$  at  $r = 6$  in and  $r = 10$  in if  $a = 4$  in,  $b = 8$  in,  $c = 12$  in. Use a shrinkage factor  $\delta/b = 0.001$ , and take  $E = 30 \times 10^6$  lb per sq in.

Answer

$$(\sigma_t)_{r=6} = -13,500 \text{ lb per sq in}$$

$$(\sigma_t)_{r=10} = 13,750 \text{ lb per sq in}$$

4 For the hub and shaft in Fig 129 find the uniform pressure  $p$  if the radius of the shaft is 6 in and the outer radius of the hub is 12 in. The initial difference in diameters between hub and shaft is 0.012 in. Take  $E = 30 \times 10^6$  lb per sq in.

**42. Rotating Disc of Uniform Thickness.**—When a circular disc rotates about the axis of symmetry which is perpendicular to the disc, the inertia forces set up stresses which may become very large at high speeds. These stresses are distributed symmetrically with respect to the axis of rotation and may be calculated by the method indicated in Art 40. It is assumed that the stresses do not vary over the thickness of the disc and this thickness is taken equal to unity.

The equation of equilibrium of an element such as  $mnmn_1n_1$  in Fig 127 is derived by adding to the forces which were considered in Art 40 the inertia force acting on the element

$$\frac{\gamma \omega^2 r^2}{\sigma} dr d\theta \quad (a)$$

In this equation,  $\gamma$  is the weight per unit volume and  $\omega$  the angular velocity of the disc. The remaining notation is the same as in Art 40. The equation of equilibrium then becomes

$$\sigma_t - \sigma_r - r \frac{d\sigma_r}{dr} - \frac{\gamma \omega^2 r^2}{g} = 0 \quad (b)$$

Substituting for the stresses  $\sigma_t$  and  $\sigma_r$  in terms of the displacement  $u$  (eqs 170, p 207), we obtain the following equation

$$\frac{d^2u}{dr^2} + \frac{1}{r} \frac{du}{dr} - \frac{u}{r^2} + (1 - \mu^2) \frac{\gamma\omega^2 r}{gE} = 0. \quad (185)$$

The general solution of this equation is obtained by adding a particular solution to the solution of the corresponding homogeneous equation (see eqs.  $e$  and  $f$ , p. 207). A particular solution is

$$u = -(1 - \mu^2) \frac{\gamma\omega^2 r^3}{gE \cdot 8}.$$

Then, using the notation

$$N = (1 - \mu^2) \frac{\gamma\omega^2}{gE}, \quad (c)$$

the general solution of eq. (185) is

$$u = -N \frac{r^3}{8} + C_1 r + \frac{C_2}{r}, \quad (d)$$

in which, as before,  $C_1$  and  $C_2$  are constants which must be determined in such a way as to satisfy the conditions at the edges of the disc.

For a *disc with a hole at the center* (Fig. 127) and with no forces acting on the edges, the conditions at the edges are

$$(\sigma_r)_{r=a} = 0; \quad (\sigma_r)_{r=b} = 0. \quad (e)$$

The general expression for  $\sigma_r$  is obtained by substituting from eq. (d) into the first of eqs. (170), p. 207, which gives

$$\sigma_r = \frac{E}{1 - \mu^2} \left[ -\frac{3 + \mu}{8} N r^2 + (1 + \mu) C_1 - (1 - \mu) C_2 \frac{1}{r^2} \right]. \quad (f)$$

When  $r = a$  and  $r = b$ , this expression must vanish, as stated in eqs. (e). Making this substitution, we obtain the following equations for calculating  $C_1$  and  $C_2$ :

$$\begin{aligned} -\frac{3 + \mu}{8} N a^2 + (1 + \mu) C_1 - (1 - \mu) C_2 \frac{1}{a^2} &= 0, \\ -\frac{3 + \mu}{8} N b^2 + (1 + \mu) C_1 - (1 - \mu) C_2 \frac{1}{b^2} &= 0, \end{aligned} \quad (g)$$

from which

$$C_1 = \frac{3 + \mu}{8(1 + \mu)} (a^2 + b^2)N; \quad C_2 = \frac{3 + \mu}{8(1 - \mu)} a^2 b^2 N. \quad (h)$$

The general expression for  $u$  is obtained when these values are substituted into eq. (d). Then substituting the resulting expression for  $u$  into eqs. (170), p. 207, we find

$$\sigma_r = \frac{3 + \mu}{8(1 - \mu^2)} EN \left( a^2 + b^2 - r^2 - \frac{a^2 b^2}{r^2} \right), \quad (186)$$

$$\sigma_t = \frac{3 + \mu}{8(1 - \mu^2)} EN \left( a^2 + b^2 - \frac{1 + 3\mu}{3 + \mu} r^2 + \frac{a^2 b^2}{r^2} \right). \quad (187)$$

If  $N$  is now replaced by its value as given by eq. (c), and if we let

$$\frac{a}{b} = \alpha, \quad \frac{r}{b} = x, \quad b\omega = v, \quad (i)$$

then eqs. (186) and (187) become

$$\sigma_r = \frac{\gamma v^2}{g} \frac{3 + \mu}{8} \left( 1 + \alpha^2 - x^2 - \frac{\alpha^2}{x^2} \right), \quad (188)$$

$$\sigma_t = \frac{\gamma v^2}{g} \frac{3 + \mu}{8} \left( 1 + \alpha^2 - \frac{1 + 3\mu}{3 + \mu} x^2 + \frac{\alpha^2}{x^2} \right). \quad (189)$$

It is seen that the radial stress  $\sigma_r$  vanishes at the edges, where  $x = 1$  or  $x = \alpha$ , and that it is positive for other values of  $x$ . The maximum value occurs where

$$x = \sqrt{\alpha} = \sqrt{\frac{a}{b}},$$

or

$$r = \sqrt{ab}. \quad (j)$$

Using eq. (j) for  $r$ , eq. (188) gives

$$(\sigma_r)_{\max} = \frac{\gamma v^2}{g} \frac{3 + \mu}{8} (1 - \alpha)^2. \quad (190)$$

The tangential stress  $\sigma_t$  is maximum at the inner edge of the disc. Substituting  $x = \alpha$  into eq. (189), we then obtain

$$(\sigma_t)_{\max} = \frac{\gamma v^2}{g} \frac{3 + \mu}{4} \left( 1 + \frac{1 - \mu}{3 + \mu} \alpha^2 \right). \quad (191)$$

It can be seen that  $(\sigma_t)_{\max}$  is always larger than  $(\sigma_r)_{\max}$ .

In Fig. 130 the values of the terms in the parentheses in eqs. (188) and (189) are plotted as ordinates, with values of  $x$  as abscissas. The full lines represent the case  $\alpha = \frac{1}{4}$ , that

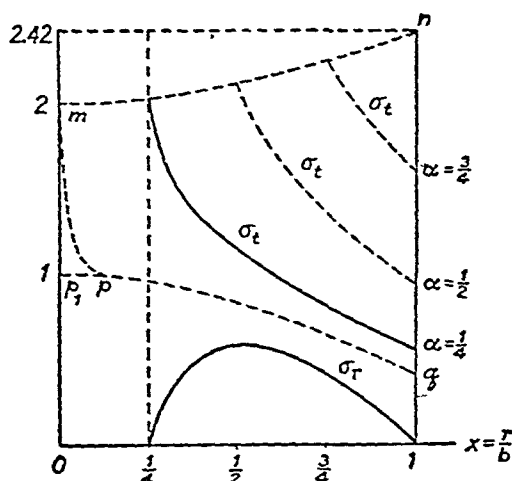


FIG. 130.

is, the inner radius is one-fourth the outer radius. The dotted lines represent the value of the term in parentheses in eq. (189) for other values of  $\alpha$ . Eq. (191) shows that the stress  $(\sigma_t)_{\max}$  at the inner edge varies with  $\alpha$  according to a parabolic law. This is shown by the curve  $mn$  in Fig. 130.

It is interesting to note that when the inner radius is very small, i.e.,  $\alpha$  approaches zero, there is a very sharp change in

the stress  $\sigma_t$  near the hole. This is shown by the curve  $mpq$ , for which

$$(\sigma_t)_{\max} = \frac{\gamma v^2}{g} \frac{3 + \mu}{4}. \quad (192)$$

For the other extreme case, when the inner radius approaches the outer radius of the disc and  $\alpha$  approaches unity, eq. (191) becomes

$$(\sigma_t)_{\max} = \frac{\gamma v^2}{g}.$$

This coincides with eq. (15), Part I, p. 32, which was obtained for a thin rotating ring. It is seen that in the case of a disc with a hole at the center, the maximum stress does not change very much with the radius of the hole; the value for a very thin ring is only about 20 per cent higher than that for a very thick ring with a small hole.

In the case of a *solid disc*, one edge condition is  $u = 0$  for  $r = 0$ ; hence the constant  $C_2$  in the general solution (eq. *d*) must be taken equal to zero. The constant  $C_1$  is found from the condition that  $\sigma_r = 0$  at the outer edge of the disc. Using the second of eqs. (g), we thus obtain

$$C_1 = \frac{3 + \mu}{8(1 + \mu)} N b^2. \quad (k)$$

The values of the constants  $C_1$  and  $C_2$  are now introduced into the general expression (eq. *d*) for the displacement  $u$ , and the resulting expression is then substituted into eqs. (170), p. 207. In this way we obtain

$$\sigma_r = \frac{\gamma v^2}{g} \frac{3 + \mu}{8} (1 - x^2), \quad (193)$$

$$\sigma_t = \frac{\gamma v^2}{g} \frac{3 + \mu}{8} \left( 1 - \frac{1 + 3\mu}{3 + \mu} x^2 \right), \quad (194)$$

where  $\kappa = r/b$ . Both the radial and tangential stresses are always positive and increase as  $\kappa$  decreases. In other words, the stresses increase as the center is approached. At the center ( $\kappa = 0$ ) the stresses are

$$(\sigma_t)_{\max} = (\sigma_r)_{\max} = \frac{\gamma v^2}{g} \frac{3 + \mu}{8}. \quad (195)$$

Comparing this with eq. (192), we see that owing to stress concentration, the stress at the edge of a small central hole is twice as great as that at the center of a solid disc. The variation of the stress  $\sigma_t$  along the radius of a solid disc is represented in Fig. 130 by the broken line  $p_1pq$ .

The equations derived above for rotating discs are sometimes used for comparatively long cylinders<sup>5</sup> such as the rotors of electric motors. In large installations the peripheral velocities may be very great. The above discussion shows that the stresses produced by the inertia forces are proportional to the square of the peripheral velocity and are therefore of primary importance in such cases. Hence, for a material of a given strength and for a given angular velocity of the rotor there is a definite maximum limit for the diameter of the rotor.

In discussing the working stresses for such rotors it is important to note that very large forgings are likely to have defects in the material at the center, which is also the point where the stress produced by the inertia forces is at a maximum. To eliminate uncertainties it is common practice to bore a central hole along the axis of the rotor. Although the maximum stress is doubled by the presence of the hole, this disadvantage is compensated for by the possibility of investigating the soundness of the material inside the forging. It is also usual to run the rotor at a certain overspeed<sup>6</sup> during the preliminary tests, so that the stresses around the hole may exceed the yield point. After stopping the rotor, the stresses will not disappear completely because of a permanent set of

<sup>5</sup> Stress distribution in thick discs is discussed in Timoshenko and Goodier, *Theory of Elasticity*, p. 352, 1951.

<sup>6</sup> In electric motors, usually 20 per cent above service speed.



the material at the hole. The inner portion of metal which has yielded is compressed by the outer portion which has not yielded, and conversely, the outer portion is in tension.<sup>7</sup> The conditions are similar to those in a thick cylinder which has been overstressed by internal pressure (see p. 212). The residual stress produced at the hole by overstressing is opposite in sign to that produced by the inertia forces; hence overstressing produces a favorable effect on the final distribution of stresses in the rotor.<sup>8</sup>

It is important to note also that the equations obtained above for the stresses (see eqs. 188 and 189) contain only ratios such as  $\alpha$  and  $x$ , in addition to  $v$  and the constants defining the properties of the material. Hence for a given material and a given peripheral velocity, the stresses are equal in similarly situated points of geometrically similar rotors. This fact simplifies the calculation of stresses in geometrically similar discs and is also used in establishing the strength of large discs from tests on models.

In the previous discussion it was assumed that the edges of the discs are free from external forces. If there are tensile or compressive forces uniformly distributed around the edges of the disc, the stresses due to them are found by using the theory of thick-walled cylinders (Art. 40). These stresses (see eqs. 171) can be represented in the following form:

$$\begin{aligned}\sigma_r &= k - \frac{n}{r^2}, \\ \sigma_t &= k + \frac{n}{r^2},\end{aligned}\tag{I}$$

in which  $k$  and  $n$  are constants depending upon the dimensions of the disc and the magnitude of the external forces acting at the edges. Stresses of eqs. (I) are to be superposed upon the stresses of eqs. (188) and (189) and the total stresses may then be represented in

<sup>7</sup> This question is discussed by C. Honegger, *Brown Bowery C. Mitt*, Nov. 1919.

<sup>8</sup> Residual stresses in rotating discs due to yielding of the metal were investigated by A. Nadai and L. H. Donnell; see *Trans. A.S.M.E., Appl. Mech. Div.*, 1928. See also H. Hencky, *Z. angew. Math. u. Mech.*, Vol. 4, p. 331, 1924, and F. Laszlo, *ibid.*, Vol. 5, p. 281, 1925.

the following form:

$$\sigma_r = A + \frac{B}{r^2} - \beta_1 \omega^2 r^2, \quad (196)$$

$$\sigma_t = A - \frac{B}{r^2} - \beta_2 \omega^2 r^2,$$

in which

$$\beta_1 = \frac{\gamma}{\varepsilon} \frac{3 + \mu}{8}; \quad \beta_2 = \frac{\gamma}{\varepsilon} \frac{1 + 3\mu}{8}, \quad (197)$$

and  $A$  and  $B$  are constants of integration which may be calculated in each particular case by using eqs. (171), (188) and (189). With the notation

$$s = \sigma_r + \beta_1 \omega^2 r^2, \quad (198)$$

$$t = \sigma_t + \beta_2 \omega^2 r^2$$

and

$$\varpi = \frac{1}{r^2}, \quad (199)$$

eqs. (196) become

$$s = A + B\varpi; \quad t = A - B\varpi. \quad (200)$$

If  $s$  and  $t$  are known for any point of the disc, their magnitudes for any other point can easily be obtained by using the following graphical method.<sup>3</sup> Let  $s_1$  and  $t_1$  denote the magnitudes of  $s$  and  $t$  for the point where  $\varpi = \varpi_1$  (see Fig. 131). Then the magnitudes  $s_2$  and  $t_2$  of  $s$  and  $t$  for any other point where  $\varpi = \varpi_2$  are obtained from the intersection of the vertical line through  $\varpi_2$  with the straight lines  $s_1 s_2$  and  $t_1 t_2$ , which have their point of intersection on the vertical axis of the coordinates ( $\varpi = 0$ ) and are equally inclined to this axis. These lines represent equations (200) graphically. They have the common ordinate  $A$  on the axis  $\varpi = 0$ , and have equal and opposite slopes ( $\pm B$ ). This graphical construction is very useful in calculating stresses in rotating discs of variable thickness, as we shall see in the next article.

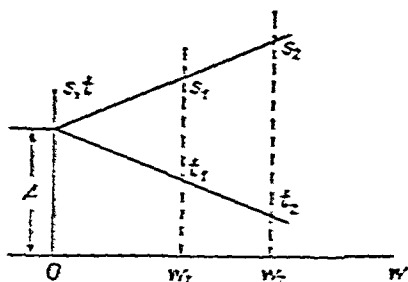


FIG. 131.

<sup>3</sup> This method was developed by R. Grammel, *Dinglers Polytech. J.*, Vol. 338, p. 217, 1923.

## Problems

- 1 Determine the stresses due to centrifugal force in a rotor with an outer radius of 26 in and with the radius of the inner hole equal to 4 in. The outer portion of the rotor is cut by slots 10 in deep for the windings (Fig 132). The rotor is of steel and revolves at 1,800 rpm. The weight of the windings in the slots is the same as that of the material removed.

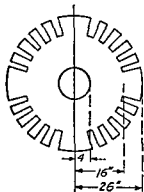


FIG 132

*Solution* Because of the radial slots, the part of the rotor between the outer radius and the 16-in radius can support no tensile hoop stresses. The centrifugal force due to this rotating ring is transmitted as a radial tensile stress

across the surface of the cylinder of 16-in radius. The magnitude of this stress is

$$p_0 = \frac{1}{2\pi \times 16} \int_{r=16}^{r=26} \frac{\gamma}{g} \omega^2 r dV = \frac{1}{2\pi \times 16} \frac{\gamma \omega^2}{g} 2\pi \int_{16}^{26} r^2 dr$$

$$= \frac{\gamma \omega^2}{g} \frac{1685}{6}$$

Substituting  $\gamma = 0.284$  lb per cu in and  $g = 32.2 \times 12$  in  $\text{sec}^{-2}$  gives

$$p_0 = 7,334 \text{ lb per sq in}$$

The maximum tangential stress at the inner edge produced by the tensile stress  $p_0$  is found from eq (177)

$$\sigma_t' = 7,334 \times \frac{2 \times 16^2}{16^2 - 4^2} = 15,700 \text{ lb per sq in}$$

The maximum tangential stress at the same edge due to the mass of the rotor between the 16 in and the 4 in radii, calculated as for a rotating disc (eq 191), is  $\sigma_t'' = 5,580$  lb per sq in. The total maximum circumferential stress at the inner edge is then  $(\sigma_t)_{\max} = \sigma_t' + \sigma_t'' = 15,700 + 5,580 \approx 21,300$  lb per sq in.

- 2 A steel ring is shrunk on a cast iron disc (Fig 128). Determine the change in the shrink fit pressure produced by inertia forces at 3,600 rpm, if  $a = 1$  in,  $b = 5$  in,  $c = 10$  in,  $E_s = 30 \times 10^6$  lb per sq in,  $E_c = 16 \times 10^6$  lb per sq in,  $\gamma_s = 0.284$  lb per cu in,  $\gamma_c = 0.260$  lb per cu in.

*Solution* Let  $p_0$  be the increase in pressure between the ring and the disc. The arbitrary constants in eq (f) for the outer ring are

determined by the equations

$$\frac{E_s}{1 - \mu^2} \left[ -\frac{3 + \mu}{8} N c^2 + (1 + \mu) C_1 - (1 - \mu) C_2 \frac{1}{c^2} \right] = 0, \quad (m)$$

$$\frac{E_s}{1 - \mu^2} \left[ -\frac{3 + \mu}{8} N b^2 + (1 + \mu) C_1 - (1 - \mu) C_2 \frac{1}{b^2} \right] = -p_0.$$

When we apply eq. (f) to the inner disc, for which the arbitrary constants are denoted by  $C_1'$  and  $C_2'$  and  $N'$  is the constant defined by eq. (c), we obtain the following equations for determining  $C_1'$  and  $C_2'$ :

$$\frac{E_{c.i.}}{1 - \mu^2} \left[ -\frac{3 + \mu}{8} N' b^2 + (1 + \mu) C_1' - (1 - \mu) C_2' \frac{1}{b^2} \right] = -p_0, \quad (n)$$

$$\frac{E_{c.i.}}{1 - \mu^2} \left[ -\frac{3 + \mu}{8} N' a^2 + (1 + \mu) C_1' - (1 - \mu) C_2' \frac{1}{a^2} \right] = 0.$$

From equations (m) and (n) the four constants  $C_1$ ,  $C_2$ ,  $C_1'$  and  $C_2'$  can be found as functions of  $p_0$ . The magnitude of  $p_0$  is now found from the condition that at the surface of contact, the radial displacements of the disc and of the ring are equal. Using eq. (d), the equation for determining  $p_0$  is therefore

$$-N \frac{b^3}{8} + C_1 b + \frac{C_2}{b} = -N' \frac{b^3}{8} + C_1' b + \frac{C_2'}{b}. \quad (o)$$

The numerical calculations are left to the reader.

3. Find the change in pressure  $p$  calculated for Prob. 4 of Art. 41 if the shaft and the hub rotate at 1,800 rpm,  $\gamma = 0.284$  lb per cu in. and  $E = 30 \times 10^6$  lb per sq in.

43. Rotating Disc of Variable Thickness.—In the case of a disc of variable thickness the problem of determining the stresses becomes more involved.<sup>10</sup> We will now discuss an approximate method of solving this problem, based on the replacement of the actual pro-

<sup>10</sup> The general equation for this case, together with a consideration of the different methods of its solution, can be found in the book by A. Stodola, *Dampf- und Gasturbinen*, 6th Ed., pp. 312–40, 1924. A rotating disc of conical profile was considered by H. M. Martin, *Engineering*, Vol. 115, p. 1, 1923; B. Hodgkinson, *Engineering*, Vol. 116, p. 274, 1923; and A. Fischer, *Z. österr. Ing. u. Architekt-Ver.*, Vol. 74, p. 46, 1922. See also the book by I. Malkin, *Festigkeitsberechnung rotierender Scheiben*, Berlin, 1935, and the book by C. B. Biezeno and R. Grammel, *Technische Dynamik*, Vol. 2, p. 5, 1953.

file by a system of discs of uniform thickness (Fig 133)<sup>11</sup> The stresses in the separate discs are calculated by the equations given in Art 42 We must then consider conditions at the boundaries between these discs, that is, at sections such as 2, 3, 4 (Fig 133), where abrupt

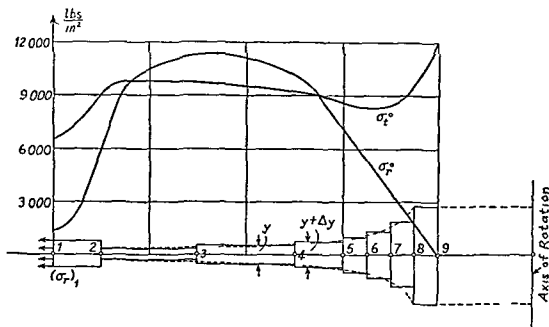


FIG 133

changes in the thickness occur. If  $y$  and  $y + \Delta y$  denote the thickness of the discs on opposite sides of the section under consideration, the corresponding change  $\Delta\sigma_r$  in the magnitude of the radial stress  $\sigma_r$  is found from the equation

$$\sigma_r y = (\sigma_r + \Delta\sigma_r)(y + \Delta y),$$

in which it is assumed, as before, that the stresses are uniformly distributed over the thickness of the disc. Solving this equation we obtain

$$\Delta\sigma_r = -\frac{\Delta y}{y + \Delta y} \sigma_r \quad (a)$$

<sup>11</sup> This method was developed by M. Donath, *Die Berechnung rotierender Scheiben und Ringe*, Berlin, 1912. It is described in English by H. Hearle in *Engineering*, Vol 106, p 131, 1918. Further development of the method was given by R. Grammel, *loc cit*, p 221, and the numerical example of Fig 133 was taken from this paper. See also the papers by M. G. Driessen, *Trans. A.S.M.E., Appl. Mech. Div.*, 1928; R. Grammel, *Ing. Arch.*, Vol 7, p 136, 1936; R. G. Olsson, *ibid*, Vol 8, p 270 and p 373, 1937; A. Held, *ibid*, Vol 10, p 339, 1939. An approximate method of handling the problem was given by G. F. Lake, *J. Appl. Mech.*, Vol 12, p A-65, 1945.

The change  $\Delta\sigma_t$  in the tangential stress at the same section is found from the condition that the unit circumferential elongation is the same on both sides of the section. Hence

$$\sigma_t - \mu\sigma_r = (\sigma_t + \Delta\sigma_t) - \mu(\sigma_r + \Delta\sigma_r),$$

from which

$$\Delta\sigma_t = \mu\Delta\sigma_r.$$

Then from eqs. (198)

$$\Delta s = \Delta\sigma_r = -\frac{\Delta y}{y + \Delta y} \sigma_r,$$

$$\Delta t = \Delta\sigma_t = \mu\Delta s. \quad (201)$$

Eqs. (197), (198), (199) and (201), together with the graphical solution given in Fig. 131, are sufficient for the calculation of a disc of variable thickness.

Consider as an example the disc represented in Fig. 133, rotating at a speed of 3,000 rpm. The dimensions of the disc are given in Table 17. In addition, assume that the centrifugal forces applied at the outer edge, such as the force due to the blades of a turbine, produce a radial stress at the outer edge equal to

$$(\sigma_r)_1 = 1,420 \text{ lb per sq in.}$$

The properties of the material are  $\mu = 0.3$  and  $\gamma = 0.283 \text{ lb per cu in.}$  Then from eqs. (197) we obtain

$$\beta_1\omega^2 = 30.0 \frac{\text{lb}}{\text{in.}^4}; \quad \beta\omega^2 = 17.3 \frac{\text{lb}}{\text{in.}^4}.$$

The first eight columns of Table 17 are computed from the above data and from Fig. 133.

We begin the stress calculation from the outer edge of the disc where  $(\sigma_r)_1$  is given. The magnitude of the tangential stress  $(\sigma_t)_1$  at the outer edge is usually unknown, and an arbitrary magnitude must be assumed at the beginning. The simplest assumption is to take  $(\sigma_t)_1$  so as to make  $s$  and  $t$  (see eq. 198) equal, in which case

$$(\sigma_t)_1 = (\sigma_r)_1 + \beta_1\omega^2 r_1^2 - \beta\omega^2 r_1^2,$$

or, by using the figures in columns 5 and 6 of the table,

$$(\sigma_t)_1 = 1,420 + 11,620 - 6,680 = 6,360 \text{ lb per sq in.}$$

Now, from eqs. (198),

$$s_1 = (\sigma_r)_1 + \beta_1\omega^2 r_1^2 = 1,420 + 11,620 = 13,040 \text{ lb per sq in.,}$$

$$t_1 = (\sigma_t)_1 + \beta\omega^2 r_1^2 = 6,360 + 6,680 = 13,040 \text{ lb per sq in.}$$

TABLE 17 STRESS CALCULATION IN A ROTATING DISC

1	2	3	4	5	6	7	8	9	10	11	12	13	14
Cross Section	$r$ in	$r^2$ in <sup>2</sup>	$10^3 w$ in <sup>-2</sup>	$\beta_1 \omega^2 r^2$ $\frac{\text{lb}}{\text{in}^2}$	$\beta_2 \omega^2 r^2$ $\frac{\text{lb}}{\text{in}^2}$	$y$ in	$-\frac{\Delta y}{y + \Delta y}$	$\sigma_r$ $\frac{\text{lb}}{\text{in}^2}$	$\Delta r$ $\frac{\text{lb}}{\text{in}^2}$	$\Delta t$ $\frac{\text{lb}}{\text{in}^2}$	$\sigma_t$ $\frac{\text{lb}}{\text{in}^2}$	$\sigma_r^0$ $\frac{\text{lb}}{\text{in}^2}$	$\sigma_t^0$ $\frac{\text{lb}}{\text{in}^2}$
1	19 7	388	2 58	11,620	6,680			1,420 0			6,360 710	1,420	6,800
2	17 7	314	3 18	9,410	5,420	985	+1 50	3,630 - 80	5,450 - 130	1,640 - 40	7,620 795	6,250	8,900
3	13 8	190	5 26	5,700	3,290	394	- 333	14,000 - 510	-4,670 + 170	-1,390 + 60	10,020 1,070	11,400	10,000
4	9 85	97 0	10 31	2,910	1,680	591	- 400	13,500 - 1,020	-5,400 + 410	-1,620 + 130	8,900 1,820	10,300	9,300
5	7 87	62 0	16 1	1,860	1,070	985	- 286	9,680 - 1,340	-2,740 + 380	825 + 110	7,300 2,640	7,600	8,600
6	6 89	47 4	21 1	1,420	820	1 38	- 263	7,550 - 1,550	-1,990 + 410	- 597 + 130	6,530 3,300	5,700	8,400
7	5 91	34 9	28 6	1,050	603	1 87	- 321	5,970 - 1,990	-1,920 + 640	- 570 + 200	6,110 4,270	3,980	8,600
8	4 92	24 2	41 3	726	418	2 76	- 300	4,280 - 2,590	-1,250 + 780	- 370 + 230	5,960 5,720	2,260	9,500
9	3 94	15 5	64 5	465	268	3 94		2,530 - 4,000			6,350 8,100	0	11,500

Since  $s_1 = t_1$ , the  $s$  and  $t$  straight lines coincide in the construction explained in Fig. 131. In Fig. 134 in which  $s$  and  $t$  are taken as ordinates and  $w = 1/r^2$  as abscissa, these lines are represented by the line  $a-a$  parallel to the  $w$  axis. The length of this line, corresponding to the radial distance 1-2 of the disc (Fig. 134), is determined from the figures in column 4 of the table. From this we obtain for section 2 (Fig. 133)

$$s_2 = t_2 = 13,040 \text{ lb per sq in.};$$

then by using eqs. (198),

$$(\sigma_r)_2 = s_2 - \beta_1 \omega^2 r_2^2 = 13,040 - 9,410 = 3,630 \text{ lb per sq in.},$$

$$(\sigma_t)_2 = t_2 - \beta_2 \omega^2 r_2^2 = 13,040 - 5,420 = 7,620 \text{ lb per sq in.}$$

At section 2 an abrupt change in the thickness of the disc takes place. To take this into account, we use eqs. (201) together with the figures in column 8 in the table. Then

$$(\Delta s)_2 = (\Delta \sigma_r)_2 = \left( -\frac{\Delta y}{y + \Delta y} \sigma_r \right) = 1.50 \times 3,630$$

$$= 5,450 \text{ lb per sq in.},$$

$$(\Delta t)_2 = (\Delta \sigma_t)_2 = \mu(\Delta s)_2 = 0.3 \times 5,450 = 1,640 \text{ lb per sq in.}$$

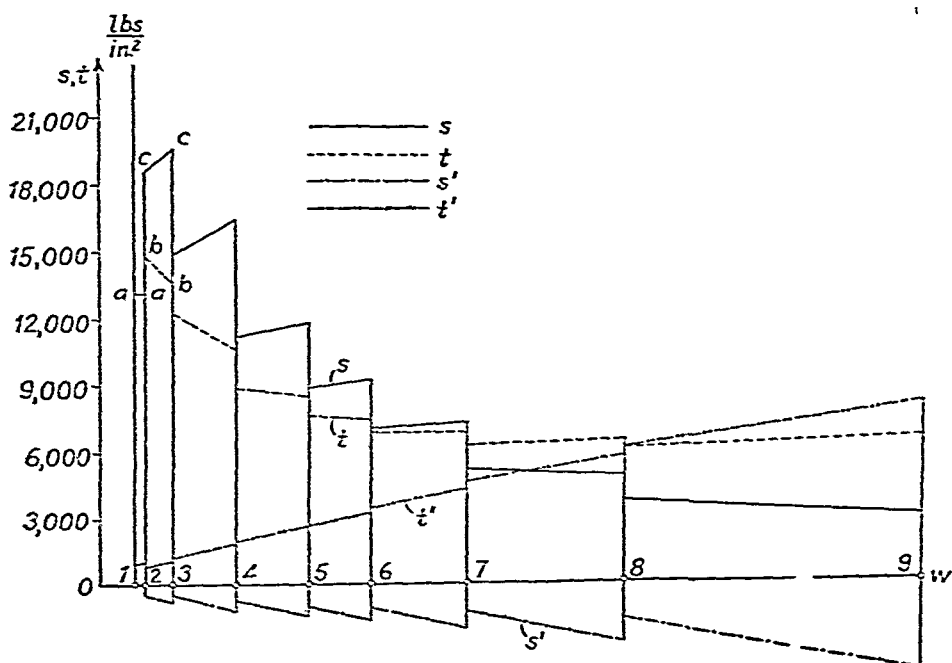


FIG. 134.



These quantities are added to the ordinate of point  $a$  in Fig. 134 to obtain points  $b$  and  $c$ , the lines  $bb$  and  $cc$  are then constructed as explained in Fig. 131. In this manner  $s_3$  and  $t_3$  are found for section 3. By repeating the above process all the necessary data for section 3 are obtained, and so on. By this method we may compute all values in the upper lines in columns 9 to 12 of the above table.

Because of the fact that the stress  $(\sigma_t)_1$  at the periphery of the disc was taken arbitrarily, the conditions at the inner edge will usually not be satisfied, and the stress  $(\sigma_r)_9$  obtained by the above method will not be the stress which actually exists there. In order to satisfy the condition at the inner edge, an additional calculation is required. We assume  $(\sigma_r)_1 = 0$ ,  $\omega = 0$ , and then take an arbitrary value for  $(\sigma_t)_1$ . In the calculations for this problem  $(\sigma_t)_1$  was taken equal to 710 lb per sq in. We then obtain the corresponding stress distribution in the same manner as before. For this case, from eqs. (198) we obtain  $s = \sigma_r$  and  $t = \sigma_t$ . The results of the calculations are given in columns 9 to 12 in the lower lines, and the corresponding constructions are given in Fig. 134 by the lines  $t'$  and  $s'$ . The solution which satisfies the actual condition at the inner edge of the disc is obtained by combining the above two stress distributions as follows. Let  $(\sigma_r)_9$  and  $(\sigma_r)_9'$  be the radial stresses at the inner edge of the disc, obtained by the first and the second calculations respectively, and let  $(\sigma_r)_9^0$  denote the actual stress at the inner edge. Then the solution for the actual condition is obtained by superposing on the first stress distribution the stresses of the second distribution multiplied by

$$n = \frac{(\sigma_r)_9^0 - (\sigma_r)_9}{(\sigma_r)_9'}$$

The average stresses at the sections where the thickness changes abruptly may be calculated as follows

$$(\sigma_r)^0 = \left( \sigma_r + \frac{\Delta s}{2} \right) + n \left( \sigma_r' + \frac{\Delta s'}{2} \right),$$

$$(\sigma_t)^0 = \left( \sigma_t + \frac{\Delta t}{2} \right) + n \left( \sigma_t' + \frac{\Delta t'}{2} \right)$$

The results of these calculations for the case when the radial stress at the inner edge is zero are given in the last two columns of table 17 and are represented by the two curves in Fig. 133.

**44 Thermal Stresses in a Long, Hollow Cylinder.**—When the wall of a cylinder is nonuniformly heated, its elements do not expand uniformly and mutual interference sets up thermal stresses. In the

following discussion the distribution of the temperature is taken to be symmetrical with respect to the axis of the cylinder and constant along this axis. The deformation of the cylinder is then symmetrical about the axis and we may use the method developed in Art. 40. A ring is cut from the cylinder by two cross sections perpendicular to the axis and unit distance apart. During thermal deformation such cross sections can be assumed to remain plane if taken sufficiently distant from the ends of the cylinder,<sup>12</sup> hence the unit elongations in the direction of the axis are constant. Let the  $z$  axis be the axis of the cylinder,  $w$  the displacement in the direction of the  $z$  axis, and the remaining notation the same as in Art. 40 and Fig. 127. Then the unit elongations in the three perpendicular directions are

$$\left. \begin{aligned} \epsilon_z &= \frac{dw}{dz} = \text{const.}, \\ \epsilon_r &= \frac{du}{dr}, \\ \epsilon_t &= \frac{u}{r}. \end{aligned} \right\} \quad (a)$$

These elongations can be represented as functions of the stresses  $\sigma_z$ ,  $\sigma_r$ ,  $\sigma_t$ , and the thermal expansion. Let  $\alpha$  denote the coefficient of linear expansion and  $t$  the increase in temperature above the uniform initial temperature. The temperature increase  $t$  varies with the radial distance  $r$  only. From eqs. (43), Part I, p. 66, the elongations are

$$\left. \begin{aligned} \epsilon_z &= \frac{\sigma_z}{E} - \frac{\mu}{E} (\sigma_r + \sigma_t) + \alpha t, \\ \epsilon_r &= \frac{\sigma_r}{E} - \frac{\mu}{E} (\sigma_z + \sigma_t) + \alpha t \\ \epsilon_t &= \frac{\sigma_t}{E} - \frac{\mu}{E} (\sigma_z + \sigma_r) + \alpha t. \end{aligned} \right\} \quad (b)$$

Using the symbol  $\Delta$  for the unit increase in volume, we obtain

$$\Delta = \epsilon_z + \epsilon_r + \epsilon_t = \frac{1 - 2\mu}{E} (\sigma_z + \sigma_r + \sigma_t) + 3\alpha t. \quad (c)$$

<sup>12</sup> At the ends the stresses in the direction of the axis of the cylinder are zero and the stress distribution is more complicated.

From eqs (b) and (c) we find

$$\left. \begin{aligned} \sigma_z &= \frac{E}{1+\mu} \left( \epsilon_z + \frac{\mu}{1-2\mu} \Delta \right) - \frac{\alpha t E}{1-2\mu}, \\ \sigma_r &= \frac{E}{1+\mu} \left( \epsilon_r + \frac{\mu}{1-2\mu} \Delta \right) - \frac{\alpha t E}{1-2\mu}, \\ \sigma_t &= \frac{E}{1+\mu} \left( \epsilon_t + \frac{\mu}{1-2\mu} \Delta \right) - \frac{\alpha t E}{1-2\mu} \end{aligned} \right\} \quad (d)$$

The equation of equilibrium of an element  $mnm_1n_1$  (Fig 127) is (see eq b, p 206)

$$\frac{d\sigma_r}{dr} + \frac{\sigma_r - \sigma_t}{r} = 0 \quad (e)$$

Substituting eqs (d) and (a) into eq (e), we obtain

$$\frac{d^2u}{dr^2} + \frac{1}{r} \frac{du}{dr} - \frac{u}{r^2} = \frac{1+\mu}{1-\mu} \alpha \frac{dt}{dr} \quad (202)$$

This equation determines the displacement  $u$  for any particular distribution of temperature. It may be written in the form

$$\frac{d}{dr} \left[ \frac{1}{r} \frac{d}{dr} (ru) \right] = \frac{1+\mu}{1-\mu} \alpha \frac{dt}{dr}.$$

Integration with respect to  $r$  gives

$$\frac{d}{dr} (ru) = \frac{1+\mu}{1-\mu} \alpha t r + 2C_1 r.$$

A second integration gives the solution

$$u = \frac{1}{r} \frac{1+\mu}{1-\mu} \int_a^r \alpha t r dr + C_1 r + C_2 \frac{1}{r}, \quad (f)$$

in which  $C_1$  and  $C_2$  are constants of integration which must be determined in such a manner as to satisfy the conditions at the inner and outer surfaces of the cylinder. If these surfaces are free from external forces,  $C_1$  and  $C_2$  are determined from the conditions

$$(\sigma_r)_{r=a} = 0, \quad (\sigma_r)_{r=b} = 0 \quad (g)$$

A general expression for  $\sigma_r$  is obtained by substituting  $\epsilon_r = du/dr$  and  $\epsilon_t = u/r$  into the second of eqs (d) and then taking  $u$  from eq

( $f$ ), which gives

$$\sigma_r = \frac{E}{1 + \mu} \left( -\frac{1 + \mu}{1 - \mu} \frac{1}{r^2} \int_a^r \alpha t r dr + \frac{C_1}{1 - 2\mu} - \frac{C_2}{r^2} + \frac{\mu}{1 - 2\mu} \epsilon_z \right). \quad (h)$$

From eqs. (g) we then obtain

$$C_2 = \frac{1 + \mu}{1 - \mu} \frac{a^2}{b^2 - a^2} \int_a^b \alpha t r dr, \quad (i)$$

$$C_1 = \frac{(1 + \mu)(1 - 2\mu)}{1 - \mu} \frac{1}{b^2 - a^2} \int_a^b \alpha t r dr - \mu \epsilon_z.$$

With these values substituted in eq. (h) the general expression for  $\sigma_r$  becomes

$$\sigma_r = \frac{E}{1 - \mu} \left[ -\frac{1}{r^2} \int_a^r \alpha t r dr + \frac{r^2 - a^2}{r^2(b^2 - a^2)} \int_a^b \alpha t r dr \right]. \quad (203)$$

The general expression for  $\sigma_t$  is obtained from the equation of equilibrium ( $\epsilon$ ) which gives

$$\sigma_t = \sigma_r + r \frac{d\sigma_r}{dr}$$

$$= \frac{E}{1 - \mu} \left[ \frac{1}{r^2} \int_a^r \alpha t r dr + \frac{r^2 + a^2}{r^2(b^2 - a^2)} \int_a^b \alpha t r dr - \alpha t \right]. \quad (204)$$

If the distribution of the temperature over the thickness of the wall is known, we can evaluate the integrals in eqs. (203) and (204) and obtain  $\sigma_r$  and  $\sigma_t$  for each particular case.

When the walls of the cylinder are at temperature  $t_i$  on the inner surface and temperature zero on the outer surface,<sup>13</sup> the equilibrium temperature distribution may be represented by the function

$$t = \frac{t_i}{b} \log_e \frac{b}{r} \quad (205)$$

<sup>13</sup> Any other temperature condition at the surfaces of the cylinder may be obtained by superposing on this condition a uniform heating or cooling, which does not produce any stresses.

With this expression for  $t$  eqs. (203) and (204) become

$$\sigma_r = \frac{E\alpha t_1}{2(1-\mu) \log_e \frac{b}{a}} \left[ -\log_e \frac{b}{r} - \frac{a^2}{b^2 - a^2} \left( 1 - \frac{b^2}{r^2} \right) \log_e \frac{b}{a} \right], \quad (206)$$

$$\sigma_t = \frac{E\alpha t_1}{2(1-\mu) \log_e \frac{b}{a}} \left[ 1 - \log_e \frac{b}{r} - \frac{a^2}{b^2 - a^2} \left( 1 + \frac{b^2}{r^2} \right) \log_e \frac{b}{a} \right]. \quad (207)$$

The maximum value of  $\sigma_t$  occurs at the inner or outer surface of the cylinder. Substituting in the above equation  $r = a$  and  $r = b$ , we obtain

$$(\sigma_t)_{r=a} = \frac{E\alpha t_1}{2(1-\mu) \log_e \frac{b}{a}} \left( 1 - \frac{2b^2}{b^2 - a^2} \log_e \frac{b}{a} \right), \quad (208)$$

$$(\sigma_t)_{r=b} = \frac{E\alpha t_1}{2(1-\mu) \log_e \frac{b}{a}} \left( 1 - \frac{2a^2}{b^2 - a^2} \log_e \frac{b}{a} \right). \quad (209)$$

The distribution of thermal stresses over the thickness of the wall for the particular case when  $a/b = 0.3$  and  $t_1$  is negative is shown in Fig. 135.

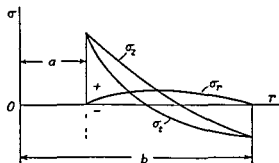


FIG 135

If the thickness of the wall is small in comparison with the outer radius of the cylinder we can simplify eqs (208) and (209) by putting

$$\frac{b}{a} = 1 + m, \quad \log_e \frac{b}{a} = m - \frac{m^2}{2} + \frac{m^3}{3} - \dots$$

and considering  $m$  as a small quantity. Then

$$(\sigma_t)_{r=a} = -\frac{E\alpha t_i}{2(1-\mu)} \left(1 + \frac{m}{3}\right) \quad (j)$$

$$(\sigma_t)_{r=b} = \frac{E\alpha t_i}{2(1-\mu)} \left(1 - \frac{m}{3}\right). \quad (k)$$

In the case of a very thin wall the second term in the parentheses of these equations is negligible, and the equations coincide with the equations derived for a nonuniformly heated plate (see eq. 87, p. 91).

In the above discussion only  $\sigma_r$  and  $\sigma_t$  were considered, and it was shown that these quantities do not depend upon the elongation  $\epsilon_z$  in the direction of the cylinder. The stress  $\sigma_z$  may be calculated from the first of eqs. (d). Substituting  $\epsilon_r = du/dr$ ,  $\epsilon_t = u/r$ , and using eq. (f) for  $u$  and eqs. (i) for the arbitrary constants, we are able to find the general expression for  $\sigma_z$ . This expression contains the constant elongation  $\epsilon_z$  in the direction of the axis of the cylinder. If we assume that the cylinder can expand freely, we calculate the magnitude of  $\epsilon_z$  from the condition that the sum of the normal forces over the cross section of the cylinder perpendicular to the  $z$  axis is equal to zero. As a result of this calculation the following final expression for  $\sigma_z$  is obtained:

$$\sigma_z = \frac{E\alpha t_i}{2(1-\mu) \log_e \frac{b}{a}} \left(1 - 2 \log_e \frac{b}{r} - \frac{2a^2}{b^2 - a^2} \log_e \frac{b}{a}\right). \quad (210)$$

It may be seen that at the inner and outer surfaces of the cylinder the stress  $\sigma_z$  is equal to  $\sigma_t$ .<sup>14</sup>

In the case of a disc without a hole at the center and having a uniform thickness which is assumed small in comparison with the radius  $b$  of the disc, the radial and the tangential stresses are given by the following expressions:

$$\sigma_r = \alpha E \left( \frac{1}{b^2} \int_0^b t r dr - \frac{1}{r^2} \int_0^r t r dr \right), \quad (211)$$

$$\sigma_t = \alpha E \left( -t + \frac{1}{b^2} \int_0^b t r dr + \frac{1}{r^2} \int_0^r t r dr \right). \quad (212)$$

<sup>14</sup> A more detailed discussion of thermal stresses in cylinders was given by C. H. Lees, *Proc. Roy. Soc. (London)*, A, Vol. 101, 1922. Charts for the rapid calculation of stresses from eqs. (206), (207) and (210) were given by L. H. Barker, *Engineering*, Vol. 124, p. 443, 1927. The numerical example which follows was taken from this paper.

In each particular case when the temperature  $t$  is known as a certain function of  $r$ , the integrals in these expressions can be readily evaluated and the thermal stresses obtained

Thermal stresses are of great practical importance, especially in large cylinders such as steam turbine rotors, heavy shafts, or large turbine discs. In all these cases, heating or cooling must be gradual in order to reduce the temperature gradient in the radial direction.<sup>15</sup> Thermal stresses are also important in Diesel engines.<sup>16</sup> In the case of materials which are weak in tension, such as stone, brick and concrete, cracks are likely to start on the outer surface of the cylinder when  $t_i$  is positive

### Problems

1 Determine the thermal stresses in a cylinder with the properties  $2a = \frac{3}{8}$  in,  $2b = 1\frac{1}{4}$  in,  $E\alpha/(1 - \mu) = 615$ , if the inner temperature is  $t_i = -1^\circ\text{C}$  and the outer temperature is zero

*Solution* From eqs (208) and (209)

$$(\sigma_t)_{r=a} = (\sigma_z)_{r=a} = 420 \text{ lb per sq in,}$$

$$(\sigma_t)_{r=b} = (\sigma_z)_{r=b} = -194 \text{ lb per sq in}$$

The maximum value of the stress  $\sigma_r$ , from eq (206), occurs at  $r = 0.3$  in and is equal to 87 lb per sq in. The distribution of the stresses over the thickness of the wall is shown in Fig. 135

<sup>15</sup> A discussion of thermal stresses in cylinders in which the temperature varies along the axis is given by A. Stodola, *loc cit*, p. 223, Appendix. See also G. Eichelberg, *Forschungsarb*, No. 220, 1923, and No. 263. For a discussion of thermal stresses in discs, see H. Quednau, *Z. Ver. deut. Ing.*, Vol. 72, p. 522, 1928. The same problem is discussed in Timoshenko and Goodier, *Theory of Elasticity*, p. 408, 1951.

<sup>16</sup> See R. Zulzer, 'Temperature Variation and Heat Stresses in Diesel Engines,' *Engineering*, Vol. 121, p. 447, 1926. A. Nagel, 'Transfer of Heat in Reciprocating Engines,' *ibid*, Vol. 127, p. 282, 1929. W. Nusselt, *Z. Ver. deut. Ing.*, Vol. 70, p. 468, 1926. J. N. Goodier, *J. Appl. Mech.*, Vol. 4, p. A-33, 1937.

## CHAPTER VII

### TORSION

**45. Shafts of Noncircular Cross Section.**—The problem of the torsion of circular shafts was considered in Part I (p. 281). Formulas for the maximum stress and for the angle of twist for rectangular shafts also were given. There are several other shapes of cross section of a twisted shaft for which the problems of stress distribution and of the angle of twist are solved. In the following pages some final results, which may be of practical interest, are given.

*Elliptic Cross Section.*<sup>1</sup>—The maximum shearing stress takes place at the ends of the minor axis  $mn$ , Fig. 136, and is

$$\tau_{\max} = \frac{16M_t}{\pi b^2 h}. \quad (213)$$

The angle of twist per unit length is

$$\theta = \frac{4\pi^2 M_t I_p}{A^4 G}, \quad (214)$$

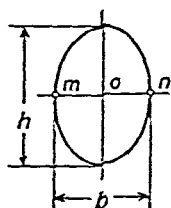


FIG. 136.

where  $I_p = (\pi/64)(bh^3 + b^3h)$  is the polar moment of inertia of the cross section (see Part I, Appendix A, p. 420), and  $A = \pi bh/4$  is the area of the cross section.

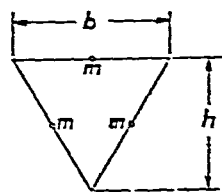


FIG. 137.

*Equilateral Triangle.*—The maximum shearing stress occurs at the middle of the sides (points  $m$  in Fig. 137) and can be calculated from the equation

$$\tau_{\max} = \frac{20M_t}{b^3}. \quad (215)$$

<sup>1</sup> The solutions of the torsion problem for an elliptic cross section and also for an equilateral triangle are due to St.-Venant, *Mém. des savans étrangers*, Vol. 14, 1855. The derivation of the formulas given here can be found in Timoshenko and Goodier, *Theory of Elasticity*, p. 258, 1951.



The angle of twist per unit length is

$$\theta = \frac{M_t}{0.6GI_p} = \frac{46.2M_t}{b^4G}. \quad (216)$$

*Regular Hexagon.*<sup>2</sup>—For this case

$$\tau_{\max} = \frac{M_t}{0.217Ad}, \quad (217)$$

$$\theta = \frac{M_t}{0.133Ad^2G}, \quad (218)$$

where  $d$  is the diameter of the inscribed circle and  $A$  is the cross sectional area.

*Regular Octagon.*—For this case

$$\tau_{\max} = \frac{M_t}{0.223Ad}, \quad (219)$$

$$\theta = \frac{M_t}{0.130Ad^2G}, \quad (220)$$

where  $A$  and  $d$  have the same meaning as in the preceding case.

*Trapezoid.*—In the case of an isosceles trapezoid approximate values for the maximum stress and the angle of twist are obtained by replacing the trapezoid by an *equivalent* rectangle, which is obtained as indicated by the dotted lines in Fig. 138. From the centroid  $C$  of the trapezoid are drawn perpendiculars,  $BC$  and  $CD$ , to the lateral sides, and then verticals are drawn through  $B$  and  $D$ . Eqs. (158) and (159) given in Part I, p. 289, if applied to the rectangular cross section thus obtained, give approximate values of  $\tau_{\max}$  and  $\theta$  for the trapezoid in Fig. 138.

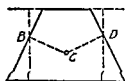


FIG 138

For any solid (nontubular) shaft an approximate value for the angle of twist is obtained by replacing the cross section by an *equivalent* elliptical one of the same area  $A$  and the same polar moment of inertia  $I_p$ . Then an approximate value for  $\theta$  is given by formula (214).

<sup>2</sup> For the solutions for a regular hexagon, octagon and trapezoid, see C. Weber, *Die Lehre von der Verdrehungsfestigkeit*, Berlin, 1921.

46. **Membrane Analogy.**<sup>3</sup>—The membrane analogy establishes certain relations between the deflection surface of a uniformly loaded membrane and the distribution of stresses in a twisted bar. Imagine a homogeneous membrane with the same outline as that of the cross section of the torsional member and subjected to uniform tension at the edges and to uniform lateral pressure. It can be shown that the differential equation of the deflection surface<sup>4</sup> of this membrane has the same form as the equation which determines the stress distribution over the cross section of the twisted bar. If  $S$  is the tensile force per unit length of the boundary line of the membrane,  $p$  the lateral pressure per unit area and  $\theta$  the angle of twist per unit length of the bar, then the two differential equations are identical if

$$\frac{p}{S} = 2G\theta. \quad (a)$$

If this condition is fulfilled, the following relationships hold between the surface of the membrane and the distribution of shearing stresses in twist: (1) The *tangent to a contour line* at any point of the deflected membrane gives the direction of the shearing stress at the corresponding point in the cross section of the twisted bar. (2) The *maximum slope* of the membrane at any point is equal to the magnitude of the shearing stress at the corresponding point in the twisted bar. (3) *Twice the volume* included between the surface of the deflected membrane and the plane of its outline is equal to the torque of the twisted bar.

All these statements can be readily proved in the case of a circular shaft. Let Fig. 139 represent the corresponding circular membrane uniformly stretched by the forces  $S$  and loaded by uniform pressure  $p$  acting upwards. Considering

<sup>3</sup> The analogy was developed by L. Prandtl; see *Phys. Z.*, Vol. 4, p. 758, 1903; *Jahresber. deut. math. Ver.*, Vol. 13, p. 31, 1904. For further development see the papers by A. A. Griffith and G. I. Taylor, *Proc. Inst. Mech. Engrg.*, p. 755, 1917, and *Advisory Comm. Aeronaut. (England)*, *Tech. Repts.*, Vol. 3, pp. 920, 938 and 950, 1917–18. See also Timoshenko and Goodier, *Theory of Elasticity*, p. 289, 1951.

<sup>4</sup> It is assumed that the deflections are small.

a concentric portion  $mn$  of radius  $r$  of the membrane, Fig 139, we observe that the total pressure on that portion is  $\pi r^2 p$ . This pressure is balanced by the tensile forces  $S$  which are uniformly distributed along the circle of radius  $r$  and have a direction tangent to the deflected membrane. Denoting by  $w$  the deflections of the membrane, we obtain

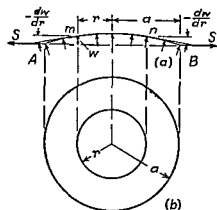


FIG 139

$$\pi r^2 p = -2\pi r S \frac{dw}{dr}$$

and

$$-\frac{dw}{dr} = \frac{pr}{2S} \quad (b)$$

Substituting in this equation the value of  $p/S$  given by formula (a), we obtain

$$-\frac{dw}{dr} = G\theta r \quad (c)$$

On the right-hand side of this equation we have the expression for the torsional stress in a twisted circular shaft (see eq (b), Part I, p 282). Hence the slope of the deflected membrane gives the magnitude of the torsional stress. The maximum slope of the membrane at each point is in the direction of a meridian, hence the torsional stress in the shaft at each point has a direction perpendicular to the radius. This conclusion again agrees with the result of the elementary theory of torsion.

To determine the torque which produces the stresses given by eq (c), let us calculate the volume included between the deflected membrane, Fig 139a, and the plane of the boundary  $AB$ . The integration of eq (c) gives the deflection surface of the membrane,

$$w = \frac{G\theta}{2} (a^2 - r^2),$$

and the required volume is

$$V = \int_0^a 2\pi r w dr = G\theta \frac{\pi a^4}{4} = \frac{1}{2} G\theta I_p.$$

Comparing this expression with the usual formula for torque (see eq. 150, Part I, p. 284), we conclude in the membrane analogy that twice the volume gives the magnitude of the torque. Hence the three statements above regarding the membrane analogy can be readily proved in the case of a circular shaft.

In other cases the shape of the surface of the deflected membrane is easily visualized for a given cross section of the

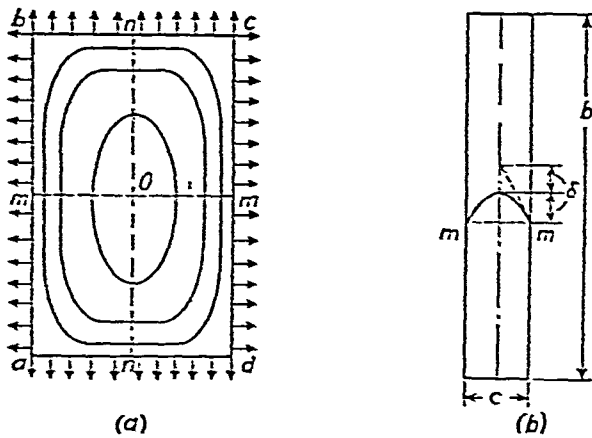


FIG. 140.

shaft; consequently qualitative conclusions are readily drawn concerning the stress distribution in torsion. For example, with a rectangular cross section the surface of the deflected membrane may be represented by contour lines as shown in Fig. 140a. The stress is inversely proportional to the distance between these lines; hence it is larger where the lines are closer to each other. The maximum stress occurs at the points  $m-m$ , where the slope of the membrane is largest. At the corners  $a$ ,  $b$ ,  $c$ ,  $d$ , where the surface of the membrane coincides with the plane of the contour  $abcd$ , the slope of this surface is zero; hence the shearing stress at these points is zero.

Consider next the case of a narrow rectangular cross section (Fig. 140b). The deflection surface of the uniformly loaded membrane at some distance from the short sides of the rectangle can be considered cylindrical. With this assumption, each strip  $mm$  of the surface behaves like a uniformly loaded

string and its maximum deflection is given by the equation

$$\delta = \frac{pc^2}{8S},$$

or, using eq (a),

$$\delta = \frac{c^2}{4} G\theta$$

The maximum stress is equal to the slope at points *m-m*. This slope is  $4\delta/c$  for a parabolic curve, hence

$$\tau_{\max} = \frac{4\delta}{c} = cG\theta \quad (d)$$

The corresponding torque is twice the volume enclosed by the membrane. Neglecting the effect of the short sides of the rectangle on the deflection of the membrane and calculating the volume as for a parabolic cylinder of length *b*, we find

$$M_t = 2 \cdot \frac{2}{3} \delta bc = \frac{1}{3} bc^3 G\theta \quad (e)$$

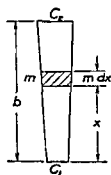


FIG 141

from which

$$\theta = \frac{M_t}{\frac{1}{3} bc^3 G} \quad (221)$$

Substituting in eq (d), we obtain

$$\tau_{\max} = \frac{M_t}{\frac{1}{3} bc^2} \quad (222)$$

These formulas coincide with formulas (158) and (159) given in Part I (pp 289 and 290) if the rectangle is assumed to be very narrow

If instead of a narrow rectangle we have a narrow trapezoid, as shown in Fig 141, an approximate solution is obtained by assuming that the surface of the deflected membrane at a sufficient distance from the narrow sides is conical. The double volume corresponding to an element *mm* of the cross section is obtained as in eq (e) above and is equal to

$$\frac{1}{3} G\theta c^3 dx, \quad (f)$$

where  $c$  is the variable width of the cross section given by the equation

$$c = c_1 + \frac{c_2 - c_1}{b} x. \quad (g)$$

Substituting from eq. (g) into eq. (f) and integrating the result, we obtain the torque as follows:

$$M_t = \int_0^b \frac{1}{3} G \theta c^3 dx = \frac{b G \theta}{12} (c_1 + c_2)(c_1^2 + c_2^2).$$

The angle of twist is then

$$\theta = \frac{M_t}{\frac{1}{12} b (c_1 + c_2)(c_1^2 + c_2^2) G}. \quad (223)$$

When  $c_1 = c_2 = c$ , this formula coincides with formula (221) obtained for the narrow rectangle.

In more complicated cases in which the form of the deflection surface of the membrane cannot easily be obtained analytically, this surface can be investigated experimentally by using a soap film for the uniformly stretched membrane and measuring the slope of its surface by optical methods. For this purpose the apparatus shown in Fig. 142 has been used.<sup>5</sup> An aluminum plate with two holes—one circular and the other of the required shape—is clamped between the two halves of the cast-iron box  $A$ . The lower part of the box, having the form of a shallow tray, is supported on leveling screws. By pumping air into this portion of the box, a soap film covering the holes is caused to deflect upward.

The contour lines on the surface of the soap film are mapped by using the screw  $B$ , which passes through a hole in a sheet of plate glass. The glass is sufficiently large to cover the box when the screw  $B$  is in any possible position. The lower end of the screw carries a hard steel point,  $C$ , whose distance from the glass plate is adjustable by the screw. The point is made to approach the film by moving the glass plate until the distortion of the image in the film shows that contact has occurred. A record is made on a sheet of paper attached to the

<sup>5</sup> See A. A. Griffith and G. I. Taylor, *loc. cit.*, p. 237.

board *E*, which can swing about a horizontal axis at the same height as the steel recording point *D*. To mark any position of the screw it is only necessary to make a dot on the paper

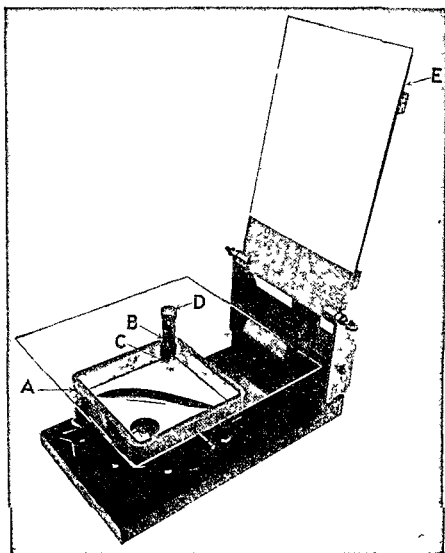


FIG 142

by swinging it down on the recording point. After the point has been made to touch the film at a number of places, the dots recorded on the paper are used for drawing a contour line. By adjusting the screw *B* this can be repeated for as many contour lines as may be required. When these lines have been mapped, the volume and the corresponding torque can be obtained by summation.

The slopes in the membrane and the corresponding stresses

in the bar are obtained by measuring the distances between neighboring contour lines. A better accuracy for measuring slopes can be obtained by projecting a beam of light onto the surface of the film and measuring the angle of the reflected ray. To establish the relation between the measured slope and the stress, the films covering the two holes are compared at the same air pressure. Since both films have the same ratio  $p/S$ , the corresponding two shafts have the same values of  $G\theta$  (see eq.  $a$ ). Hence, by measuring the slopes of the two soap films we can compare the stresses in the shaft of the given cross section with those in the circular shaft of known diameter, under the condition that they have the same angle of twist  $\theta$  per unit length and the same shearing modulus  $G$ . The corresponding ratio  $n$  of the torques is determined by the ratio of the volumes between the soap films and the plane of the plate. This ratio gives the ratio of the torsional rigidities of the two shafts. Regarding stresses for the circular shaft, the stress can be readily calculated at any point for any given torque  $M_t$ . The stress  $\tau$ , produced at any point of the noncircular shaft by the torque  $nM_t$ , is obtained by multiplying the stress  $\tau_0$  in a chosen point of the circular shaft by the experimentally determined ratio of the maximum slopes at the two points under consideration.

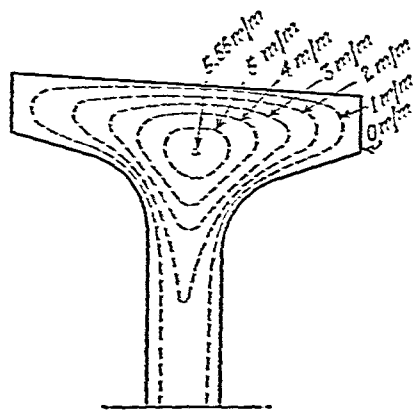


FIG. 143.

Fig. 143 represents contour lines obtained for a portion of an I section which was formerly used as a wing spar for airplanes. From the close grouping of the contour lines at the fillets of the reentrant corners and at the middle of the upper face, it follows that the shearing stresses are high at these places. The projecting parts of the flange are very lightly stressed. The maximum stress in the middle portion of the web is practically constant along the side of the web and equal to that in a narrow rectangle for the same angle of twist.



**47. Torsion of Rolled Profile Sections.**—Eqs (221) and (222), derived for a narrow rectangular cross section, can be used also for approximate solutions in other cases in which the width of the cross section is small. For example, in the case of the cross sections of uniform thickness shown in Fig 144*a* and 144*b*, the angle of twist is obtained from eq (221) by substituting for  $b$  the developed length of the center line

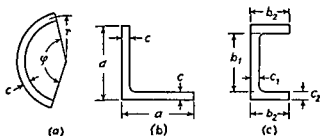


FIG 144

This length is  $b = \varphi r$  in the case of the section represented in Fig 144*a*, and  $b = 2a - c$  in the case represented in Fig 144*b*. The maximum stress for the first of these two sections is obtained from eq (222). For the angle section (Fig 144*b*) the maximum stress is at the reentrant corner. This maximum stress is obtained by multiplying the stress given by eq (222) by a stress concentration factor which is larger than unity. The magnitude of this factor is discussed later (see Art 58, p 317).

The above conclusions follow from the membrane analogy discussed in the preceding article. The reader may have anticipated from that discussion that if the thickness  $c$  of the cross section shown in Fig 144*a* is small in comparison with the radius  $r$ , the parabolic curve shown in Fig 140*b* and defining the deflection of the film can still be used with sufficient accuracy.<sup>6</sup> In such a case the maximum slope of the film and the corresponding maximum stress for the cross section in Fig 144*a* will be approximately the same as for a narrow rectangle.

<sup>6</sup> The deflection surface here is no longer cylindrical, but if  $c$  is small in comparison with  $r$ , the curvature of the film in the tangential direction is small in comparison with that in the radial direction and can be neglected.

The angle of twist  $\theta$  per unit length of a tubular member may be calculated by considering the strain energy of torsion. The strain energy per unit length of the tubular member is

$$U = \int_0^s \frac{\tau^2 h ds}{2G},$$

where  $s$  is the length of the center line of the ring cross section shown in Fig. 147 by the broken line. Substituting from eq. (226) for  $\tau$  into this equation and equating the strain energy to the work done by the torque, we obtain

$$\frac{M_t^2}{8A^2G} \int_0^s \frac{ds}{h} = \frac{1}{2} M_t \theta, \quad (c)$$

from which

$$\theta = \frac{M_t}{4A^2G} \int_0^s \frac{ds}{h} = \frac{1}{2AG} \int_0^s \tau ds. \quad (227)$$

In the case of a tube of uniform thickness,  $\tau$  is constant and eq. (227) becomes

$$\theta = \frac{\tau s}{2AG}. \quad (228)$$

From this equation the angle of twist may readily be calculated when the dimensions of the cross section are given, and the shear stress  $\tau$  may be determined by using formula (226).

Eq. (227), derived from a consideration of the strain energy of a twisted tubular member, can also be obtained from the membrane analogy. Considering the equilibrium of the plane  $n-n$  in Fig. 147, we conclude that the pressure  $pA$ <sup>11</sup> acting on this plane is balanced by the tensile forces  $S$  acting in the membrane. The tensile force  $S ds$ , acting on an element  $ds$  of the boundary, has a small slope equal to  $\tau$ ; hence the vertical component of this force is  $\tau S ds$ , and the condition of equilibrium of the plane  $n-n$  is

$$pA = \int_0^s \tau S ds. \quad (d)$$

<sup>11</sup> In the case of thin-walled members the area  $A$  bounded by the center line (shown broken) can be considered instead of the area of the plane  $n-n$ .

the quantity

$$\frac{1}{4}(c_2 + c_3)(c_2^2 + c_3^2)$$

instead of  $c_2^3$

The maximum stress usually occurs at the fillets and is of a localized character. Its magnitude will be discussed in Art 58. Considerable stress may also occur at the points  $m$ , Fig 145*b*, at the middle of the outer surfaces of the flanges. This latter stress is obtained, as before, by multiplying the angle of twist  $\theta$  by  $c_3G$ , where  $c_3$  is the maximum thickness of the flange.

It should be noted that in the derivation of eq (224) the formula for an infinitely narrow rectangle was used, and that the action of the narrow sides of the rectangle in Fig 140 on the magnitude of the volume bounded by the soap film was entirely neglected. Owing to the presence of the narrow sides, the volume will evidently be somewhat diminished. At the same time at the corners of the channel section, Fig 144*c*, where two rectangles come together, a larger deflection of the soap film may be expected than for a single rectangle. This added deflection causes an increase in the volume. These two factors, which were neglected in the derivation of eq (224), act in opposite directions and to some extent neutralize each other, so that eq (224) is sufficiently accurate for thin-walled sections.<sup>8</sup>

For cases of torsion of I beams and channels in which the thickness of the flanges is not small and varies along the width of the flange, a more elaborate formula for torsional rigidity which is in very satisfactory agreement with experiments has been developed.<sup>9</sup>

<sup>8</sup> Experiments with thin walled I beams in torsion were made by the writer, *Bull Polytech Inst (St Petersburg)*, Vol 5, 1906. These tests showed satisfactory agreement with eq (224). A very extensive series of torsional tests of rolled beams were made by A Foppl, *Sitzungsber Bayer Akad Wissensch*, p 295, 1921, and *Bauingenieur*, Vol 3, p 42, 1922. Some correction factors for eq (224) were suggested on the basis of these experiments.

<sup>9</sup> The formula was derived on the basis of experiments made by Inge Lyse and B G Johnston, *Lehigh University Publ*, Vol 9, 1935.

## Problems

1. Find the ratio of the angles of twist of a seamless and of a split circular thin tube of equal geometrical dimensions (Fig. 146) under the action of equal torques.

*Solution.* By using eq. (151), Part I, p. 284, and also eq. (221) we obtain for a seamless and for a split tube, respectively,

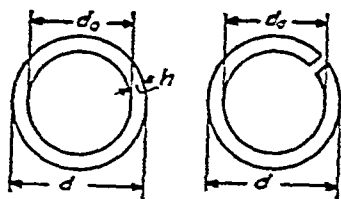


FIG. 146.

$$\theta = \frac{32M_t}{\pi d^3 \left(1 - \frac{d_0^4}{d^4}\right) G};$$

$$\theta_1 = \frac{3M_t}{\pi \left(\frac{d + d_0}{2}\right) \left(\frac{d - d_0}{2}\right)^3 G}.$$

The ratio of the angles of twist is

$$\frac{\theta}{\theta_1} = \frac{2(d - d_0)^2}{3d^2 + d_0^2}.$$

For very thin tubes  $(d^2 + d_0^2) \approx 2d^2$  and the ratio becomes

$$\frac{\theta}{\theta_1} = \frac{4}{3} \left(\frac{h}{d}\right)^2.$$

2. Determine the angle of twist per inch of length of a channel (Fig. 144c) if  $M_t = 20,000$  in. lb,  $b_1 = 10$  in.,  $b_2 = 3.5$  in.,  $c_1 = 0.4$  in.,  $c_2 = 0.6$  in.,  $G = 12 \times 10^6$  lb per sq in.

*Solution.*

$$\theta = \frac{3 \times 20,000}{(10 \times 0.4^3 + 7 \times 0.6^3) 12 \times 10^6} = 0.00233 \text{ radians per in.}$$

3. Determine the ratio of the maximum shearing stresses for the tubes discussed in Prob. 1 if the torques are equal for both tubes.

4. Determine the torsional rigidity  $C$  for the I beam considered on p. 245 if the sloping of the flanges is considered as explained on the same page.

48. Torsion of Thin Tubular Members.—In discussing the torsion of thin tubular members the membrane analogy again

may be used to advantage <sup>10</sup> In this case the outer and inner boundaries of the cross section are located in different horizontal planes with the membrane connecting the boundaries, as at  $mn$  in Fig 147 If the thickness of the tube is small, the curvature of the membrane may be neglected, i e, the lines  $mn$  may be considered straight The slope of the membrane surface is then constant over the thickness of the wall and is equal to  $f/h$ , where  $f$  is the difference in the levels of the two boundaries and  $h$  is the thickness of the tube, which may vary

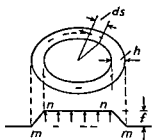


FIG 147

along the circumference of the cross section The membrane analogy indicates that in this case the shearing stresses are uniformly distributed over the thickness of the wall and are given by the slope

$$\tau = \frac{f}{h} \quad (a)$$

The stress along the circumference is therefore inversely proportional to the thickness of the wall The volume included between the surfaces  $mm$  and  $nn$  is calculated by using the center line of the ring cross section, indicated by the broken-line curve in the figure If  $A$  is the area bounded by this line, the volume  $mmnn$  is  $Af$  and from the membrane analogy we obtain

$$M_t = 2Af \quad (b)$$

From eqs (a) and (b) we then find

$$\tau = \frac{M_t}{2Ah} \quad (226)$$

This equation may be used in calculating the stresses in tubular members under torsion if the thickness of the wall is small, variations in thickness are not abrupt, and there are no reentrant corners

<sup>10</sup> Torsion of tubular members was discussed by R Bredt, *Z Ver deut Ing*, Vol 40, p 815, 1896 See also T Prescott, *Phil Mag*, Vol 60, 1920

The angle of twist  $\theta$  per unit length of a tubular member may be calculated by considering the strain energy of torsion. The strain energy per unit length of the tubular member is

$$U = \int_0^s \frac{\tau^2 h ds}{2G},$$

where  $s$  is the length of the center line of the ring cross section shown in Fig. 147 by the broken line. Substituting from eq. (226) for  $\tau$  into this equation and equating the strain energy to the work done by the torque, we obtain

$$\frac{M_t^2}{8A^2G} \int_0^s \frac{ds}{h} = \frac{1}{2} M_t \theta, \quad (c)$$

from which

$$\theta = \frac{M_t}{4A^2G} \int_0^s \frac{ds}{h} = \frac{1}{2AG} \int_0^s \tau ds. \quad (227)$$

In the case of a tube of uniform thickness,  $\tau$  is constant and eq. (227) becomes

$$\theta = \frac{\tau s}{2AG}. \quad (228)$$

From this equation the angle of twist may readily be calculated when the dimensions of the cross section are given, and the shear stress  $\tau$  may be determined by using formula (226).

Eq. (227), derived from a consideration of the strain energy of a twisted tubular member, can also be obtained from the membrane analogy. Considering the equilibrium of the plane  $n-n$  in Fig. 147, we conclude that the pressure  $pA$ <sup>11</sup> acting on this plane is balanced by the tensile forces  $S$  acting in the membrane. The tensile force  $S ds$ , acting on an element  $ds$  of the boundary, has a small slope equal to  $\tau$ ; hence the vertical component of this force is  $\tau S ds$ , and the condition of equilibrium of the plane  $n-n$  is

$$pA = \int_0^s \tau S ds. \quad (d)$$

<sup>11</sup> In the case of thin-walled members the area  $A$  bounded by the center line (shown broken) can be considered instead of the area of the plane  $n-n$ .

Observing that the tension  $S$  in the membrane is constant and that  $p/S = 2G\theta$  (see eq  $a$ , p 237), we find from eq. (d)

$$\frac{p}{S} = \frac{1}{A} \int_0^s \tau ds = 2G\theta.$$

Solving this equation for  $\theta$ , we obtain formula (227) for the angle of twist

Sometimes the torsional stresses in a tubular member with intermediate walls, as in Fig 148a, must be calculated. The boundary of the cross section in this case is formed by three closed curves. In applying the membrane analogy these curves will be located in three different horizontal planes,  $mn$ ,  $pp$ , and  $mm$ , as shown in Fig 148b. The soap film connecting these three curves forms a narrow surface, with cross sections as shown by the lines  $mn$ ,  $np$  and  $pm$ . Assuming again that the wall thicknesses— $h_1$ ,  $h_2$  and  $h_3$ —are small, and neglecting the curvature of the membrane in the directions normal to the boundaries, we consider that the lines  $mn$ ,  $np$ , and  $pm$  are straight. In such a case the slopes of the membrane, giving the stresses in the walls of the tubular member, are.

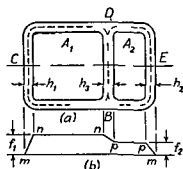


FIG 148

$$\tau_1 = \frac{f_1}{h_1}, \quad \tau_2 = \frac{f_2}{h_2}, \quad (e)$$

$$\tau_3 = \frac{f_1 - f_2}{h_3} = \frac{h_1\tau_1 - h_2\tau_2}{h_3}. \quad (f)$$

The magnitude of the torque producing these stresses is obtained by doubling the volume of the space  $mnnppm$  in Fig 148b. If we denote the areas bounded by the broken lines in Fig 148a by  $A_1$  and  $A_2$  this torque is

$$M_t = 2(A_1f_1 + A_2f_2), \quad (g)$$

or, using eqs (e), we obtain

$$M_t = 2A_1h_1\tau_1 + 2A_2h_2\tau_2. \quad (h)$$

Further equations for the solution of the problem are obtained by applying eq (227) to the two closed curves indicated by the dot-

ted lines in Fig. 148a. Assuming that the portion  $BCD$  of the wall has a constant thickness  $h_1$  and that the portions  $DEB$  and  $DB$  have the constant thicknesses  $h_2$  and  $h_3$ , respectively, equation (227) becomes

$$\tau_1 s_1 + \tau_3 s_3 = 2G\theta A_1, \quad (i)$$

$$\tau_2 s_2 - \tau_3 s_3 = 2G\theta A_2. \quad (j)$$

In these equations  $s_1$ ,  $s_2$  and  $s_3$  are the center line lengths measured along the broken lines  $BCD$ ,  $DEB$  and  $DB$ , respectively. In applying the integral of eq. (227) to the closed curves  $BCDB$  and  $DEBD$ , we pass the portion  $DB$  of the length  $s_3$  in two opposite directions. Hence the second terms on the left sides of eqs. (i) and (j) appear with opposite signs. The angle of twist  $\theta$  on the right side of eqs. (i) and (j) is evidently the same as the angle of twist of the entire tubular member. The four equations (f), (h), (i) and (j) contain the four unknowns  $\tau_1$ ,  $\tau_2$ ,  $\tau_3$  and  $\theta$ , which can be easily calculated. Eliminating  $\theta$ , we obtain for the shearing stresses the following formulas:

$$\tau_1 = M_t \cdot \frac{h_3 s_2 A_1 + h_2 s_3 (A_1 + A_2)}{2[h_1 h_3 s_2 A_1^2 + h_2 h_3 s_1 A_2^2 + h_1 h_2 s_3 (A_1 + A_2)^2]}, \quad (k)$$

$$\tau_2 = M_t \cdot \frac{h_3 s_1 A_2 + h_1 s_3 (A_1 + A_2)}{2[h_1 h_3 s_2 A_1^2 + h_2 h_3 s_1 A_2^2 + h_1 h_2 s_3 (A_1 + A_2)^2]}, \quad (l)$$

$$\tau_3 = M_t \cdot \frac{h_1 s_2 A_1 - h_2 s_1 A_2}{2[h_1 h_3 s_2 A_1^2 + h_2 h_3 s_1 A_2^2 + h_1 h_2 s_3 (A_1 + A_2)^2]}. \quad (m)$$

If the wall  $DB$  of the cross section in Fig. 148a is the plane of symmetry of the cross section we have

$$s_1 = s_2, \quad h_1 = h_2 \quad \text{and} \quad A_1 = A_2,$$

and eq. (m) gives  $\tau_3 = 0$ . Thus in this case the torque is taken entirely by the outer wall of the tube, and the intermediate web is unstressed.<sup>12</sup>

To obtain the angle of twist  $\theta$  for the tubular member, we have to substitute the calculated values of the stresses in eq. (i) or (j). Thus the torsional problem for a tubular member, such as is shown in Fig. 148, can be readily solved with sufficient accuracy provided the wall thickness is small in comparison with the general dimensions of the cross section.

In the preceding example a tubular member consisting of only two cells was considered. In practical applications we often encounter

<sup>12</sup> The small stresses corresponding to the change in slope of the membrane across the thickness of the web are neglected in this derivation.



members with a larger number of cells, in which case the algebraic solution described above becomes cumbersome. A quicker answer may be obtained by solving the problem numerically in each particular case by using the method of successive approximations<sup>13</sup>. To illustrate the numerical method let us consider the case of a tubular

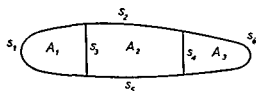


FIG 149

member with three cells, Fig 149. Following the previous notation, we will let  $f_1$ ,  $f_2$  and  $f_3$  denote the elevations of the membrane corresponding to the three cells,  $s_1$ ,  $s_6$  denote the center line lengths of the wall segments, and  $h_1$ ,  $h_6$  denote the corre-

sponding wall thicknesses. Then proceeding as before, we obtain instead of eqs (i) and (j) the following equations

$$\left. \begin{aligned} f_1 \frac{s_1}{h_1} + (f_1 - f_2) \frac{s_3}{h_3} &= 2G\theta A_1, \\ -(f_1 - f_2) \frac{s_3}{h_3} + f_2 \left( \frac{s_2}{h_2} + \frac{s_5}{h_5} \right) + (f_2 - f_3) \frac{s_4}{h_4} &= 2G\theta A_2, \\ -(f_2 - f_3) \frac{s_4}{h_4} + f_3 \frac{s_6}{h_6} &= 2G\theta A_3 \end{aligned} \right\} \quad (n)$$

In eqs (n), the quantities  $f_1 = \tau_1 h_1$ ,  $f_2 = \tau_2 h_2$ ,  $f_1 - f_2 = \tau_3 h_3$ , , called *shear flows*, are introduced instead of the shearing stresses  $\tau_1$ ,  $\tau_2$ ,  $\tau_3$ . By introducing the notation  $s_i/h_i = r_i$  we can rewrite these equations in the following simplified form

$$\left. \begin{aligned} \left( \sum_1 r_i \right) f_1 - r_3 f_2 &= 2G\theta A_1, \\ -r_3 f_1 + \left( \sum_2 r_i \right) f_2 - r_4 f_3 &= 2G\theta A_2, \\ -r_4 f_2 + \left( \sum_3 r_i \right) f_3 &= 2G\theta A_3, \end{aligned} \right\} \quad (o)$$

in which  $\sum_1 r_i$ ,  $\sum_2 r_i$ ,  $\sum_3 r_i$  are the sums of the  $r_i$  values for the first, second and third cells, respectively. Dividing these equations by the coefficients of the diagonal terms and introducing the

<sup>13</sup> See the paper by F M Baron, *J Appl Mech*, Vol 9, p A 72, 1942

notation

$$\left. \begin{aligned} \frac{2G\theta A_1}{\sum_1 r_i} &= f_1', & \frac{2G\theta A_2}{\sum_2 r_i} &= f_2', & \frac{2G\theta A_3}{\sum_3 r_i} &= f_3', \\ \frac{r_3}{\sum_1 r_i} &= d_{12}, & \frac{r_3}{\sum_2 r_i} &= d_{21}, & \frac{r_4}{\sum_2 r_i} &= d_{23}, & \frac{r_4}{\sum_3 r_i} &= d_{32}, \end{aligned} \right\} \quad (p)$$

we finally write the equations in the following form:

$$\left. \begin{aligned} f_1 - d_{12}f_2 &= f_1', \\ -d_{21}f_1 + f_2 - d_{23}f_3 &= f_2', \\ -d_{32}f_2 + f_3 &= f_3'. \end{aligned} \right\} \quad (q)$$

To these equations we add the equation for calculating the torque, similar to eq. (g),

$$M_t = 2(A_1f_1 + A_2f_2 + A_3f_3). \quad (r)$$

For a numerical solution of eqs. (q) we begin by assuming a numerical value for the angle of twist per unit length  $\theta$ . The quantities  $f_1', f_2'$  and  $f_3'$  are then determined and eqs. (q) may be solved. The resulting values for  $f_1, f_2$  and  $f_3$  are substituted into eq. (r) to find the corresponding value of  $M_t$ . For any other desired value of torque  $M_t$  we have only to change the values of  $\theta, f_1, f_2$  and  $f_3$  in direct proportion.

In applying the method of successive approximations in solving eqs. (q) we observe that all the coefficients  $d_{ij}$  are smaller than unity. Therefore as a first approximation we keep only the diagonal terms in eqs. (q) and take  $f_1', f_2'$  and  $f_3'$  as the first approximations for  $f_1, f_2$  and  $f_3$ . Substituting these first approximations into the nondiagonal terms of eqs. (q) we obtain the first corrections,

$$\Delta'f_1 = d_{12}f_2', \quad \Delta'f_2 = d_{21}f_1' + d_{23}f_3', \quad \Delta'f_3 = d_{32}f_2'. \quad (s)$$

Substituting from eqs. (s) into the nondiagonal terms of eqs. (q), we obtain the second corrections,

$$\Delta''f_1 = d_{12}\Delta'f_2, \quad \Delta''f_2 = d_{21}\Delta'f_1 + d_{23}\Delta'f_3, \quad \Delta''f_3 = d_{32}\Delta'f_2.$$

Proceeding in the same manner, we obtain the third corrections, and so on. The calculations must be repeated until any further corrections are very small. Then by adding all the corrections to the first approximations  $f_1', f_2'$  and  $f_3'$  we obtain the approximate values of

$f_1, f_2$  and  $f_3$ . Eq. (r) then gives the corresponding value of  $M_t$ , and the values of the shearing stresses are determined from equations similar to eqs. (e) and (f).

To illustrate the calculations a numerical example<sup>14</sup> for a four-cell wing section is shown in Fig. 150. The area of each cell is given by the number enclosed in a rectangle, and the values of  $r$  are shown adjacent to each wall segment. In the table below the diagram the values of  $\Sigma r_i$  for each cell are given on the first line. On the second line the coefficients  $d_{ij}$  for the intermediate cell walls are given. Be-

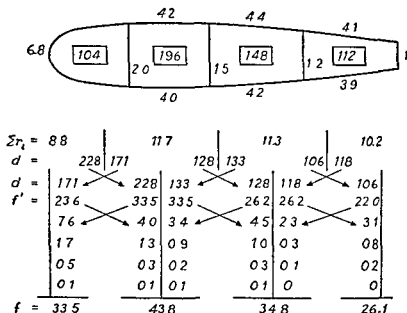


FIG. 150.

fore the calculation is started, these coefficients must be transposed as shown by the arrows and the third line. On the next line the first approximations  $f'$  for the shear flows are written, calculated on the assumption that  $G\theta = 1$ . The first corrections are calculated by multiplying each of the values of  $f'$  by the  $d$  coefficient above it and transposing the resulting values to the adjacent cells as shown by the arrows. The total correction for an internal cell consists of two numbers written one on either side of the vertical line. These numbers are added mentally and multiplied by the proper  $d$  factor in calculating the second corrections. The calculations are repeated until the corrections become negligible. The final values of shear flows, obtained by adding all the corrections to the first approximations  $f'$ , are given on the last line in Fig. 150. Substituting these values into eq. (r) the torque corresponding to  $G\theta = 1$  is obtained.

<sup>14</sup>This example is taken from the paper by Stanley U. Benscoter, *J. Aeronaut. Sci.*, Vol. 13, p. 438, 1946.

49. Torsion of Thin-walled Members of Open Cross Section in Which Some Cross Sections Are Prevented from Warping.—In our previous discussion of the twist of I beams and channels (p. 244) it was assumed that the torque was applied at the ends of the bar and that all cross sections were completely free to warp. There are cases, however, in which one or more cross sections of the bar are caused to remain plane, and the question arises how this prevention of warping affects the angle of twist and the distribution of stresses. For bars of solid cross section, such as ellipses or rectangles, warping constraint produces only a negligible effect on the angle of twist<sup>15</sup> provided the cross-sectional dimensions are small in comparison with the length of the bar. In the case of I beams, channels and other thin-walled members of open cross section, the prevention of warping during twist is accompanied by bending of the flanges and may have considerable effect on the angle of twist.

A simple case in which warping is prevented is an I beam twisted by a couple at the middle and simply supported<sup>16</sup> at the ends (Fig. 151). From symmetry, the cross section  $mn$

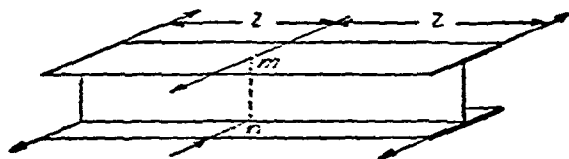


FIG. 151.

must remain plane during twist and the rotation of this cross section with respect to the end cross sections is accompanied by bending of the flanges. The end torque is balanced at any cross section partially by shearing stresses due to twist and partially by shearing stresses due to bending of the flanges.<sup>17</sup>

<sup>15</sup> For a discussion of this question see Timoshenko and Goodier, *Theory of Elasticity*, p. 302, 1951.

<sup>16</sup> Simple supports are such that the ends of the beam cannot rotate about a longitudinal axis but are free to warp.

<sup>17</sup> See the paper by the author, *Bull. Polytech. Inst. (St. Petersburg)*, 1905-6, and *Z. Math. u. Phys.*, Vol. 58, p. 361, 1910. See also K. Huber, dissertation, Munich, 1922, and C. Weber, *Z. angew. Math. u. Mech.*, Vol. 6, p. 85, 1926. Further discussion of the problem for various shapes of thin-walled members is given by A. Ostenfeld, *Lab. Baustatik Techn. Hochschule, (Copenhagen) Mitt.*, No. 6, 1931.

Fig. 152*a* represents half of the beam shown in Fig. 151. The middle cross section *mn* remains plane owing to symmetry and we may consider it as built-in, with the torque applied at the other end of the beam. Let  $\varphi$  be the angle of twist for any cross section of the beam. Then the part of the torque

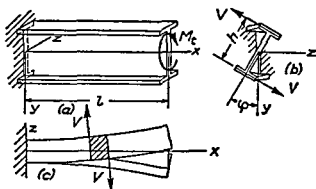


FIG. 152.

$M_t'$  which is balanced by the shearing stresses due to torsion is determined from the equation

$$M_t' = C \frac{d\varphi}{dx}, \quad (a)$$

in which  $C$  is the *torsional rigidity* of the bar (see Part I, p. 290).

In order to determine the part of the torque  $M_t''$  which is balanced by the shearing forces in the flanges due to bending, we must consider the bending of a flange (Fig. 152*c*). Denoting by  $h$  the distance between the centroids of the flanges (Fig. 152*b*), the deflection at any cross section of the upper flange is

$$z = \frac{h\varphi}{2}, \quad (b)$$

and by differentiation we obtain

$$\frac{d^3z}{dx^3} = \frac{h}{2} \frac{d^3\varphi}{dx^3}. \quad (c)$$

If we denote by  $D$  the flexural rigidity of one flange in the plane  $xz$  and observe that  $z$  is positive in the direction shown

in Fig. 152*c*, the expression for the shearing force in the flange due to bending becomes <sup>15</sup>

$$V = \frac{dM}{dx} = D \frac{d^3 z}{dx^3} = \frac{Dh}{2} \frac{d^3 \varphi}{dx^3}, \quad (d)$$

where  $M$  is the bending moment in the flange. Considering the positive direction of  $V$  as shown in Fig. 152*c*, we therefore have

$$M_t'' = -Vh = -\frac{Dh^2}{2} \frac{d^3 \varphi}{dx^3} \quad (e)$$

and the total torque is

$$M_t = M_t' + M_t'' = C \frac{d\varphi}{dx} - \frac{Dh^2}{2} \frac{d^3 \varphi}{dx^3}. \quad (229)$$

In the problem under consideration (Fig. 152*c*), the torque  $M_t$  is constant along the length  $l$  of the beam. The end conditions are <sup>19</sup>

$$\left(\frac{d\varphi}{dx}\right)_{x=0} = 0, \quad \left(\frac{d^2\varphi}{dx^2}\right)_{x=l} = 0,$$

and therefore the solution of eq. (229) is

$$\frac{d\varphi}{dx} = \frac{M_t}{C} \left( 1 - \frac{\cosh \frac{l-x}{a}}{\cosh \frac{l}{a}} \right), \quad (f)$$

in which

$$a^2 = \frac{Dh^2}{2C}. \quad (g)$$

Since the flexural rigidity  $D$  and torsional rigidity  $C$  are both measured in the same units (lb in.<sup>2</sup>), eq. (g) shows that  $a$  has the dimensions of length and depends upon the proportions of the beam.

<sup>15</sup> The influence of shearing force on the curvature of the deflection curve of the flange is neglected in this derivation.

<sup>19</sup> The conditions are determined by considering each flange as a beam with one end built in and the other end free.

Owing to the presence of the second term in eq. (f) the angle of twist per unit length varies along the length of the bar, although the torque  $M_t$  remains constant. Torsion of a bar which depends on bending of the flanges and is defined by an equation similar to eq. (229) is called *nonuniform torsion*.

When  $d\varphi/dx$  is determined, the portions  $M_t'$  and  $M_t''$  of the total torque  $M_t$  may be calculated for any cross section from eqs. (a) and (e). For the built-in section where  $x = 0$  and  $d\varphi/dx = 0$ , we obtain from eq. (a) that  $M_t' = 0$ . Hence at this point the entire torque is balanced by the moment of the shearing forces acting in the flanges, and we have  $V = -M_t/h$ . At the end  $x = l$ , using eq. (f), we obtain

$$\frac{d\varphi}{dx} = \frac{M_t}{C} \left( 1 - \frac{1}{\cosh \frac{l}{a}} \right). \quad (h)$$

If the length of the beam is large in comparison with the cross-sectional dimensions,  $l$  is large in comparison with  $a$ , and the second term in the parentheses of eq. (h) becomes negligible; hence  $d\varphi/dx$  approaches the value  $M_t/C$ .

The bending moment in the flange is found from eq. (d):

$$M = \frac{Dh}{2} \frac{d^2\varphi}{dx^2}; \quad (i)$$

or, substituting eq. (f) for  $d\varphi/dx$  and using the notation of eq. (g), we obtain

$$M = \frac{a}{h} M_t \frac{\sinh \frac{l-x}{a}}{\cosh \frac{l}{a}}. \quad (j)$$

The bending moment at the built-in end will be

$$M_{\max} = \frac{a}{h} M_t \tanh \frac{l}{a}. \quad (k)$$

When  $l$  is several times larger than  $a$ ,  $\tanh (l/a)$  approaches

To calculate the angle of twist  $\varphi$  we use eq. (f). Integrating this equation and adjusting the constant of integration to make  $\varphi = 0$  when  $x = 0$ , we obtain

$$\varphi = \frac{M_t}{C} \left( x + \frac{a \sinh \frac{l-x}{a}}{\cosh \frac{l}{a}} - a \tanh \frac{l}{a} \right). \quad (p)$$

Substituting  $x = l$  into this equation we obtain

$$(\varphi)_{x=l} = \frac{M_t}{C} \left( l - a \tanh \frac{l}{a} \right). \quad (q)$$

The second term in the parentheses represents the effect of bending of the flanges on the angle of twist. For long beams  $\tanh(l/a) \approx 1$  and eq. (q) becomes

$$(\varphi)_{x=l} = \frac{M_t}{C} (l - a). \quad (r)$$

The effect of the bending of the flanges on the angle of twist is therefore equivalent to diminishing the length  $l$  by the quantity  $a$ .

The method described above for a constant torque  $M_t$  may also be used when the torque varies along the length of the beam. It is only necessary to substitute in eq. (229) the correct expression for  $M_t$  as a function of  $x$ .

In the preceding discussion of the torsion of an I beam, Fig. 152, it was concluded from symmetry that each cross section rotates with respect to the central axis of the beam. Hence only bending of the flanges has to be considered. It is seen also that this bending does not interfere with the simple torsion of the web, since at the points of juncture of the web and flanges the bending stresses in the flanges vanish. In the case of nonsymmetrical cross sections or cross sections with only one axis of symmetry the problem becomes more complicated since not only bending of the flanges but also bending of the web will be produced during torsion. As an example



The magnitude of the force  $S$  is now determined from the condition that the strain  $\epsilon_x$  in the longitudinal direction at the juncture of the web and the flange is the same for both these parts. Calculating the curvatures of the deflection curves from eqs. (i), we find that this condition is represented by the equation <sup>22</sup>

$$\epsilon_x = e \frac{d^2\varphi}{dx^2} \cdot \frac{h}{2} = \frac{h}{2} \frac{d^2\varphi}{dx^2} \cdot \frac{b}{2} - \frac{S}{btE}. \quad (u)$$

Now using eq. (s) and noting that  $I_z = t_1 h^3/12 + bth^2/2$ , we obtain

$$S = \frac{Eb^2 h^4 t t_1}{48 I_z} \cdot \frac{d^2\varphi}{dx^2}. \quad (v)$$

Having this expression for  $S$  we can readily determine the shearing stresses in the web and the flanges and also the portion  $M_t''$  of the torque balanced by these stresses.

Let us begin by calculating the shearing stresses in the web. Taking two adjacent cross sections  $mn$  and  $m_1 n_1$ , Fig.

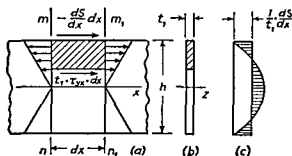


FIG. 156.

156a, and considering in the usual way the equilibrium of the shaded element, we obtain

$$\tau_{yx} t_1 dx - \frac{dS}{dx} dx + \frac{dM}{dx} \cdot \frac{Q}{I_z'} dx = 0.$$

In this equation  $Q$  is the static moment with respect to the  $z$  axis of the shaded portion of the cross section of the web, Fig. 156b,  $I_z' = t_1 h^3/12$  is the moment of inertia of the cross

<sup>22</sup> The influence of shearing forces on the curvature of the deflection curve of the flange is neglected in this derivation.

section of the web with respect to the  $z$  axis, and  $M$  is the bending moment in the web. The bending moment  $M$  is positive if it produces tension at the upper edge of the web, and is equal to

$$M = EI_z' e \frac{d^2 \varphi}{dx^2} = Sh.$$

The expression for the stresses  $\tau_{yz}$  then becomes

$$\tau_{yz} = \frac{dS}{t_1 dx} \left( 1 - \frac{Qh}{I_z'} \right).$$

Observing that the variation of  $Q$  along the depth of the cross section follows a parabolic law, we find that the distribution of  $\tau_{yz}$  is given by the shaded area in Fig. 156c and that the resultant shearing force in the web vanishes. This latter conclusion may be anticipated, since the shearing forces in the web and in the two flanges must balance the portion  $M_t''$  of the torque, and this is possible only if the shearing force in the web vanishes and the shearing forces in the two flanges form a couple.

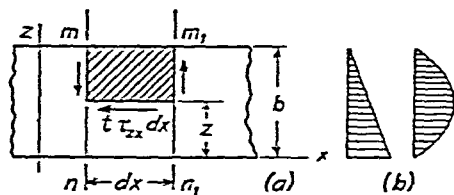


FIG. 157.

In calculating shearing stresses  $\tau_{zx}$  in the flange, Fig. 157a, we observe that at cross section  $mn$  there acts a compressive force  $S$  and a bending moment <sup>23</sup>

$$M = D \frac{d^2 \varphi}{dx^2} \cdot \frac{h}{2}. \quad (w)$$

Considering the equilibrium of the shaded element between two adjacent cross sections we obtain

$$t\tau_{zx}dx + \frac{dS}{dx} dx \cdot \frac{b-z}{b} + \frac{dM}{dx} dx \frac{Q_1}{I_1} = 0,$$

where  $Q_1$  and  $I_1$  are to be calculated for the flange in the same manner as  $Q$  and  $I_z'$  for the web. Substituting for  $M$  its

<sup>23</sup>  $D = Etb^3/12$  denotes the flexural rigidity of the flange in its plane, as previously defined (p. 256).

value from eq. (w), we obtain

$$\tau_{zx} = -\frac{1}{t} \frac{dS}{dx} \frac{b-z}{b} - \frac{E}{t} \cdot \frac{d^3\varphi}{dx^3} \cdot \frac{hQ_1}{2}.$$

The two terms on the right-hand side of this equation are represented in Fig. 157*b* by the shaded areas of the triangle and the parabolic segment respectively. The sum of these two areas multiplied by  $t$  gives the total shearing force in the flange, which is <sup>24</sup>

$$V = \frac{b}{2} \frac{dS}{dx} + E \frac{htb^3}{24} \frac{d^3\varphi}{dx^3}.$$

Then substituting from eq. (v) for  $S$ , we obtain the torque balanced by the shearing forces in the flanges as follows:

$$M_t'' = -Vh = -\frac{Dh^2}{2} \left(1 + \frac{t_1 h^3}{4I_z}\right) \frac{d^3\varphi}{dx^3}. \quad (x)$$

The total torque is

$$M_t = C \frac{d\varphi}{dx} - \frac{Dh^2}{2} \left(1 + \frac{t_1 h^3}{4I_z}\right) \frac{d^3\varphi}{dx^3}. \quad (y)$$

Hence all the conclusions obtained for an I beam can also be used for a channel if the quantity  $a^2$  given by eq. (g) is replaced by the quantity

$$a^2 = \frac{Dh^2}{2C} \left(1 + \frac{t_1 h^3}{4I_z}\right).$$

The method used in discussing torsion of a symmetrical channel, Fig. 154, can be applied also in the more general case of a nonsymmetrical channel section, Fig. 158. The position of the shear center  $O$  for this shape was determined previously (see Part I, pp. 241-3). Then proceeding as before (see eqs. *i*), we express the deflection curves of the flanges and web in terms of the angle of twist  $\varphi$ . The longitudinal forces  $S_1$  and  $S_2$  in the flanges are now determined from the conditions that at the points of juncture the longitudinal strain  $\epsilon_x$  is the same for

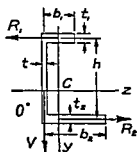


FIG. 158.

<sup>24</sup> The positive direction for  $V$  is shown in Fig. 152*c*.

Eqs. (233) and (234) are applicable between  $x = 0$  and  $x = a$ , where  $a$  defines the position of the first transverse load.

In considering the second portion of the bar ( $x > a$ ), we have to take into account the torque  $M_t^1$  applied at the cross section  $x = a$ . The expression for the angle of twist in the second portion of the bar is now obtained by adding the angle of twist produced by  $M_t^1$  to eq. (233). In this manner we obtain for  $x > a$

$$\varphi = \varphi_0 + \frac{1}{k} \varphi_0' \sinh kx + \frac{1}{k^2} \varphi_0'' (\cosh kx - 1) + \frac{M_t^0}{C} \left( x - \frac{\sinh kx}{k} \right) + \frac{M_t^1}{C} \left[ x - a - \frac{\sinh k(x-a)}{k} \right]. \quad (235)$$

The last term on the right-hand side represents the angle produced by  $M_t^1$ . It is obtained from the last term of eq. (233) by substituting  $M_t^1$  for  $M_t^0$  and  $x - a$  for  $x$ , since the distance of  $M_t^1$  from the cross section under consideration is  $x - a$ .

In a similar manner we can proceed with the third portion of the bar, and so on to the last portion. The expressions for  $\varphi$  in all portions of the bar contain the same constants  $\varphi_0$ ,  $\varphi_0'$ ,  $\varphi_0''$ , and  $M_t^0$ . All these constants can now be determined from the conditions at the two ends of the bar.

To illustrate the method let us consider several simple examples. We begin with the case in which the bar is twisted by a torque applied at the ends, and at the same time the ends are supported so that they can rotate, but warping is entirely prevented. Since there are no forces applied in the span, eq. (233) can be applied to the entire length of the bar. Assuming that the end  $x = 0$  is immovable and observing that warping is restrained, we have to put  $\varphi_0 = 0$ ,  $\varphi_0' = 0$  into eq. (233), which gives

$$\left. \begin{aligned} \varphi &= \frac{1}{k^2} \varphi_0'' (\cosh kx - 1) + \frac{M_t^0}{C} \left( x - \frac{\sinh kx}{k} \right); \\ \varphi' &= \frac{1}{k} \varphi_0'' \sinh kx + \frac{M_t^0}{C} (1 - \cosh kx). \end{aligned} \right\} \quad (236)$$

Since warping at the other end ( $x = l$ ) of the bar is also restrained,

## Problems

1. A cantilever of Z section (Fig 159) is built in at one end and twisted by a couple  $M_t$  applied at the other end. Find the angle of twist and the maximum bending moment in the flanges.

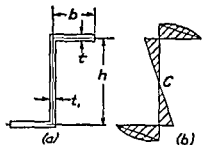


FIG 159

*Solution* In this case the shear center coincides with the centroid  $C$  of the cross section (see Part I, p. 243) and there will be no bending of the web. The forces  $S$  are identical for both flanges and the distribution of shearing stresses is

shown in Fig 159b. The resultant shearing force in the web vanishes, and the equal and opposite shearing forces  $V$  in the flanges are

$$V = \pm \frac{Eb^3ht}{12} \left( 2 - \frac{3bt}{2bt + ht_1} \right) \frac{d^3\varphi}{dx^3}$$

The torque due to the forces  $V$  is

$$M_t'' = -Vh = -Dh^2 \left( 2 - \frac{3bt}{2bt + ht_1} \right) \frac{d^3\varphi}{dx^3},$$

where  $D$  is the flexural rigidity of one flange. The angle of twist and the maximum bending moment in the flanges are calculated from eqs (k) and (l) in which, for this case,

$$a^2 = \frac{Dh^2}{C} \left( 2 - \frac{3bt}{2bt + ht_1} \right)$$

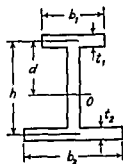


FIG 160

2. Solve Prob. 1 assuming that the cross section is as shown in Fig 160.

*Answer* The shearing forces in the flanges are

$$V = \pm Dd \frac{d^3\varphi}{dx^3},$$

where

$$D = \frac{Et_1b_1^3}{12}, \quad \frac{d}{h-d} = \frac{b_2^3t_2}{b_1^3t_1}.$$

The torque  $M_t''$  due to bending of the flanges is

$$M_t'' = -Ddh \frac{d^3\varphi}{dx^3}$$

The value of  $a$  to be substituted in eqs. (k) and (l) is

$$a^2 = \frac{Ddh}{C}.$$

3. Solve Prob. 1 for the cross sections shown in Fig. 161.

*Answer.* In both these cases the shear center  $O$  is at the intersection of the flanges. Rotation with respect to this point does not produce any bending of the flanges in their planes, and therefore the entire torque is transmitted by the torsional stresses, and  $M_t'' = 0$ .

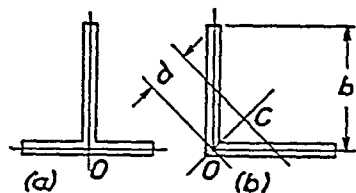


FIG. 161.

**50. Combined Bending and Torsion of Thin-walled Members of Open Cross Section.**<sup>23</sup>—Let us consider the general case of a thin-walled bar under the action of any transverse forces. Each force can be replaced by a parallel force passing through the *axis of the shear centers* and a torque. In this manner we obtain a bar loaded along its shear center axis and subjected to the action of torques applied at several cross sections. The transverse forces applied to the shear center axis produce bending only (see Part I, Art. 52, p. 235). In discussing torsion we may use the results of Art. 49. We take the origin of coordinates at the end ( $x = 0$ ) of the bar and denote by  $M_t^0$  the torque at that end. To determine the angle of twist  $\varphi$  we use eq. (230). Dividing this equation by  $C_1$  and introducing the notation

$$k^2 = \frac{C}{C_1},$$

we obtain

$$\varphi''' - k^2\varphi' = -\frac{M_t}{C_1}, \quad (231)$$

where the primes denote differentiation with respect to  $x$ . The general solution of this equation is

$$\varphi = \frac{M_t^0 x}{C} + A + A_1 \sinh kx + A_2 \cosh kx, \quad (232)$$

<sup>23</sup> See the author's paper, *J. Franklin Inst.*, Vol. 239, Nos. 3, 4 and 5, p. 258, 1945.

since in this case  $M_t = M_t^0$ . A similar equation can be written for each portion of the bar between two consecutive transverse forces. It is only necessary to replace  $M_t^0$  by the value of the torque at the beginning of that portion. The constants of integration must then be determined from the continuity conditions at the points of load application.

The calculations can be greatly simplified if instead of the constants of integration  $A$ ,  $A_1$  and  $A_2$ , we introduce quantities defining the conditions at the end  $x = 0$  of the bar.<sup>29</sup> Differentiating eq. (232) and substituting  $x = 0$ , we obtain

$$\begin{aligned}\varphi_0 &= A + A_2, \\ \varphi_0' &= \frac{M_t^0}{C} + kA_1, \\ \varphi_0'' &= k^2 A_2,\end{aligned}$$

where the subscript zero indicates that the quantities refer to the end  $x = 0$  of the bar. Solving these equations for the constants  $A$ ,  $A_1$  and  $A_2$  and substituting these values into eq. (232), we obtain

$$\begin{aligned}\varphi = \varphi_0 + \frac{1}{k} \varphi_0' \sinh kx + \frac{1}{k^2} \varphi_0'' (\cosh kx - 1) \\ + \frac{M_t^0}{C} \left( x - \frac{\sinh kx}{k} \right).\end{aligned}\quad (233)$$

In this expression the angle of twist  $\varphi$  for any cross section in the first portion of the bar is expressed in terms of the quantities  $\varphi_0$ ,  $\varphi_0'$ ,  $\varphi_0''$  and  $M_t^0$  at the end  $x = 0$ . By differentiation of eq. (233) we obtain

$$\left. \begin{aligned}\varphi' &= \varphi_0' \cosh kx + \frac{1}{k} \varphi_0'' \sinh kx + \frac{M_t^0}{C} (1 - \cosh kx); \\ \varphi'' &= k\varphi_0' \sinh kx + \varphi_0'' \cosh kx - \frac{kM_t^0}{C} \sinh kx.\end{aligned}\right\} \quad (234)$$

<sup>29</sup> This method was developed by A. N. Krylov in connection with a discussion of the bending of beams supported by an elastic foundation. See his book *Calculation of Beams on Elastic Foundation*, Russian Academy of Sciences, St. Petersburg, 1931.

Eqs. (233) and (234) are applicable between  $x = 0$  and  $x = a$ , where  $a$  defines the position of the first transverse load.

In considering the second portion of the bar ( $x > a$ ), we have to take into account the torque  $M_t^1$  applied at the cross section  $x = a$ . The expression for the angle of twist in the second portion of the bar is now obtained by adding the angle of twist produced by  $M_t^1$  to eq. (233). In this manner we obtain for  $x > a$

$$\varphi = \varphi_0 + \frac{1}{k} \varphi_0' \sinh kx + \frac{1}{k^2} \varphi_0'' (\cosh kx - 1) + \frac{M_t^0}{C} \left( x - \frac{\sinh kx}{k} \right) + \frac{M_t^1}{C} \left[ x - a - \frac{\sinh k(x-a)}{k} \right]. \quad (235)$$

The last term on the right-hand side represents the angle produced by  $M_t^1$ . It is obtained from the last term of eq. (233) by substituting  $M_t^1$  for  $M_t^0$  and  $x - a$  for  $x$ , since the distance of  $M_t^1$  from the cross section under consideration is  $x - a$ .

In a similar manner we can proceed with the third portion of the bar, and so on to the last portion. The expressions for  $\varphi$  in all portions of the bar contain the same constants  $\varphi_0$ ,  $\varphi_0'$ ,  $\varphi_0''$ , and  $M_t^0$ . All these constants can now be determined from the conditions at the two ends of the bar.

To illustrate the method let us consider several simple examples. We begin with the case in which the bar is twisted by a torque applied at the ends, and at the same time the ends are supported so that they can rotate, but warping is entirely prevented. Since there are no forces applied in the span, eq. (233) can be applied to the entire length of the bar. Assuming that the end  $x = 0$  is immovable and observing that warping is restrained, we have to put  $\varphi_0 = 0$ ,  $\varphi_0' = 0$  into eq. (233), which gives

$$\left. \begin{aligned} \varphi &= \frac{1}{k^2} \varphi_0'' (\cosh kx - 1) + \frac{M_t^0}{C} \left( x - \frac{\sinh kx}{k} \right); \\ \varphi' &= \frac{1}{k} \varphi_0'' \sinh kx + \frac{M_t^0}{C} (1 - \cosh kx). \end{aligned} \right\} \quad (236)$$

Since warping at the other end ( $x = l$ ) of the bar is also restrained,



we have

$$\varphi_l' = \frac{1}{k} \varphi_0'' \sinh kl + \frac{M_t^0}{C} (1 - \cosh kl) = 0,$$

from which

$$\varphi_0'' = - \frac{kM_t^0}{C} \frac{1 - \cosh kl}{\sinh kl}$$

Substituting into the first of eqs (236) we obtain the angle of twist

$$\varphi = \frac{M_t^0}{kC} \left[ \frac{(\cosh kl - 1)(\cosh kx - 1)}{\sinh kl} + kx - \sinh kx \right]$$

Taking  $x = l$ , we obtain the rotation of the end  $x = l$  of the bar

$$\varphi_l = \frac{M_t^0 l}{C} \left( 1 - \frac{\tanh kl/2}{kl/2} \right)$$

The second term in the parentheses gives the effect of the end restraint against warping on the magnitude of the angle of twist

As a second example let us consider the case shown in Fig 162

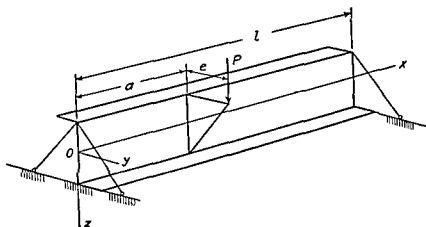


FIG 162

A bar supported at the ends is eccentrically loaded at a distance  $a$  from the left end. Denoting by  $e$  the distance of the load from the shear center axis, we reduce the problem to that of simple bending of the bar by a load  $P$ , combined with torsion produced by the torque  $Pe$ . Assume first that the ends of the bar cannot rotate with respect to the  $x$  axis but are free to warp. In such a case the end conditions are

$$\varphi = \varphi' = 0, \quad \text{for } x = 0 \text{ and } x = l$$

For the portion of the bar from  $x = 0$  to  $x = a$  we use eq (233)

Substituting in this equation  $\varphi_0 = \varphi_0'' = 0$  we obtain

$$\varphi = \frac{1}{k} \varphi_0' \sinh kx + \frac{M_t^0}{C} \left( x - \frac{\sinh kx}{k} \right).$$

For the right-hand portion of the bar ( $x > a$ ) we use eq. (235) which, for  $\varphi_0 = \varphi_0'' = 0$  and  $M_t^1 = Pe$ , gives

$$\begin{aligned} \varphi = \frac{1}{k} \varphi_0' \sinh kx + \frac{M_t^0}{C} \left( x - \frac{\sinh kx}{k} \right) \\ + \frac{Pe}{C} \left[ x - a - \frac{\sinh k(x-a)}{k} \right]. \end{aligned}$$

By differentiation we find

$$\varphi'' = k\varphi_0' \sinh kx - \frac{kM_t^0}{C} \sinh kx - \frac{kPe}{C} \sinh k(x-a).$$

Observing that at the end  $x = l$  the conditions are  $\varphi_l = \varphi_l'' = 0$ , we obtain the following equations for calculating the constants  $\varphi_0'$  and  $M_t^0$ :

$$\varphi_0' \sinh kl + \frac{M_t^0}{C} (kl - \sinh kl) = -\frac{Pe}{C} [kl - ka - \sinh k(l-a)]$$

$$\varphi_0' \sinh kl - \frac{M_t^0}{C} \sinh kl = \frac{Pe}{C} \sinh k(l-a).$$

Solving these equations we obtain

$$M_t^0 = -Pe \frac{l-a}{l}$$

$$\varphi_0' = \frac{Pe}{C} \left[ \frac{\sinh k(l-a)}{\sinh kl} - \frac{l-a}{l} \right].$$

Substituting these values into the expressions for  $\varphi$ , we obtain the angles of twist for both portions of the bar.

If the ends of the bar in Fig. 162 are built in and cannot warp, the end conditions are

$$\varphi = \varphi' = 0, \quad \text{for } x = 0 \text{ and } x = l.$$

Substituting  $\varphi_0 = \varphi_0' = 0$  into eq (235) we obtain, for  $x > a$ ,

$$\varphi = \frac{1}{k^2} \varphi_0'' (\cosh kx - 1) + \frac{M_t^0}{C} \left( x - \frac{\sinh kx}{k} \right) + \frac{Pe}{C} \left[ x - a - \frac{\sinh k(x-a)}{k} \right]$$

Applying this equation at the end  $x = l$  we obtain the following equations for calculating the constants  $\varphi_0''$  and  $M_t^0$

$$\begin{aligned} \varphi_0'' (\cosh kl - 1) + \frac{kM_t^0}{C} (kl - \sinh kl) &= -\frac{kPe}{C} [kl - ka - \sinh k(l-a)], \\ \varphi_0'' \sinh kl + \frac{kM_t^0}{C} (1 - \cosh kl) &= -\frac{kPe}{C} [1 - \cosh k(l-a)] \end{aligned}$$

From these equations the constants  $\varphi_0''$  and  $M_t^0$  can be calculated in each particular case. Substituting them in the expressions for  $\varphi$ , we again have the complete solution of the problem. Having the solution for one concentrated force, as shown in Fig 162, we can find the solution for any number of concentrated forces by superposition.

The case of a distributed load can also be handled without difficulty. As an example, consider again the bar shown in Fig 162 and assume that instead of a force  $P$ , we have a distributed load of constant intensity  $q$  applied along a line parallel to the  $x$  axis and at distance  $e$  from the shear center axis. The torque at any cross section then is

$$M_t = M_t^0 + qex$$

Substituting this value into eq (230) and solving as before, we obtain

$$\begin{aligned} \varphi = \varphi_0 + \frac{1}{k} \varphi_0' \sinh kx + \frac{1}{k^2} \varphi_0'' (\cosh kx - 1) \\ + \frac{M_t^0}{C} \left( x - \frac{\sinh kx}{k} \right) + \frac{qex^2}{2C} \end{aligned}$$

If both ends of the bar are built in rigidly, the end conditions are

$$\varphi = \varphi' = 0, \quad \text{for } x = 0 \text{ and } x = l$$

Then substituting  $\varphi_0 = \varphi_0' = 0$  into the above expression for  $\varphi$ , we obtain

$$\varphi = \frac{1}{k^2} \varphi_0'' (\cosh kx - 1) + \frac{M_t^0}{C} \left( x - \frac{\sinh kx}{k} \right) + \frac{qex^2}{2C}.$$

Applying this equation at the end  $x = l$ , and observing that from symmetry we have

$$M_t^0 = -\frac{qel}{2},$$

the following equation is obtained:

$$\frac{1}{k^2} \varphi_0'' (\cosh kl - 1) - \frac{qel}{2C} \left( l - \frac{\sinh kl}{k} \right) + \frac{qel^2}{2C} = 0,$$

from which

$$\varphi_0'' = -\frac{qekl}{2C} \cdot \frac{\sinh kl}{\cosh kl - 1}.$$

Substituting this value into the expression for  $\varphi$ , we obtain

$$\begin{aligned} \varphi = & -\frac{qel}{2kC} \cdot \frac{\sinh kl}{\cosh kl - 1} (\cosh kx - 1) \\ & - \frac{qel}{2C} \left( x - \frac{\sinh kx}{k} \right) + \frac{qex^2}{2C}. \end{aligned}$$

This expression can be simplified and put in the following form:

$$\varphi = \frac{qel}{kC} \left[ \frac{\sinh \frac{kx}{2}}{\sinh \frac{kl}{2}} \sinh \frac{k(l-x)}{2} - \frac{kx(l-x)}{2l} \right].$$

It is seen from these examples that the solution of eq. (230) can readily be obtained in any particular case.

**51. Torsional Buckling of Thin-walled Members of Open Cross Section.**<sup>30</sup>—It is known that a thin-walled bar under uniform axial compression may sometimes buckle torsionally

<sup>30</sup> See the writer's paper, *J. Franklin Inst.*, Vol. 239, Nos. 3, 4 and 5, p. 263, 1945.

while its axis remains straight. Figure 163 shows an example of this purely torsional buckling in the case of a bar having four identical flanges. The fiber coinciding with the  $x$  axis remains straight during this buckling and the moment  $M_x$  of the compressive forces applied at the end vanishes for each cross section of the bar. To determine the torque producing

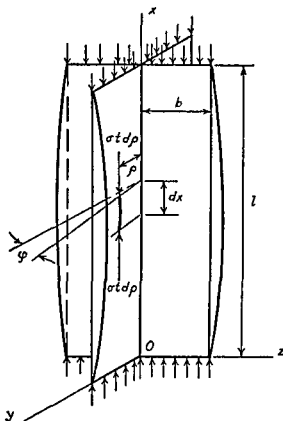


FIG 163.

twist as indicated in the figure, the deflection of the flanges during buckling must be considered.

The method to be used in the following analysis will first be explained by taking the simple case of the buckling of a strut, Fig. 164a. Initially, the strut is straight, and only a centrally applied thrust  $P$  acts on the bar. Let us now assume that the force  $P$  reaches its critical value so that the strut has a slightly deflected form of equilibrium. Owing to this deflection there will be bending stresses superposed on the initial uniformly distributed compressive stresses. At the same time the initial stresses will act on the slightly rotated cross sec-

tions as shown in Fig. 164*b*. Each element of the deflected strut between two adjacent cross sections is in equilibrium, and we can state that the bending stresses produced during buckling of the strut are in equilibrium with the initial com-

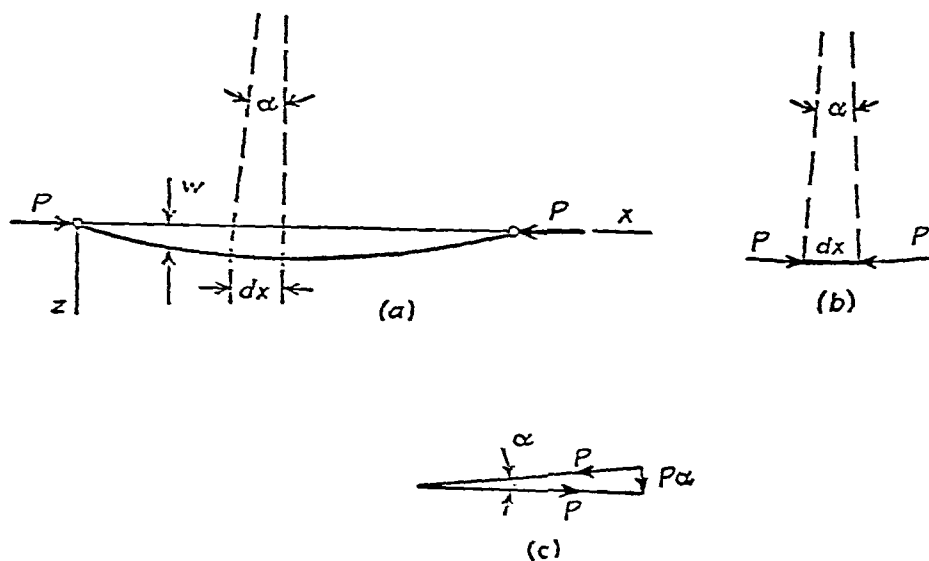


FIG. 164.

pressive stresses acting on the slightly rotated cross sections. The angle between two consecutive cross sections after deflection, Fig. 164*b*, is

$$\alpha = -\frac{d^2w}{dx^2} dx,$$

where  $w$  represents the deflection of the bar in the  $z$  direction. Therefore we conclude that the action of the compressive forces  $P$  on the rotated cross sections of the strut is equivalent to the action on each element of the strut of a transverse load, Fig. 164*c*, equal to

$$-P \frac{d^2w}{dx^2} dx.$$

We see that the deflection curve of the strut and the corresponding bending stresses can be found by assuming that the strut is loaded by a fictitious load of intensity  $-Pd^2w/dx^2$ .

The differential equation of the deflection curve in this case is

$$EI_v \frac{d^4 w}{dx^4} = -P \frac{d^2 w}{dx^2}.$$

From this equation the known critical value of the compressive force  $P_{cr}$  can be obtained in the usual way.

Returning now to the problem of torsional buckling, shown in Fig. 163, we can state that under the critical condition the buckled form of equilibrium is sustained by the longitudinal compressive stresses acting on rotated cross sections of the fibers. Assuming that the thickness  $t$  of the flanges is small and considering a strip of cross section  $t d\rho$  at a distance  $\rho$  from the axis, we see that owing to torsional buckling the deflection is  $w = \rho\varphi$ . Taking one element of this strip between two consecutive cross sections, distance  $dx$  apart, and considering the action of the initial compressive force  $\sigma t d\rho$  on the slightly rotated cross sections of the strip, Fig. 163, we obtain the transverse force

$$-(\sigma t d\rho) \frac{d^2 w}{dx^2} dx = -(\sigma t d\rho) \rho \frac{d^2 \varphi}{dx^2} dx.$$

The moment of this force with respect to the  $x$  axis is

$$-\sigma \frac{d^2 \varphi}{dx^2} dx (t \rho^2 d\rho).$$

Summing up these moments and extending the summation over the entire cross section, we obtain the torque acting on the element of the torsionally buckled bar included between two consecutive cross sections. Using the notation  $m_x$  for torque per unit length of the bar, we obtain

$$m_x = -4\sigma \frac{d^2 \varphi}{dx^2} \int_0^b t \rho^2 d\rho = -\sigma \frac{d^2 \varphi}{dx^2} I_0, \quad (a)$$

where  $I_0$  is the polar moment of inertia of the cross section of the bar with respect to the shear center, coinciding in this case with the centroid of the cross section. To establish now the equation for the buckled bar, we use eq. (230). Differen-

tiating this equation with respect to  $x$  and observing that

$$m_x = - \frac{dM_t}{dx},$$

we find

$$C_1 \varphi'''' - C \varphi'' = m_x. \quad (237)$$

Substituting for  $m_x$  its value given by eq. (a), we obtain

$$C_1 \varphi'''' - (C - \sigma I_0) \varphi'' = 0. \quad (238)$$

From this equation the critical value of the compressive stress  $\sigma$  will now be obtained.

For the case shown in Fig. 163, the middle lines of all flanges intersect in one point, and therefore the warping rigidity  $C_1$  vanishes; hence eq. (238) becomes

$$(C - \sigma I_0) \varphi'' = 0.$$

This equation is satisfied by assuming that the quantity in parentheses vanishes, which gives

$$\sigma_{cr} = \frac{C}{I_0} = \frac{\frac{4}{3} b t^3 G}{\frac{4}{3} t b^3} = G \frac{t^2}{b^2}. \quad (239)$$

Eq. (239) indicates that the critical value of compressive stress is independent of the length of the bar and of the form of buckling defined by the angle  $\varphi$ . Such a result is obtained because in the derivation of eq. (230) any resistance of the flanges to bending in the direction perpendicular to the plane of the flange was neglected. To take such bending into account we have to consider each flange as a uniformly compressed plate simply supported along three sides and entirely free to buckle along the fourth side. This more accurate investigation shows that the critical stress is <sup>31</sup>

$$\sigma_{cr} = \left( 0.456 + \frac{b^2}{l^2} \right) \frac{\pi^2}{6(1 - \mu)} \frac{G t^2}{b^2}.$$

The second term in parentheses gives the influence on the critical stress of the length of the bar. For bars of considerable

<sup>31</sup> This solution was obtained by the writer; see *Bull. Polytech. Inst. (Kiev)*, 1907, and *Z. Math. u. Phys.*, Vol. 58, p. 337, 1910.



length this term can be neglected. Then we obtain

$$\sigma_{cr} = \frac{0.75}{1 - \mu} \frac{Gt^2}{b^2}.$$

For  $\mu = 0.3$  this value is larger than the value calculated above (eq. 239) by about 7 per cent.

Eq. (238) also holds in cases when  $C_1$  does not vanish, and is valid for unsymmetrical cross sections, provided the axis of the bar remains straight during buckling. This requires, as we shall see in the next article, that the shear center axis and the centroidal axis must coincide, as in the case of a Z section. In all such cases the critical compressive stress is obtained from the solution of eq. (238). Introducing the notation

$$k^2 = \frac{\sigma I_0 - C}{C_1}, \quad (b)$$

we find that this solution is

$$\varphi = A \sin kx + A_1 \cos kx + A_2 x + A_3. \quad (240)$$

If the ends of the compressed bar cannot rotate but are free to warp, we have the following conditions at the ends:

$$\varphi = \varphi'' = 0, \quad \text{for } x = 0 \text{ and } x = l,$$

from which follows

$$A_1 = A_2 = A_3 = 0 \quad \text{and} \quad kl = n\pi.$$

Substituting this value for  $k$  into eq. (b) we obtain

$$\sigma I_0 - C = \frac{n^2 \pi^2}{l^2} C_1.$$

The smallest value of  $\sigma$  satisfying this condition is <sup>22</sup>

$$\sigma_{cr} = \frac{1}{I_0} \left( C + \frac{\pi^2}{l^2} C_1 \right). \quad (241)$$

<sup>22</sup> This solution was obtained by H. Wagner, *25th Anniversary Publication*, Technische Hochschule, Danzig, p. 329, 1929.

If the ends of the bar are built in and cannot warp, the end conditions are

$$\varphi = \varphi' = 0, \quad \text{for } x = 0 \text{ and } x = l.$$

To satisfy these conditions we must take

$$A_1 = -A_3, \quad A = A_2 = 0, \quad \text{and} \quad kl = 2n\pi.$$

The lowest critical compressive stress in this case is

$$\sigma_{cr} = \frac{1}{I_0} \left( C + \frac{\frac{1}{4}\pi^2}{l^2} C_1 \right).$$

52. Buckling of Thin-walled Members of Open Cross Section by Simultaneous Bending and Torsion.<sup>33</sup>—Let us consider now the general case of buckling where, under central thrust, not only torsion but also bending of the axis of the compressed member occurs. We assume that  $y$  and  $z$  are the principal centroidal axes of the cross section of the bar before buckling (Fig. 165) and  $y_0, z_0$  are the coordinates of the shear center  $O$ . The deflections of the shear center axis in the  $y$  and  $z$  directions during buckling are denoted by  $v$  and  $w$ , respectively, and  $\varphi$  denotes the angle of rotation of any cross section with respect to the shear center axis. In Fig. 165

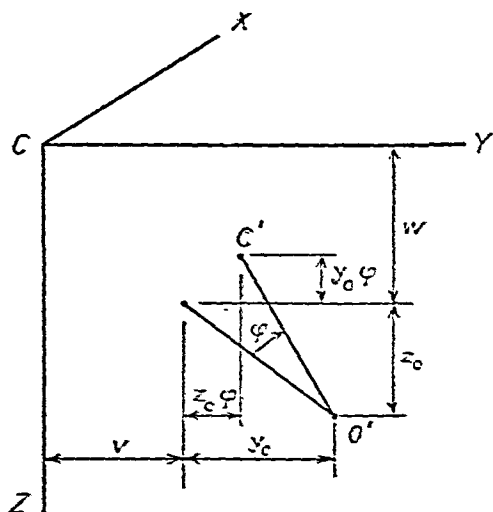


FIG. 165.

<sup>33</sup> Torsional buckling was discussed by H. Wagner, *loc. cit.*, p. 278. See also H. Wagner and W. Pretschner, *Luftfahrtforsch.*, Vol. 11, p. 174, 1934; and R. Kappus, *ibid.*, Vol. 14, p. 444, 1937. An English translation of the latter paper is given in *Nat. Advisory Comm. Aeronaut. Tech. Mem.*, No. 851, 1938. See also the writer's paper, *J. Franklin Inst.*, Vol. 239, Nos. 3, 4 and 5, p. 201, 1945; J. N. Goodier, *Cornell Univ. Eng. Exp. Sta. Bull.*, No. 27, 1941 and No. 28, 1942; and the book by V. Z. Vlasov, *Thin-walled Elastic P*, Moscow, 1940 (in Russian). Regarding experiments with torsional first see the paper by A. S. Niles, *Nat. Advisory Comm. Aeronaut.*, No. 937, and No. 733, 1939.

the points  $C'$  and  $O'$  represent the deflected positions of the centroid  $C$  and the shear center  $O$ . Then the deflections of the centroidal axis during buckling are

$$v + z_0\varphi \quad \text{and} \quad w - y_0\varphi.$$

Assuming that a thrust  $P$  acts at the ends of the bar along the  $x$  axis, as in the case of a simply supported bar, we find that the bending moments with respect to the principal axes at any cross section are

$$M_y = P(w - y_0\varphi), \quad M_z = -P(v + z_0\varphi).$$

The differential equations for the deflection curve of the shear center axis become

$$\begin{aligned} EI_z \frac{d^2 v}{dx^2} &= -P(v + z_0\varphi), \\ EI_y \frac{d^2 w}{dx^2} &= -P(w - y_0\varphi). \end{aligned} \tag{242}$$

In addition to the bending of the strut as given by eqs. (242), there will be torsional deformation. To write the equation for the angle of twist  $\varphi$ , we proceed as in Art. 51. We take a strip of cross section  $tds$ <sup>24</sup> defined by coordinates  $y$  and  $z$  in the plane of the cross section. The components of its deflection in the  $y$  and  $z$  directions during buckling are

$$v + (z_0 - z)\varphi \quad \text{and} \quad w - (y_0 - y)\varphi.$$

Taking the second derivatives of these expressions with respect to  $x$  and considering an element  $dx$  of the fiber, we find as before that the compressive forces  $\sigma t ds$  acting on the slightly rotated ends of the element  $dx$  give the following forces in the  $y$  and  $z$  directions:

$$\begin{aligned} -\sigma t ds \frac{d^2}{dx^2} [v + (z_0 - z)\varphi] dx, \\ -\sigma t ds \frac{d^2}{dx^2} [w - (y_0 - y)\varphi] dx. \end{aligned}$$

<sup>24</sup> The quantity  $ds$  is an element of length along the middle line of the section, Techn.

Again denoting by primes a derivative with respect to  $x$ , and taking the moments of the above forces with respect to the shear center axis, we obtain, as the contribution of one strip, the following torque per unit length of the bar:

$$dm_z = -\sigma t ds [\vartheta'' + (z_0 - z)\varphi''] (z_0 - z) \\ + \sigma t ds [\omega'' - (y_0 - y)\varphi''] (y_0 - y).$$

Integrating over the entire cross section and observing that

$$\sigma \int_A t ds = P, \quad \int_A z t ds = 0, \quad \int_A y t ds = 0, \\ \int_A z^2 t ds = I_y, \quad \int_A y^2 t ds = I_z,$$

we obtain

$$m_z = (y_0 \omega'' - z_0 \vartheta'') P - r_0^2 P \varphi'', \quad (a)$$

where

$$r_0^2 = y_0^2 + z_0^2 + \frac{I_y + I_z}{A}.$$

That is,  $r_0$  is the polar radius of gyration of the cross section with respect to the shear center. Substituting the calculated value of  $m_z$  (eq. *a*) into eq. (237) we obtain

$$C_1 \varphi'''' - (C - r_0^2 P) \varphi'' - P(y_0 \omega'' - z_0 \vartheta'') = 0. \quad (243)$$

This equation together with eqs. (242) will now be used to determine the critical value of the thrust  $P$ .<sup>35</sup>

It is seen that the angle of rotation  $\varphi$  enters into all three equations, indicating that, in general, torsional buckling is accompanied by bending of the axis, and we have combined torsional and flexural buckling. In the particular case when  $y_0 = z_0 = 0$ , i.e., when the shear center axis coincides with the centroidal axis, each of eqs. (242) and (243) contains only one unknown and can be treated separately. Eqs. (242) then give two values of the critical load, corresponding to buckling in two principal planes as given by the Euler theory, and

<sup>35</sup> A system of equations equivalent to eqs. (242) and (243) was first obtained by Robert Kappus; see *Jahrb. deut. Luftfahrtforsch.*, 1937, and *Luftfahrtforsch.*, Vol. 14, p. 444, 1938.

eq. (243) gives the critical load for purely torsional buckling, as already discussed in Art. 51. From these three values of the critical load, the smallest will naturally be taken into consideration in practical applications.

Returning to the general case, let us assume that the ends of the compressed bar cannot rotate with respect to the  $x$  axis, Fig. 163, but are free to warp and to rotate freely with respect to the  $y$  and  $z$  axes (simply supported ends). In such a case, the end conditions are

$$\left. \begin{aligned} v &= w = \varphi = 0 \\ v'' &= w'' = \varphi'' = 0 \end{aligned} \right\} \text{for } x = 0 \text{ and } x = l.$$

All of these conditions will be satisfied by taking the solutions of eqs. (242) and (243) in the form

$$v = A_1 \sin \frac{\pi x}{l}, \quad w = A_2 \sin \frac{\pi x}{l}, \quad \varphi = A_3 \sin \frac{\pi x}{l}. \quad (244)$$

Substituting these expressions into eqs. (242) and (243), we obtain the following equations for calculating the constants  $A_1$ ,  $A_2$  and  $A_3$ :

$$\left. \begin{aligned} \left( P - EI_z \frac{\pi^2}{l^2} \right) A_1 + Pz_0 A_3 &= 0, \\ \left( P - EI_y \frac{\pi^2}{l^2} \right) A_2 - Py_0 A_3 &= 0, \\ Pz_0 A_1 - Py_0 A_2 + \left( -C_1 \frac{\pi^2}{l^2} - C + r_0^2 P \right) A_3 &= 0. \end{aligned} \right\} \quad (245)$$

These equations are satisfied by taking  $A_1 = A_2 = A_3 = 0$ , which corresponds to the straight form of equilibrium of the compressed strut. To have a buckled form of equilibrium eqs. (245) must yield for  $A_1$ ,  $A_2$  and  $A_3$  solutions different from zero, which is possible only if the determinant of eqs. (245) vanishes. To simplify the writing we introduce here the notation

$$P_1 = \frac{\pi^2 EI_z}{l^2}, \quad P_2 = \frac{\pi^2 EI_y}{l^2}, \quad P_3 = \frac{1}{r_0^2} \left( C + C_1 \frac{\pi^2}{l^2} \right) \quad (246)$$

in which  $P_1$  and  $P_2$  are the Euler loads for buckling in two principal planes and  $P_3$  denotes the critical load for purely torsional buckling, as given by eq. (241). Then equating to zero the determinant of eqs. (245), we obtain

$$\begin{vmatrix} P - P_1 & 0 & z_0 P \\ 0 & P - P_2 & -y_0 P \\ z_0 P & -y_0 P & r_0^2(P - P_3) \end{vmatrix} = 0,$$

which, after expanding, gives the following cubic equation for calculating the critical values of  $P$ :

$$\begin{aligned} & (-r_0^2 + y_0^2 + z_0^2)P^3 \\ & + [(P_1 + P_2 + P_3)r_0^2 - y_0^2 P_1 - z_0^2 P_2]P^2 \\ & - r_0^2(P_1 P_2 + P_2 P_3 + P_1 P_3)P + P_1 P_2 P_3 r_0^2 = 0. \end{aligned} \quad (247)$$

From this equation one important conclusion can be obtained. Assuming that  $P_1 < P_2$ , i.e., that the smaller Euler load corresponds to bending in the  $xy$  plane, let us investigate the sign of the left-hand side of eq. (247) for various values of  $P$ . If  $P$  is very small, we can neglect all terms containing  $P$ , and the left-hand side of the expression reduces to  $P_1 P_2 P_3 r_0^2$ , which is positive. If  $P$  takes the value  $P_1$ , then the left-hand side of eq. (247) reduces to  $z_0^2 P_1^2 (P_1 - P_2)$  which is negative since  $P_1 < P_2$ . This indicates that eq. (247) has a root smaller than  $P_1$ . Therefore we conclude that when the possibility of torsion during buckling is considered, we always obtain a critical load smaller than the Euler load.

To find the critical load in any particular case, we calculate, by using the notation of eqs. (246), the numerical values of the coefficients in eq. (247) and then solve this cubic equation.<sup>35</sup> We thus obtain three values for  $P$  from which the smallest will be taken in practical applications. Substituting the critical values into eqs. (245), we find for each possible critical form the ratios  $A_1:A_3$  and  $A_2:A_3$ . These ratios, establishing the relations between rotation and translation of

<sup>35</sup> This solution can be greatly simplified by the use of a nomogram as shown in the paper by Kappus, *loc. cit.*, p. 281.

the cross sections, define for each critical form the position of the shear center axis and the rotation about that axis.

If the bar has very thin walls and the length  $l$  is short, then  $P_3$  may become small in comparison with  $P_1$  and  $P_2$ . In such a case the smallest root of eq. (247) approaches the value  $P_3$ . Substituting this value into eqs. (245), we find that  $A_1$  and  $A_2$  are small in comparison with the rotational displacements, which indicates that the buckled form approaches purely torsional buckling as discussed in Art. 51. In the case of a thick wall and large length  $l$ ,  $P_3$  is usually large in comparison with  $P_1$  and  $P_2$  and the smallest root of eq. (247) approaches the value  $P_1$ . The effect of torsion on the critical load is small in such a case, and the usual column formula gives satisfactory results.

If the cross section has an axis of symmetry, the calculation of  $P_{cr}$  is simplified. Let the  $y$  axis be the axis of symmetry, then  $z_0 = 0$  and the term containing  $\varphi$  in the first of eqs. (242) vanishes. The buckling of the bar in the plane of symmetry is independent of torsion, and the corresponding critical load is given by Euler's formula. We have to consider only bending perpendicular to the plane of symmetry and torsion. The corresponding equations are

$$EI_y w'' = -P(w - y_0 \varphi),$$

$$C_1 \varphi'''' - (C - r_0^2 P) \varphi'' = P y_0 w''.$$

Proceeding as before and using eq. (244), we obtain for calculating the critical load

$$\begin{vmatrix} P - P_2 & -y_0 P \\ -y_0 P & r_0^2 (P - P_3) \end{vmatrix} = 0,$$

which gives

$$r_0^2 (P - P_2)(P - P_3) - y_0^2 P^2 = 0. \quad (248)$$

This quadratic equation gives two solutions. Together with the Euler load for buckling in the plane of symmetry, they represent the three critical values for  $P$ , of which the smallest must be used in practical applications. Considering the left-

hand side of eq. (248), we see that for very small values of  $P$  it reduces to the value  $r_0^2 P_2 P_3$ , which is positive. We see also that it is negative for  $P = P_2$  and for  $P = P_3$ , since its value then reduces to  $-y_0^2 P^2$ . It is negative also for all values of  $P$  between  $P = P_2$  and  $P = P_3$ , since the first term becomes negative and the second is always negative. From this discussion we conclude that one root of eq. (248) is smaller than either  $P_2$  or  $P_3$ , while the other is larger than either. The smaller of these roots or the Euler load for buckling in the plane of symmetry gives the required critical load.

All the above conclusions are based on eq. (244). Without any complication we can take the solution in a more general form and assume

$$v = A_1 \sin \frac{n\pi x}{l}, \quad w = A_2 \sin \frac{n\pi x}{l}, \quad \varphi = A_3 \sin \frac{n\pi x}{l}, \quad (249)$$

which corresponds to the assumption that during buckling the bar is subdivided into  $n$  half-waves. Our previous conclusions will also hold in this case; we have only to substitute into eq. (246) the values  $n^2\pi^2/l^2$  instead of  $\pi^2/l^2$ . The corresponding critical values of the load will naturally be larger than those obtained for buckling in one half-wave and are of practical interest only if the bar has intermediate equidistant lateral supports.

If the ends of the bar are built in, the end conditions are

$$\left. \begin{aligned} v &= w = \varphi = 0 \\ v' &= w' = \varphi' = 0 \end{aligned} \right\} \text{for } x = 0 \text{ and } x = l.$$

Since, during buckling, end moments will appear, we will have the following equations instead of eqs. (242):

$$\begin{aligned} EI_z \frac{d^2 v}{dx^2} &= -P(v + z_0 \varphi) + EI_z \left( \frac{d^2 v}{dx^2} \right)_{x=0} \\ EI_y \frac{d^2 w}{dx^2} &= -P(w - y_0 \varphi) + EI_y \left( \frac{d^2 w}{dx^2} \right)_{x=0} \end{aligned} \quad (250)$$



These equations, together with eq. (243),<sup>37</sup> define the buckling forms of the bar and the corresponding critical loads. All these equations and the end conditions will be satisfied by taking

$$\begin{aligned} v &= A_1 \left( 1 - \cos \frac{2\pi x}{l} \right), & w &= A_2 \left( 1 - \cos \frac{2\pi x}{l} \right), \\ \varphi &= A_3 \left( 1 - \cos \frac{2\pi x}{l} \right). \end{aligned} \quad (251)$$

Substituting these expressions into eqs. (243) and (250), we obtain the same eq. (247) for calculating the critical loads; it is only necessary to use  $4\pi^2/l^2$  instead of  $\pi^2/l^2$  in the notations of eqs. (246).

**53. Longitudinal Normal Stresses in Twisted Bars.**—In discussing the torsion of circular shafts (Part I, p. 281) it was assumed that the distance between any two cross sections of the shaft remained unchanged during torsion. It will now be shown that this assumption is very accurate for small deformations, as in steel shafts. But for a material such as rubber the maximum shearing strain during torsion may be considerable. Then the change in the distances between the cross sections of the shaft during torsion must be taken into account if we wish to find the correct values of the stresses. The same conclusion also holds for steel torsional members of narrow rectangular cross section or of thin-walled cross section such as are shown in Fig. 144.

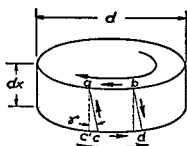


FIG. 166.

Let us begin the discussion with the case of a solid circular shaft and assume first that the distance between two consecutive cross sections, Fig. 166, remains unchanged during torsion. If  $\gamma$  is the shearing strain at the surface of the shaft, the elongation of the longitudinal fiber  $ac$  is obtained from the triangle  $acc'$  as follows:

$$ac = \frac{ac'}{\cos \gamma} = ac' \left( 1 + \frac{1}{2} \gamma^2 \right).$$

<sup>37</sup> Eq. (243) was developed from a consideration of an element of the bar between two adjacent cross sections and is not affected by changes in the end conditions.

Expressing  $\gamma$  in terms of the angle of twist per unit length  $\theta$ , we obtain

$$\alpha c = \alpha c' \left[ 1 + \frac{1}{2} \left( \frac{\theta d}{2} \right)^2 \right]$$

and the unit elongation of the fiber  $\alpha c$  is

$$\epsilon_{\max} = \frac{\alpha c - \alpha c'}{\alpha c'} = \frac{1}{2} \gamma^2 = \frac{1}{8} \theta^2 d^2 = \frac{1}{2} \frac{\tau_{\max}^2}{G^2}. \quad (a)$$

The corresponding tensile stress is

$$\sigma_{\max} = \epsilon_{\max} E = \frac{E}{2} \cdot \frac{\tau_{\max}^2}{G^2}.$$

For any other fiber at a distance  $r$  from the axis of the shaft, the unit shear is less than  $\gamma$  in the ratio  $r:d/2$ , and the tensile stress is

$$\sigma = \sigma_{\max} \left( \frac{2r}{d} \right)^2 = E \frac{2r^2}{d^2} \frac{\tau_{\max}^2}{G^2}. \quad (b)$$

The assumption that the distance between the cross sections remains unchanged during twist brings us therefore to the conclusion that a longitudinal tensile force, producing tensile stresses (eq. *b*), must be applied at the ends to keep the length unchanged. If no such force is applied, then twisting due to a pure torque will be accompanied by shortening of the shaft. Let  $\epsilon_0$  be the corresponding unit shortening. Then instead of eq. (*b*) we obtain

$$\sigma = \frac{2r^2}{d^2} \frac{E \tau_{\max}^2}{G^2} - \epsilon_0 E. \quad (c)$$

The quantity  $\epsilon_0$  is determined from the condition that the longitudinal force corresponding to the stress distribution (eq. *c*) must be equal to zero. Dividing the cross section into elemental rings and making a summation of forces corresponding to the stresses of eq. (*c*), we obtain<sup>33</sup>

$$\begin{aligned} \int_0^{d/2} 2\pi r \sigma dr &= 2\pi \int_0^{d/2} \left( \frac{2r^2}{d^2} \frac{E \tau_{\max}^2}{G^2} - \epsilon_0 E \right) r dr \\ &= \frac{\pi d^2 E}{2} \left( \frac{\tau_{\max}^2}{G^2} - \epsilon_0 \right) = 0, \end{aligned}$$

<sup>33</sup> It is assumed that the cosine of the angle between the fibers and the axis of the bar can be taken equal to unity.

from which

$$\epsilon_0 = \frac{\tau_{\max}^2}{4G^2},$$

and the stress distribution, from eq. (c), becomes

$$\sigma = \frac{E\tau_{\max}^2}{4G^2} \left( \frac{8r^2}{d^2} - 1 \right). \quad (252)$$

The maximum stress occurs at the outer surface where  $r = d/2$ , and we obtain

$$\sigma_{\max} = \frac{E\tau_{\max}^2}{4G^2} \quad (253)$$

At the center of the cross section we obtain a compressive stress of the same amount.

It is interesting to note that the stress  $\sigma$  is proportional to  $\tau_{\max}^2$ ; hence the importance of this stress increases with increasing  $\tau_{\max}$ , i.e., with increasing angle of twist. For a material such as steel  $\tau_{\max}$  is always very small in comparison with  $G$ , and the magnitude of  $\sigma_{\max}$  is therefore small in comparison with  $\tau_{\max}$  and can be neglected. But for a material like rubber  $\tau_{\max}$  may be of the same order as  $G$ ; hence  $\sigma_{\max}$  will no longer be small in comparison with  $\tau_{\max}$  and must be taken into consideration.

The first investigation of axial deformation due to torsion of a circular shaft was made by Thomas Young.<sup>39</sup> He showed that owing to tension in inclined fibers, such as fiber  $ac$  in Fig. 166, there will be an additional resistance of the shaft to torsion proportional to  $\theta^3$ .

If instead of a circular cross section we have a narrow rectangular section, it can be shown<sup>40</sup> that even for materials such as steel the stress  $\sigma$  may become of the same order of magnitude as  $\tau_{\max}$ . If the longer side  $b$  of the cross section is large in comparison with the shorter side  $c$ , the maximum elongation of the most remote fiber due to twist alone is obtained from eq. (a) by substituting  $b$  for  $d$ :

$$\epsilon_{\max} = \frac{b^2}{8} \theta^2.$$

For any fiber at distance  $y$  from the axis, the elongation is less than  $\epsilon_{\max}$  in the ratio  $(2y/b)^2$ . Combining this elongation with the longi-

<sup>39</sup> See Thomas Young, *A Course of Lectures on Natural Philosophy*, etc., London, 1807.

<sup>40</sup> See the paper by Buckley, *Phil. Mag.*, p. 778, 1914. See also C. Weber, *loc. cit.*, p. 236, and also his paper in *Festschrift zum 70. Geburtstage August Föppl*, Berlin, 1924.

tudinal unit contraction  $\epsilon_0$ , we obtain

$$\epsilon = \frac{b^2}{8} \theta^2 \left( \frac{2y}{b} \right)^2 - \epsilon_0 = \frac{\theta^2 y^2}{2} - \epsilon_0.$$

The corresponding tensile stress is

$$\sigma = E \left( \frac{\theta^2 y^2}{2} - \epsilon_0 \right). \quad (d)$$

The constant  $\epsilon_0$  is determined, as before, from the condition that the tensile longitudinal force is equal to zero; hence

$$\int_{-b/2}^{b/2} c \sigma dy = cE \int_{-b/2}^{b/2} \left( \frac{\theta^2}{2} y^2 - \epsilon_0 \right) dy = cE \left( \frac{\theta^2}{2} \cdot \frac{b^3}{12} - \epsilon_0 b \right) = 0,$$

from which

$$\epsilon_0 = \frac{\theta^2}{2} \cdot \frac{b^2}{12},$$

and we obtain from eq. (d),

$$\sigma = \frac{E\theta^2}{2} \left( y^2 - \frac{b^2}{12} \right). \quad (e)$$

The maximum tensile stress for the most remote fiber ( $y = b/2$ ) is

$$\sigma_{\max} = \frac{E\theta^2 b^2}{12}. \quad (f)$$

The maximum compressive stress at the center ( $y = 0$ ) is

$$\sigma_{\min} = -\frac{E\theta^2 b^2}{24}. \quad (g)$$

To compare these longitudinal stresses with  $\tau_{\max}$ , eqs. (221) and (222) can be used. For a narrow rectangular section we obtain from those equations

$$\theta = \frac{\tau_{\max}}{cG}. \quad (h)$$

Substituting this relation into eqs. (f) and (g) we obtain

$$\sigma_{\max} = \frac{E\tau_{\max}^2}{12G^2} \cdot \frac{b^2}{c^2}; \quad \sigma_{\min} = -\frac{E\tau_{\max}^2}{24G^2} \cdot \frac{b^2}{c^2}. \quad (254)$$

It is seen that when  $b/c$  is large, the stresses  $\sigma_{\max}$  and  $\sigma_{\min}$  may not be small in comparison with  $\tau_{\max}$ . The distribution of the stresses

(see eq *e*) is shown <sup>41</sup> in Fig 167. These stresses have the direction of the longitudinal fibers of the twisted strip, and are inclined to the axis of the strip at an angle  $\theta y$ . Their projections on a plane perpendicular to the axis of the bar are



FIG 167

$$\sigma_{\theta y} = \frac{E\theta^3}{2} \left( y^3 - \frac{b^2 y}{12} \right) \quad (i)$$

The component (eq *i*) of the stress  $\sigma$  per element  $cdy$  of the cross section gives a moment with respect to the axis of the bar equal to

$$\frac{E\theta^3}{2} \left( y^3 - \frac{b^2 y}{12} \right) c y d y$$

Hence the torque resulting from the stresses  $\sigma$  is

$$\int_{-b/2}^{b/2} \frac{E\theta^3}{2} \left( y^3 - \frac{b^2 y}{12} \right) c y d y = \frac{E c b^5}{360} \theta^3$$

Combining this torque with the torque due to shearing stresses (eq 221, p 240), we obtain the following expression for the total torque

$$M_t = \frac{1}{3} b c^3 G \theta + \frac{1}{360} E c b^5 \theta^3 = \frac{1}{3} b c^3 G \theta \left( 1 + \frac{1}{120} \frac{E b^4}{G c^2} \theta^2 \right) \quad (255)$$

It can be seen that in the case of a very narrow rectangular cross section and comparatively large angles of twist, the stress  $\sigma$  may contribute an important portion of the torque, since this portion, represented by the second term in eq (255), varies as  $\theta^3$ , while the portion due to the shearing stresses  $\tau$  varies as  $\theta$ . When the magnitude of the torque is given, the corresponding angle of twist  $\theta$  may be found from eq (255). The maximum shearing stress  $\tau_{\max}$  is then calculated from eq (h) and  $\sigma_{\max}$ ,  $\sigma_{\min}$  from eqs (254).

As an example let us take a bar of narrow rectangular cross section as follows:  $b = 4$  in,  $c = 0.05$  in,  $E/G = 2.6$ ,  $G = 11.5 \times 10^6$  lb per sq in, and  $M_t = \frac{1}{3} b c^2 \times 15,000 = 50$  in lb. If the normal stresses  $\sigma$  be neglected, eq (222) gives  $\tau_{\max} \approx 15,000$  lb per sq in, and eq (221) gives

$$\theta = \frac{\tau_{\max}}{cG} = 0.0261 \text{ in}^{-1}$$

<sup>41</sup> This stress distribution takes place at some distance from the ends of the bar. Near the ends a more complicated stress distribution than given by eq (e) is produced. It is such as to make the ends entirely free from normal stresses. This kind of stress distribution is discussed in Timoshenko and Goodier, *Theory of Elasticity*, p 167, 1951.

If the longitudinal stresses are considered, eq. (255) must be used. From this equation, after dividing by  $\frac{1}{3}bc^3G$ , we obtain

$$0.0261 = \theta(1 + 2,220\theta^2),$$

from which  $\theta = 0.0164 \text{ in.}^{-1}$ . Then from eqs. (h) and (254)

$$\tau_{\max} = cG\theta = 9,430 \text{ lb per sq in.},$$

$$\sigma_{\max} = \frac{E\tau_{\max}^2 b^2}{12G^2 c^2} = 10,700 \text{ lb per sq in.}$$

It can be seen that for a large angle of twist of a thin metallic strip, as in this example, the normal stresses  $\sigma$  are of the same order as the shearing stresses  $\tau$  and cannot be neglected in calculating the angle of twist.

From the above discussion it may also be concluded that a uniform longitudinal tension will have some influence on the angle of twist of a thin rectangular strip. Assume, for example, that a uniform longitudinal tensile stress  $\sigma_0$  is applied to the strip which was just considered. In such a case the equation for calculating  $\epsilon_0$  is

$$cE\left(\frac{\theta^2}{2} \frac{b^3}{12} - \epsilon_0 b\right) = \sigma_0 bc,$$

and we obtain

$$\epsilon_0 = \frac{\theta^2}{2} \frac{b^2}{12} - \frac{\sigma_0}{E}.$$

The expression for the longitudinal stress  $\sigma$  then becomes

$$\sigma = \frac{E\theta^2}{2} \left(y^2 - \frac{b^2}{12}\right) + \sigma_0$$

and the corresponding torque is

$$\int_{-b/2}^{+b/2} \sigma \theta y \cdot cy dy = \frac{Ec b^5}{360} \theta^3 + \frac{\sigma_0 \theta b^3 c}{12}.$$

For the total torque, instead of eq. (255), we then obtain

$$M_t = \frac{1}{3} bc^3 G \theta \left(1 + \frac{1}{120} \frac{E b^4}{G c^2} \theta^2 + \frac{1}{4} \frac{\sigma_0}{G} \cdot \frac{b^2}{c^2}\right). \quad (256)$$

It is seen that when  $b/c$  is a large number, i.e., in the case of a thin strip, the tensile stress may reduce considerably the angle of twist  $\theta$ .

54. Open-coiled Helical Spring.—In the previous discussion of helical springs (see Part I, p 290) it was assumed that the angle  $\alpha$

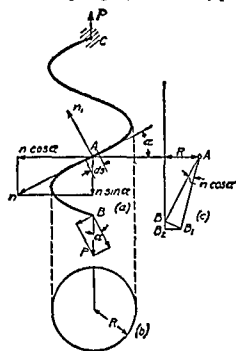


FIG 168

between the coils and a plane perpendicular to the axis of the helix was very small. With the effect of this angle neglected, the deformation consists only of the twisting of the wire. In open-coiled springs the angle  $\alpha$  is no longer small, and the deformation produced by the axial loads  $P$  consists of both twist and bending (Fig 168). At any point  $A$  the tangent to the helical center line of the spring is not perpendicular to the force  $P$ , and therefore this force produces at cross section  $A$  a bending moment about the axis  $n_1$  and a torque. The force  $P$  is resolved into two components  $P \cos \alpha$ , perpendicular to the tangent at  $A$ , and  $P \sin \alpha$ , parallel to the tangent at  $A$ . At cross section

$A$  the component  $P \cos \alpha$  produces the torque

$$M_t = PR \cos \alpha, \quad (a)$$

where  $R$  is the radius of the helix, and the component  $P \sin \alpha$  produces the bending moment

$$M = PR \sin \alpha \quad (b)$$

The maximum combined stress is (see Part I, p 297)

$$\sigma_{\max} = \frac{16}{\pi d^3} (M + \sqrt{M^2 + M_t^2}) = \frac{16PR}{\pi d^3} (1 + \sin \alpha), \quad (257)$$

in which  $d$  is the diameter of the wire. The maximum shearing stress is <sup>42</sup>

$$\tau_{\max} = \frac{16}{\pi d^3} \sqrt{M^2 + M_t^2} = \frac{16PR}{\pi d^3} \quad (258)$$

<sup>42</sup> If the diameter  $d$  of the wire is not very small in comparison with the diameter  $2R$  of the helix, this value must be multiplied by a correction factor, which, for  $\alpha < 20^\circ$ , can be taken to be the same as for close coiled springs (Part I, p 292). A further discussion of this subject is given by O Göhner, *Z Ver deut Ing*, Vol 76, p 269, 1932. See also Timoshenko and Goodier, *Theory of Elasticity*, p 391, 1951.

Let us consider now the deflection of the spring on the assumption that it is fixed at the upper end and loaded by an axial load  $P$  at the lower end. An element  $ds$  between two adjacent cross sections at  $A$  is twisted by the torque  $M_t$  through the angle

$$d\phi = \frac{PR \cos \alpha}{GI_p} ds. \quad (c)$$

Owing to this twist the lower portion of the spring rotates about the tangent at  $A$  through the angle  $d\phi$ . This small rotation is represented in Fig. 168 by the vector  $\pi$  along the tangent. The positive direction of the vector is such that between the direction of the vector and the direction of rotation there exists the same relation as between the displacement and the rotation of a right-hand screw. The small rotation  $\pi$  may be resolved into two components: (1) a rotation  $\pi \cos \alpha$  about a horizontal axis, and (2) a rotation  $\pi \sin \alpha$  about a vertical axis. The latter rotation does not produce any lowering of the end  $B$  of the spring and need not be considered here. The following discussion of the lowering of the end  $B$  due to the rotation  $\pi \cos \alpha$  is similar to the discussion for a close-coiled spring. Because of this rotation, point  $B$  is displaced to  $B_1$  (Fig. 168c) and we have  $\overline{BB_1} = \overline{AB} \pi \cos \alpha$ . The vertical component of this displacement is

$$\overline{BB_2} = \overline{BB_1} \cdot \frac{R}{\overline{AB}} = R\pi \cos \alpha. \quad (d)$$

The total deflection of the end  $B$  due to twist is the summation of elements such as are given by eq. (d), or

$$\delta_t = \int_B^C R\pi \cos \alpha, \quad (e)$$

in which the summation is taken along the total length of the spring from the lower end  $B$  to the upper fixed end  $C$ .

The deflection due to bending may be calculated in the same manner. The angular deflection due to the bending of the element  $ds$  by the moment  $M$  (eq. b) is

$$d\phi_1 = \frac{PR \sin \alpha}{EI} ds. \quad (f)$$

The corresponding rotation of the lower portion of the spring is shown in Fig. 168 by the vector  $\pi_1$ . In the same manner as above it may be shown that only its horizontal component  $\pi_1 \sin \alpha$  contributes to the vertical displacement of the end  $B$ , and that the magni-



The total rotation of the end  $B$  with respect to the  $z$  axis produced by the torque  $M_z$  is

$$\varphi_1 = sM_z \left( \frac{\sin^2 \alpha}{GI_p} + \frac{\cos^2 \alpha}{EI} \right) \quad (261)$$

Since a tensile force  $P$  produces rotation  $\varphi$  of the end  $B$  of the spring, it can be concluded from the reciprocal theorem (see Part I, p 351) that the torque  $M_z$  will produce an elongation of the spring. The magnitude  $\delta$  of this elongation is obtained from the equation

$$P\delta = M_z\varphi,$$

from which

$$\delta = \frac{M_z}{P} \varphi = M_z s R \sin \alpha \cos \alpha \left( \frac{1}{GI_p} - \frac{1}{EI} \right) \quad (262)$$

*Bending in an Axial Plane*—Sometimes we have to consider the pure bending of a helical spring in its axial plane, Fig 170. Let  $M_b$ , represented by vector  $\overline{AB}$ , Fig 170*b*, be the magnitude of the bend-

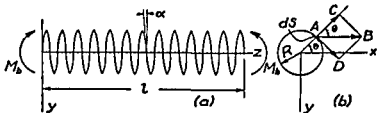


FIG 170

ing couples in the  $yz$  plane. Considering an element  $ds$  of the spring at a point  $A$  defined by the angle  $\theta$ , we resolve the vector  $\overline{AB}$  into two components  $\overline{AC} = M_b \cos \theta$  and  $\overline{AD} = M_b \sin \theta$ . The first component represents a couple which is in the plane tangent to the cylindrical surface of radius  $R$  and produces bending of the wire in that plane. The second component represents a couple acting in the axial plane of the spring and can be resolved into a torque  $M_b \sin \theta \cos \alpha$ , and a bending moment in the plane of the coil,  $M_b \sin \theta \sin \alpha$ . Hence the element  $ds$  undergoes bending by a combined bending moment equal to

$$\sqrt{M_b^2 \cos^2 \theta + M_b^2 \sin^2 \theta \sin^2 \alpha}, \quad (j)$$

and twist by a torque equal to  $M_b \sin \theta \cos \alpha$ . The strain energy of

the element, assuming a circular cross section of the wire, is

$$dU = ds \left[ \frac{M_b^2 (\cos^2 \theta + \sin^2 \theta \sin^2 \alpha)}{2EI} + \frac{M_b^2 \sin^2 \theta \cos^2 \alpha}{2GI_p} \right]. \quad (k)$$

Substituting  $ds = Rd\theta/\cos \alpha$  and integrating from  $\theta = 0$  to  $\theta = 2\pi n$ , where  $n$  is the number of coils, we obtain

$$U = \frac{\pi n R}{\cos \alpha} \left[ \frac{M_b^2 (1 + \sin^2 \alpha)}{2EI} + \frac{M_b^2 \cos^2 \alpha}{2GI_p} \right]. \quad (l)$$

The angular deflection of one end of the spring with respect to the other is  $l/\rho$ , where  $l$  is the length of the spring, Fig. 170a, and  $\rho$  is the radius of curvature of the deflection curve of the axis of the spring. The length  $l$  is determined from the expression

$$l = s \sin \alpha = \frac{2\pi R n}{\cos \alpha} \cdot \sin \alpha.$$

Equating the work done by the bending couples  $M_b$  to the strain energy (eq. l), we obtain

$$\frac{M_b}{2} \cdot \frac{l}{\rho} = U,$$

from which

$$\frac{1}{\rho} = M_b \cdot \frac{1}{\sin \alpha} \left( \frac{1 + \sin^2 \alpha}{2EI} + \frac{\cos^2 \alpha}{2GI_p} \right). \quad (263)$$

Hence the quantity

$$B = \frac{\sin \alpha}{\frac{1 + \sin^2 \alpha}{2EI} + \frac{\cos^2 \alpha}{2GI_p}} \quad (m)$$

must be taken as the flexural rigidity in the case of axial bending of a helical spring with wire of circular cross section. If the angle  $\alpha$  is small, we can assume with sufficient accuracy that  $\sin^2 \alpha = 0$  and  $\cos^2 \alpha = 1$ . Then since  $\sin \alpha = l/s$ , we may represent the flexural rigidity of a helical spring by the formula

$$B = \frac{2EI}{s} \frac{1}{1 + \frac{E}{2G}}. \quad (264)$$

In considering the bending of a helical spring by a lateral load,

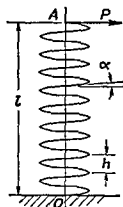


FIG 171

Fig 171, we have to take into account not only the deflection produced by the bending moment but also the deflection produced by the shearing force. Assuming that the end O of the spring is fixed and that  $\alpha$  is small, we obtain the deflection  $\delta_1$  of the upper end A of the spring due to the bending moment from the usual cantilever formula by substituting the value from eq (264) for the flexural rigidity. Hence

$$\delta_1 = \frac{Pl^3}{3} \frac{s}{2EI} \left(1 + \frac{E}{2G}\right) \quad (n)$$

In discussing the effect of shearing force on the deflections, let us consider the distortion of one coil in its plane<sup>46</sup> due to the shearing force  $V$ , Fig 172. The bending moment produced by  $V$  at any point A is  $VR \sin \theta$ , and the corresponding strain energy of one coil is

$$U = \int_0^{2\pi} \frac{M^2 R d\theta}{2EI} = \frac{V^2 R^3 \pi}{2EI}$$

The relative displacement  $e$  then is

$$e = \frac{\partial U}{\partial V} = \frac{\pi VR^3}{EI}$$

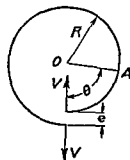


FIG 172

Dividing this displacement by the pitch  $h$  of the helix, we obtain the additional slope  $\gamma$  of the deflection curve due to the action of the shearing force

$$\gamma = \frac{e}{h} = \frac{\pi VR^3 n}{EI} \quad (o)$$

The formulas derived previously (see Part I, Art 39), for the deflection of solid beams due to shear may be adapted to the calculation of the lateral deflection of helical springs. It is only necessary to substitute the slope given by eq (o) in place of the expression  $\alpha V/AG$  previously used. In the case shown in Fig 171 the shearing force is constant along the length  $l$  and equal to  $P$ , hence the deflection due to shear is

$$\delta_2 = \gamma l = \frac{\pi n PR^3}{EI} \quad (p)$$

<sup>46</sup> The angle  $\alpha$  is assumed to be small in this discussion.

Adding eqs. (n) and (p) and assuming  $s = 2\pi Rn$ , we obtain

$$\delta = \delta_1 + \delta_2 = \frac{\pi n P l^2 R}{3EI} \left( 1 + \frac{E}{2G} + \frac{3R^2}{l^2} \right). \quad (265)$$

The last term in the parentheses represents the effect of shear action. It is negligible if the radius  $R$  of the helix is small in comparison with the length  $l$ .<sup>47</sup>

---

<sup>47</sup> Lateral buckling of helical springs under axial compression is discussed in S. Timoshenko, *Theory of Elastic Stability*, p. 165, 1936. A bibliography of the subject is also given.

## CHAPTER VIII

### STRESS CONCENTRATION

**55. Stress Concentration in Tension or Compression Members**—In discussing simple tension and compression it was assumed that the bar was of prismatic form. Then for centrally applied forces the stress is uniformly distributed over the cross section. A uniform stress distribution was also assumed in the case of a bar of variable cross section (see Fig 14, Part I, p 16), but this is an approximation which gives satisfactory results only when the variation in the cross section is gradual. Abrupt changes in cross section give rise to great irregularities in stress distribution. These irregularities are of particular importance in the design of machine parts subjected to variable external forces and to reversal of stresses. Irregularity of stress distribution at such places means that at certain points the stress is far above the average value, and under the action of reversal of stresses progressive cracks are likely to start. The majority of fractures of machine parts in service can be attributed to such progressive cracks.

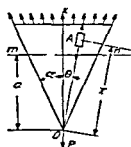


FIG 173.

To illustrate the stress distribution in a bar of variable cross section under tension, let us consider a symmetrical wedge of constant thickness  $h$  loaded as shown in Fig 173. An exact solution shows (see p 60) that there is a simple radial stress distribution. An element in the radial direction at any point  $A$  is in a condition of simple radial tension. The magnitude of this radial tensile stress is given by the equation

$$\sigma_r = k \frac{P \cos \theta}{\lambda r}, \quad (a)$$

in which  $\theta$  is the angle between the  $x$  axis and the radius  $OA$ ,  $r$  is the

distance of the point  $A$  from  $O$ , and  $k = 1/(\alpha + \frac{1}{2} \sin 2\alpha)$  is a factor depending on the angle  $2\alpha$  of the wedge.

The distribution of the normal stresses  $\sigma_x$  over any cross section  $mn$  perpendicular to the axis of symmetry of the wedge is not uniform. Using eq. (17), Part I, p. 38, and substituting  $r = a/\cos \theta$  in eq. (a) above, we find

$$\sigma_x = \sigma_r \cos^2 \theta = \frac{kP \cos^4 \theta}{ah}. \quad (b)$$

This shows that the normal stress is a maximum at the center of the cross section ( $\theta = 0$ ) and a minimum at  $\theta = \alpha$ . The difference between the maximum and minimum stresses increases with the angle  $\alpha$ . When  $\alpha = 10^\circ$ , this difference is about 6 per cent of the average stress obtained by dividing the load  $P$  by the area of the cross section  $mn$ . Analogous conclusions also may be drawn for a conical bar. It may be shown that the distribution of normal stresses over a cross section approaches uniformity as the angle of the cone diminishes.

This discussion shows that the assumption of uniform distribution of normal stresses over a cross section of a nonprismatic bar gives satisfactory results if the variation in cross section along the bar is gradual. However, the conditions are quite different when there are abrupt changes in the cross section. At such points the distribution of the stresses is very far from uniform and results obtained on the assumption of uniform stress distribution are entirely misleading. Several examples of abrupt change in cross section are discussed in the subsequent articles.

**56. Stresses in a Plate with a Circular Hole.**—If a small circular hole<sup>1</sup> is made in a plate subjected to a uniform tensile stress  $\sigma$ , a high stress concentration takes place at the points  $nn$  (Fig. 174a). The exact theory<sup>2</sup> shows that the tensile stress at these points is equal to  $3\sigma$ . The theory also shows that this stress concentration is of very localized character and is confined to the immediate vicinity of the hole.

<sup>1</sup> The diameter of the hole is less, say, than one-fifth of the width of the plate.

<sup>2</sup> This theory was given by Kirsch, *Z. Ver. deut. Ing.*, 1898. See also Timoshenko and Goodier, *Theory of Elasticity*, p. 78, 1951.

If a circle be drawn concentric with the hole and of comparatively large radius  $c$ , as shown in Fig 174*a* by the broken line, it can be assumed that the stress condition at the circumference of this circle is not materially affected by the presence of the hole. Let Fig

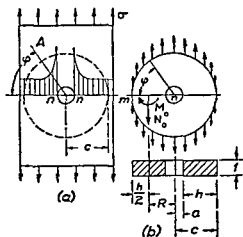


FIG 174

174*b* represent a circular ring cut out of the plate by a circular cylindrical surface of radius  $c$ . At each point of the outer surface of this ring we apply a vertically directed stress of magnitude  $\sigma \sin \varphi$ , i.e., equal to the stress on the corresponding elemental area  $A$  of the plate (see eq 16, Part I, p 37). Then the stresses in the ring will be approximately the same as in the portion of the plate bounded by the circle of radius  $c$  (Fig 174*a*). In this manner the problem of the stress distribution near the hole in the plate is reduced to that

of an annular ring of rectangular cross section subjected to known vertical forces of intensity  $\sigma \sin \varphi$  continuously distributed along its outer boundary<sup>3</sup>. This latter problem may be solved by using the method discussed in Part I, p 380. Considering one quadrant of the ring, the stresses acting across the cross section  $mn$  are reduced to a longitudinal tensile force  $N_0$  at the centroid of the cross section and a bending couple  $M_0$ . The longitudinal force can be determined from the equation of statics and is

$$N_0 = \sigma c \quad (a)$$

The moment  $M_0$  is statically indeterminate and is calculated by the theorem of least work. Eq (228), Part I, p 382, is used for the potential energy, in which the longitudinal force and the bending moment at any cross section of the ring, determined by the angle  $\varphi$  (Fig 174*b*), are

$$N = \sigma c \cos^2 \varphi,$$

$$M = M_0 + \sigma c (1 - \cos \varphi) \left[ \frac{c}{2} (1 - \cos \varphi) + \frac{h}{2} \cos \varphi \right] - \sigma c \left( c - \frac{h}{2} \right) (1 - \cos \varphi), \quad (b)$$

<sup>3</sup> The thickness of the plate is assumed to be unity

where  $h$  is the depth of the rectangular cross section. Then

$$\frac{dU}{dM_0} = \int_0^{\pi/2} \frac{Md\varphi}{AEe} - \int_0^{\pi/2} \frac{Nd\varphi}{AE} = 0,$$

from which, after integration,

$$M_0 = \frac{2\sigma c^2}{\pi} \left[ 1 - \frac{3}{8}\pi - \frac{h}{2c} \left( 1 - \frac{1}{4}\pi \right) + \frac{e\pi}{4c} + \frac{R}{2c} (\pi - 2) \right]. \quad (c)$$

Here, as before,  $R$  is the radius of the center line and  $e$  the distance of the neutral axis from the centroid of the cross section.

The stress at the point  $n$  of the cross section  $mn$  of the ring consists of two parts: (1) the tensile stress produced by the longitudinal force  $N_0$  and equal to

$$\sigma_1 = \frac{N_0}{h} = \frac{\sigma c}{h}, \quad (d)$$

and (2) the bending stress produced by  $M_0$  which is, from eq. (212), Part I, p. 365,

$$\sigma_2 = \frac{M_0 \left( \frac{h}{2} - e \right)}{Aea} = \frac{M_0}{2ea} \left( 1 - \frac{2e}{h} \right), \quad (e)$$

in which  $a$  is the radius of the hole.

The distance  $e$  is calculated (see Part I, Art. 79, p. 368) for various values of the ratio  $c/a$ , and then the quantities  $\sigma_1$  and  $\sigma_2$  are determined from eqs. (d) and (e). The maximum stress is

$$\sigma_{\max} = \sigma_1 + \sigma_2.$$

The results of these calculations are given in Table 18 below.

TABLE 18

$c/a =$	3	4	5	6	8	10
$2e/h$ .....	0.1796	0.2238	0.2574	0.2838	0.3239	0.3536
$\sigma_1/\sigma$ .....	1.50	1.33	1.25	1.20	1.14	1.11
$\sigma_2/\sigma$ .....	2.33	1.93	1.83	1.83	1.95	2.19
$\sigma_{\max}/\sigma$ .....	3.83	3.26	3.08	3.03	3.09	3.30

Comparison of the figures in the last line of the above table with the exact solution  $\sigma_{\max} = 3\sigma$  for a very small hole shows that for



$5 < c/a < 8$  the results of the approximate calculation agree closely with the exact solution. When  $c/a < 5$ , the hole cannot be considered very small, but has a perceptible effect on the distribution of stresses along the circle of radius  $c$  (Fig 174a), in which case our assumption regarding the distribution of forces along the outer boundary of the ring (Fig 174b) is not accurate enough. The deviation from the exact theory for  $c/a > 8$  is due to insufficient accuracy in the elementary theory of curved bars for the case where the inner radius is very small in comparison with the outer one.

Taking any point in the cross section  $mn$ , Fig 174b, at a distance  $r$  from the center of the hole, the normal stress at that point is, from the exact theory,

$$\sigma \left( 2 + \frac{a^2}{r^2} + \frac{3a^4}{r^4} \right), \quad (f)$$

where  $\sigma$  is the uniform tensile stress applied at the ends of the plate. This stress distribution is shown in Fig 174a by the shaded areas. It is seen that the stress concentration is highly localized in this case. At points  $n$ , i.e., at  $r = a$ , we have  $\sigma_{\max} = 3\sigma$ . The stresses decrease rapidly as the distance from this overstressed point increases, at a distance from the edge of the hole equal to the radius of the hole, i.e., for  $r = 2a$ , we obtain from eq (f) the normal stress equal to  $1\frac{7}{8}\sigma$ . The stress also decreases rapidly with an increase of the angle  $\varphi$ , Fig 174b, and for  $\varphi = \pi/2$ , i.e., for the cross section parallel to the applied tensile stresses  $\sigma$ , we find at the edge of the hole a compressive stress in the tangential direction equal to the tensile stress  $\sigma$  applied at the ends of the plate.

If instead of tension we have compression of the plate, Fig 175a, we have only to change the sign of the stresses obtained in the preceding discussion, and we conclude that there will be a compressive stress of magnitude  $3\sigma$  at points  $n$  and a tensile stress of magnitude  $\sigma$  at points  $m$ . In the case of a brittle material, such as glass, which is very strong in compression and weak in tension, the cracks usually start at points  $m$  as shown in Fig 175b.

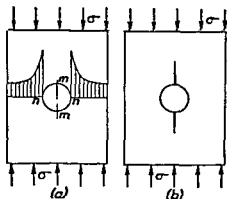


FIG 175

Having the stresses for simple tension or compression and using the method of superposition, we readily obtain the stress concentration for the cases of *combined tension or compression* in two perpendicular directions. For example, in the case shown in Fig 176 we find that the tangential stress at points  $n$  is  $3\sigma_y - \sigma_x$  and at points  $m$  the

stress is  $3\sigma_x - \sigma_y$ . In the particular case of *pure shear* we have

$$\sigma_x = -\sigma_y = \sigma$$

and we obtain for points *n* the stress  $-4\sigma$  and for the points *m* the stress  $+4\sigma$ ; thus in this case the maximum stress is four times larger than the stresses applied at the edges of the plate. Such a condition of high stress concentration is obtained in the torsion of a thin-walled circular tube with a small circular hole, Fig. 177. If the applied

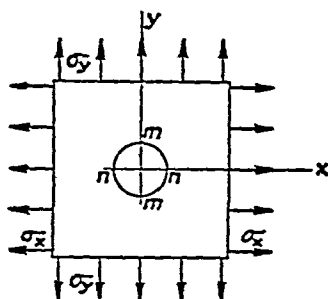


FIG. 176.



FIG. 177

torque has the direction indicated in the figure, the maximum tensile stress, four times larger than the shearing stresses applied at the ends, is produced at the edge of the hole at the points marked by plus signs. At the points marked by the minus signs, there will be a compressive stress of the same magnitude.

The approximate method described above for the calculation of stresses at a circular hole can also be used for the case of a hole with a bead (Fig. 178). The results of this calculation<sup>4</sup> for  $b/t_1 = 11$ ,  $t/2a = 0.01$ , give the following values of the ratio  $\sigma_{\max}:\sigma$  for various values of  $c/a$ :

$c/a = 4$	5	6
$\sigma_{\max}/\sigma = 2.56$	2.53	2.56

In the range considered, the ratio  $\sigma_{\max}/\sigma$  varies but slightly with  $c/a$ , so further calculations will be made for the case  $c/a = 5$  only. The influence of the cross sectional area of the bead on  $\sigma_{\max}$  can be studied by varying the dimension  $b$  of the bead. If  $\Delta_1 = 2t_1a$  denotes the decrease in the cross section

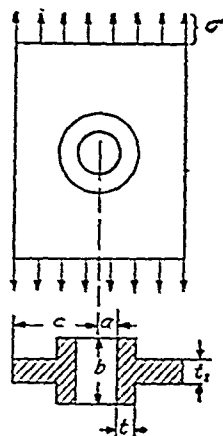


FIG. 178.

<sup>4</sup> Discussion of this problem is given in the author's paper, *J. Franklin Inst.*, Vol. 197, p. 505, 1924. It is assumed that the entire cross section of the bead is effective. For further study of the problem see L. Beskin, *J. Appl. Mech.*, Vol. 11, p. 140, 1944. See also C. Gurney, *Air Ministry Repts. and Mem.* (London), No. 1834, 1938.

of the plate due to the hole, and  $A_2 = (b - t_1)t$  denotes the cross sectional area of the bead, the ratio  $\sigma_{\max}/\sigma$  for several values of the ratio  $A_2/A_1$  is given below

$A_2/A_1 = 0.10$	0.20	0.30	0.40	0.50
$\sigma_{\max}/\sigma = 2.53$	2.17	1.90	1.69	1.53

The above figures can be used also in the case of other shapes of bead cross section provided the dimension  $t$  of the bead in the radial direction can be considered as small in comparison with the radius  $a$  of the hole. Take, for example, a wide plate in tension,  $\frac{7}{16}$  in thick, with a circular hole of 40 in diameter. Let the edge of the hole be stiffened with two angle irons  $4 \times 4 \times \frac{7}{16}$  in. In such a case  $A_2/A_1 = 0.40$  and the above table gives  $\sigma_{\max}/\sigma = 1.69$ .

**57. Other Cases of Stress Concentration in Tension Members.**—There are only a few cases in which, as in the case of a circular hole, the problem of stress concentration is rigorously solved theoretically.<sup>5</sup> In most cases information regarding the

maximum stresses at points of sharp change in cross section is obtained from experiments.<sup>6</sup> In the discussion which follows, some final results of theoretical and experimental investigations which may be of practical significance are presented.<sup>7</sup>

In the case of a small *elliptic hole in a plate*<sup>8</sup> (Fig. 179a) the

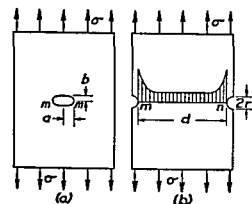


FIG. 179

maximum stress is at the ends of the horizontal axis of the hole and is given by the equation

<sup>5</sup> Theoretical solutions of stress-concentration problems for holes of various shapes are given in the book by G. N. Sawin, *Stress Concentration at Holes*, 1951 (in Russian).

<sup>6</sup> Various experimental methods of determining the maximum stresses are described in Arts. 61 and 62. See also E. Lehr, *Spannungsverteilung in Konstruktionselementen*, 1934.

<sup>7</sup> A very complete collection of information regarding stress concentrations is given in the book by R. E. Peterson, *Stress Concentration Design Factors*, 1953.

<sup>8</sup> See G. Kolosoff, dissertation, 1910, St. Petersburg, see also C. E. Inglis, *Engineering*, Vol. 95, p. 415, 1913, and *Trans. Inst. Naval Architects*, 1913.

$$\sigma_{\max} = \sigma \left( 1 + 2 \frac{a}{b} \right), \quad (a)$$

where  $\sigma$  is the tensile stress applied at the ends of the plate. This stress increases with the ratio  $a/b$ , so that a very narrow hole perpendicular to the direction of tension produces a very high stress concentration. This explains why cracks perpendicular to the direction of the applied forces tend to spread. This spreading can be stopped by drilling holes at the ends of the crack in order to eliminate the sharp corners which produce the high stress concentration.

Small *semicircular grooves*<sup>9</sup> in a plate subjected to tension (Fig. 179b) also produce high stress concentrations. Experiments<sup>10</sup> show that at points  $m$  and  $n$  the stresses are about three times the stress applied at the ends of the plate, if the radius  $r$  of the groove is very small in comparison with the width  $d$  of the minimum section. In general the maximum stress at points  $m$  and  $n$  is a function of the ratio  $r/d$ . The ratio of the maximum stress to the average stress in the minimum section  $mn$  is usually called the *stress concentration*

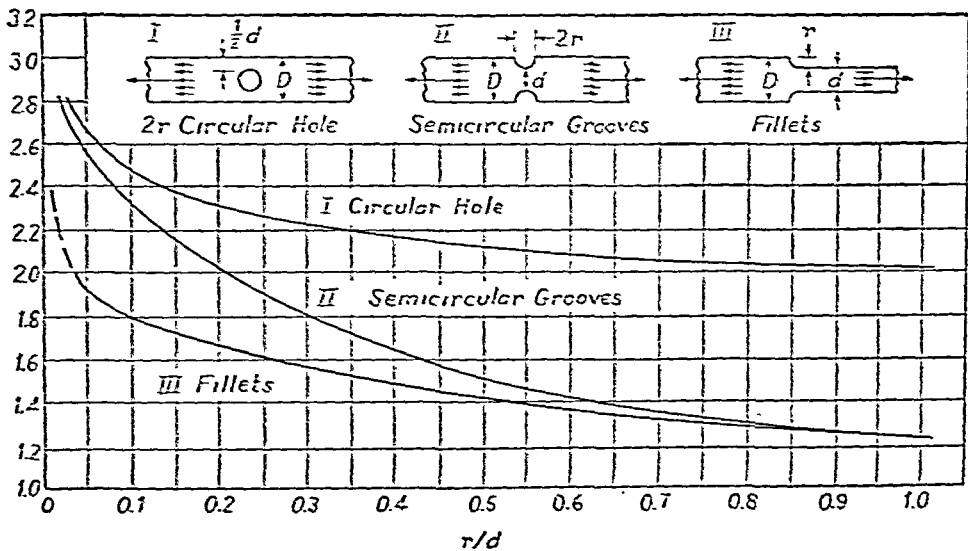


FIG. 180.

<sup>9</sup> For a theoretical solution of this problem see the paper by F. G. Maunsell, *Phil. Mag.*, Vol. 21, p. 765, 1936.

<sup>10</sup> See M. M. Frocht, *J. Appl. Mech.*, Vol. 2, p. 67, 1935.

factor and denoted by  $k$ . The values of  $k$  for various values of the ratio  $r/d$  are given in Fig. 180 by the curve II.<sup>11</sup> In the same figure are given also the factors of stress concentration for the case of a circular hole (curve I) and for the case

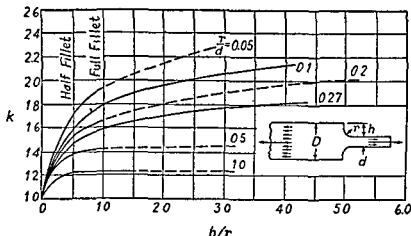


FIG. 181.

of fillets (curve III). In Fig. 181 more information regarding stress concentration at fillets is given.

In Fig. 182 the factors  $k$  are given for grooves of various depths having a circular shape at the bottom. It is seen that

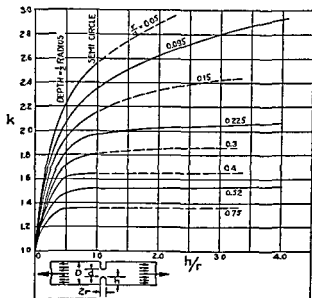


FIG. 182.

<sup>11</sup> The curves given in the following discussion are taken from the article by M. M. Frocht, *ibid*.

for deep grooves the stress concentration factors are larger than those for semicircular grooves with the same value of  $r/d$ .

The case of a plate of very large width with hyperbolic grooves, Fig. 183, can be treated theoretically.<sup>12</sup> The solution shows that the stress concentration factor, i.e., the ratio of the maximum stress at the points  $m$  and  $n$  to the average tensile stress over the cross section  $mn$ , can be represented by the following approximate formula:<sup>13</sup>

$$k = \sqrt{0.8 \frac{d}{r} + 1.2} - 0.1 \quad (b)$$

in which  $d$  is the width of the minimum section and  $r$  is the radius of curvature at the bottom of the groove. It is interesting to note that the values of  $k$  obtained from this formula are in very good agreement with experimental results obtained for deep grooves ( $h/r = 4$ ) semicircular at the bottom, Fig. 182.

Assume now that Fig. 183 represents an axial section of a circular cylinder of large diameter with deep grooves of hyperbolic profile un-

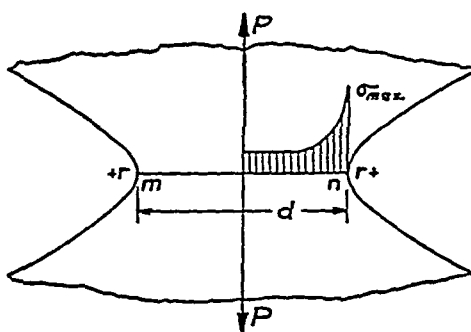


FIG. 183.

der axial tension. The maximum tensile stress again occurs at the bottom of the groove and the value of the factor of stress concentration is<sup>14</sup>

$$k = \sqrt{0.5 \frac{d}{r} + 0.85} + 0.08. \quad (c)$$

Comparison of this formula with formula (b) shows that in the case of a grooved cylinder the stress concentration is smaller than in the

<sup>12</sup> H. Neuber, *Z. angew. Math. u. Mech.*, Vol. 13, p. 439, 1933. See also Neuber's book, *Kerbspannungslehre*, 1937.

<sup>13</sup> Poisson's ratio is taken equal to 0.3 in eqs. (b), (c), and (d).

<sup>14</sup> H. Neuber, *Z. angew. Math. u. Mech.*, *ibid.*

case of a grooved plate. A further discussion of this comparison is given later (see Art. 60).

In the case of a cylinder in tension with an ellipsoidal cavity at the axis, for which Fig. 179a can be considered an axial section, the maximum tensile stress occurs at points  $m$ . Its value is given by the following approximate formula

$$\sigma_{\max} = \sigma \left( \sqrt{0.8 \frac{a}{r} + 0.05} + 0.78 \right) \quad (d)$$

where  $\sigma$  is a uniform tensile stress applied at the ends of the cylinder and  $r$  is the radius of curvature of the ellipse at points  $m$ .

The standard tensile test specimen for concrete, Fig. 184, is another example of a tension member with sharp variation in cross section. Experiments show<sup>15</sup> that the maximum stress occurs at points  $m$  and  $n$  and that this stress is about 1.75 times the average stress over the cross section  $mn$ .

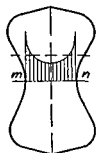


FIG. 184

Figure 185 represents a *dovetail joint* which is often used in electric motors to hold the magnetic poles to the rim of the spider. The centrifugal force acting on the pole produces large tensile stresses over the cross section  $mn$ .

The distribution of these stresses is shown in Fig. 185b<sup>16</sup>. Owing to the abrupt change in cross section a high stress concentration comes about at points  $m$  and  $n$ . The tensile stresses  $\sigma_x$  are accompanied by stresses  $\sigma_y$  in the lateral direction. The distribution of these stresses along  $mn$  is shown in Fig. 185b. The distribution of  $\sigma_x$  and  $\sigma_y$  along the vertical plane of symmetry is shown in Fig. 185a.

All of the above conclusions regarding stress distribution assume that the maximum stresses are within the proportional limit of the material. Beyond the proportional limit the stress distribution depends on the *ductility* of the material.

<sup>15</sup> See E. G. Coker, *Proc. Congr. Internat. Assoc. Testing Materials*, New York, 1913.

<sup>16</sup> See the paper by E. G. Coker, *J. Franklin Inst.*, Vol. 199, p. 289, 1925. T heads, which also have frequent application in machine design, were tested by M. Hetényi, *J. Appl. Mech.*, Vol. 6, p. 151, 1939.

A *ductile material* can be subjected to considerable stretching beyond the yield point without great increase in stress. Because of this fact, the stress distribution beyond the yield point becomes more and more uniform as the material stretches. This explains why, with ductile materials, holes and notches do not lower the *ultimate strength* when the notched piece is tested statically. Moreover, in testing mild steel specimens with deep grooves, a certain increase in the ultimate strength

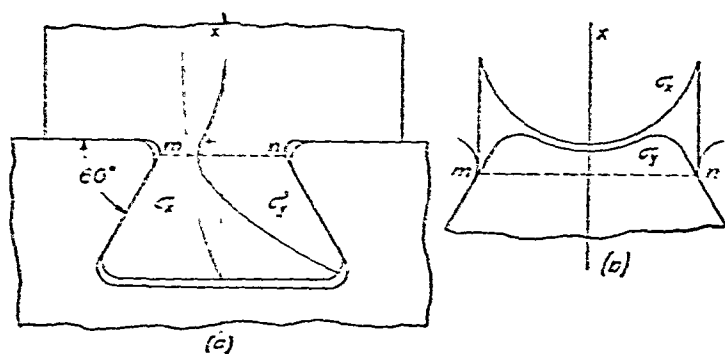


FIG. 185.

is usually obtained because the grooves prevent necking of the specimen at the cross section of fracture (see p. 434).

However, in the case of a *brittle material*, such as glass, the high stress concentration remains right up to the point of breaking. This causes a substantial weakening effect, as demonstrated by the decrease in ultimate strength of any notched bar of brittle material. It is interesting to note that very fine scratches on the surface of a glass specimen do not produce a weakening effect, although the stress concentration at the bottom of the scratch must be very high.<sup>17</sup> In explanation of this, it is assumed that common glass in its natural condition has many internal microscopic cracks, and small additional scratches on the surface do not change the strength of the specimen.

The above discussion shows, therefore, that the use of notches and reentrant corners in design is a matter of judg-

<sup>17</sup> This phenomenon was investigated by A. A. Griffith, *Phil. Trans. Roy. Soc. (London)*, A, Vol. 221, p. 163, 1920. See also the paper by I. N. Sneddon, *Proc. Roy. Soc. (London)*, A, Vol. 187, p. 229, 1946.



ment. In the case of a ductile material such as structural steel, high stress concentrations are not dangerous provided there are no alternating stresses. For example, in the dovetail joint shown in Fig. 185, the stresses are very often so high that yielding occurs at  $m$  and  $n$ , but this yielding is not considered dangerous, because the structure is subjected to the action of a constant force. In the case of brittle material, points of stress concentration may have a great weakening effect, and such places should be eliminated or the stress concentration reduced by using generous fillets.

In members subjected to reversal of stress the effect of stress concentration must always be considered, since progressive cracks are liable to start at such points even if the material is ductile (see Art. 87).

**58. Stress Concentration in Torsion.**—In discussing the twisting of bars of various cross sections (see Arts. 46 and 47) it was mentioned that reentrant corners or other sharp irregularities in the boundary line of the cross section cause high stress concentrations. Longitudinal holes have a similar effect.

As a first example let us consider the case of a *small circular hole* in a twisted circular shaft<sup>18</sup> (Fig. 186).

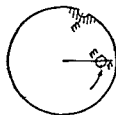


FIG. 186.

In discussing this problem the *hydrodynamical analogy* is very useful.<sup>19</sup> The problem of the twisting of bars of uniform cross section is mathematically identical with that of the motion of a *frictionless fluid* moving with uniform angular velocity inside a cylindrical shell having the same cross section as the bar. The

velocity of the circulating fluid at any point represents the shearing stress at the corresponding point of the cross section of the bar when twisted. The effect of a small hole in a shaft of circular cross section is similar to that of a stationary solid

<sup>18</sup> This case was investigated by J. Larmour, *Phil. Mag.*, Vol. 33, p. 76, 1892.

<sup>19</sup> This analogy was developed by Lord Kelvin and Tait, *Natural Philosophy*, Vol. 2; J. Boussinesq, *J. math. (Liouville)*, Vol. 16, 1871; and A. G. Greenhill, article "Hydromechanics," *Encyclopaedia Britannica*, 9th Ed. Regarding the application of the analogy in experiments, see the paper by J. P. Den Hartog and J. G. McGivern, *J. Appl. Mech.*, Vol. 2, p. 46, 1935.

cylinder of the same size in the stream in the hydrodynamical model. Such a cylinder greatly changes the velocity of the fluid in its immediate neighborhood. The velocities at the front and rear points are reduced to zero, while those at the side points  $m$  and  $n$  are doubled. A hole of this kind therefore doubles the maximum stress in the portion of the shaft in which it is located. A small *semicircular groove* on the surface parallel to the length of the shaft (Fig. 186) has the same effect. The shear stress in the neighborhood of the point  $m$  will be nearly twice the shearing stress calculated for points on the surface of the shaft far away from the groove.

The same hydrodynamical analogy explains the effect of a *hole of elliptic cross section* or of a *groove of semielliptic cross section*. If one of the principal axes  $a$  of the ellipse is in the radial direction and the other principal axis is  $b$ , the stresses at the edge of the hole at the ends of the  $a$  axis are increased in the proportion  $[1 + (a/b)]:1$ . The maximum stress produced in this case thus depends upon the magnitude of the ratio  $a/b$ . The effect of an elliptic hole on the stress is greater when the major axis of the ellipse is in the radial direction than when it runs circumferentially. This explains why a radial crack has such a weakening effect on the strength of a shaft. The above discussion also applies to the case of a semielliptic groove on the surface parallel to the axis of the shaft.

In the case of a *keyway* with sharp corners (Fig. 187) the hydrodynamical analogy indicates a zero velocity of the circulating fluid at the corners projecting outwards (points  $m-m$ ); hence the shearing stress in the corresponding torsion problem is equal to zero at such corners. At points  $n-n$ , the vertices of the reentrant angles, the velocity of the circulating fluid is theoretically infinite. In the corresponding torsion problem the shearing stress is also infinite at the points  $n-n$ , which means that even a small torque will produce permanent set at these points. The stress concentration can be reduced by rounding the corners  $n-n$ .

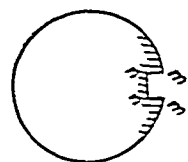


FIG. 187.

Experiments made<sup>20</sup> on a hollow shaft of outer diameter 10 in., inner diameter 5.8 in., depth of keyway 1 in., width of keyway 2.5 in., and radius of fillet in corner of keyway  $r$ , showed that the maximum stress at the rounded corners is equal to the maximum stress in a similar shaft without a keyway multiplied by the factor  $k$  given in Table 19. This shows

TABLE 19

$r$ (in) =	0.1	0.2	0.3	0.4	0.5	0.6	0.7
$k$ =	5.4	3.4	2.7	2.3	2.1	2.0	1.9

that the stress concentration can be greatly diminished by increasing the radius of the fillet at the corners  $n$ .

The weakening effect of stress concentrations in shafts due to holes and grooves depends on whether the material is ductile or not, and the conclusions reached in Art. 57 apply here also.

If a tubular member has reentrant corners, there is stress concentration at these corners, and the magnitude of the maximum stress depends on the radius of the corners. An approximate value of this maximum stress can be obtained from the membrane analogy. Let us

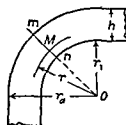


FIG 188

consider the simple case of a tube of constant thickness and assume that the corner is bounded by two concentric circles (Fig 188) with center at  $O$  and radii  $r_i$  and  $r_o$ . The surface of the membrane at the cross section  $mn$  may be assumed<sup>21</sup> to be a surface of revolution with axis perpendicular to the plane of the figure at  $O$ . We have seen that the slope of the membrane surface at any point  $M$  is numerically equal to the shearing stress  $\tau$ . Referring to Fig. 189, which shows a meridional section through  $mn$ , the principal curvatures of the membrane at this point are

<sup>20</sup> See the collective work, *The Mechanical Properties of Fluids*, New York, D Van Nostrand Company, Inc., p 245, 1924

<sup>21</sup> This assumption is satisfactory provided  $r_i$  is not small in comparison with  $r_o$ .

$$\frac{1}{R_1} = \frac{d\varphi}{ds} = \frac{d\tau}{dr}$$

for the meridian (taking an element  $ds$  of the meridian equal to  $dr$ ), and

$$\frac{1}{R_2} = \frac{\tau}{r}$$

for the section perpendicular to the meridian. The equation of equilibrium of the membrane, from eq. (122), p. 119, is then

$$\frac{d\tau}{dr} + \frac{\tau}{r} = \frac{p}{S}$$

or, by using eq. (a), p. 237,

$$\frac{d\tau}{dr} + \frac{\tau}{r} = 2G\theta. \quad (a)$$

Let  $\tau_0$  denote the average shearing stress, obtained from eq. (226). From eq. (227) we then find

$$\frac{d\tau}{dr} + \frac{\tau}{r} = 2G\theta = \frac{\tau_0 s}{A}, \quad (b)$$

in which  $s$  is the length of the center line of the section of the tubular member. The general solution of eq. (b) is

$$\tau = \frac{C}{r} + \frac{\tau_0 s r}{2A}. \quad (c)$$

The constant of integration  $C$  is obtained from the condition <sup>22</sup>

$$\int_{r_i}^{r_a} \tau dr = \tau_0 h.$$

<sup>22</sup> This condition follows from the hydrodynamical analogy (p. 312). If a fluid circulates in a channel having the shape of the cross section of the tubular member, the quantity of fluid passing each cross section of the channel must remain constant.

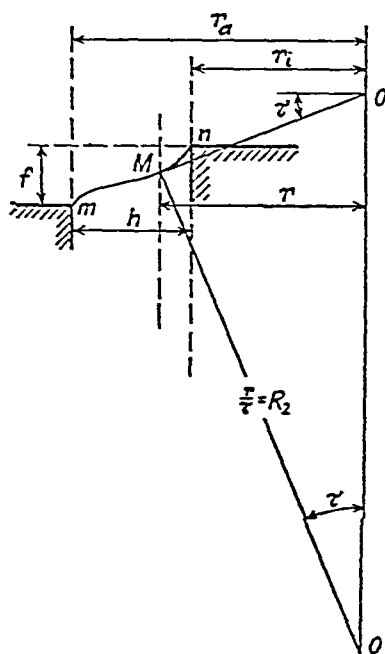


FIG. 189.

Substituting eq (c) for  $\tau$ , we find

$$C = \tau_0 h \frac{1 - \frac{s}{4A}(r_a + r_i)}{\log_e \frac{r_a}{r_i}},$$

and, from eq (c),

$$\tau = \frac{\tau_0 h}{r} \frac{1 - \frac{s}{4A}(r_a + r_i)}{\log_e \frac{r_a}{r_i}} + \frac{\tau_0 s r}{2A} \quad (266)$$

At the reentrant corners  $r = r_i$ , and substituting this value into the above equation we can calculate the stress concentration at these corners<sup>23</sup>

Take for example a square tube (Fig 190) with outer dimensions

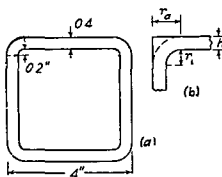


FIG 190

4 × 4 in, wall thickness  $h = 0.4$  in, and radii at the corners  $r_i = 0.2$  in,  $r_a = 0.6$  in. Then

$$A = 3.6 \times 3.6 - 0.4^2(4 - \pi) = 12.82 \text{ sq in},$$

$$s = 3.6 \times 4 - 0.4(8 - 2\pi) = 14.40 - 0.70 = 13.70 \text{ in}$$

The average stress  $\tau_0$  is given by eq (226). The stress at the reentrant corners, from eq (266), is

$$\tau = 1.54\tau_0$$

The stress concentration factor in this case is 1.54. It may be seen that this factor increases with decrease in the inner radius  $r_i$ .

Eq (266) can also be used for an approximate calculation of the stress concentration when only the reentrant corner is rounded (Fig

<sup>23</sup> Such an equation was given by C. Weber, *loc cit*, p. 236

190*b*). As the stresses are small at the projecting corners, we can take  $r_a = h + r_i$ , as indicated in the figure by the broken line.

In the case of rolled profile sections such as are shown in Fig. 144*b* and 144*c*, p. 244, the maximum stress occurs at the reentrant corners. Its value is obtained by multiplying the stress calculated from eqs. (222) or (225) (see pp. 240, 245) by the stress concentration factor for which the following expression can be used:<sup>24</sup>

$$k = 1.74 \sqrt[3]{\frac{c}{r}}, \quad (267)$$

in which  $c$  is the thickness of the flange and  $r$  the radius of the fillet. More elaborate calculations give for the stress concentration factor the values represented in Fig. 191 by the curve  $AB$ .<sup>25</sup>

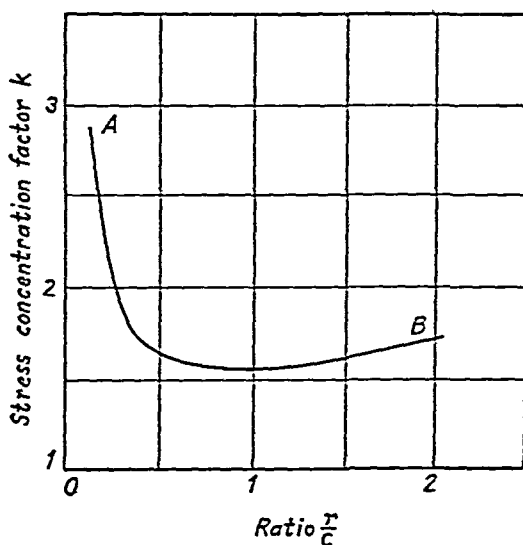


FIG. 191.

<sup>24</sup> E. Trefftz, *Z. angew. Math. u. Mech.*, Vol. 2, p. 263, 1922. Eq. (267) is derived for a corner for which the adjacent parts have equal thicknesses as in Fig. 144*b*. In the case of two different thicknesses  $c_1$  and  $c_2$ , as in Fig. 144*c*, the larger thickness must be used in eq. (267). A further discussion of this question is given by H. M. Westergaard and R. D. Mindlin, *Proc. Am. Soc. Civil Engrs.*, p. 509, 1935.

<sup>25</sup> See paper by J. H. Huth, *J. Appl. Mech.*, Vol. 17, p. 388, 1950. The results of Huth's calculations are in very good agreement with the experimental results of N. S. Waner and W. W. Soroka obtained by the conducting sheet analogy. See *Proc. Soc. Exp. Stress Anal.*, Vol. 11, p. 19, 1953.

and the corresponding stress is

$$\tau = \frac{G\Delta\varphi r}{a}. \quad (c)$$

The two systems of perpendicular lines, equimomental and equiangular, divide the diametral section of the shaft into elemental rectangles, as indicated in Fig. 193. The dimensions of these rectangles may be used to compare the shearing stresses at the corresponding points of the shaft. Using eq. (b) and comparing the shearing stresses  $\tau_1$  and  $\tau_2$  at radii  $r_1$  and  $r_2$  respectively, we find

$$\frac{\tau_1}{\tau_2} = \frac{r_2^2 h_2}{r_1^2 h_1}. \quad (d)$$

From eq. (c) we find

$$\frac{\tau_1}{\tau_2} = \frac{r_1 a_2}{r_2 a_1}. \quad (e)$$

In the case under consideration  $a_1 = a_2 = a$ , but eq. (e) will be used later for a more general case. It is evident that each system of lines may be used in calculating the shearing stresses. In one case (eq. d) the ratio of stresses depends on the ratio of the distances between equimomental lines  $h_2/h_1$ , while in the other case (eq. e) it depends on the ratio of the distances between equiangular lines  $a_2/a_1$ .

Let us consider a shaft of variable diameter as shown in Fig. 192. The irregularities in stress distribution produced at the fillets are of local character. At sufficient distance from the junction of the shafts of two diameters the stress distribution is practically the same as in a shaft of uniform cross section, and the two systems of lines described above can be constructed in the diametral section (Fig. 194). Near the cross section of discontinuity, the stress distribution is a more complicated one and the equimomental and equiangular lines become curved. Analysis of the problem shows<sup>30</sup> that although curved, these lines remain mutually orthogonal and

<sup>30</sup> See the paper by F. A. Willers, *loc. cit.*, p. 318.

subdivide the diametral section into curvilinear rectangles as indicated by the shaded areas.

Also eqs. (d) and (e), which were derived for a uniform shaft, are shown to hold here, if we take for  $h$  and  $a$  the dimensions measured at the middle of each curvilinear rectangle. Then the equimomental and equiangular lines give a complete picture of the stress distribution in the shaft. Considering, for example, the equimomental lines and using eq. (d), we see that the stresses increase with decrease in the radius and thickness of the equimomental tubes.

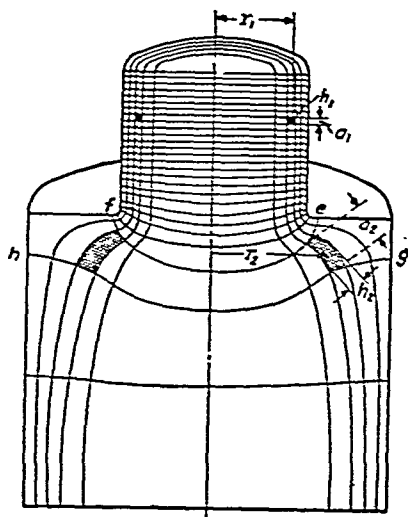


FIG. 194.

It is evident from Fig. 194 that the stress is a maximum at the fillets, where the thickness  $h$  of the outer equimomental tube is the smallest. We come to the same conclusion also by considering the equiangular lines. It can be seen from the figure that at the fillets the distance  $a$  between these lines is very small; hence, from eq. (e), the stress is large. From eq. (d) or (e) we can determine the ratio of the maximum stress at the fillet to the stress at any other point provided the equimomental or equiangular lines are known.

The electric analogy, mentioned above, p. 318, provides a means for measuring the distances  $a$  between the equiangular lines. These distances are measured at the surface of the shaft of smaller diameter  $d$ , first at a point remote from the cross section of discontinuity, and then at the fillet. The ratio of these two distances gives (see eq. e) the factor by which the stress, as calculated by the usual formula, must be multiplied to obtain the maximum stress at the fillet. In discussing the electric analogy, we begin with the case of a rectangular plate of uniform thickness (Fig. 195). If the ends of the plate are maintained at a constant difference of potential, there will flow through the plate an electric current uniformly distributed over its cross section. By dividing the electric



flow into equal parts we obtain a system of equidistant *streamlines*. The system of *equipotential lines* is perpendicular to the streamlines. With a homogeneous plate of uniform cross section the drop in potential will be uniform along the direc-

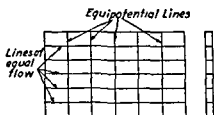


FIG. 195.

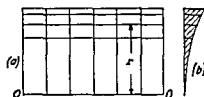


FIG. 196.

tion of the current and the equipotential lines are therefore equidistant vertical lines. In order to get two systems of lines analogous to those in Fig. 193, the thickness of the plate is varied as the cube of the distance  $r$ , as shown in Fig. 196*b*. Then the distance between the streamlines will be inversely proportional<sup>21</sup> to the cube of  $r$ , and the distance between the vertical equipotential lines remains constant as before. In this manner we can obtain the same system of mutually orthogonal lines as in Fig. 193. The edge  $O-O$  of the plate corresponds to the axis of the shaft. The equipotential lines

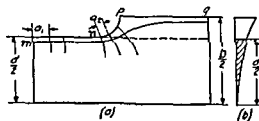


FIG. 197.

correspond to the equiangular lines, and the streamlines to the equimoment lines of the torsional problem. Investigation shows<sup>22</sup> that this analogy also holds in the case of a plate of two different widths and of thickness varying as the cube of the distance  $r$  (Fig. 197). This makes it possible to investigate the stress concentration at the fillet of a twisted shaft by an electric method. We maintain a constant difference in potential at the ends of the plate

<sup>21</sup> It is assumed that the flow per unit area of cross section is uniform over the cross section.

<sup>22</sup> See the paper by L. S. Jacobsen, *loc. cit.*, p. 318.

and measure the drop in potential along the edge  $mnp$ . The distances  $a_1$  and  $a_2$  between equipotential lines at a remote point  $m$  and at the fillet  $n$  respectively are thus obtained. The ratio  $a_1/a_2$  of these distances gives the stress concentration factor for the fillet at  $n$ .

Actual measurements were made on a steel model 24 in. long, 6 in. wide at the larger end and 1 in. maximum thickness

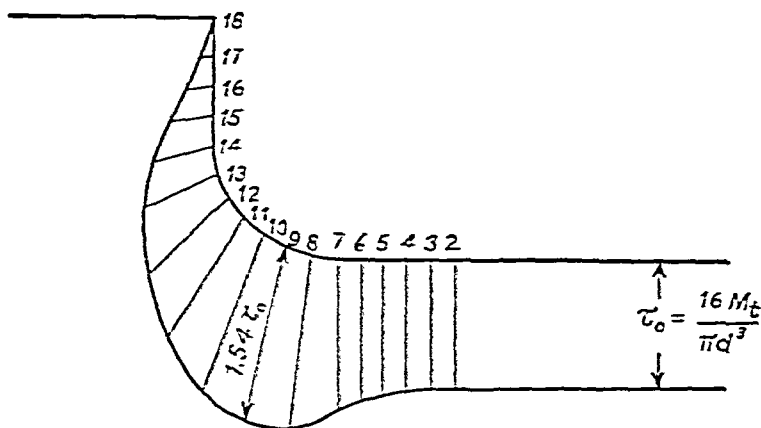


FIG. 198.

at the edge  $pq$ . The drop of potential along the edge  $mnpq$  of the model was investigated by using a very sensitive galvanometer, the terminals of which were connected to two sharp needles fastened in a block at a distance 2 mm apart. By touching the plate with the needles the drop in potential over the distance between the needle points was indicated by the galvanometer. By moving the needles along the fillet it is possible to find the place of maximum voltage gradient and to measure this maximum. The ratio of this maximum to the voltage gradient at a remote point  $m$  (Fig. 197) gives the magnitude of the stress concentration factor  $k$  in the equation

$$\tau_{\max} = k \frac{16 M_t}{\pi d^3}. \quad (268)$$

The results of such tests in one particular case are represented in Fig. 198, in which the potential drop measured at each point is indicated by the length on the normal to the edge of

the plate at this point. From this figure the stress concentration factor is found to be 1.54. The magnitudes of this factor obtained with various proportions of shafts are given in Fig. 199, in which the abscissas represent the ratios of the radius

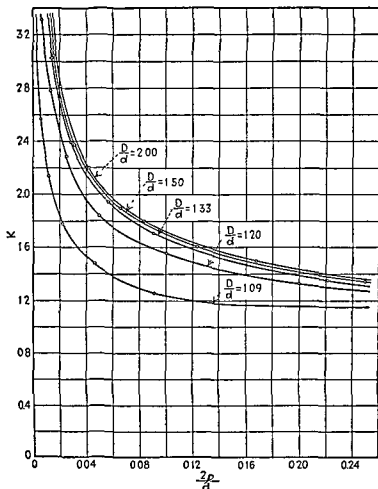


FIG. 199.

of the fillet to the smaller radius of the shaft  $2\rho/d$ , and the ordinates represent the factor  $k$  for various ratios of  $D/d$ .

**60. Stress Concentration in Bending.**—The formulas for bending and shearing stresses derived for prismatic beams are very often applied also to cases of beams of variable cross section. This is a satisfactory procedure provided the variation in the cross section is not too rapid (see Art. 9).

If the change in cross section is abrupt, there is a considerable disturbance in stress distribution at the section of dis-

continuity. The maximum stress is usually much greater than that given by the simple beam formula, and can be represented by the formula

$$\sigma_{\max} = k\sigma, \quad (a)$$

in which  $\sigma$  is the stress at the point under consideration as obtained from the prismatic beam formula and  $k$  is the stress concentration factor. In only a few cases is this factor obtained by the use of the equations of the theory of elasticity.<sup>33</sup>

A plate of large width with hyperbolic notches, Fig. 183, is one of the cases where we have a rigorous solution in bending for the stress distribution at the notches. This solution shows that in the case of the pure bending of the plate by couples acting in the middle plane, the maximum stress occurs at points  $m$  and  $n$  and the stress concentration factor in formula (a) can be represented by the following approximate formula

$$k = \sqrt{0.355 \frac{d}{r} + 0.85 + 0.08}, \quad (b)$$

where  $d$  is the minimum width of the plate and  $r$  the radius of curvature at the bottom of the notch.

In the case of a circular shaft with a hyperbolic groove, for which Fig. 183 represents an axial section, the stress concentration factor in the case of pure bending is

$$k = \frac{3}{4N} \left( \sqrt{\frac{d}{2r} + 1} + 1 \right) \left[ \frac{3d}{2r} - (1 - 2\mu) \sqrt{\frac{d}{2r} + 1} + 4 + \mu \right], \quad (c)$$

where

$$N = 3 \left( \frac{d}{2r} + 1 \right) + (1 + 4\mu) \sqrt{\frac{d}{2r} + 1} + \frac{1 + \mu}{1 + \sqrt{\frac{d}{2r} + 1}}. \quad (d)$$

As before,  $d$  is the diameter of the minimum cross section and  $r$  the smallest radius of the curvature at the bottom of the groove. For

<sup>33</sup> H. Neuber, *Ingenieur-Archiv*, Vol. 5, p. 238, 1934, and Vol. 6, p. 133, 1935.

large values of the ratio  $d/2r$  eq (c) can be replaced with sufficient accuracy by the approximate formula

$$k = \frac{3}{4} \sqrt{\frac{d}{2r}} \quad (e)$$

Most of the information regarding the magnitude of the factor  $k$  in eq (a) is obtained experimentally by the photoelastic method<sup>34</sup> The stress concentration factors for pure bending of plates with semicircular grooves and with fillets in

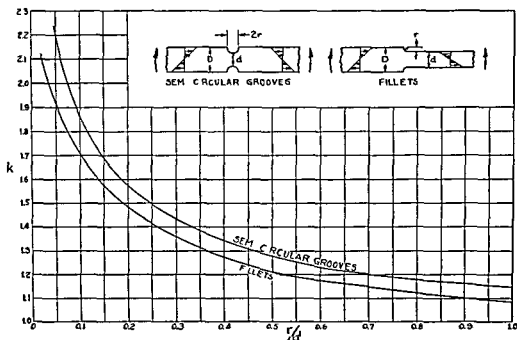


FIG 200

the form of a quarter of a circle and with  $D = d + 2r$  are given by the curves in Fig 200 In Fig 201 the stress concentration factors for fillets with various values of the ratio  $D/d$  are given In Fig 202 are given the stress concentration factors for grooves of varying depth in pure bending

For comparison of the stress concentration factors in tension and in bending for plates and for circular shafts, the

<sup>34</sup> The curves given in the following discussion are taken from the article by M M Frocht, *loc cit*, p 307 See also the paper by M M Leven and M M Frocht, *J Appl Mech*, Vol 19, p 560, 1952

curves in Fig. 203 are given.<sup>35</sup> Curves 1 and 2, which give the stress concentration factors for a hyperbolic notch in a

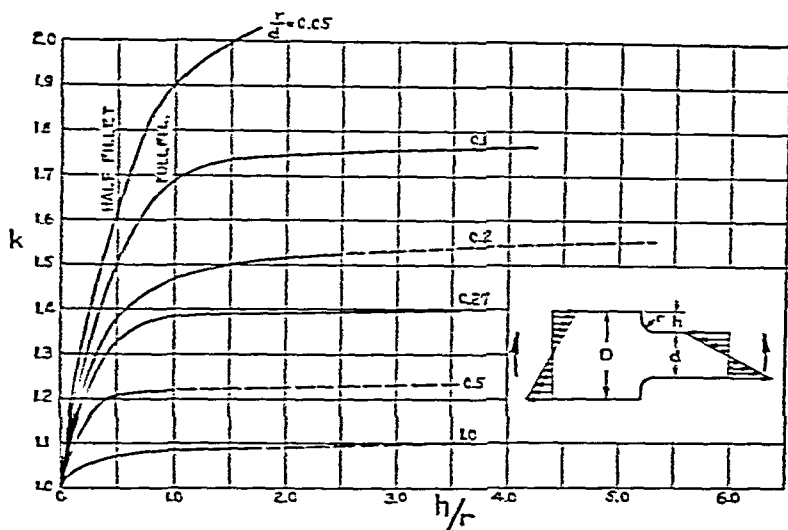


FIG. 201.

plate and in a circular shaft in tension, are calculated from eqs. (b) and (c), p. 309. Curves 3 and 4 showing similar values

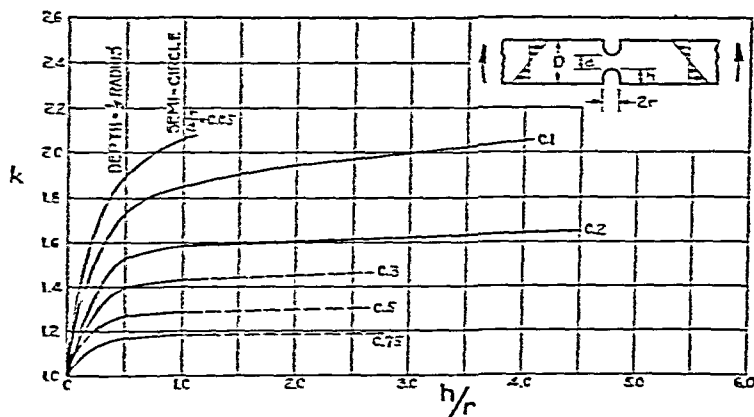


FIG. 202.

for notches in pure bending are calculated from eqs. (b) and (c), p. 325. It may be seen from these curves that the stress concentration factors are higher for plates than for circular shafts, the difference being more pronounced in the case of

<sup>35</sup> This figure and the following are taken from the paper by R. E. Peterson and A. M. Wahl, *J. Appl. Mech.*, Vol. 3, p. 15, 1936.

tension In the case of pure bending, which is of greater practical importance, the difference between the two cases is small, around 6 to 8 per cent for notches of practical dimensions The dashed curves 5 and 6 in Fig 203 are obtained from the curves in Figs 182 and 202 by extrapolating these curves to

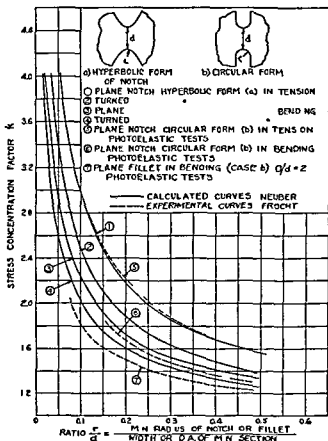


FIG 203

large values of the ratio  $h/r$ , which corresponds to a deep notch semicircular at the bottom It may be seen that curves 5 and 6 agree satisfactorily with curves 1 and 3 for hyperbolic notches for ratios  $r/d$  between 0.15 and 0.50 This indicates that in the case of deep notches the magnitude of the stress concentration factor depends principally on the magnitude of the ratio  $r/d$  and not on the shape of the notch

The dashed curve 7 is obtained from the curves in Fig 201 and represents the stress concentration factors at the fillets of a plate in pure bending with the ratio  $D/d = 2$  It is seen that for fillets the stress concentration factors are somewhat

lower than for deep notches (curves 4 and 6) with the same ratio  $r/d$ .

To obtain the stress concentration factors for fillets in circular shafts, direct tests on large steel shafts with diameter ratio  $D/d = 1.5$  were made at the Westinghouse Research Laboratories.<sup>35</sup> The values of these factors obtained by direct measurement of the strain at the fillets are given by the circular points in Fig. 204. For comparison, the results of photoelastic

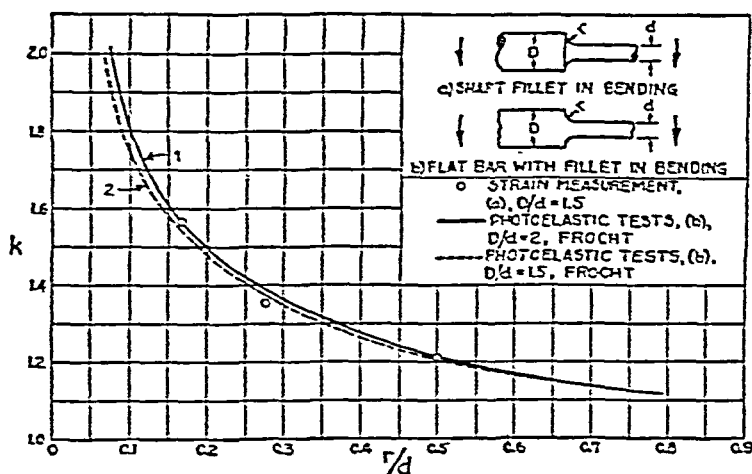


FIG. 204.

experiments on flat models with  $D/d = 2$  and  $D/d = 1.5$  are given<sup>37</sup> in the same figure by curves 1 and 2. From these experiments the very important conclusion can be made that the stress concentration factors for circular shafts agree quite well with the values obtained photoelastically on flat specimens.

#### 61. The Investigation of Stress Concentration with Models.

—It has already been stated that a complete theoretical solution for the stress distribution at a section of discontinuity exists in only a few of the simplest cases, such as that of a circular or elliptic hole and hyperbolic notch. In the majority of cases, information regarding stress concentration is obtained by experiment. For this purpose strain measurements at the section of discontinuity may sometimes be made with sensi-

<sup>35</sup> *Ibid.*

<sup>37</sup> These curves were constructed from the data given in Fig. 201.



average stress over the end cross section of the plate when yielding occurred was  $1/2$  of that necessary to produce yielding in the prismatic bar

In both the preceding examples the yielding at the place of maximum stress occurred at an average stress which is higher than indicated by the true stress concentration factors. This can be explained as follows. The small region of overstressed material is surrounded by portions where the stress does not exceed the proportional limit. This prevents the sort of sliding shown in Fig 205, along surfaces perpendicular to the plane of the figure and inclined  $45^\circ$  to the direction of tension. In the cases shown in Fig 206 and Fig 207, the Lueders' lines started on the polished surfaces of the plates as thin lines perpendicular to the maximum tensile stress. This indicates that in these cases the sliding occurred along planes through these lines and inclined  $45^\circ$  to the plane of the plates. In such a case the thickness of the plate is an important factor. This thickness must be very small in comparison with the radii of the holes or fillets in order to have the surface of sliding totally within the region of highly overstressed material. The fact that the surface of sliding, beginning at the points of maximum stress, must cross a region with smaller stresses explains<sup>41</sup> the retardation in the appearance of Lueders' lines. In the case of the circular hole above, the width of the plate was 6 in. and the diameter of the hole 1 in., while the thickness of the plate was only  $\frac{1}{8}$  in. When testing models in which the thickness and the diameter of the hole are of the same order, it was impossible to detect any substantial effect due to stress concentration on the magnitude of the load producing Lueders' lines. Another reason for the Lueders' lines' being retarded is the fact that a certain amount of permanent set may occur before Lueders' lines become visible.

The use of Lueders' lines in testing the weak points of a structure is not confined to any particular type of problem and has an advantage over the photoelastic method, described in the next article, in that it is applicable to three dimensional

<sup>41</sup> This explanation was suggested to the writer by L. H. Donnell

problems. To make the yielding of the metal visible on a rough surface, the method of covering the surface with a *brittle lacquer*, or stress coat, has been successfully used in investigating stresses in boiler heads<sup>42</sup> and in built-up compression members.<sup>43</sup> By cutting the specimens and models apart after testing and using a special etching process on the cut surfaces it is possible to reveal the interior regions which have yielded and thus obtain information regarding the flow of metal at the points of stress concentration.<sup>44</sup>

62. Photoelastic Method of Stress Measurements.—There are many stress analysis problems in which the deformation is essentially parallel to a plane. These are called *two-dimensional problems*. Illustrations are the bending of beams of narrow rectangular cross section, bending of girders, arches and gear teeth, or, more generally, plates of any shape but of constant thickness acted on by forces or couples in the plane of the plate. Their shapes may be such that the stress distributions are very difficult to determine analytically, and for such cases the *photoelastic* method has proved very useful. In this method, models cut out of a plate of an isotropic transparent material such as glass, Celluloid or Bakelite are used. It is well known that under the action of stresses these materials become *doubly refracting*; and if a beam of *polarized light* is passed through a transparent model under stress, a colored picture may be obtained from which the stress distribution can be found.<sup>45</sup>

In Fig 208  $abcd$  represents a transparent plate of uniform thickness and  $O$  the point of intersection with the plate of a beam of polarized light perpendicular to the plate. Suppose

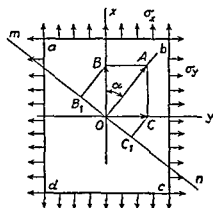


FIG 208

that  $OA$  represents the plane of vibration of the light and that the length  $\overline{OA} = a$  represents the amplitude of this vibration. If the vibration is considered to be simple harmonic (monochromatic light), the displacements may be represented by the equation

$$s = a \cos pt, \quad (a)$$

where  $p$  is proportional to the frequency of vibration, which depends on the color of the light

Imagine now that the stresses  $\sigma_x$  and  $\sigma_y$ , different in magnitude, are applied to the edges of the plate. Because of the difference in stresses the optical properties of the plate also become different in the two perpendicular directions. Let  $v_x$  and  $v_y$  denote the velocities of light in the planes  $Ox$  and  $Oy$  respectively. The simple vibration in the plane  $OA$  is resolved into two components with amplitudes  $\overline{OB} = a \cos \alpha$  and  $\overline{OC} = a \sin \alpha$  in the planes  $Ox$  and  $Oy$  respectively, and the corresponding displacements are

$$x = a \cos \alpha \cos pt, \quad y = a \sin \alpha \cos pt \quad (b)$$

If  $h$  is the thickness of the plate, the intervals of time necessary

was started by C Wilson, *Phil Mag* (Ser 5), Vol 32, 1891, and further developed by A Mesnager, *Ann ponts et chaussées*, 1901 and 1913, and E G Coker, *General Electric Co Mag*, 1920, and *J Franklin Inst*, 1925. For further development of the photoelastic method see the paper by Henry Favre, *Schweiz. Bauzeitung*, Vol 20, p 291, 1927, see also his dissertation *Sur une nouvelle méthode optique de détermination des tensions intérieures*, Paris, 1929. The use of monochromatic light, called the fringe method, was introduced by Z Tuzi, *Inst Phys Chem Research (Tokyo)*, Vol 8, p 247, 1928. The subject is very completely discussed in the book by E G Coker and L N G Filon, *Photo-Elasticity*, 1931 and also in the book by M M Frocht, *Photo-Elasticity*, 1941. The accuracy of photoelastic stress measurements is discussed in the paper by M M Frocht, R Guernsey and D Landsberg, *Proc Soc Exp Stress Anal*, Vol 11, p 105, 1953.

for the two component vibrations to cross the plate are

$$t_1 = \frac{h}{c_x} \quad \text{and} \quad t_2 = \frac{h}{c_y}, \quad (c)$$

and the vibrations (eq. *b*) after crossing the plate are given by the equations

$$x_1 = a \cos \alpha \cos p(t - t_1); \quad y_1 = a \sin \alpha \cos p(t - t_2). \quad (d)$$

These components have the phase difference  $p(t_2 - t_1)$ , due to the difference in velocities. Experiments show that the difference in the velocities of the light is proportional to the difference in the stresses; hence

$$\begin{aligned} t_2 - t_1 &= \frac{h}{c_y} - \frac{h}{c_x} = \frac{h(c_x - c_y)}{c_x c_y} \\ &\approx \frac{h(c_x - c_y)}{c^2} = k(\sigma_x - \sigma_y), \end{aligned} \quad (e)$$

where  $c$  is the velocity of light when the stresses are zero, and  $k$  is a numerical factor which depends on the physical properties of the material of the plate.

We see that the difference of the two principal stresses can be found by measuring the difference in phase of the two vibrations. This can be done by bringing them into interference in the same plane. For this purpose a Nicol prism (called the *analyzer*) is placed behind the plate in such a position as to permit the passage of vibrations in the plane  $mn$  perpendicular to the plane  $OA$  only. The components of the vibrations (*d*), which pass through the prism, have the amplitudes  $\overline{OB}_1 = \overline{OB} \sin \alpha = (a/2) \sin 2\alpha$  and  $\overline{OC}_1 = \overline{OC} \cos \alpha = (a/2) \sin 2\alpha$ . The resultant vibration in the plane  $mn$  is therefore

$$\begin{aligned} &\frac{a}{2} \sin 2\alpha \cos p(t - t_1) - \frac{a}{2} \sin 2\alpha \cos p(t - t_2) \\ &= \left( a \sin 2\alpha \sin p \frac{t_1 - t_2}{2} \right) \sin p \left( t - \frac{t_1 + t_2}{2} \right). \end{aligned} \quad (f)$$

This is a simple harmonic vibration, whose amplitude is proportional to  $\sin p[(t_1 - t_2)/2]$ ; hence the intensity of the light

is a function of the difference in phase  $p(t_1 - t_2)$ . If the stresses  $\sigma_x$  and  $\sigma_y$  are equal,  $t_1$  and  $t_2$  are also equal, and the amplitude of the resultant vibration (eq. *f*) is zero and we have darkness. There will be darkness also whenever the difference in stresses is such that

$$p \frac{t_1 - t_2}{2} = n\pi, \quad (g)$$

where  $n$  is an integer. The maximum intensity of light is obtained when the difference in stresses is such that

$$\sin p \frac{t_1 - t_2}{2} = \pm 1.$$

Imagine that instead of the element *abcd*, Fig. 208, we have a strip of transparent material under simple tension. By gradually increasing the tensile stress we obtain a dark picture of the strip on the screen each time eq. (*g*) is fulfilled. In this manner we can establish experimentally for a given material of given thickness the stress corresponding to the interval between two consecutive dark pictures of the specimen. For example, for one kind of Phenolite plate, 1 mm thick, this stress was found<sup>46</sup> to be 1,620 lb per sq in. Hence for a plate  $\frac{1}{4}$  in. thick, the corresponding stress will be  $1,620/6.35 = 255$  lb per sq in. With this information we can determine the stress in a strip under tension by counting the number of intervals between the consecutive dark images occurring during the gradual loading of the specimen.

If we use a strip in pure bending, we obtain a picture such as is shown in Fig. 209. The parallel dark fringes indicate that in the portion of the strip at a considerable distance from



FIG 209.

<sup>46</sup> Z. Tuzi, *Sci. Papers, Inst. Phys. Chem. Research (Tokyo)*, Vol. 12, p. 247, 1929.

the points of application of the loads the stress distribution is the same in all vertical cross sections. By counting the number of fringes we can determine the magnitudes of the stresses, as the stress difference between two consecutive fringes is the same as the stress difference between two consecutive dark images in simple tension. By watching the strip while the load is applied gradually, we may see how the number of dark fringes increases with increase of load. The new ones always appear at the top and the bottom of the strip and gradually move toward the neutral plane so that the fringes become more and more closely packed. The stress at any point is then obtained by counting the number of fringes which pass over the point.

The method of counting the number of dark fringes passing a chosen point can be used also for any plane stress distribution. As seen from our previous discussion, this number gives the difference between the two principal stresses at the point. For a complete determination of the stress at the point it remains to find the directions of the principal stresses and their sum. Eq. (f) shows that the intensity of the light passing through the analyzer is proportional to  $\sin 2\alpha$ , where  $\alpha$  is the angle between the plane of polarization and the plane of one of the principal stresses, Fig. 208. If these two planes coincide,  $\sin 2\alpha$  is zero and we obtain a dark spot on the screen. Hence in examining a stressed transparent model in polarized light we observe not merely the dark fringes discussed before but also dark lines connecting the points at which one of the principal stress directions coincides with the plane of polarization. By rotating both Nicol prisms, polarizer and analyzer, and marking dark lines on the image of the stressed plate for various directions of the plane of polarization, we obtain a system of *isoclinic lines* which join together points with the same directions of principal stresses. Having these lines, we can draw the lines which are tangent at each point to the principal axes of stress. These latter lines are called the *trajectories* of the principal stresses (see Part I, p. 128). Thus the directions of the principal stresses at each point of the plate can be obtained experimentally.

The sum of the principal stresses can also be obtained experimentally by measuring the change  $\Delta h$  in the thickness  $h$  of the plate due to the stresses  $\sigma_x$  and  $\sigma_y$ <sup>47</sup> and using the known relation

$$\Delta h = \frac{\mu h}{E} (\sigma_x + \sigma_y). \quad (h)$$

Having the difference of the two principal stresses from the photoelastic test and their sum from eq. (h), we can readily calculate the magnitude of the principal stresses. The fringes obtained in a plate with fillets subjected to the action of pure bending are shown as an illustration in Fig. 210. From the

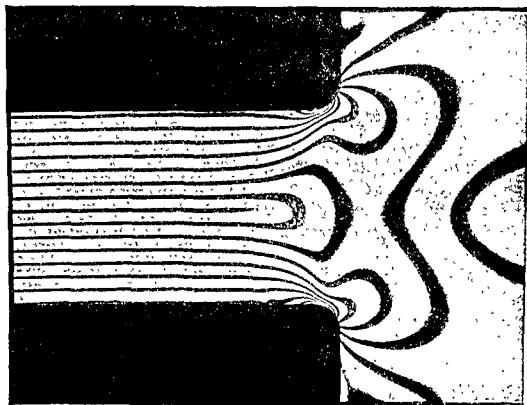


FIG. 210.

fact that the fringes are crowded at the fillets it may be concluded that a considerable stress concentration takes place

<sup>47</sup>This method was suggested by A. Mesnager, *loc. cit.*, p. 334. The necessary lateral extensometer was developed and successfully used by A. M. Wahl. See the paper by R. E. Peterson and A. M. Wahl, *J. Appl. Mech.*, Vol. 2, p. 1, 1935.

at those points. In Fig. 211 are shown the fringes for a centrally loaded beam on two supports.

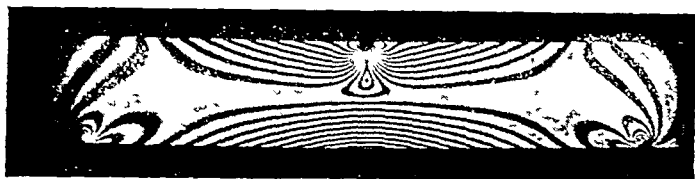


FIG. 211.

In the previous discussion of the photoelastic method of stress analysis it was always assumed that we were dealing with two-dimensional problems. More recently considerable efforts have been made to extend the photoelastic method to three-dimensional problems, and some promising results have already been obtained.<sup>48</sup>

### 63. Contact Stresses in Balls and Rollers.

—If two elastic bodies, say two balls, are pressing on each other, a small surface of contact is formed as a result of local deformation. The pressures distributed over this surface are called contact pressures. The magnitude of these pressures and the stresses produced in the bodies can be calculated by using equations of the theory of elasticity.<sup>49</sup> We will give here only the final results of such investigations.

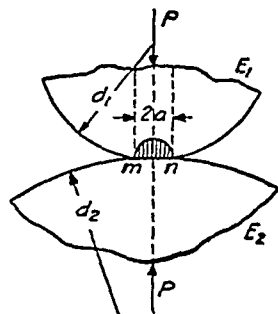


FIG. 212.

In the case of two balls compressed by forces  $P$  (Fig. 212) the pressures are distributed over a small *circle of contact*  $mn$ , the radius of which is given by the equation

$$a = 0.88 \sqrt[3]{\frac{P (E_1 + E_2) d_1 d_2}{2 E_1 E_2 (d_1 + d_2)}}. \quad (269)$$

<sup>48</sup> See the paper by M. Hetényi, *J. Appl. Mech.*, Vol. 5, p. 149, 1938. See also R. Weller, *J. Appl. Phys.*, Vol. 10, p. 266, 1939, and the article by D. C. Drucker in M. Hetényi, ed., *Handbook of Experimental Stress Analysis*, New York, 1950.

<sup>49</sup> This problem was solved by H. Hertz, *Gesammelte Werke*, Vol. 1, 1895. A discussion of the problem and a bibliography are given in Timoshenko and Goodier, *Theory of Elasticity*, p. 372, 1951. See also I. J. Steierman, *Contact Problems*, 1949 (in Russian); and N. M. Belajef, *Strength of Materials*, 1945 (in Russian).



In this expression  $E_1$  and  $E_2$  are the moduli of the two balls and  $d_1$  and  $d_2$  the corresponding diameters. The maximum pressure occurs at the center of the *circle of contact* and is given by the equation

$$p_{\max} = 1.5 \frac{P}{\pi a^2} \quad (270)$$

Because of local deformation the centers of the balls approach one another by the distance

$$\lambda = 0.77 \sqrt[3]{2P^2 \left( \frac{1}{E_1} + \frac{1}{E_2} \right)^2 \left( \frac{1}{d_1} + \frac{1}{d_2} \right)} \quad (271)$$

When the diameters of the balls and the moduli of elasticity are equal, the above equations become

$$a = 0.88 \sqrt[3]{\frac{Pd}{2E}}, \quad p_{\max} = 0.62 \sqrt[3]{\frac{4PE^2}{d^2}}, \quad \lambda = 1.54 \sqrt[3]{\frac{2P^2}{E^2 d}} \quad (272)$$

When a ball of diameter  $d$  is forced against an elastic body having a plane surface, the required formulas are obtained by substituting  $d_1 = d, d_2 = \infty$  in eqs (269)–(271). Assuming  $E_1 = E_2 = E$ , we find for this case

$$a = 0.88 \sqrt[3]{\frac{Pd}{E}}, \quad p_{\max} = 0.62 \sqrt[3]{\frac{PE^2}{d^2}}, \quad \lambda = 1.54 \sqrt[3]{\frac{P^2}{E^2 d}} \quad (273)$$

In the case of a *ball in a spherical seat* (Fig. 213), the sign of  $d_2$  in eqs (269)–(271) must be changed. Then for the case  $E_1 = E_2 = E$ , we find

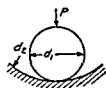


FIG. 213

$$\left. \begin{aligned} a &= 0.88 \sqrt[3]{\frac{P}{E} \frac{d_1 d_2}{d_2 - d_1}}, \\ p_{\max} &= 0.62 \sqrt[3]{PE^2 \left( \frac{d_2 - d_1}{d_2 d_1} \right)^2} \end{aligned} \right\} \quad (274)$$

It is important to note that in the cases represented by eqs (272) and (273) the maximum compressive stress at the center of the surface of contact depends on the magnitude of the ratio  $P/d^2$ , i.e., the maximum stress remains constant if the above ratio is kept constant.

This justifies the usual practice of determining the safe diameter of the ball by taking a definite magnitude of load per square inch of the diametral section of the ball. Since the material at the center of the surface of contact is prevented from lateral expansion, it is in a condition of compression from all sides and may sustain very high pressures without failure (see Art. 81). In experiments<sup>50</sup> with hardened crucible steel the allowable compressive force  $P$  in the case of a ball pressed against a plane surface was sometimes taken from the equation

$$P_{\max} = 700d^2,$$

in which  $d$  is in inches and  $P$  in pounds. Substituting in the second of eqs. (273), we find  $p_{\max}$  equal to approximately 530,000 lb per sq in.

In the general case of the compression of two bodies having the same modulus  $E$ , let  $1/r_1$  and  $1/r_1'$  denote the principal curvatures at the point of contact of one of the bodies, let  $1/r_2$  and  $1/r_2'$  denote the curvatures of the other,<sup>51</sup> and let  $\varphi$  denote the angle between the normal planes containing curvatures  $1/r_1$  and  $1/r_2$ . The *surface of contact* for the general case is an ellipse, the semiaxes of which are given by the equations

$$a = \alpha \sqrt{\frac{Pm}{n}}; \quad b = \beta \sqrt[3]{\frac{Pm}{n}}, \quad (275)$$

in which  $P$  is the compressive force and

$$m = \frac{4}{\frac{1}{r_1} + \frac{1}{r_1'} + \frac{1}{r_2} + \frac{1}{r_2'}}; \quad n = \frac{4E}{3(1 - \mu^2)}.$$

The constants  $\alpha$  and  $\beta$  are taken from Table 20 for each particular case. The angle  $\theta$  in the first column of the table is calculated from

<sup>50</sup> See Stribeck, *Z. Ver. deut. Ing.*, p. 73, 1901; Schwinning, *ibid.*, p. 332, and A. Bauschlicher, *ibid.*, p. 1185, 1908.

<sup>51</sup> The principal curvatures are the maximum and the minimum curvatures and these are in planes at right angles. The curvature of a body is considered as positive if the corresponding center of curvature is within the body.

TABLE 20 CONSTANTS FOR CALCULATING THE SEMIAXES OF THE ELLIPSE OF CONTACT

$\theta$ degrees	$\alpha$	$\beta$	$\theta$ degrees	$\alpha$	$\beta$
20	3 778	0 408	60	1 486	0 717
30	2 731	0 493	65	1 378	0 759
35	2 397	0 530	70	1 284	0 802
40	2 136	0 567	75	1 202	0 846
45	1 926	0 604	80	1 128	0 893
50	1 754	0 641	85	1 061	0 944
55	1 611	0 678	90	1 000	1 000

the equation

$$\cos \theta = \frac{B}{A}, \quad (a)$$

in which

$$A = \frac{2}{m}; \quad B =$$

$$\frac{1}{2} \sqrt{\left(\frac{1}{r_1} - \frac{1}{r_1'}\right)^2 + \left(\frac{1}{r_2} - \frac{1}{r_2'}\right)^2 + 2\left(\frac{1}{r_1} - \frac{1}{r_1'}\right)\left(\frac{1}{r_2} - \frac{1}{r_2'}\right) \cos 2\varphi} \quad (b)$$

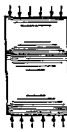
The expression for the maximum pressure at the center of the surface of contact is then

$$p_{\max} = 1.5 \frac{P}{\pi ab} \quad (276)$$

In the case of *rollers in compression*, Fig 214, the contact area is a narrow rectangle whose width  $b$  is given<sup>52</sup> by the equation



FIG 214



$$b = 2.15 \sqrt{\frac{P'}{2} \frac{d_1 d_2}{d_1 + d_2} \left(\frac{1}{E_1} + \frac{1}{E_2}\right)}, \quad (277)$$

in which  $P'$  denotes the compressive force per unit length of the roller. The maximum unit pressure at the middle of the *rectangle of contact* is

$$p_{\max} = 0.59 \sqrt{2P' \frac{E_1 E_2 (d_1 + d_2)}{(E_1 + E_2) d_1 d_2}} \quad (278)$$

<sup>52</sup> See A. Föppl, *Technische Mechanik*, Vol 5, p 351, 1907

In the particular case in which the moduli for the two rollers are equal

$$b = 2.15 \sqrt{\frac{P'd_1d_2}{E(d_1 + d_2)}}; \quad p_{\max} = 0.59 \sqrt{P'E \frac{d_1 + d_2}{d_1d_2}}. \quad (279)$$

If one of the diameters be taken infinitely large as in the case of a roller in contact with a plane surface, eqs. (279) reduce to

$$b = 2.15 \sqrt{\frac{P'd}{E}}; \quad p_{\max} = 0.59 \sqrt{\frac{P'E}{d}}. \quad (280)$$

It will be seen that the maximum stress remains constant if  $P'$  varies in the same proportion as  $d$ . This justifies the practice of determining the safe dimensions on the basis of the diametral cross-sectional area of the roller. The allowable compressive force  $P'$  in the case of ordinary steel rollers in bridges, for example, is obtained from the equation

$$P' = 700d.$$

Substituting into eq. (280), we find that the maximum pressure is about 85,000 lb per sq in.<sup>53</sup>

### Problems

1. Determine the maximum pressure at the surface of contact  $C$  in a single-row ball bearing, shown in Fig. 215. The ball diameter is  $d = 1.5$  in., the radius of the grooves is 1 in., the diameter of the outer race is 8 in. and the greatest compressive force on one ball is  $P = 5,000$  lb.

*Solution.* Using the notation of p. 341, we obtain

$$r_1 = r_1' = \frac{1.5}{2} = \frac{3}{4} \text{ in.}; \quad r_2 = -1 \text{ in.};$$

$$r_2' = -4 \text{ in.};$$

$$m = \frac{1}{\frac{2}{1.5} + \frac{2}{1.5} - \frac{1}{1} - \frac{1}{4}} = 2.823;$$

$$n = \frac{4 \times 30 \times 10^6}{3 \times 0.91};$$

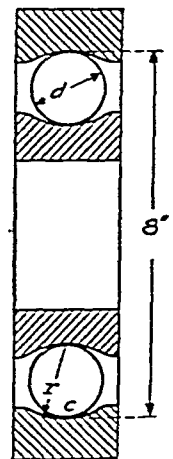


FIG. 215.

<sup>53</sup> For the testing of steel rollers see W. M. Wilson, *Univ. of Illinois Eng. Exp. Sta. Bull.*, No. 162, 1927; No. 191, 1929; No. 263, 1934. See also V. P. Jensen, *Iowa Eng. Exp. Sta. Bull.*, No. 138, 1937. Fatigue tests of rollers are discussed in Art. 89.

$$2A = \frac{4}{m} = \frac{4}{2\,823} = 1\,417, \quad 2B = \frac{1}{1} - \frac{1}{4} = 0\,750$$

Substituting in eq (a),

$$\cos \theta = \frac{0\,750}{1\,417} = 0\,529, \quad \theta = 58^\circ$$

Then from Table 20 we find by interpolation,

$$\alpha = 1\,536, \quad \beta = 0\,701$$

The semiaxes of the ellipse of contact are, from eqs (275),

$$a = 1\,536 \sqrt[3]{\frac{5,000 \times 2\,823 \times 3 \times 0\,91}{4 \times 30 \times 10^6}} = 0\,105 \text{ in},$$

$$b = 0\,701 \sqrt[3]{\frac{5,000 \times 2\,823 \times 3 \times 0\,91}{4 \times 30 \times 10^6}} = 0\,048 \text{ in},$$

and from eq (276),

$$p_{\max} = 1\,5 \frac{5,000}{\pi ab} = 475,000 \text{ lb per sq in}$$

Such high stresses can be sustained by hardened steel owing to the fact that at the center of the ellipse of contact the material is compressed not only in the direction of the force  $P$  but also in the lateral directions

2 Determine the surface of contact and the maximum pressure between two circular cylinders whose axes are mutually perpendicular. We have such a problem, for example, in contact pressures between a wheel with a cylindrical boundary and a rail<sup>54</sup>

*Solution* Denoting by  $r_1$  and  $r_2$  the radii of the cylinders and using the notation of p 341,

$$\frac{1}{r_1'} = 0, \quad \frac{1}{r_2'} = 0, \quad \varphi = \frac{\pi}{2}, \quad m = \frac{4}{\frac{1}{r_1} + \frac{1}{r_2}}, \quad n = \frac{4E}{3(1 - \mu^2)},$$

<sup>54</sup> The problem of contact pressures becomes more important as the axle loads of modern locomotives are increased. For discussion of this problem, see the paper by H. Fromm, *Z. Ver. deut. Ing.*, Vol 73, p 957, 1929, and the paper by Belajef, *Mem. Inst. Engrs. Ways of Communication* (St. Petersburg), 1907, and Föppl, 7.

$$A = \frac{1}{2} \left( \frac{1}{r_1} + \frac{1}{r_2} \right); \quad B = \frac{1}{2} \sqrt{\frac{1}{r_1^2} + \frac{1}{r_2^2} - \frac{2}{r_1 r_2}} = \pm \frac{1}{2} \left( \frac{1}{r_1} - \frac{1}{r_2} \right).$$

The sign of  $B$  must be so chosen as to make  $B$  positive. From eq. (a)

$$\cos \theta = \pm \frac{\frac{1}{r_1} - \frac{1}{r_2}}{\frac{1}{r_1} + \frac{1}{r_2}}.$$

Knowing  $\theta$ , we find the semiaxes of the ellipse of contact from eqs. (275) and the maximum pressure from eq. (276).

In the particular case of two cylinders of equal radii,  $\cos \theta = 0$ , and from Table 20 it can be concluded that the surface of contact has a circular boundary.

3. Find the maximum pressure between a wheel with a cylindrical rim of radius  $r_1 = 15.8$  in. and a rail with the radius of the head  $r_2 = 12$  in., if  $P = 1000$  lb and Poisson's ratio  $\mu = 0.25$ .

*Answer.* The semiaxes of the ellipse of contact are

$$a = 0.0946 \text{ in.} \quad \text{and} \quad b = 0.0792 \text{ in.,}$$

and the maximum pressure is

$$p_{\max} = \frac{3}{2} \frac{P}{\pi ab} = 63,600 \text{ lb per sq in.}$$

## CHAPTER IX

### DEFORMATIONS BEYOND THE ELASTIC LIMIT

64. Structures of Perfectly Plastic Materials.—In the preceding discussions it was always assumed that the material of the structure followed Hooke's law. On the basis of this law the deformations and stress distributions in a variety of cases were analyzed. There are cases, however, in which it is necessary to investigate the deformation of a structure beyond the proportional limit. To make such an investigation the mechanical

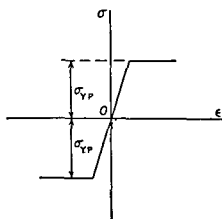


FIG. 216.

ical properties of materials beyond the proportional limit must be known. These properties are usually defined by tension and compression test diagrams. The simplest form these diagrams have is in the case of a *perfectly plastic material*. Such a material follows Hooke's law up to the proportional limit and then begins to yield under constant stress. The corresponding tension and compression test diagrams

are given in Fig. 216. Structural steels with sharply defined yield points and a considerable stretching at that point approach within certain limits the properties of a perfectly plastic material, and the stress analyses of structures on the basis of the diagram in Fig. 216 are of practical importance in many cases. In this and in the next article we will discuss several problems of this kind.

*Pure Bending.*—In discussing pure bending beyond the proportional limit we will make the same assumptions as in the case of elastic bending (see Part I, Art. 23, p. 92). Thus

we assume (1) that cross sections of the beam during bending remain plane and normal to the deflection curve, and (2) that the longitudinal fibers of the beam are in the condition of simple tension or compression and do not press on one another laterally.<sup>1</sup> Considering beams having an axial plane of symmetry and assuming that the bending couples act in that plane, we will have bending in the same plane, and during this bending cross sections of the beam will rotate about their neutral axes perpendicular to the plane of bending. The unit elongation of a fiber at distance  $y$  from the neutral axis (see Part I, p. 93) is

$$\epsilon = \frac{y}{r}. \quad (a)$$

The magnitude of the bending moment at which yielding begins will be calculated from the equation (see Part I, p. 95)

$$M_{Y.P.} = \sigma_{Y.P.} \frac{I_z}{c}, \quad (b)$$

in which  $I_z$  is the moment of inertia of the cross section of the beam with respect to its neutral axis, and  $c$  is the distance from that axis to the most remote fiber of the beam.

Considering as the simplest example a rectangular beam, Fig. 217, we obtain <sup>2</sup>

$$M_{Y.P.} = \sigma_{Y.P.} \frac{bh^2}{6}, \quad (c)$$

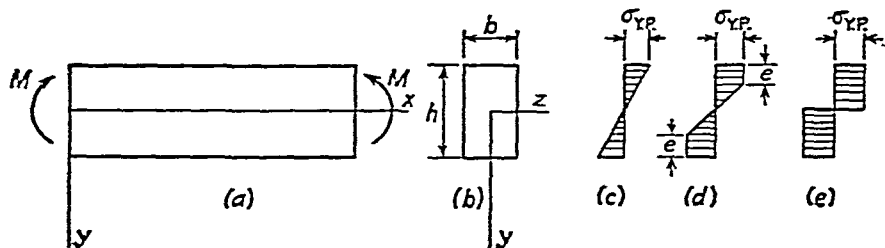


FIG. 217.

<sup>1</sup> These assumptions are in good agreement with experiments; see the paper by G. H. MacCullough, *Trans. A.S.M.E.*, Vol. 55, p. 55, 1935.

<sup>2</sup> We assume  $\sigma_{Y.P.}$  in tension and compression equal. Our derivations can be readily generalized if  $\sigma_{Y.P.}$  has different values for tension and compression.



and the corresponding stress distribution is shown in Fig. 217*c*. All the fibers of the beam are in the elastic condition, and the most remote fibers have just reached the yield point stress. If we somewhat increase the bending moment above  $M_{YP}$ , the fibers near the upper and the lower surfaces of the beam begin to yield and the stress distribution will be as shown in Fig. 217*d*. Plastic deformation penetrates further into the beam as the bending moment increases. For each value  $e$  of the depth of this penetration the corresponding bending moment, defined by the shaded area in Fig. 217*d*, is given by the equation

$$\begin{aligned} M &= \sigma_{YP} be(h - e) + \sigma_{YP} \frac{b(h - 2e)^2}{6} \\ &= \sigma_{YP} \frac{bh^2}{6} \left[ 1 + \frac{2e}{h} \left( 1 - \frac{e}{h} \right) \right]. \end{aligned} \quad (d)$$

The corresponding curvature of the deflection curve of the beam is found by using eq. (a). Applying this equation to the fibers at the distance  $(h/2) - e$  from the neutral axis and observing that the stress in these fibers just reaches the proportional limit  $\sigma_{YP}$ , we obtain

$$\sigma_{YP} = \frac{E \left( \frac{h}{2} - e \right)}{r},$$

and

$$\frac{1}{r} = \frac{\sigma_{YP}}{E \left( \frac{h}{2} - e \right)}. \quad (e)$$

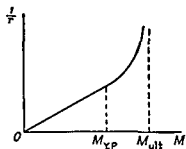


FIG. 218.

Using eqs. (d) and (e), we can represent the relation between bending moment  $M$  and curvature  $1/r$  graphically as shown in Fig. 218. Up to the value  $M = M_{YP}$ , the deformation is elastic and the curvature of the beam increases in proportion to the bending moment. When  $M$  increases beyond

$M_{Y.P.}$  the relation between  $M$  and  $1/r$  becomes nonlinear. The corresponding curve (Fig. 218) becomes steeper as the depth  $e$  of penetration of plastic deformation approaches the value  $h/2$ , and the stress distribution approaches that shown in Fig. 217*e*. Substituting  $e = h/2$  into eq. (d) we obtain the highest value of the bending moment,

$$M_{ult} = \sigma_{Y.P.} \frac{bh^2}{4}. \quad (f)$$

In Fig. 218 the value of  $M_{ult}$  defines the position of the vertical asymptote to the curve. As  $M$  approaches  $M_{ult}$  a small increment in  $M$  produces a large increase in curvature, so that  $M_{ult}$  produces complete failure of the beam.<sup>3</sup>

Eqs. (c) and (f) were developed for rectangular beams, and we can conclude that for this shape of the cross section the bending moment required to produce complete failure of the beam is 50 per cent larger than that at which plastic deformation just begins. Similar equations can be derived readily for symmetrical cross sections of other shapes.

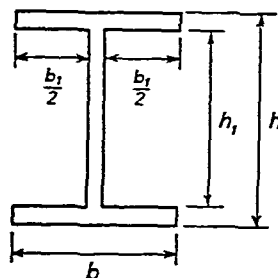


FIG. 219.

Let us consider, for example, an I beam, Fig. 219. The yield moment is again obtained by multiplying  $\sigma_{Y.P.}$  by the section modulus (see eq. b) and we obtain

$$M_{Y.P.} = \sigma_{Y.P.} \left( \frac{bh^3}{12} - \frac{b_1h_1^3}{12} \right) \frac{2}{h}. \quad (g)$$

In calculating  $M_{ult}$  we observe that the corresponding stress distribution is shown in Fig. 217*e*. The moment of all internal tensile forces with respect to the neutral axis is obtained by multiplying  $\sigma_{Y.P.}$  by the static moment of one-half of the cross section with respect to the same axis. Doubling this

<sup>3</sup> The concept of *ultimate moment* is well confirmed by experimental investigations; see the paper by J. F. Baker, *J. Inst. Aeronaut. Engrs.*, Vol. 31, p. 188, 1949.

moment, we find

$$M_{ult} = \sigma_Y P \cdot \left( \frac{bh^2}{4} - \frac{b_1 h_1^2}{4} \right). \quad (h)$$

From eqs. (g) and (h) we now obtain

$$\frac{M_{ult}}{M_{Y.P.}} = \frac{3}{2} \cdot \frac{1 - \frac{b_1 h_1^2}{bh^2}}{1 - \frac{b_1 h_1^3}{bh^3}}. \quad (i)$$

We see that for an I beam the ratio  $M_{ult}/M_{Y.P.}$  is smaller than  $\frac{3}{2}$  and that its value depends on the proportions of the cross section. Assuming, for example,  $b_1/b = h_1/h = 0.9$ , we find, from eq. (i),  $M_{ult}/M_{Y.P.} = 1.18$ . In this case,  $M_{ult}$  is only 18 per cent larger than  $M_{Y.P.}$ . In the case of ordinary rolled I beams the calculations give the values 1.15 to 1.17 for  $M_{ult}/M_{Y.P.}$ .

From this consideration it is seen that if a rectangular beam and an I beam are designed for the same factor of safety with respect to the beginning of yielding, the rectangular beam will be stronger than the I beam with respect to complete failure. After the beginning of yielding a rectangular beam has a larger supply of additional strength than an I beam. In the theoretical case of an I beam which has all its material concentrated in thin flanges, we will find  $M_{ult} = M_{Y.P.}$  and the beginning of yielding coincides with complete failure of the beam.

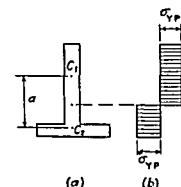


FIG. 220.

In cases of rectangular and I cross sections we have two axes of symmetry, and the neutral axis coincides with one of those axes during elastic and plastic deformation. If we have only one axis of symmetry, as for example in the case of a T section, Fig.

220, the situation is different. In calculating  $M_{Y.P.}$  all fibers of the beam are in the elastic condition and the neutral axis passes through the centroid of the cross section. In calculat-

ing  $M_{ult}$  we take the stress distribution shown in Fig. 220*b*, and since the summation of the inner tensile forces must be equal to that of the compressive forces, we conclude that the neutral axis divides the area of the cross section into two equal parts. When this position of the neutral axis is found, the magnitude of  $M_{ult}$  is calculated from the equation

$$M_{ult} = \frac{1}{2} \sigma_{Y.P.} A a,$$

in which  $A$  is the cross sectional area and  $a$  is the distance between the centroids of the two parts of the cross section.

✓ *Bending by Transverse Forces.*—Let us consider as an example the case of a simply supported and centrally loaded rectangular beam, Fig. 221. The bending moment diagram is a

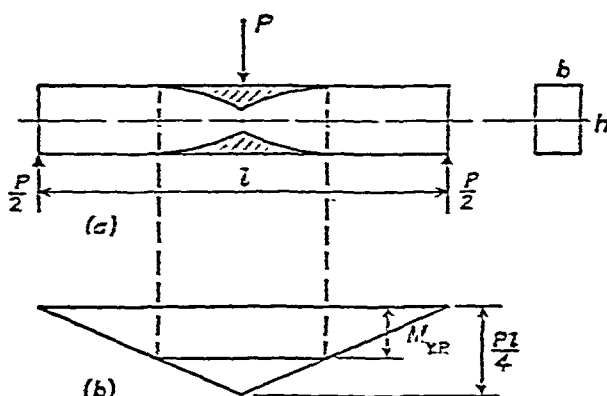


FIG. 221.

triangle, and if  $M_{Y.P.} < Pl/4 < M_{ult}$ , the length of the middle portion of the beam, in which plastic deformation occurs, can be determined as shown in Fig. 221*b*. Neglecting the effect of shearing stresses,<sup>4</sup> the depth  $e$  of penetration of plastic deformation in each cross section can be calculated from eq. (d) and in this way the regions of plastic flow, shaded in the figure, can be determined. As the maximum bending moment  $Pl/4$  approaches the value  $M_{ult}$ , the regions of plasticity approach the neutral axis of the middle cross section of the beam. The resistance to bending at this cross section is therefore at its

<sup>4</sup> Experiments by J. F. Baker and J. W. Roderick justify this assumption; see *Trans. Inst. Welding*, Vol. 3, p. 83, 1940.

maximum value, and the beam will fail. The two halves of the beam will rotate with respect to each other about the neutral axis of the middle cross section, as about a hinge. This is called a *plastic hinge* and resists rotation by the constant moment  $M_{ult}$ .

To investigate the deflection of a beam having regions of plastic deformation, Fig. 221a, we neglect the effect of shearing forces on the deflection and use eqs. (d) and (e) derived for pure bending. Eliminating  $\sigma_{YP}$  from these equations, we obtain

$$\frac{1}{r} = \frac{M}{kEI_z}, \quad (j)$$

where

$$k = \left(1 - \frac{2e}{h}\right) \left[1 + \frac{2e}{h} \left(1 - \frac{e}{h}\right)\right]. \quad (k)$$

The quantity  $k$  is a function of  $e$  and is equal to unity when  $e = 0$  and is equal to zero when  $e = h/2$ . For any cross section in the plastic region of the beam in Fig. 221a,  $e$  can be calculated from eq. (d), and  $k$  can be found from eq. (k).

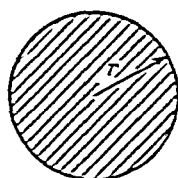
Eq. (j) for the curvature has the same form as in the case of elastic bending, provided we use  $M/k$  instead of  $M$ . In applying the *area-moment method* (see Part I, p. 147) in calculating deflections, we have to use a *modified* bending moment diagram in which the ordinates are equal to  $M/k$ . As  $M$  approaches  $M_{ult}$ ,  $k$  approaches zero, the ordinates of the modified diagram increase indefinitely and we approach the condition of a plastic hinge.

In the preceding discussion a rectangular beam was considered, but similar derivations can be made for other shapes of cross sections. In general, the deflection of a beam in a plane of symmetry beyond the proportional limit can be calculated by using the area-moment method in conjunction with a modified bending moment diagram. The quantity  $k$  in eq. (j) must be derived for each particular shape of cross section.

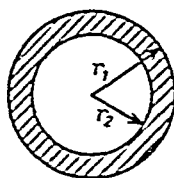
## Problems

1. Determine the ratios  $M_{ult}/M_{Y.P.}$  for the beam cross sections shown in Fig. 222.

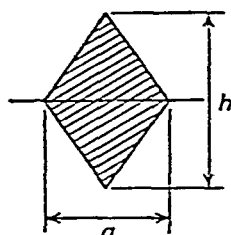
*Answer.* (a)  $\frac{16}{3\pi} = 1.70$ , (b)  $\frac{16r_1}{3\pi} \cdot \frac{r_1^3 - r_2^3}{r_1^4 - r_2^4}$ , (c) 2.



(a)



(b)



(c)

FIG. 222.

2. Find  $M_{ult}$  for the T beam cross section shown in Fig. 223 if  $a = b$ .

*Answer.*

$$M_{ult} = \sigma_{Y.P.} a h \left( \frac{a + h}{2} \right).$$

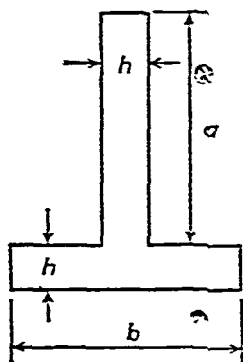


FIG. 223.

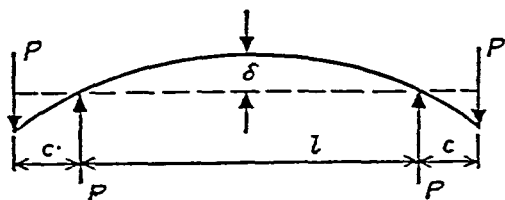


FIG. 224.

3. Find  $M_{ult}/M_{Y.P.}$  for an equilateral triangle cross section.

*Answer.*  $M_{ult}/M_{Y.P.} = 2.343$ .

4. Find the deflection  $\delta$  at the middle of the rectangular beam shown in Fig. 224 if  $Pc = 1.4M_{Y.P.}$ .

*Answer.*

$$\delta = \frac{l^2}{8r} = \frac{l^2}{8} \frac{Pc}{kEI_z}, \quad k = 0.626.$$

5 Solve the preceding problem for the T beam of Fig 223 if  $P_c = 0.90M_{ult}$

6 Find  $q_{ult}$  for a uniformly loaded square steel beam (Fig 225) if the cross sectional area  $A = 9$  sq in,  $l = 48$  in, and  $\sigma_{YF} = 32,000$  lb per sq in

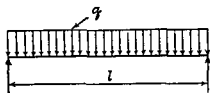


FIG 225

Answer  $q_{ult} = 750$  lb per in

7 Show graphically the modified bending moment diagram and find an approximate value of the deflection at the middle of the uniformly loaded

square beam (Fig 225) if  $ql^2/8 = 1.4M_{YF}$  and the dimensions are the same as in the preceding problem

8 Find the deflection at the middle of the rectangular beam shown in Fig 226 if  $Pl = 3.6M_{ult}$ . Show the boundaries of the plastic regions in the beam

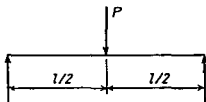


FIG 226

### / 65. Ultimate Strength of Structures.—

It is common practice in the case of metallic structures supporting static loads to select the safe dimensions of the structure in such a way that the service load multiplied by the factor of safety produces a maximum stress equal to the yield point stress of the material<sup>5</sup>. In most cases, however, the onset of yielding does not represent complete failure, and the structure usually will stand a larger load than the load at which yielding begins. To utilize this additional supply of strength it is sometimes suggested<sup>6</sup> that in selecting the

<sup>5</sup> Cases in which the dimensions are selected on the basis of elastic stability considerations are not discussed in this article

<sup>6</sup> This method of determining safe dimensions of steel structures was proposed by N. C. Kist, *Eisenbau*, Vol 11, 1920. Experiments for determining ultimate loads were made by Maier Leibnitz, *Bautechnik*, 1928, and by K. Girkmann, *Bautechnik*, 1932. A theoretical discussion of the bending of beams beyond the yield point was given by J. Fritsche, *Baugenieur*, 1930 and 1931. The combination of bending with compression was discussed by K. Girkmann, *Sitzungsber Akad Wissensch Wien, Abt IIa*, Vol 140, 1931. In more recent times important work in this field has been accomplished at Cambridge University, England, under the direction of J. F. Clark, see *J. Inst. Civil Engrs*, Vol 31, p 188, 1949, and the paper by B. G. Neal and P. S. Symonds, *Proc Inst Civil Engrs*, 1952. In the United States the question of design on the basis of the ultimate load has been discussed by

proper structural dimensions, the ultimate value of the load be calculated for the assumed structural dimensions. The safe load on the structure is then taken as a certain definite portion of that ultimate value, which is the load that produces complete collapse of the structure. The factor of safety in this latter case naturally should be higher than for the case in which the yield load is taken as the basis of design. Design procedure which takes the ultimate load as the basis for selecting the safe dimensions of a structure is called *limit design*. In the following discussion several examples of the application of limit design to various structures will be considered.

Beginning with statically determinate structures, we conclude that in such cases the forces acting on the elements of a structure are determined from equations of statics and are independent of the mechanical properties of the material, provided the deformations remain small. If such a structure consists of bars acting in tension or compression, as in the case of a pin-connected truss, the load which initiates yielding is also the ultimate load, since in the case of a perfectly plastic material (Fig. 216) yielding progresses at constant stress. In the case of the bending of beams, the ratio of the ultimate load to the load which initiates yielding will be equal to the ratio  $M_{ult}/M_{Y.P.}$  and will depend, as we have seen, on the shape of the beam cross section.

In statically indeterminate structures the problem of stress analysis is more complicated, since the forces acting on the elements of a structure depend in this case not only on the magnitude of the external forces but also on the elastic and plastic properties of the elements of the structure, and the analysis requires a consideration of the deformation of the structure. The methods used in investigating deformations within the elastic limit are different from those applied in studying plastic deformations. The differences in the two analyses will now be illustrated by several examples.

We begin with a discussion of statically indeterminate

---

J. A. Van den Broek, *Trans. Am. Soc. Civil Engrs.*, Vol. 105, p. 638, 1940. See also the paper by H. J. Greenberg and W. Prager, *Proc. Am. Soc. Civil Engrs.*, Vol. 77, 1951.



cases of the bending of beams of constant cross section. Take, for example, the case of a beam with one end built in and the other simply supported, Fig. 227. Considering first the bend-

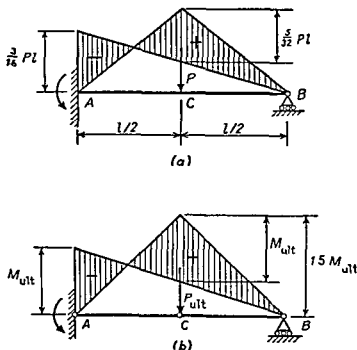


FIG 227

ing which occurs within the elastic limit and observing that the end  $A$  of the beam is built in, we find the bending moment diagram as shown in Fig. 227*a* by the shaded area (see Part I, p. 180). If we take as a basis of design the load at which yielding begins, we observe that the maximum bending moment occurs at the built-in end  $A$  of the beam and calculate the value of  $P_{YP}$  from the equation

$$\frac{3}{16} P_{YP} l = M_{YP},$$

which gives

$$P_{YP} = \frac{16}{3} \frac{M_{YP}}{l}. \quad (a)$$

In calculating  $P_{ult}$  we observe that when the load is increased beyond  $P_{YP}$ , yielding begins at the built-in end  $A$ . At a somewhat larger load than  $P_{YP}$ , yielding begins at cross section  $C$  where there is another peak in the bending moment

diagram. Continuing to increase the load, the condition of a plastic hinge is reached at the end  $A$  of the beam, but this condition does not cause complete collapse of the beam. The structure will stand some further increase in the load  $P$  until the bending moment at cross section  $C$  also reaches the value  $M_{ult}$ . Then there will be plastic hinges at  $A$  and  $C$  and free rotation at  $B$ . This is the limiting condition corresponding to complete collapse of the beam. The bending moments at  $A$  and  $C$  for this case are numerically equal to  $M_{ult}$  and the bending moment diagram is shown in Fig. 227*b*. From this diagram we see that the maximum ordinate of the bending moment triangle, corresponding to the load  $P_{ult}$ , is equal to  $1.5M_{ult}$  and calculate  $P_{ult}$  from the equation

$$\frac{P_{ult}l}{4} = 1.5M_{ult},$$

which gives

$$P_{ult} = \frac{6M_{ult}}{l}. \quad (b)$$

From eqs. (a) and (b) we now obtain

$$\frac{P_{ult}}{P_{Y.P.}} = \frac{9}{8} \frac{M_{ult}}{M_{Y.P.}}; \quad (c)$$

i.e., the ratio of the loads  $P_{ult}:P_{Y.P.}$  is larger in this statically indeterminate case than the value of the ratio  $M_{ult}:M_{Y.P.}$  which is obtained in statically determinate cases.

We see also that by introducing plastic hinges at  $A$  and  $C$ , Fig. 227*b*, we obtain a problem which can be readily solved by using equations of statics and which is much simpler than the statically indeterminate problem in Fig. 227*a*. Thus the calculation of  $P_{ult}$ , in limit design, is simpler than the calculation of  $P_{Y.P.}$  in the design based on the assumption of elastic behavior of the structure. It is also more realistic, since the results obtained on the assumption of perfect elasticity depend on the accuracy of the assumed end conditions of the beam. A slight rotation of the built-in end  $A$  or a small lowering of the support  $B$  may change considerably the magnitude of  $P_{Y.P.}$ , while imperfections of the same kind do not

affect the value of  $P_{ult}$  calculated for the statically determinate system of Fig. 227*b*. These are the two principal advantages of the limit-design method.

As a second example let us consider the case of a uniformly loaded beam with one end built in and the other end simply supported, Fig. 228. Within the elastic range the

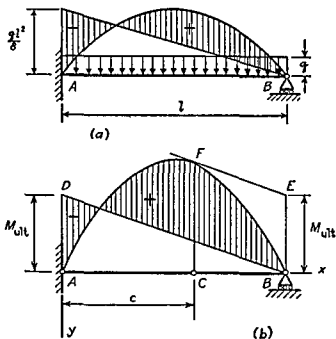


FIG. 228.

bending moment diagram will be as shown in Fig. 228*a*. The numerically maximum value of the bending moment is at the built-in end, and the magnitude of the load  $q_{Y.P.}$  is found from the equation

$$\frac{q_{Y.P.} l^2}{8} = M_{Y.P.},$$

which gives

$$q_{Y.P.} = \frac{8M_{Y.P.}}{l^2}. \quad (d)$$

If we continue to increase the load above the value  $q_{Y.P.}$ , yielding at the built-in end  $A$  will progress further and the corresponding bending moment will increase up to the value  $M_{ult}$ , when a plastic hinge will form at  $A$ . To obtain complete

collapse of the beam we have to continue increasing the load up to the value  $q_{ult}$  at which a plastic hinge will form at a certain intermediate cross section  $C$  of the beam, Fig. 228*b*. The position of the cross section  $C$  and the value of  $q_{ult}$  will be found from the conditions that the bending moment at  $C$  is a maximum and that it is equal to  $M_{ult}$ . Using the shaded bending moment diagram in Fig. 228*b*, we write these two conditions as follows:

$$M = \frac{q_{ult}l}{2}x - \frac{q_{ult}x^2}{2} - \frac{M_{ult}(l-x)}{l} = M_{ult}, \quad (e)$$

$$\frac{dM}{dx} = \frac{q_{ult}l}{2} - q_{ult}x + \frac{M_{ult}}{l} = 0. \quad (f)$$

From these equations we obtain

$$x = c = l(2 - \sqrt{2}), \quad q_{ult} = \frac{2M_{ult}}{l^2(3 - 2\sqrt{2})}, \quad (g)$$

and we conclude from eqs. (d) and (g) that

$$\frac{q_{ult}}{q_{Y.P.}} = 1.46 \frac{M_{ult}}{M_{Y.P.}}. \quad (h)$$

In discussing more general cases of plastic deformation of structures we observe that beyond the elastic limit the principle of superposition does not hold and the deformation of a structure depends not only on the final values of the loads but also on the order in which the loads are applied to the structure. Take, for example, the case shown in Fig. 229*a*. If both forces are applied simultaneously, the corresponding bending moment diagram will have the shape shown in Fig.

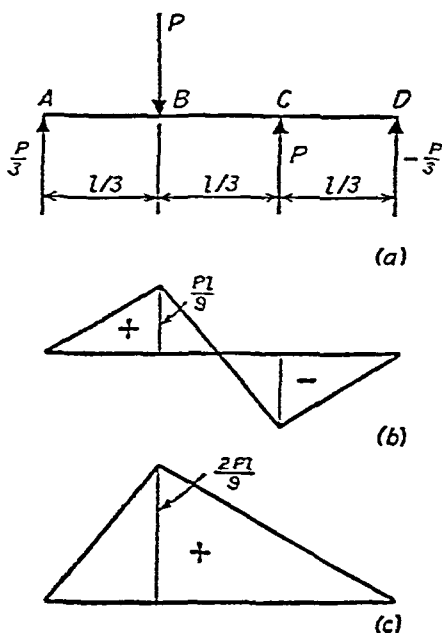


FIG. 229.

229*b* and the maximum bending moment is  $Pl/9$ . We see that the deformation will be perfectly elastic if

$$P < \frac{9M_{Y.P.}}{l} \quad (i)$$

Let us consider now the case when the load  $P$  is applied at cross section  $B$  first and the load at  $C$  is applied afterwards. After the load at  $B$  is applied, the corresponding bending moment diagram has the shape shown in Fig. 229*c*; the maximum bending moment is two times larger than in the preceding case and may produce plastic deformation although the condition of eq. (i) is satisfied. This plastic deformation will not be removed by subsequent application of the force  $P$  at cross section  $C$ , and the final deformation of the beam will

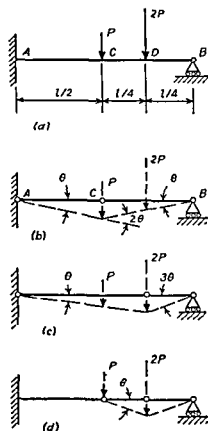


FIG. 230.

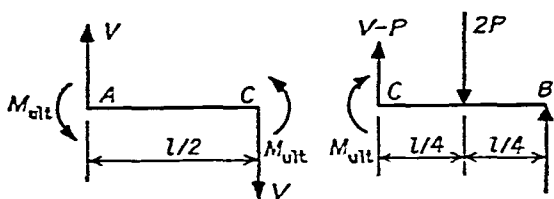
be different from the case of simultaneous application of the forces at cross sections  $B$  and  $C$ . In our further discussion we will always assume that the forces are applied simultaneously and that during the process of loading the ratios between the forces remain constant and equal to the ratios of the final values of the forces. All the forces will be denoted by the same symbol multiplied by numerical factors indicating the required ratios between the magnitudes of the forces.

In the problems previously discussed, such as those shown in Figs. 227 and 228, there was only one possible way of positioning the plastic hinges and only one form of collapse of the beam had to be considered. But if several

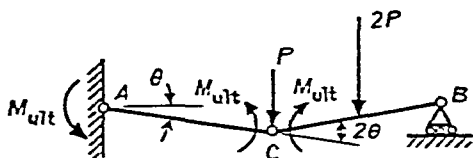
forces are acting on the beam, there will be several different possibilities for locating plastic hinges and several possible

forms of collapse of the beam. Naturally the designer has to select from all the possible forms of collapse the one which occurs at the smallest value of the loads. These loads will then be considered as the ultimate loads for the structure.

As an example of the selection of the proper locations for the plastic hinges, let us consider the beam in Fig. 230, which is built in at  $A$ , simply supported at  $B$  and carries two loads  $P$  and  $2P$ . The bending moment diagram in this case will be represented by a broken line, and the peak values of the bending moment will be located on the verticals through the cross sections  $A$ ,  $C$  and  $D$ . At the condition of complete collapse, plastic hinges will be formed at two of these three cross sections. All possible locations of these hinges and the corresponding forms of collapse are shown in Fig. 230*b-d*. Observing that at each plastic hinge the moments  $M_{ult}$  act so as to oppose any relative rotation, we can write equations of equilibrium for each portion of the beam and determine the magnitude of  $P$  corresponding to the assumed form of collapse. For example, for the form shown in Fig. 230*b*, the corre-



(a)



(b)

FIG. 231.

sponding forces are shown in Fig. 231*a* and the equations of equilibrium are

$$\frac{Pl}{2} - 2M_{ult} = 0; \quad \frac{(V - P)l}{2} + M_{ult} - \frac{Pl}{2} = 0,$$

from which we find

$$P_{\text{ult}} = \frac{3M_{\text{ult}}}{l}.$$

Instead of using equations of equilibrium such as are shown above, it is advantageous to apply the principle of virtual displacements<sup>1</sup> in calculating  $P_{\text{ult}}$ . Considering again the form of collapse shown in Fig. 230*b*, we see that by introducing plastic hinges at *A* and *C* we obtain a mechanism consisting of two hinged bars, Fig. 231*b*. To write the condition of equilibrium of this mechanism let us consider a virtual displacement defined by the small angle of rotation  $\theta$ . During this rotation the moments  $M_{\text{ult}}$  at the cross sections *A* and *C*, opposing rotation, will produce work equal to  $-\theta M_{\text{ult}}$  and  $-2\theta M_{\text{ult}}$ . At the same time the loads  $P$  and  $2P$  will produce work equal to  $P\theta l/2$  and  $2P\theta l/4$ , so that the equation of virtual displacements becomes

$$-\theta M_{\text{ult}} - 2\theta M_{\text{ult}} + \frac{P\theta l}{2} + \frac{2P\theta l}{4} = 0,$$

from which

$$P_{\text{ult}} = \frac{3M_{\text{ult}}}{l}. \quad (j)$$

Proceeding in the same way for the cases shown in Figs. 230*c* and 230*d*, we obtain the following results:

$$P_{\text{ult}} = \frac{2.5M_{\text{ult}}}{l}, \quad P_{\text{ult}} = \frac{6M_{\text{ult}}}{l}. \quad (k)$$

Comparing the results, eqs. (j) and (k), we conclude that for the beam represented in Fig. 230*a* the ultimate load is  $P_{\text{ult}} = 2.5M_{\text{ult}}/l$ , and the corresponding form of collapse is shown in Fig. 230*c*.

The method of calculating ultimate loads which was used in the preceding cases of beams can be applied also in discussing the ultimate strength of frames. Let us consider the

<sup>1</sup>This method of calculation was introduced by J. F. Baker, *J. Inst. Structural Engrs.*, Vol. 27, p. 397, 1949.

frame shown in Fig. 232*a*, which has three redundant quantities. We can take, for example, the bending moment and two components of the reactive force at *B* as the three redundants. If these three quantities are known, the moment and two components of the force at any cross section of the frame can be readily found from equations of statics. We can make the structure statically determinate also by putting three hinges in it. For example, by putting hinges at *A*, *B* and *E* we obtain

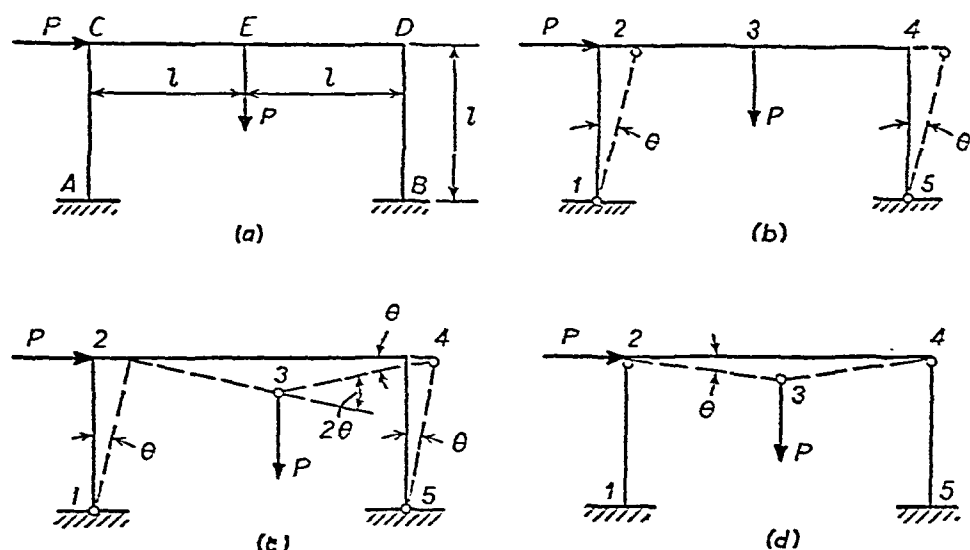


FIG. 232.

a structure which can be readily analyzed as a three-hinged arch. To make a movable system (or mechanism) out of the frame we have to introduce four plastic hinges. To determine the locations of these hinges we observe that the bending moment diagram will have peaks at the cross sections 1, 2, ... 5, (Fig. 232), where the concentrated forces are acting. The plastic hinges must be located at some of those cross sections, since the bending moment reaches its largest numerical values at those points. Two possible ways of locating the four plastic hinges, corresponding to two different forms of collapse of the frame, are shown in Fig. 232*b* and *c*.<sup>8</sup>

<sup>8</sup> For selection of all possible forms of collapse of frame structures see the paper by P. S. Symonds and B. G. Neal, *J. Inst. Civil Engrs.*, Vol. 35, p. 21, 1950.



In Fig. 232*d* we have an exceptional case of failure. By introducing only three plastic hinges we naturally do not obtain a mechanism of the same type as in the two preceding cases. As the plastic hinges at the cross sections 2, 3 and 4 are formed, there will not occur an unlimited relative rotation at these hinges with a further increase of the load  $P$ . The two bars 2-3 and 3-4, after some rotation, will be in a position to sustain a further increase of the load  $P$  by working in tension. But the corresponding displacements will be large, and we have to consider this deformation also as representing complete collapse of the frame.

To calculate the values of  $P_{ult}$  corresponding to the three different modes of collapse shown in Fig. 232 we use the dimensions shown in the figure and in addition assume that the cross section of the horizontal member  $CD$  is larger than that of the verticals, so that  $M_{ult}$  represents the ultimate moment for the verticals and  $1.5M_{ult}$  represents the ultimate moment for the horizontal member.<sup>9</sup> The virtual displacements will be defined by the small angle  $\theta$ . Then the equation of equilibrium for the case shown in Fig. 232*b* will be

$$P\theta l - 4\theta M_{ult} = 0,$$

from which

$$P_{ult} = \frac{4M_{ult}}{l}.$$

For the case in Fig. 232*c* the equation of equilibrium is

$$P\theta l + P\theta l - 2\theta M_{ult} - 1.5(2\theta)M_{ult} - 2\theta M_{ult} = 0,$$

from which

$$P_{ult} = \frac{3.5M_{ult}}{l};$$

and for the case of Fig. 232*d* we obtain in the same way

$$P_{ult} = \frac{5M_{ult}}{l}.$$

---

<sup>9</sup> The plastic hinges at the corners will be formed in the weaker members as shown by the location of the small circles in Fig. 232*b*, *c* and *d*.

From these results we conclude that the actual form of collapse will be as shown in Fig. 232c and that the ultimate load is

$$P_{\text{ult}} = \frac{3.5M_{\text{ult}}}{l}.$$

### Problems

1. Find the values of  $P_{\text{ult}}$  and  $q_{\text{ult}}$  for the beams shown in Fig. 233.

*Answer.* (a)  $P_{\text{ult}} = \frac{8M_{\text{ult}}}{l}$ , (b)  $q_{\text{ult}} = \frac{16M_{\text{ult}}}{l^2}$ , (c)  $P_{\text{ult}} = \frac{6M_{\text{ult}}}{l}$ .

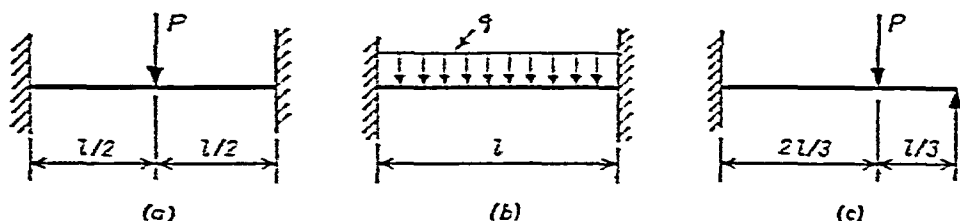


FIG. 233.

2. A two-span beam of constant cross section is uniformly loaded, Fig. 234. Find  $q_{\text{ult}}$  assuming that  $l_1 > l_2$ .

*Answer.*

$$q_{\text{ult}} = \frac{2M_{\text{ult}}}{l_1^2(3 - 2\sqrt{2})}.$$

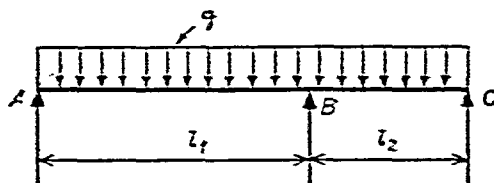


FIG. 234.

3. Find the value of  $P_{\text{ult}}$  for the continuous beam of uniform cross section shown in Fig. 235. Show the form of collapse.

*Answer.*

$$P_{\text{ult}} = \frac{16M_{\text{ult}}}{3l}.$$

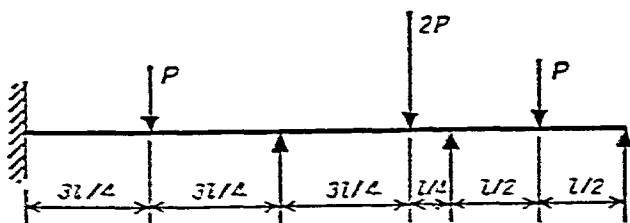


FIG. 235.

- 4 A beam with built in ends is subjected to the action of two forces  $P$  and  $2P$ , Fig 236 Find  $P_{ult}$  and show the corresponding form of collapse

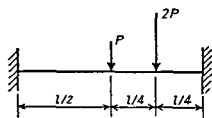


FIG 236

Answer

$$P_{ult} = \frac{4M_{ult}}{l}$$

- 5 Find  $P_{ult}$  and the corresponding form of collapse for the frame in Fig 237

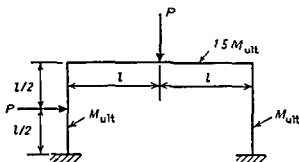


FIG 237

✓66. Pure Bending of Beams of Material Which Does Not Follow Hooke's Law.—In the preceding articles it was assumed that the material of the beams was perfectly plastic (Fig 216) Let us consider now the more general case in which the mechanical properties of the material are represented by a diagram such as curve  $AOB$  in Fig 239 In discussing the pure bending of such beams we assume, as before, that cross sections of the beam remain plane during bending, hence elongations and contractions of the longitudinal fibers are proportional to their distances from the neutral surface Taking this as a basis of our further discussion and assuming that during bending there exists the same relation between stress and strain as in the case of simple tension and compression, we can find without difficulty the stresses produced in the beam by a bending moment of any given magnitude <sup>10</sup>

Let us begin with a beam of rectangular cross section,

<sup>10</sup> This theory was developed by St Venant in his notes to Navier's book, *Résumé des leçons*, 3d Ed, p 173, 1864 See also the paper by Eugen Mayer, *Phys Z*, 1907, and H Herbert, dissertation, Göttingen, 1909

Fig. 238, and assume that the radius of curvature of the neutral surface produced by the bending moments  $M$  is equal to  $r$ .

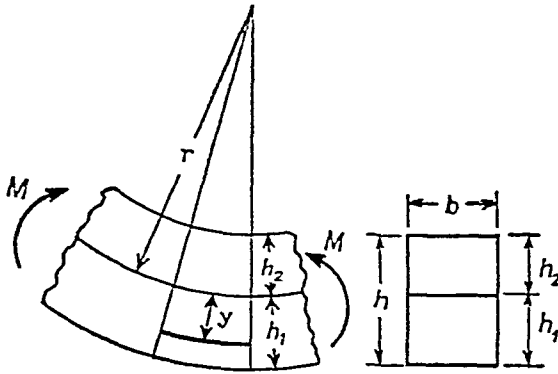


FIG. 238.

In such a case the unit elongation of a fiber at distance  $y$  from the neutral surface is

$$\epsilon = \frac{y}{r}. \quad (a)$$

Denoting by  $h_1$  and  $h_2$  the distances from the neutral axis to the lower and upper surfaces of the beam respectively, we find that the elongations in the extreme fibers are

$$\epsilon_1 = \frac{h_1}{r}, \quad \epsilon_2 = -\frac{h_2}{r}. \quad (b)$$

It is seen that the elongation or contraction of any fiber is readily obtained provided we know the position of the neutral axis and the radius of curvature  $r$ . These two quantities can be found from the two equations of statics:

$$\int_A \sigma dA = b \int_{-h_2}^{h_1} \sigma dy = 0, \quad (c)$$

$$\int_A \sigma y dA = b \int_{-h_2}^{h_1} \sigma y dy = M. \quad (d)$$

The first of these equations states that the sum of the normal forces acting on any cross section of the beam vanishes, since these forces represent a couple. The second equation states

that the moment of the same forces with respect to the neutral axis is equal to the bending moment  $M$ .

Eq. (c) is now used for determining the position of the neutral axis. From eq. (a) we have

$$y = r\epsilon, \quad dy = r d\epsilon. \quad (e)$$

Substituting into eq. (c), we obtain

$$\int_{-h_2}^{h_1} \sigma dy = r \int_{\epsilon_2}^{\epsilon_1} \sigma d\epsilon = 0. \quad (f)$$

Hence the position of the neutral axis is such that the integral

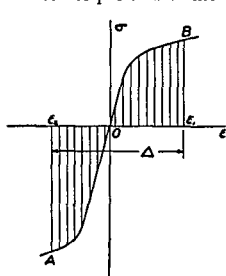


FIG. 239.

$\int_{\epsilon_2}^{\epsilon_1} \sigma d\epsilon$  vanishes. To determine this position we use the curve  $AOB$  in Fig. 239, which represents the tension-compression test diagram for the material of the beam, and we denote by  $\Delta$  the sum of the absolute values of the maximum elongation and the maximum contraction, which is

$$\Delta = \epsilon_1 - \epsilon_2 = \frac{h_1}{r} + \frac{h_2}{r} = \frac{h}{r}. \quad (g)$$

To solve eq. (f), we have only to mark the length  $\Delta$  on the horizontal axis in Fig. 239 in such a way as to make the two areas shaded in the figure equal. In this manner we obtain the strains  $\epsilon_1$  and  $\epsilon_2$  in the extreme fibers. Eqs. (b) then give

$$\frac{h_1}{h_2} = \left| \frac{\epsilon_1}{\epsilon_2} \right|, \quad (h)$$

which determines the position of the neutral axis. Observing that the elongations  $\epsilon$  are proportional to the distance from the neutral axis, we conclude that the curve  $AOB$  also represents the distribution of bending stresses along the depth of the beam, if  $h$  is substituted for  $\Delta$ .

In calculating the radius of curvature  $r$  we use eq. (d). Substituting for  $y$  and  $dy$  their values from eqs. (e), we represent eq. (d) in the following form:

$$br^2 \int_{\epsilon_2}^{\epsilon_1} \sigma \epsilon d\epsilon = M. \quad (i)$$

By observing that  $r = h'/\Delta$  from eq. (g), we can write eq. (i), after a simple transformation, as follows:

$$\frac{bh^3}{12} \cdot \frac{1}{r} \cdot \frac{12}{\Delta^3} \int_{\epsilon_2}^{\epsilon_1} \sigma \epsilon d\epsilon = M. \quad (j)$$

Comparing this result with the known equation

$$\frac{EI}{r} = M \quad (k)$$

for bending of beams following Hooke's law, we conclude that beyond the proportional limit the curvature produced by a moment  $M$  can be calculated from the equation

$$\frac{E_r I}{r} = M, \quad (281)$$

in which  $E_r$  is the *reduced modulus* defined by the expression

$$E_r = \frac{12}{\Delta^3} \int_{\epsilon_2}^{\epsilon_1} \sigma \epsilon d\epsilon. \quad (282)$$

The integral in this expression represents the moment with respect to the vertical axis through the origin  $O$  of the shaded area shown in Fig. 239. Since the ordinates of the curve in the figure represent stresses and the abscissas represent strains, the integral and also  $E_r$  have the dimensions of lb per sq in., which are the same dimensions as the modulus  $E$ .

The magnitude of  $E_r$  for a given material, corresponding to a given curve in Fig. 239, is a function of  $\Delta$  or of  $h'/r$ . Taking several values of  $\Delta$  and using the curve in Fig. 239 as previously explained, we determine for each value of  $\Delta$  the corresponding extreme elongations  $\epsilon_1$  and  $\epsilon_2$ , and from eq. (282) determine the corresponding values of  $E_r$ . In this way a curve repre-

sending  $E_r$  as a function of  $\Delta = h/r$  is obtained. In Fig. 240 such a curve is shown for structural steel with  $E = 30 \times 10^6$  lb per sq in. and the proportional limit equal to 30,000 lb per

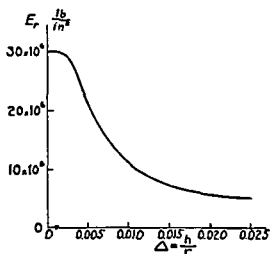


FIG. 240

sq in. In this case, for  $\Delta < 0.002$ ,  $E_r$  remains constant and equal to  $E$ . With such a curve the moment corresponding to any assumed curvature can be readily calculated from eq. (281), and we can plot a curve, Fig. 241, giving the moment  $M$

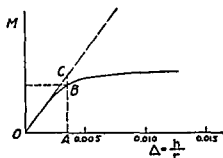


FIG. 241

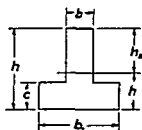


FIG. 242

as a function of  $\Delta$ . For small values of  $\Delta$  the material follows Hooke's law, and the curvature is proportional to the bending moment  $M$ , as shown in Fig. 241 by the straight line  $OC$ . Beyond the proportional limit the rate of change of the curvature increases as the moment increases.

If instead of a rectangle we have any other symmetrical shape of cross section, the width  $b$  of the cross section is var-

iable, and eqs. (c) and (d) must be written in the following form:

$$\int_{-h_2}^{h_1} b \sigma dy = r \int_{\epsilon_2}^{\epsilon_1} b \sigma d\epsilon = 0, \quad (l)$$

$$\int_{-h_2}^{h_1} b \sigma y dy = r^2 \int_{\epsilon_2}^{\epsilon_1} b \sigma \epsilon d\epsilon = M. \quad (m)$$

Take as an example the case of a  $\perp$  section, Fig. 242. If we denote by  $\epsilon'$  the longitudinal strain at the junction of the web and flange, eqs. (l) and (m) can be written in the following form:

$$\int_{\epsilon_2}^{\epsilon'} \sigma d\epsilon + \int_{\epsilon'}^{\epsilon_1} \frac{b_1}{b} \sigma d\epsilon = 0, \quad (n)$$

$$br^2 \left( \int_{\epsilon_2}^{\epsilon'} \sigma \epsilon d\epsilon + \int_{\epsilon'}^{\epsilon_1} \frac{b_1}{b} \sigma \epsilon d\epsilon \right) = M. \quad (o)$$

We see that in this case the ordinates of the tensile test curve  $AOB$ , Fig. 243, in the region corresponding to the flange of the cross section must be magnified in the ratio  $b_1/b$ . In determining the position of the neutral axis we proceed as in the preceding case and use the tension-compression test diagram, Fig. 243, and mark on the horizontal axis the position of the assumed length  $\Delta = h/r$  such that the two shaded areas become numerically equal. In this manner the strains  $\epsilon_1$  and  $\epsilon_2$  in the extreme fibers are obtained. The strain  $\epsilon'$  at the junction of the web and flange is obtained from the equation

$$\frac{\epsilon_1 - \epsilon'}{\Delta} = \frac{c}{h},$$

in which  $c$  is the thickness of the flange, Fig. 242. Having

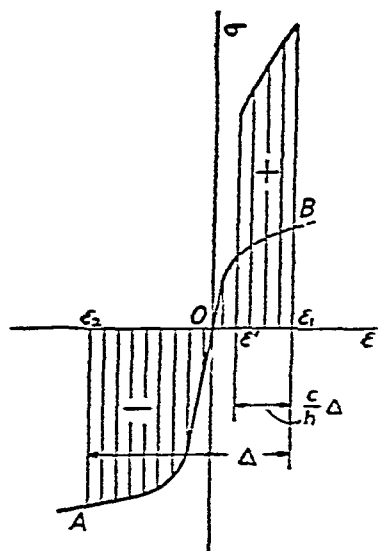


FIG. 243.



determined the position of the neutral axis and observing that the expression in the parentheses of eq (o) represents the moment of the shaded areas in Fig 243 with respect to the vertical axis through the origin  $O$ , we can readily calculate from eq (o) the moment  $M$  corresponding to the assumed value of  $\Delta = h/r$ . In this manner a curve similar to that shown in Fig 241 can be constructed for a beam of  $\perp$  section. An I beam can be treated in a similar manner.

In the preceding examples the tension compression test diagram  $AOB$  was used for determining the position of the neutral axis and the magnitude of the radius of curvature  $r$ . If there exists an analytical expression for the curve  $AOB$ , the above quantities can be obtained by calculation alone without using the graphical method shown in Fig 239 and Fig 243. A very general equation for stress strain curves was used by St Venant<sup>11</sup>. He assumed that for bending beyond the proportional limit the distribution of tensile and compressive stresses along the depth of the beam can be represented by the following equations

$$\begin{aligned}\sigma &= \sigma_0 \left[ 1 - \left( 1 - \frac{y}{a} \right)^m \right] \\ \sigma' &= \sigma_0 \left[ 1 - \left( 1 - \frac{y_1}{b} \right)^n \right]\end{aligned}\tag{p}$$

in which  $\sigma_0$  and  $\sigma'_0$  and also  $a$  and  $b$  are certain constants which, together with the exponents  $m$  and  $n$ , define the stress distribution curves shown in Fig 244. For very small distances  $y$  and  $y_1$  we can assume that

$$\left( 1 - \frac{y}{a} \right)^m \approx 1 - \frac{my}{a} \quad \text{and} \quad \left( 1 - \frac{y_1}{b} \right)^n \approx 1 - \frac{ny_1}{b}$$

and eqs (p) give

$$\sigma = \frac{\sigma_0 my}{a} = \frac{\sigma_0 m r \epsilon}{a} \quad \text{and} \quad \sigma' = \frac{\sigma'_0 n y_1}{b} = \frac{\sigma'_0 n r \epsilon}{b}$$

<sup>11</sup> *Loc cit*, p 366. See also the paper by W R Osgood, *J Aeronaut Sci*, Vol 11, p 213, 1944.

Hence

$$\frac{\sigma_0 m r}{a} = E_1, \quad \text{and} \quad \frac{\sigma_0' n r}{b} = E_2, \quad (q)$$

where  $E_1$  and  $E_2$  are the moduli of the material for very small tension and compression respectively. If these two moduli of the material are equal, the two curves given by eqs. (p) have a common tangent at the neutral axis, and we have

$$\frac{\sigma_0 m}{a} = \frac{\sigma_0' n}{b}. \quad (r)$$

By using eqs. (p) in equations of equilibrium (c) and (d), the position of the neutral axis and the radius of curvature can be calculated in each particular case. Taking, for example,  $m = n = 1$  and using eqs. (q) we obtain, from eqs. (p),

$$\sigma = \frac{E_1 y}{r}, \quad \sigma' = \frac{E_2 y_1}{r}. \quad (s)$$

This is the case in which the material of the beam follows Hooke's law but has a modulus in tension different from that in compression. Substituting from eqs. (s) into eq. (c) and assuming that the beam has a rectangular cross section, we obtain

$$E_1 k_1^2 = E_2 k_2^2,$$

which, together with the equation  $k_1 + k_2 = h$ , gives

$$k_1 = \frac{k\sqrt{E_2}}{\sqrt{E_1} + \sqrt{E_2}}, \quad k_2 = \frac{k\sqrt{E_1}}{\sqrt{E_1} + \sqrt{E_2}}.$$

From eq. (d) we then find

$$\frac{E_1 k_1}{r} \cdot \frac{b k_1}{2} \cdot \frac{2}{3} h = \frac{b k^3}{12} \cdot \frac{1}{r} \cdot \frac{4 E_1 E_2}{(\sqrt{E_1} + \sqrt{E_2})^2}.$$

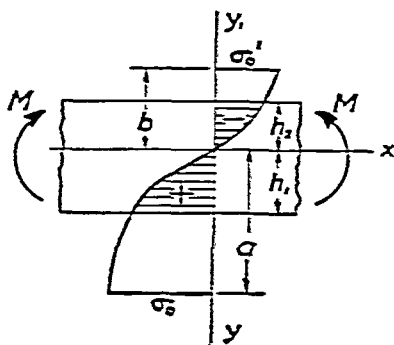


FIG. 244.

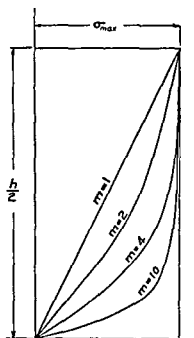


FIG 245

It is seen that in this case the curvature is obtained from eq. (281) by using for the reduced modulus the value

$$E_r = \frac{4E_1E_2}{(\sqrt{E_1} + \sqrt{E_2})^2} \quad (283)$$

This modulus is sometimes used in calculating the buckling load for a column compressed beyond the proportional limit of the material (see p. 182).

As another example let us assume that the stress-strain curves in tension and compression are identical; then  $m = n$ ,  $a = b$  and  $\sigma_0 = \sigma_0'$  in eqs. (p). Assuming also that  $a = b = h/2$ , we find, from eq. (d), for a rectangular beam

$$M = \sigma_{\max} \frac{bh^2}{6} \frac{3m(m+3)}{2(m+1)(m+2)} \quad (284)$$

The neutral axis in this case goes through the centroid of the cross section. The curves giving the stress distribution for various values of the exponent  $m$  are shown in Fig 245. With increasing values of  $m$  the moment approaches the value

$$M = \frac{3}{2} \cdot \sigma_{\max} \cdot \frac{bh^2}{6}$$

**67. Bending of Beams by Transverse Loads beyond the Elastic Limit.**—In the case of the bending of beams by transverse loads we neglect the action of shear on the deflection<sup>12</sup> and assume that the relation between bending moment and curvature is represented by eq. (281) derived for pure bending. Then the area-moment method (see Part I, p. 147) can be applied in calculating deflections beyond the proportional limit. It is only necessary to observe that the flexural rigidity in this case is not constant, but varies with the magnitude of the bending moment. To establish the relation between these

<sup>12</sup> The effect of shear has been discussed by A. Eichinger, *Final Report*, 2d Congr. Internat. Assoc. Bridge and Structural Engng, Berlin, 1938.

two quantities for rectangular beams, we use the curve in Fig. 241. For any value of  $\Delta = h/r$  the ordinate  $AB$  gives the corresponding value of the bending moment, and the ordinate  $AC$  represents the moment which we would have if the material followed Hooke's law. Hence

$$\overline{AB}:\overline{AC} = E_r:E.$$

In this way we obtain for each assumed value of the bending moment the ratio  $E_r I / EI$  of the reduced flexural rigidity to the initial flexural rigidity of the beam. Denoting this ratio by  $\beta$  we represent it as a function of the bending moment  $M$  by the curve shown in Fig. 246.

To illustrate how this curve can be used in the calculation of deflections, let us consider the case of a simply supported beam loaded at the middle, Fig.

247. The bending moment diagram in this case is the triangle  $ACB$ . Let  $M_0$  be the magnitude of the bending moment up to which the material follows Hooke's law. In such a case the portion  $mn$  of the beam is stressed beyond the proportional limit, and the reduced flexural rigidity, which varies along this portion of

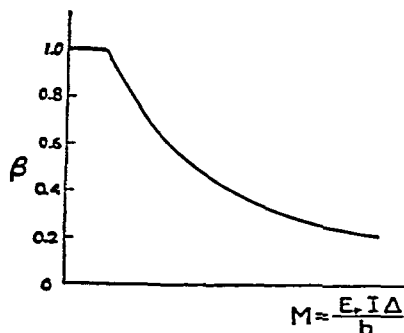


FIG. 246.

the beam, must be used instead of the initial flexural rigidity in calculating deflections. Proceeding as in the case of beams of variable cross section (see Part I, p. 212), we divide the ordinates of the bending moment diagram by the corresponding values of  $\beta$ , taken from Fig. 246. In this manner the *modified* bending moment diagram  $ADEFB$  is obtained. Considering the modified bending moment area as a fictitious load and proceeding in the usual way, we obtain the deflection at any cross section of the beam by dividing by  $EI$  the bending moment produced at that cross section by the fictitious load.

We have discussed here only the case of a rectangular

beam, but the same method is applicable in other cases provided a curve for the factor  $\beta$ , similar to that shown in Fig 246, is obtained. Such a curve can be constructed by using the method illustrated in Fig 243, or its ordinates can be calculated if the stress strain relation beyond the proportional limit of the material is given analytically as by eqs (p) in Art 66.

In our discussion of the bending of beams by transverse loads it was assumed that the problem was statically deter-

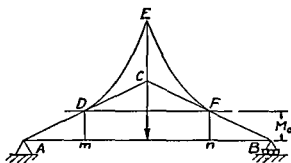


FIG 247

minate so that the construction of the bending moment diagram did not require any discussion of the deflection curve. In statically indeterminate cases the problem becomes more involved, since beyond the proportional limit redundant forces and moments are no longer proportional to the acting loads, and the principle of superposition does not hold. Sometimes, however, the problem can be simplified by using a symmetry consideration. Assuming, for example, that the ends of the beam in Fig 247 are built in, we conclude from symmetry that the bending moment vanishes at the quarter points, and the deflection curve consists of four identical portions which can be obtained in the same way as for a cantilever loaded at the end. In the case of a uniformly loaded beam with built-in ends we conclude from symmetry that the moments at the ends are equal. The magnitude of these moments can be obtained by trial and error method. It is necessary to assume some value for these moments and construct the modified bending moment diagram, as explained for the case shown in Fig 247. The correct value of the moments is evidently that

value at which the total fictitious load, represented by the modified bending moment area, vanishes.

It may be seen from the above discussion that in the case of bending beyond the proportional limit the calculation of redundant forces and redundant moments usually requires a complicated investigation. However, in the case of materials which have a pronounced yield point, such as structural steel, the analysis of statically indeterminate structures can be simplified very much if we limit our consideration to the stage of loading at which the structure reaches the ultimate load and begins to yield without a further increase in the load (see Art. 65).

§ 68. Residual Stresses Produced by Inelastic Bending.—If a beam is bent beyond the elastic limit, some permanent set is produced, and the deformation does not vanish after the load is removed. The fibers which have suffered a permanent set prevent the elastically stressed fibers from recovering their initial length after unloading, and in this way some *residual stresses* are produced. To determine the distribution of these stresses over the cross section, let us begin with the simplest case of a rectangular beam in which the stress distribution in bending beyond the yield point can be represented by two rectangles,  $Oklm$  and  $Oprn$ , shown in Fig. 248*a*. We assume also that the material, if stretched be-

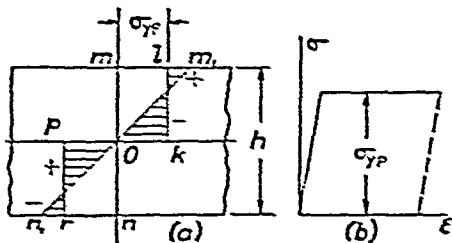


FIG. 248.

yond the yield point and then unloaded, follows Hooke's law during unloading, as shown in Fig. 248*b* by the broken line. As a result of this assumption it can be concluded that the bending stresses which are superposed while unloading the beam follow the linear law indicated in Fig. 248*a* by the line  $m_1n_1$ . The superposition of the two stress distributions, rectangular while loading and triangular while unloading, shown by the shaded areas in Fig. 248*a*, represents the stresses which remain in the beam after unloading. These are the residual stresses produced in the beam by plastic deforma-

It is seen that if the curvature  $d(1/r)$  is measured, then the magnitude of the residual tensile stress  $\sigma$  in the most remote fiber is readily calculated from eq (a)

The determination of the residual stress  $\sigma_a$  in a fiber  $mn$  at a distance  $a$  from the upper side of the beam, Fig 249b, is more involved. By taking off one layer after the other we finally reach the layer  $mn$ , and we can determine the stress in it by using an equation similar to eq (a). This stress, however, will have a magnitude  $\sigma'_a$  different from the initial residual stress  $\sigma_a$ , since the removal of the previous layers produces changes of stresses in the remaining portions of the beam. It is evident that only after investigation of these changes will the determination of the required residual stress  $\sigma_a$  be possible. Let us assume that by taking off layer after layer we reach the fibers indicated by the broken line in Fig 249b, at a distance  $2z$  from the upper side of the beam. If a new thin layer of thickness  $\Delta$  is now taken off, the stress  $\sigma'_z$  in this layer is obtained from the equation

$$d\left(\frac{1}{r}\right) = \frac{\sigma'_z b z \Delta}{EI_z} \quad \text{where} \quad I_z = \frac{b(2z)^3}{12},$$

from which

$$\sigma'_z = \frac{d(1/r)EI_z}{bz\Delta} \quad (b)$$

The removal of this layer will produce in the fiber  $mn$  a direct stress of magnitude

$$\frac{\sigma'_z b \Delta}{2bz} \quad (c)$$

and a bending stress of magnitude

$$\frac{\sigma'_z b z \Delta (a - z)}{I_z} \quad (d)$$

Eqs (c) and (d) give the changes in the stress in the fiber  $mn$  owing to the removal of one layer. Now taking into consideration all the layers by varying  $2z$  from  $h$  to  $a$ , we obtain the total change in the residual stress of the fiber  $mn$  as follows

$$\Sigma \frac{\sigma'_z \Delta}{2z} + \Sigma \frac{\sigma'_z b z \Delta (a - z)}{I_z}, \quad (e)$$

where  $\sigma'_z$  for each step is calculated from formula (b) by using the

measured values of  $d(1/r)$ . The required residual stress  $\sigma_a$  in the fiber  $mn$  is now obtained by subtracting the quantity  $(e)$  from the stress  $\sigma_a'$ , which is found by substituting  $a$  for  $2z$  in formula  $(b)$ . Hence

$$\sigma_a = \sigma_a' - \Sigma \frac{\sigma_z' \Delta}{2z} - \Sigma \frac{\sigma_z' b z \Delta (a - z)}{I_z}. \quad (f)$$

This method of experimentally determining the longitudinal residual stresses can be applied not only in the case of bending but also in other cases of prismatic bars subjected to longitudinal plastic deformation (see Art. 70). It was, for example, successfully applied in measuring residual stresses in cold-drawn brass tubes.<sup>14</sup> To take off thin layers of metal a special chemical solution was used in that work. The changes in curvature were measured optically. In this way complete information regarding residual stresses in cold-drawn tubes can be obtained. Such information is of great practical importance in developing the proper heat treatment in manufacturing tubes.

**69. Torsion beyond the Elastic Limit.**—Let us begin with the torsion of circular shafts and assume that beyond the elastic limit the cross sections of the twisted shaft continue to remain plane and their radii remain straight.<sup>15</sup> In such a case the shearing strain  $\gamma$  at a distance  $r$  from the axis of the shaft is determined by the same formula as in the case of torsion within the elastic limit (see Part I, p. 282):

$$\gamma = r\theta, \quad (a)$$

where  $\theta$  is the angle of twist per unit length of the shaft. To determine the magnitude of the torque which is required for producing the twist  $\theta$ , it is necessary to know the relation

<sup>14</sup> This method was developed by N. N. Davidenkov, *loc. cit.*, p. 392, and *Z. Metallkunde*, Vol. 24, p. 25, 1932. See also the doctor's thesis by C. G. Anderson, University of Michigan, 1935, and the paper by D. J. Demorest and D. O. Leeser, *Proc. Soc. Exp. Stress Anal.*, Vol. 11, p. 45, 1953. A description of several methods of analysis of residual stresses is given in the paper by C. S. Barrett, *ibid.*, Vol. 2, p. 147, 1944. See also the article by O. J. Horger in M. Hetényi, ed., *Handbook of Experimental Stress Analysis*, New York, 1950.

<sup>15</sup> This theory was developed by St.-Venant, *J. de math.*, Vol. 16, p. 373, 1871. See also I. Todhunter and K. Pearson, *History of the Theory of Elasticity*, Vol. 2, Part I, p. 170. For a further discussion of this subject see A. Nadai, *Theory of Flow and Fracture of Solids*, New York, p. 347, 1950.



these stresses can be obtained by repeating the same reasoning which was applied in the case of bending (p. 377). Let the ordinates of the horizontal line  $mn$  in Fig. 251 represent the shearing stress  $\tau_{YP}$  produced by the moment  $M_{ult}$  and uniformly distributed along the radius of the shaft. During unloading of the shaft the material follows Hooke's

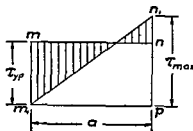


FIG 251

law, and the torsional stresses which are to be subtracted while unloading the shaft follow the linear law indicated in Fig. 251 by the line  $m_1n_1$ . The difference between the two stress distributions, rectangular while loading and triangular while unloading, represents the stresses which remain in the shaft after unloading. The distribution of these stresses along a radius of the shaft is shown in Fig. 251 by the shaded areas. The magnitude of the ordinate  $n_1p$ , denoted by  $\tau_{max}$ , is found from the fact that the rectangular and the triangular stress distributions both represent a torque of the same magnitude  $M_{ult}$ . For the rectangular stress distribution this torque is given by eq. (e). The formula for the same torque and for the triangular stress distribution is obtained by substituting  $\tau_{max}$  for  $\tau_{YP}$  in eq. (f):

$$\frac{2\pi a^3}{3} \tau_{YP} = \frac{\pi a^3}{2} \tau_{max},$$

or

$$\tau_{max} = 1\frac{1}{3} \tau_{YP}.$$

It is seen that the residual torsional stress at the surface of the shaft is equal to  $\frac{1}{3}\tau_{YP}$  and near the center is equal to  $\tau_{YP}$ .

The distribution of residual torsional stresses can also be investigated experimentally. For this purpose it is necessary to machine off successive thin layers of metal from the shaft and measure, after removing each layer, the change in the angle of twist of the shaft.

In the case of perfectly plastic materials (see p. 346) the membrane analogy (see p. 237) can be used to advantage in studying tor-

sion beyond the yield point. When the magnitude of the torque is somewhat larger than  $(M_t)_{Y.P.}$ , the outer portion of the shaft is in the condition of yielding while the inner portion continues to deform elastically. To extend the membrane analogy to this case, it is necessary to use, together with the membrane, a rigid cone  $ACB$ , Fig. 252, the slope of which represents the yield point stress  $\tau_{Y.P.}$  to the proper scale. If a small pressure  $p$  acts on the membrane, the deflections are also small, and the conical surface does not interfere with the free deflection of the membrane. Hence its surface defines the stress distribution for the case of elastic torsion, as previously discussed (see p. 237). With an increase in pressure the deflections of the membrane also increase, and finally the outer portion of the membrane comes into contact with the rigid cone as shown in Fig. 252. This condition represents torsion beyond the yield point. The outer portion of the membrane, coinciding with the cone, has a constant slope corresponding to the yield point stress  $\tau_{Y.P.}$ . The inner portion  $mn$  of the membrane corresponds to the inner portion of the shaft, which is in an elastic condition. The double volume between the membrane and the plane of the boundary  $AB$  continues to represent the torque. From this we conclude that the double volume of the cone must give us the value of  $M_{ult.}$  Since the slope of the cone is  $\tau_{Y.P.}$ , its height is equal to  $a\tau_{Y.P.}$ , and its double volume is  $\frac{2}{3}\pi a^2 a\tau_{Y.P.}$ , which coincides with eq. (e).

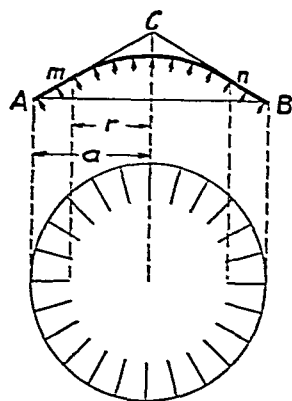


FIG. 252.

A similar method can also be used in the case of noncircular cross sections of shafts and is very useful in determining the portions of the shaft in which yielding begins. Consider as an example a rectangular shaft. In investigating torsion of this shaft beyond its yield point the membrane must be used together with a rigid roof surface, Fig. 253, which has a constant slope at all points representing to a certain scale the yield point stress  $\tau_{Y.P.}$ . It is evident that the membrane, deflecting under increasing uniform pressure, touches the roof first at points  $c$  and  $d$ , the middle points of the longer sides of the rectangle. At these points yielding begins and at a higher pressure some portions of the membrane will coincide with the roof as indicated in the figure by the shaded areas. These areas define the regions where the material yields. In the rest of the shaft we have only elastic

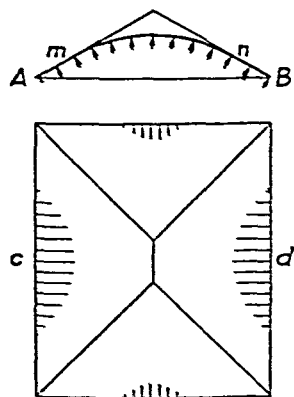


FIG. 253.

deformation. A further increase in pressure on the membrane increases the portions in contact with the roof, as well as the regions of plastic deformation. The double volume between the roof and the plane  $AB$  evidently gives the magnitude of  $M_{ult}$  for the rectangular shaft.

If a rectangular bar of wrought iron is twisted beyond the yield point, the regions of plastic flow can be revealed by a proper etching of the cross section. After etching, there appear in the plastic regions of the cross section dark parallel lines with directions as shown in Fig 253. These lines indicate sliding of the metal along layers parallel to the axis of the shaft, produced by the yield point stress.<sup>17</sup>

**70. Plastic Deformation of Thick Cylinders under the Action of Internal Pressure.**<sup>18</sup>—In discussing the elastic deformation of a thick walled cylinder under the action of internal pressure  $p$ , we found (see p 208) that the radial and tangential stresses at a radial distance  $r$  from the axis of the cylinder are represented by the formulas

$$\sigma_r = \frac{a^2 p}{b^2 - a^2} \left( 1 - \frac{b^2}{r^2} \right), \quad \sigma_t = \frac{a^2 p}{b^2 - a^2} \left( 1 + \frac{b^2}{r^2} \right), \quad (a)$$

where  $a$  and  $b$  are the inner and the outer radii respectively of the cylinder. The maximum tangential tension and the maximum radial compression occur at the inner surface of the cylinder. At that surface the maximum shearing stress also acts, and its magnitude is

$$\tau_{\max} = \left( \frac{\sigma_t - \sigma_r}{2} \right)_{r=a} = \frac{pb^2}{b^2 - a^2}. \quad (b)$$

By gradually increasing the internal pressure, we finally reach a point when the material at the inner surface begins to yield. This occurs when the maximum shearing stress (eq  $b$ )

<sup>17</sup> Interesting photographs of these lines, obtained for various shapes of twisted bars, are shown in the paper by A. Nadai, *Trans. A. S. M. E.*, Vol. 53, p. 29, 1931, see also his book, *Theory of Flow and Fracture of Solids*, p. 494, 1950.

<sup>18</sup> An investigation of plastic flow in thick cylinders submitted to internal pressure was made by St. Venant, see *Compt. rend.*, Vol. 74, p. 1009, 1872, see also I. Todhunter and K. Pearson, *History of the Theory of Elasticity*, Vol. 2, Part I, p. 172, and the paper by L. B. Turner, *Cambridge Phil. Soc. Trans.*, Vol. 21, p. 377, 1913.

becomes equal to the yield point stress  $\tau_{Y.P.}$ .<sup>19</sup> Substituting this value into formula (b), we find that the pressure at which yielding begins is

$$p_{Y.P.} = \tau_{Y.P.} \frac{b^2 - a^2}{b^2}. \quad (c)$$

Assuming, for example,  $b = 2a$ , we find that in this particular case  $p_{Y.P.} = 0.750\tau_{Y.P.}$ . With a further increase in pressure the plastic deformation penetrates deeper and deeper into the wall of the cylinder and finally at a certain pressure, which we shall call  $p_{ult}$ , the entire wall of the cylinder is brought into the state of yielding. The distribution of stresses in the wall at this yielding condition can be investigated without much difficulty if we assume that the material is perfectly plastic, which means that yielding proceeds under the action of a constant shearing stress equal to  $\tau_{Y.P.}$ . This gives for every point in the region of plastic deformation the equation

$$\frac{\sigma_z - \sigma_r}{2} = \tau_{Y.P.} \quad (d)$$

Another equation for determining the principal stresses  $\sigma_r$  and  $\sigma_z$  is obtained by considering the equilibrium of an element of the wall, shown in Fig. 127. From our previous discussion (see p. 206) the equation of equilibrium is

$$\sigma_z - \sigma_r - r \frac{d\sigma_r}{dr} = 0. \quad (e)$$

Substituting for the difference of the principal stresses its value from eq. (d), we obtain

$$\frac{d\sigma_r}{dr} = \frac{2\tau_{Y.P.}}{r}. \quad (f)$$

The integration of this equation gives

$$\sigma_r = 2\tau_{Y.P.} \log_e r + C. \quad (g)$$

<sup>19</sup> The question of the yielding of a material under various stress conditions is discussed in Art. 82. We assume here that  $\tau_{Y.P.}$  has the same value as in the case of torsion (see p. 381).

The constant of integration  $C$  is obtained from the condition that at the outer surface of the cylinder, i.e., at  $r = b$ , the radial stress  $\sigma_r$  vanishes. This gives

$$0 = 2\tau_{YP} \log_e b + C, \quad C = -2\tau_{YP} \log_e b.$$

Substituting this value of the constant of integration  $C$  into eq. (g), we obtain

$$\sigma_r = 2\tau_{YP} \log_e \frac{r}{b}. \quad (285)$$

This gives for the inner surface of the cylinder

$$(\sigma_r)_{r=a} = 2\tau_{YP} \log_e \frac{a}{b}, \quad (286)$$

and the pressure which is required to bring the entire wall of the cylinder into the state of plastic flow is

$$p_{ult} = -(\sigma_r)_{r=a} = -2\tau_{YP} \log_e \frac{a}{b}.$$

Taking again  $b = 2a$ , we find

$$p_{ult} = 2\tau_{YP} \log_e 2 = 0.693(2\tau_{YP}).$$

Having eq. (285) for the radial stresses, we obtain the tangential stresses from eq. (d), which gives

$$\sigma_t = 2\tau_{YP} \left( 1 + \log_e \frac{r}{b} \right). \quad (287)$$

If  $b = 2a$ , this expression becomes

$$(\sigma_t)_{r=a} = 2\tau_{YP} \left( 1 + \log_e \frac{a}{b} \right) = 0.307(2\tau_{YP}),$$

$$(\sigma_t)_{r=b} = 2\tau_{YP}.$$

The distribution of stresses  $\sigma_r$  and  $\sigma_t$  along the thickness of the wall for the particular case  $b = 2a$  is shown in Fig. 254 by the curves *mln* and *st* respectively. If, after bringing the material of the cylinder to the condition of yielding, we remove

the internal pressure, some residual stresses remain in the wall of the cylinder. These stresses can be readily calculated if we assume that during unloading, the material of the cylinder follows Hooke's law. In such a case the stresses which are to be subtracted while unloading the cylinder are given by eqs. (a) if we substitute in these expressions  $p_{ult}$  instead of  $p$ .

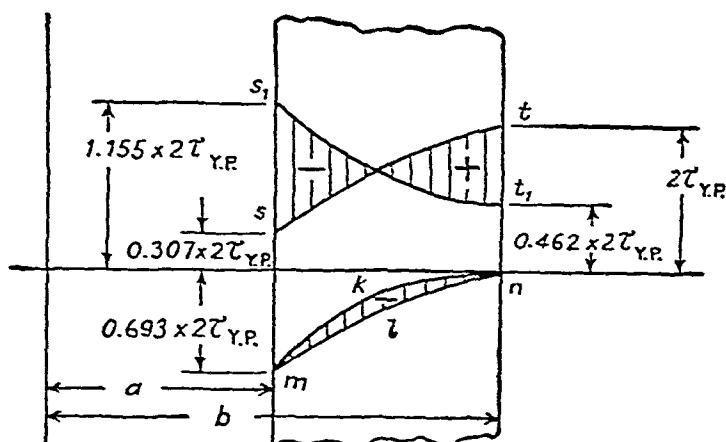


FIG. 254.

These stresses for the particular case  $b = 2a$  are shown in Fig. 254 by the curves  $s_1t_1$  and  $mkn$ . The shaded areas then give the residual stresses in the wall of the cylinder. It is seen that owing to the plastic deformation, considerable compressive tangential stresses are produced in the portion of the cylinder wall.<sup>20</sup> If a cylinder with such residual stresses is again loaded by internal pressure equal to  $p_{ult}$  the tangential stresses produced by this pressure and given by the curve  $s_1t_1$  will be superposed on the residual stresses, given by the shaded areas, so that the resultant stress distribution will be that represented by the curve  $st$ . The maximum resultant stress is  $2\tau_{Y.P.}$ , and no yielding will occur during this second application of the internal pressure. Hence the residual stresses produced by the plastic expansion of the cylinder are of such a nature as to increase the pressure which can be sustained by the cylinder elastically. This fact is sometimes used

<sup>20</sup> It is assumed that this compressive stress is less than the yield point stress and that no yielding occurs during unloading. The case of yielding during unloading was studied by L. B. Turner, *loc. cit.*, p. 386.

in manufacturing guns which must withstand high internal gas pressures.<sup>21</sup>

It has been assumed in the discussion that the applied inner pressure is such as to bring the entire cylinder to the condition of yielding, but the method can also be applied without any difficulty to cases in which only the inner portion of the cylinder wall is in the state of yielding while the outer portion is in the elastic state. Assume that a pressure  $p'$ , larger than  $p_{YP}$  but smaller than  $p_{ult}$ , is applied, and let  $c$  be the radius of the cylindrical surface separating the plastic region of the wall from the elastic region. There will be a radial pressure which we shall call  $X$  acting between these two regions. The magnitude of this pressure can be found from a consideration of the elastic outer portion of the wall. The maximum shearing stress  $\tau_{max}$  in this portion is found from eq. (b) by substituting  $c$  instead of  $a$  and  $X$  instead of  $p$  in that equation which gives

$$\tau_{max} = \frac{Xb^2}{b^2 - c^2}.$$

Since the cylindrical surface  $r = c$  separates the elastic and plastic zones, the material at that surface just reaches the yield point. Hence  $\tau_{max} = \tau_{YP}$ . The equation for determining the pressure  $X$  is then

$$\tau_{Y.P} = \frac{Xb^2}{b^2 - c^2}, \quad (h)$$

and we obtain

$$X = \frac{\tau_{YP}(b^2 - c^2)}{b^2}. \quad (i)$$

Having this pressure, we can readily calculate the stresses at any point in the elastic region of the wall by using equations similar to eqs. (a).<sup>22</sup>

<sup>21</sup> A description of this use of the initial plastic deformation can be found in the book by L. Jacob, *Résistance et construction des bouches à feu: Autofretage*, Paris. See also S. J. Brown, *U.S. Naval Inst. Proc.*, Vol. 46, p. 1941, 1920.

<sup>22</sup> The radius  $c$  instead of  $a$  and  $X$  instead of  $p$  must be used in these equations.

For calculating stresses in the plastic region of the wall we use eq. (g). The constant of integration  $C$  is found from the condition that for  $r = c$ ,  $\sigma_r = -X$ , which gives

$$-X = 2\tau_{Y.P.} \log_e c + C, \quad C = -X - 2\tau_{Y.P.} \log_e c.$$

Substituting this value of  $C$  in eq. (g) and using eq. (i), we obtain

$$\sigma_r = 2\tau_{Y.P.} \log_e \frac{r}{c} - \frac{\tau_{Y.P.}(b^2 - c^2)}{b^2}. \quad (288)$$

Taking  $r$  equal to the inner radius  $a$  of the cylinder, we obtain the magnitude  $p'$  of the pressure which must be used to produce plastic flow in the wall up to the depth corresponding to the radius  $r = c$ . This pressure is

$$p' = -2\tau_{Y.P.} \log_e \frac{a}{c} + \frac{\tau_{Y.P.}(b^2 - c^2)}{b^2}. \quad (289)$$

Taking our previous example, where  $b = 2a$ , and assuming  $c = 1.5a$ , we find from eq. (289) that  $p' = 0.624(2\tau_{Y.P.})$ .

The distribution of tangential stresses  $\sigma_t$  is obtained from eq. (d), which gives

$$\sigma_t = 2\tau_{Y.P.} + \sigma_r = 2\tau_{Y.P.} \log_e \frac{r}{c} + \tau_{Y.P.} \frac{b^2 + c^2}{b^2}. \quad (290)$$

For  $r = c$  the first term on the right-hand side vanishes and the value of  $\sigma_t$  becomes equal to the value of the tangential stress produced by pressure  $X$  in the adjacent elastic zone of the wall. Eqs. (289) and (290) give the stresses produced in the inner portion of the cylinder wall, which undergoes plastic deformation. For the outer portion, which remains elastic, equations similar to eqs. (a) must be used. In this way the problem of stress distribution for the case of a cylinder which undergoes only a partially plastic deformation is completely solved.

If after partial yielding of the cylinder wall the inner pressure  $p'$  is removed, some residual stresses will remain in the wall of the cylinder. The inner portion of the wall, in which plastic deformation occurred, does not return to its initial diameter and undergoes a pressure from the side of the elastic



outer portion of the wall. The stress distribution produced in this way is similar to that produced by shrink fit pressures in built-up cylinders (see Art. 41). To calculate these stresses we proceed in exactly the same way as was explained before and illustrated in Fig. 254.

All these calculations are based on the assumption that beyond the yield point the material yields without an increase in stress. If this is not the case, the residual stresses cannot be calculated as simply as explained above, and recourse must be had to an experimental determination of the residual stresses. In such cases a method similar to that used in determining residual bending stresses can be applied. We machine off thin layers of the metal beginning from the inner surface of the cylinder,<sup>23</sup> and after each cut measure the strain produced in the axial and circumferential directions at the outer surface of the cylinder. Such measurements furnish sufficient information for calculating residual stresses.

Residual stresses in cylinders can be produced not only by the plastic deformation described above but also by non-uniform cooling and by volume changes of the metal during recrystallization in various processes of heat treatment. Sometimes these stresses become of primary importance as, for example, in large forgings, and several methods for their determination have been developed.<sup>24</sup>

<sup>23</sup> Some experiments by machining from the outside have also been made, see H. Bühler and W. Schreiber, *Metallwissensch u. Tech.*, Sept. 1954, and the article by Bühler in the book, *Residual Stresses in Metals and Metal Construction*, 1954.

<sup>24</sup> The first investigation of this kind was made by N. Kalakoutzky, St. Petersburg, 1887. See also N. Kalakoutzky, *Investigation into the Internal Stress in Cast Iron and Steel*, London, 1888. The complete solution of the problem was given by G. Sachs, *Z. Metallkunde*, Vol. 19, p. 352, 1927, and *Z. Ver. deut. Ing.*, Vol. 71, p. 1511, 1927. These two papers contain a complete bibliography of the subject. Further improvements in the methods of measuring residual stresses in tubes were made by N. N. Davidenkov, *J. Tech. Phys. (Leningrad)*, Vol. 1, 1931. See also G. Sachs, *Trans. A S M E*, p. 821, 1939. A bibliography on plastic deformation of metals and on residual stresses is given in G. Sachs, *Handbuch der Metallphysik*, Leipzig, Vol. 3, Part I, 1937. See also the article by O. J. Horger, *loc. cit.*, p. 381. Residual stresses in oil field pump rods are discussed in the paper by R. E. Hanslip, *Proc. Soc. Exp. Stress Anal.*, Vol. 10, p. 97, 1952.

## CHAPTER X

### MECHANICAL PROPERTIES OF MATERIALS

71. General.—The preceding chapters dealt with the methods of analyzing the stress distribution produced by various kinds of forces on structures. Knowing the stresses, the designer must then select the material and the dimensions of the structure in such a way that it will stand safely various loading conditions in service. For this purpose it is necessary to have information regarding the elastic properties and strength characteristics of structural materials under various stress conditions. In analyzing stresses it is usually assumed that the material follows Hooke's law, and then for solving a problem it is sufficient to know the moduli of elasticity of the material. But for selecting the safe dimensions of a structure this knowledge is not enough. The designer must know the limits under which the material can be considered as perfectly elastic for various stress conditions, and also the behavior of the material beyond those limits. Information of this type can be obtained only by experimental investigations. Material-testing laboratories are equipped with testing machines<sup>1</sup> which produce certain typical deformations of test specimens, such as tension, compression, torsion and bending.

To make the results of tests comparable, certain proportions for test specimens have been established and are recognized as standard. The most widely used of all mechanical tests of structural materials is undoubtedly the tension test. The standard tensile test specimen in the United States is

---

<sup>1</sup> For a description of material-testing machines and a bibliography on the subject see the article by J. Marin in M. Hetényi, ed., *Handbook of Experimental Stress Analysis*, New York, 1950. See also the article by A. Eichinger in E. Siebel, ed., *Handbuch der Werkstoffprüfung*, Stuttgart, 1940.

circular, with  $\frac{1}{2}$  in diameter and 2 in gage length, so that

$$\frac{l}{d} = 4 \quad \text{or} \quad l = 4.51\sqrt{A},$$

where  $A = \pi d^2/4$  is the cross-sectional area of the specimen.<sup>2</sup> In the case of rectangular specimens it is preferable to take the same relation between the length and the cross-sectional area as for circular specimens.

The length of the cylindrical portion of the specimen is always somewhat greater than the gage length  $l$  and is usually at least  $l + d$ . The ends of the specimen are generally made with a larger cross section in order to prevent the specimen from breaking in the grips of the testing machine, where the stress conditions are more severe because of local irregularities in stress distribution. A cylindrical specimen with  $l = 10d$  is shown in Fig. 255*a*, which also shows the spherical seats in

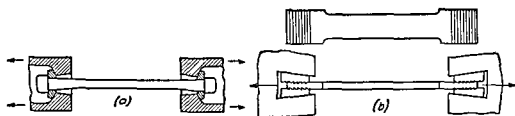


FIG 255

the grips of the machine, used to insure central application of the load. Fig. 255*b* shows a flat rectangular specimen.

Tensile test machines are usually provided with a device which automatically draws a tensile test diagram representing the relation between the load  $P$  and the extension  $\delta$  of the specimen. Such a diagram exhibits important characteristics of the material. Fig. 256, for example, shows a series of tensile test diagrams for carbon steel with various contents of carbon. It can be seen that as the carbon content increases, the ultimate strength of the steel also increases,

<sup>2</sup> In central Europe two different proportions of circular specimens are used, (1) long specimens, for which  $l = 10d = 11.3\sqrt{A}$ , and (2) short specimens, for which  $l = 5d = 5.65\sqrt{A}$ .

but at the same time the elongation before fracture decreases and the material has less ductility. High-carbon steel is relatively brittle. It follows Hooke's law up to a high value of stress and then fractures at a very small elongation. On the other hand, a mild steel with a small carbon content is ductile and stretches considerably before fracture. In the following discussion we will begin by considering tensile tests of brittle materials.

**72. Tensile Tests of Brittle Materials.**—As an example of a brittle material, let us begin by considering glass. Glass follows Hooke's law practically up to fracture, and the tensile test diagram can be represented approximately by the straight line  $OA$ , Fig. 257. Ordinary tensile tests of glass usually give very low values of ultimate strength, and the corresponding amount of work required to produce fracture (represented in Fig. 257 by the shaded area  $OAB$ ) is very small in comparison with the amount of energy theoretically required to separate the molecules. This latter quantity can be obtained experimentally by melting and then evaporating the glass. The work required to separate the molecules will then be of the same order of magnitude as the amount of heat required for vaporization. Experiments show that this quantity is thousands of times larger than the work required in a tensile test (Fig. 257).

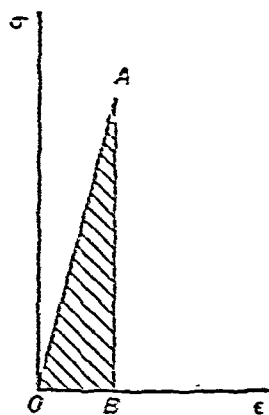


FIG. 257.

To explain this discrepancy Griffith proposed the theory<sup>2</sup> that the energy required for fracture of a glass specimen is

<sup>2</sup> A. A. Griffith, *Trans. Roy. Soc. (London)*, A, Vol. 221, pp. 163-98, 1921. See also *Proc. Internat. Congr. Appl. Mech.*, Delft, pp. 55-63, 1924.

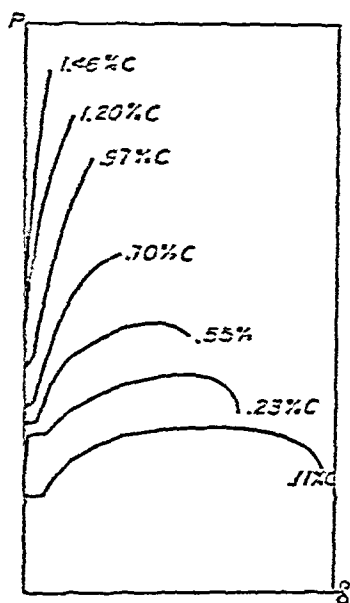


FIG. 256.

not uniformly distributed over the volume and that there are regions of energy concentration produced by microscopic cracks which act as stress raisers. Considering one of these microscopic cracks as a narrow elliptic hole in a plate which is uniformly stretched (Fig. 258) and using the known expressions

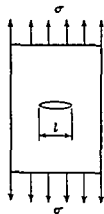


FIG. 258

for stresses around an elliptic hole (see Art. 57), we can show that the strain energy of the plate (for unit thickness) is reduced by the presence of the hole by the amount <sup>4</sup>

$$\frac{\pi l^2 \sigma^2}{4E} \quad (a)$$

In this expression  $l$  is the length of the crack,  $\sigma$  is the uniformly distributed tensile stress and  $E$  is the modulus of elasticity of the material.

Let us consider next the magnitude of stress at which the crack will start to spread across the plate and thus produce fracture. Such a spreading out of the crack becomes possible without any additional work only if the increase in *surface energy* due to an increment  $dl$  of crack length is compensated for by a corresponding reduction in strain energy of the plate. Denoting the surface tension by  $S$ , the equation for the ultimate stress is therefore

$$\frac{d}{dl} \left( \frac{\pi l^2 \sigma_{ult}^2}{4E} \right) dl = 2S \quad (b)$$

or

$$l = \frac{4SE}{\pi \sigma_{ult}^2} \quad (c)$$

In order to determine the surface tension  $S$ , Griffith made a series of tests with melted glass at various temperatures. The temperatures were such that the glass behaved as a viscous liquid. The value of  $S$  at room temperature was then obtained by extrapolation, assuming a linear variation of  $S$  with tem

<sup>4</sup> It is assumed that the distances between the cracks are comparatively large, so that the disturbances in stress distribution due to the cracks can be considered independent of one another. Then it is sufficient to consider only one crack, perpendicular to the stresses, as the most unfavorable

perature. The ultimate strength  $\sigma_{ult}$  of glass is found from ordinary tensile tests, and the length of crack  $l$  may then be computed <sup>5</sup> from eq. (c). It is also seen from eq. (c) that the ultimate tensile strength is inversely proportional to the square root of  $l$ .

To verify the theory Griffith made experiments with thin glass tubes subjected to internal pressure. By making artificial cracks with a diamond parallel to the axis of the cylinder and of different lengths, he found the ultimate stresses  $\sigma_{ult}$  experimentally. These were in satisfactory agreement with the theoretical predictions of eq. (c). Griffith conducted further experiments with thin glass fibers and found the ultimate tensile strength to be  $3.5 \times 10^4$  kg per sq cm (about 500,000 lb per sq in.) for a fiber  $3.3 \times 10^{-3}$  mm in diameter. This was about 20 times higher than previously found for thicker specimens. This relatively enormous strength of thin fibers can also be explained on the basis of Griffith's theory, if it is observed that in the process of drawing the thin fibers any cracks that were initially perpendicular to the length of the fibers are eliminated. Griffith noticed that after a period of time the fibers lost part of their strength. Experimenting with fibers immediately after they were drawn, he succeeded in obtaining the immense ultimate strength of  $6.3 \times 10^4$  kg per sq cm (about 900,000 lb per sq in.) for a diameter of 0.5 mm. This value is about one-half of the theoretical strength predicted by considering the molecular forces.

Other investigations of the tensile strength of brittle materials were made with single crystal specimens cut out from large cubic crystals of rock salt.<sup>6</sup> These experiments showed that the ultimate strength of that material was only 45 kg per sq cm when tested in air at room temperature. When the same specimen was tested while submerged in hot water, it reached the yield point at a stress of 80 kg per sq cm and then stretched plastically until final fracture occurred at a

<sup>5</sup> Griffith's experiments gave values for  $l$  of the order  $1 \times 10^{-3}$  cm.

<sup>6</sup> See the paper by A. Joffe, *Z. Phys.*, Vol. 22, p. 286, 1924. See also *Proc. Internat. Congr. Appl. Mech.*, Delft, p. 64, 1924. A further discussion of Joffe's work is given in E. Schmid and W. Boas, *Kristallplastizität*, Berlin, p. 271, 1935.

rials which have considerable plastic deformation before failure. Plastic deformation will alleviate the local stress concentrations at points of imperfection, and therefore only the average stresses are important in determining failure.

### 73. Tensile Tests of Ductile Materials—

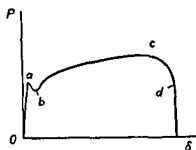


FIG 260

The mechanical properties of ductile materials, such as steel and other metals used in structures, are usually obtained from tensile tests. Fig 260 represents the tensile test diagram for mild structural steel. From this diagram the important characteristics such as *yield point*, *ultimate strength* and amount of *plastic elongation* can be obtained.

In determining the *proportional limit*, sensitive extensometers are necessary in order to detect the slightest deviation from a straight line in the tensile test diagram. Obviously the position found for this limit depends considerably on the sensitivity of the instruments. In order to obtain greater uniformity in results, a specified amount of permanent set or a certain deviation from proportionality is often taken as the basis for determining the proportional limit. The International Congress for Testing Materials at Brussels (1906) defined the proportional limit as the tensile stress at which the permanent set is 0.001 per cent. Since then there has been a tendency to increase this limiting magnitude of permanent set to 0.01 per cent.<sup>14</sup>

The *yield point* is a very important characteristic for materials such as structural steel. At the yield point stress, the specimen elongates a considerable amount without any increase in load. In the case of mild steel the elongation may be more than 2 per cent. Sometimes yielding is accompanied by an abrupt decrease in load, and the tensile test diagram has the shape shown in Fig 260. In such a case the upper and lower limits of the load at *a* and *b*, divided by the initial cross-sectional area, are called the *upper* and *lower yield points*,

<sup>14</sup> See the paper by P. Ludwik, 'Bruchgefahr und Materialprüfung', *Schweiz. Verband f. Materialprüf. d. Technik (Zurich) Ber.*, No. 13, 1928.

tity is also used as a characteristic property of the material and depends not only on the strength but also on the ductility of the material

The *ductility* of a metal is usually considered to be characterized by the *elongation* of the gage length of the specimen during a tensile test and by the *reduction in area* of the cross section where fracture occurs. In the first stage of plastic elongation, from *a* to *c* in Fig. 260, the specimen elongates uniformly along its length. This uniform elongation is accompanied by a uniform lateral contraction, so that the volume of the specimen remains practically constant.<sup>15</sup> At point *c*



FIG. 261

the tensile force reaches a maximum value, further extension of the specimen is accompanied by a decrease in the load. At this stage of plastic elongation the deformation becomes localized and *necking* begins, with the specimen taking the shape shown in Fig. 261. It is difficult to determine accurately the moment when necking begins and thereby establish separately the magnitude of the uniform stretching and the magnitude of the elongation due to necking. It is therefore customary to measure the total increase in the gage length when the specimen is fractured. The *elongation* is then defined as the ratio of this total elongation of the gage length to its initial length. In practice the elongation at fracture is usually given in percentage. If  $l$  is the original gage length and  $\delta$  the total elongation, the elongation at failure in percentage is

$$\epsilon = \frac{\delta}{l} \cdot 100 \quad (a)$$

This elongation is usually taken as a measure of the ductility of the material. Elongation obtained in this manner depends on the proportions of the specimen. The increase in the gage length due to necking is a large part of the total increase and is practically the same for a short gage length as for a long gage length. Hence the elongation defined by eq. (a) becomes

<sup>15</sup> The small elastic deformation in which the volume does change can be neglected in comparison with the comparatively large plastic deformation.



larger as the gage length decreases. For steel the elongation obtained for specimens with  $l = 5d$  is about 1.22 times the elongation for a specimen of the same material with  $l = 10d$ . Experiments also show that the shape of the cross section affects the local deformation at the neck and hence affects the elongation of the specimen. This shows that comparable results with respect to elongation can be obtained only by using geometrically similar specimens.

The *reduction in area* at the cross section of fracture is expressed as follows:

$$q = \frac{A_0 - A_1}{A_0}, \quad (b)$$

in which  $A_0$  is the initial cross-sectional area and  $A_1$  the final cross-sectional area at the section where fracture occurs.

A table giving the results of a number of static tensile tests of various steels is given at the end of the chapter.

**74. Tests of Single-Crystal Specimens in the Elastic Range.**—The metals with which we are concerned in engineering applications normally have a crystalline structure. A piece of metallic material consists of a large number of minute crystals, and the mechanical properties of the material can be better understood if the properties of a single crystal are first studied.

X-ray analyses have shown that each crystal of a particular material consists of a large number of atoms arranged in a characteristic geometric pattern. The pattern is formed by a repetition of a *unit cell*, of which two types are shown in Fig. 262. Fig. 262a represents a *body-centered cubic cell*, the crystal

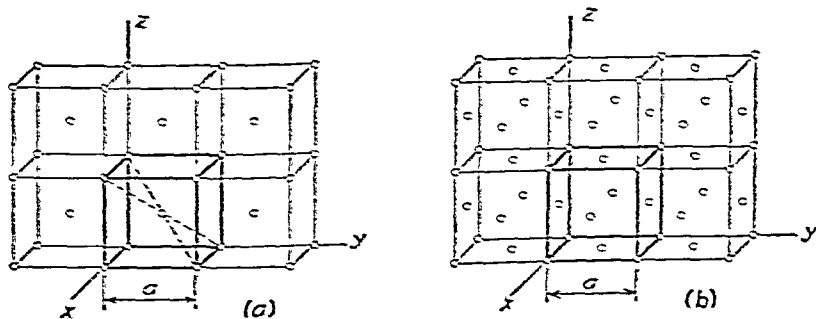


FIG. 262.

structure of iron at room temperature; while Fig. 262*b* shows a *face-centered cubic cell* representing the crystal structure for aluminum, copper and some other metals. The *lattice dimensions*, such as distance  $a$  in Fig. 262, are constant for each material and are of the order of  $1 \times 10^{-8}$  cm.

Various methods have been developed<sup>16</sup> for obtaining metal crystals of large size in order that specimens for mechanical tests may be cut out from a single crystal. Fig. 263 illus-

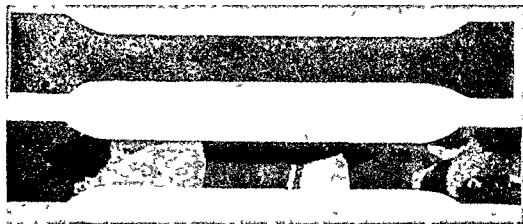


FIG 263

trates<sup>17</sup> the process of obtaining single-crystal specimens of aluminum by recrystallization. If a fine-grained aluminum specimen as shown in the upper photograph is uniformly stretched by an amount of 1-2 per cent and then annealed by a slow increase of temperature (20-50° F per day) and subsequent slow cooling, we usually obtain a specimen consisting of only a few crystals as shown in the lower picture. By carefully selecting material with great uniformity of grain size and by experimentally establishing the proper amount of stretching and the proper process of heating and cooling, it is possible to obtain single-crystal specimens after annealing. The orientation of the crystal with respect to the axis of the specimen cannot be controlled and the principal crystal axes (axes  $x$ ,  $y$ ,  $z$  in Fig. 262) will usually make different angles with the axis of the specimen for each different specimen.

<sup>16</sup> See C. F. Elam, *The Distortion of Metal Crystals*, Oxford, 1936.

<sup>17</sup> Figs. 263 and 264 were taken from E. Schmid and W. Boas, *Kristallplastizität*, Berlin, 1935; English translation by F. A. Hughes, London, 1950.

Tests of single crystal specimens in the elastic range usually show considerable variation in the elastic properties, depending on the orientation of the crystal. Fig. 264 shows the manner in which the moduli  $E$  and  $G$  for a crystal of iron vary with orientation. With the aid of this information for a single crystal, methods of calculating the average values of the moduli for polycrystalline specimens were developed<sup>18</sup>

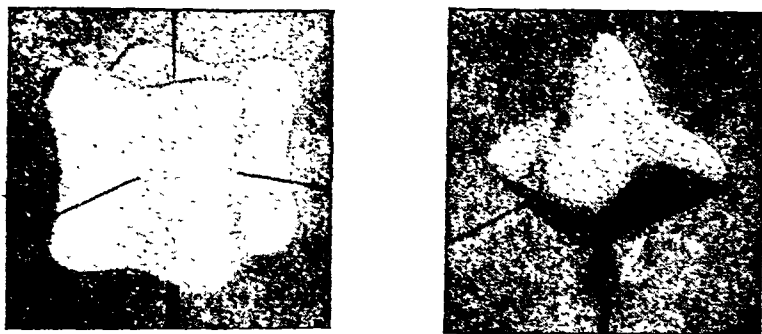


FIG. 264.

to such an extent that experimental results could be predicted with some accuracy.

With a sensitive extensometer it can be shown in a tensile test of a single-crystal specimen that even in the elastic range there exists some deviation from Hooke's law. There is also a *time effect* on the extensometer readings. To explain these phenomena thermal effects must be considered.

If a tensile test involving very slow increase of the load is carried out,<sup>19</sup> the temperature of the specimen remains equal to that of its surroundings and the stress-strain relation may be represented by the straight line  $OA$  (Fig. 265a). The slope of this line gives the magnitude of the modulus  $E$  under *isothermal* conditions. If the tensile load is applied rapidly, so that there is not enough time for heat exchange to take place, the straight line  $OB$  is obtained instead of  $OA$ , and usually the modulus  $E$  under *adiabatic* conditions is larger than that obtained isothermally. Because of its sudden

<sup>18</sup> See Boas and Schmid, *Helv. phys. acta*, Vol. 7, p. 628, 1934.

<sup>19</sup> See Lord Kelvin, *Elasticity and Heat*, Edinburgh, p. 18, 1880.

stretching, the specimen is cooled <sup>20</sup> below room temperature. If the specimen remains under constant load for a sufficient length of time, it gradually warms up until it reaches room temperature. As a result, an additional elongation of the specimen is brought about (represented in the figure by the horizontal line  $BA$ ). This is the *elastic aftereffect* and is due to the thermoelastic property of the material. If, after complete equalization of the temperature, the specimen is suddenly unloaded, its adiabatic contraction will be represented in

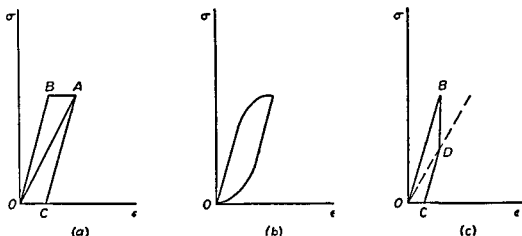


FIG. 265.

Fig. 265a by the line  $AC$  parallel to  $OB$ . Owing to this sudden shortening the specimen warms up, and the subsequent process of cooling to room temperature will give rise to a further contraction, represented by the length  $CO$ . It is seen that by deforming the specimen adiabatically and then allowing enough time for temperature equalization, a complete cycle, represented by the parallelogram  $OBAC$ , is described. The area of this parallelogram represents the loss of mechanical energy per cycle. We have assumed adiabatic deformation in our reasoning, whereas in practice there is always some heat exchange during the cycle. Thus, instead of a parallelogram, a loop such as shown in Fig. 265b is obtained.

The difference between the adiabatic and the isothermal moduli is usually small,<sup>21</sup> and the loss of mechanical energy

<sup>20</sup> The temperature change can be measured by attaching a thermocouple to the specimen.

<sup>21</sup> For steel it is about  $\frac{1}{3}$  of 1 per cent.

per cycle is also very small. But if many cycles occur in succession, as in vibration, the losses in mechanical energy become important and must be considered. They correspond to the so-called *internal friction* and are responsible for damping the vibratory motion. A loop such as is shown in Fig. 265*b* is called a *hysteresis loop*, and since after a complete cycle the specimen returns to its initial state, the term *elastic hysteresis* is sometimes used.

It was assumed above that, after sudden stretching the specimen remained under the action of a constantly applied load. Instead, the stretched specimen could be held at constant length. Then the warming up of the specimen would result in some decrease in the initially applied force. This process of *relaxation* is represented in Fig. 265*c* by the vertical line *BD*. In this case, by suddenly releasing the specimen the portion *DC* is obtained, and later, because of cooling, the closing line *CO* of the cycle *OBDC* is obtained.

The preceding discussion has been concerned with a tensile test, but actually most of our information regarding deviations from Hooke's law and the time effect in the elastic range was obtained from bending tests of strips cut out from a quartz crystal. It was shown in this way that all deviations from perfect elasticity could be completely explained by a consideration of the thermo-elastic and piezoelectric properties of the material.<sup>22</sup>

**75. Plastic Stretching of Single-Crystal Specimens.**—By increasing the load on a tensile test specimen we finally reach the point at which the specimen begins to yield and stretch plastically. Diagrams<sup>23</sup> for single-crystal specimens of aluminum tested in

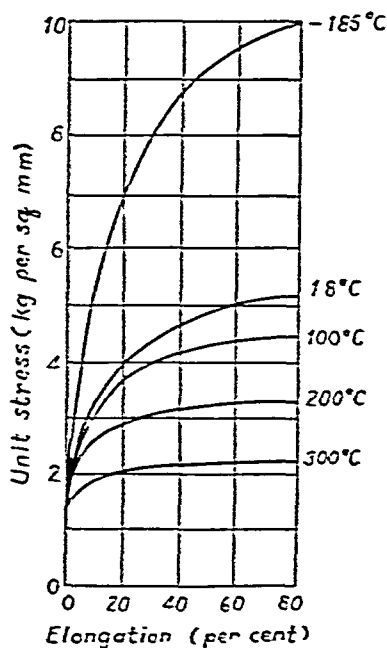


FIG. 266.

<sup>22</sup> See the paper by A. Joffe, *Ann. Phys.* (Ser. 4), Vol. 20, 1906.

<sup>23</sup> Fig. 266 is taken from Schmid and Boas, *loc. cit.*, p. 404.

tension at various temperatures are shown in Fig 266. It is seen that the proportional limit is very low, and beyond this limit the specimen stretches plastically. Because of plastic deformation the material hardens, and with increased stretching the stresses required to continue deformation become larger. This *strain hardening* phenomenon is especially pronounced at low temperatures. With increasing temperature the effect of strain hardening diminishes, and at  $300^{\circ}\text{C}$  the curve approaches a horizontal line and extension of the specimen continues at practically constant stress.

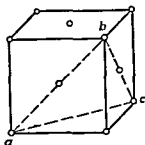


FIG 267

Observation of lines (slip bands) which appear on the surface of single-crystal specimens during plastic deformation reveals that this deformation consists of sliding of the material on certain crystallographic planes in definite directions. For example, in testing a single crystal specimen of aluminum, which has a face centered cubic lattice structure (Fig 267),

sliding will occur parallel to one of the octahedral planes (such as plane  $abc$ ) and the direction of sliding will be parallel to one of the sides of the triangle  $abc$ . In a specimen in tension, sliding will occur on the most unfavorably oriented octahedral plane, rather than on the  $45^{\circ}$  planes on which the maximum shearing stresses act. This explains why in testing single crystal specimens we obtain scattered results for the value of the tensile load at which yielding begins. These values depend not only on the mechanical properties of the material but also on the orientation of the crystal axes with respect to the axis of the specimen.

Assume, for example, that in a tensile test of a single crystal specimen (Fig 268) having a cross-sectional area  $A$ , the direction of the most unfavorably oriented octahedral plane of sliding is defined by the normal  $n$ , and the direction of sliding by the line  $pq$ . The shearing stress which acts on the plane of sliding is

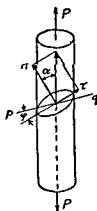


FIG 268

$$\tau = \frac{P}{A} \cos \alpha \sin \alpha. \quad (a)$$

Experiments show that the onset of sliding is brought about, not by the magnitude of  $\tau$ , but by the magnitude of the component  $\tau \cos \varphi$  of this stress in the direction of sliding  $pq$ . Sliding begins when this component reaches a definite value  $\tau_{cr}$ . From eq. (a) we then obtain

$$\tau_{cr} = \tau \cos \varphi = \frac{P}{A} \cos \alpha \sin \alpha \cos \varphi. \quad (b)$$

It is seen that, while  $\tau_{cr}$  is constant for a given material, the load  $P$  at which yielding of the specimen begins depends upon the values of the angles  $\alpha$  and  $\varphi$ .

The process by which a specimen elongates due to sliding along crystallographic planes is shown in Fig. 269. We may

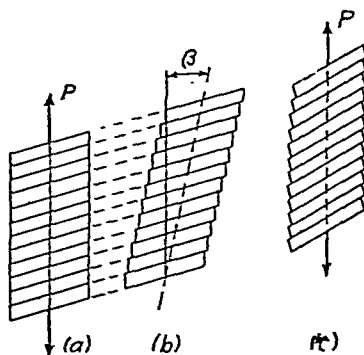


FIG. 269.

assume that stretching is produced in two steps, (1) translatory motion along the sliding planes (Fig. 269*b*) and (2) rotation of the specimen by the angle  $\beta$  to its original direction (Fig. 269*c*). From this mechanism of stretching it is apparent that the angle between the direction of the tensile force  $P$  and the planes of sliding changes during stretching. Furthermore, the initially circular cross section of the specimen becomes elliptic, with the ratio of its principal axes equal to  $1:\cos \beta$ . Numerous experiments with single crystals have yielded results that uphold these conclusions. For instance,

Fig. 270 represents a stretched copper-aluminum single-crystal<sup>24</sup> specimen.

Experiments have also shown that the magnitude of  $\tau_{cr}$  at which sliding begins is usually very small.<sup>25</sup> However, calculations for the value of  $\tau_{cr}$ , based on a consideration of the molecular forces,<sup>26</sup> give large values of the order of  $G/30$ . This indicates that the process of slipping does not consist solely of the rigid translatory motion of atomic planes relative to one another. It is necessary to assume the existence of local imperfections which permit slip to begin under the action

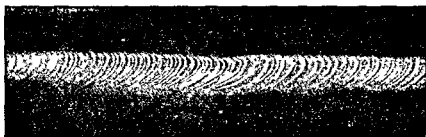


FIG. 270.

of a small force and then spread over the entire plane of sliding. A model illustrating the possibility of sliding which begins at a point of imperfection was described by L. Prandtl.<sup>27</sup> Another mechanical model was proposed by G. I. Taylor.<sup>28</sup> Assuming a local irregularity in the atomic distribution, called a *dislocation*, he showed that this irregularity would move along the plane of sliding in the crystal under the influence of a small stress  $\tau_{cr}$  and would cause a relative displacement of one portion of the crystal with respect to the other. Using his model, Taylor was able not only to explain the onset of sliding at very small values of  $\tau_{cr}$  but also the phenomenon of strain hardening.<sup>29</sup>

<sup>24</sup> See C. F. Elam, *The Distortion of Metal Crystals*, Oxford, p. 182, 1936.

<sup>25</sup> *Ibid.*

<sup>26</sup> See J. Frenkel, *Z. Phys.*, Vol. 37, p. 572, 1926.

<sup>27</sup> The model was discussed by Prandtl in a seminar on the theory of elasticity at Göttingen in 1909, and its description was published in *Z. angew. Math. u. Mech.*, Vol. 8, pp. 85–106, 1928.

<sup>28</sup> G. I. Taylor, *Proc. Roy. Soc. (London)*, A, Vol. 145, pp. 362–404, 1934.

<sup>29</sup> Taylor's work attracted the interest of physicists, and at present there is an extensive body of literature on dislocations. For a recent bibliography of the subject see A. H. Cottrell, *Dislocations and Plastic Flow in Crystals*, Oxford, 1953.



76. Tensile Tests of Mild Steel in the Elastic Range.— Leaving this brief discussion of the mechanical properties of single crystals, let us go on to consider tensile tests of polycrystal specimens, such as a specimen of structural steel. A typical tensile test diagram for steel is shown in Fig. 260, p. 400. For the lower range of stresses the corresponding portion of the diagram can be represented with satisfactory accuracy by a straight line, and the slope of this line gives the value of the modulus of elasticity  $E$ . As a result of differences in orientation, the moduli of individual crystals in the axial direction of the specimen will be different. But since the grains are minute, we can disregard this fact and consider the material as isotropic. The value of  $E$  is thus an average value obtained from a tensile test of the polycrystal specimen.

With a sensitive extensometer some deviation from Hooke's law and some aftereffect may be noticed in the elastic range of a tensile test. The explanation of this is the thermoelastic effect, as in the case of a single-crystal specimen (see p. 405). It must be noted, however, that the thermoelastic properties of a crystal depend upon the orientation of the crystal, and therefore the temperature changes produced by extension of a polycrystal specimen vary from grain to grain. This means that we have to consider not only the heat exchange between the specimen and the surroundings but also the heat flow between the individual crystals. Since the heat generated in a grain is proportional to its volume and the heat exchange depends upon the magnitude of its surface, it is evident that temperature equalization will be facilitated and the losses of mechanical energy increased by diminution of the grain size. This is of great practical importance, since there are cases in which damping of the vibrations of an elastic system depends mainly on the internal friction of the material. To increase damping in such systems, materials with small grain size should be employed.

It was assumed in this discussion that the deformation of the specimen was perfectly elastic, as may be expected with small stresses. With larger stresses the phenomenon of internal friction becomes more complicated, since we have to con-

sider not only the losses in mechanical energy due to heat exchange, as discussed above, but also the losses due to plastic deformation within the individual grains<sup>30</sup>

By polishing and etching the surface of a polycrystal specimen, the crystalline structure of the material can be observed with a microscope, and it can be seen that at loads smaller than the yield point load, slip bands appear on the surface of some grains. These bands indicate sliding along definite crystallographic planes in those grains and are of the same type as previously discussed for tests of single crystals. Since the elastic properties of a single crystal vary in different directions and since the crystals are oriented at random, the stresses in a tensile test piece are not uniformly distributed, and sliding may occur in the most unfavorably oriented individual crystals before the average tensile stress reaches the yield point value. If such a specimen is unloaded, the crystals which suffered sliding cannot return to their initial shape freely, and as a result some residual stresses will remain in the unloaded specimen. This yielding of the individual crystals also contributes to the losses of energy during loading and unloading and will increase the area of the hysteresis loop (see Fig 265*b*, p 406)

If, after unloading, the specimen is subjected to a tensile test for a second time, the grains in which sliding occurred in the first test will not yield until the tensile load reaches the value applied in the first loading. Only when the load exceeds that value will sliding begin again. If the specimen is subjected to compression after a previous loading in tension, the applied compressive stresses, combined with the residual stresses induced by the preceding tensile test, will produce yielding in the most unfavorably oriented crystals before the

---

<sup>30</sup> A considerable amount of research work in measuring the damping capacity of various materials was done by Rowett, *Proc Roy Soc (London)*, *A*, Vol 89, p 528, 1913, and by O Iöpl and his collaborators at the Wöhler Institut, Braunschweig, see *Z Ver deut Ing*, Vol 70, p 1291, 1926, Vol 72, p 1293, 1928, Vol 73, p 766, 1929. The importance of the thermoelastic cause of internal friction was shown by the investigations of C Zener and his associates, see *Phys Rev*, Vol 52, p 230, 1937, Vol 53, p 90, 1938, Vol 60, p 455, 1941. The results of these investigations are presented in C Zener, *Elasticity and Inelasticity of Metals*, 1948.

average compressive stress reaches the value at which slip bands would be produced in a specimen in its original state. Thus the tensile test cycle raises the elastic limit in tension, but lowers the elastic limit in compression. This phenomenon was first studied by Bauschinger<sup>31</sup> and is called the *Bauschinger effect*. We see that the Bauschinger effect is explained by considering sliding in individual crystals and the residual stresses produced by that sliding.

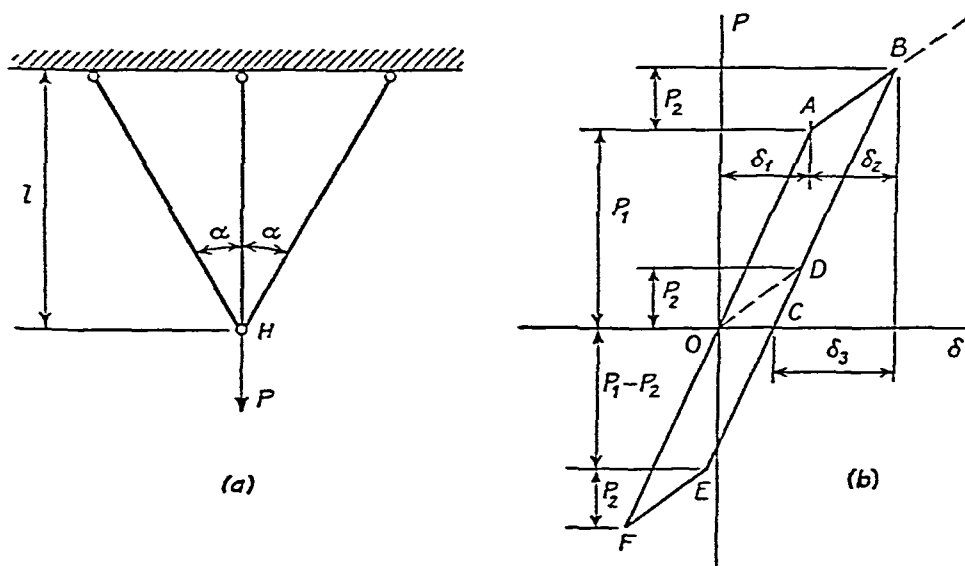


FIG. 271.

Residual stresses introduced into a material by yielding of the most unfavorably oriented grains and also the Bauschinger effect can be illustrated by the model shown in Fig. 271. The model consists of three bars of the same material and the same cross-sectional area  $A$ . The material has the same yield point stress  $\sigma_{Y.P.}$  in tension and compression. If a vertical load  $P$  is applied to the model, it will produce tensile forces  $S_1$  and  $S_2$  in the vertical and inclined bars respectively. In the elastic range these forces are (see Part I, p. 21)

$$S_1 = \frac{P}{1 + 2 \cos^3 \alpha}, \quad S_2 = \frac{P \cos^2 \alpha}{1 + 2 \cos^3 \alpha}. \quad (a)$$

<sup>31</sup> See *Mitt. Mech.-tech. Lab. München*, 1886. See also *Dinglers Polytech. J.*, Vol. 266, 1886.

Owing to elastic deformation the hinge  $H$  of the model will move vertically downward by the amount

$$\delta = \frac{Pl}{AE(1 + 2 \cos^3 \alpha)}. \quad (b)$$

The relation between the load and the displacement is represented in Fig. 271*b* by the line  $OA$ . From eqs. (a) we see that the stress in the vertical bar is larger than the stress in either of the inclined bars. The vertical bar of the model corresponds to the most unfavorably oriented crystal of the polycrystal specimen. By gradually increasing the load we reach the condition at which the vertical bar begins to yield while the inclined bars continue to deform elastically. The corresponding value  $P_1$  of the load and the corresponding displacement  $\delta_1$  are found from the equations

$$S_1' = A\sigma_{YP} = \frac{P_1}{1 + 2 \cos^3 \alpha}, \quad \delta_1 = \frac{P_1 l}{AE(1 + 2 \cos^3 \alpha)}, \quad (c)$$

which give

$$P_1 = A\sigma_{YP} (1 + 2 \cos^3 \alpha), \quad \delta_1 = \frac{\sigma_{YP} l}{E}. \quad (d)$$

This condition corresponds to point  $A$  in Fig. 271*b*.

If we continue to increase the load, the vertical bar will stretch plastically<sup>22</sup> at a constant stress  $\sigma_{YP}$  and the additional load  $P_2$  will be taken by the elastic inclined bars. The additional forces  $S_2'$  in these bars and the additional vertical displacement  $\delta_2$  will be

$$S_2' = \frac{P_2}{2 \cos \alpha}, \quad \delta_2 = \frac{P_2 l}{2AE \cos^3 \alpha}. \quad (e)$$

The relation between  $P_2$  and  $\delta_2$  is shown in Fig. 271*b* by the inclined line  $AB$ . If we begin unloading the model after reaching point  $B$  on the diagram, all three bars will behave elastically and the relation between the removed load and the upward displacement will be given by eq. (b). In the diagram we therefore obtain the line  $BC$  parallel to  $OA$ , and the total

<sup>22</sup> Strain hardening is neglected in this discussion.

vertical displacement upwards during unloading is

$$\delta_3 = \frac{(P_1 + P_2)l}{AE(1 + 2 \cos^3 \alpha)}. \quad (f)$$

We see that because of plastic stretching of the vertical bar, the model does not return to its initial state and the permanent set  $OC$  is produced. The magnitude of the permanent set is found from the equation

$$\overline{OC} = \delta_1 + \delta_2 - \delta_3 = \frac{P_2 l}{2AE \cos^3 \alpha (1 + 2 \cos^3 \alpha)}. \quad (g)$$

Owing to this permanent set there will be tensile forces  $S_2''$  in the inclined bars, and these forces will be balanced by the compressive force  $S_1''$  in the vertical bar. These are the residual forces which remain in the system after complete unloading of the model and which illustrate the residual stresses in the polycrystal specimen after a tensile test cycle.

To find the values of the residual forces in the model, we note first that the inclined bars remained in the elastic range throughout the loading cycle. Therefore the relation between the force  $S_2$  in the inclined bars and the deflection  $\delta$  may be obtained by combining eqs. (a) and (b), which gives

$$S_2 = \frac{\delta AE \cos^2 \alpha}{l}. \quad (h)$$

Substituting for  $\delta$  the value of the permanent set (eq. g) we obtain the residual tensile force  $S_2''$  in the inclined bars

$$S_2'' = \frac{P_2}{2 \cos \alpha (1 + 2 \cos^3 \alpha)}. \quad (i)$$

By a summation of vertical forces at hinge  $H$ , the residual compressive force  $S_1''$  in the vertical bar is

$$S_1'' = 2S_2'' \cos \alpha = \frac{P_2}{1 + 2 \cos^3 \alpha}. \quad (j)$$

To show the Bauschinger effect let us consider a second cycle of loading. At small values of load all three bars deform elastically, and in Fig 271*b* the second loading process will begin at point *C* and proceed along the straight line *CB*. When we reach point *D* the vertical bar will be relieved of the residual compressive force  $S_1''$  and during further loading will act in tension. At point *B* the tensile stress in this bar will reach the value  $\sigma_{YP}$  and plastic yielding of the bar will begin. It is seen that the proportional limit of the model is raised because of the residual stresses. The proportional limit was at the load  $P_1$  in the first cycle and at the load  $P_1 + P_2$  in the second cycle. The process of unloading in the second cycle is perfectly elastic and follows the line *BC*.

Let us now reverse the direction of the force and apply an upward load  $P$ . The deformation will then proceed along the straight line *CE*, which is a continuation of line *BC*. The compressive force in the vertical bar is due to the upward load  $P$  and to the residual compressive force  $S_1''$ . At point *E* the total upward force is  $P_1 - P_2$ , and the compressive force in the vertical bar is equal to the yield point value. As the load is increased, the deformation proceeds along the line *EF*. If the model is unloaded after reaching point *F*, it will return to the initial state represented by point *O*. It is seen that by loading the model in tension up to point *B*, its proportional limit in tension was increased from  $P_1$  to  $P_1 + P_2$ . At the same time the proportional limit in compression was diminished from  $P_1$  to  $P_1 - P_2$ . This illustrates the Bauschinger effect.

If the model is subjected to cyclical forces varying from  $P_1 + P_2$  in tension to  $P_1$  in compression, we obtain the hysteresis loop represented in Fig 271*b* by the parallelogram *OABCEFO*. The area of this parallelogram gives the amount of mechanical energy lost per cycle.<sup>33</sup>

This article has been concerned with tensile tests of mild steel specimens in which the deformations are small and must be measured by a sensitive extensometer. In the next article we will consider larger deformations which cause not only

therer  
 eff.<sup>33</sup> Strain hysteresis by C. F. Jenkin, see *Engineering*, Vol. 114, p. 603, 1922

the individual unfavorably oriented crystals but also the entire material of the specimen to deform plastically.

77. **Yield Point.**—In studying the tensile strength of structural steel, engineers have been particularly interested in the phenomenon of sudden stretching of the specimens at the yield point. It is well known that at a certain value of tensile stress a sudden drop in the tensile load occurs, followed by considerable stretching of the metal at a somewhat lower stress. C. Bach introduced<sup>34</sup> the terms upper and lower yield point for these two values of stress, shown in Fig. 272 by points *A* and *B*. Further experiments showed that the lower yield point is less influenced by the shape of the specimen than is the upper yield point. Thus more practical significance is attributed to the lower yield point.

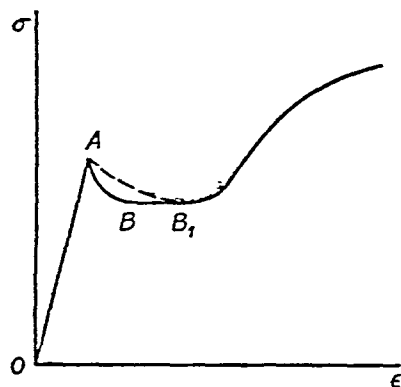


FIG. 272.

The shape of the stress-strain diagram (Fig. 272) at the yield point depends noticeably on the mechanical properties of the testing machine. If extension of the specimen is produced by an increase of distance between the grips of the machine moving at a uniform speed, the sudden plastic stretching will somewhat decrease the tensile force in the specimen, and a sharp peak *A* in the diagram will be obtained. If an elastic spring is inserted in series with the specimen, the slope of the curve *AB* of the diagram can be reduced as shown by the broken line *AB₁*. On the other hand if the tensile load itself is applied directly to the specimen, the tensile force at yielding will be affected by the small movement of the load at sudden stretching, and small vibrations may appear on the diagram.

In order to study in more detail the deformations which occur at the yield point, specimens with polished surfaces are used. Such experiments show that at the time the tensile

<sup>34</sup> *Z. Ver. deut. Ing.*, Vol. 58, p. 1040, 1904; Vol. 59, p. 615, 1905.

stress drops from point  $A$  to point  $B$  (Fig 272) fine, dull lines begin to appear on the surface of the specimen. These lines are inclined about  $45^\circ$  to the direction of tension and are called *Lueders' lines*<sup>35</sup> (see Fig 205, p 330). With further stretching the lines increase in width and in number, and during stretching from  $B$  to  $B_1$  (Fig 272) they cover the entire surface of the specimen. The first lines usually start at points of stress concentration. Fig 206 (p 330) shows, for example, a Lueders' line which started at a point of maximum stress concentration in a fillet. Instead of polishing, sometimes special paints (called stress coats) are used to indicate Lueders' lines. The paints are brittle and cannot sustain large deformations, hence they crack during loading and indicate the pattern of Lueders' lines.

Studies with a microscope show that Lueders' lines represent the intersections with the lateral surface of the specimen of thin layers of material in which plastic deformation has occurred while the adjacent portions of the material remain perfectly elastic. By cutting the specimen and using a special etching,<sup>36</sup> the thin plastic layers in the interior of the specimen can be made visible. Under a microscope it is seen that these layers consist of crystals which have been distorted by sliding, as previously described (see Art 75).

Experiments show that the values of the yield point stress and the yield point strain depend upon the rate of strain.<sup>37</sup> The curves in Fig 273 show stress-strain diagrams for mild steel for a wide range of rates of strain ( $u = d\epsilon/dt = 9.5 \times 10^{-7}$  per sec to  $u = 300$  per sec). It is seen that not only the yield point but also the ultimate strength and the total elongation depend greatly upon the rate of strain. In general, these quantities increase as the rate of strain increases.

---

<sup>35</sup> These lines were first described by W. Lueders, *Dinglers Polytech J*, 1854. See also L. Hartmann, *Distribution des déformations*, etc., Paris, 1896, and A. Nadai, *Theory of Flow and Fracture of Solids*, New York, 1950.

<sup>36</sup> See the paper by A. Fry, *loc cit*, p 333.

<sup>37</sup> M. J. Manjoine, *J Appl Mech*, Vol 11, p 211, 1944. See also R. C. Smith, T. E. Pardue and I. Vigness, *U S Naval Research Lab Rept 4468*, 1954.



To explain the sudden stretching of steel at its yield point, it has been suggested<sup>38</sup> that the boundaries of the grains consist of a brittle material and form a rigid skeleton which pre-

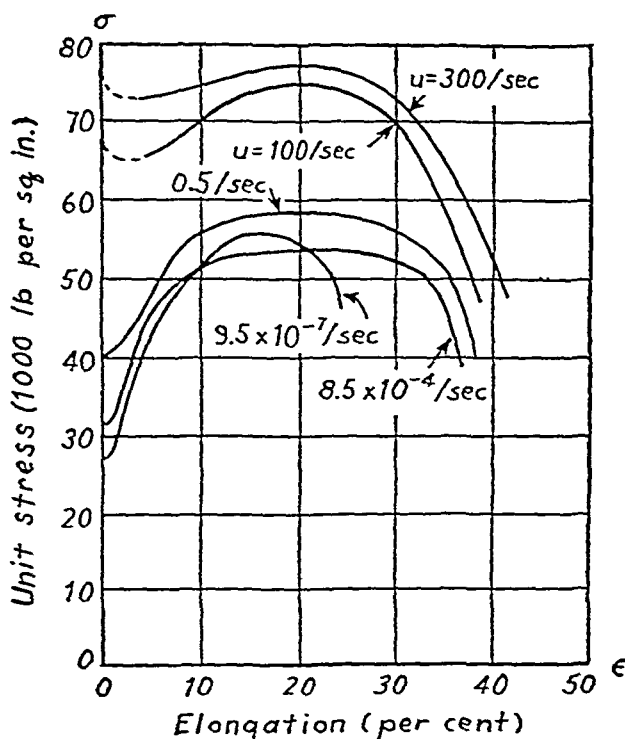


FIG. 273.

vents plastic deformation of the grains at low stress. Without such a skeleton the tensile test diagram would be like that indicated in Fig. 274 by the broken line. Owing to the presence of the rigid skeleton, the material remains perfectly elastic and follows Hooke's law up to point *A*, where the skeleton breaks down. Then the plastic grain material suddenly obtains the permanent strain *AB*, after which the material follows the usual curve *BC* for a plastic material. This theory explains the condition of instability of the material at the upper yield

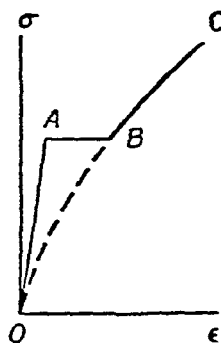


FIG. 274.

<sup>38</sup> See P. Ludwik and Scheu, *Werkstoffanschuss*, *Ver. deut. Ing. Ber.*, No. 70, 1925; W. Köster, *Archiv Eisenhüttenw.*, No. 47, 1929. See also N. N. Davidenkov, *Some Problems of Mechanics of Materials*, Leningrad, 1943 (in Russian).

point The theory also accounts for the fact that materials with small grain size usually show higher values for the yield stress As a result, such materials undergo more stretching at the yield point, as defined by the length of the horizontal line  $AB$  in Fig 274 In addition, the theory explains the fact that in high speed tests the increase in yield point stress is accompanied by an increase in the amount of stretching at yielding, as shown by the curves in Fig 273

Lueders' lines appear in steel blocks tested in compression, just as in the case of tension Furthermore, experiments in bending and torsion show that Lueders' lines also appear in these cases, but at a much higher value of stress than for a homogeneous stress distribution On the assumption that yielding begins when the brittle skeleton (formed by the grain boundaries) breaks, the theory was advanced<sup>39</sup> that the yield point stress depends upon the size of the specimen Experiments with small specimens showed higher values of the yield stress than was found for specimens of usual size

**78 Stretching of Steel beyond the Yield Point.**—During stretching of a steel specimen beyond the yield point the material hardens and the stress required for stretching the bar increases as shown by the portion  $BC$  of the stress strain diagram (Fig 275) Elongation of the specimen is combined

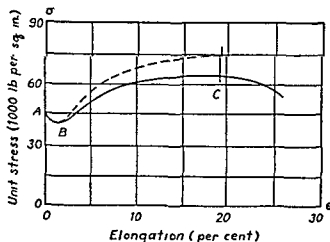


FIG 275

<sup>39</sup> C W Richards, paper presented at the 57th Annual Meeting of the American Society for Testing Materials, 1954

with uniform reduction of the cross-sectional area so that the volume of the specimen remains practically constant. The work done during stretching is transformed largely into heat and the specimen becomes hot.

Calorimetric measurements show that not all of the mechanical energy is transformed into heat, however; part of it remains in the specimen in the form of strain energy. Owing to differences in orientation of the crystals, the stresses are not uniformly distributed over the cross sections, and after unloading, some residual stress and a certain amount of strain energy remain in the specimen.

If after unloading we load the specimen a second time, we will find that its yield point stress is raised. This characteristic is shown in Fig. 276, which represents a tensile test diagram for mild steel.<sup>40</sup> After stretching the bar to the point C it was unloaded. During unloading, the material followed

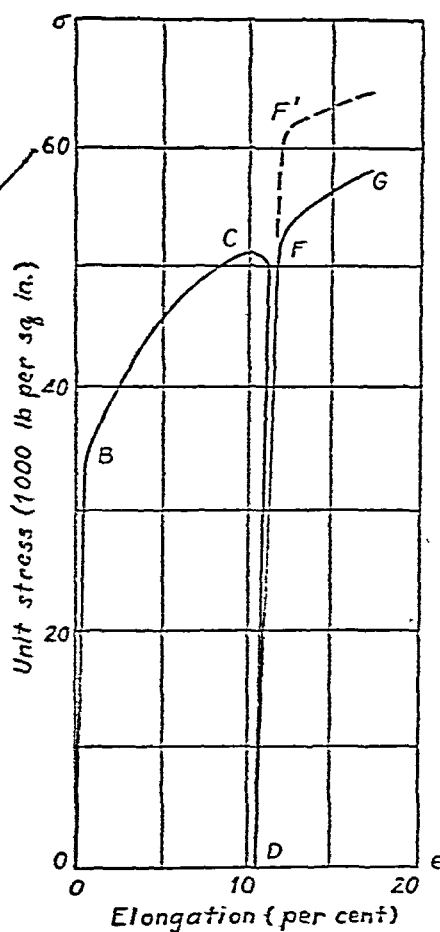


FIG. 276.

approximately a straight-line law, as shown by the line CD on the diagram. When the load was applied to the bar a second time, the material again followed approximately Hooke's law and the line DF was obtained. At point F, which corresponds to the previous loading at C, the curve abruptly changed character and traced the portion FG, which can be considered a prolongation of the curve BC. This represents a *raising of the yield point* due to previous stretching of the material. If several days are allowed to elapse after the first

<sup>40</sup> See Ewing, *Strength of Materials*, p. 35, 1914.

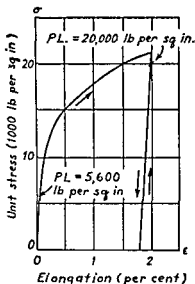


FIG. 277.

unloading, then upon reloading a still higher yield point may be obtained, as indicated by the dotted line at  $F'$  (Fig. 276). Fig. 277 shows the results of a tensile test of die-cast aluminum.<sup>41</sup> The initial proportional limit of the material was 5,600 lb per sq in. After stretching the specimen 2 per cent, the proportional limit upon reloading was found to be 20,000 lb per sq in. and the yield point about 21,000 lb per sq in.

More complete investigations show that the time which elapses between unloading and reloading is of great influence on the stress-strain curve during reloading. If reloading begins immediately after unloading, accurate measurements show that there are deviations from the straight-line law at very low stress, and the proportional limit is greatly lowered. But if a considerable interval of time elapses between unloading and reloading, the material recovers its elastic properties completely. Fig. 278 shows curves obtained<sup>42</sup> for mild steel which indicate that if reloading follows in ten minutes after overstrain, the material does not follow Hooke's law, but after five days it has partially recovered its elasticity and after twenty-one days it has almost completely recovered it.

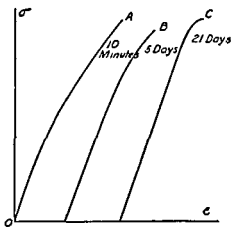


FIG. 278.

Experiments also show that if the material is subjected to mild heat treatment after unloading, say in a bath of 100° C, the recovery of elastic properties occurs in a much shorter

<sup>41</sup> Westinghouse Electric Corporation Research Laboratory.

<sup>42</sup> See Ewing, *loc. cit.*, p. 421.

interval of time. Fig. 279 shows the results of tests made on a steel bar.<sup>43</sup> The initial tensile test is represented by the curve *A*. Curve *B* represents reloading of the same bar ten minutes after unloading, and considerable deviation from Hooke's law is noticeable. Curve *C* is the diagram obtained with the same bar after a second unloading and after heat treating at 100° C for four minutes. In this case the material has completely recovered its elastic properties.

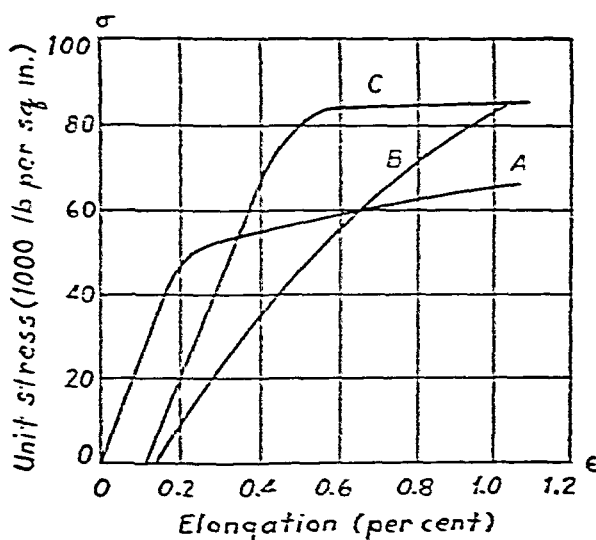


FIG. 279.

The phenomenon of strain hardening due to plastic deformation is encountered in many technological processes such as rolling bars and drawing tubes and wires at low temperature, cutting sheet metal by shears and drawing and punching holes. In all these cases the part of the material which undergoes plastic deformation becomes harder, and its ductility is greatly reduced.<sup>44</sup> To eliminate this undesirable effect of strain hardening it is customary to anneal the material, which restores the initial ductility.<sup>45</sup>

<sup>43</sup> I. Muir, *Phil. Trans. Roy. Soc. (London)*, *A*, 1899.

<sup>44</sup> For a general discussion of the properties of cold-worked metals see the paper by Z. Jeffries and R. S. Archer, *Chem. and Metallurg. Engrg.*, Vol. 27, p. 747, 1922. See also G. Masing and M. Polanyi, *Kaltreckung und Verfestigung*, Berlin, 1923.

<sup>45</sup> See the paper by Rees, *Iron and Steel Inst. J.*, 1923.

Sometimes the strain hardening of ductile materials is of practical use in manufacturing. It is common practice to subject the chains and cables of hoisting machines to a certain amount of overstrain in order to eliminate undesirable stretching of these parts in service. The cylinders of hydraulic presses are sometimes subjected to an initial internal pressure sufficient to produce permanent deformation of the walls. The strain hardening and the residual stresses produced by this pressure prevent any permanent set in service. Overstraining of the metal is sometimes used in the manufacture of guns (see p. 390). By stretching the metal in the wall of a gun beyond the initial yield point and afterwards subjecting it to a mild heat treatment, the elastic properties of the material are improved and at the same time initial stresses are produced which combine with the stresses produced by the explosion to give a more favorable stress distribution. Turbine discs and rotors are sometimes given an analogous treatment. By running these parts at overspeed, a permanent set is obtained around the central hole, which raises the yield point of the material and produces initial stresses which are in a favorable direction.<sup>46</sup> Die-cast aluminum fans are sometimes subjected to overstrain at the bore to prevent any possibility of their loosening on the shaft in service. Considerable plastic flow of the metal is sometimes produced in pressing the hubs of locomotive wheels onto their axles, and this has proved to have a favorable effect. Copper bars in the commutators of electric machinery are subjected to considerable cold work by drawing in order to give them the required strength.

In using overstrain in this manner to raise the yield point and improve the elastic properties of a structure, it is necessary to keep in mind (1) that the hardening disappears if the structure is subjected to annealing temperatures and (2) that stretching the metal in a certain direction, while making it stronger with respect to tension in that direction, does not proportionately improve the mechanical properties with respect to compression in the same direction. This phenomenon

---

<sup>46</sup> See A. Nadai and L. H. Donnell, *Trans. A.S.M.E.*, Vol. 51, p. 173, 1929.

is clearly shown in Fig. 280, which represents tests made with electrolytic copper.<sup>47</sup> Curve (a) shows the mechanical properties of the copper in the annealed condition. The proportional limit and yield strength<sup>48</sup> in this condition are very low. Such a material cannot be used in structures which are subjected to the action of appreciable stresses. Curve (b) repre-

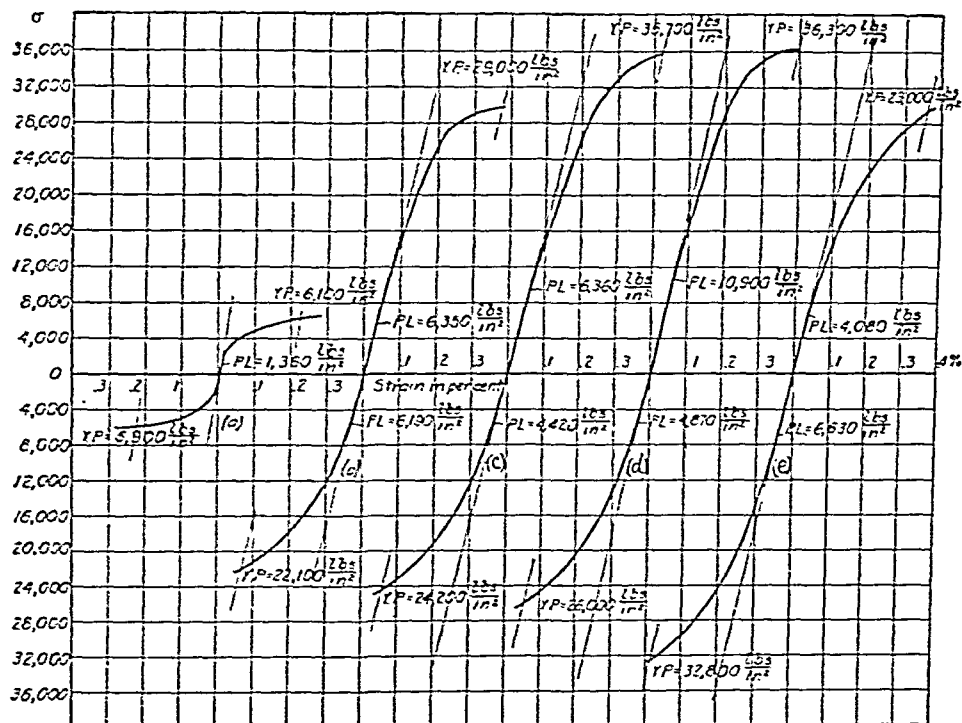


FIG. 280.

sents tension and compression tests of the same material after stretching the bar plastically by 15 per cent. The proportional limit and yield point have been raised considerably, especially in tension. Curves (c) and (d) show the results of tests which were made after plastic stretching of 20 per cent and 25 per cent. The additional stretching produces still further improvement of the mechanical properties, especially in tension. At the same time the proportional limit in compression is somewhat lowered. Curve (e) represents tension and compression tests

<sup>47</sup> Westinghouse Electric Corporation Research Laboratory.

<sup>48</sup> The yield strength is defined as the stress when the unit elongation or the unit compression is 0.2 per cent.

on a bar which has been drawn through a die, reducing the cross-sectional area of the bar by 15 per cent. In the drawing process the material is subjected not only to longitudinal tension but also to lateral compression; this accounts for the difference between curves (*b*) and (*e*). Although in both cases the bar received about the same reduction in cross-sectional area, the material drawn through the die showed better mechanical properties with respect to compression than the material which was subjected to a uniform longitudinal stretching in a testing machine.

The fact that stretching a metal in a certain direction does not improve the mechanical properties in compression in the same proportion as it does in tension must not be overlooked in cases in which the material is subjected to reversal of stresses (see Art. 84). It should also be mentioned that there are indications<sup>49</sup> that material which has yielded in a particular region is more sensitive in that region to chemical action, and there is a tendency for corrosion to enter the metal along the surfaces of sliding. This phenomenon is of particular importance in the case of boilers and other containers subjected simultaneously to stress and to chemical action.

In constructing a tensile test diagram such as curve *ABC* in Fig. 275 the tensile load is usually divided by the initial cross-sectional area  $A_0$  of the specimen in order to obtain the conventional unit stress. But for large stretching there will be a considerable reduction in cross-sectional area; and to obtain the *true stress* the actual area  $A$ , instead of  $A_0$ , should be used. From the constancy of the volume of the specimen we have

$$l_0 A_0 = l A, \quad A = \frac{A_0 l_0}{l} = \frac{A_0}{1 + \epsilon}, \quad (a)$$

and the true stress is

$$\sigma = \frac{P}{A} = \frac{P}{A_0} (1 + \epsilon). \quad (b)$$

<sup>49</sup> See F. Körber and A. Pomp, *Mitt. Kaiser-Wilh. Inst. Eisenforsch. (Düsseldorf)*, Vol. 8, p. 135, 1926; see also S. W. Parr and F. G. Straub, *Engineering*, Vol. 124, p. 216, 1927.



To obtain the true stress diagram the ordinates of the conventional diagram must be multiplied by  $1 + \epsilon$ . In Fig. 275 such a diagram is shown by the broken line. It extends as far as a vertical through point  $C$ , where the load reaches its maximum value. On further stretching of the specimen, local reduction of the cross section (necking) begins and  $\epsilon$  is no longer constant along the specimen. Then eq. (b) is no longer applicable, since the stresses over the minimum cross section are not uniformly distributed (see p. 432). In such a case, eq. (b) gives an average value of  $\sigma$ . The average unit elongation  $\epsilon$  at the minimum section may be found from eq. (a), which gives

$$\epsilon = \frac{A_0}{A} - 1. \quad (c)$$

Using the symbol  $q$  for the unit reduction of the cross-sectional area (see p. 403) we obtain

$$\frac{A_0 - A}{A_0} = q, \quad A = A_0(1 - q);$$

and eq. (c) gives

$$\epsilon = \frac{q}{1 - q}, \quad (d)$$

and the unit elongation at the minimum section can be readily calculated if the reduction in area of that section is measured. This quantity is called <sup>50</sup> the *effective elongation* and is much larger than the elongation  $\epsilon = \delta/l$  determined from the total elongation  $\delta$  of the gage length.

Let us now consider in more detail the notion of unit elongation  $\epsilon$ . For its calculation we usually use the equation  $\epsilon = (l - l_0)/l_0$ , so that an increment of unit elongation is defined by the equation

$$d\epsilon = \frac{dl}{l_0}, \quad (e)$$

in which the increment of length is divided by the initial length  $l_0$ . It seems more logical in many cases to define the increment

<sup>50</sup> See P. Ludwik, *Elemente der technologischen Mechanik*, Berlin, 1909.

of unit elongation by the equation

$$d\epsilon' = \frac{dl}{l}, \quad (f)$$

where  $l$  is the length to which the increment  $dl$  is added. Then the total unit elongation becomes

$$\begin{aligned} \epsilon' &= \int_{l_0}^l d\epsilon' = \int_{l_0}^l \frac{dl}{l} = \log_e \frac{l}{l_0} = \log_e (1 + \epsilon) \\ &= \log_e \frac{A_0}{A}. \end{aligned} \quad (g)$$

This is called the *natural strain*.<sup>51</sup> For small elongations the natural strain  $\epsilon'$  is very close to  $\epsilon$ . But for large deformations, as in the case of rubber or the plastic stretching of a steel specimen, the difference between  $\epsilon'$  and  $\epsilon$  becomes considerable and there is some advantage in using the notion of natural strain.

Let us consider, as an example, the change in volume of a cube of material having an original volume of one cubic inch and subjected to uniform elongations  $\epsilon_x$ ,  $\epsilon_y$ ,  $\epsilon_z$  in the directions of its sides. After deformation the volume of the cube will be

$$(1 + \epsilon_x)(1 + \epsilon_y)(1 + \epsilon_z).$$

If the deformation is such that the volume does not change, as in the case of plastic deformation of metals, the condition of constant volume is

$$(1 + \epsilon_x)(1 + \epsilon_y)(1 + \epsilon_z) = 1. \quad (h)$$

If the strains  $\epsilon_x$ ,  $\epsilon_y$ ,  $\epsilon_z$  are not small, so that their powers cannot be neglected, then the condition in eq. (h) will be very complicated. But if we use the notion of natural strain, the same condition takes a very simple form. For that purpose we take the logarithm of both sides of eq. (h) and obtain

$$\log_e (1 + \epsilon_x) + \log_e (1 + \epsilon_y) + \log_e (1 + \epsilon_z) = 0.$$

<sup>51</sup> It was first suggested by Mesnager; see *Proc. Congr. Internat. Phys.*, Paris, Vol. 1, p. 348, 1900.

Using the definition of natural strain (eq. *g*) we obtain the condition of constant volume in the simple form

$$\epsilon_x' + \epsilon_y' + \epsilon_z' = 0. \quad (i)$$

Tensile test diagrams for the minimum section at the neck of a tensile test specimen <sup>52</sup> can be constructed by plotting true stress (eq. *b*) against natural strain  $\epsilon'$ . These diagrams have the form shown in Fig. 281 and indicate that beyond the stress at which necking starts, the relation between the true stress and natural strain is practically linear.

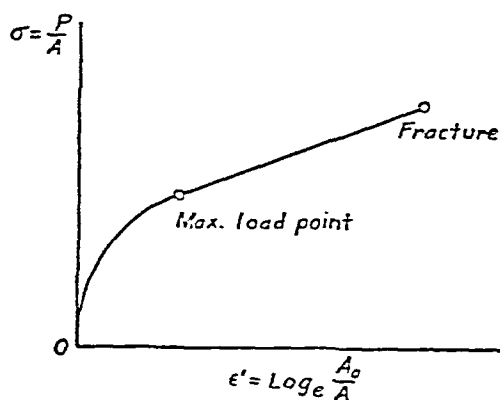


FIG. 281.

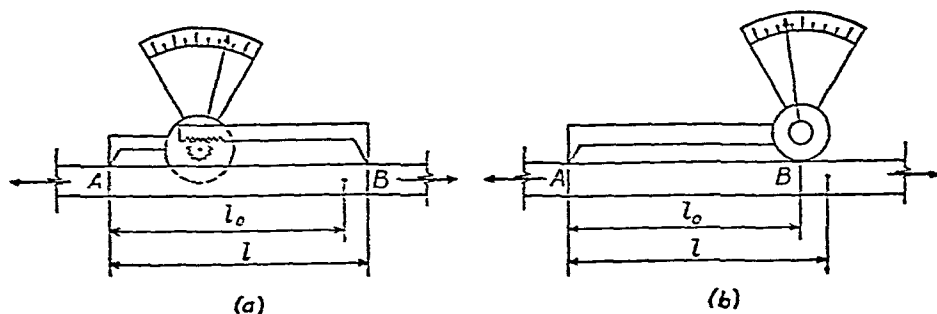


FIG. 282.

In Fig. 282 methods of measuring the conventional strain  $\epsilon$  and the true strain  $\epsilon'$  are illustrated. The extensometer in Fig. 282*a* is attached to the specimen at two fixed points *A*

<sup>52</sup> Such diagrams were used by C. W. MacGregor, *Proc. Am. Soc. Test. Mat.*, Vol. 40, p. 508, 1940; see also his article in M. Hetényi, ed., *Handbook of Experimental Stress Analysis*, 1950.

and  $B$  The distance between  $A$  and  $B$  changes during stretching of the specimen, varying from the initial distance  $l_0$  to the final distance  $l$  The extensometer in Fig 282*b* (called *Bauschinger's extensometer*) is fixed to the specimen at  $A$  and has a roller at  $B$ , so that the length  $AB$  remains equal to  $l_0$  If two identical specimens (Fig 282) are stretched from  $l_0$  to  $l$  and then two equal increments of load are applied, the changes in readings for the two instruments will evidently not be equal, but will be in the ratio  $l/l_0 = 1 + \epsilon$  But this ratio (from eqs  $e$  and  $f$ ) is equal to the ratio  $d\epsilon/d\epsilon'$  Hence the instrument in Fig 282*a* gives the conventional unit elongation  $\epsilon$ , while Bauschinger's extensometer gives the natural strain  $\epsilon'$

**79. Types of Fractures in Tension.**<sup>53</sup>—There are two kinds of fractures to be distinguished in tensile tests of single crystal specimens With a material such as rock salt, for example, we have brittle fracture without substantial plastic deformation, and failure occurs when the magnitude of the normal stress on one of the principal planes of the crystal reaches the critical value This is called *cohesive fracture* Single-crystal specimens of metal usually show, before fracture, large plastic deformation consisting of sliding along certain crystallographic planes Failure of this type is called *shear fracture*

The relation between the resistance to *separation*, as in cohesive fracture, and the resistance to *sliding* in shear fracture does not remain constant for the same material It depends upon the temperature of the specimen and upon the velocity at which the test is made There is evidence that the resistance to sliding increases as the temperature is lowered and as the velocity of deformation is increased However, the resistance to separation is not affected to the same extent by these two factors This explains why rock salt, which is brittle at room temperature, shows shear fracture if tested in warm water, when the resistance to sliding is diminished because of higher temperature It also explains why a bar

<sup>53</sup> A complete bibliography on this subject is given in the paper by P. Ludwik, *Eidg Materialprüfungsanstalt (Zurich) Ber*, No 35, 1928 See also *Forschungsarb*, No 295, 1927

of metal, such as zinc, can be bent like a ductile material under slow deformation, while the same bar shows brittleness and fractures without plastic deformation if the load is applied suddenly.<sup>54</sup>

In the case of polycrystalline materials there are again two kinds of fractures to be considered, (1) *brittle fracture*, as in the case of cast iron or glass, and (2) *shear fracture*, as in the case of mild steel, aluminum and other metals. In the first



FIG. 283.

case, fracture occurs practically without plastic deformation over a cross section perpendicular to the axis of the specimen. In the second case fracture occurs after considerable plastic stretching and has the familiar *cup-and-cone* form, Fig. 283. In discussing these two kinds of fracture the theory has again been forwarded that the strength of the material can be described by two characteristics, the resistance of the material to *separation* and the resistance to *sliding*. If the resistance to sliding is greater than the resistance to separation, we have a brittle material, and fracture will occur as a result of overcoming the cohesive forces without any appreciable deformation. If the resistance to separation is larger than the resistance to sliding, we have a ductile material. Then sliding along inclined planes begins first, and the cup-and-cone frac-

<sup>54</sup> P. Ludwik, *Stahl. u. Eisen*, Vol. 43, p. 1427, 1923.

ture occurs only after considerable uniform stretching and subsequent local reduction of the cross-sectional area (necking) of the specimen.

The stress distribution at the smallest section of the neck in the cup-and-cone type of fracture has been investigated<sup>65</sup>

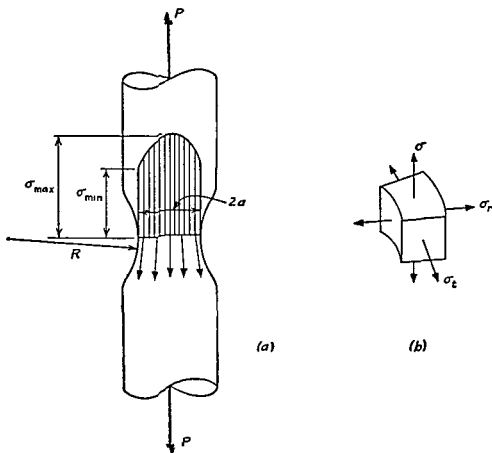


FIG. 284.

and it was found that near the neck the tensile forces in the longitudinal fibers have the directions indicated by the arrows in Fig. 284a. The horizontal components of these forces at the neck produce radial and tangential stresses so that each infinitesimal element in the plane of the minimum cross section is in the three-dimensional stress condition shown in Fig. 284b. Assuming that plastic flow requires a constant

<sup>65</sup> See the paper by N. N. Davidenkov, English translation, *Proc. Am. Soc. Test. Mat.*, 1946. See also P. Bridgman, *Trans. Am. Soc. Metals*, Vol. 32, p. 553, 1944.

maximum shearing stress, we conclude that the axial tensile stresses are not uniformly distributed over the minimum cross section of the specimen, but have a maximum value at the center of the cross section where  $\sigma_r$  and  $\sigma_t$  are also maximum. The distribution of the axial stresses is shown in Fig. 284*a* by the shaded area. The magnitudes of  $\sigma_{\max}$  and  $\sigma_{\min}$  depend upon the radius  $a$  of the minimum cross section and the radius of curvature  $R$  of the neck, and are given by the formulas

$$\sigma_{\max} = \sigma_c \frac{1 + \frac{a}{2R}}{1 + \frac{a}{4R}}, \quad \sigma_{\min} = \sigma_c \frac{1}{1 + \frac{a}{4R}},$$

where  $\sigma_c = P/\pi a^2$  is the average stress.

Because of the three-dimensional stress conditions the material near the center of the minimum cross section has its ductility reduced so that during stretching the crack starts in that region <sup>55</sup> (Fig. 285) while the material near the surface continues to stretch plastically. This fact explains why the central portion of a cup-and-cone fracture has a brittle character, while near the surface there is a ductile type of failure.

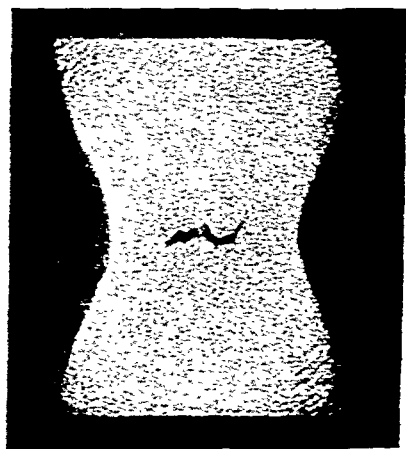


FIG. 285.

Because of the nonuniform stress distribution in the region of the neck, residual stresses will remain in the specimen if it is unloaded before the crack starts. These stresses were investigated <sup>57</sup> by the method used in the case of thick cylinders (see p. 392). By this method the stress distribution before the unloading of the specimen was computed and was found to be

<sup>55</sup> See P. Ludwik, *Z. Ver. Deut. Ing.*, Vol. 71, 1927.

<sup>57</sup> See the paper by E. R. Parker, H. E. Davis and A. E. Flanigan, *Proc. Am. Soc. Test. Mat.*, Vol. 46, pp. 1159-74, 1946.

in satisfactory agreement with the results of Davidenkov's theory (Fig. 284). In addition, examination of the fractures with a microscope showed that they occurred across the grains and were of the shear type, in both inner and outer portions of the cup-and-cone fractures.

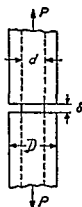


FIG. 286.

The preceding discussion refers to tensile tests of standard circular specimens of cylindrical shape. The results obtained with other shapes of specimens are quite different, as illustrated by the grooved specimen<sup>88</sup> shown in Fig. 286. During a tensile test, reduction of the cross-sectional area at the grooved section is partially prevented by the presence of the portions of larger diameter  $D$ . It is natural that this action should increase as the width  $\delta$  of the groove decreases. In Table 21 are given the

TABLE 21: ULTIMATE STRENGTH OF CYLINDRICAL AND GROOVED SPECIMENS

$\delta$ (inches)	Ultimate Strength (lb per sq in.)			
	Carbon Steel		Nickel Chrome Steel	
	Computed from Original Area	Computed from Reduced Area	Computed from Original Area	Computed from Reduced Area
$\frac{1}{4}$	163,000	176,000	193,000	237,000
$\frac{1}{8}$	164,000	177,000	184,000	232,000
$\frac{1}{16}$	143,000	158,000	154,000	199,000
Normal specimen	102,000	227,000	108,000	348,000

results of tests obtained with two different materials:<sup>89</sup> (1) *carbon steel* with proportional limit 56,000 lb per sq in., yield point 64,500 lb per sq in., ultimate strength 102,000 lb per sq in., elongation  $26\frac{1}{2}$  per cent, reduction in area 55 per cent; and (2) *nickel chrome steel* with proportional limit, 80,000 lb

<sup>88</sup> The first experiments with grooved specimens appear to have been made by D. Kirkaldy. In this way he showed that a brittle type of fracture could be produced in a ductile material. See his book *Results of an Experimental Inquiry*, etc., Glasgow, 1862.

<sup>89</sup> These tests were made at the Westinghouse Electric Corp. Research Laboratory. See also the tests made by P. Ludwik and R. Scheu, *Stahl u. Eisen*, Vol. 43, p. 999, 1923.



per sq in., yield point 85,000 lb per sq in., ultimate strength 108,000 lb per sq in., elongation 27 per cent, reduction in area 69 per cent. These figures were obtained from ordinary tensile tests on normal cylindrical specimens with  $\frac{1}{2}$ -in. diameter and 2-in. gage length. The original cross-sectional area was used in calculating the stresses. The grooved specimens of the type shown in Fig. 286 had  $d = \frac{1}{2}$  in. and  $D = 1\frac{1}{2}$  in.

The table shows that in all cases the breaking load for the grooved specimens was larger than for the corresponding cylindrical specimens. With the grooved specimens only a small reduction in area took place, and the appearance of the fracture was like that of brittle materials. The *true* ultimate strength of the cylindrical specimens was larger than for the grooved specimens because fracture of the cylindrical specimens occurred after considerable plastic flow. This resulted in strain hardening and increased not only the resistance to sliding but also the resistance to separation.

Similar conditions are sometimes encountered in engineering practice. An effect analogous to that of the narrow groove in Fig. 286 may be produced by internal cavities in large forgings, such as turborotors. Thermal stresses and residual stresses may combine with the effect of the stress concentration at the cavity to produce a crack. The resulting fracture will have the characteristics of a brittle failure without appreciable plastic flow, although the material may prove ductile in the usual tensile tests.

Because most of the grooved specimen (Fig. 286) remains elastic during a tensile test to failure, it will have a very small elongation, and hence only a small amount of work is required to produce fracture. A small impact force can easily supply the work required for failure. The specimen is brittle because of its shape, not because of any mechanical property of the material. In machine parts subjected to impact all sharp changes in cross section are dangerous and should be avoided.

**80. Compression Tests.**—The compression test is commonly used for testing brittle materials such as stone, concrete and cast iron. The specimens used in the tests are usually made in either cubic or cylindric shape. In compressing the specimens between the plane surfaces of the testing machine it is

normally assumed that the compressive force is uniformly distributed over the cross section. The actual stress distribution is much more complicated, even if the surfaces are in perfect contact and the load is centrally applied. Owing to friction on the surfaces of contact between the specimen and the heads of the machine, the lateral expansion which accompanies compression is prevented at these surfaces and the

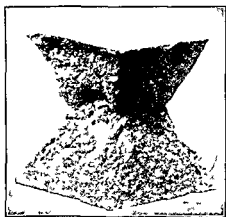


FIG. 287.

material in this region is in a more favorable stress condition. As a result the type of fracture obtained in a compression test of a cubic specimen of concrete is as shown in Fig. 287.<sup>60</sup> The material in contact with the machine remains unaffected while the material at the sides is crushed out.

In order to obtain the true resistance to compression of a material such as concrete, the influence of friction at the surfaces of contact must be eliminated or minimized. For this purpose A. Föppl covered the surfaces of contact with paraffin<sup>61</sup> and found that the ultimate strength was then greatly reduced. The type of failure was completely different, and cubic specimens failed by subdividing into plates parallel to one of the lateral sides. Another method of eliminating the effect of friction forces is to use specimens in the form of prisms having a length in the direction of compression several times larger than the lateral dimensions. The middle portion of the prism then approaches the condition of uniform compression.<sup>62</sup> A very interesting method of producing uniform compression on cylindrical specimens as developed in the Kaiser-Wilhelm Insti-

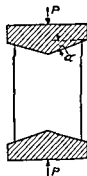


FIG. 288.

<sup>60</sup> See C. Bach, *Elastizität und Festigkeit*, 6th Ed., Berlin, p. 160, 1911.

<sup>61</sup> A. Föppl, *Mitt. Mech.-tech. Lab. München*, No. 27, 1900.

<sup>62</sup> See Prandtl and Rinne, *Neu. Jahrb. Mineral*, 1907. See also W. Gehler, *Bauingenieur*, Vol. 9, p. 21, 1928. Cylindrical specimens with height twice the diameter are used in testing concrete.

tut<sup>63</sup> is shown in Fig. 288. The head pieces of the testing machine and the ends of the cylindrical specimen are machined to conical surfaces with the angle  $\alpha$  equal to the angle of friction. Thus the effect of friction is compensated for by the wedging action and uniform compression results.

Compression tests of materials such as concrete, stone and cast iron show that these materials have a very low proportional limit.<sup>64</sup> Beyond the proportional limit the deformation increases at a faster rate relative to the load, and the compression test diagram has the shape shown in Fig. 289. Sometimes it is desirable to have an analytical expression for such a diagram. For these cases Bach proposed<sup>65</sup> an exponential law given by the equation

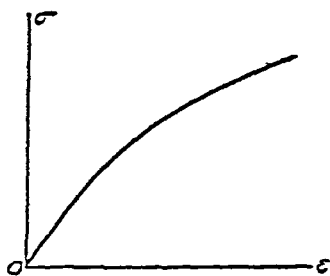


FIG. 289.

$$\epsilon = \frac{\sigma^n}{E}, \quad (a)$$

in which  $n$  is a number depending on the properties of the material. Bach found the values  $n = 1.09$  for pure cement and  $n = 1.13$  for granite.

Compression tests of ductile materials show that the shape of the diagram depends on the proportions of the specimen. As the dimension in the direction of compression decreases, the effect of friction at the ends becomes more pronounced and the compression test diagram becomes steeper. For example, Fig. 290 shows the results of compression tests<sup>66</sup> on copper cylinders with various ratios  $d/h$  of the diameter to the height of the specimen. In compression tests of such ductile materials as copper, fracture is seldom obtained. Compression is accompanied by lateral expansion and a compressed cylinder ultimately assumes the shape of a flat disc.

<sup>63</sup> *Mitt. Kaiser-Wilh. Inst. Eisenforsch. (Düsseldorf)*, Vol. 9, p. 157, 1927.

<sup>64</sup> The proportional limit for cast iron in tension was determined by Grüneisen; see *Ber. deut. physik. Ges.*, 1906.

<sup>65</sup> C. Bach, *Elastizität und Festigkeit*, 5th Ed., Berlin, p. 67, 1905.

<sup>66</sup> See G. Sachs, *Grundbegriffe der mechanischen Technologie der Metalle*, Leipzig, p. 36, 1925.

To reduce the effect of friction forces at the surfaces of contact and thereby obtain a satisfactory compression test diagram, the method of producing compression in stages<sup>67</sup> is sometimes used. After the specimen has acquired a barreled form due to lateral expansion, it is machined to its original diameter. Further compression is applied and the process

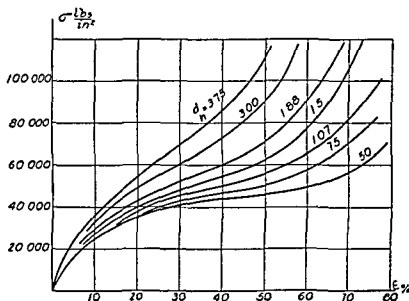


FIG 290

repeated at each stage. Thus the test proceeds with a continuous decrease in the size of the specimen.

**81. Tests of Materials under Combined Stresses**—Leaving the discussion of simple tension and compression tests, let us now consider cases in which the materials are tested under combined stresses. We begin with a discussion of materials tested under *uniform hydrostatic pressure*<sup>68</sup>. Such tests show that under uniform pressure, homogeneous materials can sustain enormous compressive stresses and remain elastic. Tests

<sup>67</sup>See G. I. Taylor and H. Quinney, *Proc Roy Soc (London), A*, Vol 143, pp 307-26, 1933-4.

<sup>68</sup>The most comprehensive tests of this kind were made by P. W. Bridgman, who developed a technique for obtaining enormous pressures; see his books, *The Physics of High Pressure*, New York, 1931, and *Studies in Large Plastic Flow and Fracture*, New York, 1952. A new triaxial stress-testing machine was described by H. A. B. Wiseman and Joseph Marin, *Proc Am Soc Test Mat*, Vol 54, 1954.

also show that the unit volume change under hydrostatic pressure  $p$  can be represented by the equation <sup>69</sup>

$$\frac{\Delta V}{V_0} = ap + bp^2.$$

Values of the constants  $a$  and  $b$  for several materials ( $p$  is measured in kg per sq cm) are given in Table 22. It is seen

TABLE 22

Material	$a \times 10^7$	$b \times 10^{12}$
Iron.....	5.87	-2.10
Copper.....	7.32	-2.70
Aluminum.....	13.34	-3.50
Silica.....	27.74	+7.17
Pyrex glass.....	30.08	+4.86

that large pressures produce only small changes in volume.

Several attempts have been made to produce *uniform tension* of materials, but up to now there has not been a satisfactory solution to this interesting problem.

Tensile tests of various steels combined with lateral pressure have shown <sup>70</sup> that the pressure has a great effect on the shape of the neck and on the reduction in area at the minimum cross section. Fig. 291 shows the yoke arrangement by which tension was applied to specimens within the pressure vessel. Figs. 292*a* and *b* illustrate fractures of medium carbon steel (0.45 per cent carbon) at atmospheric pressure and at a lateral pressure of 145,000 lb per sq in. In the first case the natural elongation was  $\log_e A_0/A = 0.92$  and the average true stress was 114,000 lb per sq in. In the second case the corresponding values were 2.37 and

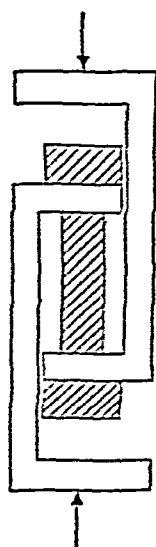


FIG. 291.

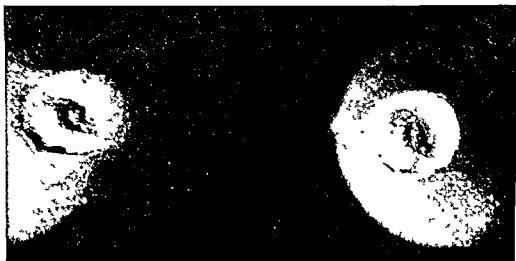
<sup>69</sup> Bridgman, *Studies in Large Plastic Flow and Fracture*.

<sup>70</sup> Bridgman, *ibid*.

474,000 lb per sq in. It was also found that with an increase in lateral pressure the relative extent of the flat part at the bottom of the cup-and-cone fracture diminishes; at a certain



(a)



(b)

FIG 292.

pressure it entirely disappears, and the fracture becomes entirely shear fracture.

The combination of *axial compression and lateral pressure* was used by Th. v. Kármán <sup>11</sup> in compression tests of marble.

<sup>11</sup> *Z. Ver. deut Ing*, p 1749, 1911.

These tests showed that with increasing lateral pressure marble becomes more and more plastic, and initially cylindrical specimens may obtain barreled forms, as in Fig. 293.

In studying two-dimensional stress conditions, thin-walled cylindrical tubes have been tested. By subjecting a tube to axial tension combined with internal pressure, the yield point

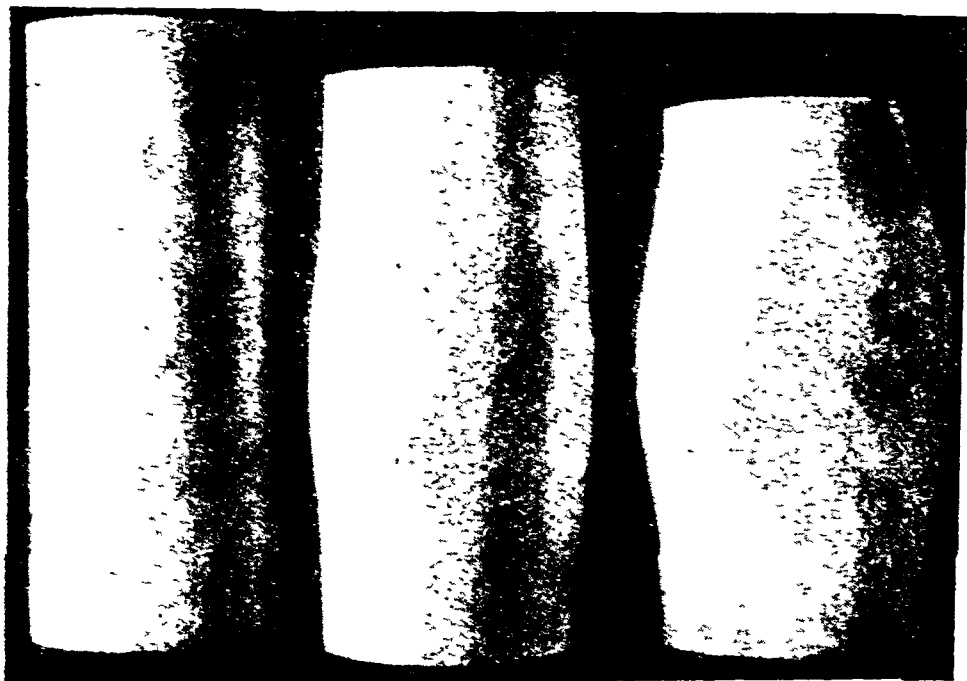


FIG. 293.

stress for various ratios of the two principal stresses was established<sup>72</sup> for several materials, including iron, copper and nickel. The results obtained in this way were in satisfactory agreement with the maximum distortion energy theory (see p. 451). Further experiments<sup>73</sup> with thin tubes of mild steel subjected to internal pressure in combination with tension, compression or torsion also gave results in agreement with the above theory. Combined tension and torsion tests of thin

<sup>72</sup> Such experiments were made by W. Lode under the direction of A. Nadai; see *Forschungsarb.*, No. 303, 1928. See also *Z. Phys.*, Vol. 36, pp. 913-939, 1926.

<sup>73</sup> See M. Roš and A. Eichinger, *Proc. Internat. Congr. Appl. Mech.*, Zürich, 1926.

tubes of steel, copper and aluminum showed<sup>74</sup> that the beginning of yielding is predicted with good accuracy by the equation

$$\sigma^2 + 3\tau^2 = \sigma_{YP}^2,$$

in which  $\sigma$  is the axial tensile stress,  $\tau$  is the torsional shear stress and  $\sigma_{YP}$  is the yield point stress in simple tension. This equation again follows from the maximum distortion energy theory.

In practical applications not only the yield point stress but also the ductility and strain hardening are of great importance in cases of combined stresses. Unusual cases of failure, such as explosions of large spherical storage tanks<sup>75</sup> and sudden cracks in the hulls of welded cargo ships, have recently called attention to those subjects. In both these types of failure, low-carbon steel plates were used which showed satisfactory strength and ductility in ordinary tensile tests. But the fractured surfaces of the plates in the exploded pressure vessels and in the damaged ships did not show plastic deformation and had a brittle character. Most of these failures occurred at low atmospheric temperatures and under two-dimensional stress conditions.

In order to determine the influence of temperature and two-dimensional stress on the strength and ductility of low-carbon steel, a considerable amount of experimental work has been done in recent times in various laboratories. Thin-walled tubes were used to produce two-dimensional stress conditions. These tubes were subjected simultaneously to axial tension and internal hydrostatic pressure, so that tensile stresses  $\sigma_t$  in the circumferential direction and  $\sigma_a$  in the axial direction could be produced in any desired ratio  $n = \sigma_t/\sigma_a$ . Using tubes of medium-carbon steel (0.23 per cent carbon) with 1.450 in. outside diameter and 0.100 in. wall thickness, E. A. Davis made tests<sup>76</sup> with five different values of the

<sup>74</sup> G. I. Taylor and H. Quinney, *Phil. Trans. Roy. Soc. (London)*, A, Vol. 230, pp. 323-62, 1931.

<sup>75</sup> See A. L. Brown and J. B. Smith, *Mech. Engr.*, Vol. 66, p. 392, 1944.

<sup>76</sup> See E. A. Davis (Westinghouse Research Laboratories), *J. Appl. Mech.*, Vol. 12, p. 13, 1945, and Vol. 15, p. 216, 1948.



ratio  $n$ . Fig. 294 shows the types of fractures obtained. For the smaller values of the ratio  $n$  the cracks were circumferential, and for the larger values they were longitudinal. By making

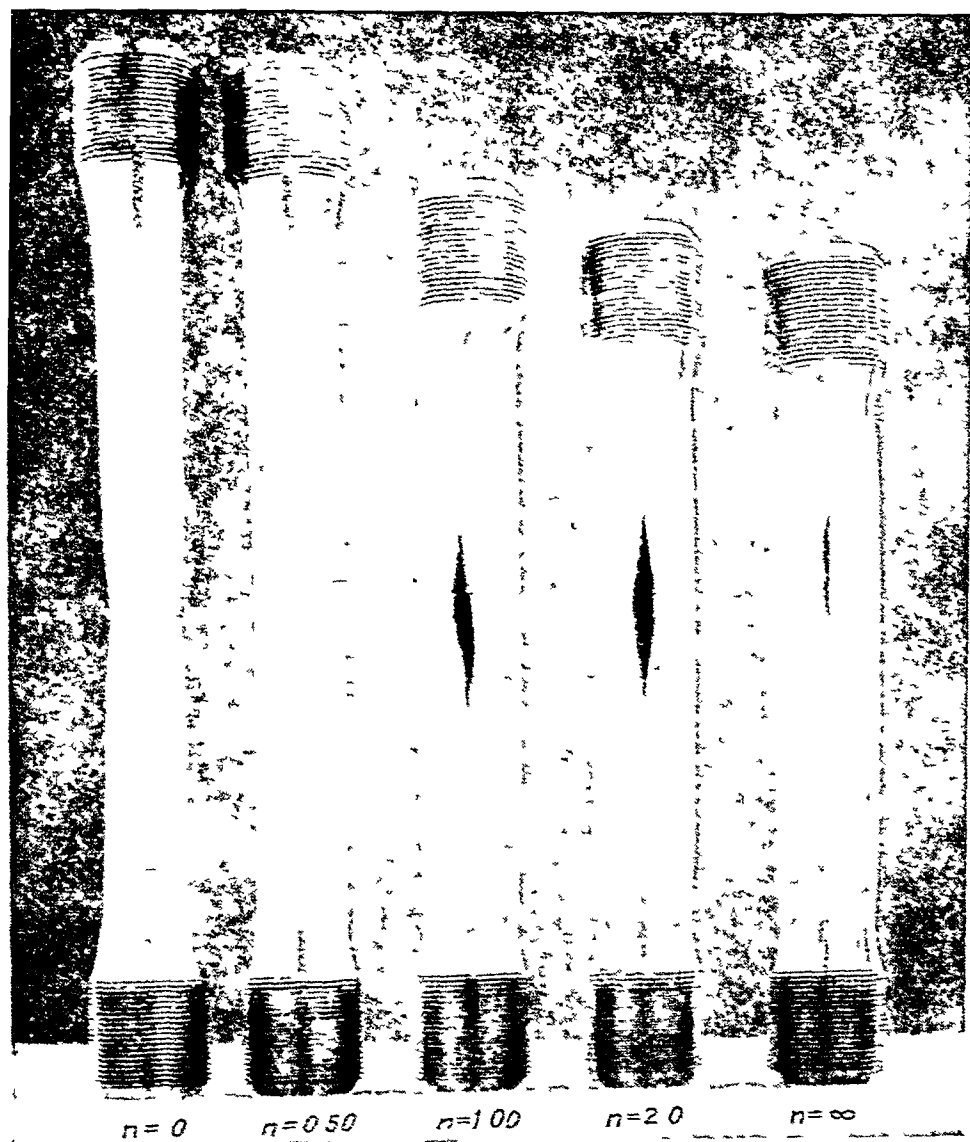


FIG. 294.

an additional series of tests it was established that the transition from one type of failure to the other occurred at the value  $n = 0.76$ . It was found that in the case of circumferential cracks the fracture occurred along the planes of maximum shearing stress and at true stresses of about the same magnitude as in the case of flat specimens prepared from the same

material as the tubes. In the case of the longitudinal cracks, rupture appeared to be more brittle. Failure usually started along the planes of maximum shearing stress, but owing to high stress concentration at the crack ends, it continued as brittle fracture in the axial plane without substantial plastic deformation. The maximum shearing stress at which the longitudinal cracks began was always much smaller than in the case of circumferential cracks. It seems that the differences in the two fractures were due largely to the shape of the specimens. In the case of circumferential cracks the material was much more free to neck down than in the case of longitudinal cracks and therefore the latter occurred with smaller local deformation and smaller decrease in load beyond the ultimate strength.

In experiments at the University of California<sup>77</sup> tests were made at two different temperatures using thin walled tubes of low carbon steel. The diameter of the tubes was  $5\frac{1}{4}$  in and the temperatures were 70° F and -138° F. The tests at room temperature always gave a shear type of fracture with considerable plastic deformation. The tests at low temperature (with  $n = 1$ ) showed brittle fracture with very small plastic deformation. This brittleness was attributed to the local stresses at the welded junctions of the tubes with the end connections.

After these tests with small tubes, large size tubular specimens of 20 in outside diameter and 10 ft length, made of  $\frac{3}{4}$ -in ship plate, were tested<sup>78</sup> at 70° F and at -40° F. The tests at low temperature, especially with the ratio  $n = 1$ , showed brittle fracture at stresses much smaller than those obtained from tensile tests of ordinary cylindrical specimens made of the same material.

**82. Strength Theories**<sup>79</sup>—The mechanical properties of structural materials are normally determined by tests which

<sup>77</sup> See H. E. Davis and E. R. Parker, *J. Appl. Mech.*, Vol 15, p 201, 1948.

<sup>78</sup> See *Welding J.*, Vol 27, p 34, 1948.

<sup>79</sup> A description of these theories can be found in papers by H. M. Westergaard, *J. Franklin Inst.*, 1920, A. J. Becker, *Univ. of Illinois Eng. Exp. Sta. Bull.*, No 85, F. Schleicher, *Z. angew. Math. u. Mech.*, Vol 5, p 199, 1925, A. Nadai, *J. Appl. Mech.*, Vol 1, p 111, 1933.

subject the specimen to comparatively simple stress conditions. For example, most of our information concerning the strength of metals was obtained from tensile tests. Similarly, compression tests have been used for studying brittle materials like stone and concrete. In addition, a small amount of information is available concerning the strength of materials under shear loading. However, the strength of materials under more complicated stress conditions has only been investigated in a few exceptional cases, such as those discussed in the preceding article.

In order to determine suitable allowable stresses for the complicated stress conditions which occur in practical design, various strength theories have been developed. The purpose of these theories is to predict when failure will occur under combined stresses, assuming that the behavior in a simple tension or compression test is known. By failure of the material is meant either yielding or actual rupture, whichever occurs first.

The most general state of stress which can exist in a body is always completely determined by specifying the principal stresses  $\sigma_1$ ,  $\sigma_2$  and  $\sigma_3$  (Fig. 295). In the following discussion tension is considered positive and compression negative, and the axes in Fig. 295 are chosen so that the relations between the algebraic values of the principal stresses are

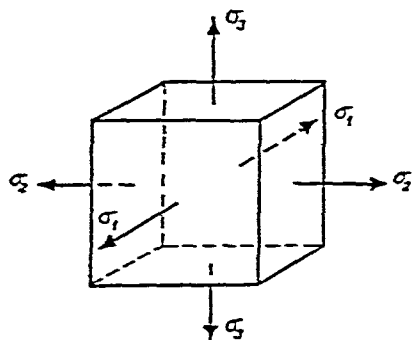


FIG. 295.

$$\sigma_1 > \sigma_2 > \sigma_3. \quad (a)$$

The *maximum stress theory*<sup>80</sup> considers the maximum or minimum principal stress as the criterion for strength. For ductile materials this means that yielding begins in an element of a stressed body (Fig. 295) when either the maximum stress reaches the yield point stress of the material in simple tension

<sup>80</sup> This is the oldest theory of failure and is sometimes called *Rankine's theory*.

or the minimum stress reaches the yield point stress in simple compression. Thus the conditions for yielding are

$$(\sigma_1)_{Y.P.} = \sigma_{Y.P.}, \quad \text{or} \quad |(\sigma_3)_{Y.P.}| = \sigma_{Y.P.}' \quad (291)$$

in which  $\sigma_{Y.P.}$  and  $\sigma_{Y.P.}'$  are the yield point stresses in simple tension and compression, respectively. There are many examples which contradict the maximum stress theory. It has already been pointed out (see p. 418) that in simple tension sliding occurs along planes inclined at  $45^\circ$  to the axis of the specimen. For these planes neither the tensile nor the compressive stresses are maximum, and failure is caused by shear stresses instead. It has also been pointed out (see p. 438) that a homogeneous and isotropic material, even though weak in simple compression, may sustain very large hydrostatic pressures without yielding. This indicates that the magnitude of the maximum stress is not sufficient to determine the conditions for the yielding of the material or its fracture.

A second strength theory is the *maximum strain theory*, usually attributed to St. Venant. In this theory it is assumed that a ductile material begins to yield either when the maximum strain (elongation) equals the yield point strain in simple tension or when the minimum strain (shortening) equals the yield point strain in simple compression. The maximum and minimum strains (see Part I, eqs. 43, p. 66) are

$$\frac{\sigma_1}{E} - \frac{\mu}{E}(\sigma_2 + \sigma_3) = \epsilon_1,$$

$$\frac{\sigma_3}{E} - \frac{\mu}{E}(\sigma_1 + \sigma_2) = \epsilon_3$$

Substituting the yield point strains  $\sigma_{Y.P.}/E$  in tension and  $\sigma_{Y.P.}'/E$  in compression for  $\epsilon_1$  and  $\epsilon_3$ , the criterion of failure according to the maximum strain theory becomes

$$\sigma_1 - \mu(\sigma_2 + \sigma_3) = \sigma_{Y.P.} \quad (292)$$

or

$$|\sigma_3 - \mu(\sigma_1 + \sigma_2)| = \sigma_{Y.P.}'$$

There are many cases in which the maximum strain theory may also be shown to be invalid. For example, if a plate is subjected to equal tensions in two perpendicular directions, the maximum strain theory indicates that the tension stress at yielding will be higher than the stress in simple tension. This result is obtained because the elongation in each direction is decreased by the tension in the perpendicular direction. However, this conclusion is not supported by experiments.<sup>81</sup> Tests of materials under uniform hydrostatic pressure also contradict the theory. For this case, the second of eqs. (292) gives

$$|\sigma_3|_{Y.P.} = \frac{\sigma_{Y.P.}'}{1 - 2\mu},$$

in which  $\sigma_3$  represents the hydrostatic pressure. Experiments show that homogeneous materials under uniform compression can withstand much higher stresses and remain elastic (see p. 438).

The *maximum shear theory* gives better agreement with experiments, at least for ductile materials which have  $\sigma_{Y.P.} = \sigma_{Y.P.'}$ . This theory assumes that yielding begins when the maximum shear stress in the material becomes equal to the maximum shear stress at the yield point in a simple tension test. Since the maximum shear stress in the material is equal to half the difference between the maximum and minimum principal stresses,<sup>82</sup> and since the maximum shear stress in a tension test is equal to half the normal stress, the condition for yielding is

$$\sigma_1 - \sigma_3 = \sigma_{Y.P.} \quad (293)$$

In machine design the maximum shear theory is usually used for ductile materials.<sup>83</sup> The theory is in good agreement with experiments<sup>84</sup> and is simple to apply.

<sup>81</sup> See Wehage, *Mitt. Tech. Versuchsanstalt. (Berlin)*, 1888, p. 89.

<sup>82</sup> See Part I, p. 66.

<sup>83</sup> A comparison of various strength theories as applied in machine design is given by J. Marin, *Product Engng.*, May 1937.

<sup>84</sup> The theory is supported by the experiments of J. J. Guest, *Phil. Mag.*, Vol. 50, p. 69, 1900. See also L. B. Turner, *Engineering*, Vol. 86, p. 169; W. A. Scoble, *Phil. Mag.*, Dec. 1906, and Jan. 1910; C. A. Smith, *Engineering*, Vol. 88, p. 238.

In the *maximum energy theory* the quantity of strain energy per unit volume of the material is used as the basis for determining failure.<sup>85</sup> By using the general expression for strain energy (eq. 195, Part I, p. 327) and equating the energy for the case shown in Fig. 295 to the energy at yielding in simple tension, the criterion for yielding becomes

$$\begin{aligned} w_{Y.P.} &= \frac{1}{2E} (\sigma_1^2 + \sigma_2^2 + \sigma_3^2) - \frac{\mu}{E} (\sigma_1\sigma_2 + \sigma_2\sigma_3 + \sigma_1\sigma_3) \\ &= \frac{\sigma_{Y.P.}^2}{2E}. \end{aligned} \quad (294)$$

To compare the preceding strength theories let us consider the case of pure shear. For this special case of two-dimensional stress the maximum tensile, compressive and shearing stresses are all numerically equal (see eq. *a*, Part I, p. 57) and we have

$$\sigma_1 = -\sigma_3 = \tau, \quad \sigma_2 = 0.$$

Assuming that the material has the same yield point in tension and compression, the conditions for yielding according to the maximum stress theory, maximum strain theory and maximum shear theory, respectively, are

$$\tau_{Y.P.} = \sigma_{Y.P.},$$

$$\tau_{Y.P.} = \frac{\sigma_{Y.P.}}{1 + \mu},$$

$$\tau_{Y.P.} = \frac{\sigma_{Y.P.}}{2}.$$

The maximum energy theory gives the relation

$$w_{Y.P.} = \frac{\sigma_1^2(1 + \mu)}{E} = \frac{\sigma_{Y.P.}^2}{2E},$$

from which

$$\tau_{Y.P.} = \frac{\sigma_{Y.P.}}{\sqrt{2(1 + \mu)}}.$$

<sup>85</sup> This theory was first proposed by Beltrami, *Rendiconti*, p. 704, 1885; *Math. Ann.*, p. 94, 1903. See also Girtler, *Sitzungsber. Wiener Akad.*, Vol. 116, IIa, p. 509, 1907; B. P. Haigh, *Engineering*, Vol. 109, p. 158, 1920, and *Brit. Assoc. Adv. Sci. (Edinburgh) Repts.*, 1921.

Taking  $\mu = 0.3$ , as for steel, we find the following results:

- Maximum stress theory.....  $\tau_{Y.P.} = \sigma_{Y.P.}$   
 Maximum strain theory.....  $\tau_{Y.P.} = 0.77\sigma_{Y.P.}$   
 Maximum shear theory.....  $\tau_{Y.P.} = 0.50\sigma_{Y.P.}$   
 Maximum energy theory.....  $\tau_{Y.P.} = 0.62\sigma_{Y.P.}$

It is seen that the difference between the various theories is considerable in this particular case.<sup>85</sup> In the design of a circular shaft in torsion, for example, it is first necessary to assume an allowable value of working stress in shear  $\tau_W = \tau_{max} = \tau_{Y.P.}/n$ . Then the diameter of the shaft may be found from eq. (152), Part I, p. 284. Using the four theories discussed above, the following ratios of the diameters are obtained:

$$1:1.09:1.26:1.17.$$

Another method for comparing the four strength theories discussed above is shown in Fig. 296. The figure is drawn for

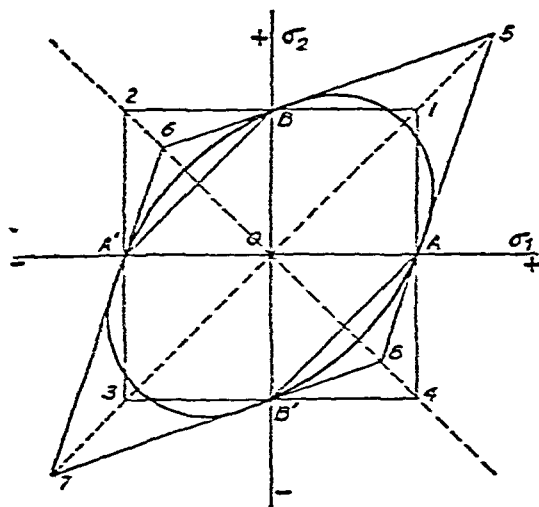


FIG. 296.

a material which has the same yield point stress in tension and compression and which is subjected to two-dimensional stress<sup>87</sup> so that  $\sigma_3 = 0$ . The lines in the figure represent the values of

<sup>85</sup> Comparisons of strength theories as applied to various design problems are given in a paper by Roth, *Z. Math. u. Phys.*, Vol. 48, 1902.

<sup>87</sup> See papers by A. J. Becker, *loc. cit.*, p. 444; and B. P. Haigh, *loc. cit.*, p. 448.

$\sigma_1$  and  $\sigma_2$  at which yielding begins. The maximum stress theory is represented by the square *1234* in which the lengths *OA* and *OB* represent the yield point stresses in simple tension in the directions of the corresponding principal stresses. In the same manner, *A'* and *B'* correspond to simple compression. Point *I* represents equal tensions in two perpendicular directions, each stress being equal to the yield point stress in simple tension. According to the maximum stress theory there is no yielding at stresses represented by points inside the square *1234*.

The maximum strain theory is represented by the rhombus *5678* (Fig. 296). Since tension in one direction reduces the strain in the perpendicular direction, this theory indicates that two equal tensions will cause yielding at much higher values (point 5) than indicated by the maximum stress theory (point *I*). The coordinates of point 5, from eq. (292), are  $\sigma_{YP}/(1 - \mu)$ . If the two principal stresses are equal in magnitude but opposite in sign, the maximum strain theory indicates yielding begins at points 6 and 8 which have coordinates numerically equal to  $\sigma_{YP}/(1 + \mu)$ . The values of stress at these points are therefore lower than indicated by the maximum stress theory (points 2 and 4).

The maximum shear theory is represented by the irregular hexagon *AIBA'3B'A* which was constructed on the basis of eq. (293). In using eq. (293) it should be observed that  $\sigma_3 = 0$  in this case, and therefore  $\sigma_2$  must be used instead of  $\sigma_3$  whenever  $\sigma_2$  is negative. This theory coincides with the maximum stress theory whenever both principal stresses have the same sign, but there is considerable difference when the principal stresses have opposite signs.

For two-dimensional stress problems eq. (294) for the maximum energy theory reduces to

$$\sigma_1^2 + \sigma_2^2 - 2\mu\sigma_1\sigma_2 = \sigma_{YP}^2.$$

By plotting this equation we obtain the ellipse shown in Fig. 296. The ellipse deviates only a comparatively small amount from the hexagon representing the maximum shear theory.



When a material is subjected to uniform hydrostatic pressure in all directions ( $\sigma_1 = \sigma_2 = \sigma_3 = -p$ ) then the maximum energy theory gives

$$p_{Y.P.} = \frac{\sigma_{Y.P.}}{\sqrt{3(1 - 2\mu)}}, \quad (b)$$

in which  $p_{Y.P.}$  is the pressure at which the yielding of the material begins. This result is not in agreement with uniform compression tests, however. As already noted (see p. 438) homogeneous isotropic materials can withstand large hydrostatic pressures and remain elastic.

To obtain better agreement between theory and experiment Huber<sup>ss</sup> proposed that the total strain energy be resolved into two parts, (1) the strain energy of uniform tension or compression, and (2) the strain energy of distortion. Then he proposed that only the strain energy of distortion be used to determine yielding and failure of the material.<sup>ss</sup> To accomplish this separation of the strain energy into two parts let us begin again with a general stress condition defined by the three principal stresses  $\sigma_1$ ,  $\sigma_2$  and  $\sigma_3$  (Fig. 295). Then Hooke's law gives

$$\epsilon_1 = \frac{\sigma_1}{E} - \frac{\mu}{E}(\sigma_2 + \sigma_3),$$

$$\epsilon_2 = \frac{\sigma_2}{E} - \frac{\mu}{E}(\sigma_1 + \sigma_3),$$

$$\epsilon_3 = \frac{\sigma_3}{E} - \frac{\mu}{E}(\sigma_1 + \sigma_2).$$

Adding these equations we obtain

$$\epsilon_1 + \epsilon_2 + \epsilon_3 = \frac{1 - 2\mu}{E}(\sigma_1 + \sigma_2 + \sigma_3), \quad (c)$$

<sup>ss</sup> M. T. Huber, *Czasopismo techniczne*, Lwów (Lemberg), 1904. See also A. Föppl and L. Föppl, *Drang und Zwang*, Munich, 2d Ed., Vol. 1, p. 50, 1924.

<sup>ss</sup> It seems that J. C. Maxwell was the first to express the opinion that "when [the strain energy of distortion] reaches a certain limit then the element will begin to give way." This was stated in Maxwell's letter (1856) to William Thomson and became known only after the publication of Maxwell's letters.

which states that the unit volume change is proportional to the summation of the three principal stresses. If this summation is zero the volume change vanishes and the material is subjected only to the deformation of distortion.

If  $\sigma_1 = \sigma_2 = \sigma_3 = p$ , we have

$$\epsilon_1 = \epsilon_2 = \epsilon_3 = \epsilon = \frac{1 - 2\mu}{E} p. \quad (d)$$

There will be no distortion in this case and the uniform tension or compression exists alone.

In the general case let us introduce the notation

$$\frac{\sigma_1 + \sigma_2 + \sigma_3}{3} = p \quad (e)$$

and then divide each of the three principal stresses into two components as follows:

$$\sigma_1 = p + \sigma_1', \quad \sigma_2 = p + \sigma_2', \quad \sigma_3 = p + \sigma_3'. \quad (f)$$

Summing up these three equations and using eq. (e) we obtain

$$\sigma_1' + \sigma_2' + \sigma_3' = 0.$$

Since the summation of  $\sigma_1'$ ,  $\sigma_2'$  and  $\sigma_3'$  vanishes, these stresses produce only distortion, and eqs. (f) provide a means for dividing the given system of stresses  $\sigma_1$ ,  $\sigma_2$  and  $\sigma_3$  into two systems: (1) uniform tension or compression  $p$ , producing only change of volume, and (2) the system of stresses  $\sigma_1'$ ,  $\sigma_2'$  and  $\sigma_3'$ , producing only distortion.

As an example of the application of eqs. (f) let us consider the case of simple tension, Fig. 297*a*. Substituting  $\sigma_2 = \sigma_3 = 0$

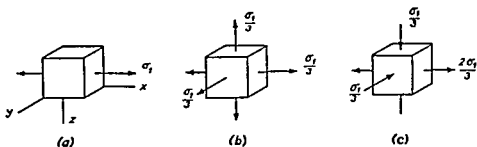


FIG. 297.

into eqs. (e) and (f) we obtain

$$p = \frac{\sigma_1}{3}, \quad \sigma_1' = \frac{2\sigma_1}{3}, \quad \sigma_2' = \sigma_3' = -\frac{\sigma_1}{3}.$$

Simple tension in the  $x$  direction can thus be resolved into uniform tension (Fig. 297*b*) and a combination of pure shear in the  $xy$  and  $xz$  planes (Fig. 297*c*). It can be seen that the work of the stresses producing only distortion (Fig. 297*c*) on the displacements produced by uniform tension (Fig. 297*b*) vanishes. The strain energies of cases (b) and (c) are thus independent of each other, and the total strain energy in simple tension (Fig. 297*a*) is obtained by adding together the strain energy of uniform tension and the strain energy of distortion.

This conclusion also holds in the general case when all three principal stresses  $\sigma_1$ ,  $\sigma_2$  and  $\sigma_3$  are acting. From this it follows that the strain energy of distortion is obtained by subtracting the strain energy of uniform tension from the total strain energy. Substituting

$$\sigma_1 = \sigma_2 = \sigma_3 = \frac{\sigma_1 + \sigma_2 + \sigma_3}{3}$$

into eq. (294) we obtain for the strain energy of uniform tension the expression

$$\frac{1 - 2\mu}{6E} (\sigma_1 + \sigma_2 + \sigma_3)^2.$$

Thus the strain energy of distortion in the general case is

$$\begin{aligned} w_1 &= \frac{1}{2E} [\sigma_1^2 + \sigma_2^2 + \sigma_3^2 - 2\mu(\sigma_1\sigma_2 + \sigma_2\sigma_3 + \sigma_1\sigma_3)] \\ &\quad - \frac{1 - 2\mu}{6E} (\sigma_1 + \sigma_2 + \sigma_3)^2 \\ &= \frac{1 + \mu}{6E} [(\sigma_1 - \sigma_2)^2 + (\sigma_2 - \sigma_3)^2 + (\sigma_1 - \sigma_3)^2]. \quad (295) \end{aligned}$$

This equation may now be taken as the basis for determining failure of ductile materials having a pronounced yield point

stress  $\sigma_{YP}$  in simple tension. According to this theory, for the general case of stresses  $\sigma_1$ ,  $\sigma_2$  and  $\sigma_3$ , yielding begins when the distortion energy (eq. 295) reaches the value of the distortion energy at the yield point in a simple tension test. This latter quantity is obtained from eq. (295) by substituting

$$\sigma_1 = \sigma_{YP}, \quad \sigma_2 = \sigma_3 = 0,$$

which gives

$$w_1 = \frac{1 + \mu}{3E} \sigma_{YP}^2.$$

Then the condition for yielding based on the distortion energy theory is

$$(\sigma_1 - \sigma_2)^2 + (\sigma_2 - \sigma_3)^2 + (\sigma_1 - \sigma_3)^2 = 2\sigma_{YP}^2. \quad (296)$$

In the particular case of two-dimensional stress we put  $\sigma_3 = 0$  into eq. (296) and the condition for yielding becomes

$$\sigma_1^2 - \sigma_1\sigma_2 + \sigma_2^2 = \sigma_{YP}^2. \quad (297)$$

Considering, for example, combined axial tension and torsion of thin tubes (see p. 442) and denoting by  $\sigma$  and  $\tau$  the corresponding stresses, the principal stresses will be (see eqs. 31 and 32, Part I, p. 50)

$$\sigma_1 = \frac{\sigma}{2} + \sqrt{\frac{\sigma^2}{4} + \tau^2}, \quad \sigma_2 = \frac{\sigma}{2} - \sqrt{\frac{\sigma^2}{4} + \tau^2},$$

and the condition of yielding (eq. 297) becomes

$$\sigma^2 + 3\tau^2 = \sigma_{YP}^2. \quad (298)$$

This equation, as previously discussed (p. 442), is in good agreement with experiments. In the case of torsion alone we have  $\sigma = 0$  and eq. (298) gives

$$\tau_{YP} = \frac{\sigma_{YP}}{\sqrt{3}} = 0.577\sigma_{YP}, \quad (299)$$

which again is in good agreement with experimental results.

At present the condition of yielding given by eq. (296) is generally accepted as valid for ductile materials, and it is

assumed that the material begins to yield when the strain energy of distortion reaches a definite value.

It was shown by Eichinger<sup>52</sup> that the same condition for yielding as given by the maximum distortion energy theory (eq. 296) may also be obtained by considering the shearing stress acting on an octahedral plane such as  $ABC$  in Fig. 298. The element in Fig. 298 is subjected to the action of principal stresses  $\sigma_1$ ,  $\sigma_2$  and  $\sigma_3$ . From geometry it can be seen that the cosine of the angle between the normal  $n$  to the octahedral plane and the coordinate axes  $x$ ,  $y$ , and  $z$  is equal to  $1/\sqrt{3}$ . Resolving the resultant unit stress  $S$  acting on the octahedral plane into three components  $X$ ,  $Y$ ,  $Z$ , and writing three equations of static equilibrium, we find

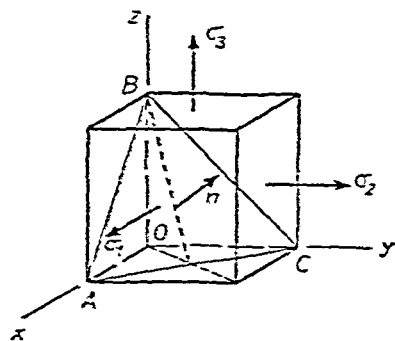


FIG. 298.

$$X = \frac{\sigma_1}{\sqrt{3}}, \quad Y = \frac{\sigma_2}{\sqrt{3}}, \quad Z = \frac{\sigma_3}{\sqrt{3}}.$$

The resultant stress acting on the octahedral plane is then

$$S = \sqrt{X^2 + Y^2 + Z^2} = \frac{1}{\sqrt{3}} \sqrt{\sigma_1^2 + \sigma_2^2 + \sigma_3^2}.$$

The normal component  $N$  of the stress  $S$  may be obtained by projecting the  $X$ ,  $Y$  and  $Z$  components into the direction of the normal  $n$ , which gives

$$N = \frac{\sigma_1 + \sigma_2 + \sigma_3}{3}.$$

The shearing stress  $\tau_{oct}$  on the octahedral plane then is

$$\begin{aligned} \tau_{oct} &= \sqrt{S^2 - N^2} = \frac{1}{3} \sqrt{3(\sigma_1^2 + \sigma_2^2 + \sigma_3^2) - (\sigma_1 + \sigma_2 + \sigma_3)^2} \\ &= \frac{1}{3} \sqrt{(\sigma_1 - \sigma_2)^2 + (\sigma_2 - \sigma_3)^2 + (\sigma_1 - \sigma_3)^2}. \end{aligned}$$

<sup>52</sup> A. Eichinger, *Proc. 2d Internat. Congr. Appl. Mech.*, Zürich, p. 325, 1926.

On comparing this result with eq. (296) it is seen that the condition for yielding based on the distortion energy theory is equivalent to the statement that yielding begins when the octahedral shear stress reaches a critical value equal to

$$(\tau_{\text{oct}})_{cr} = \frac{\sqrt{2}}{3} \sigma_{Y P} = 0.47 \sigma_{Y P}.$$

G. Sachs used the critical value  $\tau_{cr}$  for a single crystal (see p. 409) as the basis for calculating the yield point stress for a polycrystalline specimen.<sup>91</sup> From eq. (b), p. 409, we know that the yield point load on a single-crystal specimen depends on the orientation of the crystal. By considering a polycrystalline specimen as a system of crystals distributed at random, Sachs calculated the relation between  $\sigma_{Y P}$  for a specimen in tension and  $\tau_{cr}$  for a single crystal specimen, by means of an approximate averaging method. The calculations neglected the effect of the crystal boundaries and assumed that at the yield point all the crystals yielded simultaneously. For crystals with face-centered cubic lattice structure (such as aluminum, copper and nickel) he found

$$\sigma_{Y P} = 2.238 \tau_{cr}.$$

Repeating the calculations for torsion he found the yield point stress in shear for a polycrystalline specimen to be

$$\tau_{Y P} = 1.293 \tau_{cr}.$$

From the last two equations we obtain

$$\tau_{Y P} = \frac{1.293}{2.238} \sigma_{Y P} \approx 0.577 \sigma_{Y P},$$

which coincides with the results of the distortion energy theory (see eq. 299). Sachs assumed that a similar result would be obtained for crystals with body-centered cubic lattice structure (as in iron). We thus see that there is some physical

<sup>91</sup> G. Sachs, *Z. Ver. deut. Ing.*, Vol. 72, p. 734, 1928. See also H. L. Cox and D. G. Sopwith, *Proc. Phys. Soc. (London)*, Vol. 49, p. 134, 1937, and U. Dehlinger, *Z. Metallkunde*, Vol. 35, p. 182, 1943.

foundation for the result obtained previously by assuming that yielding of a crystalline material begins when the amount of strain energy of distortion reaches a certain value for each material.

In the preceding discussion we were concerned with the establishment of criteria for the beginning of yielding in ductile materials under general stress conditions. In the case of brittle materials, which fracture without plastic deformation, we also need a criterion for fracture under the general system of stresses  $\sigma_1$ ,  $\sigma_2$  and  $\sigma_3$ . Such a criterion is furnished by the strength theory developed by Mohr,<sup>92</sup> in which not only yielding but also fracture is considered. In developing his theory Mohr made use of the graphical representation of the stress conditions on an element of a body by the use of circles, as explained in Art. 18, Part I, p. 65. In this representation (Mohr's circle) the normal and shearing components of the stress acting on any plane are given by the coordinates of a certain point in the shaded areas (Fig. 299). Points lying on the same vertical line (such as  $MN$ ) represent stresses on planes with the same normal stress  $\sigma$  and with various shearing stresses.

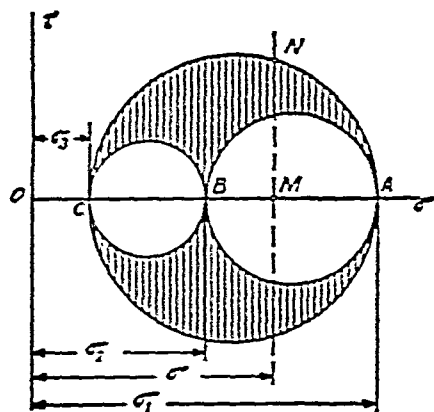


FIG. 299.

It is natural to assume that the weakest of all these planes is the plane with the maximum shearing stress, represented by point  $N$  on the outer circle. Repeating the same reasoning with points on any other vertical line, we finally arrive at the conclusion that the weakest plane must be one of the planes whose stress conditions are represented by points on the outer circle  $ANC$ . Hence the outer circle alone is sufficient to determine the *limiting stress condition*, i.e., the stress condition at which either yielding

<sup>92</sup> O. Mohr, *Z. Ver. deut. Ing.*, Vol. 44, p. 1524, 1900. See also his *Abhandlungen aus dem Gebiet der technischen Mechanik*, 2nd Ed., Berlin, p. 192, 1914.

begins or fracture occurs, depending on whether the material is ductile or brittle.

Let us begin with the determination of the stresses at yielding. Then in Fig. 300 the circle with diameter  $OA$  represents

the condition for yielding in simple tension. In the

same manner the circle with diameter  $OC$  represents the

condition for yielding in simple compression, and the

circle with diameter  $DB$  represents the condition for

yielding in pure shear. If

several circles of this kind are obtained by making ex-

periments with a given material, the envelopes of these circles ( $MN$  and  $M_1N_1$ ) can be constructed. Then Mohr assumed that yielding would begin only at stress conditions represented by one of the circles tangent to these envelopes.

Assume, for example, that the envelopes  $MN$  and  $M_1N_1$  can be replaced by straight lines (Fig. 301). Then, knowing the limiting conditions in simple tension ( $\sigma_1 = \sigma_{YP}$ ) and in simple compression ( $\sigma_3 = -\sigma_{YP}'$ ), the conditions for yielding

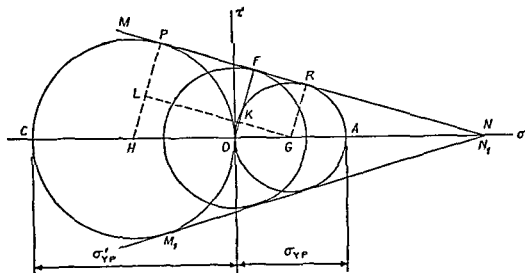


FIG. 301.



in pure shear can easily be obtained. It is only necessary to find the radius  $OF$  of the circle drawn with center at  $O$  and tangent to  $MN$ . From Fig. 301 we have  $\overline{OK} = \overline{OF} - \overline{KF} = \tau_{Y.P.} - \sigma_{Y.P.}/2$  and  $\overline{HL} = \overline{HP} - \overline{LP} = \sigma_{Y.P.}'/2 - \sigma_{Y.P.}/2$ . Then from the similarity of triangles  $GOK$  and  $GHL$  we obtain

$$\overline{OK}/\overline{HL} = \overline{GO}/\overline{GH} \quad \text{or} \quad \frac{2\tau_{Y.P.} - \sigma_{Y.P.}}{\sigma_{Y.P.}' - \sigma_{Y.P.}} = \frac{\sigma_{Y.P.}}{\sigma_{Y.P.}' + \sigma_{Y.P.}},$$

from which

$$\tau_{Y.P.} = \frac{\sigma_{Y.P.}\sigma_{Y.P.}'}{\sigma_{Y.P.} + \sigma_{Y.P.}'} \quad (g)$$

When  $\sigma_{Y.P.} = \sigma_{Y.P.}'$ , eq. (g) coincides with the maximum shear theory.

Let us now apply Mohr's theory to the case of brittle materials in two-dimensional stress and assume that, in Fig. 302,  $OA$  represents the ultimate strength of the material in

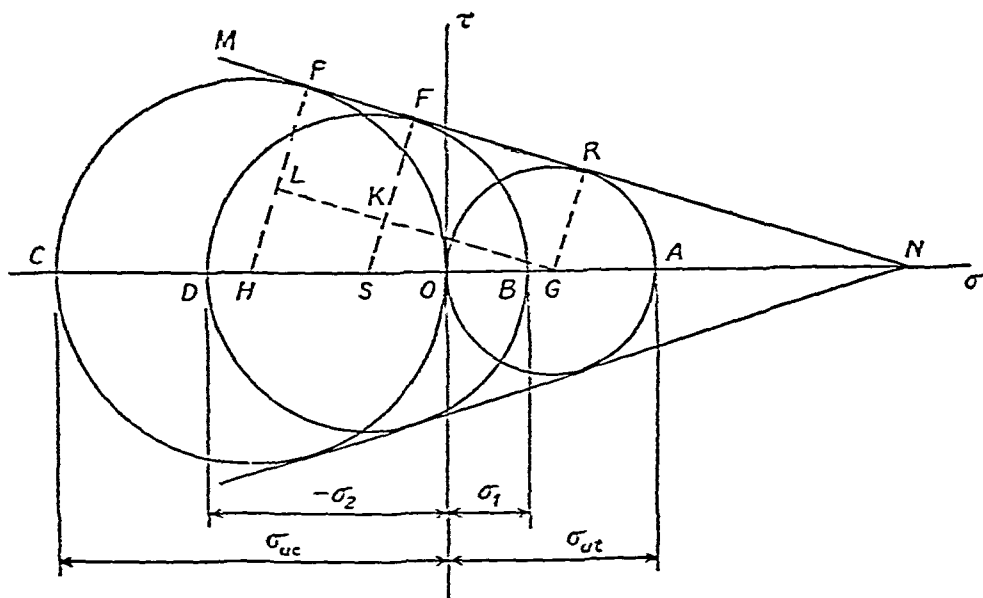


FIG. 302.

tension  $\sigma_{ut}$  and  $OC$  represents the ultimate strength in compression  $\sigma_{uc}$ . Then, for any ratio  $\sigma_{\max}/\sigma_{\min} = \sigma_1/\sigma_2$ , the ultimate values of these stresses are obtained by drawing a circle

with diameter  $\overline{BD} = \sigma_1 - \sigma_2$  and tangent to the line  $MN$ .<sup>22</sup> From Fig. 302 the following relations are now obtained:

$$\overline{SK} = \overline{SF} - \overline{KF} = (\sigma_1 - \sigma_2)/2 - \sigma_{ut}/2,$$

$$\overline{HL} = \overline{HP} - \overline{LP} = \sigma_{uc}/2 - \sigma_{ut}/2,$$

$$\overline{GS} = \overline{GO} + \overline{OS} = \sigma_{ut}/2 + (-\sigma_2 - \sigma_1)/2,$$

$$\overline{GH} = \overline{GO} + \overline{OH} = \sigma_{ut}/2 + \sigma_{uc}/2;$$

and from the similarity of triangles  $GSK$  and  $GHL$  we obtain

$$\overline{SK}/\overline{HL} = \overline{GS}/\overline{GH} \quad \text{or} \quad \frac{\sigma_1 - \sigma_2 - \sigma_{ut}}{\sigma_{uc} - \sigma_{ut}} = \frac{\sigma_{ut} - \sigma_2 - \sigma_1}{\sigma_{ut} + \sigma_{uc}},$$

from which

$$\frac{\sigma_1}{\sigma_{ut}} - \frac{\sigma_2}{\sigma_{uc}} = 1. \quad (h)$$

Thus for any given value of the ratio  $\sigma_1/\sigma_2$  the values of  $\sigma_1$  and  $\sigma_2$  at fracture can be calculated.

It was assumed in the preceding paragraph that  $\sigma_1$  represented the maximum principal stress  $\sigma_{\max}$  and that  $\sigma_2$  represented the minimum principal stress  $\sigma_{\min}$ . Since the third principal stress is zero in the case of two-dimensional stress, it follows that  $\sigma_1$  and  $\sigma_2$  must have opposite signs, as shown in Fig. 302, and the ratio  $\sigma_1/\sigma_2$  must be negative. However, in the case of tension in two perpendicular directions the third principal stress  $\sigma_3 = 0$  will represent  $\sigma_{\min}$ , and the corresponding Mohr's circle will be the circle with diameter  $OA$  in Fig. 302. Fracture will then occur when the larger of the two tensions reaches the value  $\sigma_{ut}$ . Similarly, in the case of compression in two perpendicular directions the stress  $\sigma_3 = 0$  represents  $\sigma_{\max}$ , and the circle with diameter  $OC$  in Fig. 302 is obtained. Fracture then occurs when the larger compressive stress reaches the value  $\sigma_{uc}$ .

<sup>22</sup> Note that  $\sigma_1$  and  $\sigma_2$  are algebraic quantities and hence distance  $OD = -\sigma_2$ .

Constructing for Mohr's theory a figure similar to Fig. 296, p. 449, we obtain for tension in two perpendicular directions the limiting lines  $AB$  and  $BC$  (Fig. 303) indicating that in this case fracture occurs when the larger tension reaches the value  $\sigma_{ut}$ . Similarly, for compression in two directions we obtain the lines  $DE$  and  $EF$ . If we have  $\sigma_1$  in tension and  $\sigma_2$  in compression, the conditions for fracture are represented by eq. (h), which gives line  $AF$  in Fig. 303. The line  $CD$  is ob-

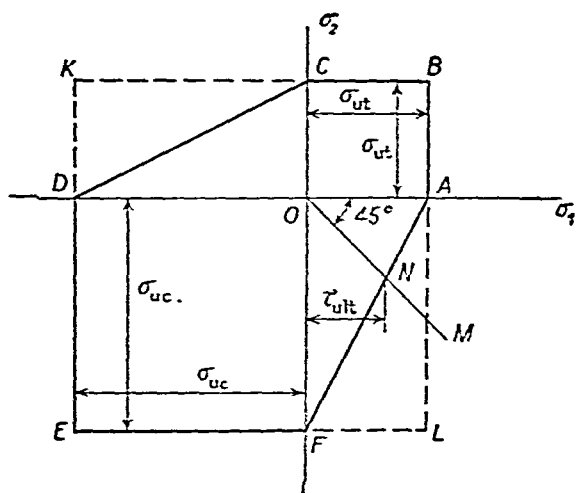


FIG. 303.

tained similarly. No fracture will occur for stress conditions defined by points within the hexagon  $ABCDEF$ , and the ultimate stresses can be obtained from this hexagon for any value of the ratio  $\sigma_1/\sigma_2$ . For example, to find the ultimate strength of a brittle material in pure shear we observe that in this case  $\sigma_1 = -\sigma_2$  and the corresponding limiting point will be the intersection point  $N$  of the line  $OM$  (Fig. 303) and the side  $AF$  of the hexagon. The value of  $\tau_{ult}$  can be determined from the figure or calculated from eq. (h) which, for  $\sigma_1 = -\sigma_2$ , gives

$$\sigma_1 = \tau_{ult} = \frac{\sigma_{ut}\sigma_{uc}}{\sigma_{ut} + \sigma_{uc}}. \quad (i)$$

This equation has the same form as eq. (g) for yielding.

If we apply eq. (i) to a material such as cast iron and assume that the ultimate stress in compression is four times the ulti-

mate stress in tension we find the ultimate stress in shear to be

$$\tau_{ult} = 0.8\sigma_{ult},$$

which is in satisfactory agreement with the experiments of Bach <sup>94</sup>

The square *BKEL* shown by the broken lines in Fig 303 represents the conditions of failure according to the maximum stress theory. It is seen that by using Mohr's theory the designer will be on the safe side as compared to the maximum stress theory, when the principal stresses are of opposite sign. Mohr's theory may be recommended in the case of brittle materials, although the assumption that only the outer stress circle (Fig 299, p 457) must be considered is not always supported by experiments <sup>95</sup>

**83 Impact Tests**—Impact tests are used in studying the *toughness* of materials, i.e. the ability of the material to absorb energy during plastic deformation. In static tensile tests this energy is represented by the area under the tensile test diagram, and it can be concluded that in order to have high toughness the material must have high strength and at the same time large ductility. Brittle materials have low toughness since they have only small plastic deformation before fracture. The use of such materials in structures is dangerous since fracture may occur suddenly without any noticeable deformation.

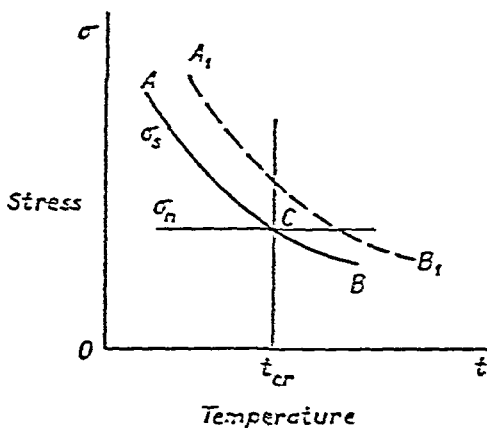
In discussing various kinds of fractures (see Art 79) it was indicated that the same material may behave as a brittle or a plastic material, depending on the external conditions. A tensile test of a single crystal specimen of rock salt gives a brittle fracture (cleavage) along one of the principal crystallographic planes if tested at room temperature. The same specimen, if tested in hot water, deforms plastically by sliding along octahedral planes. Similar conditions may also exist in such an important case as mild structural steel. Under

<sup>94</sup> C. Bach, *Elastizität und Festigkeit*, 7th Ed., p. 362.

<sup>95</sup> Th. v. Karman, *Forschungsarb.*, No. 118, and *Z. Ver. deut. Ing.*, Vol. 55, 1911. See also R. Boker, *Forschungsarb.*, Nos. 175/176.

ordinary tensile tests, steel may have large plastic deformation, while if tested at some lower temperature it may fracture entirely as a brittle material. Disastrous examples of such fractures occurred during World War II in the numerous failures of welded cargo ships.<sup>55</sup> Subsequent research work showed that the brittleness temperature of the steel plates used in the hulls of the ships was in the same range as the service temperature.

To explain the transition from brittle to plastic fracture of a single-crystal tensile test specimen of rock salt, A. F. Joffe<sup>57</sup> distinguished between two kinds of tensile stresses, (1) tensile stress  $\sigma_n$  producing brittle fracture by separation along one of the principal crystallographic planes and (2) tensile stress  $\sigma_s$  corresponding to the beginning of sliding along one of the octahedral planes of the crystal.<sup>58</sup> In Fig. 30 $\frac{1}{2}$  these two quantities are represented as functions of the specimen temperature  $t$ . In Joffe's experiments the resistance to separation remained practically independent of temperature, and in Fig. 30 $\frac{1}{2}$  the diagram for  $\sigma_n$  is given by the horizontal line. At the same time the resistance to

FIG. 30 $\frac{1}{2}$ .

sliding was influenced considerably by the temperature of the specimen, and the ordinates of the curve for  $\sigma_s$  decrease as the temperature increases. The point of intersection  $C$  of the two curves defines the critical value  $t_{cr}$  of the temperature. If the temperature of testing is higher than  $t_{cr}$ , the resistance to sliding is smaller than the resistance to separation and the specimen will yield plastically. For temperatures lower than  $t_{cr}$  we have  $\sigma_n < \sigma_s$ ,

<sup>55</sup> See the paper by Finn Jonassen in W. M. Murray (ed.), *Fatigue and Fracture of Metals*, 1952.

<sup>57</sup> *Z. Phys.*, Vol. 22, p. 286, 1924.

<sup>58</sup> It is assumed that the axis of the specimen is parallel to one of the crystallographic axes.

and the specimen will fail by a separation fracture without plastic deformation.

There are other important conclusions which can be obtained on the basis of the diagram in Fig. 304. Let us consider the effect of speed of loading on the test results. It is known that with an increase of speed the resistance of the material to sliding increases while its resistance to separation remains practically constant. As a result of this the ordinates of the  $\sigma_s$  curve will increase, and the curve will move to the new position  $A_1B_1$  (Fig. 304) while the line  $\sigma_n$  remains stationary. Thus the intersection point of the two curves is displaced to the right, indicating that with an increase in the speed of loading the critical temperature increases. This conclusion is verified by impact tests, which give brittle fractures at higher temperatures than in static tests.

Now assume that the specimen is subjected to torsion and that the axis of the specimen is taken perpendicular to one of the octahedral planes. Yielding of the specimen in shear will begin at about the same value of shearing stress as in the tension tests, but the corresponding value of the maximum normal stress  $\sigma_n$ , equal in this case to the maximum shearing stress, will be about one-half of the value of  $\sigma_n$  in a tension test. Hence in constructing for torsion tests a diagram similar to Fig. 304, we must take values of the ordinates of the  $\sigma_s$  curve about one-half the values for tension tests. As a result the intersection point  $C$  of the curves will be displaced to the left, and we conclude that in torsion tests the critical temperature must be lower than in tensile tests. This conclusion is in agreement with experiments.

Considering further the influence of the state of stress on the value of the critical temperature, let us assume that a uniform tension in all three directions is superposed on simple tension, so that we obtain a three-dimensional stress condition. It is known (see the preceding article) that such a superposition does not affect the value of the maximum shearing stress at which yielding begins. The value of  $\sigma_s$  increases, however, and the ordinates of the  $\sigma_s$  curve in Fig. 304 increase and the intersection point  $C$  moves to the right. Thus the

critical temperature for the assumed three-dimensional stress condition will be higher than for simple tension. Similar three-dimensional stress conditions are produced at the notch in a grooved specimen. Such specimens have higher values of  $t_{cr}$  than in the case of smooth specimens.<sup>99</sup>

The fundamental ideas regarding the critical temperature at which the transition occurs from brittle to plastic fracture were extended by N. N. Davidenkov and applied to crystalline materials, especially to various kinds of steel. Using a diagram similar to Fig. 304 he was able to predict the influence of various factors on the value of the critical temperature and showed by his experimental work that the predictions were in satisfactory agreement with the experimental facts.<sup>100</sup> For determining the critical temperature impact tests were used. Since in the case of brittle fracture the amount of work required to produce failure is many times smaller than for plastic fracture, the tests showed at the critical temperature a sharp change in the amount of energy absorbed. Fig. 305 represents the results of impact tensile tests of smooth cylindrical steel specimens. It can be seen that a sharp change occurs in the energy absorbed in the interval  $-130^{\circ}$  to  $-110^{\circ}$  C.

By changing the process of heat treatment the grain size of steel can be varied considerably, and it is of practical interest to investigate the influence of grain size on the magnitude of the critical temperature. It is known that with an increase in grain size the resistance of steel to separation diminishes. Hence for coarse-grained steels the horizontal line for  $\sigma_n$  (Fig. 304) will be lowered and the critical temperature will be higher than for fine-grained steels. To verify this conclusion

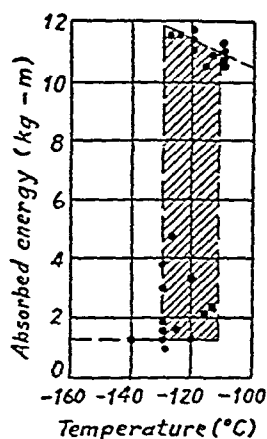


FIG. 305.

<sup>99</sup> For more details on stresses at grooves see E. Orowan's article in W. M. Murray (ed.), *Fatigue and Fracture of Metals*, 1952.

<sup>100</sup> See Davidenkov's books, *Dynamical Testing of Metals*, 1936, and *Problems of Impact in Metal Study*, Ed. Acad. Science, Moscow, 1938 (in Russian). The results given in the following discussion, if not specifically noted, are taken from the latter book.

specimens of medium carbon steel (0.23 per cent carbon) were subjected to two different heat treatments. In the first case the temperature was raised to  $1,100^{\circ}\text{C}$  for two hours and then the specimens were slowly cooled in a furnace. In the second case, after maintaining the specimens at  $950^{\circ}\text{C}$  for twenty minutes, they were cooled in air. By this process coarse grains were obtained in the first case and fine grains in the second case. Smooth cylindrical specimens were then tested in impact and the results are shown in Fig. 306. It is seen that the

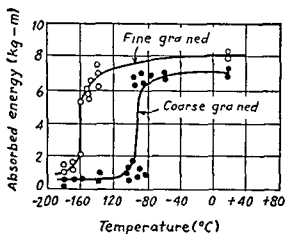


FIG 306

critical temperature for the coarse grained steel was about  $-95^{\circ}\text{C}$ , while in the case of the fine-grained steel it was  $-160^{\circ}\text{C}$ .

The effect of the size of the specimen on the value of the critical temperature was also investigated. But here the simple diagram of Fig. 304 does not give a clear interpretation of the experimental results. With an increase in dimensions we may expect a decrease in the resistance to brittle fracture, since the probability of having critical imperfections increases with volume<sup>101</sup> (see p. 398). Hence for larger volumes the horizontal line for  $\sigma_n$  will be lowered in Fig. 304, producing a displacement of point *C* to the right. But it also appears that an increase in volume reduces the value of  $\sigma_s$  (see p. 410) and the corresponding lowering of the  $\sigma_s$  curve in Fig. 304

<sup>101</sup> For an extension of the Griffith criterion to ductile materials see E. Orowan, *loc. cit.*, p. 465.



results in a displacement of  $C$  in the opposite direction. Thus the final result depends on the relative importance of the two factors. Experiments with smooth cylindrical specimens indicate that the lowering of the  $\sigma_n$  line is more important and point  $C$  moves to the right, showing that the critical temperature increases with an increase in volume of the specimen. This factor must be considered when applying the results of tests on small specimens to the design of large-sized structures.

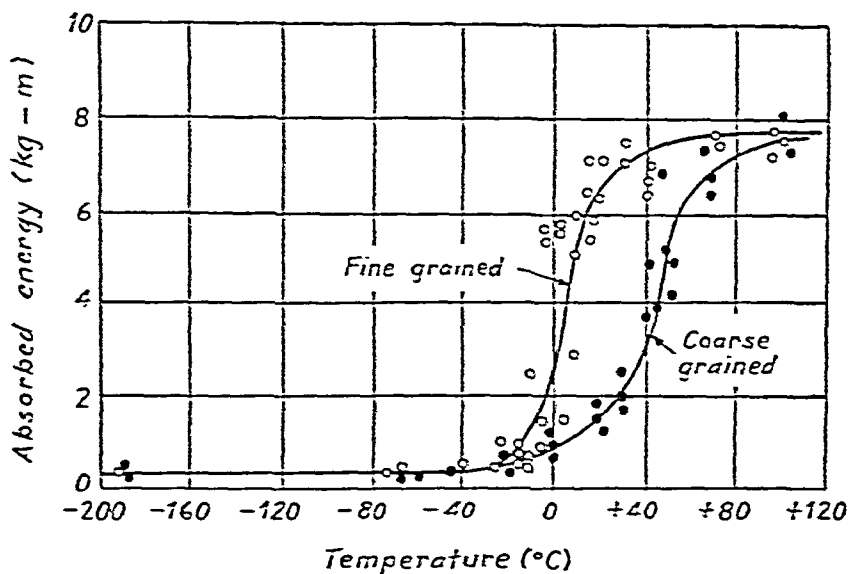


FIG. 307.

In the preceding discussion we have considered only tensile tests of cylindrical specimens in which the stress distribution was uniform. In practice, however, notched specimens are used in impact tests and stress concentrations are present. To investigate the effect of nonuniform stress distribution on the magnitude of the critical temperature let us begin with the case of bending of a smooth cylindrical specimen. Experiments in bending with static loads indicate that the yielding of the steel begins at a much higher stress than in the case of uniform tension. The yield point stress is first reached in the thin layer of fibers at the farthest distance from the neutral axis, and the formation of planes of yielding in those fibers is prevented by the presence of the adjacent material at lower stress. The resulting increase in the value of the yield stress

must be considered in applying the diagram of Fig. 304 to bending tests. The ordinates of the  $\sigma_s$  curve must be increased, which results in a displacement of the intersection point  $C$  to the right. The critical temperature, as obtained from bending tests, will then be higher than the value obtained from tensile tests. This conclusion agrees with experimental results.

Similar reasoning can be applied to cases of stress concentration produced by grooves and notches (see p. 420) and we may expect an increase in  $t_{cr}$  for notched bars. In Fig. 307 the results of impact tests in bending are given for the same two steels (fine- and coarse-grained) discussed before<sup>102</sup> (see Fig. 306). The type of groove used (Fremont type) is shown in Fig. 308. Comparing Figs. 306 and 307, we see that owing to the presence of the groove the critical temperature was

considerably increased. We see also that the temperature interval during which the transition from brittle to plastic fracture occurs is much larger in the case of notched specimens, and the critical temperature is not as sharply defined as for unnotched specimens. Static

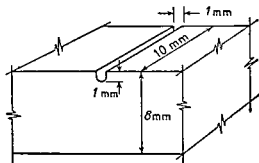


FIG. 308.

tests of notched specimens in the transition interval<sup>103</sup> showed that the character of fracture changed gradually and the portion of the fracture surface which had a brittle character increased as the temperature was lowered. At the same time the amount of work required to produce fracture decreased. Fig. 309 represents several load deflection diagrams obtained in static bending tests of notched specimens at various temperatures. Davidenkov suggested that the critical value be taken as the temperature at which the work absorbed in impact tests is 40 per cent of the maximum work obtained at some higher temperature. To obtain load deflection diagrams in impact tests, special piezo-quartz dynamometers were constructed.

<sup>102</sup> See N. N. Davidenkov and F. F. Wittman, *J. Tech. Phys. (Leningrad)*, Vol. 7, p. 343, 1937.

<sup>103</sup> Davidenkov and Wittman, *ibid.*

After this general discussion let us now consider the type of impact test which should be used in practice to determine  $t_{cr}$ . The correct determination of  $t_{cr}$  is important in order to avoid the dangerous situation in which the critical temperature of the material is the same as the service temperature of the structure. It is apparent that impact tests at room temperature are not sufficient and in important situations a series of tests over a range of temperatures should be made. A transition curve, similar to Fig. 307, should be constructed and from it  $t_{cr}$  determined. Bending tests of notched bars are preferable since they give a transition curve at higher temperatures and thereby reduce the amount of experimental work at very low temperatures. When the critical temperature has been determined, and knowing the service temperature  $t_0$  of the structure, Davidenkov recommends that the measure of safety be taken as the ratio

$$\frac{T_0 - T_{cr}}{T_0}, \quad (a)$$

in which  $T_0$  and  $T_{cr}$  are the absolute temperatures corresponding to  $t_0$  and  $t_{cr}$ . This ratio diminishes and approaches zero as  $T_0$  approaches  $T_{cr}$ . The result is a very dangerous situation in which small external impulses may produce brittle fracture of the structure. On the other hand, the ratio approaches unity as  $T_{cr}$  approaches absolute zero. In this case brittle fractures will not occur and it is only necessary to select the dimensions of the structure so that it will be strong enough to carry the loads without plastic deformation.

In selecting a reasonable value of the ratio (a) for use in design, the conditions which actually exist in the structure

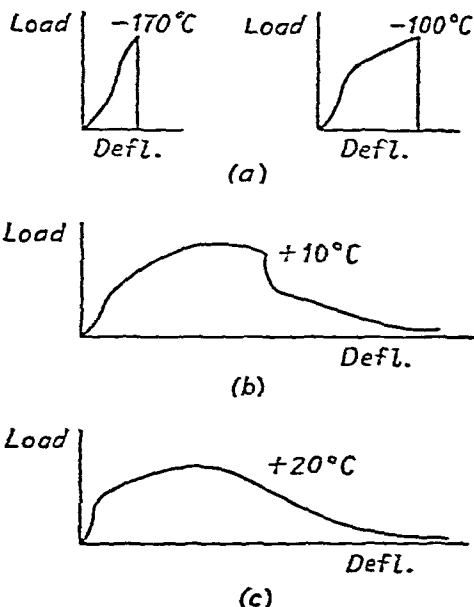


FIG. 309.

must be considered. Such stress raisers as sharp reentrant corners and imperfections in welding contribute to an increase in  $t_{cr}$ . An increase in size of the structure has the same effect. To have sufficient safety and to keep the ratio ( $a$ ) as large as possible, materials with low value of  $t_{cr}$  should be used. The critical temperature can be lowered not only by changing the chemical content of the material but also by the proper heat treatment. A fine-grained steel has a lower value of  $t_{cr}$  than a coarse-grained steel. Considerable interest in the brittle character of metals at low temperatures has developed recently in this country and we can expect an improvement in our knowledge of this important subject.<sup>104</sup>

**84. Fatigue of Metals**<sup>105</sup>—Machine parts are frequently subjected to varying stresses and it is important to know the strength of materials under such conditions.<sup>106</sup> It is well known that materials fail under repeated loading and unloading, or under reversal of stress, at stresses smaller than the ultimate strength of the material under static loads. The magnitude of the stress required to produce failure decreases as the number of *cycles* of stress increases. This phenomenon of the decreased resistance of a material to repeated stresses is called *fatigue*, and the testing of a material by the application of such stresses is called an *endurance test*.

If  $\sigma_{\max}$  and  $\sigma_{\min}$  are the maximum and minimum values of

<sup>104</sup> A bibliography on this subject can be found in the book by N. N. Davidenkov, *Problems of Impact in Metal Study*, 1938 (in Russian). See also the article by C. W. MacGregor in W. M. Murray (ed.), *Fatigue and Fracture of Metals*, p. 229, 1952.

<sup>105</sup> This subject is discussed in H. J. Gough, *The Fatigue of Metals*, London, 1924, and H. F. Moore and J. B. Kammers, *The Fatigue of Metal*, New York, 1927. These books contain bibliographies on the subject. For additional information see the mimeographed lectures given by H. J. Gough at the Massachusetts Institute of Technology, summer, 1937. See also R. Cazaud, *Fatigue of Metals* (English translation), London, 1953, Battelle Memorial Institute, *Prevention of the Failure of Metals under Repeated Stress*, New York, 1941, M. Roš and A. Eichinger, "Die Bruchgefahr fester Körper bei wiederholter Beanspruchung Ermüdung," *Eidg. Materialprüfungsanstalt (Zürich) Ber.*, No. 173, 1950.

<sup>106</sup> J. O. Roos found from examinations of a large number of fractures of machine parts that 80 per cent could be attributed to fatigue, see *Proc. Internat. Assoc. Test. Mat.*, 1912.



ward and the specimen rotates at constant speed. The stress therefore changes sign every half revolution, and the number of cycles of stress is equal to the number of revolutions of the machine. The stress is a completely reversed stress, the average stress being zero and the range of stress twice  $\sigma_{\max}$ .

By taking several specimens and testing them at various loads  $P$ , a curve such as is shown in Fig. 311 can be obtained.

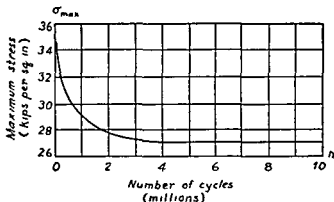


FIG. 311.

Here  $\sigma_{\max}$  is represented as a function of the number of cycles  $n$  required to produce fracture. The curve shown was obtained with mild steel. At the beginning  $\sigma_{\max}$  decreases rapidly as  $n$  increases, but after about 4 million cycles there is no longer any appreciable change in  $\sigma_{\max}$ , and the curve approaches asymptotically the horizontal line  $\sigma_{\max} = 27,000$  lb per sq in. The stress corresponding to such an asymptote is called the *endurance limit* of the material. It is now the usual practice in endurance tests to plot  $\sigma_{\max}$  against  $\log n$ . In this manner the magnitude of the endurance limit is disclosed by a definite discontinuity in the curve.<sup>108</sup> An example of such a curve is shown in Fig. 312.

There is a great difference between the fractures of mild steel specimens tested statically and those tested by alternating stresses. In the first case considerable plastic flow precedes fracture, and the surfaces at the ruptured section

<sup>108</sup> The results of fatigue tests usually have wide scatter. To improve their presentation and interpretation the use of statistical methods has been recommended by several investigators. See *Symposium on Statistical Aspects of Fatigue*, American Society for Testing Materials, 1951.

show a silky, fibrous structure due to the great stretching of the crystals. A fatigue crack, however, appears entirely different. A crack begins at some point in the material owing to a local defect or to a stress concentration produced by an abrupt change in the cross section. Once formed, the crack spreads owing to the stress concentrations at its ends. This spreading progresses under the action of the alternating stresses until the cross section becomes so reduced in area that the remaining portion fractures suddenly under the load.

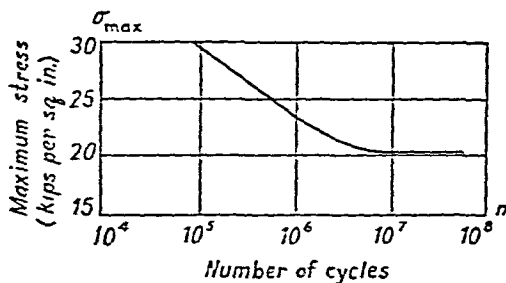


FIG. 312.

Two zones can usually be distinguished in a fatigue fracture, one due to the gradual development of the crack and the other due to sudden fracture. The latter zone resembles the fracture of a tensile test specimen with a deep, narrow groove (see p. 434) in which the shape of the specimen prevents sliding, and therefore fracture occurs as a result of overcoming the cohesive forces. This fracture is of the brittle type even though the material is ductile. In the case of cantilever test specimens (Fig. 310) the maximum stresses are at the outer fibers. Hence the fatigue crack usually starts at the circumference and spreads towards the center. Where there are stress concentrations due to fillets, grooves or holes, the crack usually starts at the most highly stressed portion and spreads outward from this point. In such cases the fracture surface shows concentric rings with respect to this starting point. This is a very common type of fracture in machine parts which have been subjected to alternating stresses. It is thus evident that the brittle type of fatigue fracture is due to the peculiar mechanism of fracture, not to crystallization of the material as was once thought.

W Fairbairn was the first to state, on the basis of experiments on a full-size wrought-iron girder,<sup>109</sup> that there is a *limiting stress* which can be applied safely an infinite number of times. Although it cannot be proved by direct test, all experimental evidence<sup>110</sup> supports this statement and it is now generally accepted that for steels and ferrous alloys there is a definite limiting range of stress which can be resisted for an infinite number of cycles without fracture.

It is of great practical importance to know how quickly the  $\sigma$ - $n$  curve approaches the asymptote, since this determines the number of cycles necessary to establish the endurance limit. Experiments show that for ferrous metals the endurance limit can be established with sufficient accuracy on the basis of from 6 to 10 million cycles. For nonferrous metals such as aluminum there is no definite endurance limit, and the ordinates of the  $\sigma$ - $n$  curve diminish indefinitely as the number of cycles is increased.

It is evident from the above discussion that the determination of the endurance limit for a particular material requires a large number of tests and considerable time. Hence it is of practical interest to establish relations between the endurance limit and other mechanical properties which can be determined by static tests. The large amount of experimental data accumulated has not yet made it possible to establish such a correlation.<sup>111</sup> As a rough estimate, the endurance limit for ferrous metals under reversal of stresses can be taken equal to 0.40 to 0.55 times the ultimate strength obtained in the usual way from a tensile test. When working with materials whose mechanical characteristics are very well known, such as carbon steels, estimates of this type can be considered reliable. Otherwise such estimates are likely to be misleading, and direct endurance tests should be used instead. Some results of endurance tests of steels are given in Fig. 313 and also in Table 26 at the end of the chapter.

<sup>109</sup> See W Fairbairn, *Phil Trans Roy Soc (London)*, 1864.

<sup>110</sup> A large number of endurance test curves were analyzed by O H Basquin, *Proc Am Soc Test Mat*, Vol 10, 1910.

<sup>111</sup> See the book by H J Gough, *loc cit*, p 470, and his lectures, *ibid*.



In the majority of cases, endurance tests are carried out for completely reversed stresses ( $\sigma_{\max} = -\sigma_{\min}$ ), while in many cases in machine design the stresses vary but are not completely reversed. It is necessary to know the endurance limits under these varying stresses. Wöhler was the first experimenter who studied the phenomenon of fatigue system-

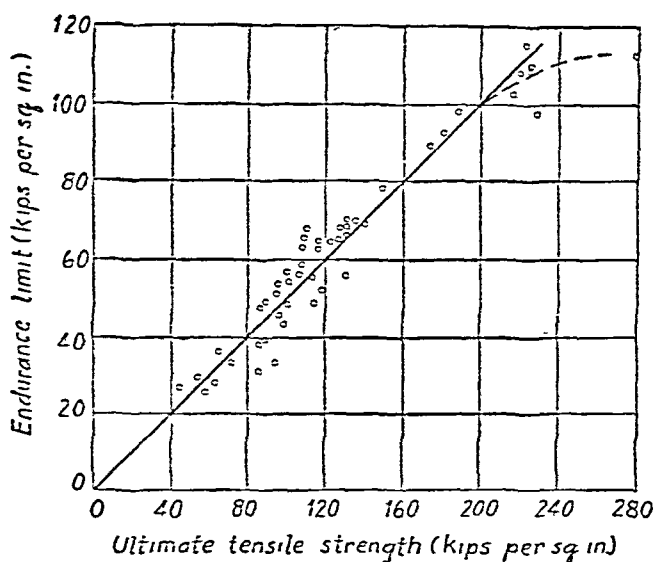


FIG. 313.

matically.<sup>112</sup> He showed that the range of stress  $R$  necessary to produce fracture decreases as the mean stress  $\sigma_m$  increases. On the basis of these tests and of Bauschinger's work<sup>113</sup> Gerber proposed<sup>114</sup> a parabolic law relating the range of stress  $R$  and the mean stress  $\sigma_m$ . This is illustrated by the parabolic curves in Fig. 314, in which the mean stress and the range of stress are expressed as fractions of the ultimate strength. The range is a maximum when the stress is completely reversed ( $\sigma_m = 0$ ) and it approaches zero when the mean stress approaches the ultimate strength. If the endurance limit for reversed stress and the ultimate strength are known, the

<sup>112</sup> A. Wöhler, *Z. Bauwesen*, Vols. 8, 10, 13, 16 and 20, 1858-70. An account of this work in English is given in *Engineering*, Vol. 11, 1871; see also Unwin, *The Testing of Materials of Construction*, 3d Ed., 1910.

<sup>113</sup> J. Bauschinger, *Mitt. Mech.-tech. Lab. München*, Nos. 13 and 25.

<sup>114</sup> W. Gerber, *Z. bayer. Architekt Ing.-Ver.*, 1874. See also Unwin, *Elements of Machine Design*, Vol. 1, Chap. 2.

endurance limit for any varying stress can be obtained from such curves. Other investigations show that there is no general law connecting the mean stress and the range of stress<sup>115</sup>. For instance, there are materials<sup>116</sup> for which the relation between  $R$  and  $\sigma_m$  is represented more accurately by the broken lines (Goodman law) in Fig. 314 than by parabolas.

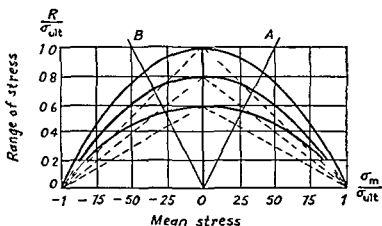


FIG. 314

The straight lines  $OA$  and  $OB$  in Fig. 314 have a slope of 2 and determine the region  $AOB$  in which the stress changes sign during a cycle. Outside this region the stress always remains tension or compression. Experimentally determined values within the region  $AOB$  usually lie between the parabolas and the corresponding straight lines<sup>117</sup>. When the stress is always tension or always compression, the values of the range  $R$ , as found by test, are sometimes not only below Gerber's parabolas but also below the corresponding straight lines.

Instead of presenting the range of stress  $R$  as a function of  $\sigma_m$  (Fig. 314) sometimes  $\sigma_{\max}$  and  $\sigma_{\min}$  are plotted as functions of  $\sigma_m$  (Fig. 315). The stresses  $\sigma_{\max}$  and  $\sigma_{\min}$  are obtained from eqs. (c) and are plotted graphically by adding  $\pm R/2$  to the ordinates of the straight line  $AOB$  inclined at an angle of

<sup>115</sup> An extensive discussion of this question is to be found in the book by H. J. Gough, *loc. cit.*, p. 470. See also his lectures, *ibid.*

<sup>116</sup> See the paper by B. P. Haigh, *J. Inst. Metals*, Vol. 18, 1927.

<sup>117</sup> Some experiments with mild steel indicate that the mean stress  $\sigma_m$  has little influence on the magnitude of the range  $R$ . See H. J. Gough lectures, *loc. cit.*, p. 470, and his paper, *J. Appl. Mech.*, Vol. 17, p. 113, 1950.

45°. The vertical line through point  $O$  (Fig. 315) corresponds to complete reversal of stress. The vertical through point  $D$  corresponds to a *pulsating* tensile stress, in which the load changes from zero to a maximum and then returns to zero. Similarly the vertical line through  $E$  corresponds to a pulsating

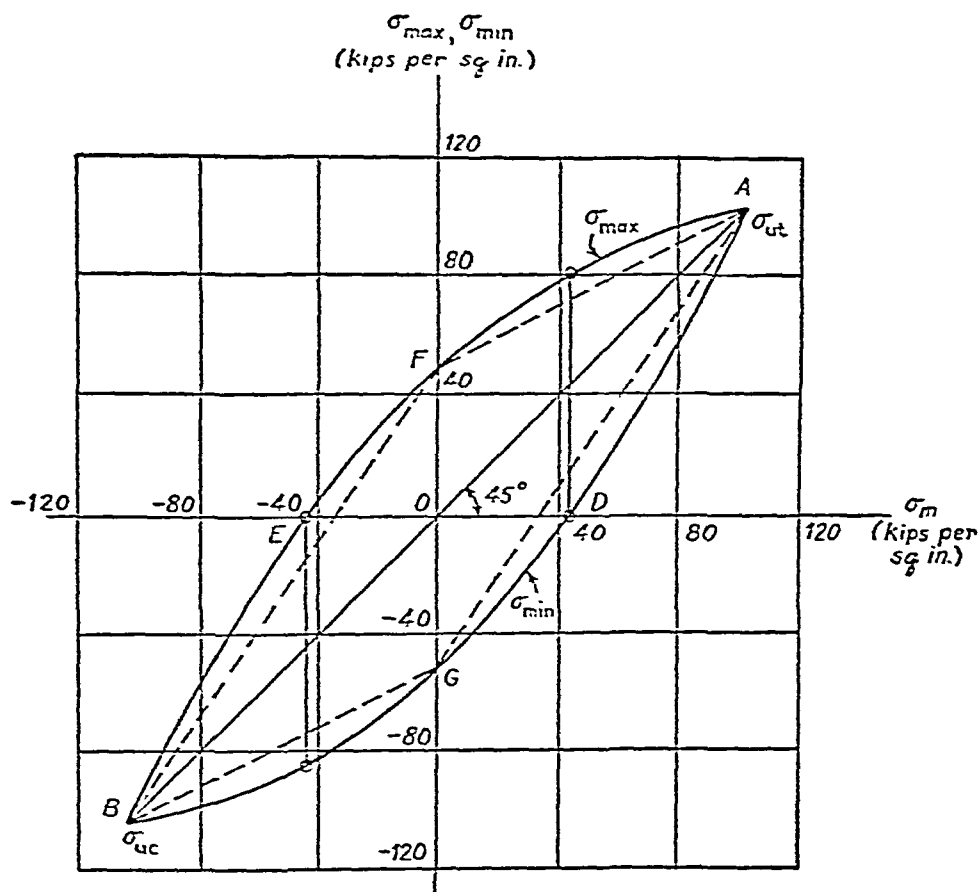


FIG. 315.

compressive stress. Point  $A$  represents the ultimate strength of the material in tension and point  $B$  gives the ultimate strength in compression. The curves for  $\sigma_{\max}$  and  $\sigma_{\min}$  represent the limiting conditions for fluctuating stresses. If the points corresponding to some actual variable stress lie within the area  $AEBDA$  then the material can withstand that stress an infinite number of cycles without fracture. The curves for  $\sigma_{\max}$  and  $\sigma_{\min}$  (Fig. 315) were obtained from a parabolic curve as in Fig. 314. But as mentioned before, the parabola

is replaced in many cases by two inclined lines, and the region of safety in Fig. 315 then becomes the parallelogram  $AFBG$ .

It has been assumed in the preceding discussion that the range of stress is represented by a symmetrical curve, such as the parabolas of Fig. 314; but many experiments show that the range of stress depends not only on the magnitude but also on the sign of the mean stress  $\sigma_m$ . When this stress is compressive the material can withstand a higher range of variable stress than when it is a tension stress. In addition, the ultimate strength in compression  $\sigma_{uc}$  is higher than the

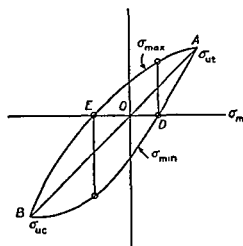


FIG. 316.

ultimate strength in tension  $\sigma_{ut}$ . Thus, instead of the symmetrical parabolas of Fig. 314 we obtain nonsymmetrical

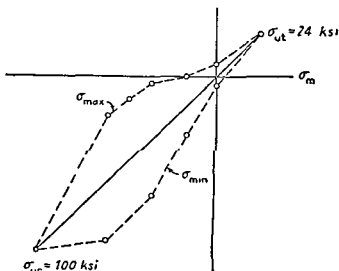


FIG. 317.

curves<sup>118</sup> and the region of safety for a ductile material has the shape shown in Fig. 316. The difference between  $\sigma_{ut}$  and

<sup>118</sup> See the paper by R. E. Peterson in *Fatigue and Fracture of Metals*, 1952.

$\sigma_{uc}$  is especially large for brittle materials and the region of safety has a wide bulge on the compression side as shown in Fig. 317 for cast iron.<sup>119</sup>

85. Fatigue under Combined Stresses.—Most of our experimental information on the fatigue strength of materials

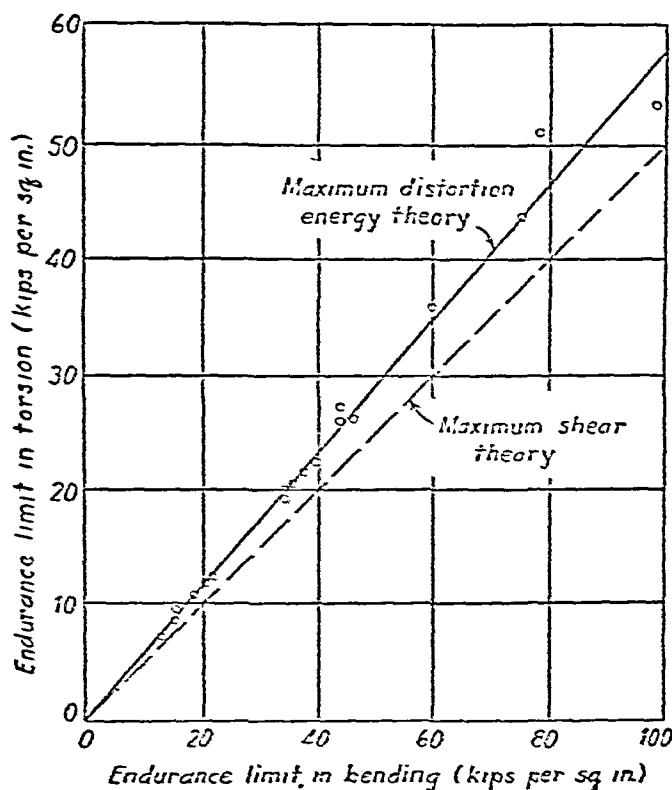


FIG. 318.

was obtained under conditions of uniaxial stress, as in rotating bending-test specimens. But in practical problems we frequently encounter cases of combined stress, and it is important to know the fatigue strength for such conditions. To obtain the fatigue strength of various ductile materials in pure shear, torsion tests were made in which the angle of twist was reversed. The results of some of these tests are shown<sup>120</sup> in Fig. 318. For purposes of comparison the endurance limit

<sup>119</sup> A. Pomp and M. Hempel, *Mitt. Kaiser-Wilh. Inst. Eisenforsch. (Düsseldorf)*, Vol. 22, p. 169, 1940.

<sup>120</sup> This figure is taken from R. E. Peterson, *Stress Concentration Design Factors*, New York, 1953.

in bending is taken as the abscissa (Fig. 318) and the endurance limit in shear is plotted as the ordinate. It is seen that the ratio of these limits for all the materials tested is very nearly equal to  $\sqrt{3}$ . This is the value given by the maximum distortion energy theory for the ratio of the yield point stresses in bending and shear (see eq. 299).

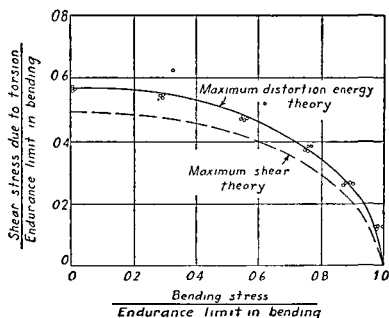


FIG. 319.

Fatigue tests under combined stresses produced by the simultaneous action of alternating bending and torsion<sup>121</sup> have also been made and the results are shown<sup>122</sup> in Fig. 319. Here again the test results are in good agreement with the maximum distortion energy theory, as might be expected, since slip generally precedes the development of a fatigue crack.<sup>123</sup> To obtain the equation for calculating the endurance limit for combined bending and torsion we have only to substitute into the corresponding equation for yielding (see eq. 298) the value of the endurance limit  $\sigma_E$  for reversed bending, in place of

<sup>121</sup> See H. J. Gough and H. V. Pollard, *Engineering*, Vol. 140, p. 566, 1935. See also Nisihara and Kawamoto, *Trans. Soc. Mech. Engr. (Japan)*, Vol. 6, p. S-2, 1940.

<sup>122</sup> See R. E. Peterson, *Proc. Soc. Exp. Stress Anal.*, Vol. 11, p. 118, 1943.

<sup>123</sup> H. J. Gough, *Proc. Am. Soc. Test. Mat.*, Vol. 33, p. 3, 1933.

$\sigma_{Y.P.}$ , which gives

$$\sigma^2 + 3\tau^2 = \sigma_E^2. \quad (a)$$

The corresponding ellipse is shown in Fig. 319, and it is apparent that the test results are in good agreement with the equation.

Other fatigue tests <sup>124</sup> with biaxial tension or tension and compression, and with the ratio  $\sigma_1/\sigma_2$  remaining constant during a cycle, are also in satisfactory agreement with the maximum distortion energy theory. Thus we can use for determining the fatigue limit in the case of complete reversal of stresses the following equation (see p. 454):

$$\sigma_1^2 - \sigma_1\sigma_2 + \sigma_2^2 = \sigma_E^2 \quad (b)$$

in which  $\sigma_E$  is the endurance limit for uniaxial stress conditions. Assuming that  $\sigma_1 > \sigma_2$  and using the notation  $\sigma_2 = \alpha\sigma_1$ , we obtain from eq. (b)

$$\sigma_1\sqrt{1 - \alpha + \alpha^2} = \sigma_E. \quad (c)$$

In the case of pulsating stresses in which the stress varies from zero to some maximum value, the corresponding uniaxial pulsating stress  $\sigma_{\max}$  should be substituted <sup>125</sup> for  $\sigma_E$  in eq. (c).

To establish the limiting conditions in cases of three-dimensional stress we use eq. (296). Substituting  $\sigma_2 = \alpha\sigma_1$ , and  $\sigma_3 = \alpha_1\sigma_1$  we obtain the following equation for cases of complete reversal of stress:

$$\sigma_1\sqrt{1 - \alpha - \alpha_1 + \alpha^2 + \alpha_1^2 - \alpha\alpha_1} = \sigma_E. \quad (d)$$

From this equation the limiting value of  $\sigma_1$  for any given values of  $\alpha$  and  $\alpha_1$  can be calculated.

There is only a small amount of available information which can be applied to cases in which the ratios  $\sigma_1/\sigma_2$  and  $\sigma_1/\sigma_3$  do not remain constant during the loading cycle. Gough investigated <sup>126</sup> the case in which static bending and torsion

<sup>124</sup> A. F. Maier, *Stahl u. Eisen*, Vol. 54, p. 1289, 1934; C. W. MacGregor, *J. Appl. Mech.*, Vol. 16, p. 269, 1949.

<sup>125</sup> If there are no experimental data, Gerber's parabola or Goodman's law can be used to determine  $\sigma_{\max}$ .

<sup>126</sup> H. J. Gough, *J. Appl. Mech.*, Vol. 17, p. 113, 1950.

was superimposed on complete reversal of stress. It was found that the influence of the static moments on the limiting values of the variable moments was quite small,<sup>127</sup> and that for calculating the limiting values of the variable stresses an ellipse of the same type as in Fig 319 could be used. The axes of the ellipse are equal to the ranges of variable stress<sup>128</sup> in bending and torsion. The ranges correspond to the applied static stresses, since they are the mean stresses in this case.

For brittle materials Mohr's theory is used for calculating the limiting combined stresses in fatigue. If both these stresses have the same sign, then only the numerically larger stress need be considered. Its limiting value can be obtained from a diagram for uniaxial stress such as shown in Fig 317 for cast iron. If the stresses are of opposite sign we can use eq (h), p 460, derived for static loads. Denoting the numerically larger principal stress by  $\sigma_1$  and the smaller stress by  $\sigma_2 = -\alpha\sigma_1$  we obtain

$$\sigma_1 = \sigma_{ut} \frac{\sigma_{uc}}{\sigma_{uc} + \alpha\sigma_{ut}}$$

We can now assume<sup>129</sup> that the limiting value of  $\sigma_1$  for alternating stresses will be

$$\sigma_1 = \sigma_E \frac{\sigma_{uc}}{\sigma_{uc} + \alpha\sigma_{ut}}, \quad (e)$$

where  $\sigma_E$  is the endurance limit for uniaxial stress conditions. Applying this equation to the case of pure shear ( $\alpha = 1$ ) we obtain

$$\tau_E = \sigma_E \frac{\sigma_{uc}}{\sigma_{uc} + \sigma_{ut}},$$

which is in satisfactory agreement with test results<sup>130</sup>

<sup>127</sup> The material used was alloy steel with a high value of the ratio  $\sigma_{Y.P.}/\sigma_{ult}$ .

<sup>128</sup> These ranges can be taken from Fig 318 if the endurance limits for bending and torsion alone are determined experimentally.

<sup>129</sup> This is equivalent to the assumption that the influence of  $\sigma_2$  on the value of  $\sigma_1$  is the same for both fatigue and static tests.

<sup>130</sup> H. J. Gough and H. V. Pollard, *Proc Inst Mech Engrs (London)*, Vol 131, p 1, and Vol 132, p 549, 1935.



There is only sparse information regarding the fatigue strength of brittle materials for cases in which static stresses are superimposed on alternating stresses. Uniaxial pulsating tests in which the stress varied from zero to a maximum were made with cast iron.<sup>131</sup> The tests were made in both tension and compression and showed that the limiting values of stress for these two cases, denoted by  $\sigma_{pt}$  and  $\sigma_{pc}$ , are in the same ratio as  $\sigma_{ut}/\sigma_{uc}$  in static tests. Thus for a pulsating torque, using the same reasoning as in the preceding case, we can write

$$\tau_p = \sigma_{pt} \cdot \frac{\sigma_{uc}}{\sigma_{uc} + \sigma_{ut}}.$$

For cast iron  $\sigma_{uc}/\sigma_{ut}$  is usually in the range between 3 and 4.

**86. Factors Affecting the Endurance Limit.**—After the general discussion of the preceding articles let us consider next the various factors which affect the results obtained by endurance tests.

*Effect of Cold-Working.*—In discussing stretching, drawing and rolling of ductile metals at room temperature it was pointed out (see Art. 78) that owing to cold-working, the material becomes stronger, the yield point is raised and the ultimate strength is somewhat increased. Hence we may expect that cold-working will also affect the endurance limit of the material. Experiments made with steel specimens submitted to cold-stretching<sup>132</sup> showed that a moderate degree of stretching produces some increase in the endurance limit. With a further increase in cold-working a point may be reached at which a drop in the endurance limit occurs due to overworking.<sup>133</sup> An improvement of a cold-worked material can

<sup>131</sup> H. F. Moore, S. W. Lyon and N. P. Inglis, *Univ. of Illinois Eng. Exp. Sta. Bull.*, No. 164, 1927. See also the paper by A. Pomp and M. Hempel, *loc. cit.*, p. 479.

<sup>132</sup> H. F. Moore and J. B. Kommers, *Univ. of Illinois Eng. Exp. Sta. Bull.*, No. 124, 1921; and O. J. Horger, *Trans. A.S.M.E.*, Vol. 57, p. A-128, 1935. In Moore's experiments carbon-steel specimens (0.18 per cent carbon) were stretched 8 per cent and 18 per cent. In Horger's experiments the same percentage stretching was used, but with steel containing 0.48 per cent carbon.

<sup>133</sup> See H. F. Moore and T. M. Jasper, *Univ. of Illinois Eng. Exp. Sta. Bull.*, No. 136, and R. M. Brown, *Trans. Inst. Engrs. Shipbuilders Scot.*, 1928.

be obtained by subjecting the material, after cold-working, to a mild heat treatment, such as by leaving the material in boiling water for some time

*Effect of Overstress and Understress*—Experiments have been made in which cycles of stress above the endurance limit were applied a number of times before starting a normal endurance test. This *overstressing* of the specimens showed that there is a *limiting number* of cycles of overstress. The magnitude of the limiting number of cycles depends on the amount

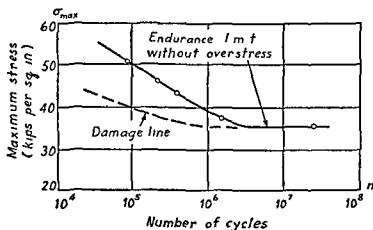


FIG 320

of overstress. Below the limiting number the endurance limit is not affected by overstress, whereas above that number of cycles the endurance limit was observed to decrease. By plotting the magnitude of overstress against the limiting number of cycles of overstress, a *damage curve*<sup>134</sup> for the tested material is obtained. An example of such a curve is shown<sup>135</sup> in Fig 320 for a material having an endurance limit of 35,000 lb per sq in. The area below this curve defines all those degrees of overstress which do not cause damage.

The damage curve is of practical importance in dealing with machine parts which normally operate at cycles of stress below the endurance limit, but are subjected from time to

<sup>134</sup> H J French, *Trans Am Soc Steel Treat*, Vol 21, p 899, 1933, and H W Russell and W A Welcker, *Proc Am Soc Test Mat*, Vol 36, 1936

<sup>135</sup> See H F Moore, *Metals and Alloys*, Vol 7, p 297, 1936. For a bibliography on this subject see Battelle Memorial Institute, *Prevention of the Failure of Metals under Repeated Stress*, New York, 1941

time to cycles of overstress. If the magnitude of overstress is known, the safe number of cycles of overstress is readily obtained from the damage curve.<sup>135</sup> It can be seen from the curve in Fig. 320, for example, that cycles of overstress of  $\pm 40,000$  lb per sq in. do not produce damage if the number of cycles of overstress is less than 100,000.

In the field of airplane design the problem of fatigue strength becomes more complicated since the parts are subjected in service to stress cycles of various intensities. Statistical methods are used to plan the necessary fatigue tests. On the basis of stress and acceleration measurements made in flight it is possible to establish the probable number of cycles of each intensity. Then fatigue tests are made in which the stress intensity is varied according to the statistical information.<sup>137</sup>

By running an endurance test at a load just below the endurance limit and then increasing the load by small increments the endurance limit can be raised. This phenomenon is called the *understressing* effect. The amount by which the endurance limit can be raised in this way depends on the material.<sup>138</sup> For mild steel this amount is sometimes as high as 30 per cent of the original endurance limit, whereas Armco iron and copper are practically unaffected by understressing.

*Frequency Effect.*—The effect of the frequency of the cycles in endurance tests has also been studied, but no appreciable effect was observed up to a frequency of about 5,000 cycles per minute. For higher frequencies some increase in the observed endurance limit was found. Very interesting experiments of this kind were made by C. F. Jenkin.<sup>139</sup> Increasing

<sup>135</sup> B. F. Langer suggested a formula for calculating the number of cycles of overstress which a machine part can withstand before failure. See *J. Appl. Mech.*, Vol. 4, p. A-160, 1937. See also M. A. Miner, *ibid.*, Vol. 12, 1945.

<sup>137</sup> For a bibliography see the article by H. L. Dryden, R. V. Rode and P. Kuhn, in W. M. Murray (ed.), *Fatigue and Fracture of Metals*, 1952. See also A. M. Freudenthal, *Proc. Am. Soc. Test. Mat.*, Vol. 53, p. 896, 1953.

<sup>138</sup> H. F. Moore and T. M. Jasper, *Univ. of Illinois Eng. Exp. Sta. Bull.*, No. 142, 1924; J. B. Kommers, *Engng. News Record*, 1932.

<sup>139</sup> C. F. Jenkin, *Proc. Roy. Soc. (London)*, A, Vol. 109, p. 119, 1925, and C. F. Jenkin and G. D. Lehmann, *ibid.*, Vol. 125, 1929.

the frequency to over a million cycles per minute, he found an increase in the endurance limit of more than 30 per cent for such materials as Armco iron and aluminum. To obtain these high frequencies Jenkin used forced vibrations of small specimens. A rotating beam machine was used by G. N. Krouse<sup>140</sup> for high-speed tests at 30,000 cycles per minute. For aluminum and brass he found an 8 per cent increase in the endurance limit at this speed.

*Temperature Effect*—In the previous discussion we were concerned with endurance tests made at room temperature. There are, however, cases where materials are submitted to the action of cycles of stress at low temperature, such as certain parts of airplanes. Other materials, as in steam turbines and internal-combustion engines, operate at very high temperatures. Hence, endurance tests at low and high temperatures are of practical importance. Comparative endurance tests made<sup>141</sup> at  $+20^{\circ}\text{C}$  and  $-40^{\circ}\text{C}$  with Monel metal, stainless steel, nickel steel and chromium molybdenum steel showed in all cases an increase in the endurance limit with a decrease in temperature. Similar conclusions were also obtained for other materials.<sup>142</sup>

Endurance tests at high temperatures made with various kinds of steels on rotating beam machines<sup>143</sup> and also on reversed direct stress machines<sup>144</sup> all indicate that up to  $300^{\circ}\text{C}$  to  $400^{\circ}\text{C}$  there is no great effect of temperature on the endurance limit. The maximum endurance limit is usually obtained in the range  $300^{\circ}\text{C}$  to  $400^{\circ}\text{C}$ , while at  $100^{\circ}\text{C}$  to  $200^{\circ}\text{C}$  the endurance limit is usually somewhat less than at room temperature. Experiments also show that the  $\sigma$ - $n$  curves do not approach their asymptotes as rapidly as at room temperature,

<sup>140</sup> G. N. Krouse, *Proc Am Soc Test Mat*, Vol 34, 1934

<sup>141</sup> H. W. Russell and W. A. Welcker, *ibid*, Vol 31, p 122, 1931. See also *Nat Advisory Comm Aeronaut Tech Notes*, No 381, 1931

<sup>142</sup> W. D. Boone and H. B. Wishart, *Proc Am Soc Test Mat*, Vol 35, 1935

<sup>143</sup> H. F. Moore and T. M. Jasper, *Univ of Illinois Eng Exp Sta Bull*, No 152, 1925, and H. F. Moore, S. W. Lyon and N. P. Inglis, *ibid*, No 164, 1927

<sup>144</sup> H. J. Tapsell and J. Bradley, *J Inst Metals*, Vol 35, 1926

and that more than  $10^7$  cycles are required for determining the magnitude of the endurance limit.

*Corrosion Fatigue.*—The phenomenon of corrosion fatigue is also of practical importance. This term is used to designate the simultaneous action of corrosion and fatigue. In 1917 Haigh<sup>145</sup> published the results of some very interesting endurance tests on brass, in which he found a lowering of the endurance limit under alternating stress when the specimen was subjected to the action of salt water, ammonia, or hydrochloric acid. He also pointed out that the damaging effect of ammonia on brass was not produced unless the corrosive substance and the alternating stresses were applied simultaneously.

Further progress in the investigation of corrosion fatigue was made by McAdam,<sup>146</sup> who investigated the combined effect of corrosion and fatigue on various metals and alloys. These tests proved that in most cases a severe corrosion prior to an endurance test is much less damaging than a slight corrosion which takes place simultaneously. Tests were made with steels of various carbon contents and having endurance limits<sup>147</sup> in reversed stress varying from 20,000 to 40,000 lb per sq in. When the specimens were subjected to the action of fresh water during the tests, the endurance limits were greatly diminished and varied from 16,000 to 20,000 lb per sq in. These lowered endurance limits are called *corrosion fatigue limits*. The tests showed that while the endurance limit increases approximately in the same proportion as the ultimate strength of the steel when tested in air, the results obtained when testing in fresh water are quite different. The corrosion fatigue limit of steel having more than about 0.25 per cent carbon cannot be increased and may be decreased by heat treatment.<sup>148</sup> It was also shown that the addition of

<sup>145</sup> B. P. Haigh, *ibid.*, Vol. 18, 1917.

<sup>146</sup> D. J. McAdam, *Proc. Am. Soc. Test. Mat.*, Vol. 26, 1926; Vol. 27, 1927; *Trans. Am. Soc. Steel Treat.*, Vol. 2, 1927; *Proc. Internat. Congr. Test. Mat.*, Amsterdam, Vol. 1, p. 305, 1928. See also H. F. Moore in *Metals Handbook*, American Society for Metals, pp. 147–53, 1939.

<sup>147</sup> Determined by tests in air.

<sup>148</sup> McAdam, *Proc. Internat. Congr. Test. Mat.*, Amsterdam, Vol. 1, p. 308, 1928.

chromium in an amount sufficient to increase the ordinary corrosion resistance of the steel also raises the corrosion fatigue limit considerably above the limit for carbon or nickel steels <sup>149</sup>

Endurance tests in an atmosphere of dry steam <sup>150</sup> showed no effect on the endurance limit, but in the case of steam containing air or water a lowering of the endurance limit was observed. Experiments in a vacuum <sup>151</sup> showed that the endurance limit of steel is about the same as in air, while experiments with copper and brass in a vacuum demonstrated an increase in the endurance limit of at least 14 and 16 per cent, respectively

There are many known cases of failures in service which may be attributed to corrosion fatigue. These include failures of such parts as marine propeller shafts, water-cooled piston rods of marine oil engines, turbine blades, locomotive springs, pump rods in oil wells, boilers and superheater tubes, etc. In many cases corrosion fatigue failures were eliminated by introducing corrosion resistant materials. McAdam's experiments with corrosion resistant steels showed that such steels give very satisfactory results in corrosion fatigue tests. Later experiments with special bronzes <sup>152</sup> showed that phosphor bronze and aluminum bronze, tested under extremely corrosive conditions, have a remarkable corrosion fatigue resistance, comparing favorably with the best stainless steels.

Protective coatings <sup>153</sup> and surface cold working <sup>154</sup> of parts subjected to corrosive fatigue have also been successfully used in eliminating failures.

*Effect of Residual Stresses*—Residual stresses are usually produced during heat treatment of machine parts and during welding of structures, and the question arises as to the effect of these stresses <sup>Pr</sup> on the endurance limit. Experiments with quenched steel <sup>anc</sup> <sup>comm</sup>imens tested in a rotating-beam fatigue-

<sup>149</sup> See McAdam and F<sub>3</sub>, *ASME, Appl Mech Div*, 1928

<sup>150</sup> See T S F<sub>1</sub> er, *Trans Am Soc Steel Treat*, Vol 19, p 97, 1931

<sup>151</sup> H J Gough and D G Sopwith, *J Inst Metals*, Vol 49, p 93, 1932

<sup>152</sup> H J Gough and D G Sopwith, *J Inst Metals*, Vol 60, p 143, 1937

<sup>153</sup> D G Sopwith and H J Gough, *J Iron and Steel Inst*, 1937

<sup>154</sup> O Föppl, O Behrens and T Dusold, *Z Metallkunde*, Vol 25, 1933

testing machine showed<sup>155</sup> that the residual stresses are reduced to less than one-quarter of their initial value by the application of cycles of reversed stress. The effect of the residual stresses on the endurance limit was negligible. Similar conclusions were also obtained from fatigue tests of welded I beams.<sup>156</sup> E. E. Weibel showed the unfavorable effect of residual stresses produced in coil springs.<sup>157</sup>

*Effect of Surface Finish.*—The effect of surface finish on the endurance limit has also been studied. Tests were made on 0.49 per cent carbon steel with an ultimate strength of 95,000 lb per sq in. and an ordinary endurance limit of 48,000 lb per sq in. By taking 100 as the endurance limit for highly polished specimens, the following results were obtained for various finishes:<sup>158</sup> ground finish 89, smooth-turned finish 84, rough-turned finish 81. Tests with 0.02 per cent carbon steel (Armco iron) gave for the last two types of finish 92 and 88, respectively. Similar experiments were made with 0.33 per cent carbon steel by W. N. Thomas,<sup>159</sup> who measured the magnitude of the scratches in various finishes with a microscope. Other experiments were made by W. Zander.<sup>160</sup>

Table 26 at the end of this chapter gives the results obtained in static and endurance tests of certain steels used in engineering.

**87. Fatigue and Stress Concentrations.**—In discussing the stress concentrations produced by sharp variations in the cross sections of bars and shafts (see Chap. 8) it was indicated that such stress concentrations are especially damaging in the

<sup>155</sup> See H. Bühler and H. Buchholtz, *Stahl u. Eisen*, Vol. 53, p. 1330, 1933, and *Mitt. Forsch.-Inst., Verein. Stahlwerke (Dortmund)*, Vol. 3, p. 235, 1933.

<sup>156</sup> E. H. Schulz and H. Buchholtz, *Stahl u. Eisen*, Vol. 53, p. 545, 1933.

<sup>157</sup> *Trans. A.S.M.E.*, Vol. 57, p. 501, 1935. See also F. Wever and G. Martin, *Mitt. Kaiser-Wilh. Inst. Eisenforsch. (Düsseldorf)*, Vol. 21, p. 218, 1939, and C. W. MacGregor, in W. R. Osgood, ed., *Residual Stresses in Metals and Metal Construction*, New York, 1954.

<sup>158</sup> See H. F. Moore and J. B. Kommers, *Univ. of Illinois Eng. Exp. Sta. Bull.*, No. 124, p. 683, 1921.

<sup>159</sup> *Engineering*, Vol. 116, p. 483, 1923. Later developments in investigating surface roughness are discussed in the paper by S. Way, *loc. cit.*, p. 505.

<sup>160</sup> Dissertation, Technische Hochschule, Braunschweig, 1928.

case of varying stresses. In machines, stress concentrations are always present owing to fillets, grooves, holes, keyways, etc., and experience shows that most fatigue cracks begin at points of stress concentration. Several examples of such failures will now be briefly discussed.

Figure 321 represents <sup>161</sup> fatigue failures of circular shafts with transverse holes and subjected to the action of reversed

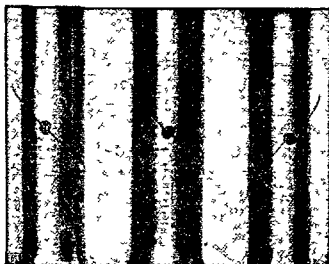


FIG 321

torsion. The maximum stress in this case occurs at the edge of the hole along a plane inclined  $45^\circ$  to the axis of the shaft (see p. 305). At these points the cracks begin and gradually develop along a helical path following the direction of one of the principal stresses.

Figure 322 shows the torsional fatigue failure of a shaft of a large motor-generator set which unfortunately operated near resonance.<sup>162</sup> The crack started at the keyway, where a high stress concentration took place, and gradually developed along the helical path. The helical crack corresponding to the direc-

<sup>161</sup> See the paper by A. Thum, *Forschung*, Vol 9, p 57, 1938.

<sup>162</sup> Figs 322-325 are taken from a paper by R. E. Peterson presented at a conference on Strength of Materials Problems in Industry, at the Massachusetts Institute of Technology, July 1937. The mechanism of crack growth is also discussed by Peterson, *J. Appl. Mech.*, Vol 1, p 157, 1933. Many examples of fatigue failures of prime movers are described in the paper by L. W. Schuster, *Proc. Inst. Mech. Engrs. (London)*, April 1933.



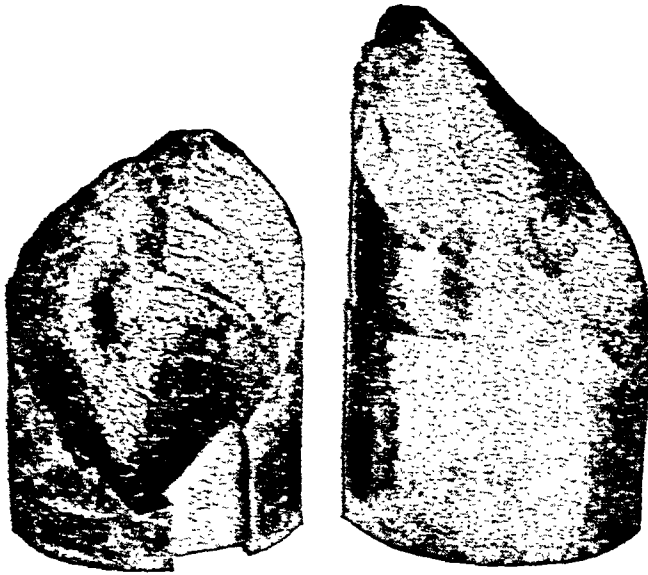


FIG. 322.

tion of the second principal stress can also be seen on the photograph. Figure 323 represents a torsion failure of a shaft of a Diesel-driven generator. A high stress concentration at the

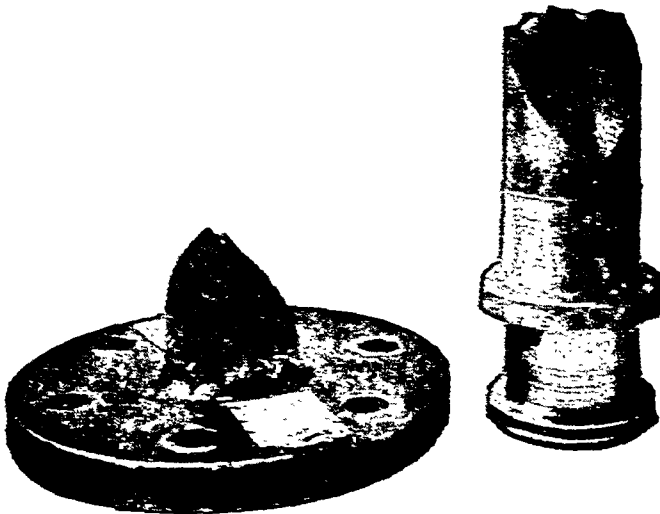


FIG. 323.

small fillet resulted in several helical cracks, which when joined together produced the saw-toothed appearance. In Fig. 324 are shown fatigue cracks which developed gradually

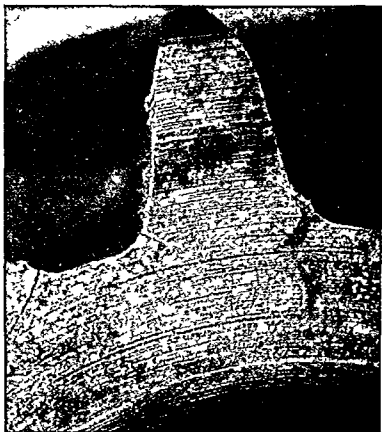


FIG 324

at the roots of gear teeth. The points of high stress concentration were produced by the bending of the teeth as cantilevers.

Finally, Fig. 325 represents a characteristic fatigue failure of a heavy helical spring. The crack started from the inside,

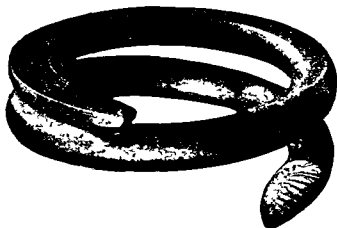


FIG 325

as theory predicts (see Part I, p. 291), and again followed the direction of one of the principal stresses. All these pictures clearly demonstrate the damaging action produced by stress concentration, and it is clear that this factor must be seriously considered in the design of machine parts.<sup>163</sup>

The early fatigue tests made with specimens having sharp changes of cross section showed that there was a reduction in strength due to the stress concentration, but this reduction was usually smaller than expected from the magnitude of the calculated stress concentration factor. For instance, in the case of flat steel specimens with small circular holes subjected to direct stress, the theoretical factor of stress concentration is 3 (see p. 301). If the magnitude of the peak stress is the controlling factor in endurance tests, it would be expected that the tension-compression load required to produce fatigue failure of a specimen with a hole would be about one-third of the load for a specimen without a hole. However, experiments showed that in this case the reduction in strength due to the stress concentration is small as compared with the calculated effect.<sup>164</sup>

To explain this discrepancy and to give the necessary information for designers, a very extensive series of tests were made by R. E. Peterson at the Westinghouse Research Laboratories.<sup>165</sup> Geometrically similar cantilever test specimens varying in diameter from 0.1 in. to 3 in., with a fillet or with a transverse circular hole and of different materials, as given in Table 23, were tested in special fatigue-testing machines.<sup>166</sup> The results of these tests for specimens with fillets are given

---

<sup>163</sup> It is very important in practice to have some means for detecting cracks as soon as they appear. Various methods of crack detection are described by Charles Lipson in his article in M. Hetényi, ed., *Handbook of Experimental Stress Analysis*, 1950.

<sup>164</sup> B. P. Haigh and J. S. Wilson, *Engineering*, Vol. 115, p. 446, 1923.

<sup>165</sup> R. E. Peterson, *J. Appl. Mech.*, Vol. 1, pp. 79 and 157, 1933; and R. E. Peterson and A. M. Wahl, *ibid.*, Vol. 3, p. 15, 1936. See also the progress reports of the Research Committee on Fatigue of Metals, *Proc. Am. Soc. Test. Mat.*, Vol. 42, p. 145, 1942, and Vol. 43, 1943.

<sup>166</sup> A description of these machines is given in the paper by R. E. Peterson, *Proc. Am. Soc. Test. Mat.*, Vol. 29, p. 371, 1929.

TABLE 23 MATERIALS USED IN FATIGUE TESTS BY PETERSON

Steel	Chemical Composition, %								Y P lb/in. <sup>2</sup>	Ult. lb/in. <sup>2</sup>	Elong, %
	C	Mn	Si	S	P	Ni	Cr	Mo			
Medium carbon*	0.45	0.79	0.18	0.03	0.013	—	—	—	32,500	76,000	32
Ni-Mo†	0.52	0.68	0.19	—	0.014	2.96	—	0.38	45,500	97,000	26
Ni-Cr‡	0.54	0.65	—	—	—	1.38	0.64	—	91,000	120,000	24

\* Normalized 1560° F, air-cooled

† Normalized and drawn 1750° F, air-cooled 1460° F, air-cooled, 1160° F, furnace-cooled

‡ Quenched and drawn 1475° F, oil-quenched, 1200° F, furnace-cooled

in Fig. 326. The smaller diameters of the specimens are taken as abscissas while the ordinates represent the ratios  $k_f$  of the endurance test loads for plain specimens to the endurance

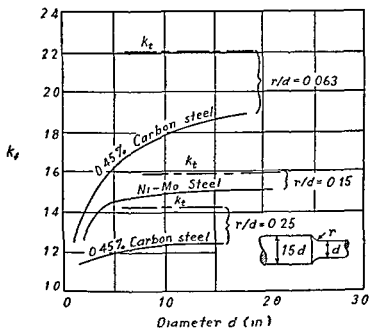


FIG. 326

test loads for the corresponding specimens with stress concentrations. Similar results were obtained for specimens with transverse holes.

The horizontal lines in Fig. 326 give the values of the stress concentration factors obtained for each fillet size by a direct measurement of strain at the points of maximum stress

concentration (see p. 329). These values are designated by  $k_t$  and are called *theoretical values* of stress concentration in the following discussion. If the fatigue strength of the specimen depends only on the peak stress, then  $k_t$  must evidently be equal to  $k_f$ .

On a basis of his tests, Peterson came to the following conclusions:

(1) In some cases fatigue results are quite close to theoretical stress concentration values. This conclusion is of great practical importance, since a general idea seems to exist, based on some early experiments, that fatigue data for stress concentration cases are always well below theoretical values, i.e., on the safe side for design purposes.

(2) Fatigue results for alloy steels and quenched carbon steels are usually closer to the theoretical values than are the corresponding fatigue results for carbon steels not quenched. It was expected in these tests that the theoretical values of  $k_t$  would be reached for all steels provided the specimens were made large enough, but Fig. 326 shows that the curves for normalized 0.45 per cent carbon steel are apparently asymptotic to values considerably below the theoretical.

(3) With a decrease in the size of the specimen the reduction in fatigue strength due to a fillet or hole becomes somewhat less; and for very small fillets or holes the reduction in fatigue strength is comparatively small. This can be clearly seen from the curves in Fig. 326.

Another way of presenting fatigue test results in order to show the extent to which the theoretical values  $k_t$  are reached, is obtained by introducing the quantity

$$q = \frac{k_f - 1}{k_t - 1}, \quad (a)$$

which is called the *sensitivity factor*. As  $k_f$  approaches the value  $k_t$ , the value of  $q$  approaches unity, and when the stress concentration has only a small effect on fatigue strength,  $k_f$  is close to unity and  $q$  approaches zero. The values of  $q$  for several forms of stress raiser and for two kinds of steel are

presented<sup>167</sup> in Fig. 327, in which the fillet or hole radius is taken as abscissa. It is seen that the sensitivity index is not a constant. It depends not only on the kind of material but also on the size of the specimens. In the case of alloy steels

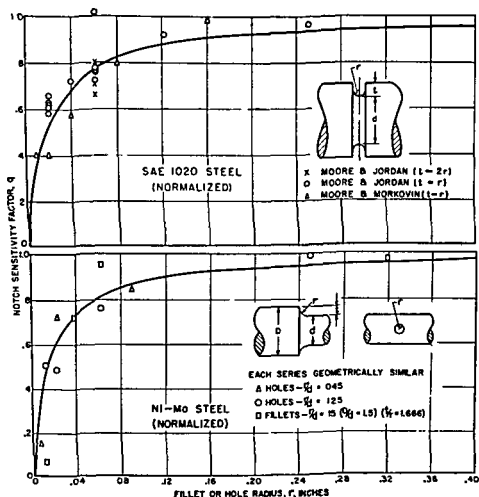


FIG 327.

and for larger specimens,  $q$  approached unity; while for a coarser material, 0.45 per cent carbon steel,  $q$  approximates a somewhat lower value.<sup>168</sup>

On the basis of the above discussion the use of the theoretical value  $k_t$  of stress concentration can be recommended

<sup>167</sup> See R. E. Peterson's book, *loc. cit.*, p. 479.

<sup>168</sup> Tests of cast iron show that stress concentrations have little effect on fatigue test results; see A. Thum and H. Ude, *Z. Ver. deut. Ing.*, Vol. 74, p. 257, 1930.

in the design of large-size machine parts, and also in the case of the finer-grained steels, such as alloy steels and heat-treated carbon steels. For parts of small dimensions and for coarse materials the reduced value of the stress concentration factor can be used. This value, from eq. (a), is

$$k_f = q(k_t - 1) + 1. \quad (b)$$

The values of  $q$  obtained experimentally for fillets, holes and grooves, and represented in Fig. 328, can be used as a guide

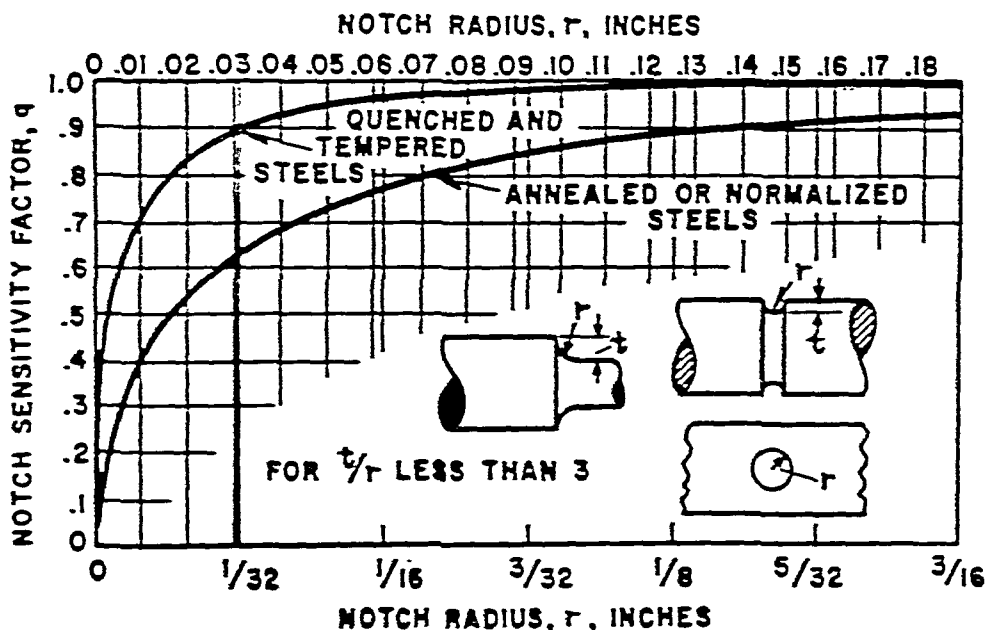


FIG. 328.

in selecting the proper values of  $k_f$  for other cases of stress concentration.<sup>153</sup>

Fatigue fractures resemble static fractures of brittle materials in that they occur practically without plastic deformation. The crack starts at some local imperfection and progresses in the direction normal to the tensile stress. It is

<sup>153</sup> See R. E. Peterson's book, *loc. cit.*, p. 479, and C. E. Phillips and R. B. Heywood, *Proc. Inst. Mech. Engrs. (London) Appl. Mech.*, Vol. 165, p. 113, 1951. Torsional fatigue tests on  $9\frac{3}{4}$ -in.-diameter shafts made by T. W. Bunyon and H. H. Attla, *Trans. Engrs. Shipbuilders Scot.*, 1955, showed for the sensitivity factor a smaller value ( $q = \frac{2}{3}$ ) than the values obtained in bending tests by R. E. Peterson.

therefore reasonable to expect that the probability theory developed in studying fracture of brittle materials (see p 399) can also be used in fatigue tests<sup>170</sup> Pursuant to this idea we must expect that the endurance limit of a material will decrease with an increase in size of the test specimen Working with fatigue tests in bending, several experimenters noticed a diminution of fatigue strength with an increase in diameter of the specimens<sup>171</sup> Much larger *size effect* was found in testing specimens with various kinds of stress concentrations, but it seems that no attempt has yet been made to study this phenomenon by applying probability theory<sup>172</sup> The problem becomes very complicated because the volume of highly stressed material in such cases is usually very small, and it becomes necessary to consider the grain size of crystalline materials While we speak of geometrically similar specimens of the same material, it is obvious that their metallographic structure is not geometrically similar, and this fact may affect the fatigue tests Considering a region of peak stress, a different result may be expected when only a few grains are contained in that region from the result if many thousands of grains are contained in the same region The relationship between the sensitivity factor  $q$  obtained from fatigue tests and the grain size of the materials is discussed in a paper by R E Peterson<sup>173</sup>

**88. Reduction of the Effect of Stress Concentrations in Fatigue.**—It can be appreciated that the problem of reducing the damaging effect of stress concentrations is of primary importance to designers Some lowering of stress concentrations can be obtained by a suitable change in design For example, a design can be improved considerably by eliminating sharp

<sup>170</sup> See the paper by W Weibull, *Trans Roy Inst Technol (Stockholm)*, No 27, 1949

<sup>171</sup> R E Peterson, *Proc Am Soc Test Mat*, Vol 29, p 371, 1929, R Faulhaber, *Mitt Forsch Inst, Verein Stahlwerke (Dortmund)*, Vol 3, p 153, 1933, and O J Horger and H R Neifert, *Proc Am Soc Test Mat*, Vol 39, p 723, 1939

<sup>172</sup> This problem was discussed by R E Peterson, *Proc Am Soc Metals*, 1948

<sup>173</sup> See *Contributions to the Mechanics of Solids, Dedicated to Stephen Timoshenko by His Friends*, New York, p 179, 1938



reentrant corners and introducing fillets of generous radius, by designing fillets of proper shape, by introducing relieving grooves, etc. In Fig. 329 are shown methods for reducing the

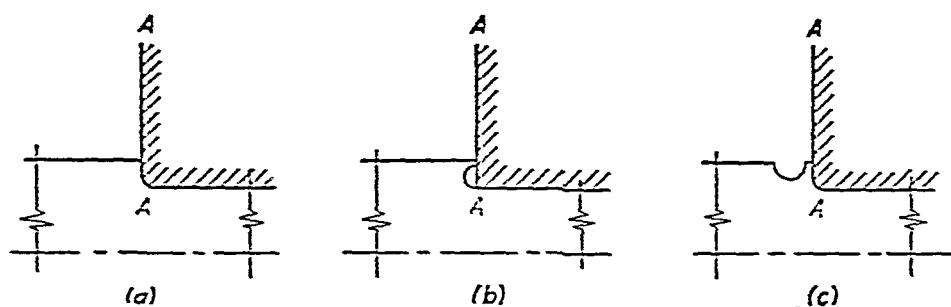


FIG. 329.

stress concentration at a shoulder of a shaft, while maintaining the positioning line  $AA$ . The stress can be reduced by cutting into the shoulder and introducing a fillet of larger radius without developing interference with the fitted member, as shown in Fig. 329*b*. If the shoulder height is too small, a relief groove may be used as shown in Fig. 329*c*.

In Fig. 330 two different bolt-and-nut designs are shown. In Fig. 330*a* the nut is in compression while the bolt is in

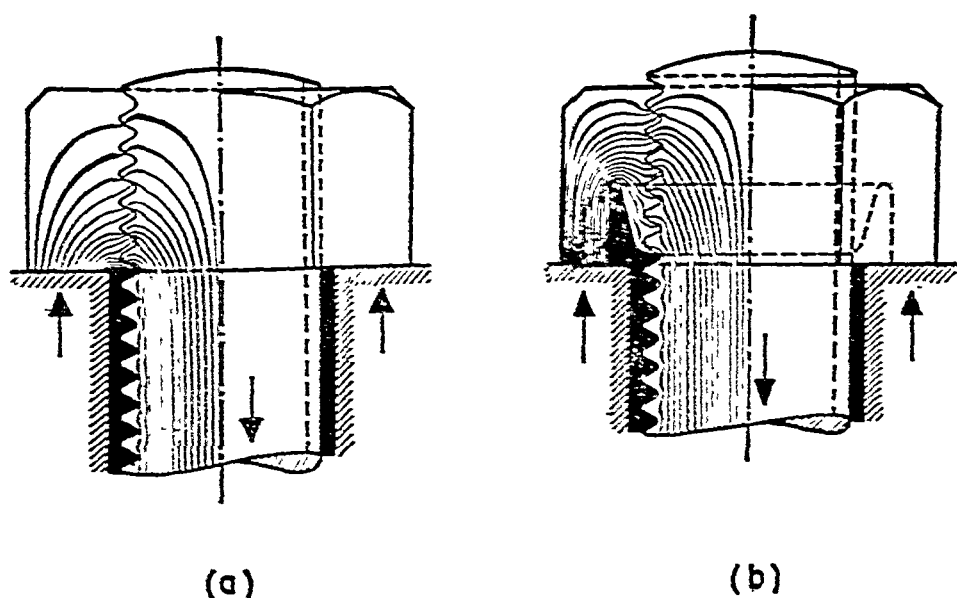


FIG. 330.

tension. High stress concentration takes place at the bottom of the thread in the face of the nut, and under the action of variable forces, fatigue fracture occurs in that plane.<sup>174</sup> In the lip design, Fig. 330*b*, the peak stress is somewhat relieved because the lip is stressed in the same direction as the bolt. Fatigue tests show <sup>175</sup> the lip design to be about 30 per cent stronger.

Sometimes these relieving measures are not sufficient to eliminate fatigue failures. As an important example let us consider the typical failures which occur at the wheel seats of locomotive and railroad-car axles, at the wheel or bearing seats of automobile axles, at the pressed or fitted bits of long drill rods in oil-well operations, etc. All these cases of fitted members subjected to the action of variable stresses have been a constant source of fatigue failures. Considering, for example, the case of a wheel hub pressed on an axle, Fig. 331*a*,

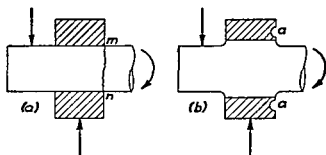


FIG. 331.

we can see that a high stress concentration combined with friction <sup>176</sup> is produced at the reentrant corners *m* and *n*. During rolling of the axle a reversal of stress at points *m* and *n* takes place, and finally a fatigue failure over the cross section *mn*, as shown in Fig. 332, may occur. Stress concentrations

<sup>174</sup> J. N. Goodier, *J. Appl. Mech.*, Vol. 62, p. 11, 1940. See also M. Hetényi, *Proc. Soc. Exp. Stress Anal.*, Vol. 11, p. 147, 1943.

<sup>175</sup> H. Wiegand, thesis, Tech. Hochschule, Darmstadt, 1933. See also S. M. Arnold, *Mech. Engrg.*, Vol. 65, p. 497, 1943.

<sup>176</sup> Regarding fretting corrosion and fatigue, see G. A. Tomlinson, P. L. Thorpe and H. J. Gough, *Proc. Inst. Mech. Engrs. (London)*, Vol. 141, p. 223, 1939. See also O. J. Horger, *Symposium on Fretting Corrosion*, American Society for Testing Materials, 1953.

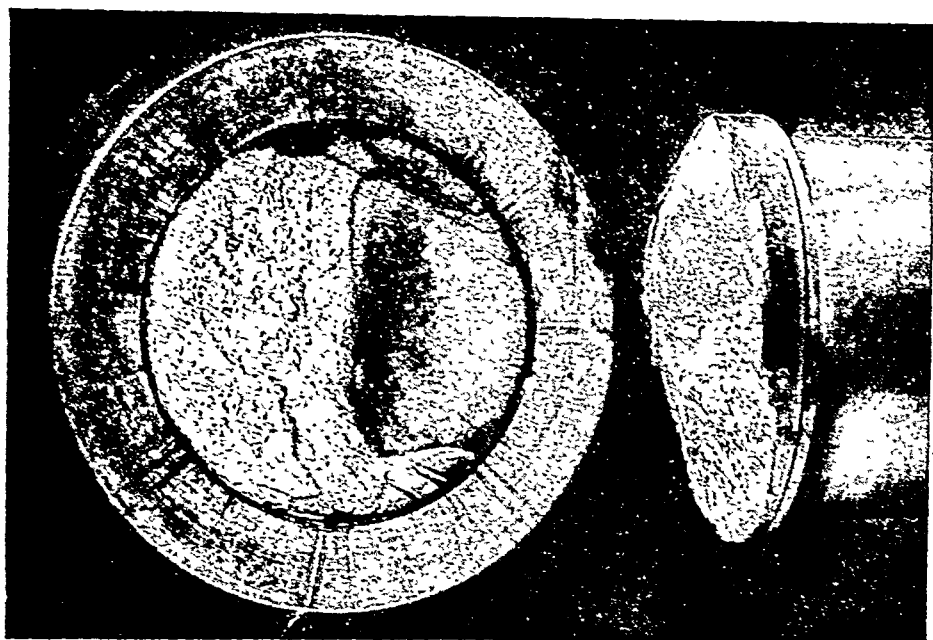


FIG. 332.

can be somewhat reduced by introducing raised seats and fillets as shown in Fig. 331*b*. A further improvement is obtained by introducing the relief groove *a*, Fig. 331*b*. Although such changes are an improvement, they are not sufficient in this case. Experience shows that the mere press fit of a hub on an axle, Fig. 331*a*, reduces the fatigue strength of the axle to less than half of its initial strength, while the changes shown in Fig. 331*b* raise the fatigue strength of the axle perhaps no more than 20 per cent.

To improve this condition and eliminate fatigue failures, surface cold-rolling of the axle in the region of stress concentration has been successfully applied. The early experiments <sup>177</sup> with surface cold work were made on small specimens, and in order to obtain sufficient information for practical applications, an extensive series of laboratory tests with large specimens

<sup>177</sup> Improvement of fatigue strength by surface cold-working was introduced by O. Föppl, *Stahl u. Eisen*, Vol. 49, p. 575, 1929. It was applied in various fatigue tests at the Wöhler-Institut. See *Mitt. Wöhler-Inst.*, Vols. 1-37, 1929-40. See also A. Thum and F. Wunderlich, *Mitt. Materialprüfungsanstalt, Tech. Hochschule (Darmstadt)*, Vol. 5, 1934; and R. Kühnel, *Stahl u. Eisen*, Vol. 110, p. 39, 1932.

were made Three types of fatigue tests made by O J Horger at the laboratory of the University of Michigan<sup>178</sup> are shown in Fig 333 The properties of the materials used in these tests are listed in Table 24 The endurance limits obtained for the S A E and for the nickel steel from the usual cantilever

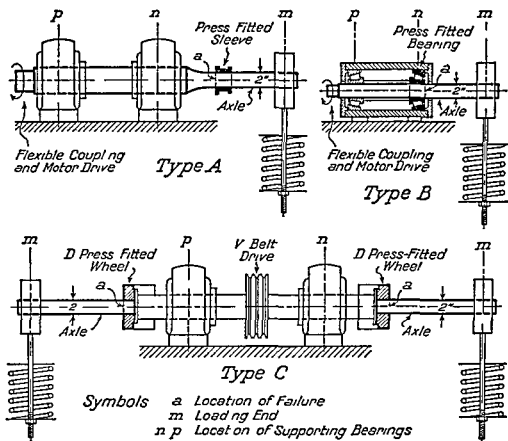


FIG 333

beam fatigue tests are 34,000 and 48,000 lb per sq in respectively After pressing on the sleeve, as in type *A* tests, Fig 333, the endurance limit of the S A E steel was reduced to 15,000 lb per sq in In tests of types *B* and *C* the endurance limits were found to be 12,000 and 14,000 lb per sq in, respectively

<sup>178</sup> A description of these experiments is given in the papers by O J Horger, *J Appl Mech*, Vol 2, p A 128, 1935, and O J Horger and J L Maubetsch, *ibid*, Vol 3, p A 91, 1936 The work done at the Westinghouse Research Laboratories is described in the paper by R E Peterson and A M Wahl, *ibid*, Vol 2, 1935, p A 1.

TABLE 24: MATERIALS USED FOR TESTS IN FIG. 333

Steel	Chemical Composition, %							Y.P.	Ult.	Elong., %
	C	Mn	P	S	Si	Cr	Ni	Lb/in. <sup>2</sup>	Lb/in. <sup>2</sup>	
S.A.E. <sup>1</sup> 1045.....	0.47	0.72	0.015	0.034	0.23	0.03	0.05	47,800	88,800	32
2.75% Nickel <sup>2</sup> .....	0.24	0.86	0.034	0.021	0.24	—	2.79	86,300	111,000	23

<sup>1</sup> Normalized 1620° F and drawn 1115° F.<sup>2</sup> Quenched 1475° F and tempered 1150° F.

This indicates that owing to the press fit the fatigue strength of the specimens was diminished to less than one-half its initial value. Similar results were also obtained for nickel steel specimens. To improve the fatigue strength the surface of the remainder of the specimens was cold-rolled, before pressing on the sleeves or hubs, by using the device shown in Fig. 334. A lathe was adapted for this rolling operation by supporting the specimen in lathe centers and

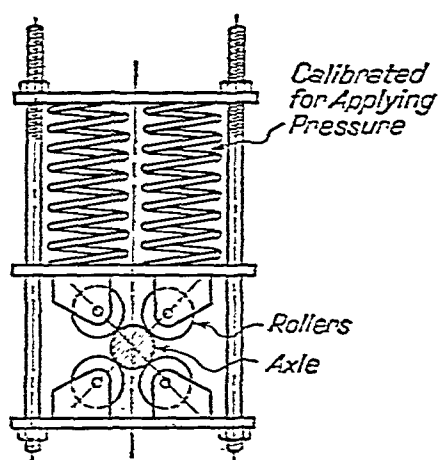


FIG. 334.

supporting the rolling device in a transverse slide fixed to the lathe carriage. To secure a sufficiently smooth surface after rolling, feeds giving more than 40 threads per in. were used.

The results of fatigue tests of type C, Fig. 333, made with cold-rolled specimens, are shown in Fig. 335. It is seen from these tests that the fatigue strength of the S.A.E. steel specimens increased owing to cold-rolling to a value more than twice their initial strength. Similar results were also obtained with the nickel steel specimens.

A further step in the investigation of the effect of cold-rolling on fatigue strength was made by building large fatigue-testing machines in which full-size locomotive axles could be

tested Fig 336 represents one of these machines<sup>179</sup> The arrangement is similar to the type C tests in Fig 333, and is the same as used by Wöhler in his famous fatigue tests of axles The laboratory results with large-size specimens were so promising that some railroads introduced the requirement of surface-rolling of axles and other locomotive parts such as piston rods, connecting rods, crankpins and tires<sup>180</sup>

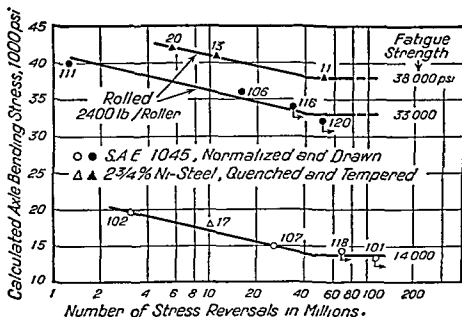


FIG 335

To produce a layer of cold-worked material of sufficient thickness, considerable roller pressure is required for surface-rolling of large diameter axles. In the case of small-diameter shafts and light machine parts, even a thin layer of cold-worked metal will show a considerable improvement in fatigue strength. A simple way of producing such surface cold work is *shot peening*. This process has found extensive application in the automobile industry<sup>181</sup>

<sup>179</sup> Three machines of this type are in use at the research laboratory of the Timken Roller Bearing Company, Canton, Ohio. Fig 332 is taken from one of these tests.

<sup>180</sup> See the paper by O J Horger presented at the Annual Meeting, American Society for Metals, Feb 1946.

<sup>181</sup> See O J Horger and H R Neifert, *Proc Soc Exp Stress Anal*, Vol 2, p 178, 1944.

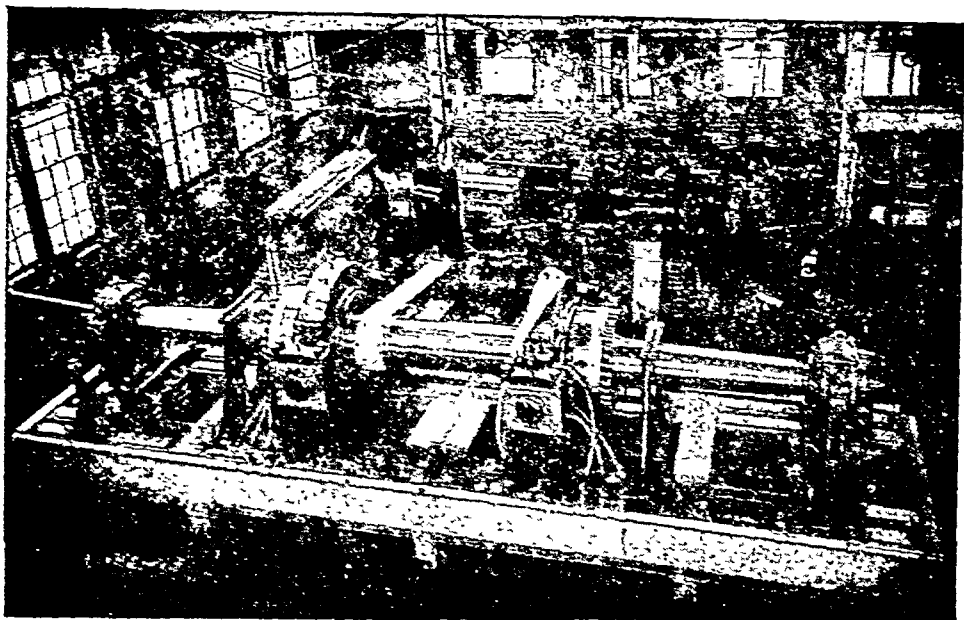


FIG. 336.

89. **Surface Fatigue Failure.**—Another case of fatigue failure under the action of highly concentrated stresses is represented by the *surface failure* of rollers and gears under the repeated action of contact pressures during rotation. Considering two rotating rollers pressed together by forces  $P$ , Fig. 337, we can calculate the maximum compressive stress at the surface of contact by using the formulas of Art. 63. In the case of an ideally smooth surface this calculated stress is the true stress, and the surface fatigue strength of rollers of a given material will depend only on the magnitude of this stress. In actual cases the roller surface has various kinds of unevenness, the magnitudes of which depend on the kind of surface finish. Several examples of surface finish are shown <sup>182</sup> in magnified form in Fig. 338. Naturally the surface roughness will affect the

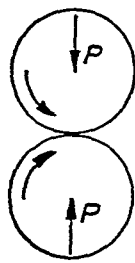


FIG. 337.

<sup>182</sup> This figure and the two following are taken from a paper by S. Way, presented at a meeting of the American Gear Manufacturers Association, May 1940. Various methods of investigation of surface finish are described by S. Way in a paper published in the *Proc. Special Summer Conferences on Friction and Surface Finish*, Massachusetts Institute of Technology, June 1940. A bibliography of the subject is given in this paper.

pressure distribution at the surface of contact of the rollers, Fig. 337. As a result of local overstressing at the peaks of the most unfavorable irregularities, fatigue cracks will start earlier than in the case of smooth rollers. This indicates that the fatigue strength of rollers depends on the degree of roughness of their surface.

Experiments show that if surface fatigue tests are made with lubricated rollers, surface fatigue cracks grow into pits.

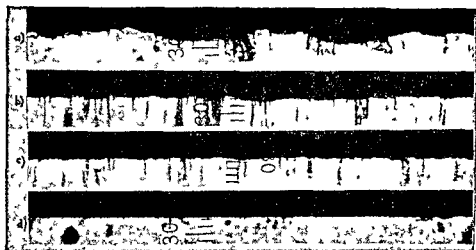


FIG 338

*Pitting cracks*, which sometimes develop in rollers and gears under service conditions, are very undesirable, and considerable effort has been expended in studying the causes of pitting.<sup>183</sup> These investigations showed that the causes of the growth of pitting cracks are of a hydrodynamical nature. Pitting cracks assume a direction that slopes obliquely into the metal and are roughly in the form of a conical surface. They meet the surface in a curve with the shape of a parabola or a  $V$ , the vertex of the  $V$  being the part that first comes into contact during rotation. In Fig. 339, showing a magnified view of a roller surface, the starting point of a pit crack is shown by the arrow. It is seen that any oil that enters such a crack will tend to be trapped as the crack passes under the loaded region. The high oil pressure in the crack will pro-

<sup>183</sup> Such investigations were made at the Westinghouse Research Laboratories by S. Way. See his paper in *J. Appl. Mech.*, Vol. 2, 1935.



duce high tensile stresses at the end of the crack, and the crack may be driven further into the metal. This theory explains why oil is necessary for the growth of pitting cracks and why the growth of cracks may be stopped by either chang-



FIG. 339.

ing the direction of rotation or reducing the oil pressure in the crack.

To obtain comparative values of pitting resistance for different materials, fatigue tests were made<sup>184</sup> with pairs of rollers, Fig. 337. In these tests one roller was 1.576 in. in diameter, the second roller was 1.500 in. in diameter, and the width of the test surface was 0.500 in. All rollers had a fine-ground surface on which the maximum depth of irregularities was between 0.0001 in. and 0.00018 in. The speed of rotation was between 300 and 500 rpm, with lubrication by a bath of

<sup>184</sup> See paper by S. Way, *ibid.*

machine oil of viscosity 700–900 sec Saybolt at the operating temperature. The maximum compressive stress, given by eq. (279), p. 343, and calculated for a compressive load just sufficient to cause at least 1 pit per sq in. of test surface in 10

### COMPARISON OF APPROXIMATE PITTING RESISTANCE OF GEARS AND ROLLERS

**CURVE A** - COMPRESSIVE STRESS ON GEAR TEETH JUST BELOW PITCH POINT (CALCULATED ASSUMING SMOOTH TEETH WITH NO PROFILE ERRORS BUT TAKING ACCOUNT OF LEAD ERRORS AND MISALIGNMENT) SUFFICIENT TO CAUSE ABOUT SIX PITS, OR ONE PIT PER SQ IN. OF AREA BETWEEN PITCH LINE AND END OF ONE TOOTH CONTACT. - GROUND TEETH -  $10^7$  GEAR REVS.

**CURVE B** - COMPRESSIVE STRESS ON TEST ROLLERS (1.500" 1.576" DIAMS.) WITH GROUND SURFACES SUFFICIENT TO CAUSE ONE PIT PER UNIT AREA IN  $10^7$  CYCLES.

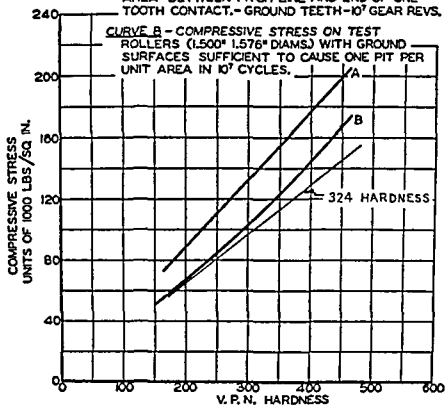


FIG. 340

million cycles, was defined as the *pitting limit* of the material. The results of these tests for the case of 0.45 per cent carbon steel and for various heat treatments are represented in Fig. 340 by the curve *B*. The hardness numbers<sup>133</sup> of the rollers are taken as the abscissas, and the corresponding pitting limits are the ordinates. For comparison, a straight line is

<sup>133</sup> The hardness numbers can be considered proportional to the ultimate strength of the surface layer of the roller.

shown which corresponds to pitting limits having values 324 times the hardness number. Since pitting is a fatigue failure, we would expect the pitting strength to increase in proportion to the hardness. The experiments showed that the assumption of a linear relationship between pitting strength and hardness is on the conservative side.

Curve *A* in Fig. 340 gives the values of the pitting limits found from experiments with gears made of the same material as the previously discussed rollers. The conditions at the surfaces of contact of gear teeth are somewhat different from those in rollers, the principal difference being the fact that rolling is associated with sliding. This difference of conditions results in an increase in the pitting limit.

90. Causes of Fatigue.—Although a large amount of data concerning the fatigue strength of materials has been accumulated, there has not been established any fundamental theory to explain the cause and the mechanism of the phenomena. A fatigue fracture was formerly attributed to “crystallization” of the metal, making it brittle. Such a theory was advanced on the basis of the appearance of the fracture (see p. 473). We now know that the individual crystals remain unchanged during an endurance test, except that there may be some slipping within these crystals.

Bauschinger was the first to investigate cycles of stress. He loaded and unloaded the specimens slowly and used sensitive extensometers to establish the stress-strain relations under these conditions.<sup>188</sup> In this manner he showed that the proportional limits in tension and compression are not fixed points for a given material, but that they may be displaced by subjecting the specimen to cycles of stress. To explain the fact that the endurance limit for steel under reversed stress is sometimes lower than the proportional limit obtained from static tests, Bauschinger advanced the theory that the material as received from the manufacturer may have its proportional limits in tension and compression raised by cold work and that the true or *natural proportional limits* are those which are

<sup>188</sup> J. Bauschinger, *Mitt. Mech.-tech. Lab. München*, 1886. See also *Dinglers Polytech. J.*, Vol. 266, 1886.

established after subjecting the material to cycles of stress. These natural proportional limits are supposed to define the *safe range* in fatigue tests.

Bauschinger's idea was further developed by Bairstow<sup>187</sup>. Using a loading and unloading machine at slow speed (2 cycles per min) and with a Martens mirror extensometer mounted on the specimen, he obtained stress strain relations for cycles of stress with various ranges. Figure 341 represents some of

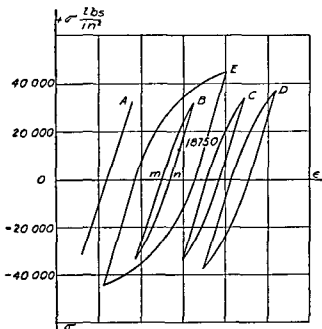


FIG 341

Bairstow's results obtained with axle steel (yield point 50,000 lb per sq in and ultimate strength 84,000 lb per sq in) under reversed stress (mean stress equal to zero). Line *A* represents the initial tension compression test with a semirange of 31,400 lb per sq in. Within these limits the stress strain relation evidently follows accurately a straight line law<sup>188</sup>.

Then the specimen was subjected to cycles of reversed stress of 31,400 lb per sq in, and it was observed that the initial straight line *A* developed gradually into a loop of definite shape. This loop as obtained after 18,750 cycles is repre-

<sup>187</sup> L. Bairstow, *Phil Trans Roy Soc (London)*, A, Vol 210, p 35, 1911

<sup>188</sup> The gage length in these tests was only 0.5 in, and the small elastic hysteresis could not be detected by Martens extensometers.

sented by the curve *B*. It can be seen that in this case the initial proportional limits were higher than the so-called natural proportional limits shown after many cycles of reversed stress. Since these limits are below 31,400 lb per sq in., a *cyclical permanent set* equal to the width *mn* was produced. The loops *C*, *D* and *E* were obtained after cycles of reversed stress equal to 33,500, 37,500 and 47,000 lb per sq in., respectively. The number of cycles in each case was apparently sufficient to stabilize the size of the loops. When the width of these loops was plotted against the corresponding maximum stress, Bairstow obtained approximately a straight line. The intersection of this line with the stress axis determines the range of stress at which there is no looping effect. The range of stress defined in this manner was assumed by Bairstow to be the *safe range of stress*, and subsequent endurance tests have verified this assumption with sufficient accuracy. Since then, various methods for the rapid determination of fatigue ranges on this basis have been developed.<sup>189</sup>

The measurement of hysteresis loops in order to determine the safe range of stress can be done in another way by using calorimetric measurements. The area of the loop represents the energy dissipated per cycle. This energy is transformed into heat which can be measured. The first experiments of this kind were made by Hopkinson and Williams,<sup>190</sup> who showed that the areas of the loops as determined by calorimetric methods agreed within 6 per cent with the areas as determined by extensometer measurements. In those tests it was also shown that it is possible to have a certain amount of hysteresis which will never cause destruction, and this can be considered as the true elastic hysteresis. More rapid methods for determining endurance limits have also been developed on the basis of these calorimetric measurements.

The first attempt to explain the mechanism of fracture in

---

<sup>189</sup> See the book by H. J. Gough, *The Fatigue of Metals*, London, Chap. 10, 1924. See also E. Lehr, *Die Abkürzungsverfahren*, dissertation, Stuttgart, 1925.

<sup>190</sup> B. Hopkinson and G. T. Williams, *Proc. Roy. Soc. (London)*, *A*, Vol. 87, 1912.

endurance tests was made by Ewing and Humfrey.<sup>191</sup> They used a rotating specimen of Swedish iron with a polished surface and examined this surface with a metallurgical microscope after applying cycles of reversed stress. They found that if stresses above a certain limit were applied, slip bands appeared on the surface of some of the crystals after a number of cycles. As the cycles were repeated the number of slip bands increased, and some of the previous slip bands seemed to broaden out. This broadening process continued until finally cracking occurred, the crack following the path of the broadened slip bands. They found that a reversed stress of 11,800 lb per sq in. could be applied millions of times without producing any slip bands. A stress of 15,400 lb per sq in. produced only one isolated slip band after 3 million cycles and this line was confined to the middle portion of the crystal. From these tests it was concluded that 15,400 lb per sq in. was the endurance limit for Swedish iron. On the basis of such investigations the theory was advanced that cycles of stress above the safe range will produce slip bands in individual crystals. If the cycles of stress are continued there will be continual sliding along the surfaces. The sliding is accompanied by friction similar to the friction between sliding surfaces of rigid bodies. As a result of this friction, according to this theory, the material gradually wears along the surfaces of sliding and a crack results.

Further investigation<sup>192</sup> showed that slip bands may occur at stresses which are much lower than the endurance limit of the material. They may develop and broaden without leading to the formation of a crack. This shows that the appearance of slip bands cannot be taken as the basis for determining the endurance limit and cannot explain the mechanism of fatigue cracks.

To obtain a deeper insight into the mechanism of failure in fatigue tests, Gough applied a new method of attack by

---

<sup>191</sup> J. A. Ewing and J. C. W. Humfrey, *Phil. Trans. Roy. Soc.*, (London), *A*, Vol. 200, p. 241, 1903.

<sup>192</sup> H. J. Gough and D. Hanson, *Proc. Roy. Soc. (London)*, *A*, Vol. 104, 1923.

using a precision X-ray technique.<sup>193</sup> Beginning with single-crystal specimens, he showed that the mechanism of deformation of ductile metallic crystals under cycles of stress is the same as under static conditions, i.e., sliding occurs along certain crystallographic planes in definite directions and is controlled by the magnitude of the shearing stress component in the direction of sliding. The X-ray analyses showed that if the cycles were outside the safe range, "the crystallographic planes became distorted in such a manner that, while their average curvature was inappreciable . . . yet severe local curvatures existed. It was suggested that large local strains—also, possibly, actual lattice discontinuities—must occur in such distorted planes, which, under the application of a sufficiently great range of external stress or strain, would lead to the formation of a progressive crack; under a lower magnitude of cyclic straining, the condition might be stable."

In experimenting with crystalline materials such as mild steel, the preliminary static tests showed that no permanent change occurs in perfect grains if they are kept within the elastic range. Between the elastic limit and the yield point, slip lines appear on the surface of some unfavorably oriented grains. These slip lines show the planes of sliding in the crystals. If cycles of stress larger than the endurance limit of the material are applied to the specimen, the weakest grain begins to deteriorate along the plane of sliding and a thin crack develops along that plane. The crack widens with the number of cycles, extends to the adjacent grains and finally produces fracture of the specimen. This shows that fatigue deterioration begins at a localized spot where plastic yielding occurs, while the surrounding material remains perfectly elastic.

In studying the deformation at the spot where fatigue deterioration begins under reversal of stress, we again consider the model composed of three bars, Fig. 271, p. 413, which was used for illustrating Bauschinger's effect. Assuming a complete reversal of the force  $P$ , which is larger than the elastic limit of the model, and proceeding as explained on

<sup>193</sup> A summary of this work was presented to the Royal Aeronautical Sociey. See *J. Roy. Aeronaut. Soc.*, Aug. 1936.

p. 416, we obtain a loop in the form of a parallelogram  $abcd$ , Fig. 342. In the previous derivation, hardening of the material of the vertical bar due to plastic deformation was neglected, and it was assumed that the yield point stress of the bar remained constant during cycles of loading. Under this assumption the size of the loop

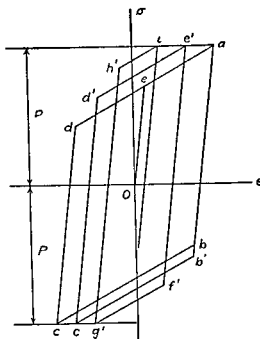


FIG 342

remained constant and independent of the number of cycles. If strain hardening is taken into consideration, we obtain quite different results. Starting with point  $a$ , which corresponds to the beginning of the unloading of the model, we obtain the line  $ab$ , Fig. 342. At point  $b$  the vertical bar will not yet begin to yield, since its yield point stress has been raised somewhat by the preceding plastic deformation (portion  $ac$  of the diagram). The bar will continue to act elastically up to some higher

value of the load, such as point  $b'$  on the diagram. Starting from this value of the load, the vertical bar yields, and we obtain portion  $b'c'$  of the diagram. Point  $c'$  corresponds in the model to the force  $P$  acting upwards. Now unloading the model and then reloading it in the reversed direction we find that the elastic deformation continues up to some point  $d'$ , because of strain hardening of the vertical bar. At point  $d'$  yielding begins and we obtain the portion  $d'e'$  on the diagram.

Proceeding further with cycles of loading and unloading, the points  $f'g'h'i' \dots$  are obtained. We see that owing to strain hardening of the vertical bar, which represents a weak spot in the fatigue specimen, the hysteresis loops become narrower and narrower with an increase in the number of cycles. This indicates that the amplitude of plastic deformation of the bar decreases with each cycle, while the amplitude of the external load remains constant ( $\pm P$ ). At the same time the



amplitude of the stresses in the bar grows with the number of cycles and approaches the value which would be obtained under the action of the load  $P$  on a perfectly elastic model.

Returning now to the discussion of weak spots in fatigue specimens, the principal question is whether a grain which is deforming plastically will safely withstand the progressive strain hardening, or whether a fatigue crack will begin to develop. To answer this question Orowan investigated<sup>154</sup> strain hardening of the weak spot, under cycles of stress, by using a strain hardening curve giving yield stress as a function of plastic deformation.<sup>155</sup> He considered two cases, as shown in Fig. 343*a* and *b*. In both cases the line  $OPA$  represents the

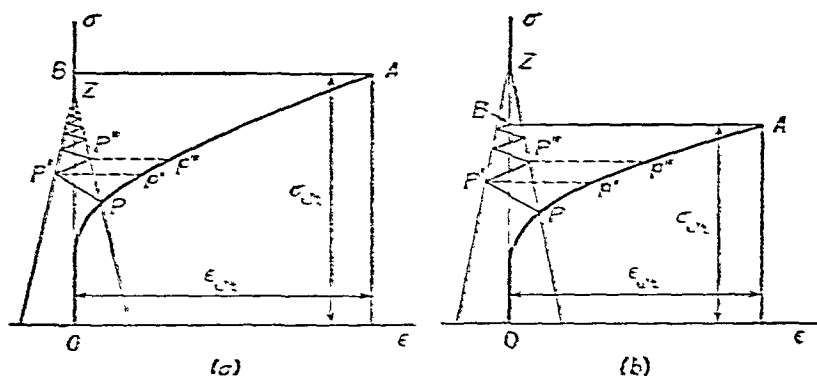


FIG. 343.

strain hardening curve for the material. The ordinate of point  $P$ , corresponding to point  $a$  in Fig. 342, gives the stress at the weak spot of the fatigue specimen at the beginning of the first cycle. The zigzag curve  $PP'P'' \dots$  gives the consecutive alternating plastic deformations of the weak spot during the cycles of the external load. Assuming that strain hardening is independent of the direction of strain, but depends only on the summation of their absolute values during the cycles, we obtain the strain hardening of the weak spot from points  $p', p'' \dots$  on the strain hardening curve  $OPA$ . We can see for the case in Fig. 343*a*, where point  $Z$  is below  $B$ ,

<sup>154</sup> E. Orowan, *Proc. Roy. Soc. (London)*, *A*, Vol. 171, p. 79, 1939.

<sup>155</sup> Because of reversal in direction of the plastic strain, this curve will be somewhat different from the curve obtained by static stretching of the specimen, but this difference is not essential in our further discussion.

that even for an unlimited number of cycles the strain hardening always remains smaller than its ultimate value (point  $A$ ). Thus we conclude that in this case the alternating load is safe.

In the case shown in Fig. 343*b*, where point  $Z$  is above point  $B$ , the strain hardening at the weak spot reaches its ultimate value at point  $B$ . With a further increase in the number of cycles, a crack will begin to develop and the specimen will fail in fatigue. It is seen that the two cases, the safe and the unsafe cycles, differ only by the position of the point  $Z$ . Therefore the endurance limit will correspond to the case in which point  $Z$  coincides with  $B$ . The ordinate  $OZ$  represents the limiting stress, which is approached by the amplitude of stresses in the weak spot as the number of cycles increases.<sup>196</sup> It is a local stress depending on the orientation of the weak grain, and may be higher than  $\sigma_{ult}$  calculated as an average stress over the cross section of the specimen.

On the basis of the diagrams in Fig. 343, Orowan drew some conclusions regarding fatigue strength which are in satisfactory agreement with experimental data.

(1) Since the effect of cycles of stress depends only on the relative value of the ordinates  $OZ$  and  $OB$ , it can be expected that the endurance limit of a material is related to its ultimate strength and is independent of such characteristics as proportional limit, yield stress and ductility.

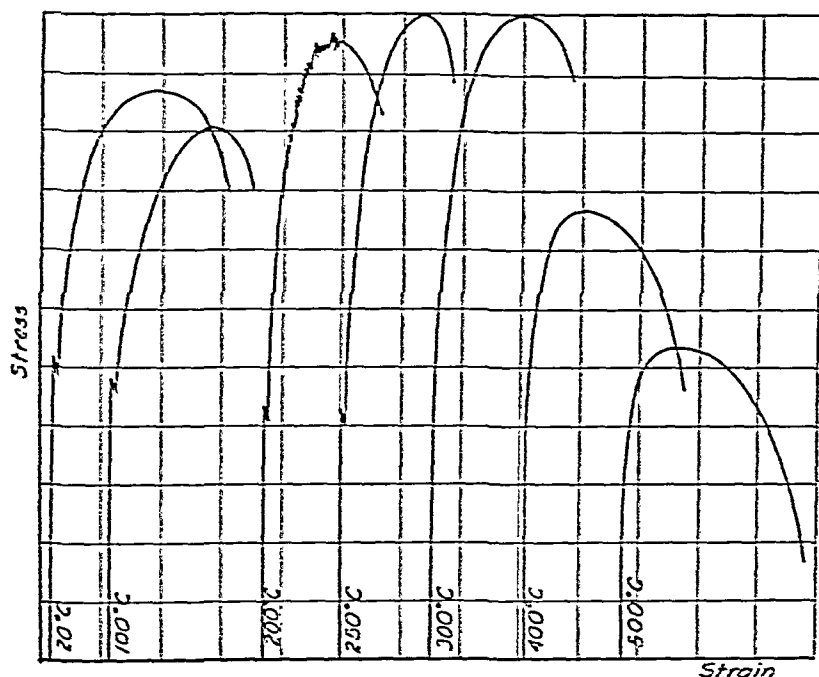
(2) Assuming that the portion  $PA$  (Fig. 343) of the strain hardening curve can be replaced by an inclined straight line, it can be shown that a  $\sigma$ - $n$  curve (Fig. 312) must have a characteristic shape consisting of an inclined and a horizontal straight line. A rough estimate of the number of cycles corresponding to the point of intersection of those two lines (the endurance limit) can also be made.

(3) The influence of mean stress on the magnitude of the range of stress can also be investigated by using a diagram similar to those in Fig. 343.

**91. Mechanical Properties of Metals at High Temperatures.**—There are many cases in which parts of engineering structures are subjected simultaneously to the action of stresses

<sup>196</sup> It corresponds to the amplitude of stress in the vertical bar of the externally discussed model.

and of high temperatures. Such conditions are found, for instance, in power plants and in the chemical industries. Because of the tendency to continually increase the initial temperature of steam <sup>127</sup> in power plants and because of the development of gas turbines, the question of the strength of materials



✓ FIG. 344.

at high temperature has become of practical importance, and a considerable amount of research work has been done in this field.<sup>128</sup>

Experiments show that the yield point and the ultimate strength of a metal in tension depend considerably on the temperature. Several tensile test diagrams for medium-carbon steel at different temperatures are shown <sup>129</sup> in Fig. 344. Up to about 250° C the ultimate strength of the steel increases, but with further increase in temperature it drops off rapidly.

<sup>127</sup> Mellanby and Kerr, *Proc. Inst. Mech. Engrs. (London)*, 1927; H. L. Guy, *ibid.*, 1929, and *Engineer*, Vol. 147, p. 136, 1929.

<sup>128</sup> For a bibliography see G. V. Smith, *Properties of Metals at Elevated Temperatures*, New York, 1950. See also H. J. Tapsell, *Creep of Metals*, Oxford, 1931.

<sup>129</sup> See report of work done at the Westinghouse Research Laboratory by R. B. Wilhelm, *Proc. Am. Soc. Test. Mat.*, Vol. 24-2, p. 151, 1924.

Also the yield point becomes less pronounced as the temperature increases, and at 300° C it cannot be distinguished on the diagram. In Fig 345 the first portions of the same diagrams are shown on a larger scale. This figure shows that the proportional limit of the steel diminishes as the temperature in-

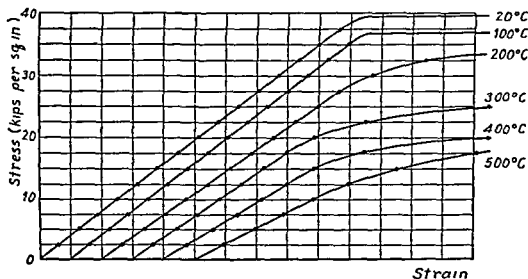


FIG 345

creases. At the same time there is a decrease in the slope of the straight portions of the diagrams, and hence in the modulus of elasticity. The results obtained in the above tests are summarized in Fig 346, which shows that the strength of the material decreases as the temperature increases, while the ductility, as characterized by elongation and reduction in area, increases.

Experiments at high temperatures show that the results of tensile tests also depend on the duration of the test. As the duration of the tensile test increases, the load necessary to produce fracture becomes smaller and smaller. In Fig 347 are shown the tensile test diagrams for the same steel as in the preceding figures, but tested at 500° C for durations of 6 min, 70 min and 240 min. It is evident that tensile test data obtained from the usual short duration tests (lasting say 15 or 20 min), as given in Fig 346, are useful only for cases in which the loads act for a short time.<sup>200</sup>

<sup>200</sup> To eliminate the time effect, vibration tests have been used in determining the modulus of elasticity. See G. Versé, *J Appl Mech*, Vol 2, 1935, and his doctoral thesis, University of Michigan.

For loads acting over a long period of time and at high temperature—for example, the dead weight of a structure or the steam pressure in power plants—we need additional infor-

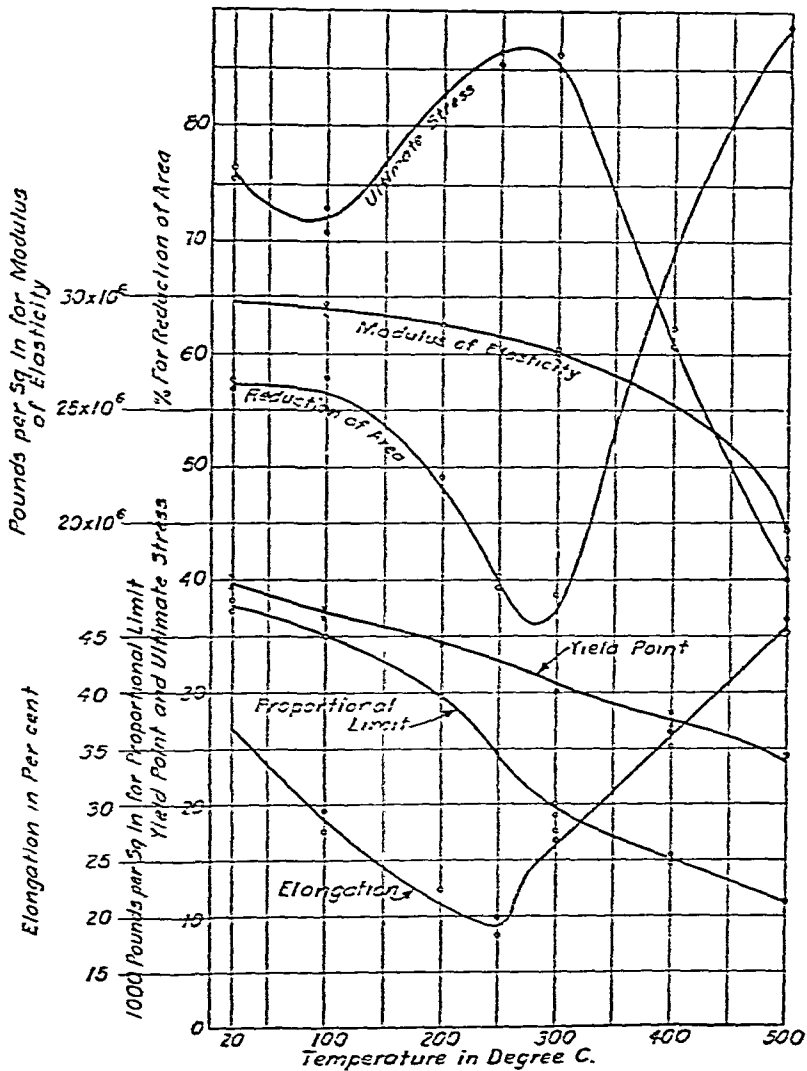


FIG. 346.

mation regarding the *time effect*. Experience shows that under such conditions a continuous deformation or *creep* takes place, which is an important factor to be considered in design. Although a considerable amount of research work has been carried out on this subject<sup>201</sup> and much more is now in progress, the question of the behavior of metals under high temperature

<sup>201</sup> For a bibliography see the book by G. V. Smith, *loc. cit.*, p. 517.

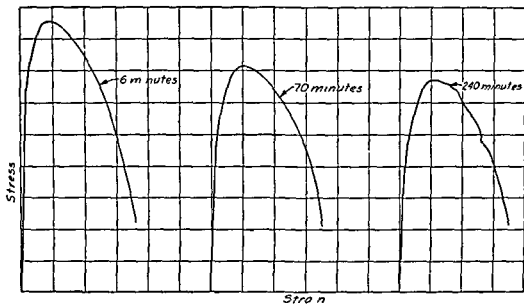


FIG 347

and prolonged loading cannot be considered completely answered

In most experiments pertaining to creep the gradual elongation of a material under prolonged tension is studied. Tensile

test specimens at high temperature are subjected to a certain constant load and temperature, and the *progressive creep* under this load is investigated. The results of such experiments for a given temperature and for various values of the load can be represented by time extension curves, such as shown in Fig 348.<sup>202</sup> Curve A represents a typical *creep curve* for a relatively high stress. After application of the load, creep proceeds at a gradually diminishing rate. At point *a* an inflection occurs and the creep rate begins to increase, until the

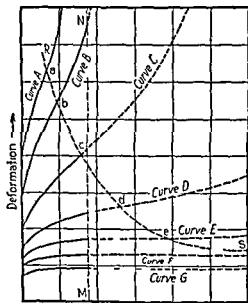


FIG 348

At point *a* an inflection occurs and the creep rate begins to increase, until the

<sup>202</sup> Figs 348-353 were taken from papers by McVetty, *Mechanical Engineering*, p 149, 1934, and *Proc Am Soc Test Mat*, Vol 34, 1938

test specimen breaks. The curve *B*, corresponding to a somewhat smaller load, has a similar shape, but because of the lower creep rates it takes a longer time to produce fracture.

As the load is further reduced, similar tests on different specimens give curves *C*, *D*, *E*, *F* and *G*. As the stress diminishes, a longer and longer time is required to reach the inflection point on the creep curve. To determine the inflection points for such curves as *F* and *G*, tests of extremely long duration would be required. As the stress decreases, it is seen that the creep curve is essentially a straight line for a progressively longer period of time. The working stresses encountered in practice are usually below curve *G*, hence the assumption that the creep curve approaches a straight line is sufficiently accurate for practical purposes. The slope of this line gives the *minimum creep rate* for a given stress and a given temperature. The magnitude of this creep rate diminishes as the stress decreases, but there is no conclusive evidence that it will ever vanish, i.e., that there is a *limiting stress* at which the specimen can indefinitely resist the stress at the high temperature.

— In studying the *progressive creep* of tensile test specimens under constant load and high temperature, two phenomena must be kept in mind, (1) hardening of the material due to plastic strain and (2) removal of this hardening, or “softening” of the material, due to the prolonged action of the high temperature. The mechanism of plastic flow at high temperature is the same as at room temperature. The plastic deformation is due to sliding of the metal. This sliding is accompanied by an increase in the resistance to sliding, which represents strain hardening (p. 423).

The rate at which the effect of strain hardening is removed depends on the temperature. It was mentioned earlier (p. 423) that the effect of strain hardening can be eliminated in a short time by *annealing* the metal at a certain specific high temperature depending on the kind of metal. The same effect can be obtained at a much lower temperature if the temperature acts for a longer period of time. It has been shown,<sup>203</sup> for

<sup>203</sup> See Pilling and Halliwell, *ibid.*, Vol. 25, 1925. See also R. W. Bailey, *J. Inst. Metals*, Vol. 35, 1926.

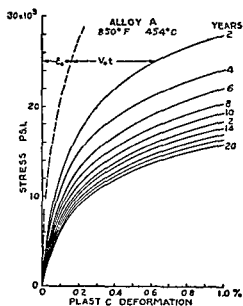


FIG 351

where  $\epsilon_0$  is a constant. Applying this equation to some specific value of  $t$  for which the plastic elongation is known from Fig 349, the value of  $\epsilon_0$  can be calculated. Hence all the constants entering into eq (b) are determined by using the curves of Figs 349 and 350. We can now apply this equation for calculating  $\epsilon$  for any given interval of time. In this way the curves shown in Fig 351 were obtained. Having such a system of curves for a definite material and a definite temperature, a designer

can readily select the proper values of working stress if the lifetime of the structure and the permissible plastic deformation are given.

In calculating  $\epsilon$  for large values of  $t$  we find that the last term in eq (b) is very small and can be neglected. This means

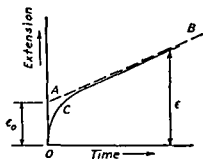


FIG 352

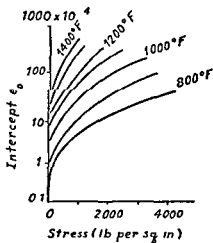


FIG 353

that instead of the curve shown in Fig 352 we can use the broken straight line. The value of  $\epsilon$  is then defined by the magnitude of the creep intercept  $\epsilon_0$  and the value of the min-



imum creep rate  $\dot{\epsilon}_0$ . The experimental values of  $\dot{\epsilon}_0$  can be represented by curves such as are shown in Fig. 353, which were obtained for 12 per cent chromium steel.

Regarding the minimum creep rate, experiments show that  $\dot{\epsilon}_0$  can be represented with satisfactory accuracy by a power function of stress, so that

$$\dot{\epsilon}_0 = k\sigma^n, \quad (c)$$

where  $k$  and  $n$  are constants for a given material and temperature. The values of these constants<sup>205</sup> are given in Table 25

TABLE 25: VALUES OF CONSTANTS  $k$  AND  $n$ 

Material	Temp.	$k$	$n$
0.39% C forged steel.....	400° C	$16 \times 10^{-45}$	8.6
0.30% C steel.....	400° C	$48 \times 10^{-33}$	6.9
Ni-Cr-Mo steel .....	932° F	$91 \times 10^{-20}$	2.7
12% Cr steel.....	850° F	$10 \times 10^{-27}$	4.4

for several steels tested at the Westinghouse Research Laboratories. In the table,  $k$  is the unit elongation per 24 hours and  $\sigma$  is stress in lb per sq in. With these constants, creep deformations and stress distributions can be calculated for structural elements in various particular cases.

In our previous discussion it has been assumed that plastic flow is accompanied by strain hardening. Experiments show that with an increase in temperature the strain hardening becomes less and less pronounced. The maximum temperature at which strain hardening is observed varies with the material, and in the case of steels it varies with the composition of the steel. For instance, no strain hardening was observed<sup>205</sup> with mild carbon steel (0.17 per cent carbon) at a stress of 2,200 lb per sq in. and a temperature of 647° C. Under such conditions the time-extension curve has the shape shown in

<sup>205</sup> See McVetty, *loc. cit.*, p. 520.

<sup>206</sup> See H. J. Tapsell, *Creep of Metals*, 1931.

Fig 354, i e, the rate of creep increases continuously with time

It is interesting to note that the two kinds of time extension curves, shown in Figs 348 and 354, are associated with different types of fracture. When strain hardening is present, yielding at any point in the specimen increases the resistance at this point, and therefore the next sliding occurs at some other cross section. As a result of this, a uniform elongation takes place and the specimen re-

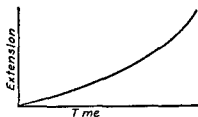


FIG 354

mains cylindrical up to the beginning of necking. When strain hardening is absent, the local yielding which begins at the weakest cross section spreads at a decreasing rate towards the ends of the specimen. As a result, the two parts of a broken specimen are tapered from the ends to the cross section of fracture.

In making extrapolations by using eq (b), it is assumed that the quantities  $v_0$ ,  $c$  and  $\alpha$  characterizing the material remain constant during the lifetime of the structure. But under the prolonged action of high temperatures the resistance of steel to creep is somewhat reduced. To compensate for this *thermal action*, laboratory tests at temperatures above the working temperature are sometimes recommended.<sup>207</sup> The thermal action is more pronounced in the case of high carbon steels. To reduce the structural transformation it is necessary to apply a suitable heat treatment which will assure structural stability.<sup>208</sup>

Before concluding this discussion it should be noted that progressive creep may produce a redistribution of stresses in parts subjected to the simultaneous action of stresses and of

<sup>207</sup> See the paper by R. W. Bailey, *J. Appl. Mech.*, Vol 21, p 309, 1954.

<sup>208</sup> See F. R. Hensel and E. I. Larsen, *Trans. Am. Inst. Min. Metallurg. Engrs.*, Vol 99, p 55, 1932. The effect of prolonged action of high temperatures on the properties of various steels is discussed in the book by G. V. Smith, *loc. cit.*, p 517. The case of intercrystalline fracture of high creep resistance steels at high temperature is discussed by R. W. Bailey, *Proc. Inst. Mech. Engrs. (London)*, Vol 131, pp 131-349, 1935.

high temperatures. At points of high stress concentration the rate of creep is larger, and hence creep will result in a more favorable stress distribution. This fact must be considered in design. Several examples of this kind have been discussed by Bailey.<sup>219</sup>

92. Bending of Beams at High Temperatures.—We will consider in this article the bending of prismatic beams of symmetrical cross section and assume that the bending forces act in the plane of symmetry. Then from symmetry it follows that bending will proceed in the same plane. In our further discussion we start with pure bending (Fig. 355) and assume

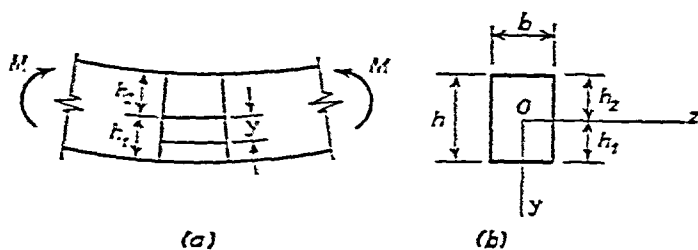


FIG. 355.

that during bending: (1) cross sections remain plane,<sup>220</sup> (2) each longitudinal fiber is in a condition of simple tension or compression, and (3) the creep equation (eq. *b*, p. 523) established for tension also holds for compression. If we denote by *y* the distances of the fibers from the neutral axis and by *r* the radius of curvature of the deflection curve, the unit elongation or compression of any fiber will be

$$\epsilon = \frac{y}{r}. \quad (a)$$

In calculating the corresponding stress we assume that a considerable time has elapsed since the application of the load.

<sup>219</sup> R. W. Bailey, *ibid.*, 1927 and 1935; *Engineering*, Vol. 124, p. 44, 1927, and Vol. 129, 1930. See also C. R. Soderberg, *J. Appl. Mech.*, Vol. 1, p. 131, 1933; G. H. MacCullough, *ibid.*, p. 87; J. Marin, *J. Franklin Inst.*, Vol. 226, p. 645, 1938.

<sup>220</sup> This assumption is in satisfactory agreement with experiments; see G. H. MacCullough, *Trans. A.S.M.E.*, Vol. 55, p. 55, 1935; H. J. Tapsell, *J. Inst. Metals*, p. 387, 1935.

Then the transient period, represented by the curve in Fig. 352, can be neglected and we can use eq. (c), p. 525, in calculating creep. We then obtain

$$\epsilon = \frac{y}{r} = k\sigma^n t \quad (b)$$

and

$$\sigma = \left( \frac{y}{rkt} \right)^{1/n}. \quad (c)$$

Denoting by  $h_1$  and  $h_2$  the distances of the most remote fibers from the neutral axis, we obtain for the largest tensile and compressive stresses the values

$$(\sigma_{\max})_t = \left( \frac{h_1}{rkt} \right)^{1/n}, \quad (\sigma_{\max})_c = \left( \frac{h_2}{rkt} \right)^{1/n}. \quad (d)$$

The tensile and compressive stresses at a distance  $y$  from the neutral axis are

$$\sigma_t = (\sigma_{\max})_t \cdot \left( \frac{y}{h_1} \right)^{1/n}, \quad \sigma_c = (\sigma_{\max})_c \cdot \left( \frac{y}{h_2} \right)^{1/n}. \quad (e)$$

To determine the position of the neutral axis and the distances  $h_1$  and  $h_2$ , we use the equation of statics which states that the sum of the tensile stresses over the lower portion of the cross section (Fig. 355) must be equal to the sum of the compressive stresses over the upper portion. This equation is

$$(\sigma_{\max})_t \int_0^{h_1} \left( \frac{y}{h_1} \right)^{1/n} dA = (\sigma_{\max})_c \int_0^{h_2} \left( \frac{y}{h_2} \right)^{1/n} dA. \quad (f)$$

When the width of the cross section is a known function of  $y$ , we can perform the indicated integrations and obtain an equation for calculating the ratio  $h_1/h_2$ .

The problem is much simpler if the cross section has an axis of symmetry perpendicular to the plane of bending. In such cases we conclude at once that this axis is the neutral axis of the cross section, since then eq. (f) is satisfied. Thus we obtain

$$h_1 = h_2 = \frac{h}{2}; \quad (\sigma_{\max})_t = (\sigma_{\max})_c = \sigma_{\max} = \left( \frac{h}{2rkt} \right)^{1/n}, \quad (g)$$

and we can use for both the tensile and compressive stresses the formula

$$\sigma = \sigma_{\max} \left( \frac{2y}{h} \right)^{1/n}. \quad (h)$$

For calculating  $\sigma_{\max}$  we use the equation of statics which states that the moment of the internal forces distributed over the cross section is equal to the external bending moment  $M$ . Thus we have

$$M = 2\sigma_{\max} \int_0^{h/2} \left( \frac{2y}{h} \right)^{1/n} y dA. \quad (i)$$

Let us consider now, as a simple example, the case of a rectangular beam of width  $b$ . For this case, eq. (i) gives

$$M = 2b\sigma_{\max} \int_0^{h/2} \left( \frac{2y}{h} \right)^{1/n} y dy = \frac{n}{2n+1} \cdot \frac{bh^2}{2} \cdot \sigma_{\max},$$

and we obtain

$$\sigma_{\max} = \frac{Mh}{2I} \cdot \frac{2n+1}{3n},$$

where  $I$  is the moment of inertia of the cross section about the neutral axis. Substituting into eq. (h), we obtain for the stress at any fiber

$$\sigma = \frac{Mh}{2I} \cdot \frac{2n+1}{3n} \left( \frac{2y}{h} \right)^{1/n}.$$

In Fig. 356 the distribution of the stress  $\sigma$  for  $n = 10$  and  $n = 6$  is shown. It is seen that for larger values of  $n$  the stress is only slightly affected by a variation in  $n$ . For comparison, the stress distribution for the elastic condition is shown by the straight line  $OA$ .

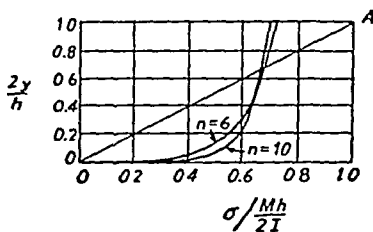


FIG. 356.

Knowing the value of  $\sigma_{\max}$ , we find the curvature of the beam from eq. (d). If the neutral axis is a symmetry axis of the

cross section, the curvature is

$$\frac{1}{r} = \frac{2kt}{h} \sigma_{\max}^n \quad (j)$$

When a beam is bent by transverse loads, the bending stresses and curvature at any cross section of the beam are calculated by substituting the value of the bending moment  $M$  into the formulas for pure bending. Thus in cases in which the neutral axis is an axis of symmetry, the stresses will be calculated by using eqs (h) and (i) and the curvature will be found from eq (j). For a rectangular beam the differential equation of the deflection curve will be

$$\frac{d^2y}{dx^2} = \pm \frac{2kt}{h} \sigma_{\max}^n = \pm \frac{2kt}{h} \left( \frac{h}{2I} \right)^n \left( \frac{2n+1}{3n} \right)^n M^n.$$

This equation can be readily integrated for each particular case of load distribution, and the constants of integration can be determined from the conditions at the ends of the beam. In a similar way, bending of a rectangular beam under combined bending and direct stresses can be investigated.<sup>211</sup>

**93 Stress Relaxation.**—In the preceding articles, creep under constant load was considered. There are cases, however, in which creep proceeds under gradually diminishing forces. A bolted assembly subjected to high temperatures is an important case of this type. By tightening the bolts, considerable initial tensile stress is produced, but because of creep the stress gradually diminishes with time. This phenomenon is called *relaxation*. The decrease in the initial stresses in the bolts may result in undesirable effects, such as leakage of steam in a turbine or in a pipe line at high temperature. Because of these effects, a considerable amount of theoretical and experimental work has been done in studying the phenomenon of relaxation.<sup>212</sup>

<sup>211</sup> This case is discussed by R. W. Bailey, *loc cit*, p. 527.

<sup>212</sup> Several methods of solving this problem are discussed by E. P. Popov, *J. Appl. Mech.*, Vol. 14, p. A 135, 1947, a bibliography on the subject is given in this article. See also G. W. Housner, *ibid.*, p. 352. For an experimental investigation of relaxation stresses see A. Nadai and J. Boyd, *Proc. 5th Internat. Congr. Appl. Mech.*, p. 245, 1939.

We will begin our discussion of this problem by considering the simple case in which the ends of the bolt are held a fixed distance apart. Assume that by tightening the bolt an initial tensile stress  $\sigma_0$  and a corresponding elastic strain  $\sigma_0/E$  are produced. With the passing of time the tensile stress and the elastic tensile strain in the bolt will gradually diminish because of creep. At the same time, plastic deformations will take place. Since the ends of the bolt are fixed, the total elongation must remain constant and equal to the initial elastic elongation. Denoting by  $\sigma$  the tensile stress in the bolt at any time  $t$ , and by  $\epsilon_p$  the plastic elongation due to creep, we obtain the equation

$$\epsilon_p + \frac{\sigma}{E} = \frac{\sigma_0}{E}. \quad (a)$$

In this equation,  $\epsilon_p$  and  $\sigma$  are functions of the time  $t$ . Differentiating eq. (a) with respect to  $t$ , we obtain

$$\frac{d\epsilon_p}{dt} = -\frac{1}{E} \frac{d\sigma}{dt}. \quad (b)$$

In solving this equation let us begin with the assumption that eq. (c), p. 525, for the creep rate is accurate enough for our problem. Then

$$k\sigma^n = -\frac{1}{E} \frac{d\sigma}{dt},$$

and we obtain

$$dt = -\frac{1}{kE} \frac{d\sigma}{\sigma^n}.$$

Integration then gives

$$t = \frac{1}{(n-1)kE} \cdot \frac{1}{\sigma^{n-1}} \left[ 1 - \left( \frac{\sigma}{\sigma_0} \right)^{n-1} \right], \quad (c)$$

and the stress-time relation for the bolt will be represented

by a curve as shown <sup>213</sup> in Fig. 357. Experience shows that the stress in the bolt as predicted by this curve is too high.

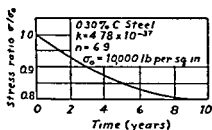


Fig. 357

The bolt loses its initial stress in a much shorter time, and the straight line *AB* in Fig. 352 cannot be used with sufficient accuracy in solving eq. (b).

To obtain a more satisfactory result the curve *OCB* in Fig. 352 should be used. Then the creep

rate is given by the more general expression <sup>214</sup>

$$\frac{d\epsilon_p}{dt} = f(\sigma, t). \quad (d)$$

Substituting (d) into eq. (b), we obtain

$$f(\sigma, t) = -\frac{1}{E} \frac{d\sigma}{dt}. \quad (e)$$

This equation is usually solved by using step-by-step numerical integration. Starting with  $t = 0$  and  $\sigma = \sigma_0$ , we calculate the left-hand side of eq. (e). This gives, on a certain scale, the initial slope of the stress-relaxation curve. By using that value, the stress  $\sigma$  at time  $t = \Delta t$  can be calculated. Substituting this new stress into eq. (e) the value of the slope for  $t = \Delta t$  is obtained. The calculation of  $\sigma$  for  $t = 2\Delta t$  can next be made, and the process continued. The calculations made by Popov showed that by following this procedure a stress relaxation curve can be obtained which is in satisfactory agreement with experiments.

It has been assumed in the preceding discussion that the ends of the bolt were absolutely fixed; but in practice there is usually some elasticity in the end fastenings, which must be

<sup>213</sup> See J. Marin, *Mechanical Properties of Materials and Design*, p. 241, 1942.

<sup>214</sup> Several forms of  $f(\sigma, t)$  are discussed in the above-mentioned paper by E. P. Popov. It should be noted that eq. (a), p. 523, for creep at constant stress has to be changed in studying relaxation in which the material is initially highly stressed and then creeps under continuously diminishing stress.



taken into account in calculating stress-relaxation curves. In Fig. 358 a bolted pipe joint subjected to high temperature is shown. During the tightening of the bolts  $m$  the flanges  $n$  will be deflected elastically. During relaxation this deflection diminishes and the length of the bolt increases. Let  $\beta\sigma/E$  represent the elastic deflection of the two flanges, per unit distance between the flanges, due to stress  $\sigma$  in the bolts.<sup>215</sup> Then, during relaxation, we will obtain the following equation instead of eq. (a):

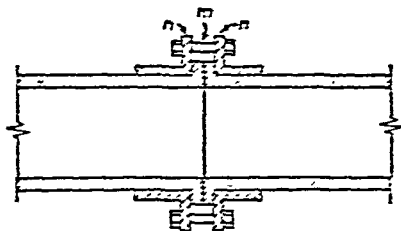


FIG. 358.

$$\epsilon_{pb} + \frac{\sigma}{E} = \frac{\sigma_0}{E} + \frac{\beta(\sigma_0 - \sigma)}{E} - \epsilon_{pf}. \quad (f)$$

The last two terms on the right-hand side of this equation represent the unit elongation of the bolt, during relaxation, due to the elastic and plastic change in distance between the flanges. Finally, eq. (f) can be written in the form

$$\epsilon_{pb} + \epsilon_{pf} = \frac{(1 + \beta)(\sigma_0 - \sigma)}{E},$$

and differentiating with respect to  $t$ , we obtain

$$\frac{d\epsilon_{pb}}{dt} + \frac{d\epsilon_{pf}}{dt} = -\frac{1 + \beta}{E} \frac{d\sigma}{dt}. \quad (g)$$

For the creep rate of the bolt we again use eq. (d). A similar expression can be used for the creep rate of the flanges. Eq. (g) will then have the same form as eq. (e) and can be solved using step-by-step integration. We then find that owing to the elasticity in the end fastenings, the gradual diminishing of the bolt stress proceeds more slowly than in the case of fixed ends.

94. Creep under Combined Stresses.—Only a few experiments have been conducted concerning creep under combined

<sup>215</sup> For calculating  $\beta$ , the elastic deformation of the flanges must be investigated (see p. 142).

stresses. At room temperature, R. W. Bailey<sup>216</sup> tested lead pipes subjected to internal pressure and to combined internal pressure and axial loading. Lead has a low melting point, and creep phenomena occur at room temperature. He also investigated the properties of steel pipes at 900° F and 1,020° F under combined axial tension and torsion. F. L. Everett<sup>217</sup> tested steel pipes in torsion at high temperatures. This kind of test has some advantages as compared with the usual tensile tests, since the plastic torsion does not affect the cross-sectional dimensions of the specimen and since small volume changes due to temperature fluctuation and to structure transformation do not affect the measured angle of twist.

In the absence of additional experimental information regarding creep under combined stress, it is necessary to adapt the results of simple-tension creep tests to the solution of these more complicated problems. This is usually accomplished by assuming (1) that during plastic deformation, the directions of the principal stresses  $\sigma_1$ ,  $\sigma_2$  and  $\sigma_3$  coincide with the directions of the principal strains  $\epsilon_1$ ,  $\epsilon_2$  and  $\epsilon_3$ , (2) that the volume of the material remains constant, so that for small deformations

$$\epsilon_1 + \epsilon_2 + \epsilon_3 = 0, \quad (a)$$

and (3) that the maximum shearing stresses are proportional to the corresponding shearing strains. It can be shown that the values of shearing strain on the planes bisecting the angles between the principal planes are  $\epsilon_1 - \epsilon_2$ ,  $\epsilon_2 - \epsilon_3$  and  $\epsilon_3 - \epsilon_1$ . This result can be obtained by considering a cube, Fig. 359, having unit elongations  $\epsilon_1$  and  $\epsilon_2$  in the directions 1 and 2.

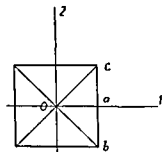


FIG. 359.

The shearing strain  $\gamma$  corresponding to the planes  $Ob$  and  $Oc$  will be found from the triangle  $Oab$ .

<sup>216</sup> World Power Conference, Tokyo, 1929; *Engineering*, Vol. 129, pp. 265-266, 327-329 and 772, 1930.

<sup>217</sup> *Trans. A.S.M.E.*, Vol. 53, 1931; *Proc. Am. Soc. Test. Mat.*, Vol. 39, pp. 215-224, 1939. See also H. J. Tapsell and A. E. Johnson, *Engineering*, Vol. 150, 1940.

Assuming that  $\epsilon_1 > \epsilon_2$ , we obtain

$$\tan\left(\frac{\pi}{4} - \frac{\gamma}{2}\right) \approx \frac{1 - \frac{\gamma}{2}}{1 + \frac{\gamma}{2}} = \frac{1 + \epsilon_2}{1 + \epsilon_1},$$

from which

$$\gamma = \epsilon_1 - \epsilon_2.$$

Similarly, we can find the shearing strains for the other two bisecting planes, and assumption (3) then takes the following form:

$$\frac{\epsilon_1 - \epsilon_2}{\sigma_1 - \sigma_2} = \frac{\epsilon_2 - \epsilon_3}{\sigma_2 - \sigma_3} = \frac{\epsilon_3 - \epsilon_1}{\sigma_3 - \sigma_1} = \theta, \quad (b)$$

where  $\theta$  is a function of  $\sigma_1$ ,  $\sigma_2$  and  $\sigma_3$  which must be determined from experiments.<sup>222</sup> From eqs. (a) and (b) it follows that

$$\left. \begin{aligned} \epsilon_1 &= \frac{2\theta}{3} \left[ \sigma_1 - \frac{1}{2}(\sigma_2 + \sigma_3) \right], \\ \epsilon_2 &= \frac{2\theta}{3} \left[ \sigma_2 - \frac{1}{2}(\sigma_1 + \sigma_3) \right], \\ \epsilon_3 &= \frac{2\theta}{3} \left[ \sigma_3 - \frac{1}{2}(\sigma_1 + \sigma_2) \right]. \end{aligned} \right\} \quad (c)$$

These equations are similar to the stress-strain relations of Hooke's law (see Part I, p. 66) but they differ in two respects. The quantity  $2\theta/3$  appears instead of the constant  $1/E$ , and the factor  $\frac{1}{2}$  replaces Poisson's ratio.

To adapt eqs. (c) to creep at a constant rate, we can divide these equations by the time  $t$ . Using the notations  $\tau_1$ ,  $\tau_2$  and  $\tau_3$  for the principal creep rates and denoting the factor before the brackets by  $m$ , we arrive at the equations

$$\left. \begin{aligned} \tau_1 &= m \left[ \sigma_1 - \frac{1}{2}(\sigma_2 + \sigma_3) \right], \\ \tau_2 &= m \left[ \sigma_2 - \frac{1}{2}(\sigma_1 + \sigma_3) \right], \\ \tau_3 &= m \left[ \sigma_3 - \frac{1}{2}(\sigma_1 + \sigma_2) \right]. \end{aligned} \right\} \quad (d)$$

<sup>222</sup> The above three assumptions are essentially the same as those used by the pioneers in theory of plasticity, Barré de St.-Venant (*Compt. rend.*, Vol. 70, p. 473, 1870) and M. Lévy (*ibid.*, p. 1323).

Applying these equations to simple tension, where  $\sigma_1 = \sigma$  and  $\sigma_2 = \sigma_3 = 0$ , we obtain

$$v = m\sigma. \quad (e)$$

We have already stated (see p. 525) that experimental results for the creep rate in simple tension at constant temperature can be represented satisfactorily by a power function

$$v = k\sigma^n, \quad (f)$$

where  $k$  and  $n$  are two constants of the material. To bring eqs. (e) and (f) into agreement, we must take

$$m = k\sigma^{n-1}. \quad (g)$$

To establish the form of the function  $m$  for the general case of creep, represented by eqs. (d), we use eq. (296), p. 454, which gives the relation between the yielding condition for a three-dimensional stress system and for simple tension. Introducing the value of equivalent stress

$$\sigma_e = \frac{1}{\sqrt{2}} \sqrt{(\sigma_1 - \sigma_2)^2 + (\sigma_2 - \sigma_3)^2 + (\sigma_3 - \sigma_1)^2} \quad (300)$$

into eq. (g), instead of  $\sigma$ , we obtain

$$m = k\sigma_e^{n-1}.$$

Eqs. (d) then become

$$\left. \begin{aligned} v_1 &= k\sigma_e^{n-1}[\sigma_1 - \tfrac{1}{2}(\sigma_2 + \sigma_3)], \\ v_2 &= k\sigma_e^{n-1}[\sigma_2 - \tfrac{1}{2}(\sigma_3 + \sigma_1)], \\ v_3 &= k\sigma_e^{n-1}[\sigma_3 - \tfrac{1}{2}(\sigma_1 + \sigma_2)]. \end{aligned} \right\} \quad (301)$$

For simple tension ( $\sigma_1 = \sigma = \sigma_e$ ,  $\sigma_2 = \sigma_3 = 0$ ) these equations give

$$v_1 = k\sigma^n, \quad v_2 = v_3 = -\frac{k\sigma^n}{2}. \quad (h)$$

In the general case, eqs. (301) provide a means of calculating the creep rates  $v_1$ ,  $v_2$  and  $v_3$  using the values  $k$  and  $n$  obtained from tensile tests. Similar formulas have been used by several

authors<sup>219</sup> in solving problems of creep in cases of combined stress.

95. Particular Cases of Two-dimensional Creep.—Let us now use eqs. (301) to investigate two-dimensional stress conditions and assume

$$\sigma_3 = 0, \quad \sigma_1 > \sigma_2, \quad \sigma_2/\sigma_1 = \alpha.$$

Then we obtain from eq. (300)

$$\sigma_e = \sigma_1 \sqrt{1 - \alpha + \alpha^2}$$

and eqs. (301) become

$$\left. \begin{aligned} \epsilon_1 &= k\sigma_1^n(1 - \alpha + \alpha^2)^{(n-1)/2}(1 - \alpha/2), \\ \epsilon_2 &= k\sigma_1^n(1 - \alpha + \alpha^2)^{(n-1)/2}(\alpha - 1/2), \\ \epsilon_3 &= -\frac{1}{2}k\sigma_1^n(1 - \alpha + \alpha^2)^{(n-1)/2}(1 + \alpha). \end{aligned} \right\} \quad (302)$$

It is seen that the expressions for the creep rates in the principal directions differ from the expressions for simple tension (eqs. *h*, Art. 94) only by numerical factors. The magnitude of these factors can be calculated readily if the constant  $n$  of the material and the ratio  $\alpha$  are known.

*Thin Pipes.*—If the allowable strains in the principal directions during the lifetime of the structure are given, the allowable stress  $\sigma_1$  is found from eqs. (302). In this way, one can solve such problems as the selection of the proper thickness of a thin pipe subjected to internal pressure combined with axial force or torque at high temperatures. Taking  $\epsilon_1$  in the circumferential and  $\epsilon_2$  in the axial direction, and assuming that the internal pressure acts alone, we have  $\alpha = \frac{1}{2}$  and  $\epsilon_2 = 0$ . There is then no creep in the axial direction, but only in the circumferential direction. This conclusion agrees with the results of the experiments with lead pipes made by R. W. Bailey.<sup>220</sup>

In the case of a torque acting alone, the principal stresses are numerically equal and are directed at  $45^\circ$  to the axis of

<sup>219</sup> F. K. G. Odqvist, "Plasticitetsteori," *Proc. Roy. Swed. Inst. Engrg. Research*, 1934; R. W. Bailey, *J. Inst. Mech. Engrs.*, Vol. 131, p. 131, 1935; C. R. Soderberg, *Trans. A.S.M.E.*, Vol. 58, pp. 733-743, 1936.

<sup>220</sup> *Loc. cit.*, p. 534.

the pipe. In this case  $\alpha = -1$ , and we obtain for the creep in the principal directions

$$v_1 = -v_2 = \frac{3}{2} k \sigma_1^n (3)^{(n-1)/2}.$$

We have pure shearing strain and no creep in the axial direction of the pipe. Thus no axial creep is produced either by a torque acting alone or by internal pressure acting alone. However, axial creep is produced when pressure and torque act simultaneously. To calculate the creep for this case we have to calculate, in each particular problem, the magnitudes and directions of the principal stresses. Eqs (302) will then give the creep rates in the principal directions. The axial and circumferential creep rates are then obtained from simple geometrical considerations. For any direction at an angle  $\varphi$  with the direction of  $v_1$ , the creep rate is

$$v = v_1 \cos^2 \varphi + v_2 \sin^2 \varphi$$

The values of creep rates calculated in this manner are in satisfactory agreement with experiments.

*Thick Pipes*—In the preceding cases we had homogeneous stress distribution. As an example of nonhomogeneous stresses let us consider a thick pipe under internal pressure  $p$  (Fig 360).

Assuming that the pipe is in a condition of plane strain, the axial strain  $\epsilon_z$  vanishes and eqs (301) give

$$\left. \begin{aligned} v_t &= k \sigma_e^{n-1} [\sigma_t - \frac{1}{2}(\sigma_r + \sigma_z)], \\ v_r &= k \sigma_e^{n-1} [\sigma_r - \frac{1}{2}(\sigma_t + \sigma_z)], \\ v_z &= 0 = k \sigma_e^{n-1} [\sigma_z - \frac{1}{2}(\sigma_t + \sigma_r)], \end{aligned} \right\} \quad (a)$$

and from the last equation we conclude that

$$\sigma_z = \frac{1}{2}(\sigma_t + \sigma_r) \quad (b)$$

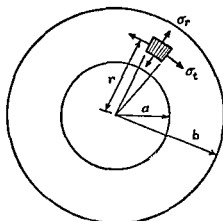


FIG 360

From the condition of equilibrium of the element shown in Fig. 360 we have (see p. 206)

$$r \frac{d\sigma_r}{dr} = \sigma_t - \sigma_r. \quad (c)$$

To determine  $\sigma_t$  and  $\sigma_r$  we have to consider the deformation of the pipe. Denoting by  $u$  the radial displacements during expansion of the tube, we conclude that (see p. 206)

$$\epsilon_t = \frac{u}{r}, \quad \epsilon_r = \frac{du}{dr},$$

and

$$\frac{d\epsilon_t}{dr} = \frac{1}{r} \frac{du}{dr} - \frac{u}{r^2} = \frac{1}{r} (\epsilon_r - \epsilon_t).$$

Assuming a steady state of creep, we obtain by dividing by time  $t$ ,

$$\frac{dv_t}{dr} = \frac{1}{r} (v_r - v_t). \quad (d)$$

Substituting for  $v_t$  and  $v_r$  from eqs. (a), an additional equation for determining the principal stresses is obtained. This equation can be greatly simplified by using equation (b). The equivalent tension then becomes

$$\sigma_e = \frac{\sqrt{3}}{2} (\sigma_t - \sigma_r),$$

and we obtain, from eqs. (a),

$$v_t = -v_r = k \left( \frac{\sqrt{3}}{2} \right)^{n+1} (\sigma_t - \sigma_r)^n. \quad (e)$$

Eq. (d) then becomes

$$\frac{d}{dr} (\sigma_t - \sigma_r)^n = -\frac{2}{r} (\sigma_t - \sigma_r)^n,$$

and we conclude that

$$(\sigma_t - \sigma_r)^n = \frac{C}{r^2}, \quad (f)$$

where  $C$  is a constant of integration. Eq. (c) now gives

$$\frac{d\sigma_r}{dr} = \frac{1}{r} \left( \frac{C}{r^2} \right)^{1/n};$$

and after integrating we obtain

$$\sigma_r = -\frac{n}{2} C_1 r^{-(2/n)} + C_2, \quad (g)$$

where  $C_1 = C^{1/n}$ .

The constants  $C_1$  and  $C_2$  will now be determined from the conditions at the inner and the outer surfaces of the pipe, which are

$$(\sigma_r)_{r=a} = -p = -\frac{n}{2} C_1 a^{-(2/n)} + C_2,$$

$$(\sigma_r)_{r=b} = 0 = -\frac{n}{2} C_1 b^{-(2/n)} + C_2.$$

From these equations we obtain

$$C_1 = -\frac{2p}{n(b^{-(2/n)} - a^{-(2/n)})}, \quad C_2 = -\frac{pb^{-(2/n)}}{b^{-(2/n)} - a^{-(2/n)}},$$

and eq. (g) gives

$$\sigma_r = -p \frac{\left(\frac{b}{r}\right)^{2/n} - 1}{\left(\frac{b}{a}\right)^{2/n} - 1}. \quad (h)$$

From eq. (f) we then obtain

$$\sigma_t = p \frac{1 + \frac{2-n}{n} \left(\frac{b}{r}\right)^{2/n}}{\left(\frac{b}{a}\right)^{2/n} - 1}. \quad (i)$$

Eqs. (b), (h) and (i) give the stresses in the pipe under conditions of steady creep rates. The magnitudes of the creep rates are obtained from eq. (e), which gives

$$v_t = -v_r = \frac{1}{2} (3)^{(n+1)/2} k \frac{b^2}{r^2} \left(\frac{1}{n}\right)^n \left[ \frac{p}{\left(\frac{b}{a}\right)^{2/n} - 1} \right]^n.$$



It is assumed in the derivation that the temperature of the pipe does not change with  $r$ . The case of heat transmission through the pipe wall can be treated in a similar way.<sup>221</sup>

In the preceding discussion a simple solution was obtained by assuming a steady state of creep. It gives satisfactory results for the creep which takes place after a long period of action of the forces. If we wish to ascertain what the creep is after only a short duration of load, the formulas derived on the assumption of steady creep are not satisfactory; we must have recourse to the creep curve  $CB$  in Fig. 352, p. 524. The problem becomes complicated, and creep can be calculated only by using a step-by-step process.<sup>222</sup> Such calculations show that with an increase in the duration of the action of the forces, the results obtained approach those found for steady creep. After a duration of perhaps a year or more, the two methods of calculation give approximately the same values of creep.

*Rotating Disc.*—In conclusion we will give a brief discussion of the method of calculating creep by successive approximations for the case of a rotating disc,<sup>223</sup> Fig. 361. It will be assumed that the variable thickness  $z$  of the disc is small in comparison with its radius, that the stresses  $\sigma_t$  and  $\sigma_r$  are uniformly distributed along the thickness

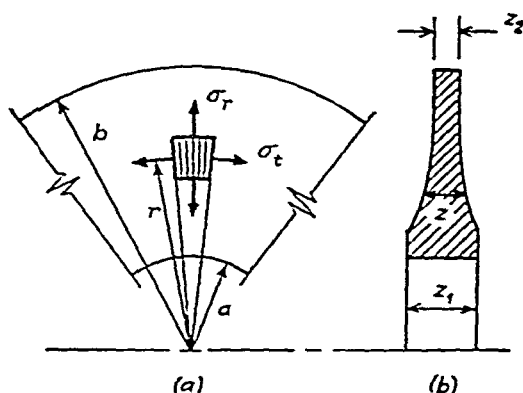


FIG. 361.

<sup>221</sup> See R. W. Bailey, *loc. cit.*, p. 537.

<sup>222</sup> Examples of such calculations are given in the paper by C. R. Soderberg, *loc. cit.*, p. 537. See also the paper by L. F. Coffin, Jr., P. R. Shepler and G. S. Cherniak, *J. Appl. Mech.*, Vol. 16, p. 229, 1949.

<sup>223</sup> R. W. Bailey, *loc. cit.*, p. 537. See also E. P. Popov, doctoral dissertation, Stanford University, 1946.

and that  $\sigma_z$  vanishes. Thus we have a two-dimensional stress distribution and can use eqs (302) for the creep rates. In these equations  $\alpha = \sigma_r/\sigma_t$  is now a function of  $r$ , say  $\alpha = \varphi(r)$ . Assuming steady creep and again denoting the radial displacements by  $u$ , we obtain

$$\begin{aligned}\epsilon_t = \frac{u}{r} = v_{t,t} &= kt\sigma_t^n(1 - \alpha + \alpha^2)^{(n-1)/2} \left(1 - \frac{\alpha}{2}\right), \\ \epsilon_r = \frac{du}{dr} = v_{r,t} &= kt\sigma_t^n(1 - \alpha + \alpha^2)^{(n-1)/2} \left(\alpha - \frac{1}{2}\right)\end{aligned}\quad (j)$$

The condition of equilibrium of the element shown shaded in Fig 361a is (see p 214)

$$\frac{d}{dr}(rz\sigma_r) - z\sigma_t + \frac{\gamma\omega^2 r^2 z}{g} = 0$$

and by integration we obtain

$$rz\sigma_r - (rz\sigma_r)_{r=a} = \int_a^r \sigma_t z dr - \frac{\gamma\omega^2}{g} \int_a^r r^2 z dr \quad (k)$$

It is seen that if the distribution of stresses  $\sigma_t$  is known, the value of  $\sigma_r$  for any value of  $r$  can be calculated from eq (k), provided also that  $(\sigma_r)_{r=a}$  and  $z$ , as a function of  $r$ , are given.

In applying the method of successive approximations we start with the assumption that  $\sigma_t$  is uniformly distributed over the diametral section of the disc, shown shaded in Fig 361b. This average value of  $\sigma_t$  is obtained from eq (k) by carrying out the integration from  $r = a$  to  $r = b$  and gives as the first approximation for  $\sigma_t$

$$(\sigma_t)_1 = \frac{1}{A} \left[ (rz\sigma_r)_{r=b} - (rz\sigma_r)_{r=a} + \frac{\gamma\omega^2 I}{g} \right], \quad (l)$$

where

$$A = \int_a^b z dr, \quad I = \int_a^b r^2 z dr$$

The quantities  $(rz\sigma_r)_{r=b}$  and  $(rz\sigma_r)_{r=a}$  can be obtained readily in each particular case, since the forces acting on the inner and outer boundaries of the disc are known.

Having  $(\sigma_t)_1$  from eq (l), we calculate  $\sigma_r$  as a function of  $r$  from eq (k) and obtain the first approximation for the ratio

$$\left(\frac{\sigma_r}{\sigma_t}\right)_1 = \alpha_1 = \varphi_1(r).$$

With these values of  $\alpha_1$ , the first approximation for the creep will be obtained from the first of eqs. (j), which gives

$$\left(\frac{u}{r}\right)_1 = kt(\sigma_t)_1^n (1 - \alpha_1 + \alpha_1^2)^{(n-1)/2} \left(1 - \frac{\alpha_1}{2}\right). \quad (m)$$

To obtain a better approximation we take the ratio of the two eqs. (j) which gives

$$\frac{du}{dr} \frac{r}{u} = \frac{2\alpha_1 - 1}{2 - \alpha_1} = \psi_1(r). \quad (n)$$

The value of  $\psi_1(r)$  can be calculated readily since  $\alpha_1 = \varphi_1(r)$  is already known. From eq. (n) we then obtain

$$\frac{du}{u} = r^{-1} \psi_1(r) dr$$

and by integration we find

$$\frac{u}{r} = \frac{(u)_{r=a}}{r} e^{\int_a^r r^{-1} \psi_1(r) dr}.$$

Substituting this value instead of  $(u/r)_1$  into eq. (m), the second approximation for  $\sigma_t$  is obtained

$$(\sigma_t)_2 = \frac{(u)_{r=a}}{r} \frac{e^{\int_a^r r^{-1} \psi_1(r) dr}}{kt(1 - \alpha_1 + \alpha_1^2)^{(n-1)/2} (1 - \alpha_1/2)}. \quad (o)$$

The constant  $(u)_{r=a}$  is found from an equation of statics similar to eq. (l), which gives

$$\int_a^b (\sigma_t)_2 r dr = (r\sigma_r)_{r=b} - (r\sigma_r)_{r=a} + \frac{\gamma\omega^2 I}{g}.$$

When  $(u)_{r=a}$  is found from this equation, the quantity  $(\sigma_t)_2$  is completely determined, and proceeding as before, we find the second approximations  $(\sigma_r)_2$ ,  $\alpha_2$ ,  $\psi_2(r)$  and  $(u/r)_2$ , and so on.

Calculations show that the process is rapidly converging and the second approximation gives satisfactory results for stresses and creep. All calculations should be made in tabular form. After calculating  $(\sigma_t)_1$  from eq. (l), we divide the distance from  $r = a$  to  $r = b$  into (say) ten equal parts. Using eq. (k) and step-by-step integration, prepare a table of values of  $(\sigma_r)_1$ . Having these values, the quantities  $\alpha_1$  and  $\psi_1$  for each value of  $r$  can be calculated and a table of  $u/r$  values prepared. With these values, and using eq. (o), a table of values of  $(\sigma_t)_2$  can be calculated, and so on.

96. **Working Stresses.**—*General.*—The problem of choosing an adequate factor of safety when designing structures and machine parts is of the utmost practical importance. If this factor is taken too low and the working stresses are too high, the structure may prove weak in service. On the other hand, if the working stresses are too low, the structure becomes unnecessarily heavy and uneconomical.

In discussing the various factors to be considered in choosing working stresses let us take the simple example of tension of a prismatic bar. We assume that the yield point of the material is taken as the basis for determining the working stress; then the safe cross-sectional area  $A$  is obtained from the equation

$$\frac{\sigma_{Y.P.}}{n} = \frac{P}{A}. \quad (a)$$

We see that the cross-sectional area depends on the magnitude of the external load  $P$ , on the yield point of the material  $\sigma_{Y.P.}$ , and on the factor of safety  $n$ . Obviously the magnitude of this factor, which is sometimes called the *factor of ignorance*, depends on the accuracy with which we know the external load and the mechanical properties of the material, and on the accuracy with which this equation represents the maximum stress.

There are cases where the external forces are known with good accuracy. For example we know very accurately the hydrostatic pressure acting on a dam if the depth of water is known. We know accurately the centrifugal forces acting in a rotor having a definite angular velocity. But in the majority of cases the forces are known only approximately, and the most unfavorable loading condition for a structure can be estimated only on the basis of long experience. Consider, for example, the design of a bridge. The weight of the bridge itself and the weight of the train moving across the bridge may be known with satisfactory accuracy. But in designing the bridge dynamic effects must be taken into account. Because of the balance weights the pressure of a locomotive wheel on the rail is not constant, and the maximum pressure is larger than the static pressure. Under the action of the moving and

varying loads the bridge will be brought into vibration, and under such conditions the problem of determining the forces in individual members of the bridge becomes extremely involved. Another type of force acting on the bridge which we do not know accurately is wind pressure. The magnitude of such forces is usually estimated on the basis of experience with existing structures. From this discussion it is obvious that if eq. (a) represents the condition of safety for a member of a bridge, the force  $P$  is not known exactly and can be estimated only with some approximation. Naturally the accuracy with which the estimate can be made will affect the magnitude of the factor of safety.

The magnitude of  $\sigma_{Y.P.}$  is also not known exactly. It may vary to a certain extent for different specimens of the same material, and this variation depends on the homogeneity of the material. It is quite natural therefore that in the case of such homogeneous materials as steel the factor of safety may be taken lower than in the case of such materials as wood or stone.

The accuracy of the formula itself must also be considered in choosing the factor of safety. Eq. (a) can be considered very accurate for calculating the stresses in a tensile test specimen (see Fig. 255, p. 394) because special precautions are taken to apply the load centrally and to distribute it uniformly over the weakest cross section. But again taking as an illustration the design of a member of a bridge, it can be appreciated that eq. (a) is only a rough approximation depending usually on the assumption that there are ideal hinges at the joints. The actual stress condition in such a member is very far from simple tension. Owing to the rigidity of the joints the members of a bridge truss undergo not only direct stress but also bending. The corresponding bending stresses are sometimes of considerable magnitude, and if they are not taken into account the inaccuracies in using eq. (a) are usually compensated for by increasing the factor of safety.

From this discussion it can be seen how difficult it would be to give any definite recommendations regarding the magnitude of the factor of safety. The choice of the factor always depends upon the experience and judgment of the designer.

In the following discussion it is assumed that the forces are established on the basis of experience and that the mechanical properties of the material are known. Methods are then considered for determining the effect of various kinds of stress conditions on the choice of the working stresses. The engineer is then able to design a structure in such a manner as to have the same factor of safety in all parts of the structure. It is obvious that this latter requirement must always be fulfilled if the design is to be economical, because the ultimate strength of a structure is determined by its strength at the weakest place.

*Working Stresses for Static Conditions.*—Let us begin with a discussion of working stresses under static conditions, which is the case when a structure is subjected to constant (or nearly constant) loads. We will distinguish between two kinds of materials, *ductile materials*, especially various kinds of structural steel, and *brittle materials*, such as cast iron, stone and concrete.

In the case of ductile materials the yield point stress  $\sigma_{Y.P.}$  is usually taken as the basis for selecting the working stresses, since the large deformations which take place at yielding are not permissible in engineering structures. For a known yield point stress  $\sigma_{Y.P.}$  for a material, the factor of safety in simple tension or compression is <sup>224</sup>

$$n = \frac{\sigma_{Y.P.}}{\sigma_w} \quad (b)$$

The allowable stress  $\sigma_w$  is calculated by using eq. (a), based on the nominal stress. The stress concentrations produced by holes or grooves are usually disregarded, on the assumption that these stresses tend to equalize owing to plastic deformation at places of peak stress. Such an assumption is justified only as long as the loads are applied statically. In the case of impact action the brittle character of bars with deep grooves

<sup>224</sup> It is assumed here that  $\sigma_{Y.P.}$  is the same for tension and compression. For materials which do not have a pronounced yield point the tensile stress at which the permanent set reaches the value 0.2 per cent is usually taken for  $\sigma_{Y.P.}$ .

or sharp changes in cross section should be considered (see p. 434).

In the general case of homogeneous stress distribution we use the equivalent stress given by eq. (300), p. 536, and obtain the factor of safety from the equation

$$n = \frac{\sigma_{Y.P.}}{(\sigma_e)_W} \quad (c)$$

For two-dimensional stress distribution, with the notation  $\sigma_2/\sigma_1 = \alpha$  this equation gives

$$n = \frac{\sigma_{Y.P.}}{(\sigma_1)_W \sqrt{1 - \alpha + \alpha^2}} \quad (d)$$

In the particular case of pure shear  $\sigma_1 = -\sigma_2 = \tau$ ,  $\alpha = -1$  and we obtain

$$n = \frac{\sigma_{Y.P.}}{\sqrt{3} \tau_W} \quad (e)$$

In the case of nonhomogeneous stress distribution, as in bending or torsion, we must take into consideration the fact that the beginning of yielding in the region of maximum stress does not result in a large deformation of the entire structure. To obtain a large deformation, equivalent to the deformation of a prismatic bar at a tensile stress equal to  $\sigma_{Y.P.}$ , we have to use higher loads than those at which  $\sigma_{max}$  reaches the value  $\sigma_{Y.P.}$ . Take, for example, bending of a rectangular beam. In loading the beam, if the maximum stress in the fibers farthest from the neutral axis reaches the  $\sigma_{Y.P.}$  value, no serious plastic deformation of the beam occurs. To obtain conditions equivalent to those in a bar stretched to the tensile stress  $\sigma_{Y.P.}$ , we have to apply a bending moment 50 per cent higher than the moment at which  $\sigma_{max}$  reaches the value  $\sigma_{Y.P.}$  (see p. 349). To take account of this fact, the equation for calculating the *factor of safety in bending* is

$$n = \frac{\beta \sigma_{Y.P.}}{\sigma_W} \quad (f)$$

in which  $\beta$  is a factor depending on the shape of the cross section. It is equal to 1.5 for rectangular beams, 1.3 for thin circular tubes ( $d_1/d_0 = 0.95$ ) and depends on the cross-sectional proportions in the case of I beams (see p. 349).

Similar considerations are applicable also in the case of *torsion*, and the equation for the factor of safety in this case is

$$n = \frac{\beta_1 \sigma_Y P.}{\sqrt{3} \tau_W}. \quad (g)$$

For solid circular shafts,  $\beta_1 = 1.33$  (see p. 383). For thin circular tubes,  $\beta_1$  approaches the value 1 and eq. (g) coincides with eq. (e).

In the case of homogeneous combined normal and shearing stresses, eq. (298), p. 454, is sometimes used instead of the general eq. (d). This gives

$$n = \frac{\sigma_Y P.}{\sqrt{\sigma^2 + 3\tau^2}}. \quad (h)$$

In deriving the equation for  $n$  in the case of combined bending and torsion we have to modify eq. (h) in the same manner as was done in deriving eqs. (f) and (g). Then we obtain

$$n = \frac{\sigma_Y P.}{\sqrt{\left(\frac{\sigma}{\beta}\right)^2 + 3\left(\frac{\tau}{\beta_1}\right)^2}}. \quad (i)$$

If  $\tau$  vanishes, this equation coincides with eq. (f), and if the normal stress vanishes, it coincides with eq. (g).

It has been assumed in the above discussion that the principle of superposition holds, which means that the maximum stress is proportional to the load. Hence the factor of safety  $n$ , which was used in determining the working stress, may be applied also to the external loads. We can then state that yielding in the structure begins under a load which is  $n$  times the actual safe load. If the principle of superposition does not hold, it is necessary to apply the factor of safety to the



load and determine the dimensions of the structure in such a manner that yielding begins only if the acting loads are increased  $n$  times. The application of this method to the case of combined bending and direct stress is discussed in Art. 4 (see p. 34). This method is recommended also in the design of columns on the basis of assumed inaccuracies (see Part I, p. 27 $\frac{1}{2}$ ).

In the case of *brittle materials* the ultimate strengths in tension and compression are taken as the basis for selecting the working stresses. Local peak stresses, such as occur at grooves and holes, must be taken into consideration. The nominal stresses as obtained from the elementary formulas must be multiplied by a theoretical factor of stress concentration.<sup>22</sup> Experiments with cast iron do not show a weakening effect of grooves and holes as severe as the theoretical factor indicates. The reason for this is the nonhomogeneous character of cast iron. Various inclusions and flaws, which are always present in cast iron, act as stress raisers, and the additional peak stresses due to grooves and holes do not lower substantially the strength of the material. The introduction of stress concentration factors in the design of cast-iron structures is justified as a compensation for the poor shock resistance of the material, and the possibility of the occurrence of shock stresses in transportation and installation must always be considered. The formulas for calculating factors of safety in tension and compression are then

$$n = \frac{\sigma_{ut}}{k\sigma_w}, \quad n = \frac{\sigma_{uc}}{k\sigma_w} \quad (f)$$

in which  $\sigma_{ut}$  and  $\sigma_{uc}$  are the ultimate strengths in tension and compression, respectively. These formulas may also be used for bending.

In the case of *combined stresses* in brittle materials we use Mohr's theory (see p. 457). If  $\sigma_{max}$  and  $\sigma_{min}$  are both of the same sign we have to use eqs. (f) in calculating  $n$ . If  $\sigma_{max}$

<sup>22</sup> For stress concentration factors in various cases see Chap. 8. See also the book by R. E. Peterson, *loc. cit.*, p. 306.

and  $\sigma_{\min}$  are of opposite sign, we use eq. (h), p. 460. Denoting  $\sigma_{\min}/\sigma_{\max}$  by  $\alpha$ , we obtain

$$\left. \begin{aligned} (\sigma_{\max})_{\text{ult}} &= \frac{\sigma_{\text{ut}}}{1 - \alpha \frac{\sigma_{\text{ut}}}{\sigma_{\text{uc}}}}, \\ (\sigma_{\min})_{\text{ult}} &= \frac{\alpha \sigma_{\text{ut}}}{1 - \alpha \frac{\sigma_{\text{ut}}}{\sigma_{\text{uc}}}} \end{aligned} \right\} \quad (k)$$

For pure shear  $\sigma_{\max} = -\sigma_{\min} = \tau$ ,  $\alpha = -1$  and eqs. (k) give

$$\tau_{\text{ult}} = \frac{\sigma_{\text{ut}}}{1 + \frac{\sigma_{\text{ut}}}{\sigma_{\text{uc}}}}.$$

Then the factor of safety for torsion will be

$$n = \frac{\sigma_{\text{ut}}}{k_1 \tau_{\text{W}} \left( 1 + \frac{\sigma_{\text{ut}}}{\sigma_{\text{uc}}} \right)}, \quad (l)$$

where  $k_1$  is the theoretical stress concentration factor in torsion.

When normal and shear stresses act simultaneously, as in the case of combined bending and torsion, we have (see Part I, p. 297)

$$\sigma_{\max} = \frac{1}{2} [k\sigma + \sqrt{(k\sigma)^2 + 4(k_1\tau)^2}],$$

$$\sigma_{\min} = \frac{1}{2} [k\sigma - \sqrt{(k\sigma)^2 + 4(k_1\tau)^2}],$$

$$\alpha = \frac{\sigma_{\min}}{\sigma_{\max}},$$

where  $k$  and  $k_1$  are the theoretical stress concentration factors for bending and torsion. Now using the ultimate values (eqs. k) for the same stresses, we obtain the factors of safety for tensile and compressive principal stresses

$$\left. \begin{aligned} n &= \frac{2\sigma_{ut}}{[k\sigma + \sqrt{(k\sigma)^2 + 4(k_1\tau)^2}] \left[1 - \alpha \frac{\sigma_{ut}}{\sigma_{uc}}\right]}, \\ n &= \frac{2\alpha\sigma_{ut}}{[k\sigma - \sqrt{(k\sigma)^2 + 4(k_1\tau)^2}] \left[1 - \alpha \frac{\sigma_{ut}}{\sigma_{uc}}\right]} \end{aligned} \right\} \quad (m)$$

If  $\tau = 0$ , these equations coincide with eqs. (j), and if  $\sigma = 0$ , we obtain eq. (l).

*Working Stresses for Alternating Loads.*—In the case of alternating loads the value of the endurance limit  $\sigma_E$  of the material is taken as the basis for calculating the factor of safety. Beginning with ductile materials we take for uniaxial stress conditions the equation

$$n = \frac{\sigma_E}{k_f \sigma_w} \quad (n)$$

Since stress concentrations have a great influence on the fatigue strength of ductile materials, the factor  $k_f$  is introduced in eq. (n). This factor is somewhat smaller than the theoretical factor of stress concentration (see p. 495) and can be obtained from the fatigue test results given in Fig. 327 or may be calculated by using the curves of Fig. 328.

In the case of a two-dimensional stress distribution the ultimate value of maximum stress is (see p. 481)

$$\sigma_{\max} = \frac{\sigma_E}{\sqrt{1 - \alpha + \alpha^2}} \quad (o)$$

Using this expression, we find for torsion ( $\alpha = -1$ )

$$n = \frac{\sigma_E}{\sqrt{3} k_f' \tau_w} \quad (p)$$

where  $k_f'$  is obtained from torsional fatigue tests or from the curves in Fig. 328. In the case of combined bending and torsion we obtain

$$n = \frac{\sigma_E}{\sqrt{(k_f \sigma)^2 + 3(k_f' \tau)^2}} \quad (q)$$

For  $\sigma = 0$  this equation coincides with eq (p), and for  $\tau = 0$  it coincides with eq (n)

For the case of *brittle materials* there exists only sparse experimental information. In order to be on the safe side the full theoretical factors of stress concentration are usually applied in formulas for calculating factors of safety. For uniaxial stress conditions we then have

$$n = \frac{\sigma_E}{k\sigma_W} \quad (r)$$

For torsion, using Mohr's theory, we obtain

$$n = \frac{\sigma_E}{k_1\tau_W \left(1 + \frac{\sigma_{ut}}{\sigma_{uc}}\right)} \quad (s)$$

For combined bending and torsion we have

$$n = \frac{2\sigma_E}{[k\sigma + \sqrt{(k\sigma)^2 + 4(k_1\tau)^2}] \left[1 + \alpha \frac{\sigma_{ut}}{\sigma_{uc}}\right]}, \quad (t)$$

where  $\alpha$  is the ratio of the smaller to the larger of the amplitudes of the two principal stresses

*Combined Alternating and Steady Stresses*—The limiting stress conditions in such cases are defined by the curves shown in Figs 315 and 316. In our further discussion we will limit our attention to the case in which cycles of stress are superposed on steady tensile stress. This case is the one most likely to be encountered in practical applications, and a sufficient amount of experimental information is available.

Starting with the case of *ductile materials* the limiting conditions for specimens without stress concentrations are represented by curves *BCA* and *DFA* in Fig 362, for 0.7 per cent carbon steel. Point *A* represents the stress  $\sigma_{ut}$ . The curves *B<sub>1</sub>C<sub>1</sub>A* and *D<sub>1</sub>F<sub>1</sub>A* are obtained for *notched* specimens. It is seen that owing to stress concentrations the range of the cycles of stress is somewhat reduced, while the mean stress remains unchanged. On the basis of such experimental data, it is established practice in machine design to apply the stress con

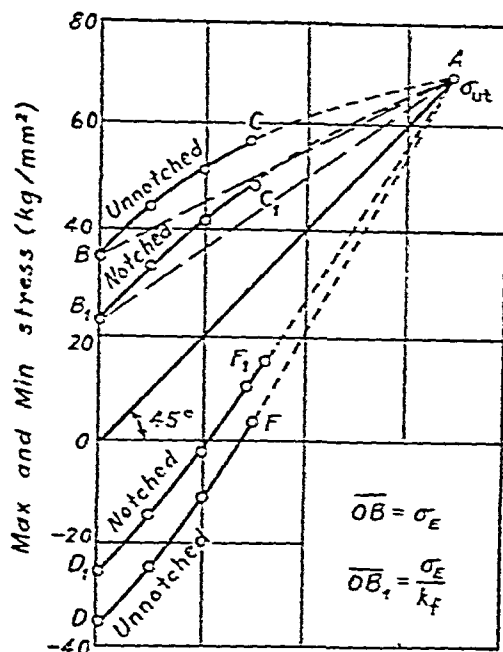


FIG. 362.

centration factor to the alternating component of stress, but not to the steady component.

It is also the usual practice to replace the curves  $BCA$  and  $B_1C_1A$  by straight lines (shown dashed in Fig. 362). For our further discussion we can then use triangles  $OBA$  and  $OB_1A$  of Fig. 363, in which the abscissas give the steady component

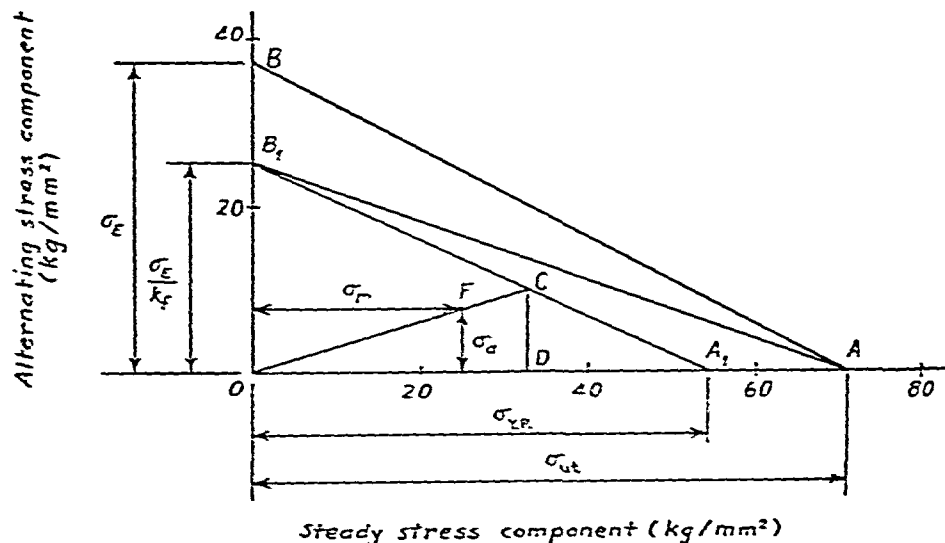


FIG. 363.

of stress  $\sigma_m$  and the ordinates give the alternating component  $\sigma_a$ . Since for steady stress and for ductile materials the stress  $\sigma_{YP}$  was taken previously as the basis for selecting working stresses, we replace point  $A$  by point  $A_1$  having  $\sigma_{YP}$  as abscissa. The line  $B_1A_1$  is considered to define the limiting stress condition for a specimen with stress concentrations.<sup>226</sup> If the steady stress on the specimen is given by the abscissa  $OD$ , Fig. 363, then the limiting amplitude of the alternating stress is given by the ordinate  $DC$ , and point  $C$  will represent the limiting stress condition. The corresponding safe condition will be represented by point  $F$  with coordinates  $\sigma_m$  and  $\sigma_a$ . These coordinates are obtained by dividing the coordinates of point  $C$  by the factor of safety  $n$ . From the similarity of triangles  $OB_1A_1$  and  $DCA_1$  we have

$$\frac{\overline{CD}}{\sigma_E/k_f} = \frac{\overline{DA}}{\sigma_{YP}} = \frac{\sigma_{YP} - \overline{OD}}{\sigma_{YP}}$$

or

$$\frac{\overline{CD}}{\sigma_E/k_f} + \frac{\overline{OD}}{\sigma_{YP}} = 1.$$

Dividing this equation by  $n$ , we obtain for the safe stress condition (point  $F$ )

$$\frac{\sigma_a}{\sigma_E/k_f} + \frac{\sigma_m}{\sigma_{YP}} = \frac{1}{n},$$

or

$$n = \frac{1}{k_f \frac{\sigma_a}{\sigma_E} + \frac{\sigma_m}{\sigma_{YP}}} \quad (u)$$

This is the expression for the factor of safety in the case of uniaxial stress conditions with stress concentrations.<sup>227</sup>

<sup>226</sup> This change is in the direction of increasing safety.

<sup>227</sup> Since we are discussing here fatigue failures which occur without plastic deformation, we may also use eq (u) for bending, without introducing the factor  $\beta$  which was used in eq (f). The form (eq u) of the equation for  $n$  was suggested by C. R. Soderberg, *Trans. A.S.M.E.*, Vol. 52, APM 52-2, 1930

In the case of combined stresses the equivalent stresses for  $\sigma_a$  and  $\sigma_m$  should be substituted<sup>228</sup> in eq. (u). For two dimensional stress conditions we then obtain

$$n = \frac{1}{\left[ k_f \frac{(\sigma_1)_a}{\sigma_E} + \frac{(\sigma_1)_m}{\sigma_{Y.P.}} \right] \sqrt{1 - \alpha + \alpha^2}}. \quad (v)$$

Applying this equation to the case of torsion, we have  $\sigma_1 = \tau$ ,  $\alpha = -1$  and using  $k_f'$  instead of  $k_f$  we obtain

$$n = \frac{1}{\sqrt{3} \left( k_f' \frac{\tau_a}{\sigma_E} + \frac{\tau_m}{\sigma_{Y.P.}} \right)}. \quad (w)$$

For the combined action of bending and torsion the factor of safety is obtained from the equation

$$n = \frac{1}{\sqrt{\left( k_f \frac{\sigma_a}{\sigma_E} + \frac{\sigma_m}{\sigma_{Y.P.}} \right)^2 + 3 \left( k_f' \frac{\tau_a}{\sigma_E} + \frac{\tau_m}{\sigma_{Y.P.}} \right)^2}}. \quad (x)$$

If bending acts alone,  $\tau_a$  and  $\tau_m$  vanish and this equation coincides with eq. (u). When  $\sigma_a$  and  $\sigma_m$  vanish, the equation coincides with eq. (w). When  $\sigma_m$  and  $\tau_m$  vanish, we have complete reversal of stresses and the equation coincides with eq. (q).<sup>229</sup>

For *brittle materials* there is little experimental information regarding the action of combined alternating and steady stresses. Introducing  $\sigma_{ut}$  instead of  $\sigma_{Y.P.}$  and using theoretical stress concentration factors  $k$  and  $k_1$ , instead of the reduced factors  $k_f$  and  $k_f'$ , we obtain for uniaxial stress conditions

$$n = \frac{1}{k \left( \frac{\sigma_a}{\sigma_E} + \frac{\sigma_m}{\sigma_{ut}} \right)}. \quad (y)$$

<sup>228</sup> It is assumed that the ratios  $\sigma_1:\sigma_2:\sigma_3$  remain constant during the stress cycles.

<sup>229</sup> Eq. (x) is also used in cases where the ratio of the principal stresses  $\sigma_1/\sigma_2$  changes during a cycle.

TABLE 26: MECHANICAL PROPERTIES OF STEELS

Source	Material, %	State	Prop Limit lb/in <sup>2</sup>	Yield Point lb/in <sup>2</sup>	Ult Strength lb/in <sup>2</sup>	Elong (2 in. gage) %	Reduction in Area %	Endurance Limit lb/in <sup>2</sup>	Remarks
1	37 C, .55 Mn	Annealed at 850° C	36,500	37,800	70,000	32	49	±29,000	Bar 2 $\frac{1}{2}$ in diameter
		Normalized at 850° C	38,000	41,500	79,200	29	46	±29,300	
		Heat treated, water at 850° C, temp at 550° C	65,000	69,000	105,000	22	56	±51,000	
2	49 C, 46 Mn	Normalized at 910° C	44,700	47,100	91,500	27	40	±33,000	Bar 1 $\frac{1}{2}$ in sq
		Heat treated, oil at 790° C, temp at 430° C	75,800	78,800	121,800	11.3	51	±64,000	
1	.35 C, .45 Mn, 3.4 Ni	Rolled	47,000	60,000	105,000	21	42	±41,000	Plate 3 $\frac{1}{2}$ ft × 2 ft × 2 in
		Annealed at 840° C	52,000	60,000	104,000	22	49	±44,000	
		Normalized at 840° C, temp at 730° C	52,000	56,000	94,000	25	48	±47,500	
2	24 C, 37 Mn, 3.3 Ni, 87 Cr	Heat treated, water at 800° C, temp at 600° C	72,000	77,000	107,000	23	56	±52,000	Bar 2 in × 1 in
		Annealed at 780° C	56,700	60,000	87,000	33	67	±49,000	
		Heat treated, oil 830° C	115,000	128,000	138,000	18	62	±68,000	
3	30 C, 56 Mn, 4.3 Ni, 1.4 Cr	Air hardened from 800° C	45,000	177,000	244,000	10.8	37	±102,000	Bar 1 $\frac{1}{2}$ in diameter
		Air hardened from 800° C, temp 600° C	92,000	142,000	157,000	17.5	55	±80,000	
1	32 C, 74 Mn, 37 Si	Cast	20,000	33,500	76,000	26	34	±30,500	Bar 2 $\frac{1}{4}$ in × 1 $\frac{1}{4}$ in
		Annealed at 925° C	37,000	41,000	80,000	27	40	±35,000	
		Normalized at 925° C	40,500	46,000	85,000	28	46	±35,000	

Source 1 Research Laboratory, Westinghouse Elec Corp See S Timoshenko and J M Lessells, *Applied Elasticity*, p 522, 1924  
 2 H F Moore and T Jasper, *Univ of Illinois Eng Exp Sta Bul*, No 136, p 33  
 3 L. Atchison, *Engineering Steels*, p 209, 1921



For torsion, using Mohr's theory, we obtain

$$n = \frac{1}{k_1 \left( \frac{\tau_c}{\sigma_E} + \frac{\tau_{cr}}{\sigma_{ut}} \right) \left( 1 + \frac{\sigma_{ut}}{\sigma_{uc}} \right)} \quad (z)$$

In the preceding discussion it has been assumed that the dimensions are determined by strength considerations only. There are sometimes additional requirements which must be considered in design. There are cases in which a limiting deflection is prescribed and must be taken as a basis for calculating the dimensions. The deflection is of great importance in cases where the vibration of the system is to be considered. Shafts must sometimes satisfy requirements regarding the angle of twist per unit length.

In the case of structures subjected to the action of high temperatures the design must be based on the assumption of a certain duration of service of the structure and of a certain amount of deformation which can be considered as permissible. The working stresses are chosen so that the deformation of the structure during its lifetime will not exceed a definite limit depending on the type of structure (see Art. 91).

In the case of slender bars and thin-walled structures the question of elastic stability (see Chap. 5) must be considered in selecting the working stresses.

From all this discussion it may be seen that the choice of working stresses is a very important problem and at the same time a very complicated one. In establishing the safety factor  $n$  the designer must always be guided by past experience. The above discussion giving a comparison of the working stresses for various stress conditions is not intended to replace the use of past experience, but may be helpful in interpreting this experience and in arriving at a design which is equally strong in all its parts. It may also be useful in making comparisons of different designs and in comparing the strengths of existing structures. The investigation of actual failures in the light of the above theoretical discussion forms a very useful method for acquiring a deeper knowledge of the strength of struc-

tures.<sup>230</sup> Combining analyses of failures with theoretical investigations of stress distributions and with laboratory investigations of the strength of materials under various stress conditions will enable us to accumulate a more reliable knowledge of the actual strength of structures. When we have such knowledge, the present specifications for working stresses in various branches of engineering can be considerably improved. This will without doubt result in an economy of material and in greater reliability for structures and machines.

---

<sup>230</sup> In this respect such publications as *Technical Reports*, British Engine, Boiler, El Insurance Co. are of great practical importance.

## AUTHOR INDEX

- Aitchison, L., 558  
 Almen, J. O., 144  
 Anderson, C. G., 381  
 Archer, R. S., 423  
 Arnold, S. M., 500  
 Attla, H. H., 497  
 Axelson, K., 128  
  
 Bach, C., 417, 436, 437, 462  
 Bailey, R. W., 521, 526, 527, 534, 537  
 Bairstow, L., 510  
 Baker, J. F., 349, 351, 362  
 Barker, L. H., 233  
 Baron, F. M., 252  
 Barrett, C. S., 381  
 Basquin, O. H., 474  
 Baugher, J. W., 212  
 Bauschinger, J., 413, 475, 509  
 Bauschlicher, A., 341  
 Becker, A. J., 444  
 Behrens, O., 488  
 Belajef, N. M., 339, 344  
 Bell, H. C., 141  
 Beltrami, 448  
 Benscoter, S. U., 254  
 Beschkine, L., 65  
 Beskin, L., 305  
 Biezeno, C. B., 138, 223  
 Biot, M. A., 1  
 Bleich, F., 178, 182  
 Boas, W., 397, 404, 405  
 Böker, R., 462  
 Boobnov, I. G., 20, 78  
 Boone, W. D., 486  
 Boussinesq, J., 312  
 Boyd, J., 530  
 Bradley, J., 486  
 Brecht, W. A., 144  
 Bredt, R., 248  
 Bresse, M., 188  
 Brewster, D., 333  
 Bridgman, P. W., 432, 438, 439  
  
 Brown, A. L., 442  
 Brown, R. M., 483  
 Brown, S. J., 390  
 Bryan, G. H., 195  
 Buchholtz, H., 489  
 Buckley, 288  
 Bühler, H., 392, 489  
 Bunyon, T. W., 497  
 Burges, R. W., 151  
 Byerly, 47  
  
 Carrington, H., 100  
 Cazaud, R., 470  
 Chabloz, E., 102  
 Charpy, M., 398  
 Cherniak, G. S., 541  
 Chien, W. Z., 265  
 Chitty, L., 330  
 Christensen, N. B., 265  
 Chwalla, E., 65, 188, 198, 199  
 Clapeyron, 208  
 Clark, J. F., 354  
 Clausen, I. M., 141  
 Clebsch, 107  
 Coates, W. M., 128  
 Codron, C., 112  
 Coffin, L. F., 128, 541  
 Coker, E. G., 310, 334  
 Cook, G., 131, 190  
 Cottrell, A. H., 410  
 Cox, H. L., 68, 456  
 Crumbiegel, J., 330  
  
 Davidenkov, N. N., 381, 392, 399, 419,  
     432, 465, 468, 470  
 Davis, E. A., 442  
 Davis, H. E., 433, 444  
 de Forest, A. V., 333  
 Dehlinger, U., 456  
 Demorest, D. J., 381  
 Den Hartog, J. P., 312  
 Dietrich, 333

- Dinnik, A N , 169, 188  
 Domke, O , 151  
 Donath, M , 224  
 Donnell, L H , 220, 424  
 Driessen, M G , 224  
 Drucker, D C , 339  
 Dryden, H L , 485  
 Dusold, T , 488  
  
 Ebner, H , 68  
 Eck, B , 102  
 Eichelberg, G , 234  
 Eichinger, A , 374, 393, 441, 455, 470  
 Elam, C F , 404, 410  
 Ellis, G , 333  
 Engesser, F , 173, 180  
 Ensslin, M , 112  
 Euler, L , 146  
 Everett, F L , 534  
 Ewing, J A , 421, 512  
  
 Fairbairn, W , 194, 474  
 Faulhaber, R , 498  
 Favre, H , 102, 334  
 Filon, L N G , 334  
 Fischer, A , 223  
 Flanagan, A E , 433  
 Föppl, A , 246, 318, 342, 436, 451  
 Föppl, L , 451  
 Föppl, O , 412, 488, 501  
 French, H J , 484  
 Frenkel, J , 410  
 Freudenthal, A M , 485  
 Fritzsche, J , 354  
 Frocht, M M , 307, 326, 334  
 Fromm, H , 344  
 Fry, A , 333  
 Fuller, T S , 488  
  
 Garabedian, G A , 107  
 Gehler, W , 436  
 Gerber, W , 475  
 Girkmann, K , 65, 354  
 Girtler, 448  
 Göhner, O , 292  
 Goodier, J N , 234, 279, 500  
 Gough, H J , 470, 476, 480, 481, 482, 488,  
     500, 511, 512, 513  
 Grammel, R , 138, 221, 223, 224  
  
 Greenberg, H J , 355  
 Greenhill, A G , 312  
 Griffith, A A , 237, 311, 395  
 Gross, S , 144  
 Grüneisen, 437  
 Guernsey, R , 334  
 Guest, J J , 447  
 Gurney, C , 305  
 Guy, H L , 517  
  
 Hadji Argyris, J , 68  
 Haugh, B P , 448, 476, 487, 493  
 Halliwell, 521  
 Halphen, 151  
 Hanslip, R E , 392  
 Hanson, D , 512  
 Hartmann, E C , 183  
 Hartmann, L , 418  
 Hayashi, 1  
 Hearle, H , 224  
 Held, A , 224  
 Hempel, M , 479  
 Hencky, H , 101, 105, 220  
 Hendry, A W , 60  
 Hensel, F R , 526  
 Herbert, H , 366  
 Hertz, H , 339  
 Hetényi, M , 1, 15, 53, 310, 333, 339,  
     500  
 Heywood, R B , 497  
 Hodgkinson, E , 194  
 Hodgkinson, B , 223  
 Höhn, E , 128  
 Holmberg, E O , 128  
 Holt, M , 183  
 Honegger, C , 220  
 Hopkinson, B , 511  
 Horger, O J , 212, 381, 483, 498, 500, 502,  
     504  
 Horvay, G , 141  
 Housner, G W , 530  
 Huber, K , 255  
 Huber, M T , 451  
 Huggenberger, A , 128, 212  
 Hughes, F A , 404  
 Humfrey, J C W , 512  
 Hummel, 330  
 Hurlbrink, E., 188  
 Huth, J H , 317

- Inglis, C. E., 306  
 Inglis, N. P., 483, 486  
  
 Jacob, L., 390  
 Jacobsen, L. S., 318  
 Janicki, W., 212  
 Jasper, T. M., 483, 585, 486, 558  
 Jeffries, Z., 423  
 Jenkin, C. F., 416, 485  
 Jensen, V. P., 343  
 Joffe, A. F., 397, 407, 463  
 Johnson, A. E., 534  
 Johnston, B. G., 246  
 Johnston, R. S., 333  
 Jonassen, F., 463  
  
 Kalakoutzky, N., 392  
 Kappus, R., 279, 281  
 Kármán, T. von, 65, 152, 265, 440, 462  
 Kawamoto, 480  
 Kayser, H., 333  
 Kent, C. H., 137  
 Kerr, 517  
 Kirkaldy, D., 434  
 Kirsch, 301  
 Kist, N. C., 354  
 Koerber, F., 333  
 Kollbrunner, C. F., 188  
 Kolosoff, G., 306  
 Kommers, J. B., 470, 483, 485, 489  
 Körber, F., 426  
 Köster, W., 419  
 Krouse, G. N., 486  
 Krylov, A. N., 268  
 Kuhn, P., 68, 485  
 Kühnel, R., 301  
  
 Lake, G. F., 224  
 Lamb, H., 77  
 Lamé, 208  
 Landsberg, D., 334  
 Langer, B. F., 1, 485  
 Larmour, J., 312  
 Larsen, E. I., 526  
 Laszlo, A., 144  
 Laszlo, F., 220  
 Lees, C. H., 233  
 Leeser, D. O., 381  
 Lehmann, G. D., 485  
  
 Lehr, E., 306, 333, 511  
 Lessells, J. M., 558  
 Leven, M. M., 326  
 Lévy, M., 535  
 Lewe, V., 117  
 Lipson, C., 493  
 Lobo, G., 113  
 Lode, W., 441  
 Lorenz, R., 131  
 Ludwik, P., 400, 419, 427, 430, 431, 433, 434  
 Lueders, W., 418  
 Lyon, S. W., 483, 486  
 Lyse, I., 246  
  
 MacCullough, G. H., 347, 527  
 MacGregor, C. W., 128, 429, 470, 481, 489  
 Maier, A. F., 481  
 Maier-Leibnitz, 354  
 Malkin, I., 223  
 Manjoine, M. J., 418  
 Marin, J., 393, 438, 447, 522, 527, 532  
 Martin, G., 489  
 Martin, H. M., 223  
 Masing, G., 423  
 Mattimore, J. D., 141  
 Maulbetsch, J. L., 502  
 Maunsell, F. G., 307  
 Maxwell, J. C., 333, 451  
 Mayer, E., 366  
 McAdam, D. J., 471, 487, 488  
 McGivern, J. G., 312  
 McVetty, 520  
 Meissner, E., 127  
 Mellanby, 517  
 Memmler, K., 152  
 Mesnager, A., 334, 428  
 Metzger, W., 65  
 Mitchell, A. G. M., 199  
 Mitchell, J. H., 318  
 Miller, J. A., 330  
 Mindlin, R. D., 317  
 Miner, M. A., 485  
 Mises, R. von, 151, 193  
 Mohr, O., 457  
 Moore, H. F., 470, 483, 484, 485, 486, 487, 489, 558  
 Muir, I., 423  
 Murray, W. M., 463

- Nadai, A , 105, 220, 381, 386, 418, 424,  
     441, 444, 530  
 Nagel, A , 234  
 Navier, 366  
 Neal, B G , 354, 363  
 Neifert, H R , 498, 504  
 Nelson, C W , 212  
 Neuber, H , 309, 325  
 Neumann, F E , 333  
 Newell, J S , 40  
 Nicolai, E L , 189  
 Niles, A S , 40, 279  
 Nishihara, 480  
 Nusselt, W , 234  
  
 Odqvist, F K G , 537  
 Olsson, R G , 224  
 Orowan, E , 398, 465, 515  
 Osgood, W R , 372, 489  
 Ostenfeld, A , 255  
  
 Papkovitch, P F , 20  
 Pardue, T E , 418  
 Parker, E R , 433, 444  
 Parkes, E W , 57  
 Parr, S W , 426  
 Pasternak, I  
 Pearson, K , 381, 386  
 Perry, I , 294  
 Peterson, R E , 306, 327, 338, 398, 478,  
     479, 480, 490, 394, 498, 502  
 Pfeiderer, 112  
 Phillips, C E , 497  
 Pichler, O , 102  
 Pilling, 521  
 Pippard, A J S , 330  
 Poisson, 92  
 Polanyi, M , 423  
 Pollard, H V , 480, 482  
 Pomp, A , 426, 479  
 Popov, E P , 530, 541  
 Poschl, T , 128  
 Prager, W , 1, 355  
 Prandtl, L , 173, 199, 237, 410, 436  
 Prescott, T , 248  
 Pretschner, W , 279  
 Preuss, E , 330  
  
 Quednau, H , 234  
 Quinney, H , 438, 442  
  
 Rees, 423  
 Reissner, E , 65, 68  
 Reissner, H , 65, 128, 195, 265  
 Richards, C W , 420  
 Rinne, 436  
 Rode, R V , 485  
 Roderick, J W , 351  
 Roos, J O , 470  
 Roš, M , 441, 470  
 Roth, 449  
 Rotscher, F , 330  
 Rowett, 412  
 Runge, C , 128  
 Russell, G M , 100  
 Russell, H W , 484, 486  
  
 Saalschütz, 151  
 Sachs, G , 392, 437, 456  
 St Venant, 107, 235, 294, 366, 381, 386,  
     535  
 Sanden, K von, 1, 131  
 Sawin, G N , 306  
 Scheffler, H , 126  
 Scheu, R , 419, 434  
 Schilhansl, M , 112  
 Schleicher, F , 1, 444  
 Schmid, E , 397, 404, 405  
 Schreiber, W , 392  
 Schulz, E H , 489  
 Schuster, L W , 490  
 Schwinning, 341  
 Scoble, W A , 447  
 Searle, G F C , 77  
 Shanley, F R , 184  
 Shearer, G W , 294  
 Shepler, P R , 541  
 Siebel, E , 333  
 Slater, A , 117  
 Smith, C A , 447  
 Smith, G V , 517  
 Smith, J B , 442  
 Smith, R C , 418  
 Smith Petersen, N O , 141  
 Sneddon, I N , 311  
 Soderberg, C R , 527, 537, 554  
 Sonntag, R , 318  
 Sopwith, D G , 456, 488  
 Soroka, W W , 317  
 Southwell, R V , 189

- Steierman, I. J., 339  
 Stodola, A., 223, 330  
 Stokey, W. F., 333  
 Straub, F. G., 426  
 Stribeck, 341  
 Sturm, R. G., 183  
 Stüssi, F., 265  
 Symonds, P. S., 354, 363  
  
 Tait, 294, 312  
 Tapsell, H. J., 486, 517, 525, 527, 534  
 Taylor, G. I., 237, 410, 438, 442  
 Taylor, J. H., 112  
 Templin, R. L., 183  
 Terzaghi, K., 128  
 Thomas, W. N., 489  
 Thomson, W. (Lord Kelvin), 294, 312, 405  
 Thorpe, P. L., 500  
 Thum, A., 490, 496, 501  
 Timoshenko, S., 1, 8, 47, 54, 77, 90, 161, 173, 188, 189, 190, 195, 198, 199, 202, 203, 246, 255, 267, 273, 277, 279, 305, 331  
 Todhunter, I., 381, 386  
 Tomlinson, G. A., 500  
 Trefftz, E., 317  
 Trumpler, W. E., 113  
 Turner, L. B., 386, 447  
 Tuzi, Z., 334, 336  
  
 Ude, H., 496  
 Unwin, 475  
  
 Van den Broek, J. A., 355  
 Van der Fleet, A. P., 33  
 Versé, G., 518  
 Vigness, I., 418  
 Vlasov, V. Z., 279  
 Voropaev, M. A., 331  
  
 Wagner, H., 278, 279  
 Wahl, A. M., 113, 144, 327, 338, 493, 502  
 Waner, N. S., 317  
 Waters, E. O., 112, 141  
 Way, S., 84, 505, 506  
 Weber, C., 236, 255, 288  
 Wehage, 447  
 Weibel, E. E., 489  
 Weibull, W., 399, 498  
 Welcker, W. A., 484, 486  
 Weller, R., 339  
 Westergaard, H. M., 47, 117, 317, 444  
 Westphal, M., 131  
 Wever, F., 489  
 Wiegand, H., 500  
 Wieghardt, 1  
 Wilhelm, R. B., 517  
 Willers, F. A., 318  
 Williams, G. T., 511  
 Wilson, C., 334  
 Wilson, J. S., 493  
 Wilson, W. M., 343  
 Winkler, E., 1  
 Wiseman, H. A. B., 438  
 Wishart, H. B., 486  
 Wittman, F. F., 468  
 Wöhler, A., 378, 475  
 Wunderlich, F., 501  
 Wyss, T., 330  
  
 Young, D. H., 178  
 Young, Thomas, 288  
  
 Zander, W., 489  
 Zariiev, K. S., 35  
 Zener, C., 412  
 Zimmermann, H., 1, 37  
 Zulzer, R., 234  
 Zwicky, F., 398

## SUBJECT INDEX

*Numbers refer to pages*

- Alternating loads, safety factor for, 551
- Analogy, electric, 318
  - hydrodynamical, 312
  - membrane, 237, 244, 248, 314, 385
- Angle section, torsion of, 244, 267
  - stress concentrations in, 317
- Annealing, effect of, 423, 424, 521
- Arch, buckling of, 188
- Area-moment method, 352
- Axial loads on beams, 26-56
- Axial stress due to torsion, 286
  
- Ball bearings, contact stresses in, 339
- Bauschinger effect, 413, 416
- Bauschinger's extensometer, 430
- Beam deflections, beyond the elastic limit, 352, 375
  - by trigonometric series, 46
  - with initial curvature, 54
- Beams, bending at high temperature, 527
  - bending beyond the elastic limit, 346, 366, 374, 377
  - box, 68, 250
  - lateral buckling of, 199
  - limit design of, 354
  - local stresses in, 57, 324
  - of variable cross section, 62
  - on elastic supports, 20
  - shearing stresses in, 62
  - stress concentrations in, 324
  - ultimate moment for, 348-353
  - ultimate strength of, 354
  - with axial loads, 26-56
  - with initial curvature, 54
  - with thin flanges, 64
  - yield moment for, 347
- Beams on elastic foundation, 1-25
  - finite length, 15
  - infinite length, 1
  - semi-infinite length, 11
- Beams with axial and lateral loads, 26-56
- Belleville spring, 143
- Bending of a spring, 296
- Bending of beams (also see *Beams*)
  - at high temperature, 527
  - beyond the elastic limit, 346, 366, 374, 377
  - combined with torsion, 267
  - factor of safety for, 547
  - stress concentrations in, 324
- Bending of continuous struts, 37
- Bending of plates (see *Plates*)
- Body-centered cubic cell, 403
- Boils, stress relaxation in, 531
- Box beam, bending of, 68
  - torsion of, 250
- Brittle lacquer method, 333, 418
- Brittle materials, factor of safety for, 549
  - fracture of, 430, 462
  - Mohr's theory for failure of, 457, 482
  - size effect in, 398
  - stress concentrations in, 311
  - tensile test of, 395
- Brittleness temperature, 463-470
- Buckling, 145-204
  - by combined torsion and bending, 279
  - due to distributed load, 167
  - effect of shear on, 171
  - energy method for, 161
  - inelastic, 178
  - lateral, 199
  - of an arch, 188
  - of bars, 145
  - of beams laterally, 199
  - of continuous struts, 155
  - of latticed struts, 173
  - of members with variable cross section, 169
  - of plates, 193
  - of rectangular frames, 157



- Buckling, *cont*  
     of rings, 186  
     of shells and tubes, 189  
     of webs of plate girders, 197  
     torsional, 273, 279
- Cell structure of crystals, 403
- Channel section, stress concentrations in, 317  
     torsion of, 244, 260, 264
- Circular arch, buckling of, 188
- Circular hole, in a plate, 109  
     in a shaft, 312  
     in a tube, 305  
     in rotating disc, 215  
     in tension member, 301, 307  
     with a bead, 305
- Circular membrane, 101
- Circular plates, 92-114  
     concentrically loaded, 107  
     large deflections of, 101  
     of variable thickness, 102  
     shear deflection of, 100  
     symmetrically loaded, 92  
     uniformly loaded, 96  
     with a hole, 109  
     with concentrated load, 103
- Circular ring, buckling of, 186  
     twist of, 138
- Circular tubes, buckling of, 189
- Cohesive fracture, 430
- Cold rolling of surface, 501
- Cold working, effect in tension, 420  
     effect on endurance limit, 483, 503
- Columns, 145-186  
     effect of shear, 171  
     energy method for, 161  
     inelastic buckling of, 178  
     latticed, 173  
     of variable cross section, 169  
     torsional buckling of, 273, 279  
     with distributed axial load, 167
- Combined axial and lateral load, 26-56
- Combined bending and torsion, 267
- Combined bending and torsional buckling, 279
- Combined stresses, creep under, 533-543  
     factor of safety for, 549  
     fatigue under, 549  
     tests under, 438-444
- Compression tests, 435-444
- Concentrated load on a beam, 57
- Concentration of stress (see *Stress concentration*)
- Concrete, compression test of, 436  
     tensile test of, 310
- Conical ring, 143
- Conical vessel, 119
- Contact stresses, 339
- Continuous struts, bending of, 37  
     buckling of, 155
- Corrosion, 426
- Corrosion fatigue, 487
- Creep, 519-543  
     curves for, 520-526  
     in rotating disc, 541  
     in thick pipes, 538  
     in thin pipes, 537  
     in torsion, 537  
     under combined stresses, 533-543
- Creep rate, 520
- Critical load, 145-204  
     by energy method, 161  
     effect of shear on, 171  
     for combined bending and torsional buckling, 279  
     for inelastic buckling, 178  
     for torsional buckling, 273  
     (also see *Buckling and Columns*)
- Critical pressure, for an arch, 188  
     for a ring, 186  
     for a tube, 189
- Critical temperature, 463-470
- Crystals, fracture of, 430  
     modulus of elasticity of, 405  
     plastic stretching of, 407  
     structure of, 403  
     tensile tests of, 397, 403-410, 463
- Cubic cell, 403
- Cup and cone fracture, 431
- Curvature, initial, beams with, 54  
     plates with, 84
- Curvature (see *Beams and Plates*)
- Cylinders, compound, 210  
     contact stresses between, 339  
     creep in, 538  
     local stresses in, 124  
     plastic deformation of, 386  
     rotating, 219  
     thermal stresses in, 228

- Cylinders, *cont.*  
   thick-walled, 205  
   thin-walled, 121, 124, 134, 189  
 Cylindrical bending of a plate, 76  
 Cylindrical shell, 121, 124, 134  
   buckling of, 189  
   with reinforcing ring, 130, 132  
  
 Damage curve, 484  
 Damping, 407  
 Deflection of beams (also see *Beams*)  
   beyond the elastic limit, 352, 375  
   by trigonometric series, 46  
   on elastic foundation, 1-25  
   with axial and lateral loads, 26-56  
   with initial curvature, 54  
 Deflection of a spring, 292  
 Deflection of plates (see *Plates*)  
 Disc, rotating, 214, 223  
   creep in, 541  
 Discontinuity stresses in shells, 124  
 Dislocation, 410  
 Distortion energy theory, 441, 451-456, 480  
 Dovetail joint, 310  
 Drum, rotating, 129  
 Ductile materials, factor of safety for, 546  
   stress concentrations in, 311  
   tensile test of, 400  
   theories of failure for, 444  
 Ductility, 402  
  
 Effective elongation, 427  
 Effective width of thin flanges, 64  
 Elastic aftereffect in tensile tests, 406  
 Elastic foundation, beams on, 1-25  
 Elastic hysteresis, 407  
 Elastic limit, 413  
 Elastic stability (see *Buckling*)  
 Electric analogy for torsion, 318  
 Elliptic hole, in glass, 396  
   in tension member, 306  
   in twisted shaft, 313  
 Elliptic shaft, torsion of, 235  
 Elongation, effective, 427  
   unit, 427  
 Endurance limit, 470-489, 558  
   factors affecting the, 483  
   for combined stress, 480  
  
 Endurance limit, *cont.*  
   for ferrous metals, 474  
   for reversed stress, 475  
   in bending, 471  
   in torsion, 479  
 Endurance test, 470  
 Energy method for critical loads, 161  
 Energy theory of failure, 448  
 Equivalent T-beam, 66  
 Extensometer, Bauschinger's, 430  
  
 Face-centered cubic cell, 403  
 Factor of safety, 544-557  
   for bending, 547  
   for brittle materials, 549  
   for combined stresses, 549  
   for ductile materials, 546  
   for torsion, 548  
 Failure theories, 444-462  
   for brittle materials, 457  
   for ductile materials, 444  
 Fatigue, 470-516  
   and stress concentrations, 489  
   causes of, 509  
   corrosion, 487  
   factors affecting, 483  
   size effect in, 498  
   surface, 505  
   under combined stresses, 479  
 Fatigue failure, 473  
   examples of, 490  
   surface, 505  
 Fillets, stress concentrations due to, 306, 318, 326  
 Flange of a pipe, stresses in, 141  
 Flanges, effective width of, 64  
 Flexural rigidity of a plate, 77  
 Foundation modulus, 1  
 Fracture, cohesive, 430  
   cup and cone, 431  
   examples of, 490  
   fatigue, 473  
   of brittle materials, 430, 462  
   of crystals, 430  
   of steel, 430  
   shear, 430  
   tensile, 430-435  
 Frames, rectangular, buckling of, 157  
   ultimate strength of, 362  
 Friction, internal, 407, 411

- Gears, fatigue failures in, 492, 508  
 Gerber's law, 475  
 Girders, buckling of webs of, 197  
 Glass, tensile test of, 395  
     stress concentrations in, 311  
 Goodman law, 476  
 Grooved specimens, tests of, 434  
 Grooves, stress concentrations due to, 306,  
     312, 325  
  
 Hardening, strain, 408, 423, 525  
 Helical spring, 292  
 Hexagonal shaft, torsion of, 236  
 High temperature, bending of beams at,  
     527  
     properties of materials at, 516  
 Hinge, plastic, 351  
 Hole, circular, in a plate, 109  
     in a shaft, 312  
     in a tube, 305  
     in rotating disc, 215  
     in tension member, 301, 307  
     with a bead, 305  
 Hole, elliptical, 306, 313, 396  
 Hydrodynamical analogy, 312  
 Hydrostatic pressure, tests under, 438  
 Hyperbolic notches, 309, 325  
 Hysteresis loop, 407, 511  
  
 I beams, lateral buckling of, 199  
     stress concentrations in, 317  
     torsion of, 245, 255, 266  
     ultimate moment for, 349  
 Impact tests, 462-470  
 Inelastic bending, 346, 366, 374  
     residual stresses due to, 377  
 Inelastic buckling, 178  
 Inelastic torsion, 381  
     residual stresses due to, 383  
 Initial curvature, beams with, 54  
     plates with, 84  
 Initial ellipticity, tubes with, 190  
 Internal friction, 407, 411  
 Isoclinic lines, 337  
  
 Keyway, stress concentrations due to, 313  
  
 Lamé's theory for thick walled cylinder,  
     208  
  
 Lateral buckling of beams, 199  
 Lattice, crystal, 403  
 Latticed struts, buckling of, 173  
 Limit design, 354-366  
 Lines, isoclinic, 337  
 Lines, Lueders', 330, 418, 420  
 Local stresses (also see *Stress concentra-  
     tions*)  
     in beams, 57, 324  
     in cylinders, 124  
 Longitudinal stresses in torsion, 286  
 Loop, hysteresis, 407, 511  
 Lower yield point, 400, 417  
 Lueders' lines, 330, 418, 420  
  
 Marble, tests of, 440  
 Materials, mechanical properties of, 393-  
     558  
 Maximum distortion energy theory, 441,  
     451-456, 480  
 Maximum energy theory, 448  
 Maximum shear theory, 447  
 Maximum strain theory, 446  
 Maximum stress theory, 445  
 Mechanical properties of materials, 393-  
     558  
 Mechanical properties of steels, table of,  
     558  
 Membrane analogy, 237, 244, 248, 250  
     for torsion beyond elastic limit, 385  
     stress concentrations by, 314  
 Membrane, circular, 101  
 Membrane stresses, 118  
 Mica, tensile tests of, 398  
 Middle surface of a plate, 84  
 Models, in stress analysis, 329  
 Modulus of elasticity, for single crystals,  
     405  
     reduced, 182, 369, 374  
     tangent, 179  
 Modulus of foundation, 1  
 Mohr's theory of failure, 457, 482  
 Moment, ultimate, for beams, 348-353  
 Moment area method, 352  
  
 Natural strain, 428  
 Necking, in tensile test, 402, 427  
 Nonuniform torsion, 255, 258, 265  
 Notch, hyperbolic, 309, 325

Octagonal shaft, torsion of, 236  
 Octahedral plane, 408  
     stresses on, 455  
 Open-coiled spring, 292  
 Overstrain, effect of, 420, 424, 484  
     (also see *Residual stresses* and *Strain hardening*)  
  
 Perfectly plastic materials, 346  
 Permanent set, 400  
 Photoelastic method, 333  
 Pipe flange, stresses in, 141  
 Pipes (see *Tubes*)  
 Pitting cracks, 506  
 Pitting limit, 508  
 Plane, octahedral, 408  
     stresses on, 455  
 Plastic bending (see *Beams*)  
 Plastic deformation of cylinders, 386  
 Plastic hinge, 351  
 Plastic stretching of crystals, 407  
 Plastic torsion (see *Torsion*)  
 Plasticity, 346-392  
 Plates, 76-117  
     buckling of, 193  
     circular, 92-114  
         concentrically loaded, 107  
         large deflections of, 101  
         of variable thickness, 102  
         shear deflection of, 100  
         symmetrically loaded, 92  
         uniformly loaded, 96  
         with a hole, 109  
         with concentrated load, 103  
     cylindrical bending of, 76  
     flexural rigidity of, 77  
     middle surface of, 84  
     pure bending of, 86  
     rectangular, 76-92, 114  
         buckling of, 193  
         cylindrical bending of, 76  
         uniformly loaded, 78, 114  
         with initial curvature, 84  
     stress concentrations in, 301, 306, 324  
     thermal stresses in, 90  
     with initial curvature, 84  
 Pressure, between balls and rollers, 339  
     critical, 186  
     hydrostatic, tests under, 438

*Pressure, cont.*  
     shrink-fit, 210  
 Properties of materials, 393-558  
     at high temperature, 516  
 Properties of steel (table), 558  
 Proportional limit, 400, 509, 558  
 Pure bending, of beams, 366  
     of plates, 86  
  
 Radial stresses, 57, 300  
 Rails, stresses in, 8  
 Raising of yield point, 421  
 Range of stress, 471, 475-478, 511  
 Rankine's theory, 445  
 Rate of strain, effect of, 418  
 Rectangular beam, ultimate moment for, 348  
 Rectangular frame, buckling of, 157  
     ultimate strength of, 362  
 Rectangular plates, 76-92, 114  
     buckling of, 193  
     cylindrical bending of, 76  
     uniformly loaded, 78, 114  
     with initial curvature, 84  
 Rectangular ring, twisting of, 140  
 Rectangular shaft, torsion of, 239, 290, 385  
 Reduced length, 150  
 Reduced modulus, 182, 369, 374  
 Reduction in area in tensile test, 403  
 Relaxation of stress, 530  
 Residual stresses, 212, 220, 413  
     due to inelastic bending, 377  
     due to inelastic torsion, 383  
     effect on endurance limit, 488  
     in thick cylinders, 389  
 Rigid frame, ultimate strength of, 362  
 Rigidity, flexural, 77  
     torsional, 256  
     warping, 265  
 Ring, buckling of, 186  
     conical, 143  
     rotating, 214  
     twisting of, 138-144  
 Rollers, contact stresses in, 339  
     pitting resistance of, 508  
     surface fatigue failure of, 505  
 Rotating cylinder, 219  
 Rotating disc, 214, 223  
     creep in, 541

- Rotating drum, 129
- Rotating ring, 214
- Rotor, stresses in, 222
- Safety factor (see *Factor of safety*)
- Salt crystals, tests of, 397, 430, 463
- Sensitivity factor, 495
- Shafts (see *Torsion*)
- Shear, effect on critical load, 171
  - effect on deflection of plates, 100
  - in beams of variable cross section, 62
- Shear deflection of circular plates, 100
- Shear flow, 248-254
- Shear fracture, 430
- Shear lag, 68
- Shear theory of failure, 447
- Shells, 117-137
  - buckling of, 189
  - conical, 119
  - cylindrical, 121, 124, 134, 189
  - discontinuity stresses in, 124
  - spherical, 119, 124
  - thermal stresses in, 134
- Shrink fit stresses, 210
- Simple radial stress, 57, 300
- Size effect, in fatigue tests, 498
  - in tensile tests, 398
- Slenderness ratio, 150
- Slip bands, 408, 412, 512
- Spherical seat, 340
- Spherical vessel, 119, 124
- Spring, bending of, 296
  - Belleville, 143
  - deflection of, 292
  - fatigue failure of, 492
  - helical, 292
  - torsion of, 295
- Stability (see *Buckling*)
- Steel, effect of carbon content, 394
  - fracture of, 430
  - in elastic range, 411
  - stretching beyond the yield point, 420
  - table of properties, 558
  - tensile test of, 394, 400
  - under combined stresses, 439
  - yielding of, 417
- Strain energy theory for failure, 448
- Strain, natural, 428
  - unit, 427
- Strain hardening, 408, 423
  - effect on creep, 525
- Strain rate, effect of, 418
- Strength theories, 444-462
  - for brittle materials, 457
  - for ductile materials, 444
- Stress, range of, 471, 475-478, 511
  - true, 426
- Stress coat, 333, 418
- Stress concentration factor, definition, 307
- Stress concentrations, 300-345, 489-504
  - and fatigue, 489
  - by membrane analogy, 314
  - by photoelastic method, 333
  - due to grooves, 306, 312, 325
  - due to keyway, 313
  - in beams, 324
  - in bending, 324
  - in brittle materials, 311
  - in concrete tensile test specimen, 310
  - in dovetail joint, 310
  - in ductile materials, 311
  - in glass, 311
  - in plate with a hole, 301
  - in plates, 301, 306, 324
  - in rolled sections, 244, 317
  - in rotating disc, 219
  - in shafts, 312-324
  - in tension or compression, 300
  - in torsion, 312-324
  - in tubes, 305, 314
  - model investigations of, 329
  - reduction of, 498
- Stress relaxation, 530
- Stress trajectories, 337
- Stresses, contact, 339
  - critical (see *Buckling*)
  - in a spring, 292
  - in a wedge, 60, 300
  - in pipe flange, 141
  - in rails, 8
  - in rotating cylinder, 219
  - in rotating disc, 214, 223
  - in shafts (see *Torsion*)
  - in thick walled cylinder, 205
  - local, in beams, 57, 324
  - local, in shells, 124
  - membrane, 118
  - on octahedral plane, 455

- Stresses, *cont.*  
 residual (see *Residual Stresses*)  
 shrink-fit, 210  
 simple radial, 57, 300  
 thermal (see *Thermal Stresses*)  
 working, 544-557
- Struts (also see *Columns*)  
 buckling of, 145-186  
 continuous, 37, 155  
 latticed, 173  
 with lateral load, 26
- Superposition, applied to struts, 30  
 limitations of, 69, 359
- Surface fatigue failure, 505
- Surface finish, effect on endurance limit, 489
- T beams, 64, 267, 350
- Tangent modulus, 179
- Tanks (see *Shells*)
- Temperature, brittleness, 463-470  
 effect on bending of beams, 527  
 effect on endurance limit, 486  
 effect on properties of metals, 516  
 effect on tensile test, 405, 411
- Tensile tests, 393, 435  
 at high temperature, 517  
 elastic aftereffect in, 406  
 fractures in, 430  
 hysteresis loops in, 407  
 of brittle materials, 395  
 of concrete, 310  
 of ductile materials, 400  
 of glass, 395  
 of grooved specimens, 434  
 of mica, 398  
 of perfectly plastic materials, 346  
 of salt crystals, 397, 430, 463  
 of single crystals, 403-410  
 of steel (see *Steel*)  
 size effect in, 398  
 standard specimens for, 310, 394  
 temperature effect in, 405, 411  
 time effect in, 405, 519
- Tests, compression, 435-444  
 impact, 462-470  
 tensile (see *Tensile Tests*)  
 under combined stresses, 438-444  
 under hydrostatic pressure, 438
- Theories of strength, 444-462  
 for brittle materials, 457  
 for ductile materials, 444
- Thermal stresses, in a cylinder, 228  
 in plates, 90  
 in shells, 134
- Thick-walled cylinder, 205 ✓  
 creep in, 538  
 plastic deformation of, 386  
 rotating, 219  
 thermal stresses in, 228
- Thin flanges, beams with, 64
- Thin plates and shells, 76-144
- Thin tubes (see *Tubes*)
- Thin-walled vessels (see *Shells*)
- Three-moment equation, 39
- Tie rod with lateral loading, 41
- Time effect in tensile tests, 405, 519
- Torsion, 235-299  
 beyond the elastic limit, 381  
 combined with bending, 267  
 electric analogy for, 318  
 factor of safety for, 548  
 hydrodynamical analogy for, 312  
 longitudinal stresses in, 286  
 membrane analogy for, 237, 244, 248, 385  
 nonuniform, 255, 258, 265  
 of a channel, 244, 260, 264  
 of a ring, 138-144  
 of a spring, 295  
 of box beams, 250  
 of I beams, 245, 255, 266  
 of noncircular cross sections, 235  
 of rectangular shaft, 239, 290, 385  
 of rolled sections, 244, 255, 266  
 of shafts with varying diameter, 318  
 of thin rectangle, 239, 288  
 of thin trapezoid, 240  
 of thin tubes, 247  
 of wing section, 252  
 of Z section, 266  
 residual stresses in, 383  
 stress concentrations in, 312-324  
 ultimate strength in, 381  
 with warping prevented, 255
- Torsional buckling, 273, 279
- Torsional rigidity, 256
- Torus, with internal pressure, 123

- Toughness, 462  
 Trajectories of stress, 337  
 Trapezoidal shaft, torsion of, 236, 240  
 Triangular shaft, torsion of, 235  
 Trigonometric series, beam deflections by, 46  
 True stress, 426  
 Tubes, buckling of, 189  
     effect of creep in, 537  
     stress concentrations in, 305, 314  
     tests of, 441  
     torsion of, 247  
     with initial ellipticity, 190  
     with reinforcing ring, 130, 132  
 Twist (see *Torsion*)  
 Twisting of a ring, 138-144  
  
 Ultimate moment for beams, 348-353  
 Ultimate strength of beams, 354-362  
     of frames, 362-366  
     by virtual displacements, 362  
 Ultimate strength in tensile tests, 401  
 Ultimate torque of a shaft, 381  
 Upper yield point, 400, 417  
  
 Variable cross section, beams of, 62  
     columns of, 169  
  
 Variable, cross section, *cont*  
     shafts of, 318  
 Variable thickness, circular plates of, 102  
     rotating disc of, 223  
 Vessels, thin walled (see *Shells*)  
 Virtual displacements, ultimate strength by, 362  
  
 Warping due to torsion, 255  
 Warping rigidity, 265  
 Wedge, stresses in, 60, 300  
 Wing section, torsion of, 252  
 Working stresses, 544-557  
     for alternating loads, 551  
     for bars in tension, 544, 552  
     for bending, 547  
     for brittle materials, 549, 552, 555  
     for ductile materials, 546, 552  
     for static loads, 546  
     for torsion, 548  
  
 Yield moment in a beam, 347  
 Yield point, 417-420, 558  
     effect of temperature on, 517  
     raising of, 421  
     upper and lower, 400, 417  
  
 Z section, torsion of, 266